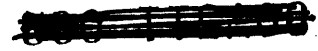


Well Completion Rpt  
Vol. 2 , Part 2 of 2  
Turrum-7  
(W1300)



TURRUM 7  
WELL COMPLETION REPORT  
VOLUME 2  
INTERPRETIVE DATA  
Part 2 of 2

GIPPSLAND BASIN  
VICTORIA

ESSO AUSTRALIA LIMITED

Petroleum Development

6 APR 2000

COMPILED BY:

Michael Gilbert  
Simon Grope  
Pamela McKean

March, 2000

**TURRUM 7**  
**VOLUME 2: INTERPRETIVE DATA**

**Part 1 of 2****CONTENTS**

1. INTRODUCTION
2. SUMMARY OF WELL RESULTS
  - Objectives
  - Uncertainties
  - Results
3. OVERVIEW
  - Regional Setting
  - Stratigraphy
  - Structure
4. GEOLOGICAL DISCUSSION
  - L110/L132 Reservoir
  - L133/L137 Reservoir
  - L170 Reservoir
  - L180 Reservoir
  - L190 & L193 Reservoirs
  - L200 Reservoir
  - L360 Reservoir
    - MDT Data
    - Core Analysis
    - L360 East Flank Oil Column Height
5. GEOPHYSICAL DISCUSSION
  - Geophysical Data
  - Time Interpretation
  - Depth Conversion

**TABLES**

1. PREDICTED VS ACTUAL FORMATION TOPS

**FIGURES**

1. LOCALITY MAP
2. STRATIGRAPHIC TABLE
3. TURRUM L360 PRESSURE vs DEPTH PLOT
4. TURRUM L360 EAST FLANK PRESSURE vs DEPTH PLOT

**ENCLOSURES**

1. STRUCTURAL CROSS SECTION
2. STRATIGRAPHIC CROSS SECTION
3. POST DRILL L360 DEPTH STRUCTURE MAP
4. SYNTHETIC SEISMOGRAM
5. SEISMIC INLINE 540

**ATTACHMENTS**

1. COMPOSITE WELL LOG

**TURRUM 7**  
**VOLUME 2: INTERPRETIVE DATA**

**Part 2 of 2**

**APPENDICES**

1. MDT ANALYSIS
2. QUANTITATIVE FORMATION EVALUATION
3. PALYNOLOGICAL ANALYSIS
4. GEOCHEMISTRY
5. CORE ANALYSIS
  - Routine Core Analysis: Permeability & Porosity
  - Special Core Analysis: Petrology
  - Special Core Analysis: Mercury Injection Capillary Pressure
6. WELL SEISMIC PROCESSING REPORT

907511 005

APPENDIX 1

907511 006

**APPENDIX 1**

**TURRUM 7**

**MDT Analysis**

907511 007

**TURRUM-7 MDT INTERPRETATION**

VIC/L4 Bass Strait

Sedco 702 Semi-Submersible

13th September 1999

C.P. Sullivan  
M.B. Gilbert

**Contents**

- 1.0 Summary and Conclusions
- 2.0 Turrum Sands - General Interpretation
- 3.0 L110/L132 Gas Sands Interpretation
- 4.0 L170 Gas Sands Interpretation
- 5.0 L180 Gas Sands Interpretation
- 6.0 L200 Oil Sands Interpretation
- 7.0 Turrum-7 MDT Sampling Program

**Attachments:**

- Figure 1 - Turrum-7 MDT; -2200 to -2800 m TVDSS (Full Pressure Dataset)
- Figure 2 - Turrum-7 MDT; -2200 to -2400 m TVDSS (Upper Turrum Sands)
- Figure 3 - Turrum-7 MDT; -2400 to -2750 m TVDSS (Lower Turrum Sands)
- Figure 4 - Turrum-7 MDT; -2170 to -2290 m TVDSS (L110/L132 Gas Interpretation)
- Figure 5 - Turrum-7 MDT; -2290 to -2410 m TVDSS (L170 Gas Interpretation)
- Figure 6 (a), (b) - Turrum-7 MDT; -2290 to -2410 m TVDSS (L180 Gas Interpretation)
- Figure 7 (a), (b) - Turrum-7 MDT; -2380 to -2480 m TVDSS (L200 Oil Interpretation)
- Esso Australia Ltd - MDT Pressure Data Field Input Forms (8 pages)



## 1.0 Summary and Conclusions

Turrum-7 was spudded @ 10:15hrs on 24th August 1999, reached TD @ 13.15hrs on 13th September 1999 and the rig was released from location at 18:00hrs on 20th September 1999. The well is located in VIC production licence L4 at 5,764,066 m North and 610,550 m South (Longitude: 148 15' 49.226" E, Latitude: 38 15' 52.256" N) and lies approximately 5.5 km south-east of the Marlin-A platform in 62m of water.

Turrum-7 is a near vertical well with a maximum deviation of 4.0 degrees, drilled to a total depth of 2830 m MDRKB with a KB height of 26 metres. The well encountered the top of Latrobe group at 1765 m MDRKB (-1738 m TVDSS), and several small gas sands between 2265m MDRKB (-2238 m TVDSS) and TD. Potential oil sands were also encountered at 2439 m MDRKB (-2412 m TVDSS, L200 oil transition zone) and 2613 MDRKB (-2586 m TVDSS, (L360 oil shows but inconclusive if live oil or residual oil). All other sands encountered within the Turrum reservoirs appear to be wet.

56 pressure surveys were attempted during the MDT program (41 + 15 repeats). 12 attempts were made to obtain pretests & samples in the L200 and L360 without success (formation too tight). The full MDT pressure dataset is plotted in Figure 1.

The main conclusions of the Turrum-7 MDT interpretation are:

1. The drawdown in water sands intersected by Turrum-7 varied from zero to 70 psia relative to the original aquifer (Figures 1, 2 & 3). The general trend was consistent with other Turrum wells in that the degree of drawdown tended to decrease with depth (with the exception of the deepest, higher quality sands). Because of this complex pressure regime it is difficult to interpret definitive hydrocarbon-water contacts for the Turrum reservoir systems.
2. The L110/L132 gas sand at -2239 to -2246 m TVDSS (Figure 4) has a gradient of 0.32 psi/m. Due to the unknown aquifer pressure in this area a definitive gas-water contact cannot be determined. Using the Turrum-7 water gradient from the overlying L100 water sand, a lowest likely gas/free-water level is interpreted at -2278m TVDSS. Although the L110 and L132 sands appear to be geologically separated at Turrum-7 (consistent with other Turrum wells), pressure points in these sands were found to lie on the same gas gradient (Figure 4), indicating that they could be in communication away from well control.
3. The Turrum-7 L133 and L137 sands were found to lie on a common water gradient of 1.37 psi/m (Figure 4). These sands have previously been seen as independent sands separated by shale in other Turrum wells but appear to represent a common system at this location.

4. The L170 gas sand at -2321 to -2324 m TVDSS (Figure 5) has a gradient of 0.33 psi/m. Due to the unknown aquifer pressure in this area; a definitive gas-water contact cannot be determined. Using L170 water gradient data from Turrum-6, the highest likely gas/free-water level is interpreted as being at -2334 m TVDSS. Using Turrum-7 water gradient data from the overlying L160 water zone; the lowest likely gas/free-water level is interpreted at -2353m TVDSS.
5. The L180 gas sand at -2327 to -2332 m TVDSS (Figure 6a) has a gradient of 0.37 psi/m. Using Turrum-6 and Turrum-7 MDT pressure data, the lowest likely gas/free-water level is estimated to be between -2348m TVDSS and -2353m TVDSS (Figures 6 a, b).
6. Pressure data in the L200 sand at -2413 to -2423 m TVDSS (Figure 7 (a)) indicates a gradient of 1.18 psi/m which is interpreted as an oil/water transition zone, suggesting the possibility of an updip oil column. If there is oil in the L200 sand, the estimated largest likely oil column is 31m (See Figure 7 (b)). MDT samples were attempted in this zone without success due to the tight formation and concerns over differentially sticking the tool.
7. Due to the inability to obtain MDT pressure readings or samples in the main target L360 sand, no conclusions can be drawn from the MDT analysis as to the contents of these zones. Log and core analysis indicates that Turrum-7 failed to intersect any net rock at the L360 level. The L360 Upper is interpreted as being absent and the L360 Lower as being of much poorer quality than expected. The presence of hydrocarbon in this interval has been independently confirmed by Geochemical Analysis (see EPR Report 96ES.99).

## **2.0 Turrum-7 MDT: -2200 to -2750m TVDSS, General Interpretation (Water Sands)**

The drawdown in water sands intersected by Turrum-7 varied from zero to 70 psia relative to the original aquifer (Figures 1, 2 & 3). The general trend was consistent with other Turrum wells in that the degree of drawdown tended to decrease with depth (with the exception of the deepest, higher quality sands). Because of this complex pressure regime it is difficult to interpret definitive hydrocarbon-water contacts for the Turrum reservoir systems.

## **3.0 Turrum-7 MDT: -2200 to -2290 m TVDSS Interpretation (L110/L132 Gas Sands)**

The L110/L132 sands at -2239 to -2246 m TVDSS are interpreted from the MDT pressure analysis as being gas sands with a gradient of 0.32 psi/m (Fig 4). Although the L110 and L132 sands appear to be geologically separated at Turrum-7 (consistent with other Turrum wells), pressure points in these sands were found to lie on the same gas gradient, indicating that they could be in communication within the gas cap away from well control. The base of the sand, from log analysis, is at -2246 m TVDSS which is interpreted as lowest known gas.

The L100 water sands (stratigraphically extensive, high permeability rock) are relatively well connected to the regional aquifer, as demonstrated by the 70 psi drawdown. The L110 and L132 sands are more poorly connected fluvial sands of limited extent, hence are likely to experience less pressure drawdown. A lowest likely gas/free-water level was identified in the L110/L132 sands @ -2278m TVDSS by extrapolating Turrum-7 L110/L132 gas gradient to the Turrum-7 L100 water gradient line (Fig 4). As the L110/L132 sands would probably be drawn down less than the L100, the gas water contact is likely to be higher than this.

The Turrum-7 L133 and L137 sands were found to lie on a common water gradient of 1.37 psi/m. These sands have previously been seen as separate sands separated by shale in other Turrum wells but do not appear to be separated at this location.

## **4.0 Turrum-7 MDT: -2290 to -2410 m TVDSS Interpretation (L170 Gas)**

The L170 reservoir sands at -2321 to -2324 m TVDSS are interpreted from the MDT pressure analysis as being gas sands with a gradient of 0.33 psi/m (Figure 5).

Water gradient data has been plotted for the Turrum-7 L160 and L193 sands (closest Turrum-7 water sands above and below the L170 gas sands) and Turrum-6 L170 water sands. No water gradient data is available in the L170 water sands in the adjacent Turrum-4 well.

The following conclusions can be drawn from this chart:

- A highest likely gas/free-water level in the Turrum-7 L170 sands is identified on Figure 5 at -2334 m TVDSS. This assumes that Turrum-7 and Turrum-6 are in stratigraphic communication and that drawdown of pressure between Turrum-6 and Turrum-7 (approximately 4 years) is minimal. This represents a conservative estimate, as any pressure drawdown of the Turrum-6 water gradient has not been accounted for (ie. the actual contact could be deeper than this).
- If Turrum-7 and Turrum-6 sands are not in stratigraphic communication, the L170 water gradient at Turrum-7 probably lies somewhere between the Turrum-7 L160 and L193 water gradients shown on Figure 5. Using Turrum-7 water gradient data from the overlying L160 water zone; a lowest likely gas/free-water level is interpreted at -2353m TVDSS. As the L170 water sands would probably be drawn down less than the L160 water sands, the gas water contact is likely to be higher than this.

#### **5.0 Turrum-7 MDT; -2290 to -2410 m TVDSS Interpretation (L180 Gas)**

The L180 reservoir sands at -2327 to -2332 m TVDSS are interpreted from the MDT pressure analysis as being gas sands with a gradient of 0.37 psi/m (Fig 6 (a)). A lowest likely gas/free-water level is identified at -2348 m TVDSS by extrapolating T7 L180 gas gradient to T7 L160 water gradient.

An alternative lowest likely gas/free-water level of -2353m TVDSS in the Turrum-7 L180 sands was inferred by extrapolating the Turrum-7 L180 gas gradient to the estimated Turrum-7 L180 water gradient (figure 6 (b)). This approach assumed that the L180 water sands were drawn down by the same amount as the L160 sands between Turrum- 4 and Turrum-7 (27 psia between 1992 and 1999).

The actual gas-water contact is likely to be higher than both of the above interpretations as the L180 water sands will probably be less drawn down than the L160 sands if they follow the regional trend.

#### **6.0 Turrum-7 MDT; -2380-2480 m TVDSS Interpretation (L200 Oil)**

The pressure data in the sand at -2413 to -2423 m TVDSS (Figure 7(a)) has a gradient of 1.18 psi/m. Petrophysical analysis of this zone at Turrum-7 demonstrates a hydrocarbon saturation of +/- 28% in good reservoir (~ 19% porosity). This saturation could represent residual hydrocarbon or a hydrocarbon transition zone. The absence of a water gradient in the MDT analysis supports the interpretation that this represents an oil transition zone.

Insufficient data is available to accurately estimate the potential L200 oil column height; hence a non-rigorous qualitative approach was used (see Fig 7 (b)). For the purposes of this analysis, the shallowest Turrum-7 L200 MDT point at -2419m was assumed to be the OWC (this point effectively represents the lowest likely oil).

An estimated Turrum-7 (1999) L200 gas gradient was derived by plotting Turrum-3 (1985) L200 data and drawing down by 0.4 psi/year (the average drawdown seen in the L200 series sands between Turrum 3 (1985) and Turrum 5 (1995)) to 1999.

Gradients of 1.42 psi/m and 0.93 psi/m were assumed for the water and oil respectively. This approach yielded an estimated highest likely GOC at 2388m TVDSS and lowest likely gas at 2403m TVDSS. **This qualitative approach indicates that if there is oil in the L200 sand, the estimated largest likely oil column is approximately 31m.**

### **7.0 Turrum-7 MDT Sampling**

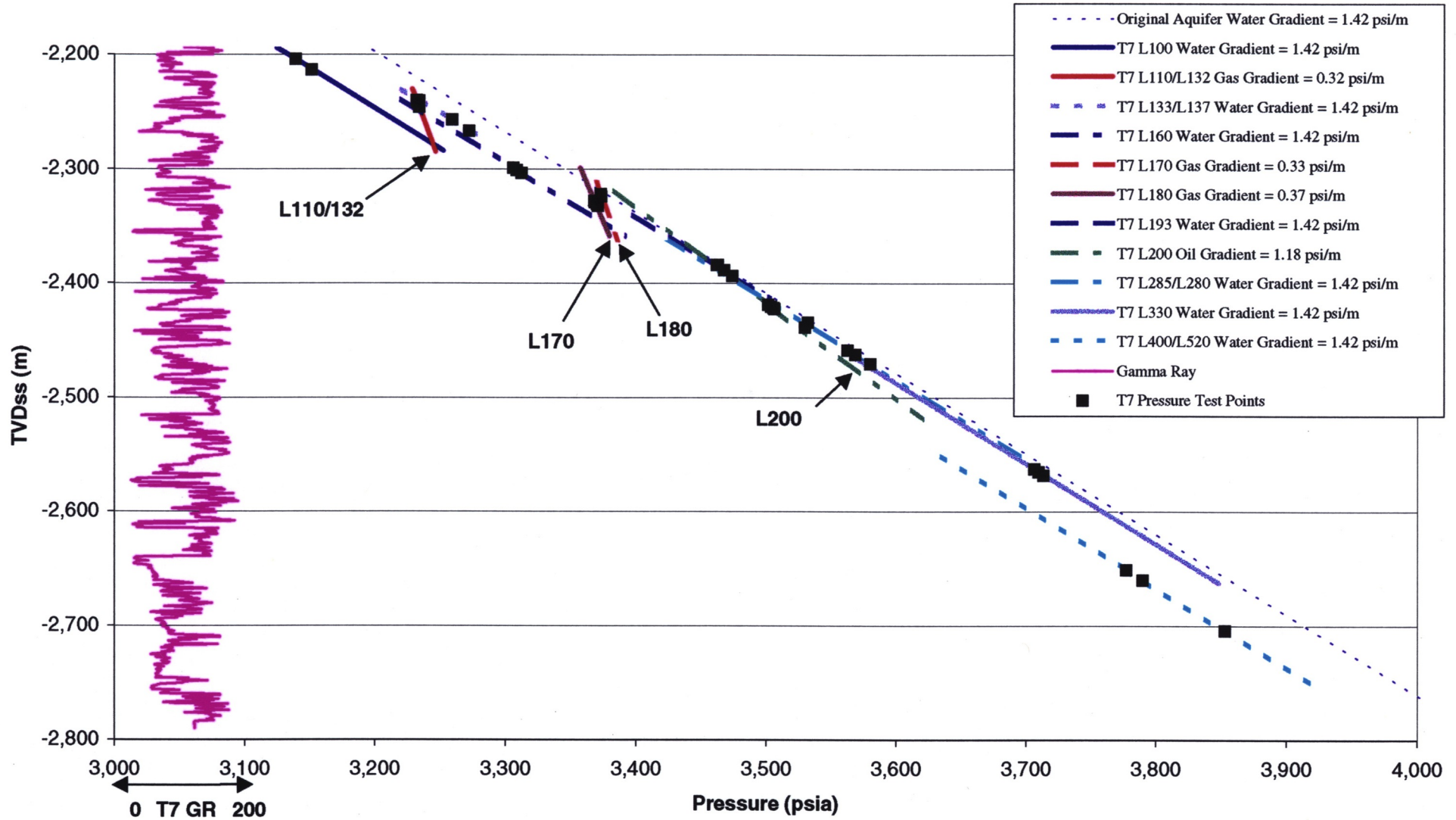
The objective of the MDT sampling program was to obtain two samples in both the L200 and L360 Upper sands. Two samples and one pretest were attempted in the L200 sands without success due to poor formation quality and concerns over differentially sticking the tool.

*Note - operating procedures specified that sample acquisition was only to be attempted if there was minimal risk of differentially sticking the tool, hence ruling out extended sampling times.*

Nine pre-tests were attempted in the L360 sands (four in the L360 upper and five in the L360 lower) without success due to poor formation quality (eight attempts) and failure to achieve a pressure seal (one attempt).

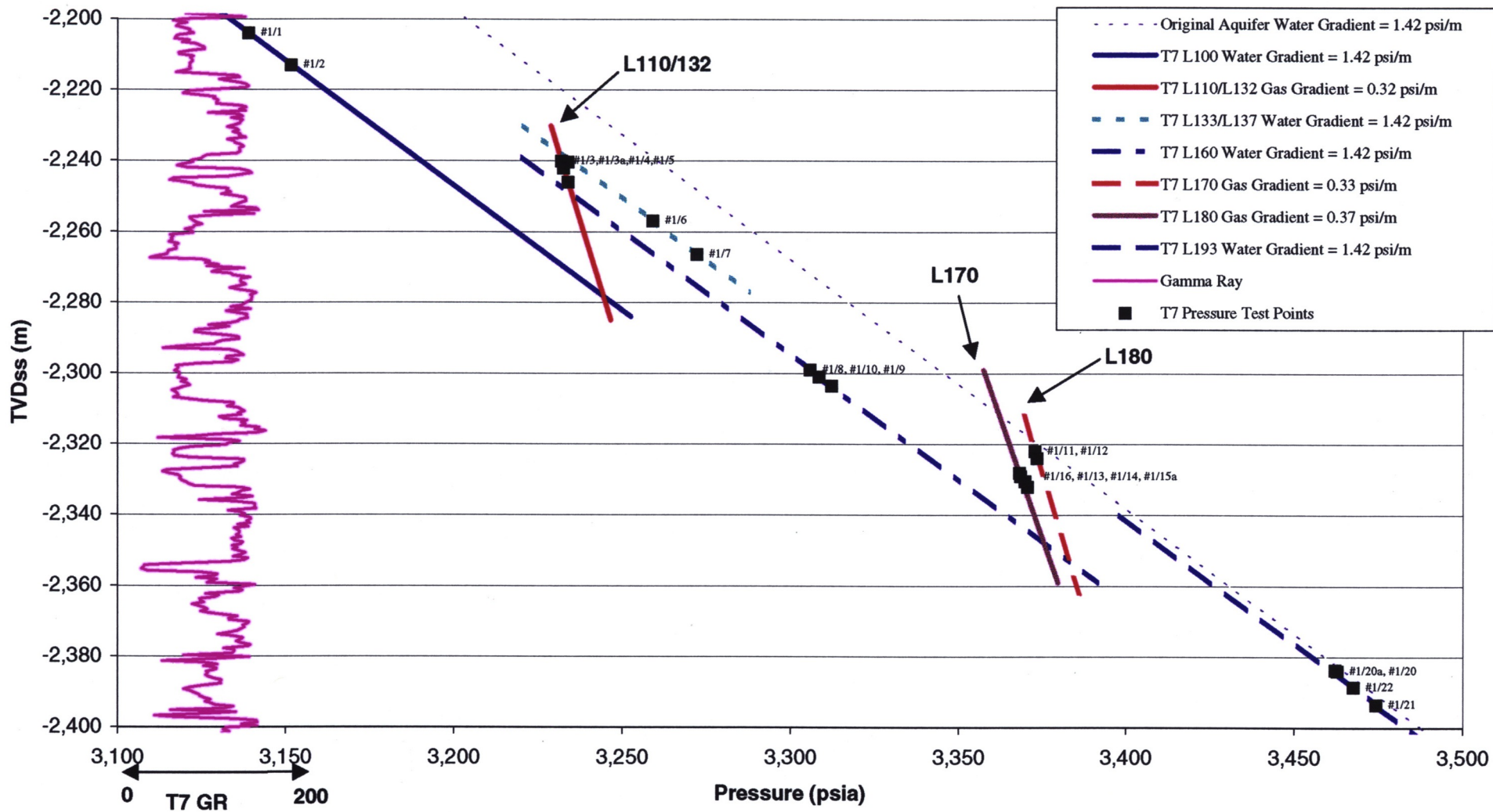
It was recognised prior to commencing the MDT sampling program that obtaining samples was likely to be extremely difficult. This was demonstrated in the preceding MDT pressure program where the L200 sands exhibited very low mobility ratios and not one pressure test was achieved on the L360 sands despite numerous attempts.

Figure 1; Turrum 7 - Depth v MDT Pressure Plot (Full Dataset)



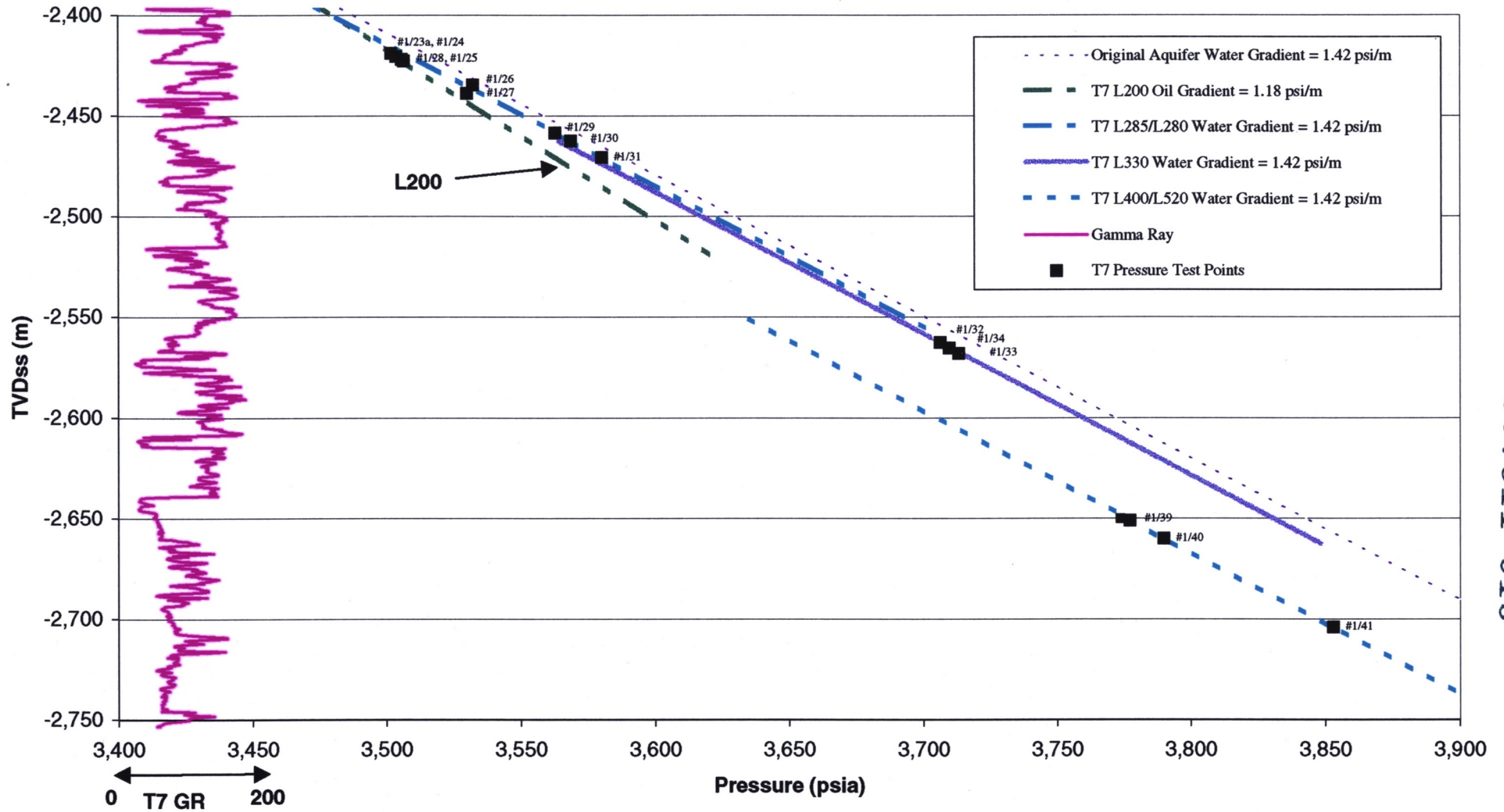
907511 014

Figure 2; Turrum 7 - Depth v MDT Pressure Plot - Upper Turrum Sands (-2200 to -2400 m TVDss m)



907511 015

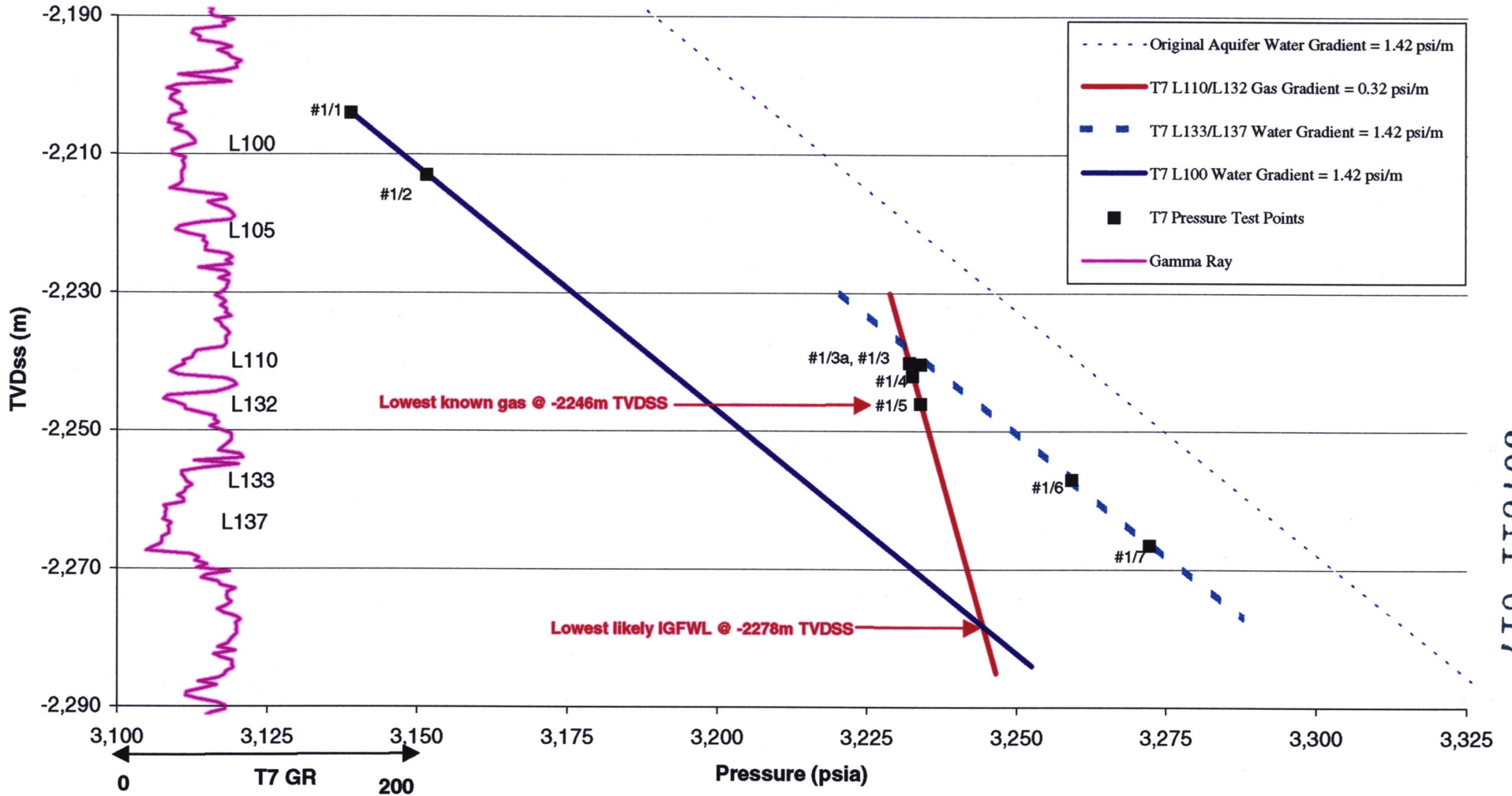
Figure 3; Turrum 7 - Depth v MDT Pressure Plot - Lower Turrum Sands (-2400 to -2750 m TVDss)



907511 016

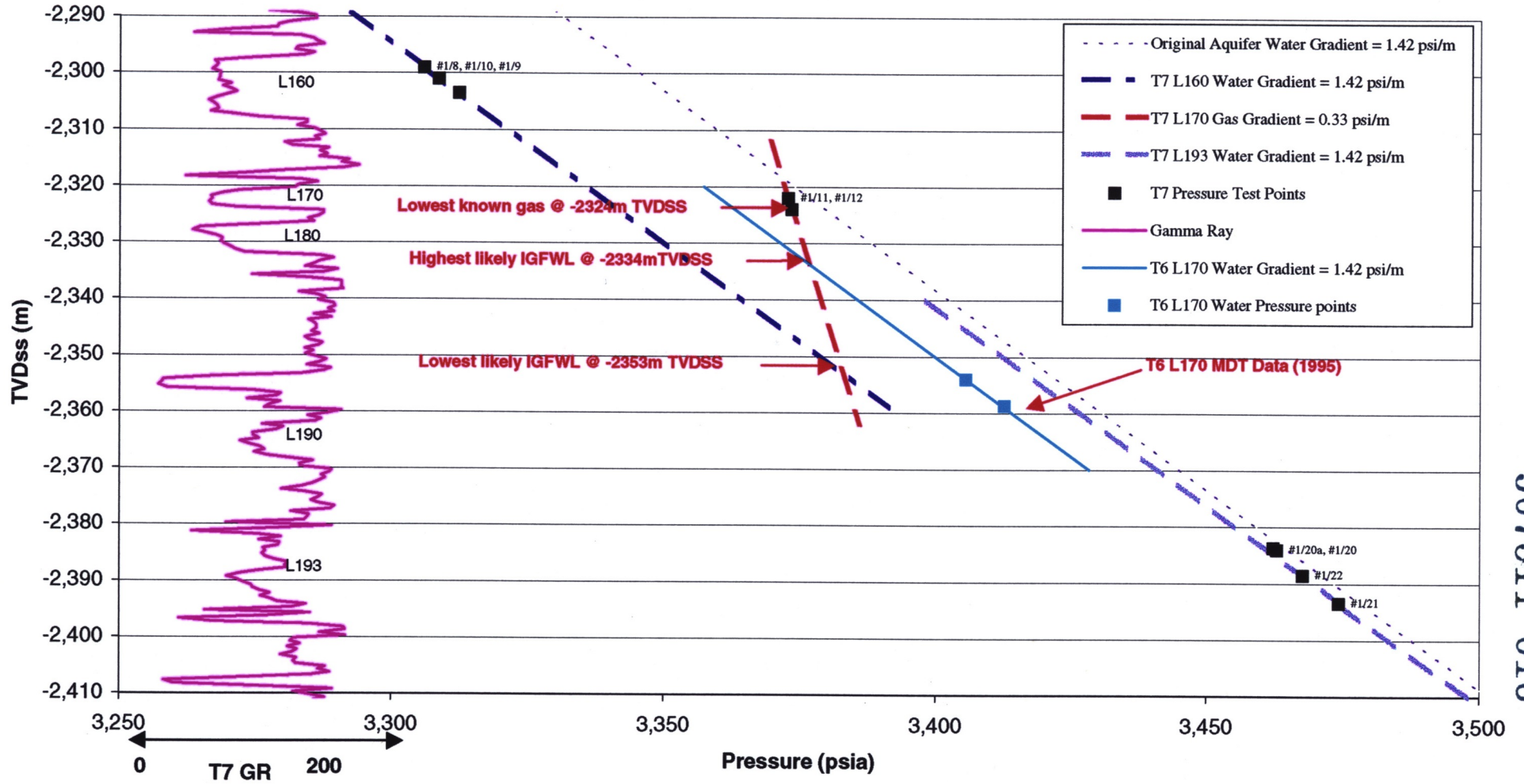


Figure 4; Turrum 7 - Depth v MDT Pressure Plot (L110/L132 Gas Interpretation)



907511 017

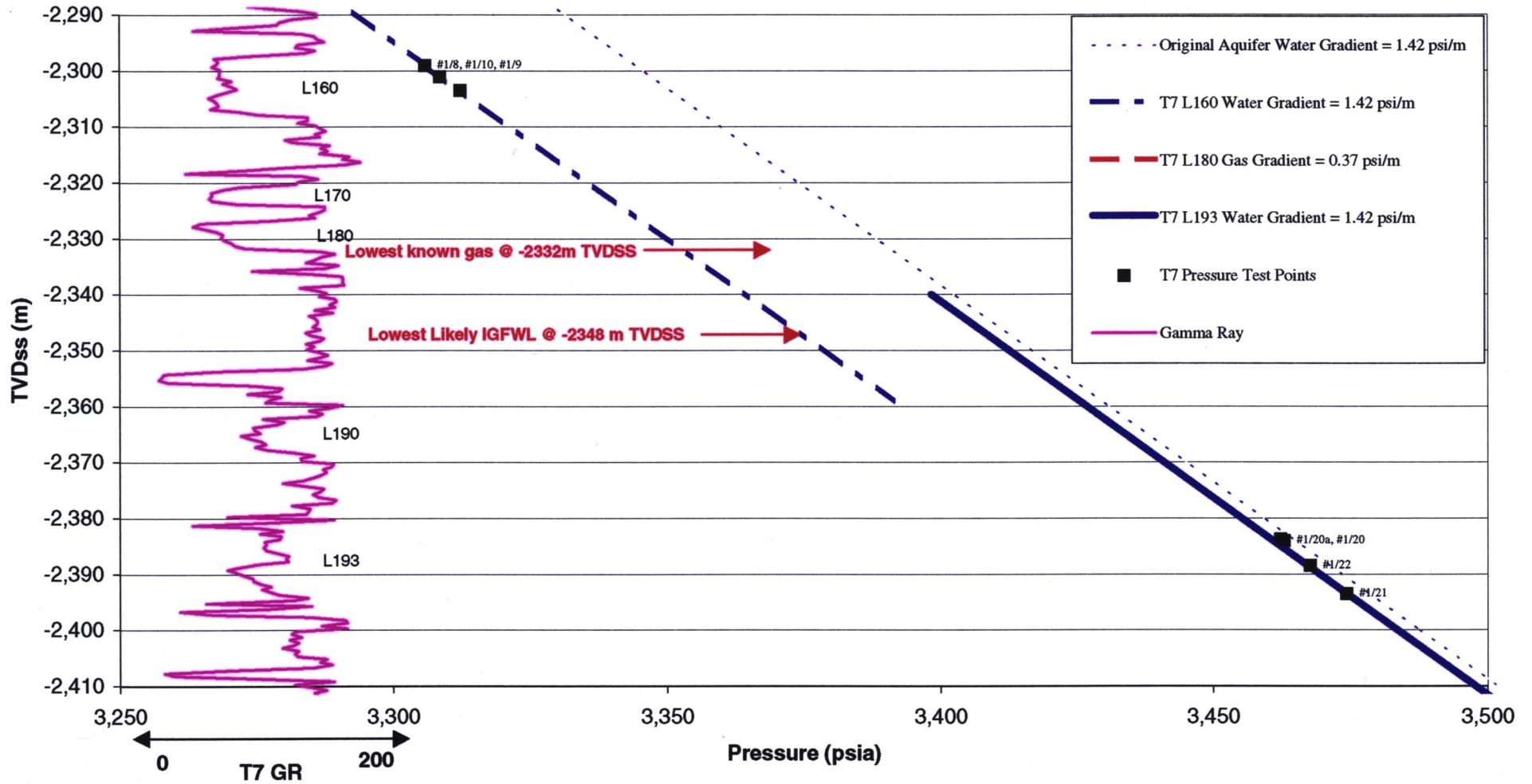
Figure 5; Turrum 7 - Depth v MDT Pressure Plot (L170 Gas Interpretation)



907511 018

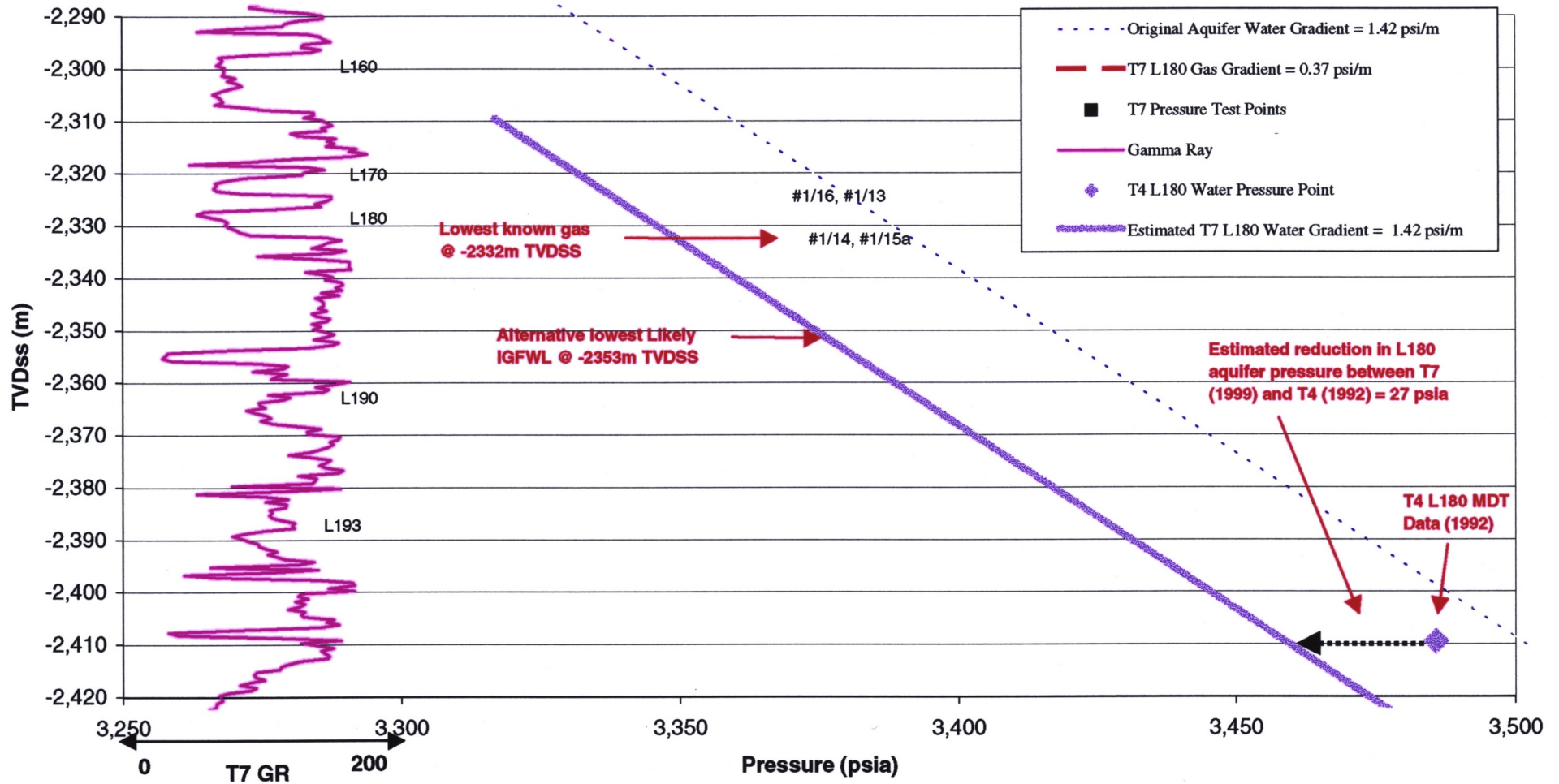
PE907511\_05

Figure 6 (a): Turrum 7 - Depth v MDT Pressure Plot (L180 Gas Interpretation)



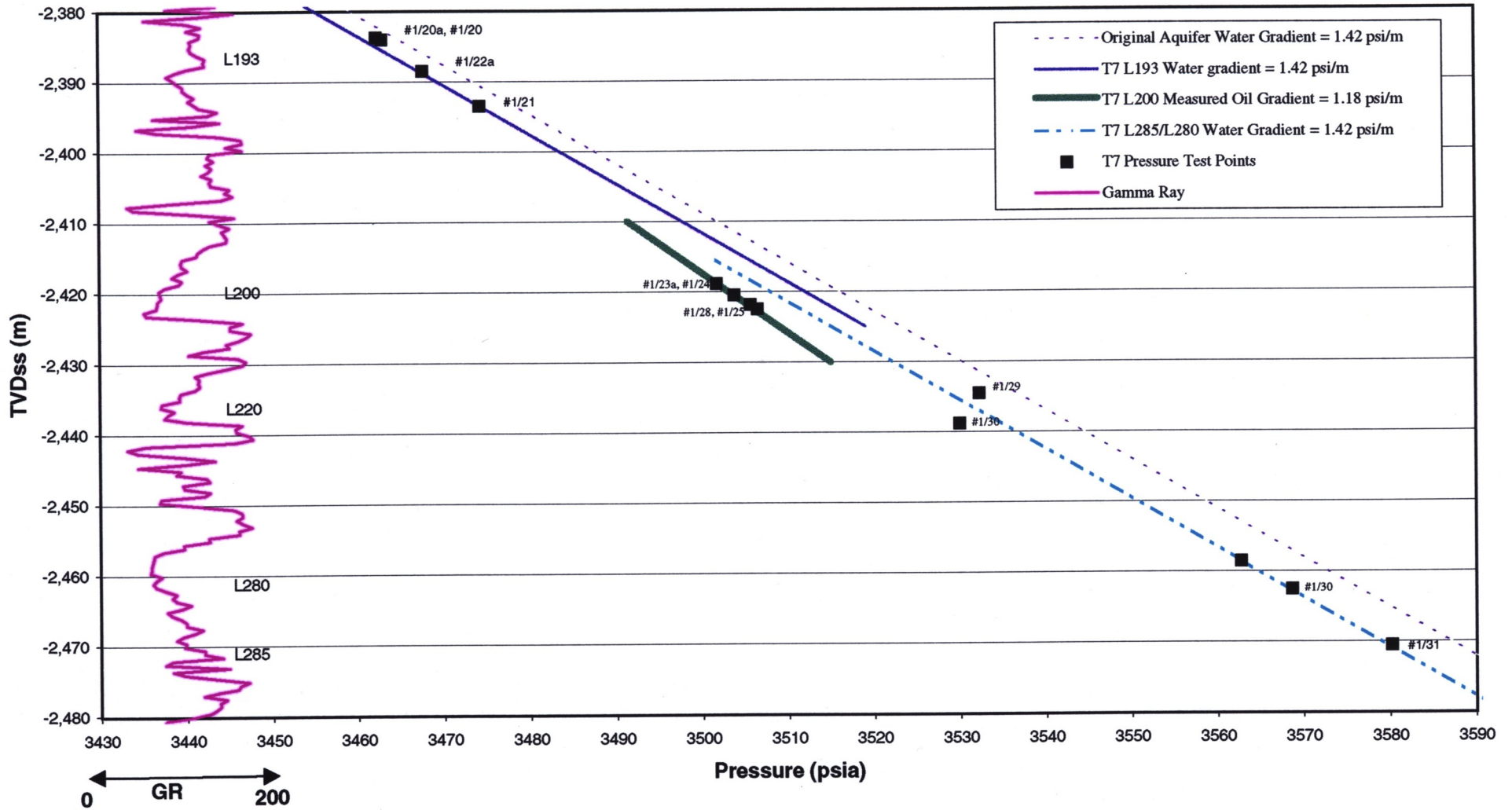
907511 019

Figure 6 (b); Turrum 7 - Depth v MDT Pressure Plot (L180 Gas Interpretation)



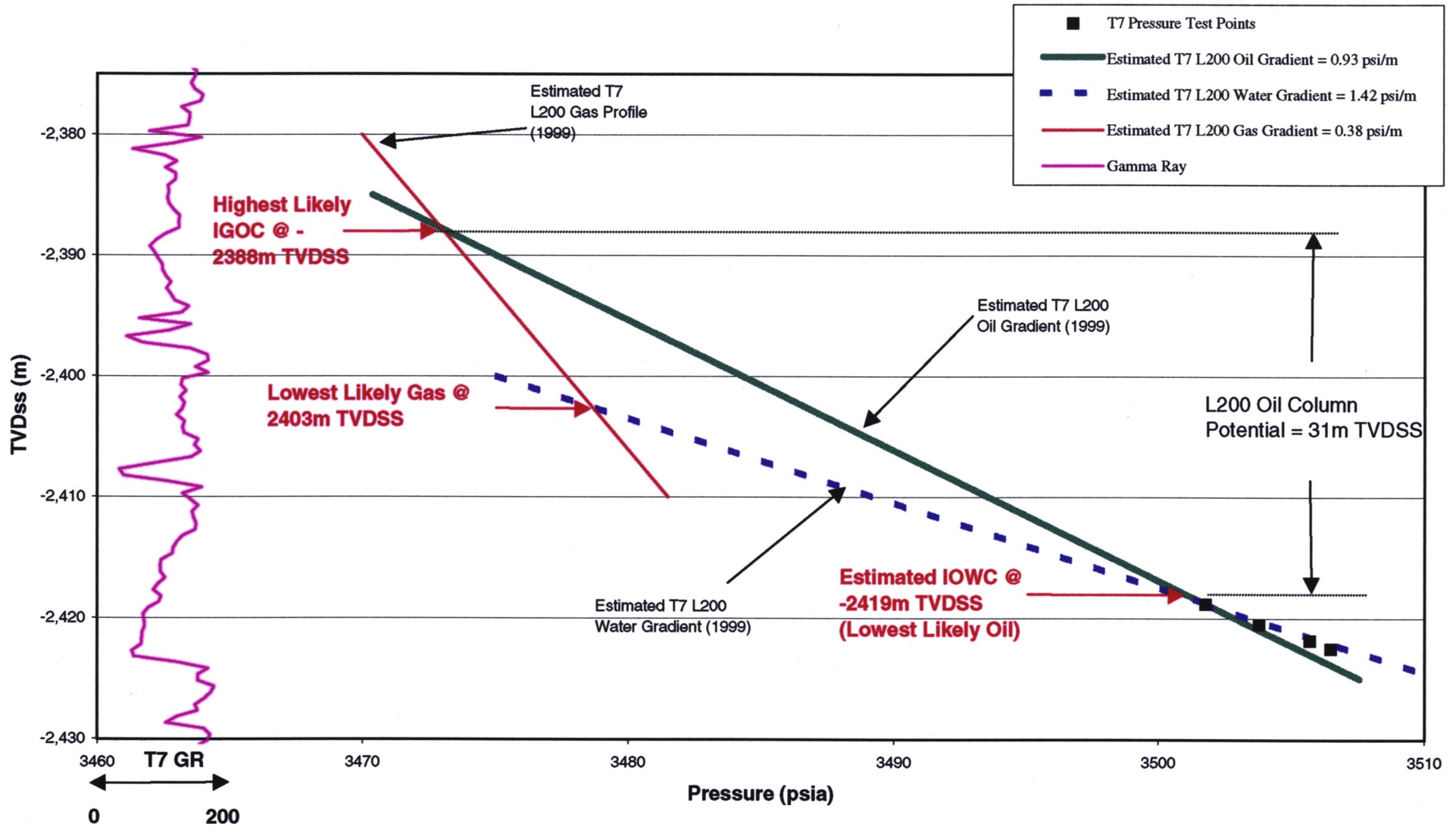
907511 020

Figure 7 (a); Turrum 7 - Depth v MDT Pressure Plot (L200 Oil Interpretation)



907511 021

Figure 7 (b); Turrum 7 - Depth v MDT Pressure Plot (L200 Oil Interpretation)



907511 022

**ESSO AUSTRALIA LTD - PRESSURE DATA FORM**

Well		TURRUM-7		Page		1		of		8	
Date		14-15/9/99		Geologist-Engineer		Greg Clota/Martin Turner					
Tool Type (MDT, RFT)		Schlumberger MDT		KB (metres):		26					
Gauge Type		CQG		Probe type		Long nose					
Pressure units (psia, psig)		PSIA		Temperature units (degF, degC)		degC					
Run-Seat Number	Depth		Initial Hydrostatic Pressure	Time Set (HH:MM)	Minimum Flowing Pressure	Formation Pressure	Temp	Time Retract (HH:MM)	Final Hydrostatic Pressure	Delta Time (MM:SS)	Comments including Test Quality and Fluid Type.
	m MDRKB	m TVDSS									
1/1	2230.0	2204.0	4010	23:34	3121.4	3138.9	84.4	23:39	4016	05:00	Good Perm 20cc vert ptest MD/CP= 285.4 (20cc DD)
1/2	2239.0	2213.0	4041	23:47	2916.5	3151.5	86.0	23:51	4013	04:00	Good Perm MD/CP= 24.1 (20cc DD)
1/3	2266.3	2240.3	4085	0:00	3223.3	3233.9	88.2	0:05	4077	05:00	Good perm MD/CP= 317.4 (20cc DD)
1/4	2268.0	2242.0	4081	0:14	3228.0	3232.4		0:18	4078	04:00	Good perm MD/CP= 1174.7 (20cc DD)
1/5	2272.0	2246.0	4085	0:26	3231.5	3233.9	90.0	0:31	4084	05:00	Good perm MD/CP= 3025.7 (20cc DD)
1/3A	2266.1	2240.1	4074	0:41	3221.0	3232.0	90.5	0:46	4074	05:00	Good Perm MD/CP= 534.3 (20cc DD)
1/6	2283.0	2257.0	4105	0:57	3205.6	3259.1	90.7	1:00	4104	03:00	Good Perm MD/CP= 121.8 (20cc DD)
1/7	2292.5	2266.5	4122	1:10	3270.9	3272.2	91.0	1:15	4121	05:00	Good Perm MD/CP= 4952.5 (20cc DD)
1/8	2325.0	2299.0	4179	1:24	3288.2	3305.9	91.7	1:30	4179	06:00	Good Perm MD/CP= 326.8 (20cc DD)
1/9	2329.5	2303.5	4187	1:37	3303.5	3312.1	92.3	1:42	4187	05:00	Good Perm MD/CP= 21.7 (20cc DD)

907511 023

ESSO AUSTRALIA LTD - PRESSURE DATA FORM

Well		TURRUM-7		Page 2 of 8				
Date	14/12/99	Geologist/Engineer	Greg Clift/Martin Turner <th>KB (metres)</th> <td>26</td>	KB (metres)	26			
Tool Type (MDT, RFT)	Schlumberger MDT <th>COG</th> <td>F81A <th>Long nose</th> <td>degC</td> </td>	COG	F81A <th>Long nose</th> <td>degC</td>	Long nose	degC			
Gauge Type		Probe type		Temp	degC			
Pressure units (psi, psig)		Temperature units (degF, degC)		Formation Pressure	PPk			
Run-Seat Number	Depth	Initial Hydrostatic Pressure	Time Set (HH:MM)	Minimum Flowing Pressure	Temp Retract (HH:MM)	Final Hydrostatic Pressure	Delta Time (MM:SS)	Comments Including Test Quality and Fluid Type.
m MDRKB	m TVDSS	PPk	PPk	PPk	PPk	PPk		
1/10	2327.0	2301.0	1:52	3292.5	92.8	4182	04:00	Good Perm
					8.4	4182		MD/CF= 418.1 (20cc DD)
					10.5	4182		Good Perm
1/11	2348.0	2322.0	2:07	3367.5	92.1	4220	03:00	Good Perm
					8.5	4220		MD/CF= 1168.3
					10.5	4220		Good Perm
1/12	2350.0	2324.0	2:18	3359.5	93.1	4223	05:00	Good Perm
					8.5	4223		MD/CF= 720.3 (20cc DD)
					10.5	4223		Good Perm
1/13	2355.0	2329.0	2:40	3366.3	93.6	4232	05:00	Good Perm
					8.5	4232		MD/CF= 2975.4 (20cc DD)
					10.5	4232		Mod perm
1/14	2356.5	2330.5	2:54	3269.7	93.7	4235	04:00	MD/CF= 57.3 (20cc DD)
					8.5	4235		Low perm.
					10.5	4235		Test curtailed
1/15	2358.5	2332.5	3:05	1861.6	93.8	(1967.03)	07:00	MD/CF= 17.0 (20cc DD)
					-	(1967.03)		Good Perm
					10.5	(1967.03)		MD/CF= 3677 (20cc DD)
1/16	2354.0	2328.0	3:18	3352.6	93.8	4230	06:00	Good Perm
					8.5	4230		MD/CF= 73.8 (20cc DD)
					10.5	4230		Low perm.
1/15A	2358.0	2332.0	3:25	3364.0	93.8	4237	04:00	Test curtailed
					8.5	4237		MD/CF= 671.1 (20cc DD)
					10.5	4237		Low perm.
1/17	2384.5	2358.5	4:16	1914.4	93.4	(1976.19)	06:00	Test curtailed
					-	(1976.19)		MD/CF= 671.1 (20cc DD)
					10.5	(1976.19)		Low perm.
1/18	2390.0	2364.0	4:29	1888.4	93.7	(1947.49)	07:00	Test curtailed
					-	(1947.49)		MD/CF= 3.1 (20cc DD)
					10.5	(1947.49)		Low perm.



**ESSO AUSTRALIA LTD - PRESSURE DATA FORM**

Well		TURRUM-7				Page		3 of 8			
Date		14-15/99				Geologist-Engineer		Greg Clots/Martin Turner			
Tool Type (MDT, RFT)		Schlumberger MDT				KB (metres):		26			
Gauge Type		COG				Probe type		Long nose			
Pressure units (psia, psig)		PSIA				Temperature units (degF, degC)		degC			
Run-Seat Number	Depth		Initial Hydrostatic Pressure	Time Set (HH:MM)	Minimum Flowing Pressure	Formation Pressure	Temp	Time Retract (HH:MM)	Final Hydrostatic Pressure	Delta Time (MM:SS)	Comments Including Test Quality and Fluid Type.
	m MDRKB	m TVDSS									
1/19 F	2394.1	2368.1	4300 10.5	4:45	1391.1	(1561.22) -	94.4	4:52	4300 10.5	07:00	Command to limit DD to 10cc not accepted by computer. Test not charged. Low perm. TEST curtailed
1/19A F	2394.1	2368.1	4300 10.5	4:54	2030.9	(2162.68) -	94.7	5:00	4300 10.5	06:00	Low perm Test curtailed MD/CP- ? (10cc DD)
1/20 F	2410.0	2384.0	4328 10.5	5:09	3405.4	3462.9 8.5	95.1	5:17	4328 10.5	08:00	Low perm Pressure stabilised MD/CP- 4.7 (20cc DD)
1/21 F	2419.5	2393.5	4345 10.5	5:24	2408.9	3474.3 8.5	95.3	5:30	4345 10.5	06:00	Low perm Pressure stabilised MD/CP- 4.7 (20cc DD)
1/22 F	2414.5	2388.5	4337 10.5	5:40			95.8	5:45	4337 10.5	05:00	Test accidentally aborted by Engineer. Not charged MD/CP-
1/22A F	2414.5	2388.5	4337 10.5	5:45	2876.7	3467.7 8.5	95.8	5:54		09:00	Mod perm MD/CP- 8.2 (20cc DD)
1/23 F	2444.7	2418.7	4390 10.5	6:05	1121.7	1130.0 -	95.7	6:10	4390 10.5	05:00	Tight abort test. MD/CP-
1/23a F	2444.8	2418.8	4391 10.5	6:17	3481.9	3501.8 8.5	96.5	6:22	4390 10.5	05:00	Good test MD/CP- 255.1
1/24 F	2446.5	2420.5	4394 10.5	6:29	3472.4	3503.8 8.5	96.6	6:32	4394 10.5	03:00	Good test. MD/CP- 165.4

ESSO AUSTRALIA LTD - PRESSURE DATA FORM

Well	TURRUM-7		Page	4 of 8							
Date	14-15/9/99		Geologist-Engineer	Gret. Clots/Marla Turner							
Tool Type (MDT, RFT)	Schlumberger MDI		KB (metres)	26							
Gauge Type	CQG		Probe type	Long nose							
Pressure units (psi, psi <sub>g</sub> )	PSIA		Temperature units (deg <sub>f</sub> , deg <sub>C</sub> )	deg <sub>C</sub>							
Run-Seat Number	Depth m MDRKB	Depth m TVDSS	Initial Hydrostatic Pressure	Time Set (HH:MM)	Minimum Flowing Pressure	Formation Pressure	Temp	Time Retract (HH:MM)	Final Hydrostatic Pressure	Delta Time (MM:SS)	Comments Including Test Quality and Fluid Type.
			PPg			PPg			PPg		
1/25	P	2448.5	2422.5	4397	3372.8	3506.5	96.7	6:40	4397	04:00	Good test MD/CP=38.1
				10.5		8.5			10.5		
1/20*	P	2409.7	2383.7	4328	3261.1	3462.3	96.4	6:54	4328	06:00	Good test MD/CP=27.8
				10.5		8.5			10.5		
1/26	P	2460.5	2434.5	4418	1002.9	3532.3	96.2	7:22	4419	18:00	Low perm. MD/CP=0.2
				10.5		8.5			10.5		
1/27	P	2464.8	2438.8	4426	3493.7	3530.0	96.9	7:35	4426	05:00	Good test. MD/CP=135.6
				10.5		8.5			10.5		
1/28	P	2447.8	2421.8	4396	3448.3	3505.7	97.2	7:47	4396	04:00	Good test. MD/CP=96.2
				10.5		8.5			10.5		
1/29	P	2484.5	2458.5	4461	3482.9	3562.8	97.0	7:58	4462	03:00	Good test. MD/CP=62.1
				10.5		8.5			10.5		
1/30	P	2488.5	2462.5	4469	3548.7	3568.7	97.4	8:08	4469	05:00	Good test. MD/CP=283.4
				10.5		8.5			10.5		
1/31	P	2496.5	2470.5	4483	2526.3	3580.2	97.8	8:17	4483	04:00	Good test. MD/CP=5.8
				10.5		8.5			10.5		
1/32	P	2588.5	2562.5	4648	3047.0	3723.0	98.0	8:35	4648	10:00	Lost seat, re-seat
				10.5		8.5			10.5		
1/32*	P	2588.5	2562.5	4648	2858.9	3706.3	99.0	8:37	4648	01:00	Good test. MD/CP=6.7
				10.5		8.5			10.5		

**ESSO AUSTRALIA LTD - PRESSURE DATA FORM**

Well		TURRUM-7				Page		5 of 8			
Date		14-15/9/99				Geologist-Engineer		Greg Clota/Martin Turner			
Tool Type (MDT, RFT)		Schlumberger MDT				KB (metres):		26			
Gauge Type		CQG				Probe type		Long nose			
Pressure units (psia, psig)		PSIA				Temperature units (degF, degC)		degC			
Run-Seat Number	Depth		Initial Hydrostatic Pressure	Time Set (HH:MM)	Minimum Flowing Pressure	Formation Pressure	Temp	Time Retract (HH:MM)	Final Hydrostatic Pressure	Delta Time (MM:SS)	Comments Including Test Quality and Fluid Type.
	m MDRKB	m TVDSS									
1/33 F	2594.0	2568.0	4657 10.5	8:40	3574.2	3713.3 8.5	100.0	8:47	4657 10.5	07:00	Good test. MD/CP= 37.4
1/34 P	2591.3	2565.3	4653 10.5	8:53	3554.4	3709.7 8.5	101.0	8:56	4652 10.5	03:00	Good test. MD/CP= 33.5
1/35 P	2614.8	2588.8	4695 10.5	9:05	-	-	101.0	9:10	4695 10.5	05:00	No seat; 2 attempts.
1/35a P	2614.7	2588.7	4694 10.5	9:15	-	-	101.0	9:17	4694 10.5	02:00	No seat.
1/35b P	2614.5	2588.5	4694 10.5	9:23	-	-	102.0	9:25	4694 10.5	02:00	Lost seat.
1/36 P	2624.8	2598.8	4712 10.5	9:31	912.0	1025.0 2.3	102.0	9:36	4713 10.5	05:00	Tight; abort
1/36a P	2624.5	2598.5	4712 10.5	9:38	892.0	1195.0 2.7	102.0	9:40	4712 10.5	02:00	Tight; abort.
1/36b P	2625.0	2599.0	4713 10.5	9:45	875.0	907.0 2.0	102.0	9:50	4716 10.5	05:00	Tight; abort.
1/37 P	2630.0	2604.0	4722 10.5	9:55	854.0	1115.0 2.5	102.0	9:58	4722 10.5	03:00	Tight; abort.
1/37a P	2629.9	2603.9	4721 10.5	10:04	2019.8	3847+	102.0	10:25	4721 10.5	21:00	See Pretest Supercharged; abort.

ESSO AUSTRALIA LTD - PRESSURE DATA FORM

Well		TURRUM-7		Page 6 of 8				
Date	14-15/9/99	Geologist-Engineer	Greg Clots/Martin Turner	Page	6 of 8			
Tool Type (MDT, RET)	Schlumberger MDT	KB (metres)	26	Probe Type	Long nose (Run 1), Martinex (Run 2)			
Gauge Type	COG	Temperature units (degF, degC)	degC	Comments	Including Test Quality (MMSS) and Fluid Type.			
Pressure units (psia, psig)	FBI/A	Formation Pressure	PPg	Final Hydrostatic Pressure	PPg			
Run-Start Number	Depth m MDRKB	Depth m TVDSS	Time Set (HH:MM)	Minimum Flowing Pressure	Temp	Retract Time (HH:MM)	Delta Time (MM:SS)	Comments
1/38	2632.5	2606.5	10:30	2140.0	102.0	10:32	02:00	5cc Pretest; Tight, abort.
1/38a	2632.0	2606.0	10:35	1972.0	102.0	10:40	05:00	5cc Pretest; Tight, abort.
1/38b	2632.0	2606.0	10:55	1956.0	102.0	10:57	02:00	5cc Pretest; Tight, abort.
1/37b	2629.4	2603.4	11:01	2180.4	102.0	11:11	10:00	5cc Pretest; Tight, abort.
1/39	2677.0	2651.0	11:15	3776.0	103.0	11:21	06:00	15cc Pretest, good test. MD/CP=4263.4
1/40	2686.0	2660.0	11:28	3784.0	103.6	11:32	04:00	20cc Pretest, good test. MD/CP=408.6
1/41	2750.0	2704.0	11:38	3830.3	104.0	11:42	04:00	20cc Pretest, good test. MD/CP=47.2
2/42	2444.8	2418.8	16:15	584.0	(780)	16:20	05:00	Low permeability Test Curtailed
2/42A	2444.9	2418.9	16:20	2704.6	3503.0	16:50	30:00	Pump 0.75gal into bore Chamber Rv=0.03 Filtrate pump only pumping in one direction about sample attempt

**ESSO AUSTRALIA LTD - PRESSURE DATA FORM**

Well		TURRUM 7				Page		7 of 8			
Date		14-15/99				Geologist-Engineer		M Turner/G Clota			
Tool Type (MDT, RFT)		Schlumberger MDT				KB (metres):		26			
Gauge Type		CQG				Probe type		Martineaux			
Pressure units (psia, psig)		PSIA				Temperature units (degF, degC)		degC			
Run-Seat Number	Depth		Initial Hydrostatic Pressure	Time Set (HH:MM)	Minimum Flowing Pressure	Formation Pressure	Temp	Time Retract (HH:MM)	Final Hydrostatic Pressure	Delta Time (MM:SS)	Comments including Test Quality and Fluid Type.
	m MDRKB	m TVDSS									
2/42B P	2446.5	2420.5	4393 10.5	16:55	3444.0	3504.2 8.5	97.8	17:40	4393 10.5	45:00	Pump 2.2gal to bore, fill 6gal chmbr 4.0 gal to bore Tot =12.2 gal OFA showing water Rw=0.04. Abandon due to time constraints
2/43 F	2614.5	2588.5	4693 10.5	18:05	2050.6	(3771)		18:12	4693 10.5	07:00	Supercharged Test curtailed
2/43A F	2614.3	2588.3	4693 10.5	18:17	1857.0	(2350)	103.0	18:22	4693 10.5	05:00	Low perm test curtailed
2/43B P	2614.1	2588.1	4692 10.5	18:25	1624.0	(1687)	103.0	18:29	4692 10.5	04:00	Low perm Test Curtailed
2/43C F	2614.8	2588.8	4693 10.5	18:33							No seal
2/44 P	2620.5	2594.5	4709 10.5	18:39	1629.1	(1690.2)	103.9	18:42	4703 10.5	03:00	Low perm test curtailed
2/45 P	2621.0	2595.0	4705 10.5	18:50	1608.6	(1680.5)	104.8	18:52	4705 10.5	02:00	Low perm test curtailed
2/46 P	2624.0	2598.0	4710 10.5	18:57	1841.0	(1879.7)	104.8	18:59	4710 10.5	02:00	Low perm test curtailed
2/47 P	2624.6	2598.6	4711	19:07	1697.3	(1690.17)	105.0	19:08	4711	01:00	Low perm test curtailed

ESSO AUSTRALIA LTD - PRESSURE DATA FORM

Well	TURRUM 7			Page	8	of	8			
Date	14-12/99			Geologist/Engineer	M Turner/G Chota					
Tool Type (MDT, RFT)	Schlumberger MDT			KB (metres)	26					
Gauge Type	COG			Probe type	Marineaux					
Pressure units (psia, psig)	PSIA			Temperature units (deg F, deg C)	deg C					
Run-Seat Number	Depth m MDRKB	Depth m TVDSS	Initial Hydrostatic Pressure	Minimum Flowing Pressure	Formation Pressure	Temp	Time Retract (HH:MM)	Final Hydrostatic Pressure	Delta Time (MM:SS)	Comments Including Test Quality and Fluid Type.
			PPG	PPG	PPG				PPG	
2/48	2624.9	2598.9	4712	1636.1	(1704.66)	104.9	19:17	4712	03:00	Low perm test curtailed
									10.5	

907511 031

APPENDIX 2

907511 032

**APPENDIX 2**

**TURRUM 7**


**Quantitative Formation Evaluation**



**Esso Australia Ltd**  
**Exploration Department**

**Turrum 7**  
**Formation Evaluation**  
**Log Analysis Report**

**Petrophysicist: P.J. Burnett**  
**November 1999**

Endorsed by:   
FE Team Leader

Date: 2.1.12.99

## Turrum 7 LOG ANALYSIS

Turrum 7 was a vertical well drilled as an outpost/extension test specifically to target the oil potential of the L-360 reservoir, along with the hydrocarbon potential of other reservoirs on the east flank of the structure. The well was spudded 5.2 km south-east of the Marlin-A Platform on 24 August 1999 in 62m of water, with an RKB of 26m. After running 30" casing, 17 1/2" surface hole was drilled to 670m and 13 3/8" casing ran to 664.5m. The 12 1/4" hole was then drilled to 2609m where a 9 7/8" coring BHA was run and 27m (2609-2636m) of 5 1/4" core was cut and 26.1m recovered. The cored interval was reamed out to 12 1/4" and the hole drilled on to a total depth of 2830m (Note that all depths quoted to this point are MD Drlr) on 13 September 1999. Wireline logs were acquired in open-hole on six consecutive runs in KCl-Polymer-Gem mud. Note that all depths quoted below are logged MDKB unless specified otherwise.

Turrum 7 electric log data acquired over the Latrobe section have been analysed for effective porosity and water saturation from 1750 to 2809m. An Esso in-house analysis model (designated K12) was used to derive effective porosity from density and neutron log responses and saturation using the Dual Water model. The results of the analysis are included as Attachment 1. Correlating to the core Gamma Ray log, a shift of +3.9m was made to the drillers depths resulting in a loggers depth interval of 2612.9 to 2639.0m MDKB.

### DATA

#### Open Hole Logs Acquired

##### *Schlumberger W/L data:*

1. PEX: HILT-DSI-HALS (O-H Quad-Combo)	2830-300m
2. FMI-HNGS	2830-1685m
3. MDT (Pressure Surveys, 55 tool sets)	2230.0-2730.0
4. MDT (Formation Sampling, 12 Tool Sets)	2444.8-2624.9m
5. VSP/Checkshot	2800-200m
6. CST (Sidewall Cores)	2806.7-1767.3m

#### Mud Data

Mud Type	Weight	K <sup>+</sup>	Cl <sup>-</sup>	Barite	Rmf
KCl-Polymer-Gem	10.5 ppg	6%	35,000	5%	0.113@19°C

#### Log Quality

- The wireline logs used in this interpretation were acquired on the first run in the hole.
- Although the tension curves indicated very little variation with no significant tight spots or major pulls and despite the data being acquired with the vendor's automatic speed correction turned on, small depth discrepancies were common throughout.

- Within the Latrobe, the hole was predominantly in gauge with rarely more than 0.5" overgauge in the coals and shaly sections resulting in minimal effects on the logs.
- The data were found to be of good quality throughout, with little need for editing.
- Although not used in this interpretation, the high Barite content of the mud appears to have affected (see Attachment 2, Track 3) the measurement of photoelectric effect with the PEA (SS apparent  $P_{ef}$ ) reading high (ie. around 3 in clean sands) and the PEFZ (formation photoelectric factor) reading low (ie. around 1 in sands).
- The Potassium and Uranium yields from the HNGS are similar to Turrum 4, 5 & 6 with a regional variation in the Thorium being evident.

### **Log Processing**

- Detailed depth alignment was performed to correct the numerous minor depth discrepancies and optimise the analysis. The approach of simultaneously depth-aligning the nuclear logs to the GR and then the resistivity logs was adopted.
- No corrections have yet been made to the PE or HNGS data but further attention may be required before use in any multiple mineral modelling analysis.
- The RT curve provided by the vendor (HART), derived from the laterolog data acquired by the HALS tool has been used as presented.

## **INTERPRETATION**

### **Logs Used**

ECGR, HART, RHOB, TNPH.

### **Analysis Parameters**

a	1
m	2
n	2
GRmin	Input curve based on log responses
GRmax	Input curve based on log responses
Apparent Shale Neutron Porosity	Input curve based on log responses
Apparent Shale Bulk Density	Input curve based on log responses
Input Hydrocarbon Density	Input curve; 0.65 g/cc for oil, 0.19 g/cc for gas
Shale Resistivity	Input curve based on log responses
Lower Grain Density Limit	2.645 g/cc
Upper Grain Density Limit	2.675 g/cc
Formation Water Salinity	Input curve based on Rwa and regional data
Bottom Hole Temperature	110 degC (based on regional gradient)
Measured Rmf	0.113@19°C

### Free Formation Water Resistivity

The calculated RWA from Turrum 4, 5, 6 and 7 were compared and representative RW's chosen from the cleanest water sands in each section for use in the interpretation. The corresponding free formation water salinities of between 20,000 and 30,000 ppm are reasonable based on regional experience.

### Shale Volume, Total Porosity and Water Saturation

An initial VSH calculated from the GR was compared to a calculated neutron-density value to test for input into an iterative log analysis model. Initial neutron-density total porosity and dual-water total water saturation were then calculated and hydrocarbon and shale corrections applied to the neutron and density data using those values. The resulting calculated grain density was compared to a supplied grain density window and the initial VSH increased or decreased until the calculated GD fell within the window. To overcome a tendency for the analysis to underestimate SW in the shalier zones by undercorrecting for shale, the input curve of RSH was doubled resulting in a more consistent SW in the shalier zones while not affecting the interpretation in the cleaner rock.

### Effective Porosity and Water Saturations

Effective porosity was calculated using the final values of total porosity and VSH and the effective water saturation from the total water saturation using the following equations:

$$\begin{aligned} \text{PHIE} &= (\text{PHIT} - (\text{VSH} * \text{PHISH})) \\ \text{SWE} &= (1 - ((\text{PHIT}/\text{PHIE}) * (1 - \text{SWT}))) \end{aligned}$$

### DISCUSSION

1. The W-L data required detailed minor depth alignment.
2. Table 1 summarises the shale volume, effective porosity and effective water saturation results from the analysis.
3. Although comparable sandy intervals are not common because of regional reservoir variation, the validity of porosities calculated from Turrum 7 data can be demonstrated by comparison to those calculated from the W-L data in a nearby well. Figure 2 shows a crossplot with histograms of the density response and calculated PHIE over two equivalent sandy intervals in Turrum 7 & 4. Similar ranges and values are present indicating similar log responses and interpretation.

Further support for the results of the analysis used at Turrum 7 is demonstrated on Attachment 3. Using the same input data from Turrum 5, the results of two analysis streams are compared (Tracks 4, 5 & 6). The PHIE calculated using the alternate model and the analysis used in this report show little difference, especially in the better quality sands.

4. Attachment 1 shows the measured core porosity plotted alongside the calculated total and effective porosity. The match is poor with the core porosity being about 5 PU lower than the calculated total porosity. This is considered to be caused by the large amount of fluid retained in the core during the humidity drying process.

Figure 3 is a crossplot comparison between the core porosities to calculated total porosities for Turrum 5, 6 & 7, indicating that the same is true for the poorer quality rock in all of the wells. This discrepancy may need to be resolved later.

5. The presence and type of hydrocarbon in each interval was determined by an examination of the calculated SW, the hydrocarbon crossover on the nuclear logs, separation between the near and far neutron counts curves (Attachment 2, Track 4), a sonic-neutron overlay technique (Track 6), mudgas level (Track 4) and gas wetness ratios (Track 5) and MDT pressures (Pressure Gradients for individual sands are shown on Figure 4). Qualifiers indicate perceived levels of certainty based on how definitive the indicators are and whether they support or conflict with each other.

Several sands stand out as being gas bearing on all of the criteria including the MDT pressures (see Figure 4). These sands are currently designated L110, L133, L170 and L180. Many sands are considered to be clearly water bearing and the remaining sands with moderately high SW's are interpreted to have probable residual hydrocarbon. For these the labels probably residual gas or probably residual oil have been applied based on gas-wetness ratios or other data.

6. The L360 is a special case because of its importance as a target for this well, but is problematic because none of the section qualifies as reservoir rock. There were only 2 core permeability measurements over 1 md (2.46 and 1.12 md) out of 84 measurements, with most (71 of 84) being less than 0.1 md. This was evident when taking MDT pressures and samples – numerous attempts failed to achieve any drawdown.

The best apparent reservoir quality from the log interpretation (2614-2615m) occurs adjacent to washed out hole which precluded successful seats with the MDT and which could have affected the log responses. The core does support this section as being the best quality rock in the L360, albeit still poor.

Evidence supportive of the possibility of liquid hydrocarbon in the vicinity comes from the core with fluorescence shows being noted near the top in an interval of better rock, prompting the speculation that the lack of shows below this is because of the poorness of the reservoir quality.

The gas-wetness ratios (Attachment 2, Track 5) are more encouraging. Over a large interval (2500 to 2700m) there was very little 'oil type' separation although the coals stand out clearly as 'gas type' crossover, whereas the whole of the L360 interval (2613-2532m) looks 'oily', again except for the coaly intervals.

7. Similarly for the L-200, although the rock quality is better the high water saturations preclude the definitive interpretation of oil. However, the MDT pressures are interpreted (C.Sullivan; Res Eng) to be indicative of an oil/water transition zone and not residual oil, suggesting the possibility of oil up-dip.

8. Other details and contact information are in Table 1.

Attached are the following presentations of results:

- Table 1 Summary of Results Turrum 7
- Figure 1 Xplot of PHIE vs Density; Equivalent Intervals in Turrum 7 and 4
- Figure 2 Xplot of Measured Core and Calculated PHIT, Turrum 7, 5 & 6
- Figure 3 Turrum 7 Depth vs MDT Pressure Plot
- Attachment 1 - Depth Plot of Analysis; Turrum 7
- Attachment 2 - Depth Plot of Input Logs to Analysis; Turrum 7
- Attachment 3 - Depth Plot Comparing Results of Alternate Analyses; Turrum 5

Table 1

TURRUM 7

PETROPHYSICS ANALYSIS SUMMARY

Net porosity cut-off: 0.120 volume per volume  
 Depth reference: MDKB  
 Net Porous Interval based on Porosity cut-off only.

GROSS INTERVAL (metres)		NET POROUS INTERVAL		Net to Gross	Mean Vsh	Mean Porosity	Mean Sw	Comments
(top)	(base)	Gross Metres	Net Metres	%	%	%	%	
1818.9	1827.7	8.8	8.3	94%	9%	21%	98%	Water
1835.7	1875.6	39.9	5.9	15%	29%	16%	99%	Water
1878.9	1893.6	14.7	13.1	89%	3%	27%	97%	Water
1895.8	1922.4	26.6	4.4	17%	28%	16%	98%	Water
1964.5	1972.3	7.8	3.5	45%	23%	19%	100%	Water
1978.8	2015.0	36.2	2.3	6%	33%	15%	100%	Water
2022.2	2038.6	16.4	2.2	14%	20%	18%	100%	Water
2046.3	2053.0	6.7	4.2	63%	16%	19%	97%	Water
2067.1	2111.1	44.0	2.7	6%	22%	16%	100%	Water
2128.7	2142.0	13.3	3.1	23%	31%	13%	100%	Water
2154.9	2200.3	45.4	3.9	9%	24%	15%	100%	Water
2215.4	2225.6	10.2	2.2	22%	28%	15%	100%	Water
2226.2	2241.5	15.3	13.8	91%	10%	19%	98%	L100, Water
2247.1	2250.2	3.1	0.7	22%	7%	17%	100%	Water
2265.9	2268.4	2.5	2.4	95%	21%	20%	50%	L110, Gas, good gas response on indicators and MDT pressures (0.323 psi/m)
2271.3	2272.8	1.5	1.4	92%	0%	22%	60%	L132, Gas, good gas response on indicators and MDT pressures (0.323 psi/m)
GWC placed at 2272.8m MDKB								
2272.8	2274.1	1.3	0.9	71%	18%	17%	97%	L132, Water
2280.6	2287.0	6.4	5.9	92%	17%	17%	99%	L133, Water
2287.0	2293.1	6.1	6.0	99%	4%	24%	95%	L137, Water
2294.7	2318.4	23.7	2.8	12%	20%	18%	98%	Water
2324.0	2334.7	10.7	7.8	73%	8%	21%	97%	L160, Water
2347.2	2350.8	3.6	3.4	95%	8%	21%	30%	L170, Gas, good gas response on indicators and MDT pressures (0.330 psi/m)
2353.6	2358.8	5.2	4.7	90%	6%	21%	39%	L180, Gas, good indications although possible GOC at 2355.5m (see Note 3)
2383.8	2394.5	10.7	1.0	9%	30%	13%	65%	L190, possible residual Gas
2408.6	2420.8	12.2	5.2	42%	28%	14%	86%	L193, possible residual hydrocarbon, indeterminate type
2440.0	2450.0	10.0	4.9	49%	10%	19%	72%	L200, possible Oil transition interpreted from MDT pressures (Note 4)
2459.0	2465.0	6.0	0.5	8%	29%	14%	100%	L220, Water
2473.6	2477.0	3.4	1.3	39%	18%	17%	100%	Water

2482.1	2490.8	8.7	7.7	89%	13%	19%	83%	L280, possible residual Oil
2492.1	2498.1	6.0	0.5	8%	31%	13%	100%	L285, Water
2506.9	2511.0	4.1	2.8	69%	23%	14%	96%	L300, Water
2520.8	2522.2	1.4	0.6	46%	28%	13%	100%	Water
2549.4	2554.4	5.0	1.4	28%	20%	15%	95%	L310, Water
2584.5	2594.3	9.8	3.8	38%	18%	15%	98%	L330, water
2613.7	2632.2	18.5	0.8	4%	38%	13%	73%	L360, indications of oil (see Note 5)
2673.8	2787.0	113.2	83.5	74%	3%	17%	100%	Water
2793.0	2804.0	11.0	0.5	5%	15%	12%	90%	Water

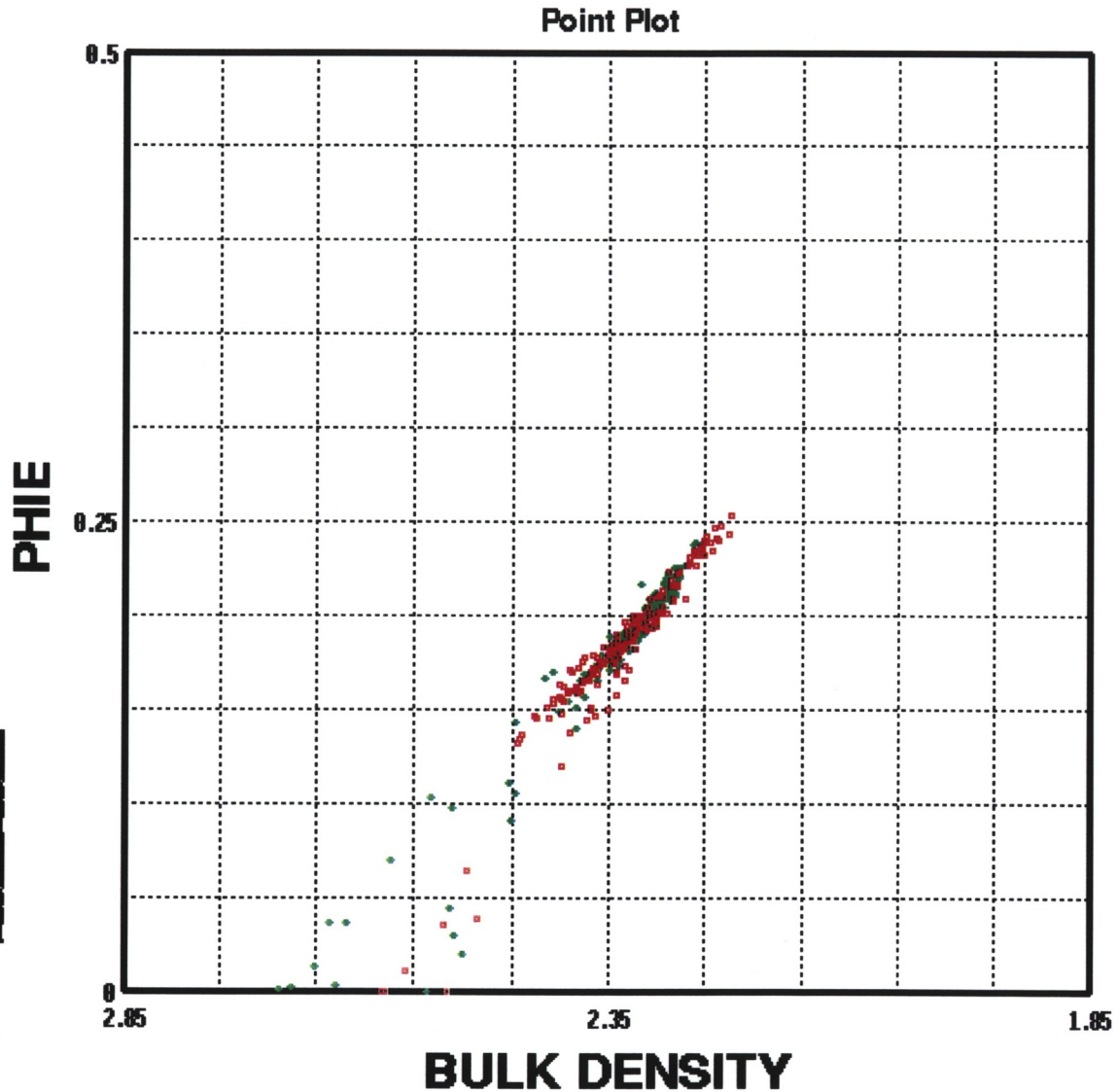
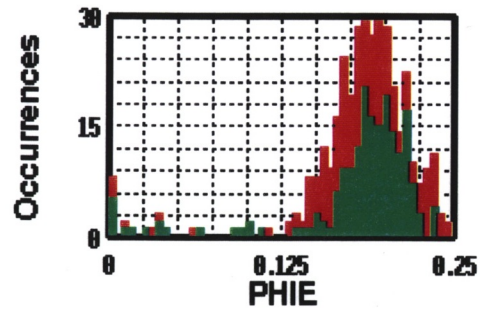
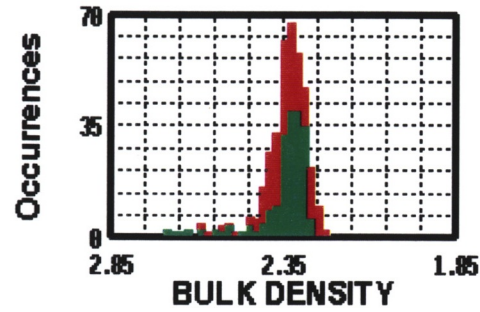
Notes

1. Discrimination between gas and oil was achieved through a variety of techniques (mainly nuclear log responses, mud-gas measurements and MDT pressures) outlined in the report. As the upper gas sand exhibited some good fluorescence, fluorescence was not considered to be a good hydrocarbon discriminator.
2. Reservoir nomenclature may not be final and may change following the release of this report.
3. Many of the criteria used to discriminate between gas and oil show a change of character at this depth suggesting the possibility of a GOC - the density-neutron crossover reduces as do the separation between the near and far counts and the sonic-neutron crossover, whereas a comparison between the nuclear log character at 2356 and 2348m suggests similar quality rock. A lithological change, such as reduced grain size, could also explain the character change of the indicators through increased capillary water leaving the interpretation uncertain. A small change in the MDT pressure gradient from 0.37 to 0.40 psi/m also occurs lending some support to the possibility of the reservoir fluid becoming more liquids rich.
4. The magnitude of the saturations and the effect on the pressure gradient was considered to be consistent with an oil/water transition although the mud-gas is more suggestive of gas.
5. As mentioned in the body of the report, core fluorescence and mud-gas ratios suggest the possibility of oil in this section of rock.



PE907511-10

Figure 1; Xplot of PHIE vs Density, over Equivalent Intervals in Turrum 7 and 4

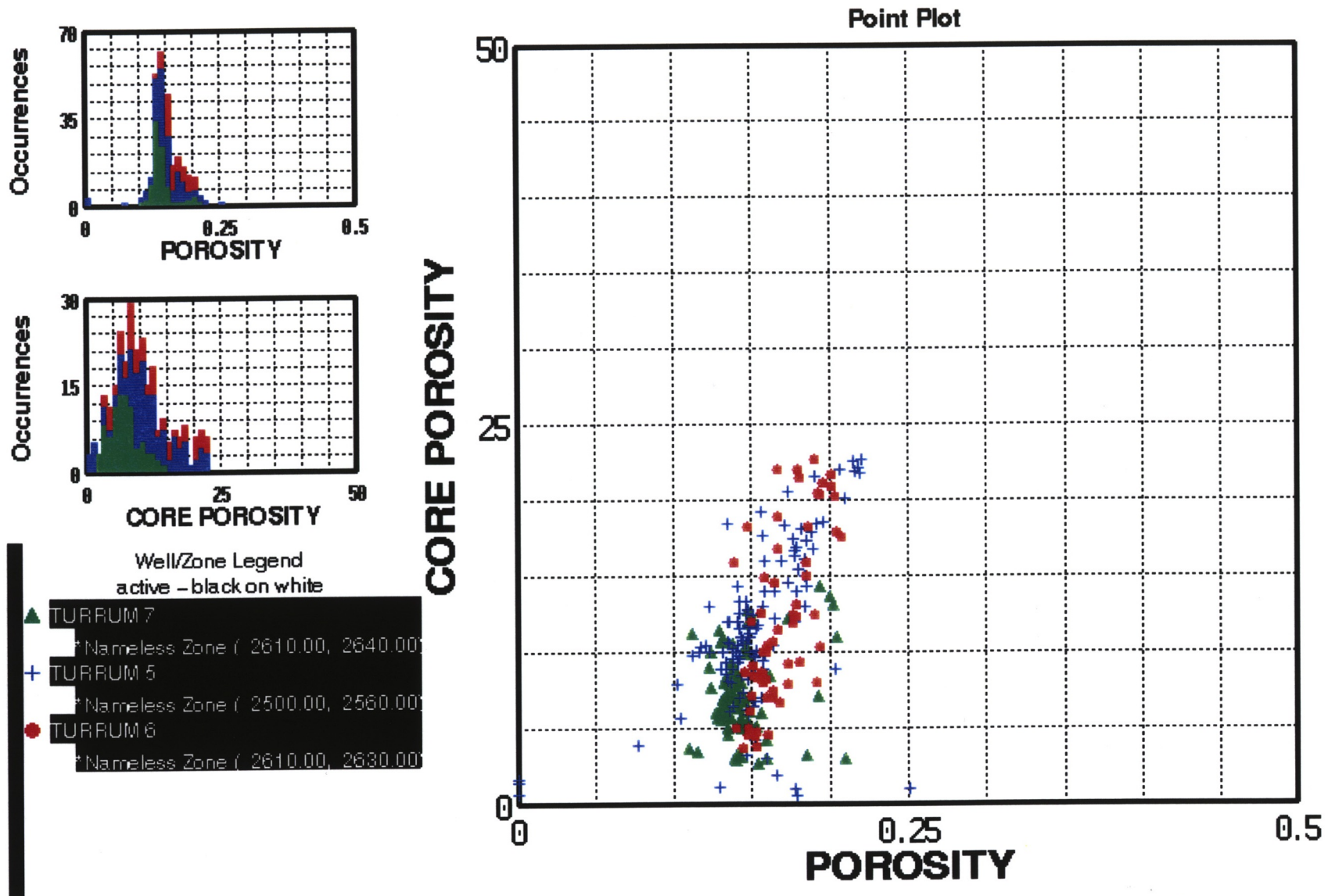


- Well/Zone Legend  
active - black on white
- ◆ TURRUM 7
    - \* Nameless Zone ( 2226.00, 2242.00 )
    - \* Nameless Zone 1 ( 2675.00, 2687.00 )
  - TURRUM 4
    - \* Nameless Zone ( 2310.00, 2323.00 )
    - \* Nameless Zone 2 ( 2728.00, 2743.00 )

907511 041

PE907511-11

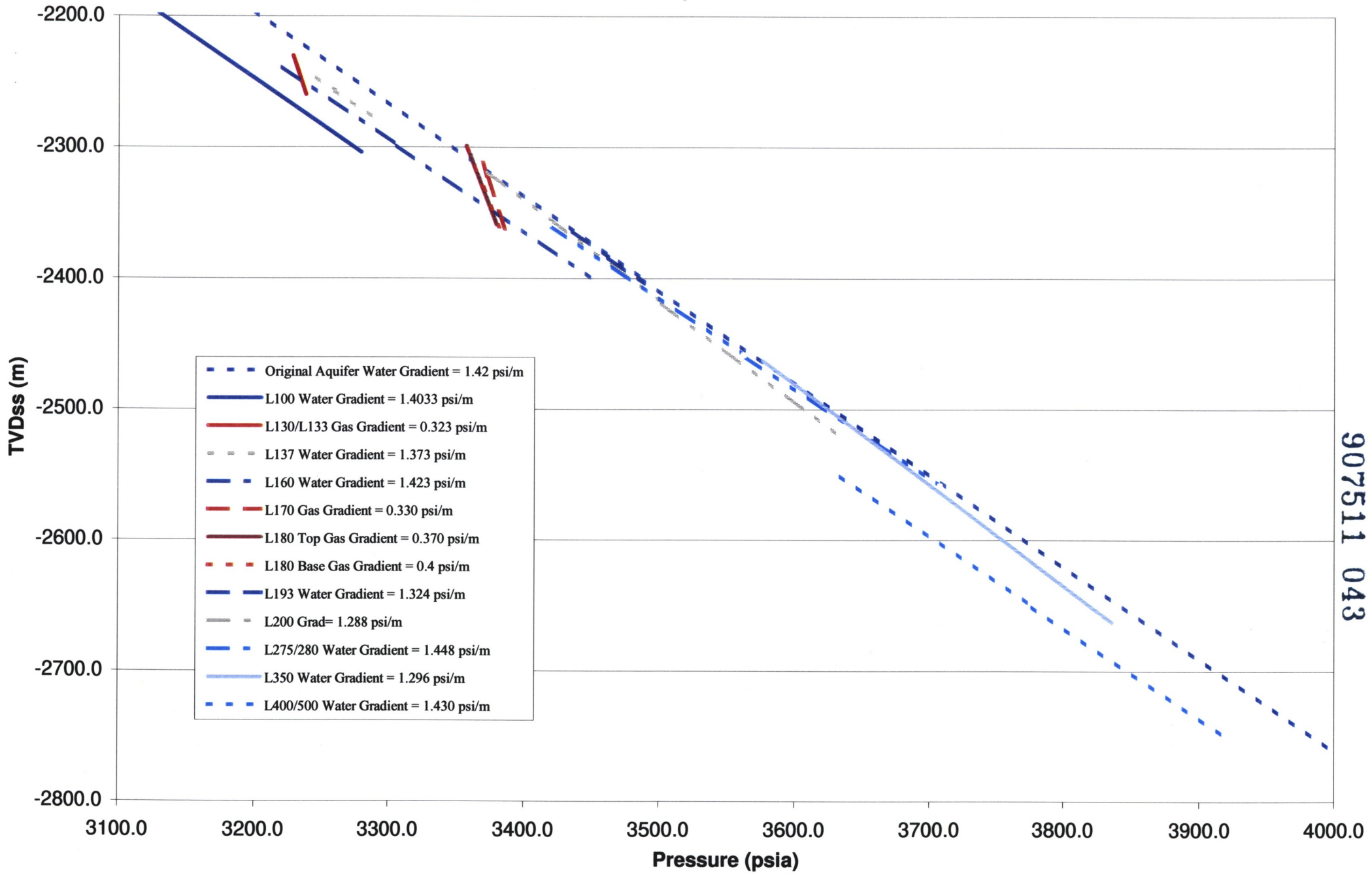
Figure 2; Xplot of L-360 Measured Core Porosity vs Log Calculated PHIT, Turrum 7, 5 and 6



907511 042

PE907511\_12

Figure 3; Turrum 7 - Depth v MDT Pressure Plot



907511 043

PE602969

This is an enclosure indicator page.  
The enclosure PE602969 is enclosed within the  
container PE907511 at this location in this  
document.

The enclosure PE602969 has the following characteristics:

- ITEM\_BARCODE = PE602969
- CONTAINER\_BARCODE = PE907511
- NAME = Turrum-7 Depth Plot Log
- BASIN = GIPPSLAND
- ONSHORE? = N
- DATA\_TYPE = WELL
- DATA\_SUB\_TYPE = WELL\_LOG
- DESCRIPTION = Turrum-7 Log Analysis Depth Plot, Scale  
1:200, by Esso Australia Ltd, W1300,  
VIC/L4. Attachment 1 contained within  
"Well Completion Report" [PE907511]
- REMARKS =
- DATE\_WRITTEN = 15-DEC-1999
- DATE\_PROCESSED =
- DATE\_RECEIVED = 06-APR-2000
- RECEIVED\_FROM = Esso Australia Ltd
- WELL\_NAME = Turrum-7
- CONTRACTOR =
- AUTHOR =
- ORIGINATOR = Esso Australia Ltd
- TOP\_DEPTH = 1750
- BOTTOM\_DEPTH = 2840
- ROW\_CREATED\_BY = DN07\_SW

(Inserted by DNRE - Vic Govt Mines Dept)

907511 ~~045~~  
045

PE602970

This is an enclosure indicator page.  
The enclosure PE602970 is enclosed within the  
container PE907511 at this location in this  
document.

The enclosure PE602970 has the following characteristics:

ITEM\_BARCODE = PE602970  
CONTAINER\_BARCODE = PE907511  
NAME = Turrum-7 Depth Plot Log  
BASIN = GIPPSLAND  
ONSHORE? = N  
DATA\_TYPE = WELL  
DATA\_SUB\_TYPE = WELL\_LOG  
DESCRIPTION = Turrum-7 Log Analysis Depth Plot, Scale  
1:200, by Esso Australia Ltd, W1300,  
VIC/L4. Attachment 2 contained within  
"Well Completion Report" [PE907511].  
REMARKS =  
DATE\_WRITTEN = 15-DEC-1999  
DATE\_PROCESSED =  
DATE\_RECEIVED = 06-APR-2000  
RECEIVED\_FROM = Esso Australia Ltd  
WELL\_NAME = Turrum-7  
CONTRACTOR =  
AUTHOR =  
ORIGINATOR = Esso Australia Ltd  
TOP\_DEPTH = 1750  
BOTTOM\_DEPTH = 2840  
ROW\_CREATED\_BY = DN07\_SW

(Inserted by DNRE - Vic Govt Mines Dept)

907511 ~~XXXX~~  
046

PE602971

This is an enclosure indicator page.  
The enclosure PE602971 is enclosed within the  
container PE907511 at this location in this  
document.

The enclosure PE602971 has the following characteristics:

ITEM\_BARCODE = PE602971  
CONTAINER\_BARCODE = PE907511  
NAME = Turrum-5 Depth Plot Log  
BASIN = GIPPSLAND  
ONSHORE? = N  
DATA\_TYPE = WELL  
DATA\_SUB\_TYPE = WELL\_LOG  
DESCRIPTION = Turrum-5 Log Analysis Depth Plot  
Comparison, Scale 1:500, by Esso  
Australia Ltd, W1300, VIC/L4.  
Attachment 3 contained within "Well  
Completion Report" [PE907511].  
REMARKS =  
DATE\_WRITTEN = 15-DEC-1999  
DATE\_PROCESSED =  
DATE\_RECEIVED = 06-APR-2000  
RECEIVED\_FROM = Esso Australia Ltd  
WELL\_NAME = Turrum-5  
CONTRACTOR =  
AUTHOR =  
ORIGINATOR = Esso Australia Ltd  
TOP\_DEPTH = 2125  
BOTTOM\_DEPTH = 2675  
ROW\_CREATED\_BY = DN07\_SW

(Inserted by DNRE - Vic Govt Mines Dept)

907511 ~~0000~~

047

907511   
048

**APPENDIX 3**

**TURRUM 7**

**Palynological Analysis**



907511 ~~032~~  
049

**ExxonMobil Exploration Company**

**Biostratigraphic Subdivision and Paleocology of the Paleocene  
Turrum Reservoir Section from the Turrum-7 Well,  
Gippsland Basin, Australia**

**Thomas D. Davies**

**TECHNOLOGY DEPARTMENT  
GEOLOGICAL SERVICE DIVISION  
EMEC.32.BIO.99  
NOVEMBER 1999**

**UNCLASSIFIED**

---

**BIOSTRATIGRAPHY REPORT**

907511 ~~6~~  
050

**Exxon Exploration Company**

**Biostratigraphic Subdivision and Paleocology of the Paleocene  
Turrum Reservoir Section from the Turrum-7 Well,  
Gippsland Basin, Australia**

**Thomas D. Davies**

**Geological Services Division  
EEC.32.BIO.99  
November 1999**

**UNCLASSIFIED**

## EXECUTIVE SUMMARY

- Palynology and kerogen analysis of core, SWC and cuttings samples from Turrum-7 provide: 1) a detailed biostratigraphic subdivision of the Turrum reservoir for EAL's full reassessment of Turrum, 2) bio-events that have local and potentially regional correlatable value to tie with EAL's lithologic/seismic surfaces, and 3) paleoenvironmental interpretations to better constrain sequence stratigraphic interpretations, facies models, and paleogeographic reconstructions for this field.
- Eight of the nine palynozones previously developed for the Turrum field are identified and allow incorporation of these results with the work EEC previously did on Turrum.
- Biostratigraphically correlative horizons of those previously picked for Turrum-3 and Turrum-4 are summarized. Sections of maximum marine influence are identified and provide additional points of correlation.
- Marine dinocysts are found most frequently in the upper two-thirds of the well from 2205, 2235-2245.8, 2300-2403.4, 2480.5, and 2525-2540.7 m, and again in the base of the well in the sandy section at 2775.8 m and just below the sands at 2788 m.
- Re Zone samples 2515-20 and 2525-30 m are interpreted as lagoonal-marginal marine. SWC 2540.7 m likely represents a period of maximum marine ingress. The types of dinoflagellate species here are consistent with a lagoonal-marginal marine setting. Cuttings sample 2565-70 m contains only few restricted marine-type dinocysts and is interpreted as lagoonal to very marginal marine. Samples 2570-80 m contains no marine microfossils and is interpreted to be nonmarine.
- Zone Rf? sample 2595-2600 m is barren of marine forms and is interpreted as nonmarine. The three uppermost Rf zone samples from 2608.8-2633 m contain isolated to extremely rare, poorly preserved, restricted marine forms, whereas sample 2634.7 m is barren of marine dinocysts. These are interpreted as probably nonmarine. Sample 2655-65 m contains rare marine forms, which indicate a possible lagoonal-marginal marine setting.

**TABLE OF CONTENTS**

EXECUTIVE SUMMARY ..... III  
TABLE OF CONTENTS ..... IV  
INTRODUCTION ..... 1  
ZONATION AND DEPOSITIONAL ENVIRONMENTS ..... 2  
    Turrum-7 Zonation ..... 2  
    Zones of Maximum Flooding ..... 2  
STRATIGRAPHIC DISCUSSION ..... 3  
PALYNOSTRATIGRAPHIC CORRELATION ..... 10  
REFERENCE ..... 12  
APPENDIX A ..... 14

## INTRODUCTION

At the request of Esso Australia Limited (Michael Gilbert), I studied core, sidewall core, and cuttings samples from the Paleocene Turrum reservoir section of the Turrum-7 well. Samples were analyzed for biostratigraphic zonation, correlation, and age. The purposes of the project were: 1) to subdivide the Paleocene Turrum clastic reservoir in Turrum-7; 2) to gain more confidence in the current stratigraphic correlations and reservoir continuity with detailed, high-resolution biostratigraphic subdivisions; and 3) to more accurately estimate the distribution and quality of the reservoir rocks within the Turrum Field.

The objectives of this study were to subdivide the Paleocene Lower *L. balmei* spore/pollen Zone using the zonation previously developed at EEC, and to provide a detailed biostratigraphic zonation through the reservoir interval that can be incorporated with the work previously done on other Turrum wells.

Microscope slides from forty-four Turrum-7 core, sidewall core, and cuttings samples were studied for palynology and paleoenvironments in the section from 2170 to 2810 m. Most of the samples were highly fossiliferous and most of the fossils used to define these zones were recognized in this well. Appendix A gives the sample-by-sample description, zonation, and interpreted ages.

ZONATION AND DEPOSITIONAL ENVIRONMENTS

TURRUM-7 ZONATION

<u>Tops (m MD)</u>	<u>Palynozones</u>	<u>Depositional Environments</u>
2170 (top sample)	Sz	Non-marginal marine
2205	Ra	Marginal marine-lagoonal
2235	Rb	Marine to 2245.8m, marginal below
2300	Rc	Marine
2375	Indeterm (mixed Rc/Rd)	Marginal marine
2395	Rd1	Marine to 2403.4m, marginal to 2460m, nonmarine to 2475
2480.5	Rd2?	Marine at 2480.5, nonmarine at 2500m
2515	Re	Marginal marine, marine at 2540.7m
2570	Indeterm (sparse fossils)	Nonmarine
(?2595) 2608.8	Rf	Nonmarine to 2634.7m, non-?marginal marine at 2655m
2665	Indeterm (sparse fossils)	Non-?marginal marine
2736	Rg	Marginal marine-marine
2788	Ma	Marginal marine-marine

ZONES OF MAXIMUM FLOODING

Marine dinocysts are found most frequently in the upper two-thirds of the well from 2205, 2235-2245.8, 2300-2403.4, 2480.5, and 2525-2540.7 m, and again in the base of the well in the sandy section at 2775.8 m and just below the sands at 2788 m (Appendix A).

Sample 2205 m is interpreted as lagoonal-marginal marine. Samples from 2235, 2240, and 2245.8 m likely represent a maximum marine flooding event. The four samples from 2300, 2305, 2335, and 2360 m are interpreted as marginal-shallow marine. Of these, samples 2305 and 2360 m likely represent intervals of maximum flooding.

Other sections with significant marine influence are recognized at 2395, 2403.4, 2525, 2540 (diversity increase), possibly 2565, 2775.8, and in Zone Ma at 2788m.

### STRATIGRAPHIC DISCUSSION

This section describes the results of the biostratigraphic analyses. The zones assigned here are for the Turrum field and may have limited utility outside the area.

Relatively rich and diversified, terrestrially-derived, spore-pollen assemblages occur in most of the samples studied from this well. Marine dinocysts are found most frequently in the upper two-thirds of the well from 2205, 2235-2245.8, 2300-2403.4, 2480.5, and 2525-2540.7 m, and again in the base of the well in the sandy section at 2775.8 m and just below the sands at 2788 m (Appendix A).

**Interval:** 2170-2195 m MD

**Age:** Eocene-uppermost Paleocene, Palynozone Sz

**Interval zone:**

2170m - Palynozone Sz

**Palynology:**

- the highest sample analyzed at 2170 m is assigned to the Eocene-uppermost Paleocene, Palynozone Sz (Appendix A). Taxa present include *Lygistepollenites balmei*, *Nothofagidites. spp.* and *Proteacidites annularis*.
- marine dinoflagellate cysts are very rare to barren suggesting that this section is non-to marginal marine.

**Interval:** 2205-2225 m MD

**Age:** Uppermost Paleocene, Palynozone Ra

**Interval zone:**

2205m - palynozone Ra

**Palynology:**

- the palynomorph assemblage at 2205-10 m is place in Zone Ra.
- taxa recorded include *Proteacidites annularis*, *Proteacidites angulatus*, *?Apectodinium* spp., *Australopollis obscurus*, and *Nothofagidites* spp. (Appendix A).
- marine dinoflagellate cysts are common. The environment of deposition of sample 2205-10 m is interpreted as marginal-lagoonal. Samples 2210 and 2220 m are interpreted as marginal marine (Appendix A).
- this assemblage is similar to that recovered in Turrum-3 at 2125-30m and in Turrum-4 about at 2290-95m (Davies, 1995).

**Interval:** 2235-2245.8 (-?2280) m MD

**Age:** Upper Paleocene, Palynozone Rb

**Interval zone:**

2235m - palynozone Rb

**Palynology:**

- sample 2235 m is placed in Zone Rb.
- this sample contains *?Apectodinium* spp., *Glaphyrocysta* spp., *Nothofagidites* spp., *Proteacidites angulatus*, and *Australopollis obscurus*.
- other taxa consistent with this zone are *Paleocystodinium golzowense* at 2240-45 m and *Cerodinium* spp. at 2245.8 m.
- cuttings samples 2235-40 and 2240-45 m, and SWC 2245.8 m are interpreted as marine, and likely represents a time of maximum flooding.
- the four samples from 2260-2280 are interpreted as marginal to perhaps nonmarine at sample 2275-80 m (Appendix A).
- the assemblage found in cuttings 2235-40 m correlates biostratigraphically to that recovered in Turrum-3 at 2155-60 m and in Turrum-4 at 2320-25 m.



The zonation of the three samples from 2260 to 2280 m is not well established. However, the biofacies assemblage at 2260 m suggests possible penetration of Zone Rc at this level. Because of the uncertainty this section is assigned broadly to Rb/?Rc.

**Interval:** 2300-2370 m MD

**Age:** Lower part of the Upper Paleocene, Palynozone Rc

**Interval zone:**

2300m - palynozone Rc

**Palynology:**

- the palynomorphs at 2300 m indicate this sample is in the Rc Palynozone.
- taxa present in this zone include: *Apectodinium* spp., *Paleocystodinium golzowense*, *Glaphyrocysta* spp., *Cerodinium* spp., *Nothofagidites* spp., *Proteacidites angulatus*, and *Australopollis obscurus*.
- cuttings samples 2300-05, 2305-10, 2335-40 and 2360-70 m are interpreted as shallow marine. Samples 2305-15 and 2360-70 m may represent intervals of maximum marine incursions.
- this assemblage recovered at 2300-2305 m is similar to that recovered in Turrum-3 at about 2215-20 m and in Turrum-4 at 2390 m.

**Interval:** 2375-2380 m MD

**Age:** Indeterminate, mixed Rc/Rd

**Interval zone:**

2375m - mixed Rc/Rd

**Palynology:**

- Because of the poor fossil recovery and poor preservation, this sample is placed broadly in zones Rc/Rd.
- palynomorphs suggest this sample was deposited in a marginal marine setting.

**Interval:** 2395-2475 m MD

**Age:** Lower Paleocene, Palynozone Rd

**Interval zones:**

2395m - palynozone Rd1

**Palynology:**

- this zone is subdivided into two subzones. Palynomorphs at sample 2395-2400 m indicates penetration of the lower Paleocene, Palynozone Rd1.
- taxa present include: *Apectodinium* spp., *Paleocystodinium golzowense*, *Glaphyrocysta* spp., *Cerodinium* spp., *Spinidinium densispinatum*, *Vozzhennikovia* spp., *Isabelidinium* spp., *Nothofagidites* spp., *Proteacidites angulatus*, and *Australopollis obscurus*.
- samples 2395-2400 and 2403.4 m are interpreted as shallow to marginal marine. This section likely represents a period of maximum flooding.
- the assemblage recovered here at 2395-2400 m is similar to that seen in Turrum-3 at 2305-10 m and in Turrum-4 at 2470-75 m.

**Interval:** 2480.5-2510 m MD

**Age:** Lower Paleocene, Palynozone Rd2?

**Interval zone:**

2480.5m - palynozone Rd2?

**Palynology:**

- the top of second subdivision of zone Rd (Rd2) is tentatively placed at 2480.5 m.
- taxa recorded include: *Apectodinium* spp., *Paleocystodinium* spp., *Cerodinium* spp., *Spinidinium densispinatum*, *Vozzhennikovia* spp., *Nothofagidites* spp., *Proteacidites angulatus*, *Australopollis obscurus*, *Tetracolporites verrucosus*, and *Ephedripites* spp. (Appendix A).
- SWC sample 2480.5 m is interpreted as shallow to marginal marine. This section likely represents a marine ingressión. The cuttings sample from 2500-10 m is barren of marine forms and is likely nonmarine (Appendix A).

- a similar assemblage to that recorded here at 2480.5 m was seen in Turrum-4 at 2540-45 m. The precise palynostratigraphic correlation into Turrum-3 is uncertain, which is perhaps due to sample gap issues.

**Interval:** 2515-2570 m MD

**Age:** Lower Paleocene, Palynozone Re

**Interval zone:**

2515m - palynozone Re  
2565m - palynozone Re2?

**Palynology:**

- sample 2515-20 m is placed in Palynozone Re.
- taxa consistent with this zonal assignment include *Glaphyrocysta retiintexta*, *Spinidinium densispinatum*, *Vozzhennikovia* spp., *Proteacidites* spp., and *Australopollis obscurus*.
- the assemblage at 2565-70 m suggests possible penetration of subzone Re2.
- samples 2515-20 and 2525-30 m are interpreted to be marginal marine. The SWC at 2540.7 m likely represents a period of maximum marine ingression. Palynomorphs present are consistent with a lagoonal to marginal marine setting. The cuttings sample from 2565-70 m is interpreted as lagoonal to very marginal marine.
- the palynomorph assemblage in Turrum-7 at 2525-30 and 2540.7 m is most similar to that recovered in Turrum-3 at 2415-20 m and in Turrum-4 at 2580-85 m.

**Interval:** 2570-80 m MD

**Age:** Indeterminate

**Palynology:**

- this sample yielded very sparse microfossils and is indeterminate for age.
- samples 2570-80 m contains no marine microfossils and is interpreted to be nonmarine (Appendix A).

**Interval:** 2595-2600 m MD

**Age:** Probably Lower part of Lower Paleocene, Palynozone Rf?

**Interval zone:**

2595m - palynozone Rf?

**Palynology:**

- the palynomorph assemblage suggests probable penetration of Zone Rf at 2595-2600 m.
- this sample is barren of marine forms and is interpreted as nonmarine (Appendix A).

**Interval:** 2608.8-2665 m MD

**Age:** Lower part of Lower Paleocene, Palynozone Rf

**Interval zone:**

2608.8m - palynozone Rf

**Palynology:**

- the assemblage at 2608.8 m is indicative of palynozone Rf.
- taxa present at this interval include *Nothofagidites* spp., *Tetracolporites verrucosus*, *Tricolpites* spp., *Proteacidites angulatus* and *Australopollis obscurus*. Marine dinocysts are extremely rare to barren (Appendix A).
- marine dinoflagellates are barren or nearly barren in the four samples from 2608.8 to 2634.7 m (Appendix A) and are probably nonmarine. The uppermost three samples contain extremely rare, poorly preserved, restricted marine forms, whereas sample 2634.7 m is barren of marine dinocysts (Appendix A). Sample 2655-65 m contains rare marine forms, which indicate a possible lagoonal-marginal marine setting.
- the assemblage at 2608.8 m (and possible up at 2595-2600 m) is most similar to those recovered in Turrum-3 at 2485-90 m and in Turrum-4 at 2655-60 m.

**Interval:** 2665-2720 m MD

**Age:** Indeterminate

**Palynology:**

- the four samples in this section yielded sparse microfossils and are indeterminate for age.
- these samples contains no definitive marine microfossils and are interpreted to be nonmarine.

**Interval:** 2736.6-2775.8 m MD

**Age:** Probably Uppermost Maastrichtian, Palynozone Rg

**Interval zone:**

2736.6m - palynozone Rg

**Palynology:**

- sample 2736.6 m is assigned to Palynozone Rg.
- taxa present include *Hystrichosphaeridium* spp., *Tricolpites*, spp., *Gambierina rudata*, and *Australopollis obscurus* at 2736.6, and *Paleocystodinium* spp., *Glaphyrocysta retiintexta*, *Manumiella* spp., *Nothofagidites* spp., *Proteacidites angulatus*, and *Australopollis obscurus* at 2775.8 m (Appendix A).
- sample 2736.6 m is interpreted to be marginal to possibly shallow marine. The depositional environment at 2775.8 m is interpreted to be shallow-marginal marine, and may represent a horizon of maximum flooding.
- the assemblage recovered at 2736.6 m in this well is most similar to that found in Turrum-3 at 2645-50 m and Turrum-4 at 2750-55 m.

**Interval:** 2788-2810 m MD

**Age:** Upper Maastrichtian, Palynozone Ma

**Interval zone:**

2788m - palynozone Ma

The palynomorph assemblage in Turrum-7 at 2525-30 and 2540.7 m, which is assigned to zone Re, is most similar to that recovered in Turrum-3 at 2415-20 m and in Turrum-4 at 2580-85 m.

The top of zone Rf in Turrum-7 is placed at 2608.8 m and its assemblage is most comparable to those recovered in Turrum-3 at 2485-90 m and in Turrum-4 at 2655-60 m. The assemblage in Turrum-7 at 2595-2600 m, tentatively placed in zone Rf, is also somewhat similar.

The assemblage recovered at 2736.6 m in this well, assigned to zone Rg, is most similar to that found in Turrum-3 at 2645-50 m and Turrum-4 at 2750-55 m.

## REFERENCE

- Cookson, I.C., and Eisenack, A., 1965. Microplankton from the Dartmoor Formation, S.W. Victoria. *Proc. Royal Soc. Vic.*, 79(1): p. 133-137.
- Cookson, I.C., and Eisenack, A., 1967. Some microplankton from the Paleocene, Rivernook bed, Victoria. *Proc. Royal Soc. Vic.*, 80(2): p. 247-258.
- Damassa, S.P., Williams, G.L., and Brinkhuis, H., 1994. Short course in Paleogene dinoflagellate cysts. Conducted at Amoco Prod. Co., Houston, Texas, Nov. 7-10, 1994.
- Davey, R.J., Downie, C., Sargeant, W.A.S., and Williams, G.L., 1966. Studies of Mesozoic and Cainozoic dinoflagellate cysts. *Bull. Brit. Mus. (Nat. Hist.) Geol., Suppl. 3*, p. 1-248.
- Davies, T. D., 1995. New biostratigraphic subdivision and paleoecology of the Paleocene Turrum Field reservoir section from seven Gippsland Basin wells, Australia. Exxon Exploration Co. rept. EEC.16A.BIO.95.
- Davies, T. D., 1996b. Palynostratigraphic zonation and paleoenvironments of the Turrum-6 well, Gippsland Basin, Australia. Exxon Exploration Co. rept. EEC.19A.BIO.96.
- Davies, T. D., 1996c. Palynology, paleoenvironments and biostratigraphic zonation of the Marlin A6 well, Gippsland Basin, Australia. Exxon Exploration Co. rept. EEC.27A.BIO.96.
- Helby, R., Morgan, R., and Partridge, A.D., 1987. A palynological zonation of the Australian Mesozoic; in Jell, P.A. (ed.), *Assoc. Australasian Palaeont., Mem. 4*. p. 1-94.
- Partridge, A.D., 1976. The geological expression of eustacy in the early Tertiary of the Gippsland Basin. *Aust. Pet. Explor. Assoc. Jour.*, v. 16, pt.1: p. 73-79.
- Powell, A.J., 1992. Dinoflagellates of the Tertiary system; in Powell, A.J. (ed.), *A Stratigraphic Index of Dinoflagellate Cysts*, Chapman and Hall, London: p. 155-252.
- Stover, L.E. and Evans, P.R., 1973. Upper Cretaceous-Eocene spore-pollen zonation, offshore Gippsland Basin, Australia. *Geol. Soc. Aust. Spec. Publ. 4*: p. 55-72.
- Stover, L.E. and Partridge, A.D., 1973. Tertiary and Late Cretaceous spores and pollen from the Gippsland Basin, Southeastern Australia. *Proc. Royal Soc. Vic.*, 85 (2): p. 237-286.

907511 ~~064~~

064

Williams, G. L., and Bujak, J. P., 1985. Mesozoic and Cenozoic dinoflagellates. *In*: H. M. Bolli, et al., (editors), *Plankton Stratigraphy*, Cambridge University Press: p. 847-964.

Wilson, G.J., 1984. New Zealand Late Jurassic to Eocene dinoflagellate biostratigraphy - a summary. *Newsletters on Stratigraphy* 13 (2): p. 104-117.

Wilson, G.J., 1988. Paleocene and Eocene dinoflagellate cysts from Waipawa, Hawkes Bay, New Zealand. *New Zealand Geol. Surv. Paleo. Bull.* 57: 96 p.



**Palynozone Ra**  
(2205-2225m)

- 2205-10      **Paleoenvironment: Marginal marine-lagoonal; Palynozone Ra**  
Kerogen: woody/coaly (A); amorphous (R), S/P (F); biodegraded terrestrial (C);  
          indeter fines (C); dinoflagellates/acritarchs (VR); pyrite (EA)  
Dinoflagellate cysts (F)  
?Apectodinium sp. short spines (F)  
Spiniferites spp. (VR)  
Nothofagidites spp. (F)  
Nothofagidites emarcidus-heterus (R)  
Tricolpites phillipsii (VR)  
Proteacidites spp. (F)  
Proteacidites annularis (VR)  
Proteacidites sp. S (R)  
Proteacidites angulatus (VR) s98.5/12; 95/10.5  
Australopollis obscurus (~Sz and lower) (F)  
Stereisporites antiquasporites (R)  
Lygistipollenites balmei (F)  
Phyllocladidites mawsonii (F-C)  
Phyllocladidites microsaccatus (R)  
Fern spores (C-A)  
Gleicheniidites spp. (C)  
Lycopodiumsporites spp. (VR)  
Laevigatosporites spp. (F)
- 2210-15      **Paleoenvironment: Marginal marine; Palynozone Ra**  
Kerogen: woody/coaly (A); amorphous (R), S/P (VR); biodegraded terrestrial (C);  
          indeterm fines (C-A); dinoflagellates/acritarchs (nearly barren); pyrite (VA)  
Dinoflagellate cysts (R)  
?Apectodinium sp. short spines (R-F)  
Cassidium filosum (VR) s103/14.8  
Nothofagidites spp. (R)  
Nothofagidites emarcidus-heterus (VR)  
Proteacidites spp. (F)  
Proteacidites sp. S (R)  
Australopollis obscurus (F)  
Stereisporites antiquasporites (R)  
Lygistipollenites balmei (F)  
Lygistipollenites florinii (VR)  
Phyllocladidites mawsonii (F)  
Phyllocladidites microsaccatus (R)  
Podospores antarcticus (R-F)  
Bisaccates (A)  
Fern spores (C)  
Gleicheniidites spp. (F-C)  
Lycopodiumsporites spp. (VR)  
Laevigatosporites spp. (F)
- 2220-25      **Paleoenvironment: Marginal marine; Palynozone Ra**  
Kerogen: woody/coaly (A); amorphous (R), S/P (R-F); biodegraded terrestrial (C);  
          indeterm fines (A); dinoflagellates/acritarchs (nearly barren); pyrite (VA)  
Dinoflagellate cysts (VR)  
Spiniferites spp. (VR)

Paleocystodinium cf. golzowense (VR) s91.1/16.9  
 Nothofagidites spp. (VR)  
 Nothofagidites emarcidus-heterus (VR)  
 Tricolpites phillipsii (VR)  
 Proteacidites spp. (F)  
 Proteacidites sp. S (VR)  
 Proteacidites angulatus (VR) s96/11  
 Australopollis obscurus (F)  
 Tetradopollenites spp. (VR)  
 Stereisporites antiquasporites (VR-R)  
 Lygistipollenites balmei (R)  
 Phyllocladidites mawsonii (C-A)  
 Phyllocladidites microsaccatus (F)  
 Podosporites antarcticus (R)  
 Bisaccates (VA)  
 Fern spores (C)  
 Gleicheniidites spp. (F)  
 Laevigatosporites spp. (R)

**Palynozone Rb**  
 (2235-2245.8 (-?2280) m)

2235-40

Paleoenvironment: Marine (shallow); **Palynozone Rb**  
 Kerogen: woody/coaly (A); amorphous (VR), S/P (F); biodegraded terrestrial (C);  
 indeterm fines (F); dinoflagellates/acritarchs (F); pyrite (A)  
 Dinoflagellate cysts (C)  
 Dinoflagellate indeterminate (VR-R)  
 ?Apectodinium sp. short spines (R)  
 Apectodinium homomorphum (VR)  
 Spiniferites spp. (VR)  
 Glaphyrocysta retiintexta (C-A)  
 Cleistosphaeridium spp. (VR)  
 Nothofagidites spp. (R-F)  
 Nothofagidites emarcidus-heterus (R)  
 Nothofagidites cf. brachyspinulosus (VR)  
 Nothofagidites endurus (VR)  
 Proteacidites spp. (F)  
 Proteacidites sp. S (R)  
 Proteacidites angulatus (VR) s97.5/12.4  
 Haloragacidites harrisii (VR)  
 Australopollis obscurus (~Sz and lower) (C)  
 Tetradopollenites spp. (VR)  
 Stereisporites antiquasporites (VR)  
 Lygistipollenites balmei (R)  
 Phyllocladidites mawsonii (F)  
 Podosporites antarcticus (R)  
 Bisaccates (F-C)  
 Fern spores (C)  
 Gleicheniidites spp. (F)  
 Lycopodiumsporites spp. (VR)  
 Laevigatosporites spp. (R)

- 2240-45      Paleoenvironment: Marine (shallow); Palynozone Rb  
Kerogen: woody/coaly (VA); amorphous (VR), S/P (F); biodegraded terrestrial (C);  
              indeterm fines (R); dinoflagellates/acritarchs (F); pyrite (A); scanned  
Dinoflagellate cysts (VA)  
Dinoflagellate indeterminate (VR-R)  
Apectodinium spp. (VR)  
Spiniferites spp. (VR)  
Paleocystodinium cf. golzowense (R-F) +  
Paleocystodinium golzowense (VR) +100/15.4  
Glaphyrocysta retiintexta (VA)  
Impagidinium spp. (VR)  
Nothofagidites spp. (R-VR)  
Nothofagidites endurus (lowermost Eocene to Maast.) (VR)  
Proteacidites spp. (R)  
Proteacidites sp. S (R)  
Australopollis obscurus (R)  
Stereisporites antiquasporites (VR)  
Lygistipollenites balmei (R)  
Phyllocladidites mawsonii (F)  
Phyllocladidites microsaccatus (R)  
Podosporites antarcticus (R)  
Fern spores (F)  
Gleicheniidites spp. (R)  
Laevigatosporites spp. (R)
- 2245.8      Paleoenvironment: Marine (shallow); Palynozone Rb  
SWC 51      Kerogen: woody/coaly (VA); amorphous (VR), S/P (F); biodegraded terrestrial (C-A);  
              indeterm fines (F); dinoflagellates/acritarchs (F); pyrite (VA)  
Dinoflagellate cysts (EA)  
Dinoflagellate indeterminate (VR-R)  
Apectodinium spp. (VR)  
Spiniferites spp. (VR)  
Paleocystodinium cf. golzowense (R) +  
Paleocystodinium golzowense (R) +  
Glaphyrocysta retiintexta (EA)  
Cleistosphaeridium spp. (VR)  
Impagidinium spp. (VR)  
Deflandrea/Cerodinium spp. (VR) +97/13.1; 100.4/10.9  
Nothofagidites spp. (R-VR)  
Nothofagidites emarcidus-heterus (VR)  
Nothofagidites endurus (VR)  
Tricolpites spp. (VR)  
Proteacidites spp. (R-F)  
Proteacidites sp. S (R)  
Proteacidites angulatus (VR)  
Haloragacidites harrisii (VR)  
Australopollis obscurus (R)  
Stereisporites antiquasporites (VR)  
Lygistipollenites balmei (R)  
Phyllocladidites mawsonii (F)  
Fern spores (F)  
Gleicheniidites spp. (R)  
Ischyosporites spp. (R)  
Laevigatosporites spp. (R)

- 2260-65      Paleoenvironment: Marginal marine; Palynozone Rb/?Rc  
Kerogen: woody/coaly (VA); amorphous (VR), S/P (R); biodegraded terrestrial (VA);  
              indeterm fines (C); dinoflagellates/acritarchs (nearly barren); pyrite (VA)  
Dinoflagellate cysts (R)  
Dinoflagellate indeterminate (VR)  
?Apectodinium sp. short spines (R)  
Achromosphaera spp. (crassipellis-type) (VR) +102/20  
Paleocystodinium golzowense (VR) +  
Deflandrea/Cerodinium spp. (VR)  
Nothofagidites spp. (R-VR)  
Nothofagidites endurus (VR)  
Proteacidites spp (VR)  
Australopollis obscurus (F)  
Lygistipollenites balmei (VR)  
Phyllocladidites mawsonii (F)  
Phyllocladidites microsaccatus (VR)  
Podosporites antarcticus (VR)  
Bisaccates (F)  
Fern spores (R)  
Gleicheniidites spp. (R)
- 2270.8      Paleoenvironment: Marginal marine; Palynozone Rb/?Rc  
Kerogen: woody/coaly (EA); amorphous (VR), S/P (F); biodegraded terrestrial (C);  
              indeterm fines (F-C); dinoflagellates/acritarchs (nearly barren); botryococcus  
              (VR); pyrite (VA)  
Dinoflagellate cysts (R)  
Dinoflagellate indeterminate (VR)  
Spiniferites spp. (VR)  
cf. Paleocystodinium golzowense (VR) +  
Glaphyrocysta spp. (VR)  
Deflandrea cf. medcalfii (VR)  
Nothofagidites spp. (VR)  
Proteacidites spp. (VR)  
Proteacidites sp. S (VR)  
Australopollis obscurus (F)  
Stereisporites antiquasporites (VR)  
Lygistipollenites balmei (VR)  
Phyllocladidites mawsonii (F)  
Fern spores (F)  
Gleicheniidites spp. (R)  
Laevigatosporites spp. (R)
- 2275-80      Paleoenvironment: Non-marginal marine; Palynozone Rb/?Rc  
Kerogen: woody/coaly (VA); amorphous (R), S/P (R); indeterm fines (A);  
              dinoflagellates/acritarchs (barren); botryococcus (VR); pyrite (VA)  
?Paleocystodinium spp. (ER, piece) +  
Proteacidites spp. (VR)  
Australopollis obscurus (~Sz and lower) (R)  
Lygistipollenites balmei (VR)  
Phyllocladidites mawsonii (F-R)  
Fern spores (R)  
Gleicheniidites spp. (VR)

2278.2  
SWC 45

Paleoenvironment: Marginal marine; Prob. Palynozone Rb; (poor pres)  
Kerogen: woody/coaly (va); amorphous (vr), S/P (c); biodegraded terrestrial (c);  
indeterm fines (r); dinoflagellates/acritarchs (); pyrite (c)  
Algal cysts (C)  
Dinoflagellate cysts (r-f)  
?Apectodinium sp. short spines (r)  
Senegalinium spp. (R)  
Glaphyrocysta spp. (R)  
Glaphyrocysta retiintexta (vr)  
Deflandrea/Cerodinium spp. (VR)  
Proteacidites spp. (f)  
Proteacidites angulatus (r)  
Australopollis obscurus (~Sz and lower) (r-f)  
Stereisporites antiquasporites (r-f)  
Lygistipollenites balmei (r)  
Phyllocladidites mawsonii (f)  
Fern spores (f)  
Gleicheniidites spp. (r)

**Palynozone Rc**  
(2300-2370m)

2300-05

Paleoenvironment: Marginal-shallow marine; Palynozone Rc  
Kerogen: woody/coaly (VA); amorphous (R), S/P (F); biodegraded terrestrial (C);  
indeterm fines (C); dinoflagellates/acritarchs (R-F); pyrite (VA)  
Dinoflagellate cysts (C)  
Dinoflagellate indeterminate (R)  
?Apectodinium sp. short spines (F-C)  
Apectodinium homomorphum (F)  
Apectodinium spp. (C)  
Spiniferites spp. (VR)  
?Achomosphaera spp. (crassipellis-type) (VR, broken)  
Paleocystodinium cf. golzowense (VR) +  
Glaphyrocysta spp. (R)  
Glaphyrocysta retiintexta (R)  
Senegalinium spp. (R)  
Spinidinium-type (D) (VR)  
Systematophora spp. (VR) s+99.5/16.5  
Nothofagidites spp. (R-VR)  
Nothofagidites endurus (VR)  
Proteacidites spp. (F)  
Proteacidites sp. S (VR)  
Proteacidites angulatus (VR)  
Haloragacidites harrisii (VR)  
cf. Gambierina rudata (VR)  
Australopollis obscurus (~Sz and lower) (F)  
Stereisporites antiquasporites (VR)  
Lygistipollenites balmei (VR)  
Phyllocladidites mawsonii (F)  
Bisaccates (F)  
Fern spores (R)  
Gleicheniidites spp. (VR)  
Ischyosporites spp. (R)

- Laevigatosporites spp. (R)
- 2305-15      Paleoenvironment: Marginal-shallow marine; Palynozone Rc  
Kerogen: woody/coaly (VA); amorphous (R), S/P (F); biodegraded terrestrial (C);  
                  indeterm fines (F); dinoflagellates/acritarchs (R-F); pyrite (VA)  
Dinoflagellate cysts (C-A)  
Dinoflagellate indeterminate (R)  
?Apectodinium sp. short spines (VR)  
Apectodinium homomorphum (VR)  
Spiniferites spp. (VR)  
Spiniferites septatus (VR)  
Paleocystodinium spp. (F) s+  
Paleocystodinium golzowense (R-F)  
Glaphyrocysta spp. (R)  
Glaphyrocysta retiintexta (A)  
Deflandrea/Cerodinium spp. (VR)  
Cerodinium spp. (R)  
Cerodinium dartmooria (VR)  
Deflandrea cf. medcalfii (VR)  
Alisocysta reticulatus (VR, top) s+102/13.4  
Nothofagidites spp. (R)  
Nothofagidites cf. brachyspinulosus (VR)  
Nothofagidites endurus (lowermost Eocene to Maast.) (VR)  
Proteacidites spp. (F)  
Proteacidites angulatus (R)  
Australopollis obscurus (~Sz and lower) (F)  
Stereisporites antiquasporites (Paleocene to Upper Campanian) (VR)  
Lygistipollenites balmei (R-F)  
Lygistipollenites florinii (VR)  
Phyllocladidites mawsonii (F-C)  
Fern spores (F)  
Gleicheniidites spp. (R)  
Laevigatosporites spp. (R)
- 2335-45      Paleoenvironment: Marginal-shallow marine; Palynozone Rc  
Kerogen: woody/coaly (A); amorphous (F), S/P (F); biodegraded terrestrial (F);  
                  indeterm fines (F-C); dinoflagellates/acritarchs (F); botryococcus (VR); pyrite (C)  
Cyclopsiella spp. (VR)  
Dinoflagellate cysts (C-A)  
Dinoflagellate indeterminate (R)  
?Apectodinium sp. short spines (F-C)  
Apectodinium homomorphum (VR)  
Spiniferites spp. (VR)  
Achomosphaera spp. (crassipellis-type) (VR)  
Paleocystodinium spp. (R-F) s+  
Paleocystodinium golzowense (R)  
Glaphyrocysta retiintexta (F)  
Cerodinium spp. (R-F)  
Senegalinium spp. (F)  
Nothofagidites spp. (VR)  
Tricolpites spp. (VR)  
Proteacidites spp. (F)  
Proteacidites sp. S (VR)  
Proteacidites angulatus (R)

- Australopollis obscurus (~Sz and lower) (C)  
 Stereisporites antiquasporites (VR)  
 Lygistipollenites balmei (R)  
 Phyllocladidites mawsonii (R)  
 Fern spores (F-C)  
 Gleicheniidites spp. (F)  
 Laevigatosporites spp. (R)
- 2360-70
- Paleoenvironment: Marginal-shallow marine; Palynozone Rc  
 Kerogen: woody/coaly (A); amorphous (F), S/P (F); biodegraded terrestrial (F);  
 indeterm fines (C); dinoflagellates/acritarchs (F); pyrite (VA)  
 Dinoflagellate cysts (A)  
 Dinoflagellate indeterminate (R)  
 ?Apectodinium sp. short spines (F)  
 Spiniferites spp. (VR)  
 Spiniferites septatus (VR)  
 Achomosphaera spp. (crassipellis-type) (R-F)  
 Paleocystodinium spp. (F) s+  
 Paleocystodinium cf. golzowense (R)  
 Paleocystodinium golzowense (R)  
 Glaphyrocysta spp. (R)  
 Glaphyrocysta retiintexta (A)  
 Deflandrea/Cerodinium spp. (VR)  
 Cerodinium spp. (VR)  
 Cerodinium dartmooria (VR) s+96.1/4  
 Deflandrea cf. medcalfii (VR)  
 Senegalinium spp. (F-C)  
 Senegalinium dilwynensis (F)  
 Nothofagidites spp. (VR)  
 Nothofagidites cf. endurus (VR)  
 Proteacidites spp. (R-F)  
 Proteacidites sp. S (VR)  
 Proteacidites cf. angulatus (R)  
 Gambierina rudata (VR)  
 Australopollis obscurus (~Sz and lower) (F)  
 Lygistipollenites balmei (R)  
 Phyllocladidites mawsonii (F-C)  
 Fern spores (F)  
 Gleicheniidites spp. (R)  
 Laevigatosporites spp. (R)

**Palynozone Rc/Rd**

(2375-80m)

- 2375-80
- Paleoenvironment: Marginal marine; Palynozone Rc?/Rd (V. poor preservation)  
 Kerogen: woody/coaly (A); amorphous (F), S/P (VR); biodegraded terrestrial (F);  
 indeterm fines (A); dinoflagellates/acritarchs (VR); pyrite (EA)  
 Dinoflagellate cysts (F)  
 Dinoflagellate indeterminate (R)  
 Paleocystodinium spp. (R)  
 Glaphyrocysta spp. (R)  
 Glaphyrocysta retiintexta (F)  
 Senegalinium spp. (R)

cf. *Spinidinium densispinatum* (VR-R)  
*Nothofagidites* spp. (VR)  
*Australopollis obscurus* (~Sz and lower) (R)  
*Lygistipollenites balmei* (VR)  
*Phyllocladidites mawsonii* (R)  
Fern spores (R)

**Palynozone Rd**  
(2395-2510m)

- 2395-2400      Paleoenvironment: Marginal-shallow marine; Palynozone Rd  
                 Kerogen: woody/coaly (VA); amorphous (R-F), S/P (F); biodegraded terrestrial (F);  
                                         indeterm fines (F); dinoflagellates/acritarchs (F); pyrite (EA)  
*Dinoflagellate* cysts (C-A)  
*Dinoflagellate* indeterminate (R)  
*?Apectodinium* sp. short spines (R)  
*Paleocystodinium* cf. *golzowense* (R) +  
*Glaphyrocysta* spp. (R)  
*Glaphyrocysta retiintexta* (F)  
*Cerodinium* spp. (R)  
*Senegalinium* spp. (R)  
*Spinidinium densispinatum* (R) 98/12.6; 98/12.6  
*Fibrocysta* spp. (VR)  
*Vozzhennikovia* spp. (VR-R)  
*Vozzhennikovia angulata* (R-F) +s975.9; 100.8/23  
*Tricolpites gillii* (VR)  
*Proteacidites* spp. (F)  
*Proteacidites angulatus* (R)  
*Australopollis obscurus* (F-C)  
*Lygistipollenites balmei* (VR)  
*Phyllocladidites mawsonii* (F)  
Fern spores (R)
- 2403.4      Paleoenvironment: Marginal-shallow marine; Palynozone Rd  
                 Kerogen: woody/coaly (A); amorphous (F), S/P (F); biodegraded terrestrial (C);  
                                         indeterm fines (VA); dinoflagellates/acritarchs (R); pyrite (F-C)  
*Cyclopsiella* spp. (VR)  
*Dinoflagellate* cysts (C)  
*Dinoflagellate* indeterminate (R)  
*?Apectodinium* sp. short spines (R)  
*Paleocystodinium golzowense* (VR)  
*Glaphyrocysta* spp. (R)  
*Glaphyrocysta retiintexta* (F-C)  
*Cerodinium* spp. (R) +s100/22  
*Cerodinium dartmooria* (VR) s+  
*Deflandrea* spp. (VR)  
*Isabelidinium* spp. (R-F)  
*Isabelidinium cingulatum* (R) +s100/20.5  
*Senegalinium dilwynensis* (R-F)  
*Spinidinium densispinatum* (R)  
*Spinidinium* cf. *macmurdoense* (VR)  
*Vozzhennikovia* spp. (VR-R)  
*Nothofagidites* spp. (F)



- Nothofagidites brachyspinulosus (VR)  
 Nothofagidites endurus (R)  
 Proteacidites spp. (F)  
 Proteacidites sp. S (R)  
 Proteacidites angulatus (VR)  
 Gambierina rudata (VR)  
 Gambierina edwardsii (VR)  
 Australopollis obscurus (F-C)  
 Stereisorites antiquasporites (R)  
 Lygistipollenites balmei (F-C)  
 Phyllocladidites mawsonii (C)  
 Phyllocladidites microsaccatus (R)  
 Podosporites spp. (VR)  
 Bisaccates (C)  
 Fern spores (C)  
 Gleicheniidites spp. (F)  
 Laevigatosporites spp. (R)
- 2435-40      Paleoenvironment: Non- marginal marine; Prob. Palynozone Rd  
 Kerogen: woody/coaly (VA); amorphous (R), S/P (R); biodegraded terrestrial (R);  
                   indeterm fines (F-C); dinoflagellates/acritarchs (ER); pyrite (F-C)  
 Dinoflagellate cysts (VR-R)  
 Glaphyrocysta spp. (VR)  
 Vozzhennikovia spp. (VR)  
 Nothofagidites spp. (vr)  
 Tricolpites spp. (VR)  
 Proteacidites spp. (F)  
 Proteacidites sp. S (R)  
 Gambierina rudata (VR)  
 Gambierina edwardsii (VR)  
 Australopollis obscurus (C)  
 Stereisorites antiquasporites (VR)  
 Phyllocladidites mawsonii (C)  
 Phyllocladidites microsaccatus (R)  
 Bisaccates (C)  
 Fern spores (F)  
 Gleicheniidites spp. (F)
- 2450-60      Paleoenvironment: Non- marginal marine; Prob. Palynozone Rd; (poor pres)  
 Kerogen: woody/coaly (VA); amorphous (F-C?), S/P (F); biodegraded terrestrial (R);  
                   indeterm fines (F-C?); dinoflagellates/acritarchs (barren); pyrite (F-C)  
 Dinoflagellate cysts (f)  
 Paleocystodinium golzowense (VR)  
 Senegalinium spp. (r-f)  
 Spinidinium densispinatum (vr)  
 Vozzhennikovia spp. (VR)  
 Tricolpites spp. (VR)  
 Proteacidites spp. (f)  
 Proteacidites sp. S (vr)  
 Proteacidites angulatus (VR)  
 Gambierina rudata (VR)  
 Gambierina edwardsii (VR)  
 Australopollis obscurus (C)  
 Stereisorites antiquasporites (VR)

- Lygistipollenites balmei (f)  
Phyllocladidites mawsonii (f)  
Phyllocladidites microsaccatus (R)  
Bisaccates (C)  
Fern spores (c)  
Gleicheniidites spp. (r)  
Laevigatosporites spp. (R)  
Verrucatosporites spp. (VR)
- 2467.5      Paleoenvironment: Nonmarine; Prob. Palynozone Rd; (poor pres)  
Kerogen: woody/coaly (A); amorphous (R), S/P (C); biodegraded terrestrial (R);  
              indeterm fines (R); dinoflagellates/acritarchs (); pyrite (r-f)  
Nothofagidites spp. (vr)  
Tricolpites spp. (R)  
cf. Tricolpites gillii (VR)  
Proteacidites spp. (c)  
Proteacidites sp. S (r)  
Proteacidites angulatus (VR)  
Australopollis obscurus (C)  
Stereisporites antiquasporites (f)  
Lygistipollenites balmei (C)  
Phyllocladidites mawsonii (f)  
Phyllocladidites microsaccatus (R)  
Fern spores (c)  
Gleicheniidites spp. (r)
- 2470-75      Paleoenvironment: Prob nonmarine; Prob. Palynozone Rd; (poor pres)  
Kerogen: woody/coaly (VA); amorphous (R), S/P (r-f); biodegraded terrestrial (R);  
              indeterm fines (f); dinoflagellates/acritarchs (); pyrite (f)  
Dinoflagellate cysts (R-F)  
Glaphyrocysta retiintexta (r)  
Spinidinium densispinatum (vr)  
Vozzhennikovia spp. (r) 96.5/15.5  
Cerodinium spp. (vr)  
Tricolpites spp. (R)  
Proteacidites spp. (f)  
Proteacidites angulatus (r)  
Australopollis obscurus (C-F)  
Lygistipollenites balmei (f)  
Phyllocladidites mawsonii (f)  
Phyllocladidites microsaccatus (R)  
Stereisporites antiquasporites (r)  
Fern spores (f)  
Gleicheniidites spp. (r)  
Laevigatosporites spp. (R)
- 2480.5      Paleoenvironment: Marginal-shallow marine; Prob. Palynozone Rd (?); (poor pres)  
Kerogen: woody/coaly (VA); amorphous (VR), S/P (f); biodegraded terrestrial (f-c);  
              indeterm fines (r); dinoflagellates/acritarchs (vr); pyrite (f)  
Dinoflagellate cysts (f-c)  
Dinoflagellate indeterminate (R)  
?Apectodinium sp. short spines (f)  
Spiniferites spp. (R)  
Hystrichosphaeridium cf. tubiferum (vr)

Paleocystodinium spp. (vr)  
 Cerodinium spp. (r)  
 Senegalinium dilwynensis (R-F)  
 Spinidinium densispinatum (r-f)  
 Vozzhennikovia spp. (r-f)  
 Cassidium fragile (vr)  
 ?Tetracolporites verrucosus (vr)  
 Proteacidites spp. (f)  
 Proteacidites angulatus (VR)  
 Nothofagidites spp. (vr)  
 Nothofagidites cf. brachyspinulosus (VR)  
 Australopollis obscurus (C)  
 Ephedripites spp. (vr)  
 Stereisorites antiquasporites (f)  
 Lygistipollenites balmei (r)  
 Phyllocladidites mawsonii (f)  
 Fern spores (f)  
 Gleicheniidites spp. (r)  
 Laevigatosporites spp. (R)

- 2500-10      Paleoenvironment: Prob Nonmarine; Prob. Palynozone Rd (?); (poor pres)  
 Kerogen: woody/coaly (c); amorphous (c), S/P (vr); biodegraded terrestrial (f-c);  
                   indeterm fines (f); dinoflagellates/acritarchs (barren); pyrite (f)  
 Dinoflagellate cysts (barren)  
 Nothofagidites spp. (r-f)  
 Nothofagidites cf. brachyspinulosus (VR)  
 Nothofagidites endurus (vr)  
 Tricolpites spp. (R)  
 Proteacidites spp. (f)  
 Proteacidites angulatus (VR)  
 Australopollis obscurus (f-c)  
 Stereisorites antiquasporites (r-f)  
 Lygistipollenites balmei (r)  
 Phyllocladidites mawsonii (f)  
 Phyllocladidites microsaccatus (R)  
 Podosporites spp. (VR)  
 Fern spores (R)  
 Gleicheniidites spp. (r)  
 Laevigatosporites spp. (vr)

**Palynozone Re**  
 (2515-2570m)

- 2515-20      Paleoenvironment: Marginal marine; Palynozone Re; (poor pres)  
 Kerogen: woody/coaly (a); amorphous (f), S/P (r); biodegraded terrestrial (f-c);  
                   indeterm fines (f-c); dinoflagellates/acritarchs (vr); pyrite (f);  
 Dinoflagellate cysts (f)  
 Apectodinium spp. (barren)  
 Glaphyrocysta spp. (r)  
 Spinidinium densispinatum (r-f)  
 Vozzhennikovia angulata (vr)  
 Proteacidites spp. (f)  
 Proteacidites sp. S (vr)  
 Australopollis obscurus (r)

- Ephedripites spp. (vr)  
Stereisporites antiquasporites (vr)  
Lygistipollenites balmei (r)  
Phyllocladidites mawsonii (f)  
Phyllocladidites microsaccatus (vr)  
Podosporites spp. (VR)  
Fern spores (f)
- 2525-30      Paleoenvironment: Marginal marine; Palynozone Re  
Kerogen: woody/coaly (a); amorphous (f), S/P (f); biodegraded terrestrial (f-c);  
                  indeterm fines (f-c); dinoflagellates/acritarchs (r); pyrite (c);  
Dinoflagellate cysts (a)  
Cerodinium spp. (f-c)  
Cerodinium striatum (VR) +99/9.7  
Isabelidinium spp. (r)  
Spinidinium-type (D) (f)  
Spinidinium densispinatum (a) k101.2/14.9; +  
Vozzhennikovia angulata (vr)  
Proteacidites spp. (f)  
Proteacidites angulatus (VR)  
Australopollis obscurus (r-vr)  
Lygistipollenites balmei (vr)  
Phyllocladidites mawsonii (r)  
Fern spores (f)
- 2540.7      Paleoenvironment: Marine; Palynozone Re (max flood)  
Kerogen: woody/coaly (va); amorphous (r), S/P (r); biodegraded terrestrial (f-c);  
                  indeterm fines (f); dinoflagellates/acritarchs (r); pyrite (ea);  
Dinoflagellate cysts (VA)  
Spiniferites septatus (VR)  
Cerodinium spp. (a)  
Cerodinium striatum (r-f) +  
Cerodinium dartmooria (r-f) +  
Deflandrea spp. (VR)  
Isabelidinium spp. (r)  
Isabelidinium cingulatum (R) +s100/20.5  
Senegalinium spp. (r)  
Spinidinium densispinatum (f) +  
Vozzhennikovia angulata (vr)  
Turbiosphaera cf. filosa (vr-r)  
Proteacidites spp. (f)  
Australopollis obscurus (r)  
Lygistipollenites balmei (r)  
Phyllocladidites mawsonii (r)  
Fern spores (f)
- 2565-70      Paleoenvironment: Marginal marine; Palynozone Re (?)  
Kerogen: woody/coaly (va); amorphous (r), S/P (r); biodegraded terrestrial (f-c);  
                  indeterm fines (c); dinoflagellates/acritarchs (r); pyrite (ea)  
Dinoflagellate cysts (f)  
Spiniferites septatus (VR)  
Glaphyrocysta spp. (vr)  
Cerodinium spp. (f)  
Spinidinium densispinatum (f) +

Vozzhennikovia spp. (r)  
 Nothofagidites spp. (vr)  
 cf. Tetracolporites verrucosus (vr)  
 Tricolpites cf. confessus (vr) -101/14.5  
 Proteacidites spp. (f)  
 Gambierina rudata (vr)  
 Australopollis obscurus (f)  
 Lygistipollenites balmei (r)  
 Phyllocladidites mawsonii (r)  
 Phyllocladidites microsaccatus (R)  
 Fern spores (f)  
 Gleicheniidites spp. (r)  
 Laevigatosporites spp. (R)

**Indeterminate**  
(2570-80m)

2570-80      Paleoenvironment: Nonmarine; Palynozone Indeterminate (v. sparse fossils)  
 Kerogen: woody/coaly (a); amorphous (vr), S/P (vr); biodegraded terrestrial (f-c);  
                   indeterm fines (f); dinoflagellates/acritarchs (barren); pyrite (f)  
 Dinoflagellate cysts (barren)  
 Lygistipollenites balmei (r)  
 Bisaccates (r)  
 Fern spores (r)

**Palynozone Rf**  
(2595?-) 2608.8-2665m)

2595-2600      Paleoenvironment: Nonmarine; Poss. Palynozone Rf  
 Kerogen: woody/coaly (va); amorphous (r-f), S/P (r); biodegraded terrestrial (f);  
                   indeterm fines (f); dinoflagellates/acritarchs (barren); pyrite (f)  
 Dinoflagellate cysts (barren)  
 Nothofagidites spp. (vr)  
 cf. Tetracolporites verrucosus (vr)  
 Tricolpites spp. (f)  
 Tricolpites gillii (vr)  
 Tricolpites phillipsii (vr)  
 Proteacidites spp. (f-c)  
 Australopollis obscurus (r)  
 Ephedripites spp. (vr-r)  
 Stereisorites antiquasporites (c)  
 Stereisorites (Tripunctisporis) sp. (r)  
 Phyllocladidites mawsonii (c)  
 Phyllocladidites microsaccatus (f)  
 Podosporites spp. (f)  
 Fern spores (c)  
 Gleicheniidites spp. (f)  
 Laevigatosporites spp. (f)

2608.8      Paleoenvironment: Nonmarine; Prob. Palynozone Rf (poor pres)  
 SWC 22      Kerogen: woody/coaly (va); S/P (f); biodegraded terrestrial (f); indeterm fines (vr);  
                   dinoflagellates/acritarchs (barren); pyrite (r)  
 Dinoflagellate cysts (barren-ER)  
 Nothofagidites spp. (r)

Nothofagidites endurus (R)  
 Tetracolporites verrucosus (r)  
 Tricolpites spp. (r)  
 Tricolpites gillii (vr)  
 Tricolpites phillipsii (vr)  
 Tricolpites cf. reticulatus (vr)  
 Tricolpites gillii (vr)  
 Proteacidites spp. (f-c)  
 Proteacidites angulatus (f)  
 Australopollis obscurus (r-f)  
 Stereisorites antiquasporites (vr)  
 Stereisorites (Tripunctisporis) sp. (vr)  
 Lygistipollenites balmei (r)  
 Lygistipollenites florinii (VR)  
 Phyllocladidites mawsonii (c)  
 Phyllocladidites microsaccatus (f)  
 Bisaccates (f)  
 Fern spores (r-f)

2615-20 Paleoenvironment: Non-?marginal marine; Prob. Palynozone Rf (poor pres)  
 Kerogen: woody/coaly (va); amorphous (vr), S/P (f); biodegraded terrestrial (f);  
 indeterm fines (vr); dinoflagellates/acritarchs (nearly barren); pyrite (r)  
 Dinoflagellate cysts (vr, v poor pres)  
 ?Senegalinium spp. (vr)  
 Nothofagidites spp. (r)  
 Tetracolporites verrucosus (vr)  
 Tricolpites spp. (r)  
 Tricolpites cf. reticulatus (vr)  
 Tricolpites gillii (vr)  
 Tricolpites phillipsii (vr)  
 Tricolpites cf. confessus (vr) –  
 Tricolporites marginatus (vr) –94/10.9  
 Proteacidites spp. (f-c)  
 Proteacidites angulatus (r)  
 Australopollis obscurus (r)  
 Ephedripites spp. (vr)  
 Stereisorites antiquasporites (c)  
 Lygistipollenites balmei (r)  
 Phyllocladidites mawsonii (f-c)  
 Phyllocladidites microsaccatus (f)  
 Bisaccates (f)  
 Fern spores ()  
 Gleicheniidites spp. (r)  
 Laevigatosporites spp. (vr)

2622-30 Paleoenvironment: Non-?marginal marine; Prob. Palynozone Rf (poor pres)  
 Core Kerogen: woody/coaly (va); amorphous (), S/P (f); biodegraded terrestrial (f);  
 indeterm fines (r); dinoflagellates/acritarchs (barren); pyrite (r)  
 Dinoflagellate cysts (barren-nearly barren)  
 ?Senegalinium spp. (vr)  
 Nothofagidites spp. (f)  
 Tricolpites spp. (f)  
 Tricolpites gillii (vr-r)  
 Tricolpites phillipsii (vr)

- Proteacidites spp. (c)  
 Proteacidites angulatus (f)  
 Gambierina rudata (vr)  
 Australopollis obscurus (f-c)  
 Stereisporites antiquasporites (vr)  
 Lygistipollenites balmei (r)  
 Lygistipollenites florinii (r-f)  
 Phyllocladidites mawsonii (r-f)  
 Phyllocladidites microsaccatus (f)  
 Bisaccates (f)  
 Fern spores (r-f)  
 Gleicheniidites spp. (r)  
 Laevigatosporites spp. (r)
- 2634.7  
 SWC 14
- Paleoenvironment: Nonmarine; Palynozone Rf (poor pres)  
 Kerogen: woody/coaly (va); amorphous (r), S/P (f); biodegraded terrestrial (f-c);  
 indeterm fines (r); dinoflagellates/acritarchs (barren); pyrite (f)  
 Dinoflagellate cysts (barren)  
 Tetracolporites verrucosus (vr)  
 Tricolpites spp. (r)  
 Tricolpites gillii (vr)  
 Tricolpites cf. confessus (vr) -  
 Proteacidites spp. (c)  
 Proteacidites sp. S (r)  
 Proteacidites angulatus (f)  
 Gambierina rudata (vr)  
 Australopollis obscurus (r)  
 Lygistipollenites balmei (r)  
 Phyllocladidites mawsonii (f)  
 Phyllocladidites microsaccatus (f)  
 Fern spores (f)  
 Gleicheniidites spp. (r)
- 2655-65
- Paleoenvironment: Marginal-non marine; Palynozone Rf (poor pres)  
 Kerogen: woody/coaly (a); amorphous (r-f), S/P (r); biodegraded terrestrial (f);  
 indeterm fines (c); dinoflagellates/acritarchs (er); pyrite (va)  
 Dinoflagellate cysts (vr-r)  
 Dinoflagellate indeterminate (vr) Pereodinia-type+99.2/14  
 Hystrichosphaeridium sp. T (vr) 104/15.5  
 Glaphyrocysta retiintexta (vr)  
 ?Senegalinium spp. (vr)  
 cf. Spinidinium densispinatum (vr) +  
 Nothofagidites spp. (r)  
 Tricolpites spp. (vr)  
 Proteacidites spp. (c)  
 Proteacidites angulatus (f)  
 Australopollis obscurus (~Sz and lower) (r)  
 Stereisporites (Tripunctisporis) sp. (vr)  
 Phyllocladidites mawsonii (f)  
 Phyllocladidites microsaccatus (f)  
 Fern spores (r)

**Indeterminate**  
 (2665-2720m)

- 2665-70 Paleoenvironment: Non-marginal marine; Zone Indeterminate (poor recovery & pres)  
Kerogen: woody/coaly (va); amorphous (r), S/P (r); biodegraded terrestrial (f);  
indeterm fines (f); dinoflagellates/acritarchs (barren); pyrite (va)  
Dinoflagellate cysts (prob barren)  
?Spinidinium densispinatum (vr) +  
Nothofagidites spp. (r)  
Proteacidites spp. (r)  
Phyllocladidites mawsonii (r)  
Fern spores (r)
- 2690-95 Paleoenvironment: Non-marine; poss. Palynozone Indeterminate (poor recovery & pres)  
Kerogen: woody/coaly (c-a); amorphous (f), S/P (r); biodegraded terrestrial (f);  
indeterm fines (c-a); dinoflagellates/acritarchs (barren); pyrite (ea)  
Dinoflagellate cysts (barren)  
Phyllocladidites mawsonii (r)  
Phyllocladidites microsaccatus (vr)  
Fern spores (r)
- 2705-20 Paleoenvironment: Non marine; Palynozone Indeterminate (poor recovery & pres)  
Kerogen: woody/coaly (c); amorphous (c), S/P (r); biodegraded terrestrial (f);  
indeterm fines (c-a); dinoflagellates/acritarchs (barren); pyrite (ea)  
Tetracolporites verrucosus (vr)  
Phyllocladidites mawsonii (r)  
Phyllocladidites microsaccatus (vr)

**Palynozone Possible Rg**  
(2735-40m)

- 2735-40 Paleoenvironment: Non-marine; Zone Indeterminate (poss Rg) (poor recovery & pres)  
Kerogen: woody/coaly (f-c); amorphous (c-a), S/P (vr); biodegraded terrestrial (f);  
indeterm fines (c-a); dinoflagellates/acritarchs (barren); pyrite (ea)  
Dinoflagellate cysts (barren)  
Nothofagidites spp. (r)  
Tricolpites spp. (vr)  
Tricolpites confessus (vr) -  
Proteacidites spp. (r)  
Proteacidites angulatus (vr)  
Gambierina spp. (vr)  
Australopollis obscurus (r-f)  
Phyllocladidites mawsonii (r)  
Phyllocladidites microsaccatus (vr)  
Bisaccates (f)  
Fern spores (f)  
Gleicheniidites spp. (vr)  
Laevigatosporites spp. (r-f)

**Palynozone Rg**  
(2736.6-2775.8m)

- 2736.6 Paleoenvironment: Marginal-shallow marine; poss. Palynozone Rg  
SWC 6 Kerogen: woody/coaly (va); amorphous (vr), S/P (f); biodegraded terrestrial (f);  
indeterm fines (f); dinoflagellates/acritarchs (r); pyrite (ea)  
Dinoflagellate cysts (f)



Hystrichosphaeridium sp. (f) 94/6  
 Hystrichosphaeridium sp. T (r) 99/9.8  
 Glaphyrocysta spp. (vr)  
 Deflandrea/Cerodinium spp. (VR)  
 Senegalinium dilwynensis (er)  
 Tricolpites spp. (r)  
 Tricolpites cf. reticulatus (vr)  
 Tricolpites gillii (vr)  
 Proteacidites spp. (r)  
 Gambierina rudata (r)  
 Australopollis obscurus (f)  
 Stereisorites antiquasporites (vr)  
 Stereisorites (Tripunctisporis) sp. (r)  
 Phyllocladidites mawsonii (r)  
 Phyllocladidites microsaccatus (r)  
 Fern spores (f)

2775.8  
SWC 4

Paleoenvironment: Marginal-shallow marine; Palynozone Rg  
 Kerogen: woody/coaly (va); amorphous (vr), S/P (f); biodegraded terrestrial (f);  
 indeterm fines (r); dinoflagellates/acritarchs (r); pyrite (ea)  
 Cyclopsiella spp. (VR)  
 Dinoflagellate cysts (c)  
 Dinoflagellate indeterminate (r)  
 Spiniferites spp. (vr)  
 Paleocystodinium spp. (vr)  
 Glaphyrocysta spp. (f)  
 Glaphyrocysta retiintexta (vr) 90.5/20  
 Deflandrea spp. (f)  
 Turbiosphaera spp. (r)  
 cf. Trythyrodinium spp. (vr)  
 Manumiella spp. (r-f) 93/17.4  
 Nothofagidites spp. (vr)  
 Tricolpites spp. (r)  
 Tricolpites cf. longus (vr, broken) -s99.5/15.8  
 Proteacidites spp. (f)  
 Proteacidites angulatus (vr)  
 Gambierina edwardsii (vr)  
 Australopollis obscurus (f)  
 Stereisorites (Tripunctisporis) sp. (vr)  
 Phyllocladidites microsaccatus (r)  
 Bisaccates (f)  
 Fern spores (f)  
 Gleicheniidites spp. (vr)  
 Lycopodiumsporites spp. (VR)  
 Laevigatosporites spp. (r)

**Palynozone Ma**  
(2788m)

2788  
SWC 3

Paleoenvironment: Marginal-shallow marine; Palynozone Ma  
 Kerogen: woody/coaly (va); amorphous (r), S/P (f); biodegraded terrestrial (f);  
 indeterm fines (r); dinoflagellates/acritarchs (r-f); pyrite (a)  
 Acritarch spp. (Micyhystridium) (vr)  
 Dinoflagellate cysts (c-a)

Dinoflagellate indeterminate (r)  
 Spiniferites spp. (vr)  
 Glaphyrocysta spp. (r)  
 Deflandrea-type spp. (vr)  
 Systematophora/Areoligera spp. (f) s+  
 Cordosphaeridium spp. (vr)  
 Nothofagidites spp. (r)  
 Tricolpites spp. (r)  
 Tricolpites confessus (r) –  
 Tricolpites cf. longus (vr, broken)  
 Triporopollenites sectillis (vr) –s95.5/14.2  
 Proteacidites spp. (c)  
 Proteacidites angulatus (r-f)  
 Gambierina rudata (r)  
 Australopollis obscurus (f)  
 Stereisorites antiquasporites (r)  
 Stereisorites (Tripunctisporis) sp. (r)  
 Phyllocladidites mawsonii (r)  
 Phyllocladidites microsaccatus (r)  
 Bisaccates (f)  
 Fern spores (c)  
 Gleicheniidites spp. (f)

**Indeterminate**  
(2790-95m)

2790-95      Paleoenvironment: Marginal marine; Palynozone Indeterminate  
 Kerogen: woody/coaly (va); amorphous (r-f), S/P (r); biodegraded terrestrial (f);  
                   indeterm fines (f); dinoflagellates/acritarchs (vr); pyrite (a)  
 Dinoflagellate cysts (f)  
 Dinoflagellate indeterminate (vr)  
 Systematophora/Areoligera spp. (r) s+  
 Nothofagidites spp. (vr)  
 Proteacidites spp. (f)  
 Proteacidites angulatus (vr)  
 Gambierina rudata (vr-r)  
 Australopollis obscurus (r)  
 Stereisorites antiquasporites (r)  
 Phyllocladidites mawsonii (r)  
 Phyllocladidites microsaccatus (r)  
 Bisaccates (f)  
 Fern spores (f)  
 Laevigatosporites spp. (r)

**Probably Palynozone Ma**  
(2795-2810m)

2795-2810      Paleoenvironment: Marginal-non marine; Palynozone prob. Ma  
 Kerogen: woody/coaly (va); amorphous (f), S/P (r); biodegraded terrestrial (f);  
 indeterm fines (f); dinoflagellates/acritarchs (er); pyrite (a)  
 Dinoflagellate cysts (r)  
 Dinoflagellate indeterminate (r)  
 Systematophora/Areoligera spp. (vr-r) s+  
 Nothofagidites spp. (vr)

Nothofagidites senectus (vr)  
cf. Tetracolporites verrucosus (vr)  
Tricolpites spp. (r)  
Tricolpites gillii (vr)  
Tricolpites confessus (vr) –  
Proteacidites spp. (r)  
Proteacidites angulatus (vr)  
Proteacidites amolosexinus (vr)  
Gambierina rudata (r)  
Gambierina edwardsii (vr)  
Australopollis obscurus (r-vr)  
Stereisporites antiquasporites (r)  
Lygistipollenites balmei (vr)  
Phyllocladidites mawsonii (r)  
Bisaccates (r)  
Fern spores (f)  
Laevigatosporites spp. (r)  
Perotriletes cf. majus (vr) 91/17

907511



084


907511 ~~085~~  
085

907511 ~~XXXX~~  
086

**APPENDIX 4**

**TURRUM 7**

**Geochemistry**

907511   
087

ExxonMobil Upstream Research Company

# Identification of Fluid Types in the Turrum-7 Well, Australia, using Geochemistry and Fluid Inclusions

R. J. Pottorf  
C. Gong  
M. Richardson  
M. O. Vityk

This study of fluid inclusions and reservoir geochemistry falls under the OIMS category, Secondary Migration for Hydrocarbon Flow and Trap Charge, of the URC Geoscience Excluded List. This technical product is not intended for use in drilling operations.

## FOR COMPANY USE ONLY

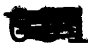
*This report was prepared on a research application basis for Esso Australia Ltd (EAL) and their partners. The information herein is confidential, and is not to be disclosed to or used by others without authorization by EAL and ExxonMobil Upstream Research Company. Copyright © 2000 by ExxonMobil Upstream Research Company. All rights are reserved under the copyright laws.*

Hydrocarbon Systems Analysis Division  
URC.2000ES.025  
March, 2000



# Geoscience Research Application Report

**ExxonMobil**  
**Upstream Research Company**  
P.O. Box 2189  
Houston, TX 77252-2189

907511   
088

**ExxonMobil**  
*Upstream Research*

Mr. Glen Nash  
Gippsland Group Manager  
Production Department  
ESSO Australia Ltd.  
Rm. 5.53, 12 Riverside Quay,  
SOUTHBANK, Victoria, 3006  
Australia

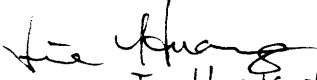
March 21, 2000

Dear Glen,

The attached report, URC.2000ES.025, is entitled "Identification of Fluid Types in the Turrum-7 Well, Australia, using Geochemistry and Fluid Inclusions" by R. J. Pottorf, C. Gong, M. Richardson, and M. O. Vityk. This work documents the use of geochemistry and fluid inclusion technologies to establish fluid types within the recently drilled Turrum-7 well. This work has been charged to URC research applications project #58816.

The Turrum-7 well is interpreted to have penetrated a "live" or movable oil leg in the L360 reservoir unit down to 2588.52m TVDSS with wet sandstones below from 2596.3-2607.3 TVDSS. There is no evidence to suggest that hydrocarbons ever migrated through the lower, wet zone, but the rocks have exceptionally low permeabilities. These rocks may be too impermeable to allow hydrocarbons to enter or may represent an uncharged, stratigraphically isolated unit from the L360 above. Because of these uncertainties, the presence of an OWC within the sampled interval cannot be confirmed or denied. Thus a significant oil column on the east flank of the field within the L360 reservoir cannot be ruled out.

We welcome your comments and suggestions on this work, and we would be happy to discuss any of these results or follow-up items in more detail at your convenience.

  
JIE HUANG for Bill Clendenen  
Bill Clendenen  
TCR Section Supervisor



**ExxonMobil Upstream Research Company**

**Identification of Fluid Types in the Turrum-7  
Well, Australia, using Geochemistry and Fluid  
Inclusions**

R. J. Pottorf, C. Gong, M. Richardson, and M. O. Vityk  
*ExxonMobil Upstream Research Company*

This study of fluid inclusions and reservoir geochemistry falls under the OIMS category, Secondary Migration for Hydrocarbon Flow and Trap Charge, of the URC Geoscience Excluded List. This technical product is not intended for use in drilling operations.

**Hydrocarbon Systems Analysis  
Division  
URC.2000ES.025  
April 2000**

**FOR COMPANY USE ONLY**

This report was prepared on a research-application basis for Esso Australia Ltd. (EAL) and their partners. The information herein is confidential and is not to be disclosed to or discussed by others without authorization by EAL and ExxonMobil Upstream Research Company. All rights are reserved under the copyright laws.

# Identification of Fluid Types in the Turrum-7 Well, Australia, using Geochemistry and Fluid Inclusions

## Summary

---

### Study Objectives

The main objectives of this work are to use geochemical and fluid inclusion analysis to establish the following for the L360 reservoir in the Turrum-7 well:

- fluid type (gas, oil, water)
  - possible fluid contacts
  - whether the hydrocarbons encountered are "live" or residual
  - likelihood of communication between the oils within the L360 reservoir at Turrum-5 with the L355 gas reservoir at Turrum-6ST1
- 

### Conclusions

Results of geochemical and fluid inclusion analysis suggest the following conclusions:

- The Turrum-7 well penetrated a "live" or movable oil leg in the L360 reservoir unit down to 2610.62m MD (2588.52 TVDSS) with wet sandstones below from 2618.4-2629.4m MD (2596.3-2607.3 TVDSS).
  - There is no evidence that hydrocarbons ever migrated through the lower, wet zone at 2618.4-2629.4m MD, but the rocks have exceptionally low permeabilities, generally measured in hundredths of millidarcies. These rocks may be too impermeable to allow hydrocarbons to enter or may represent an uncharged, stratigraphically isolated unit from the L360 above.
  - Because of these uncertainties, the presence of an OWC (oil-water contact) within the sampled interval cannot be confirmed or denied. Thus a significant oil column on the east flank of the field within the L360 reservoir cannot be ruled out.
  - We cannot determine from these data whether the L355 gas reservoir at Turrum-6ST1 is in communication with the L360 oil leg at Turrum-5.
-

**Contacts**      Contact information for authors involved in this project

<b>Name</b>	<b>Affiliate</b>	<b>Phone</b>	<b>email</b>
Bob Pottorf	URC	(713) 431-7390	americas(rjpotto)
Changrui Gong	URC	(713) 431-4590	americas(c9gong1)
Mark Richardson	URC	(713) 431-4630	americas(m9richa)
Max Vityk	URC	(713) 431-6468	americas(movityk)

**Table of Contents**

<b>Topic</b>	<b>Page</b>
Summary	1
Introduction	3
Samples	3
Analytical Procedures	6
Results and Interpretations	8
Conclusions	14
References	15
Appendix I: Gas Chromatograms	16
Appendix II: Turrum-7 Core Properties	17

## Introduction

---

**Background** The Turrum-7 well was drilled on the east flank of the Turrum Field in a location thought to maximize the potential for intersecting an oil column in the L360 reservoir. Unfortunately, the reservoir permeability of the L360 was sufficiently low that no reliable pressure data could be obtained to assess the fluid type and column height. It was suggested that a combination of geochemical and fluid inclusion analyses conducted on conventional core samples from the Turrum-7 well might help to identify whether the L360 reservoir contains oil, gas, or water at this location. The identification of fluid types has an impact on reserve volumes and further appraisal.

---

## Geochemistry and Fluid Inclusion Samples

---

**Samples collected and analyzed** In order to evaluate the unknown fluid encountered in the Turrum-7 well, samples of conventional core from other Turrum wells that cut gas, oil, and water legs in the L360 reservoir were sought for calibration purposes. Representative samples of conventional cores from gas legs were obtained from Turrum-3 (two samples, L500U zone), Turrum-5 (10 samples, L360 zone), and Turrum-6ST1 (two samples, L355 zone). Cores from oil legs were sampled in the Turrum-5 well (seven samples, L360L zone). Since only one sample of core intersecting a water leg was available from the Turrum-3 L500L zone, cuttings from the Turrum-4 L360 zone were used to calibrate water leg characteristics. Geochemical and fluid inclusion results for the unknown fluid type within cores of the Turrum-7 L360 zone were compared to the calibration data set. Subsets of the cores and cuttings were selected for fluid inclusion optical examination, Iatroscan, and extraction and gas chromatography (GC) analysis. In addition, thermal extract/GC analysis was performed on two core samples (Turrum-5, 2546.92m MD; Turrum-7, 2610.62m MD). For a complete list of analyzed samples, see Table 1.

---

**Table 1. Fluid inclusion and geochemical analyses performed on Turrum Field samples**

Well	core depth m, samples	log depth m, samples	log dep. m, fluid contacts	TVDSS	reser- voir	fluid type	elev- ation	FIV	optical FI	Iatro- scan	ext GC	EPR#
Turrum 3	2598.4	2598.8		2577.8	L500U	Gas	21 m	X	X	X	X	208101B
Turrum 3	2599.83	2600.23		2579.23	L500U	Gas	21 m	X	X	X		208101C
Turrum 3			2601.3	2580.3	L500U	IGOC	21 m					
Turrum 3			2612.3	2591.3	L500U	IOWC	21 m					
Turrum 3	2621.38	2622.38		2601.38	L500L	Water	21 m	X	X	X	X	208101D
Turrum 4	2670-2675			2647	L360U	Water	23m	X	X	X		208108A
Turrum 4	2675-2680			2652	L360U	Water	23m	X				208108B
Turrum 4	2680-2685			2657	L360L	Water	23m	X	X	X		208108C
Turrum 4	2685-2690			2662	L360L	Water	23m	X				208108D
Turrum 4	2690-2695			2667	L360L	Water	23m	X	X	X		208108E
Turrum 4	2695-2700			2672	L360L	Water	23m	X				208108F
Turrum 4	2675-2690#				L360	Water	23m	X	X		X	208108G
Turrum 5	2525	2528.4		2503.4	L360U	Gas	25 m	X	X			208102A
Turrum 5	2527.2	2530.6		2505.6	L360U	Gas	25 m	X		X		208102B
Turrum 5	2529.93	2533.33		2508.33	L360U	Gas	25 m	X	X			208102C
Turrum 5	2531.3	2534.7		2509.7	L360L	Gas	25 m	X		X		208102D
Turrum 5	2533	2536.4		2511.4	L360L	Gas	25 m	X	X			208102E
Turrum 5	2534.94	2538.34		2513.34	L360L	Gas	25 m	X		X		208102F
Turrum 5	2535.97	2539.37		2514.37	L360L	Gas	25 m	X				208102G
Turrum 5	2536.98	2540.38		2515.38	L360L	Gas	25 m	X	X	X	X	208102H
Turrum 5	2537.97	2541.37		2516.37	L360L	Gas	25 m	X		X		208102I
Turrum 5	2538.97	2542.37		2517.37	L360L	Gas	25 m	X				208102J
Turrum 5			2543	2518	L360L	GOC	25 m					
Turrum 5	2539.97	2543.37		2518.37	L360L	Oil	25 m	X	X	X	X	208102K
Turrum 5	2540.98	2544.38		2519.38	L360L	Oil	25 m	X				208102L
Turrum 5	2541.96	2545.36		2520.36	L360L	Oil	25 m	X	X	X		208102M
Turrum 5	2543.48	2546.88		2521.88	L360L	Oil	25 m	X	X	X	X	208102N
Turrum 5	2544.85	2547.05		2522.05	L360L	Oil	25 m	X		X		208102O
Turrum 5	2545.91	2548.11		2523.11	L360L	Oil	25 m	X	X			208102P
Turrum 5	2546.92	2549.12		2524.12	L360L	Oil	25 m	X	X	X	X*	208102Q
			2549	2524	L360L	LKO	25 m					
Turrum 6ST1	2611.85	2614.65		2589.65	L355	Gas	25 m	X	X			
Turrum 6ST1	2619.85	2622.65		2597.65	L355	Gas	25 m	X	X			
Turrum 6ST1			2624	2599	L355	LKG	25 m					
Turrum 6ST1			2625	2600	L355	IGWC	25 m					
Turrum 7	2610.2	2614.1		2588.1	L360	Oil	26 m	X	X	X	X	208096A

Turrum 7	2610.4	2614.3		2588.3	L360	Oil	26 m	X	X	X		208096B
Turrum 7	2610.62	2614.52		2588.52	L360	Oil	26 m	X	X	X	*	208096C
Turrum 7	2618.4	2622.3		2596.3	L360	Water	26 m	X	X	X		208096D
Turrum 7	2620.39	2624.29		2598.29	L360	Water	26 m	X	X	X	X	208096E
Turrum 7	2622.53	2626.43		2600.43	L360	Water	26 m	X	X	X		208096F
Turrum 7	2625.54	2629.44		2603.44	L360	Water	26 m	X	X	X		208096G
Turrum 7	2626.18	2630.08		2604.08	L360	Water	26 m	X	X	X		208096H
Turrum 7	2627.79	2631.69		2605.69	L360	Water	26 m	X	X	X		208096I
Turrum 7	2629.4	2633.3		2607.3	L360	Water	26 m	X	X	X	X	208096J

FIV = fluid inclusion volatiles; FI = fluid inclusions; ext. GC = extraction of hydrocarbons followed by gas chromatography; IGOC = interpreted gas/oil contact; IOWC = interpreted oil/water contact; LKO = lowest known oil; \* = thermal extract/gas chromatography performed on these samples; all samples are from conventional cores with the exception of Turrum-4, which are cuttings samples; # = composite sample from three 5m cuttings intervals. The following depth shifts were used to convert core depths to log depths:

- Turrum-3 - Core #2 (2597.30-2598.46 m MD) - log depth (measured) = driller's depth (measured) + 0.4m
- Turrum-3 - Core #3 (2599.30-2601.00 m MD) - log depth = driller's depth + 0.4m
- Turrum-3 - Core #4 (2618.00-2623.00 m MD) - log depth = driller's depth + 1.0m
- Turrum-5 - Core #4 (2526.8-2543.5 m MD) - log depth = driller's depth + 3.4m
- Turrum-5 - Core #5 (2544.8-2549.8 m MD) - log depth = driller's depth + 2.2m
- Turrum-6 - Core #1 - log depth = driller's depth + 2.8m
- Turrum-7 - Core #1 - log depth = driller's depth + 3.9m

## Analytical Procedures

---

### **FIV analysis**

Reservoired hydrocarbons are commonly trapped in pore spaces and as inclusions in mineral cements and fractures, and those hydrocarbons can be extracted and analyzed via mass spectrometry (Hall et al., 1997; Smith, 1991a; Smith, 1991b). This technique is collectively called fluid inclusion volatiles (FIV) analysis. Samples of core or cuttings are placed in a chamber and subjected to a high vacuum. After evacuation, the samples are crushed to release volatile components that are measured by mass spectrometry.

As many as 120 different masses are analyzed by the mass spectrometer. At the present time, only 13 of these masses, representing a variety of organic and inorganic compounds, are being used in geologic interpretation. The compounds represented by these masses are interpreted to include methane, ethane, C3+ hydrocarbons, paraffins, naphthenes, benzene, toluene, acetic acid, carbon dioxide, hydrogen sulfide, helium, and nitrogen. The mass spectrometer analyses are displayed versus depth, usually adjacent to a well log.

Fluid type and fluid contacts are usually distinguished best by methane (gas legs), C3+ (oil legs), and the paraffin/naphthene ratio (gas, wet gas, oil). A sharp drop in C3+ response relative to values above is consistent with an OWC. The general absence of hydrocarbons and erratic paraffin/naphthene ratio is also consistent with water legs. Fluid inclusion volatiles (FIV) analyses were performed on all samples by contractor Advanced Hydrocarbon Stratigraphy (AHS) of Tulsa.

---

### **Optical Fluid Inclusion Analysis**

Standard fluid inclusion optical techniques were undertaken to help define fluid type, migration timing, and possible communication of gas in the Turrum-6ST1 to an oil leg in the Turrum-5. Doubly polished thin sections roughly 50µm thick were prepared from core and cuttings for optical analysis. These sections were examined for optical discrimination of associated water-rich and hydrocarbon fluid inclusions, or fluid inclusion assemblages (FIA's). After petrographic investigation, selected fluid inclusions are generally heated and frozen (microthermometry) to determine the inclusion composition, and the temperature and pressure of entrapment (Goldstein and Reynolds, 1994). Optical analysis was conducted by Jim Reynolds of Fluid Inc. (Denver, CO).

---

**Iatroscan  
analysis**

Iatroscan is a Thin Layer Chromatography (TLC) technique that can measure quantities of bulk fractions (saturates, aromatics, NSOs and asphaltenes) in extracts. Briefly, about 1 gram of core sample is crushed and mixed with 1-3 ml solvent. One microliter of this extract solution is spotted on a silica gel-coated rod and the rod is developed in a series of solvents for different fractions. After the development, the rod is passed through a hydrogen flame and a signal is recorded by the Flame Ionization Detector. The recorded signal can be converted to percentages or concentrations of the fractions if the instrument is properly calibrated.

Total Iatroscan signal strength is generally interpreted to indicate the intensity of oil staining in rock samples. Live or residual oil legs in core samples are commonly associated with higher Iatroscan signals than gas or water legs. Due to preferential dissolution of compound types, there are generally higher saturate/aromatic ratios in the gas caps and lower saturate/aromatic ratios in water legs when compared to associated oil leg core samples. Sharp increases in the asphaltene fraction of rock extracts are sometimes correlated with the current or paleo oil/water contact.

---

**Whole  
extract/GC  
analysis**

Whole extract/GC analysis was performed to determine the amount of extractable hydrocarbons and the molecular compositions of GC-amenable compounds ( $C_{15+}$ ) in rock extracts. A crushed rock sample was extracted with methylene chloride:methanol (9:1) solution in a Decator Soxhlet extraction system. After the solvent was evaporated and a constant weight was obtained for the extract, the weight of the extract was recorded and converted to mg/g (ppm) of rock extracted. The extract is redissolved in  $CS_2$  and analyzed in an HP 6890A Gas Chromatograph to determine its molecular composition. The amount of extract can be related to the intensity of oil staining. Molecular compositions can be used for fluid type comparisons and reservoir compartmentalization studies.

---

**Thermal  
extract/GC  
analysis**

Because low molecular weight hydrocarbons are lost during the Soxhlet extraction process, thermal extract/GC was performed on two core samples (Turrum-5, 2546.92m MD; Turrum-7, 2610.62m MD) to determine any  $C_{15}$ -compositional differences between these two samples. Crushed core samples were loaded directly in a thermal extraction/pyrolysis injector. Hydrocarbons released at an injector temperature of  $320^{\circ}C$  were cryogenically trapped for two minutes at  $-10^{\circ}C$  before they were injected into a Varian Gas Chromatograph. Thermal extraction GC was conducted by Humble Geochemical Services (contact Paul R. Walker at 281-540-6050).

---



## Results and Interpretation

---

### Results Summary

Table 2 summarizes the general characteristics of gas, oil, and water legs from the calibration data set at Turrum as well as interpreted results from Turrum-7. FIV parameters are not included in Table 2 because this technology was not effective in discriminating fluid types for the low permeability rocks encountered (generally <10md). Summaries of FIV data are included with optical fluid inclusion and Iatroskan results for the main calibration well, Turrum-5 (Fig.1), and for the unknown fluid types in Turrum-7 (Fig. 2).

---

### Interpretation Summary

Our most likely interpretation is that "live" or movable oil was encountered down to 2610.62m MD (oil down to or ODT 2588.52m TVDSS) in the L360 reservoir unit of Turrum-7. This conclusion is based primarily on the presence of oil "inclusions" observed optically, the total Iatroskan response, and the similarity of the GC trace of the extracted HC's in Turrum-7 to the extracted oil leg samples and crude oil from the Turrum-5 calibration well.

Only water-bearing samples were observed below the ODT depth. From 2618.4 - 2629.4m MD (2596.3 - 2607.3m TVDSS) there is no geochemical or fluid inclusion evidence that either oil or gas ever entered these rocks. With these technologies we cannot distinguish whether this lower stratigraphic interval is an isolated body from the L360 that was never charged, or whether the permeabilities of these rocks, generally measured in hundredths of millidarcies, are simply too low to allow HC entry (Appendix II).

An alternative, but unlikely, hypothesis from our favored interpretation is that gas or water with residual oil was encountered. This alternative cannot be completely ruled out because we did not have rock samples containing residual oil in a gas or water leg with which to compare geochemical and fluid inclusion characteristics. However, the extracted HC's from the L360 at Turrum-7 do not as closely match the calibration geochemical data for a gas/condensate. Also the fluid inclusions and total Iatroskan signal look very similar to the rocks with movable oil in Turrum-5.

---

**Table 2.** Analytical results of the calibration wells are summarized and compared with Turrum-7 results. Turrum-7 is interpreted to have intersected oil and water zones.

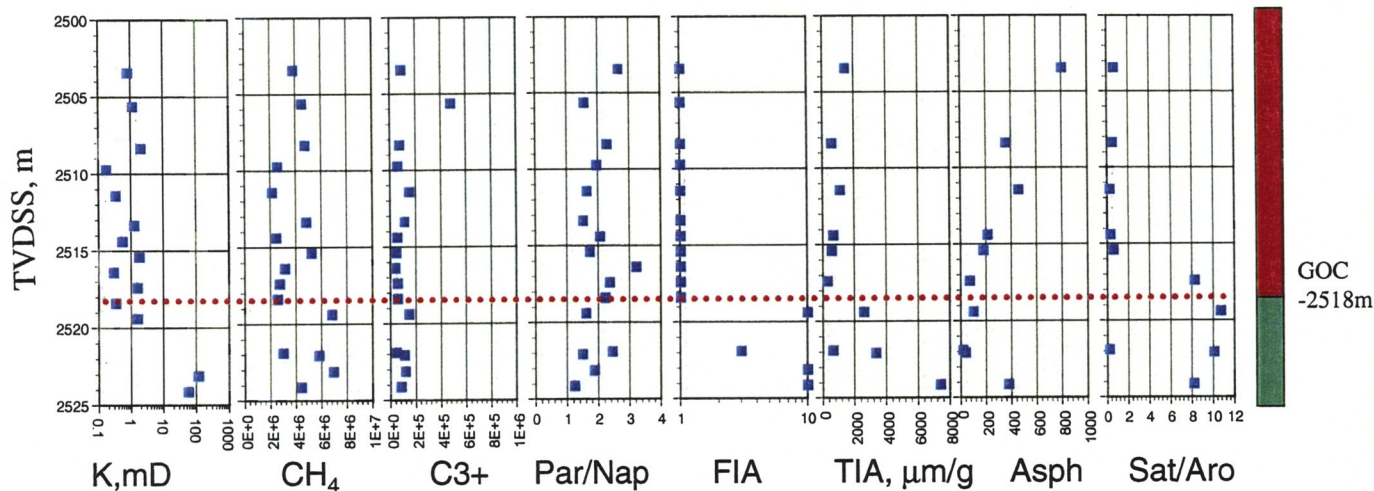
	<b>Fluid type</b>	<b>FIA</b>	<b>TIA</b>	<b>Asph</b>	<b>Sat/Aro</b>
Calibration	Gas	None	Low	Moderate	Low
Calibration	Oil	Mod-High	Mod-High	None-Low	Mod-High
Calibration	Water	None	Low		
Turrum-7 interp.	<b>Oil</b>	High	Moderate	None-Low	Moderate
Turrum-7 interp.	<b>Water</b>	None	Low	None-Low	Low

FIA = fluid inclusion abundance determined optically; TIA = total Iatroscan abundance; Asph = asphaltene fraction by Iatroscan; Sat/Aro = saturate to aromatic ratio by Iatroscan.

**Interpretation basis**

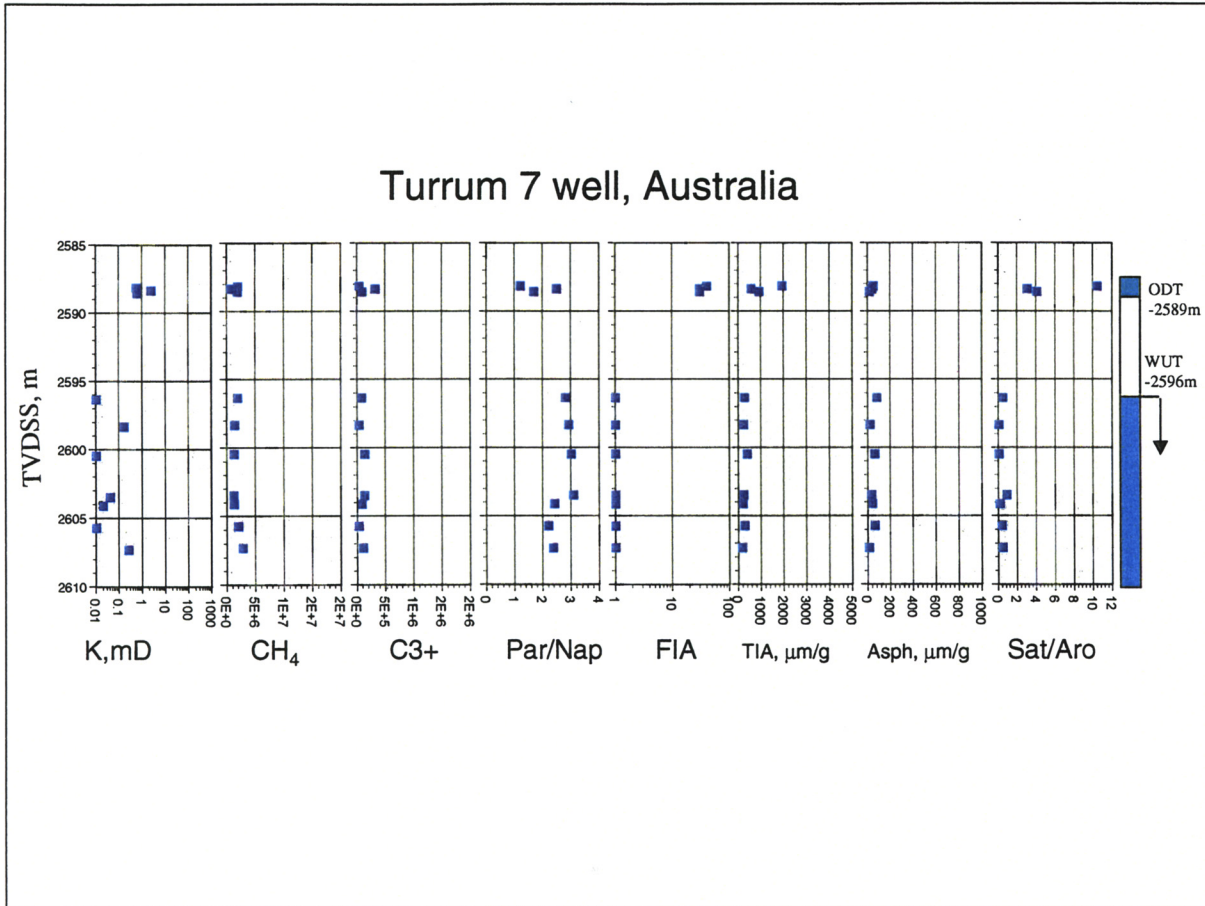
Interpretations are based upon comparisons between core or cuttings samples containing known fluid types (gas, oil, water) to rocks within Turrum-7 with unknown fluid types. The intervals used for comparison include Turrum-5 (oil and gas-bearing core), Turrum-4 (water-bearing cuttings), and Turrum-3 (oil and gas-bearing core). For details, see Table 1. Previous geochemical data from Turrum-5, Marlin A-6 and Marlin A-24 oil and condensate samples were also used in the comparison with hydrocarbons extracted from Turrum-7 cores. The results for each of the technologies used to analyze these samples will now be discussed.

### Turrum 5 well, Australia



PE 907511-13

**Figure 1.** Analytical results for FIV (CH<sub>4</sub> = methane, C<sub>3+</sub> = mass 41 propane and higher HC's, P/N = mass 57/mass 55 or "paraffin/naphthene" ratio), optical fluid inclusions (FIA = number of fluid inclusion assemblages noted), and Iatroscan techniques (TIR = total Iatroscan response, Asp = asphaltenes, Sat/Aro = saturate/aromatic ratio) plotted against permeability (K, mD) for the Turrum-5 calibration well. Gas and oil legs appear to be distinguished by optically observed fluid inclusions (FIA) and combined Iatroscan data (TIR, Asp, Sat/Aro). Fluid types could not be discriminated using FIV, perhaps because of the generally low permeabilities (<10 md) of the rocks. Other proprietary ExxonMobil studies have shown that FIV becomes less effective in determining fluid type at permeabilities <10 md.



PE907511-14

**Figure 2.** Results of FIV (CH<sub>4</sub>, C3+, P/N), optical FI (FIA), and Iatroscan (TIR, Asp, Sat/Aro) techniques for core samples in the Turrum-7 well. The results suggest an ODT -2588.52m TVDSS with water below (WUT -2596.3m TVDSS).

**Optical fluid inclusion analysis**

Eighteen optical sections were examined for HC inclusions in the calibration data set (eight gas, five oil, five water). The only samples found to contain oil inclusions were those in the oil leg, where inclusions were relatively common. Inclusions were also present in all three samples at the top of the Turrum-7 core (2610.2 - 2610.62m MD) and were not found below in the remaining seven samples (Table 1, Fig. 1-2).

The term inclusion is used loosely here, because the "inclusions" observed are at incipient stages of formation and are not yet completely sealed within cements. These inclusions do not show consistent liquid to vapor ratios and do not give reliable homogenization temperature results upon heating. However, these "inclusions" are reliable for the purpose of identifying fluid type.

Because of the unreliability of the inclusions for microthermometry, we could not investigate whether there was any evidence for communication between the L360 oil leg at Turrum-5 with the L355 gas reservoir in Turrum-6ST1. Similarly, the timing of oil arrival into the trap could not be determined.

**Iatroscan (bulk composition)**

The interval down to 2610.62m MD (2588.52 TVDSS) in Turrum 7 has very similar hydrocarbon content and bulk geochemical signature to the oil-bearing L360 interval in Turrum 5. These results suggest the interval down to 2610.62m MD in the Turrum 7 is oil-bearing. The Iatroscan data from this L360 interval in Turrum 7 (down to 2610.62m MD) have significant differences from the calibration Iatroscan data for gas/condensates.

Below 2610.62 m MD in Turrum 7, the Iatroscan data indicates the lack of any hydrocarbons within this lower interval.

Normalization of Iatroscan data to reservoir rock properties (permeability and porosity data) does not change this geochemical interpretation.

---

**Whole-extract  
gas chroma-  
tography (GC)**

Gas chromatograms of solvent-extracted hydrocarbons from the 2610.10-2610.62m MD interval in Turrum 7 are very similar to GCs of oil extracted from the L360 in Turrum 5 (Appendix 1). These same extracted hydrocarbons from the L360 Turrum 7 (down to 2610.62 m MD) have differences from the calibration GCs for gas/condensates.

Gas chromatograms from extracted cores below 2610.62 m MD in Turrum 7 do not correlate well with GCs from any of the calibration oil or gas/condensate-bearing intervals we analyzed from the Turrum Field. The GCs from the deeper L360 Turrum 7 cores (below 2610.62m MD) do not show *any* indication of in-migrated oil or gas/ condensate.

---

**Thermal extract  
/ gas chroma-  
tography  
(TE/GC)**

This technique was carried out to compare reservoir rocks from the oil leg in the L360 Turrum 5 with the possible oil zone in the L360 of Turrum 7 (down to 2610.62m MD). The TE/GC data from both the 2610.62m MD interval of the L360 of Turrum 7 and the oil leg sample at 2546.92m MD L360 at Turrum 5 are very similar. This suggests the Turrum 7 core contains oil above 2610.62m MD.

---

**FIV analysis**

FIV analysis was conducted on samples from Turrum-3, 4, 5, 6ST1, and 7 wells. The results did not clearly distinguish gas, oil, and water legs in the calibration data set and was therefore not used to make interpretations for the Turrum-7 well (Figs. 1-2).

---

## Conclusions

---

### Summary

Results of geochemical and fluid inclusion analysis suggest the following conclusions:

- The Turrum-7 well penetrated a "live" or movable oil leg in the L360 reservoir unit down to 2610.62m MD (2588.52 TVDSS) with wet sandstones below from 2618.4-2629.4m MD (2596.3-2607.3 TVDSS).
  - There is no evidence that hydrocarbons ever migrated through the lower, wet zone at 2618.4-2629.4m MD, but the rocks have exceptionally low permeabilities, generally measured in hundredths of millidarcies. These rocks may be too impermeable to allow hydrocarbons to enter or may represent an uncharged, stratigraphically isolated unit from the L360 above.
  - Because of these uncertainties, the presence of an OWC (oil-water contact) within the sampled interval cannot be confirmed or denied. Thus a significant oil column on the east flank of the field within the L360 reservoir cannot be ruled out.
  - We cannot determine from these data whether the L355 gas reservoir at Turrum-6ST1 is in communication with the L360 oil leg at Turrum-5.
-

## References

---

Bhullar, H. G., Karlsen, D. A., Lachapagne, J. C., and Holm, K., 1999, Reservoir Screening using Iatroscan TLC-FID and Identification of Palaeo-Oil Zones, Oil-Water Contacts, Tar-Mats and Residual Oil Saturations in the Froy and Rind Petroleum Accumulations: *Journal of Petroleum Science and Engineering*, v. 23, p.41-63.

Goldstein, R. H., and Reynolds, T. J., 1994, Systematics of Fluid Inclusions in Diagenetic Minerals, SEPM Short Course 31, 199 p.

Hall, D., Wells, S., Sterner, M., and Wagner, P., 1997, Using fluid inclusions to explore for oil and gas: *Hart's Petroleum Engineer International*, Nov., p. 29-34.

Smith, M. P., 1991a, Method for Exploring the Earth's Subsurface: Patent number EP 415672.

Smith, M. P., 1991b, Apparatus and Method for use in the Analysis of Fluid Inclusions: Patent number EP 414564.

---

## Acknowledgments

The authors wish to thank Peter Glenton for his helpful discussions on the Turrum Field stratigraphy, structure, and fluid distribution. Peter Vrolijk also contributed his thoughts on fluid dynamics at Turrum. Special thanks are due to Michael Gilbert of Esso Australia Ltd, for his exchange of data, questions, and ideas on the Turrum Field. Michael also provided editorial assistance with the manuscript.

---

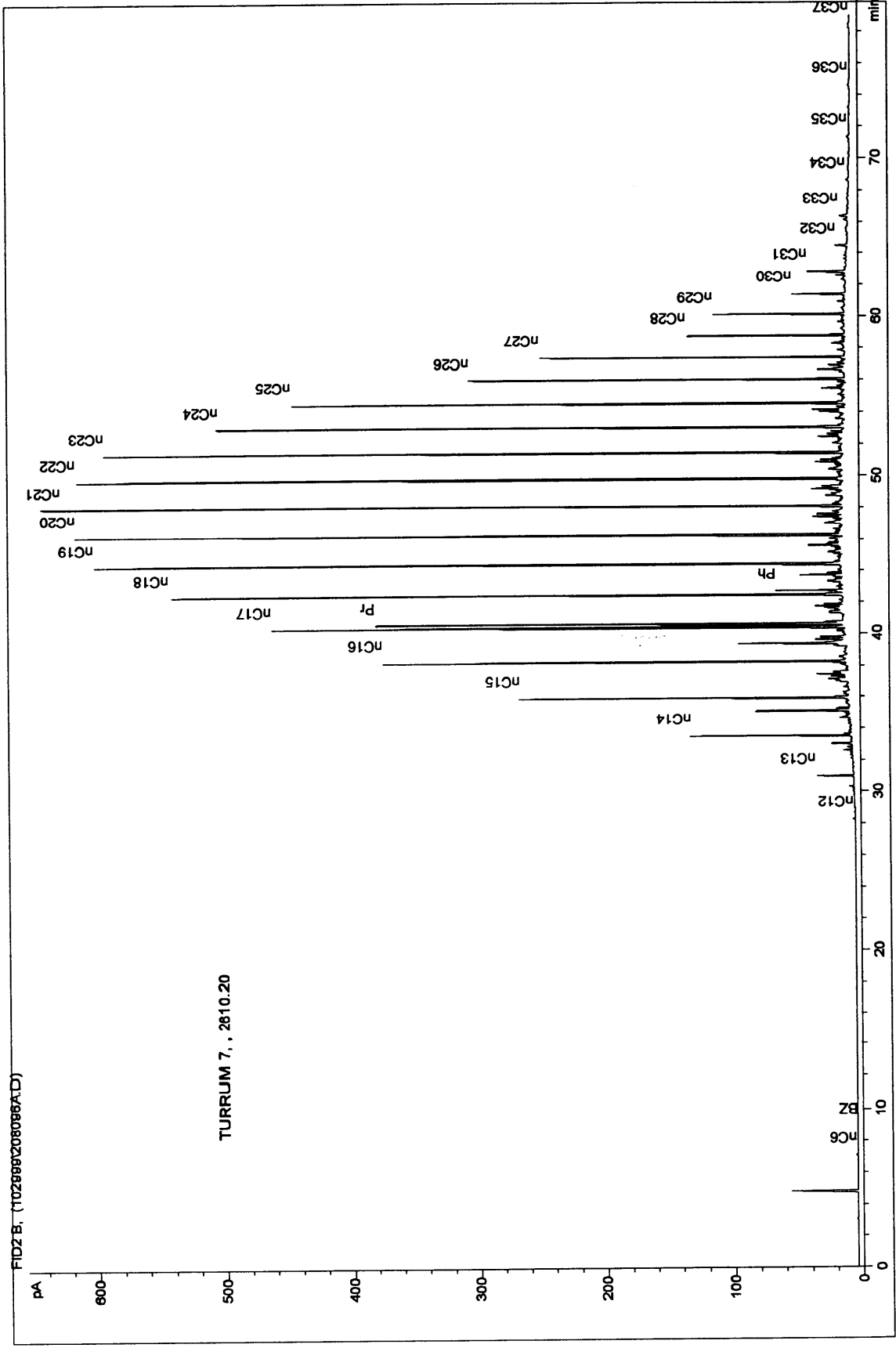


## Appendices

---

Appendix I contains gas chromatograms of samples from the Turrum-3, 4, 5, and 7 wells. Appendix II tabulates rock properties of the Turrum-7 core.

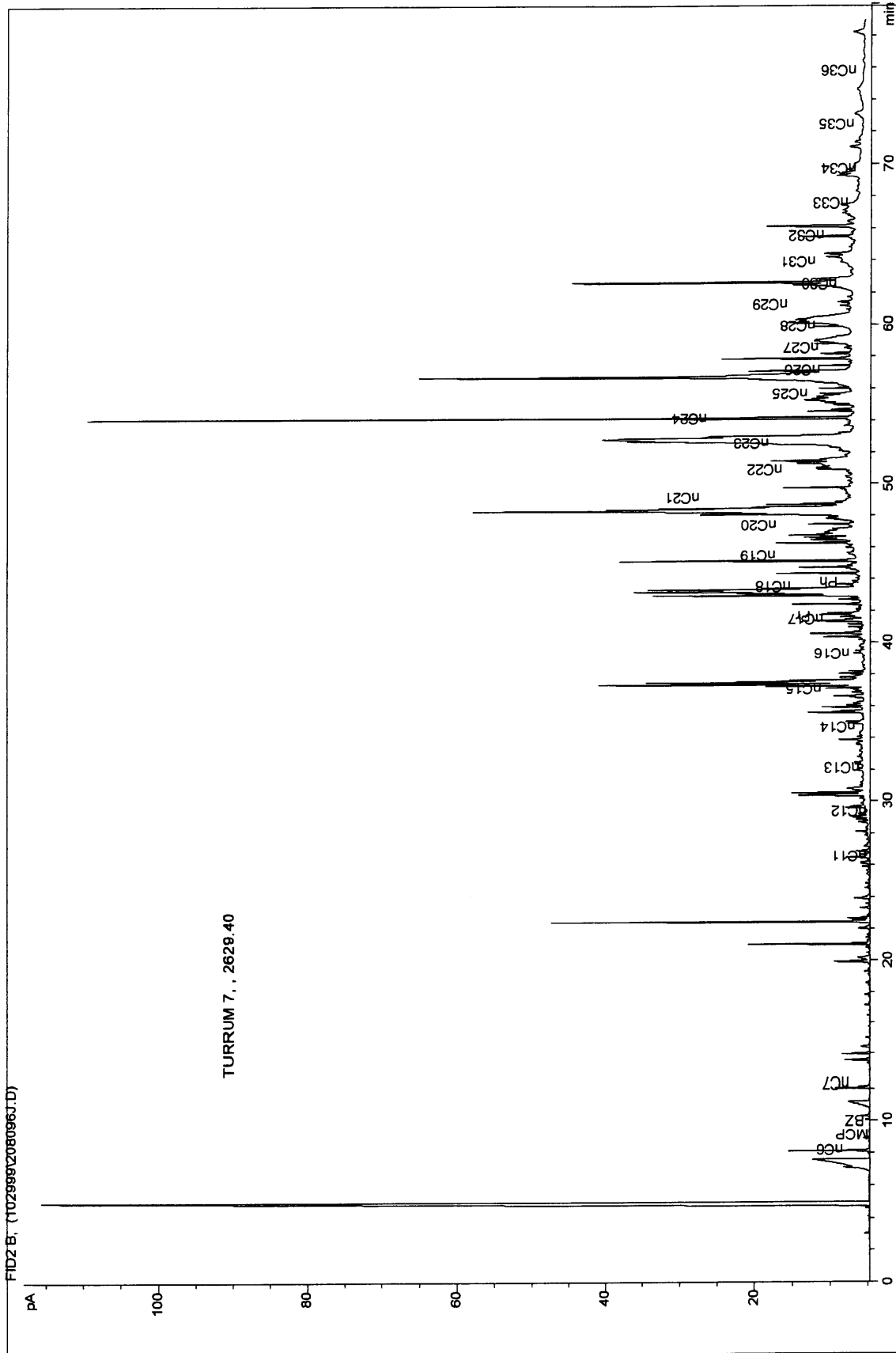
---



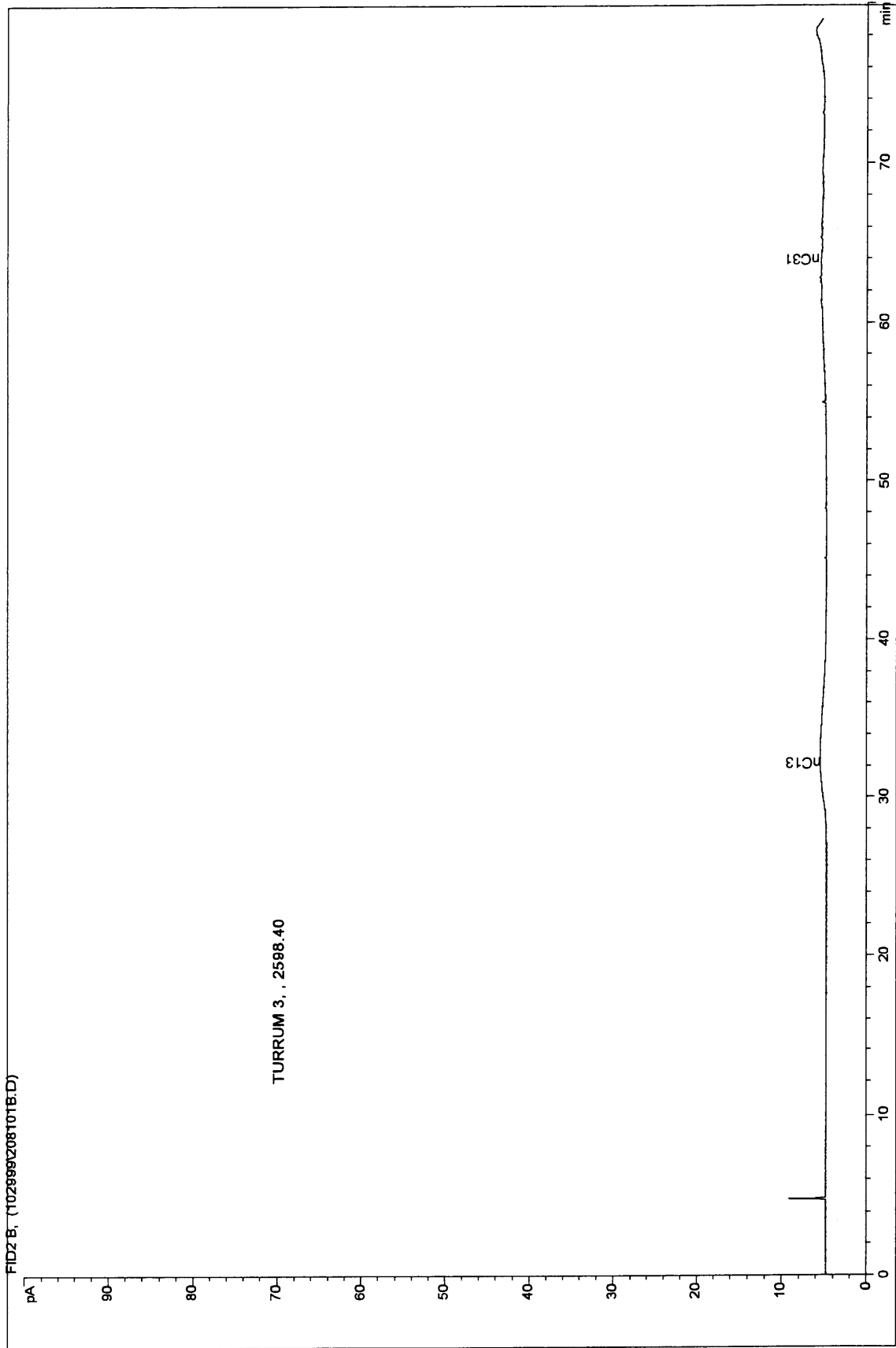
Whole-oil Gas Chromatogram of extract from Turrum 7, 2610.20 m

FID2 B, (1028991208066A.D)

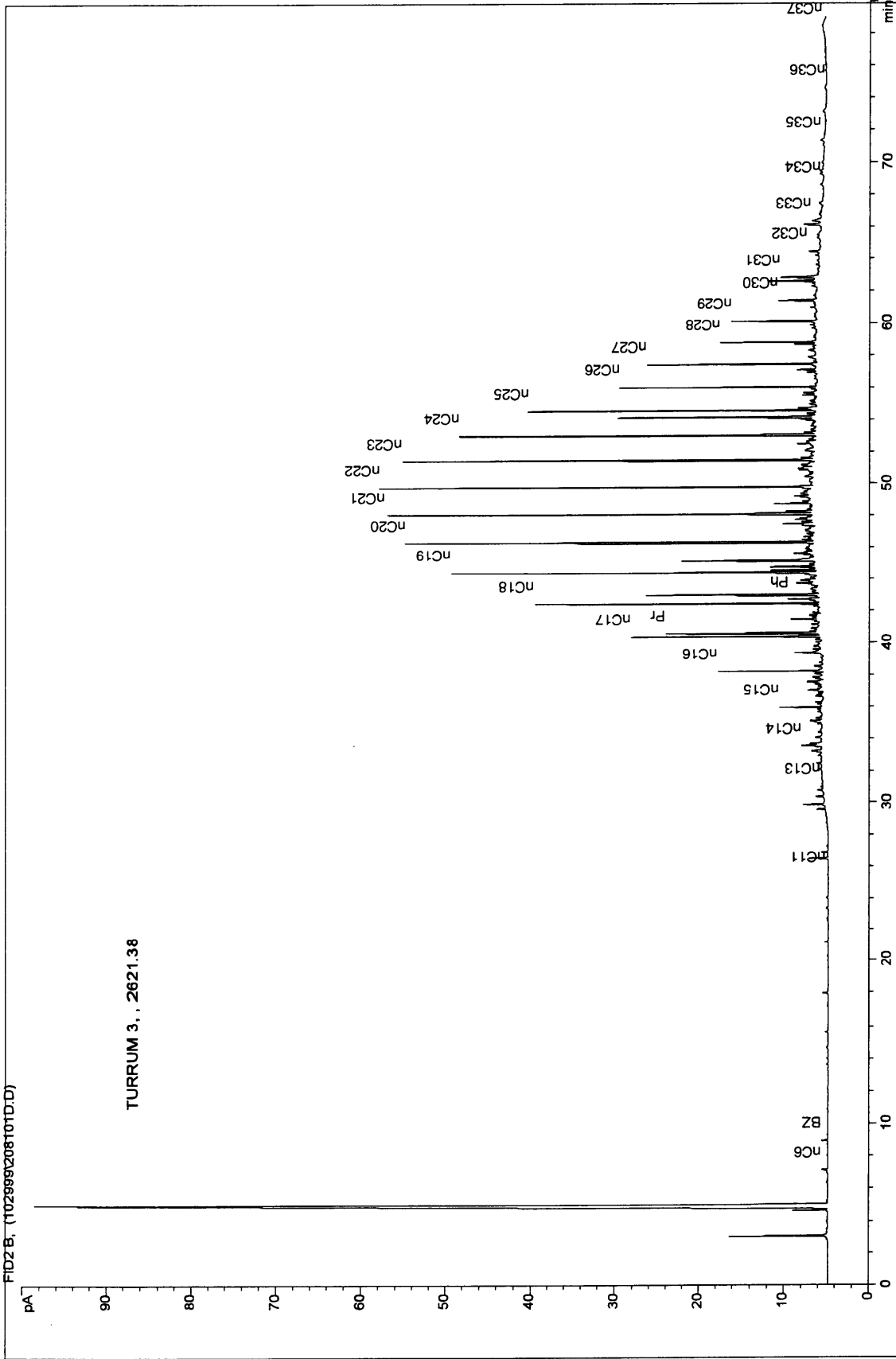
TURRUM 7, , 2810.20



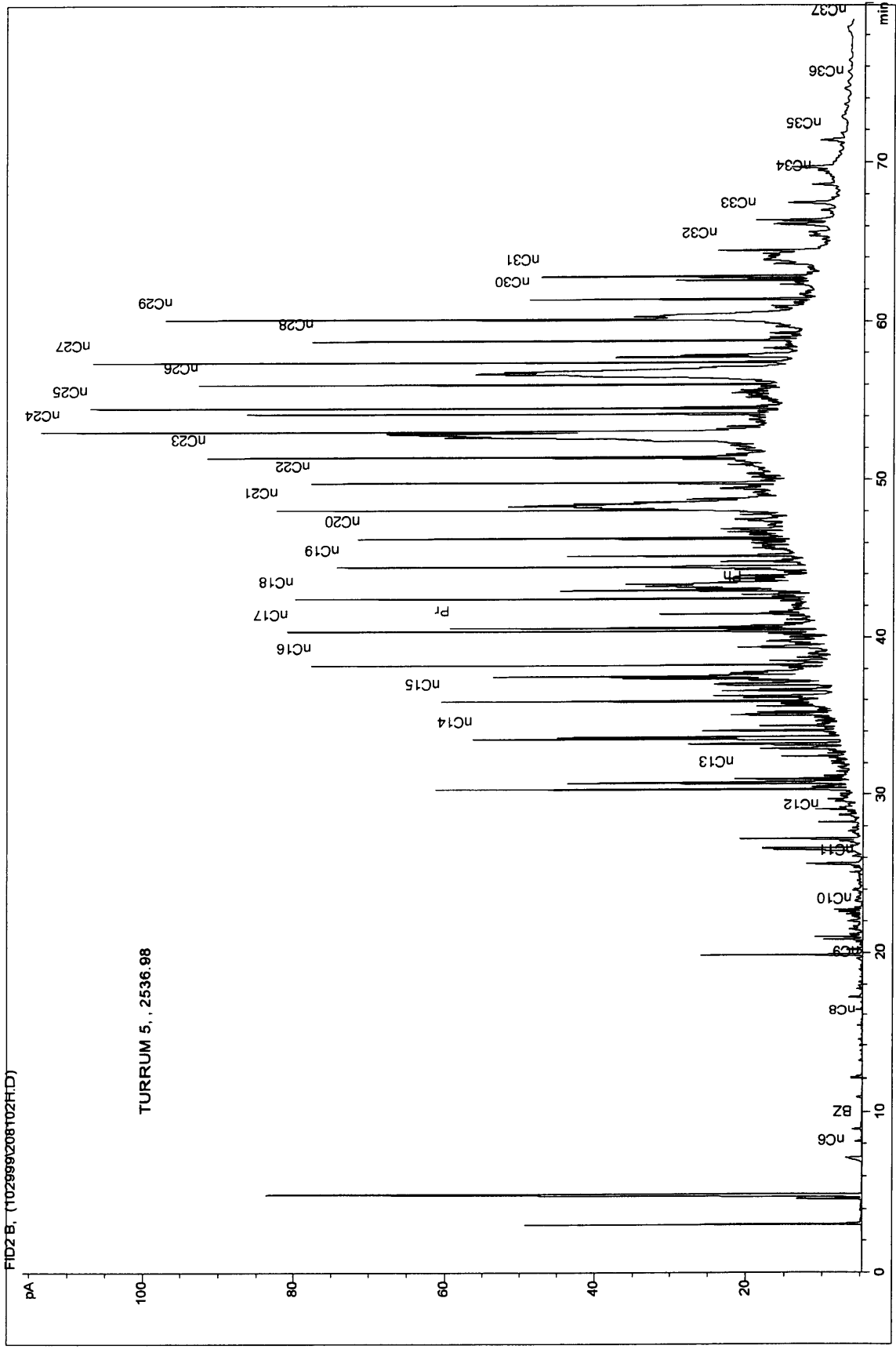
Whole-oil Gas Chromatogram of extract from Turrum 7, 2629.40 m



Whole-oil Gas Chromatogram of extract from Turrum 3, 2598.40 m



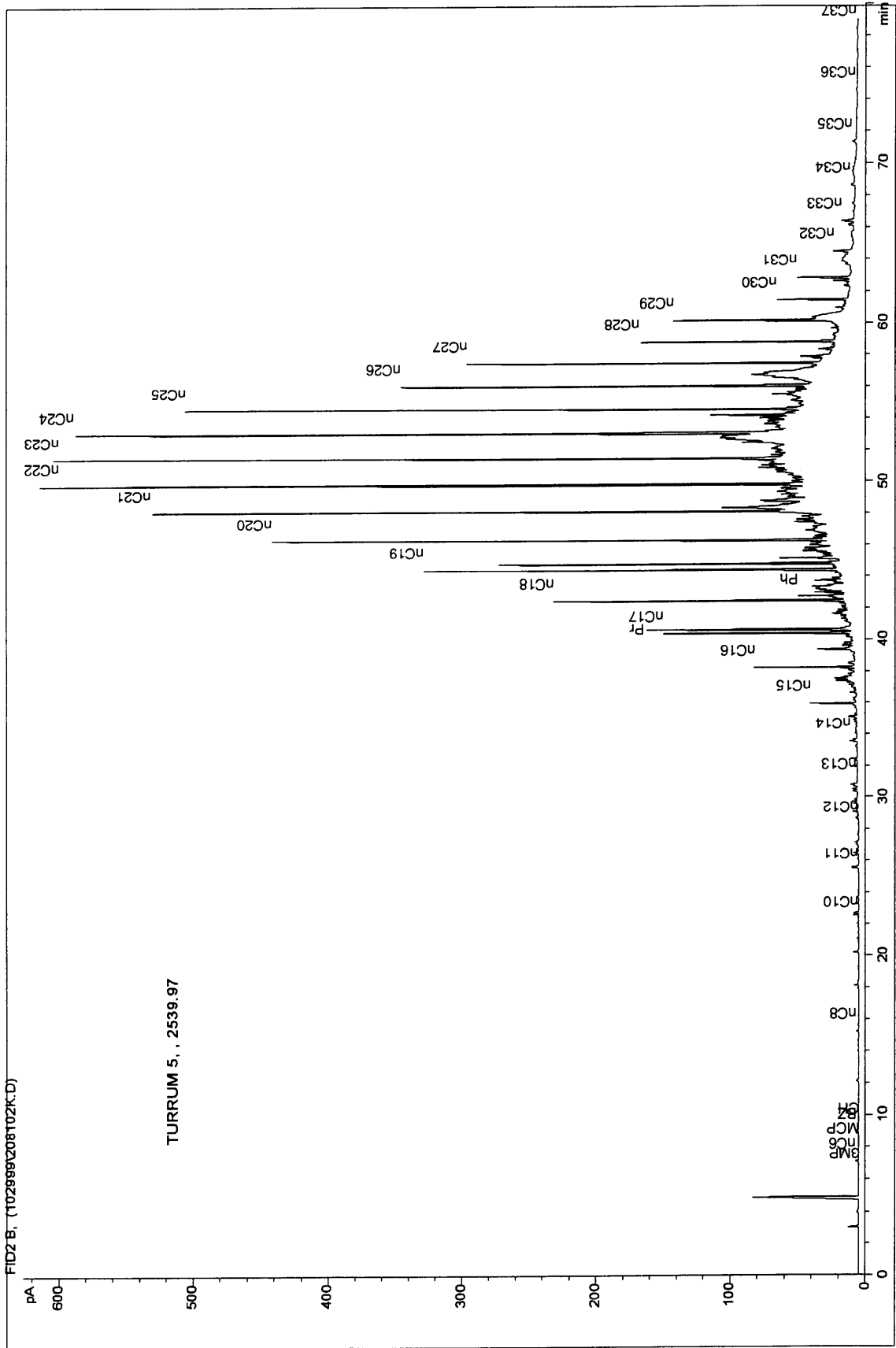
Whole-oil Gas Chromatogram of extract from Turrum 3, 2621.38 m



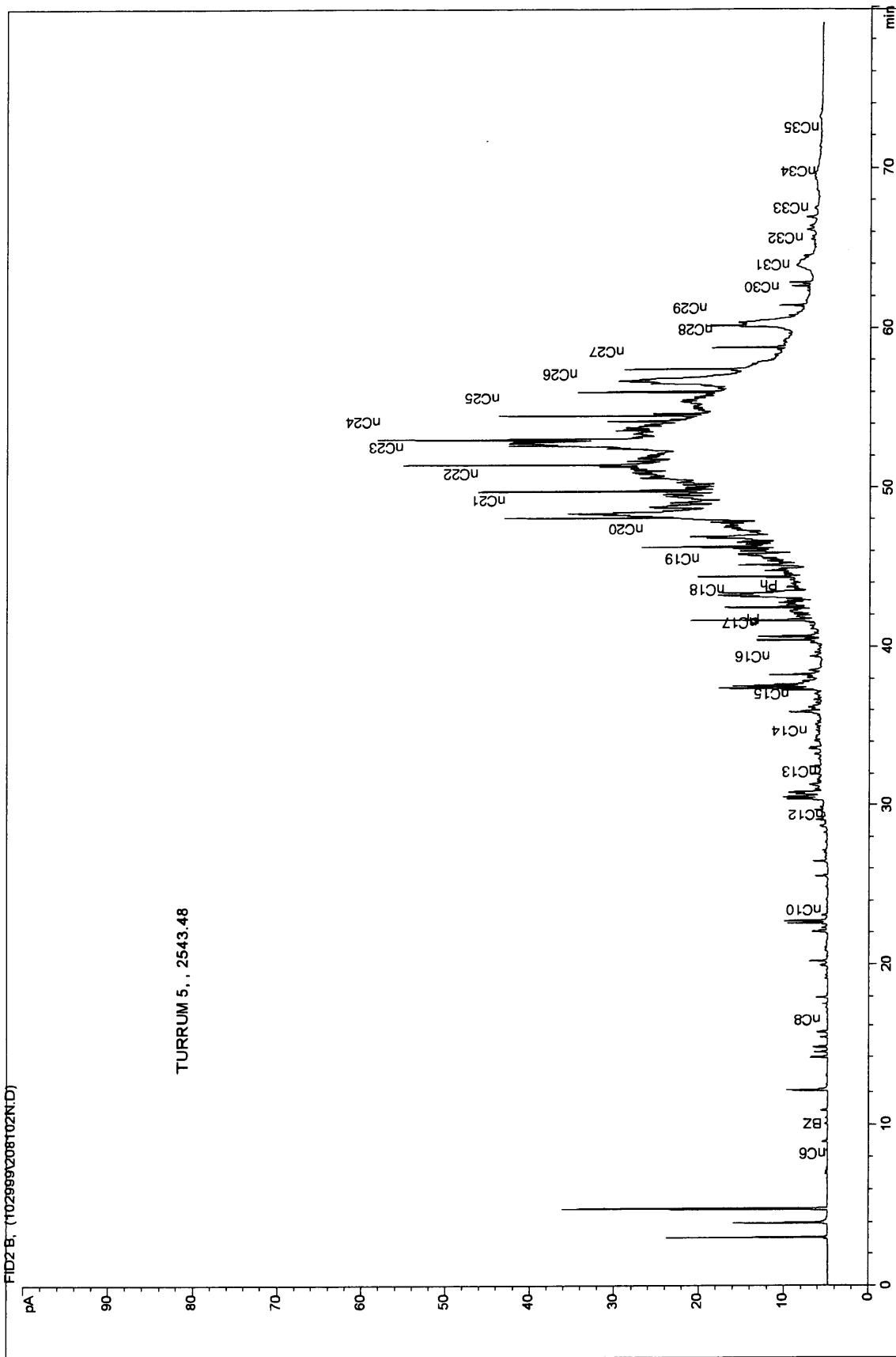
Whole-oil Gas Chromatogram of extract from Turrum 5, 2536.98 m

907511

111

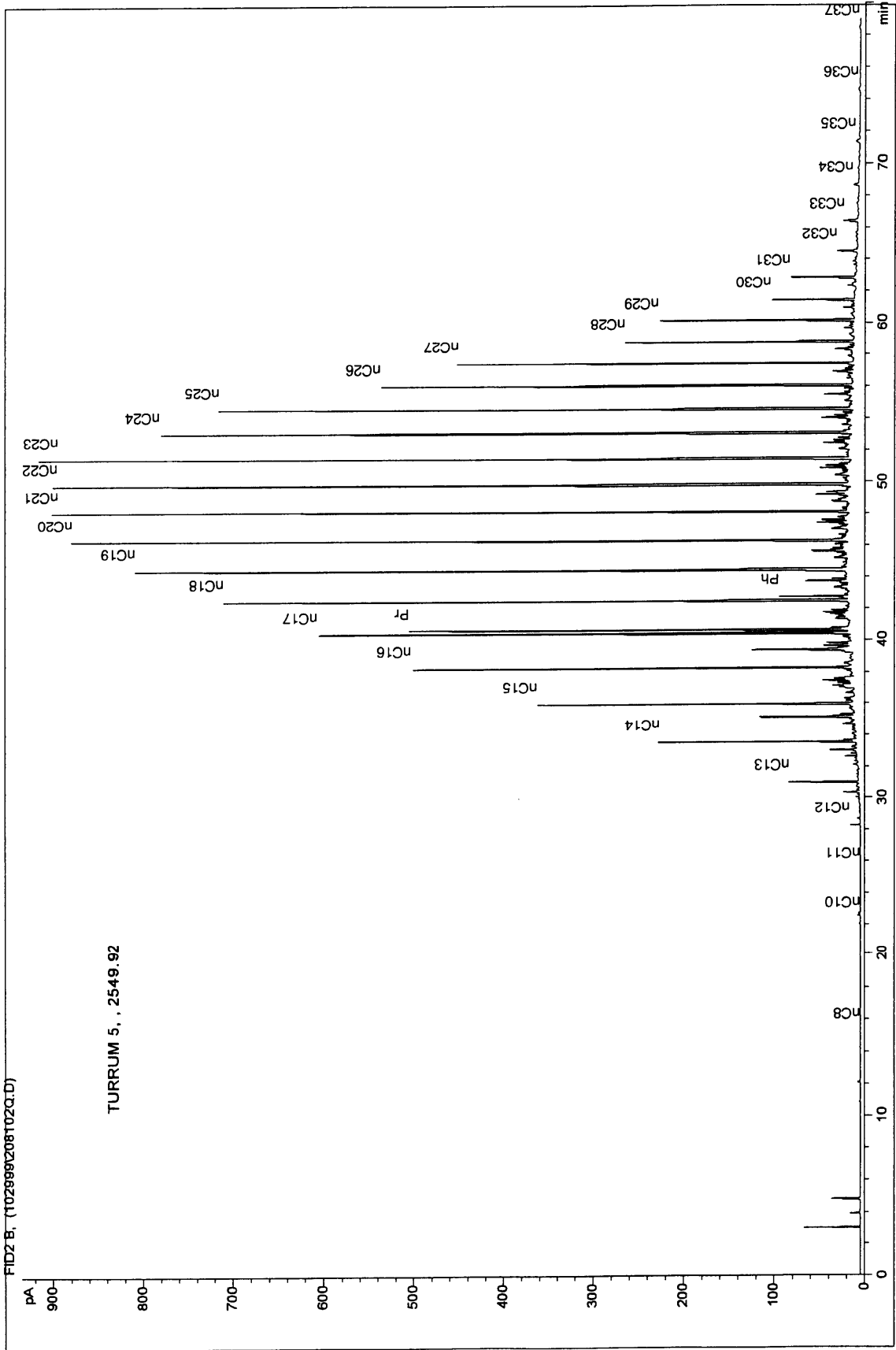


Whole-oil Gas Chromatogram of extract from Turrum 5, 2539.97 m



Whole-oil Gas Chromatogram of extract from Turrum 5, 2543.48 m

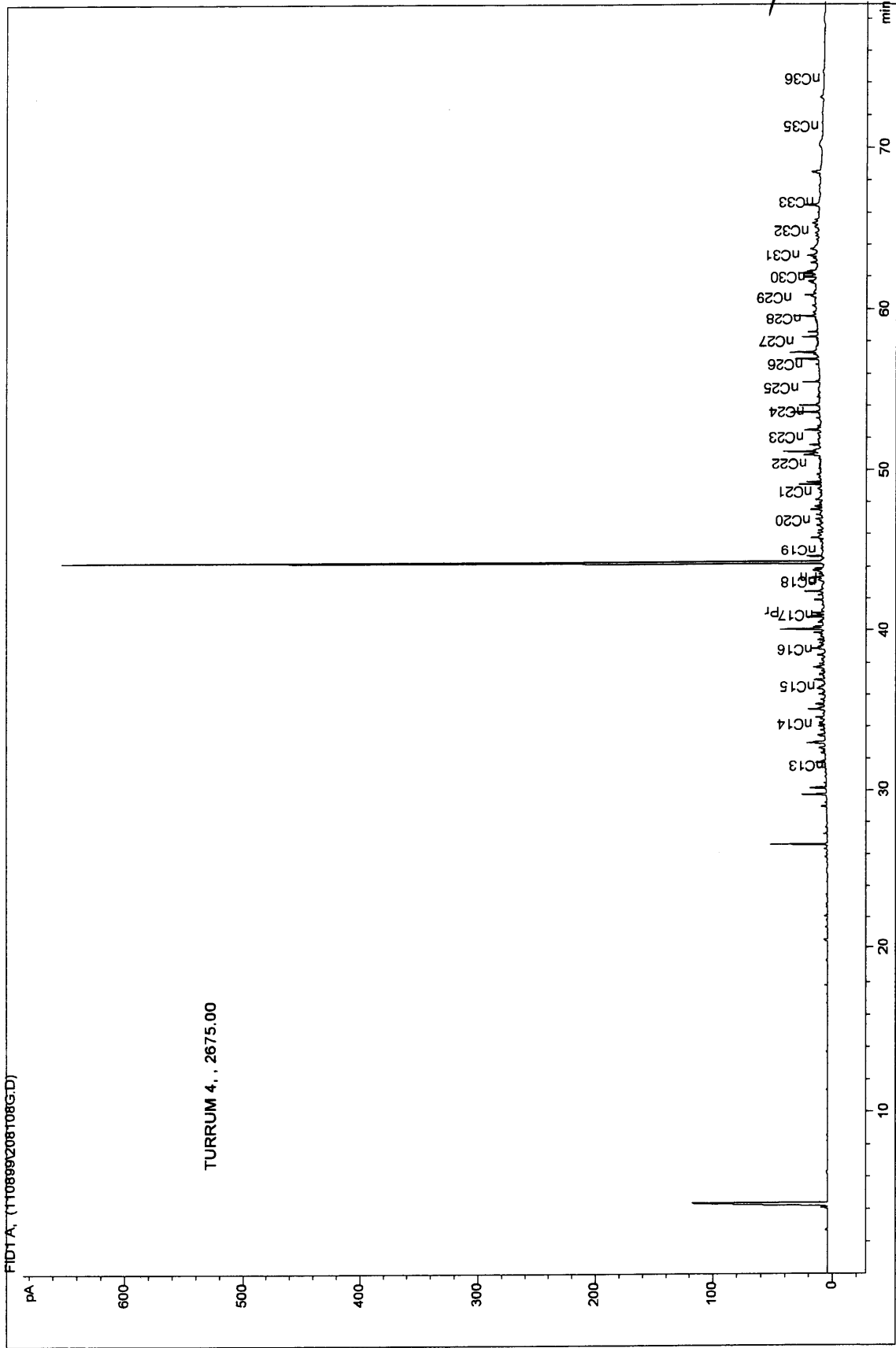




Whole-oil Gas Chromatogram of extract from Turrum 5, 2549.92 m

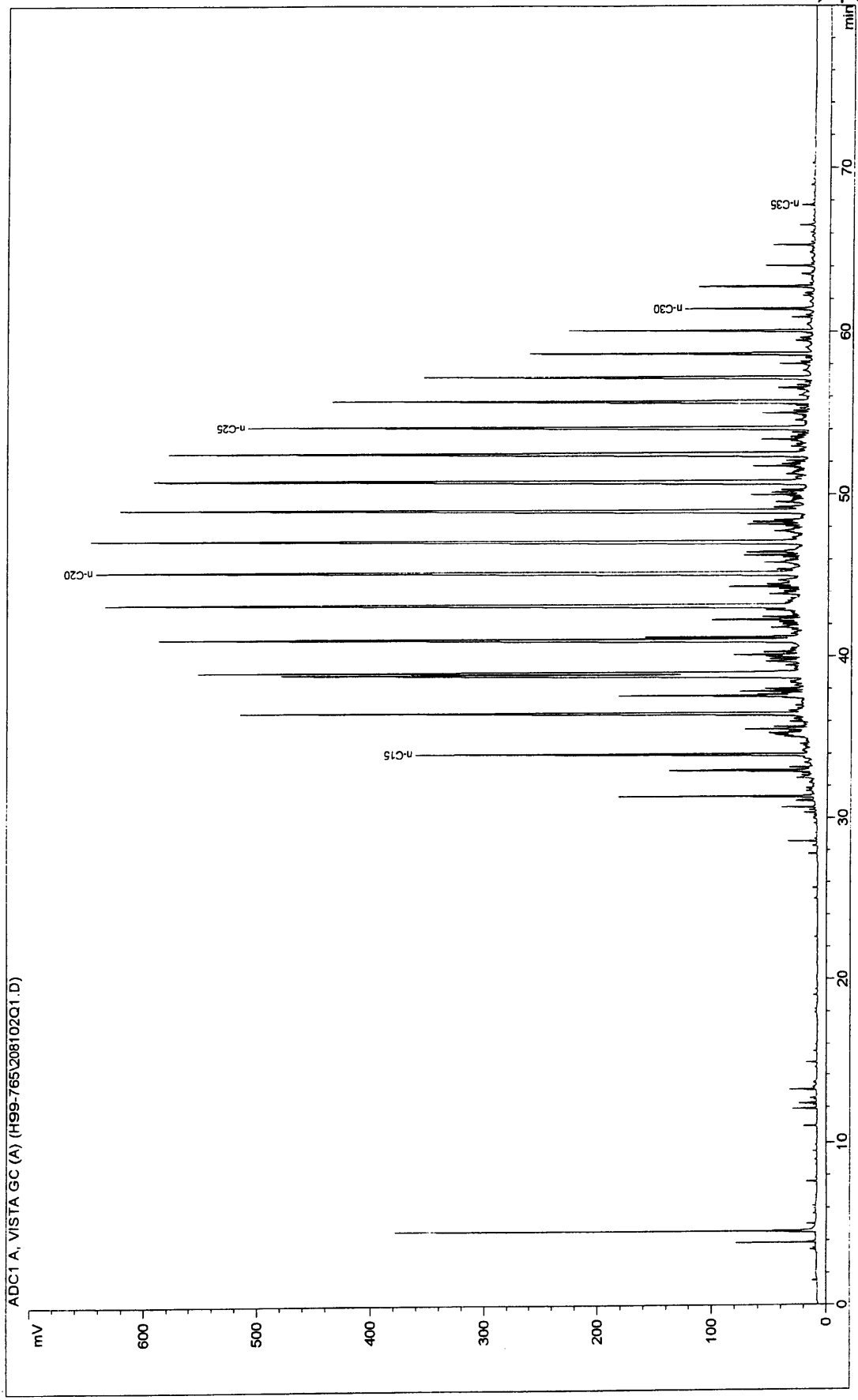
907511

114

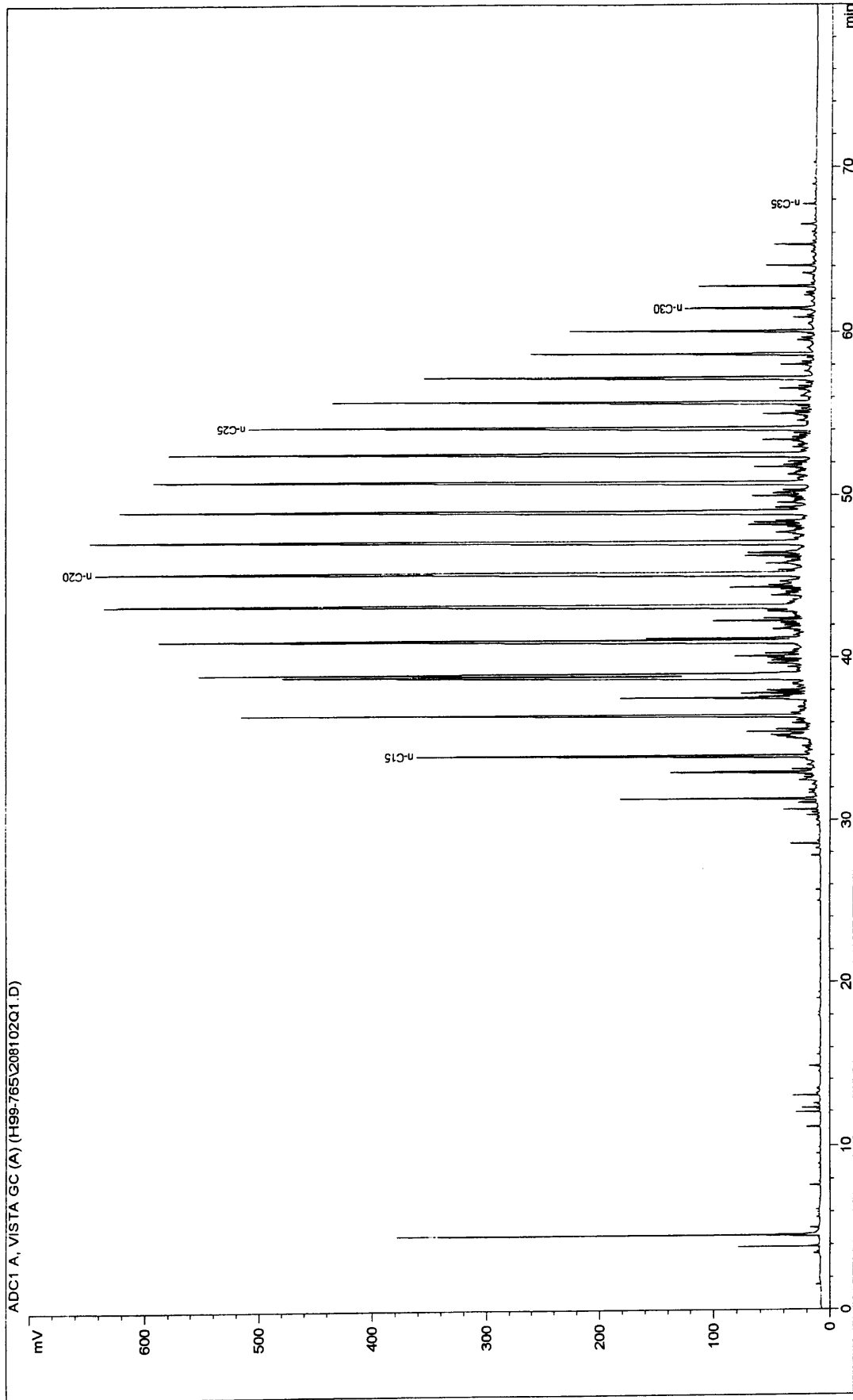


FID1A: (1108991208108.G)

Whole-oil Gas Chromatogram of extract from Turrum 4, 2675.00 m



Thermal Extraction Gas Chromatogram of Turrum 5, 2546.92 m



ADC1 A, VISTA GC (A) (H99-765\208102Q1.D)

Thermal Extraction Gas Chromatogram of Turrum 7, 2610.2 m

**Appendix II - Turrum 7 Core Properties**

OVERBURDEN ANALYSIS PRELIMINARY REPORT

**Client** : Esso Australia Ltd  
**Well** : Turrum-7  
**Field** : Turrum  
**Core 1** : 2609.00m - 2635.10m

**Date** : 10/22/1999  
**File** : 0306-02  
**Location** : Bass Strait, Victori  
**ACS Lab.** : Brisbane (02)  
**Analysts** : pnc ijm kw

**OVERBURDEN PRESSURE:** 4500 psi

Sample Number	Depth (metres)	Permeability to Air (milliDarcys)	Porosity (percent)	Grain Density		Fluid Saturations		Remarks
				Calculated (g/cm <sup>3</sup> )	Absolute (g/cm <sup>3</sup> )	Water (%)	Oil (%)	
11	2609.93	0.62	12.5	2.67		65.3	4.0	
13	2610.10	0.55	12.2	2.67		67.2	5.8	
15	2610.30	2.46	14.3	2.68		61.2	12.5	
17	2610.55	0.60	13.1	2.66		72.5	3.6	
19	2610.70	0.26	10.9	2.66		70.4	4.1	
21V	2610.78	0.20	13.6	2.66		70.8	5.6	
23	2610.90	0.04	7.1	2.63				
25	2611.10	0.05	8.4	2.65		56.9	2.4	
27	2611.30	0.01	5.6	2.97				pyr
29	2611.50	0.02	8.0	2.70				pyr
31	2611.74	0.00	3.2	2.60				frac
33V	2611.82	0.00	3.0	2.58				short sample
109	2618.05	0.00	3.0	2.63		55.7	2.7	
111	2618.25	0.00	2.6	2.59				
113	2618.48	0.01	5.4	2.64				
115	2618.65	0.01	5.4	2.66				
117	2618.85	0.05	6.1	2.67		59.9	2.5	frac/mounted
119V	2618.97	0.00	7.1	2.82				pyr
121	2619.05	0.02	7.1	2.71				
123	2619.25	0.01	5.1	2.65		55.9	2.2	
125	2619.45	0.01	4.8	2.64				
127	2619.65	0.01	6.9	2.62				
129	2619.80	0.22	11.4	2.67		73.0	0.8	
131V	2619.97	0.03	11.2	2.68				
133	2620.05	0.00	3.6	2.73				pyr
135	2620.25	0.00	3.4	2.72				pyr
137	2620.45	0.16	10.6	2.65		65.3	1.5	frac
139	2620.65	0.01	6.9	2.85				pyr
141	2620.85	0.16	10.4	2.85		70.3	3.9	pyr
143V	2620.92	0.01	9.8	2.76				pyr
145	2621.05	1.12	12.4	2.66				

Sample Number	Depth (metres)	Permeability to Air (milliDarcys)	Porosity (percent)	Grain Density		Fluid Saturations		Remarks
				Calculated (g/cm <sup>3</sup> )	Absolute (g/cm <sup>3</sup> )	Water (%)	Oil (%)	
147	2621.25	0.87	12.7	2.67				
149	2621.45	0.03	7.9	2.67		63.4	6.3	
151	2621.65	0.00	2.8	2.63				
153	2621.85	0.01	4.9	2.65				
155V	2621.95	0.00	3.1	2.62				short sample
157	2622.05	0.01	5.6	2.65		60.0	3.1	
159	2622.25	0.01	6.3	2.66				
161	2622.45	0.01	5.6	2.64				
163	2622.65	0.02	7.7	2.66		78.7	2.9	
165	2622.85	0.02	8.4	2.67				
167V	2622.93	0.00	6.4	2.66				
169	2623.05	0.01	6.3	2.66				
171	2623.25	0.00	3.3	2.64		84.4	2.6	
173	2623.45	0.00	3.0	2.63				frac/mounted
175	2623.65	0.01	4.5	2.66				C lam
177	2623.85	0.01	5.8	2.65		79.4	1.9	
179V	2623.97	0.01	7.1	2.66				
181	2624.05	0.01	4.9	2.65				
183	2624.25	0.01	5.7	2.65				short sample
185	2624.45	0.02	5.5	2.67		71.3	2.0	
187	2624.65	0.08	9.9	2.69				
189	2624.80	0.07	8.9	2.74				
191V	2624.97	0.02	7.6	3.11		62.0	3.2	pyr
193	2625.05	0.02	6.0	2.75				frac
195	2625.27	0.03	7.8	2.68				
197	2625.47	0.04	9.0	2.68				
199	2625.65	0.03	8.8	2.67		66.4	2.2	
201	2625.85	0.06	8.7	2.69				
203V	2625.97	0.01	8.1	2.68				
205	2626.05	0.06	8.7	2.68				
207	2626.25	0.02	6.5	2.68		85.5	3.7	
209	2626.45	0.08	8.3	2.73				
211	2626.65	0.03	6.6	2.73				
213	2626.85	0.03	6.9	2.70				frac/mounted
215V	2626.97	0.04	10.7	2.72		69.7	2.2	
217	2627.05	0.04	7.9	2.70				
219	2627.25	0.01	6.8	2.69				
221	2627.42	0.01	5.6	2.79				pyr
223	2627.65	0.01	6.3	2.68		75.8	0.0	
225	2627.85	0.02	7.3	2.67				
227V	2627.97	0.01	8.1	2.67				
229	2628.05	0.05	8.4	2.67				

Sample Number	Depth (metres)	Permeability to Air (milliDarcys)	Porosity (percent)	Grain Density		Fluid Saturations		Remarks
				Calculated (g/cm <sup>3</sup> )	Absolute (g/cm <sup>3</sup> )	Water (%)	Oil (%)	
231	2628.25	0.05	9.2	2.67		67.4	3.3	
233	2628.45	0.10	10.5	2.67				
235	2628.63	0.06	7.1	2.66				
237	2628.85	0.05	7.2	2.74				
239V	2628.97	0.01	7.2	2.66		70.5	5.5	
241	2629.05	0.02	6.7	2.65				frac
243	2629.27	0.03	4.9	2.65				frac
245	2629.45	0.25	11.8	2.67		73.2	2.9	
247	2629.65	0.04	5.9	2.66				
249	2629.85	0.02	4.2	2.70				
251V	2629.93	0.00	2.9	2.60		72.3	0.0	frac



907511 ~~121~~  
121

907511 ~~122~~  
122

907511 ~~123~~  
123

**APPENDIX 5**

**TURRUM 7**

**Core Analysis**

907511 ~~XXXX~~  
124



**ROUTINE CORE ANALYSIS FINAL REPORT**  
**of**  
***TURRUM-7***  
**for**  
***ESSO AUSTRALIA LTD***  
**by**  
**ACS LABORATORIES PTY LTD**

23 December, 1999

907511 ~~125~~  
125



Esso Australia Ltd  
Esso House  
12 Riverside Quay  
SOUTHBANK VIC 3006

Attention: Mr Phil Burnett

**FINAL REPORT: 0306(a)-02**  
**TURRUM-7**

**CLIENT REFERENCE:** Contract Number 2710080 RFS No.5  
AFE No. L61019005

**MATERIAL:** Core Plugs and Core Plug Offcuts

**LOCALITY:** Gippsland Basin, Bass Strait

**WORK REQUIRED:** Routine Core Analysis

Please direct technical inquiries regarding this work to the signatory below under whose supervision the work was conducted.

A handwritten signature in black ink, appearing to read 'Peter Crozier', with a horizontal line underneath.

**PETER CROZIER**  
Operations Manager

ACS Laboratories Pty. Ltd. shall not be liable or responsible for any loss, cost, damages or expenses incurred by the client, or any other person or company, resulting from any information or interpretation given in this report. In no case shall ACS Laboratories Pty. Ltd. be responsible for consequential damages including, but not limited to, lost profits, damages for failure to meet deadlines and lost production arising from this report.

Address: P.O. Box 396, Chermide South, Qld. 4032 Australia  
Telephone: 61 7 3350 1222 Facsimile: 61 7 3359 0666  
E-mail: acs.bris@acslabs.com.au

ACS Laboratories Pty Ltd  
ACN: 008 273 005

**CONTENTS**

**PAGE**

***CHAPTERS***

<b>1.</b>	<b>INTRODUCTION .....</b>	<b>1</b>
<b>2.</b>	<b>STUDY AIMS .....</b>	<b>3</b>
<b>3.</b>	<b>SAMPLE PREPARATION</b>	
	<b>3.1 Sample Extraction .....</b>	<b>7</b>
	<b>3.2 Sample Drying .....</b>	<b>7</b>
<b>4.</b>	<b>SAMPLE TEST PROCEDURES</b>	
	<b>4.1 Dean-Stark Residual Fluid Saturation .....</b>	<b>9</b>
	<b>4.2 Helium Injection Porosity at Overburden .....</b>	<b>9</b>
	<b>4.3 Air Permeability at Overburden .....</b>	<b>10</b>
	<b>4.4 Calculated Grain Density .....</b>	<b>10</b>
	<b>4.5 Absolute Grain Density .....</b>	<b>11</b>
<b>5.</b>	<b>COMMENTS .....</b>	<b>12</b>

***APPENDICES***

- I. ROUTINE CORE ANALYSIS RESULTS**
- II. POROSITY vs PERMEABILITY AT OVERBURDEN CROSSPLOT**
- III. CORE PLOT**

907511 ~~100~~  
127

***CHAPTER 1***

**INTRODUCTION**

## 1. INTRODUCTION

A suite of 100 core plug samples and off-cuts from Turrum-7 was delivered to ACS Laboratories, Brisbane in two consignments. The first 84 samples arrived on 27<sup>th</sup> September, 1999, with the remaining 16 samples arriving on 4<sup>th</sup> November, 1999.

This final report presents the results from a routine core analysis study performed on plug samples from Turrum-7. The study was undertaken as per instructions received from Esso Australia Ltd on the following facsimiles:

1. Reference Job No. T7001, dated 27 September, 1999 and
2. Reference Job No. T7002, dated 29 October, 1999.

The following report includes tabular data of residual fluid saturation, permeability to air and helium injection porosity at net overburden conditions, density determinations, both calculated and absolute.

Data presented graphically includes a core log plot, porosity versus permeability to air.

A brief commentary of the data is found in Chapter 5.



907511 ~~129~~  
129

## ***CHAPTER 2***

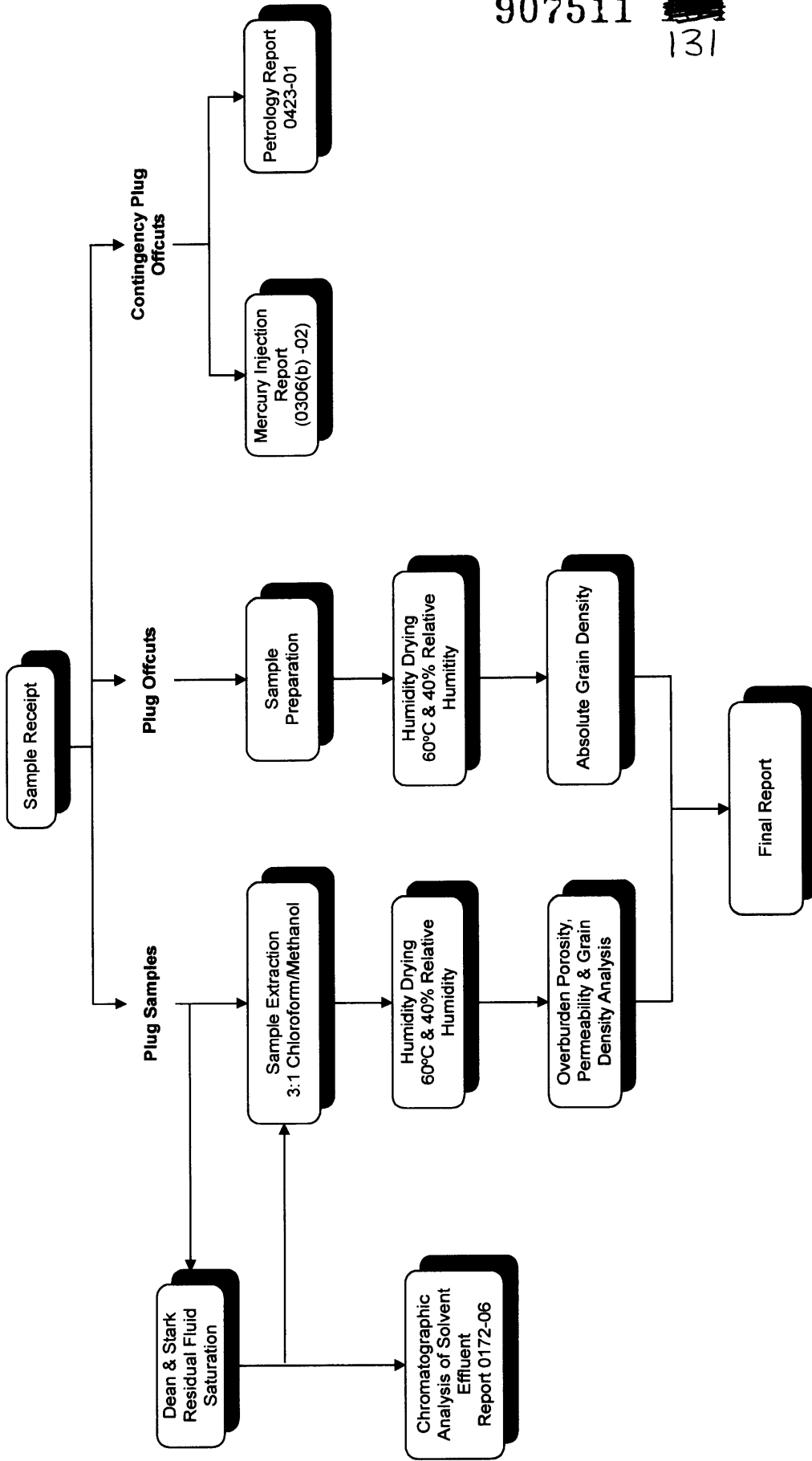
### **STUDY AIMS**

**2. STUDY AIMS**

The analyses were performed with the following aims:

1. To provide residual fluid saturation data at selected points across the cored interval.
2. To provide overburden permeability to air, helium injection porosity and density data.

# STUDY OUTLINE



907511

131

***CHAPTER 3***

**SAMPLE PREPARATION**

### 3. SAMPLE PREPARATION

The samples were prepared as follows:

#### 3.1 Sample Extraction

The samples were placed in a soxhlet extractor to remove hydrocarbons and residual salt. The samples were cleaned using 3:1 chloroform/methanol azeotrope as the solvent. When the solvent in the extractor chamber tested negative for silver nitrate ( $\text{AgNO}_3$ ) induced salt precipitation and the samples tested negative for fluorescence under ultra-violet light, the samples were removed.

#### 3.2 Sample Drying

After cleaning, all plugs were humidity dried to a constant weight at 60°C and 40% relative humidity. Once dried, the plugs were stored in individual airtight containers and allowed to cool to room temperature before analysis.

907511 ~~137~~

134

## ***CHAPTER 4***

### **SAMPLE TEST PROCEDURES**

#### 4. SAMPLE TEST PROCEDURES

##### 4.1 Dean-Stark Residual Fluid Saturation

The fresh state sample is placed in the Dean-Stark fluid extraction apparatus where it is suspended above a reservoir of boiling toluene. The solvent vapours together with the extracted pore fluids, are condensed at the top of the glassware and the water collected in a calibrated side arm. Oil and toluene are collected in the reservoir and continue boiling so that clean toluene vapour continues extracting pore fluids. The process is continued until the water production ceases.

From the collected water volume and the latter determined helium injection pore volume of the sample, water saturation is calculated as follows.

$$S_w = (\text{Pore Water Volume} / \text{Pore Volume}) \times 100\%$$

From the wet sample weight (pre-analysis), the dry sample weight (post extraction and oven drying), the extracted water volume, the pore volume and the density of the oil, the oil saturation is calculated as follows:

$$\text{Oil Weight} = \text{Sample Wt (wet)} - \text{Sample Wt (dry)} - \text{Pore Water Wt}$$

$$\text{Oil Volume} = \text{Oil Weight} / \text{Density of Oil}$$

$$S_o = (\text{Oil Volume} / \text{Pore Volume}) \times 100\%$$

(A value of 0.80 g/cm<sup>3</sup> was used as the density of oil in this case.)

The effluent solvent (and oil) was retained for chromatographic oil typing. The results of this study are found in ACS report No. 0172-06.

##### 4.2 Helium Injection Porosity at Overburden

The porosity of the cleaned and dried core plugs was determined as follows. Each plug was first placed in a sealed matrix cup. Helium held at 100 psi reference pressure was then introduced to the cup. From the resultant pressure change the unknown grain volume was calculated using Boyle's Law.

$$\begin{aligned} P_1 V_1 &= P_2 V_2 \\ \Rightarrow P_1 V_r &= P_2 (V_r + V_c - V_g) \end{aligned}$$

where:

$$\begin{aligned} P_1 &= \text{initial pressure (atmospheres)} \\ P_2 &= \text{final pressure (atmospheres)} \\ V_r &= \text{reference cell volume (cm}^3\text{)} \\ V_c &= \text{matrix cup volume (cm}^3\text{)} \\ V_g &= \text{grain volume (cm}^3\text{)} \end{aligned}$$

To determine the pore volume of the core plug at overburden pressure, the sample was placed in a thick walled rubber sleeve. This assembly was then loaded into a hydrostatic cell. A simulated overburden pressure was then applied to the samples and the pore volume determined.

The bulk volume is determined by the addition of the pore volume and the grain volume. The porosity is calculated as the volume percentage of the pore space with respect to the bulk volume.

$$V_b = V_p + V_g$$

$$\text{Porosity \%} = \frac{V_p}{V_b} \times 100$$

where:

$$\begin{aligned} V_p &= \text{pore volume (cm}^3\text{)} \\ V_b &= \text{bulk volume (cm}^3\text{)} \\ V_g &= \text{grain volume (cm}^3\text{)} \end{aligned}$$

#### 4.3 Air Permeability at Overburden

The sample was loaded into a thick walled rubber sleeve before being loaded into a hydrostatic cell and a simulated overburden pressure applied. A known air pressure was applied to the upstream face of the sample, creating a flow of air through the sample. Air permeability for each plug sample was calculated using Darcy's law through a knowledge of the upstream and downstream pressure, flow rate, viscosity of air and the sample dimensions.

$$K_a = \frac{2000 \cdot BP \cdot \mu \cdot q \cdot L}{(P_1^2 - P_2^2) A}$$

where:

$$\begin{aligned} K_a &= \text{air permeability (milliDarcy's)} \\ BP &= \text{barometric pressure (atmospheres)} \\ \mu &= \text{gas viscosity (cP)} \\ q &= \text{flow rate (cm}^3\text{/s)} \\ P_1 &= \text{upstream pressure (atmospheres)} \\ P_2 &= \text{downstream pressure (atmospheres)} \\ A &= \text{sample cross sectional area (cm}^2\text{)} \\ L &= \text{sample length (cm)} \end{aligned}$$

#### 4.4 Calculated Grain Density

The apparent grain density was calculated by dividing the weight of the plug by the grain volume, determined from the helium injection porosity measurement.



907511 ~~XXXX~~  
137

#### 4.5 Absolute Grain Density

An uncleaned, oven dried plug off-cut was used for this measurement. The sample was crushed to approximately grain size and weighed. The volume of the grains was determined by pycnometry and the density calculated accordingly.

***CHAPTER 5***

**COMMENTS**

## 5. COMMENTS

The reservoir quality of the cored interval of Turrum-7 is poor. The porosity across the cored interval ranges from 2.6% to 14.3% (av. 7.2%) and the permeability from < 0.01 mD to 2.46 mD (av. 0.10 mD).

The oil bearing reservoir section of the core between 2609.90 m and 2610.80 m exhibits a bright yellow fluorescence in the plugs ranging from approximately 60% to trace proportions. This interval of core has an average porosity of 12.5% and an average permeability of 0.90 mD. The most permeable rock measured in this interval (2610.30 m) has a porosity of 14.3% and a permeability of 2.46 mD. It has the best visual fluorescence (60%) and a residual oil saturation of 12.5%. Very dull orange fluorescence is observed in other tighter sections of the cored interval. This fluorescence is either due to traces of dead relic oil or minerals.

A good correlation exists between the absolute grain densities and the calculated grain densities. On average the absolute grain densities run 0.01 g/cm<sup>3</sup> lower than the calculated densities. Local variations in these densities is due to lithology, with the largest variations due to relative amounts of pyrite.

A good porosity versus permeability trend is evident on the cross-plot in Appendix II, with only minor scatter of the data. Data on the vertical plugs, plotted in red, are evident on the bottom of the trend.

907511 ~~140~~  
140

*APPENDIX I*

**ROUTINE CORE ANALYSIS RESULTS**

907511 

141

**OVERBURDEN ANALYSIS FINAL REPORT**

**Client** : Esso Australia Ltd  
**Well** : Turrum-7  
**Field** : Turrum  
**Core 1** : 2609.00m - 2635.10m

**Date** : 30/11/99  
**File** : 0306-02  
**Location** : Bass Strait, Victoria  
**ACS Lab.** : Brisbane (02)  
**Analysts** : pnc ijm kw

**OVERBURDEN PRESSURE:** 4500 psi

Sample Number	Depth (metres)	Permeability to Air (milliDarcys)	Porosity (percent)	Grain Density		Fluid Saturations		Remarks
				Calculated (g/cm <sup>3</sup> )	Absolute (g/cm <sup>3</sup> )	Water (%)	Oil (%)	
1	2609.05	<0.01	3.2	2.63	2.64			
3	2609.25	<0.01	3.4	2.63	2.63			
5	2609.45	0.06	5.1	2.63	2.64			frac
7	2609.65	0.01	6.7	2.64	2.64			
9V	2609.82	<0.01	6.4	2.65	2.65			
11	2609.93	0.62	12.5	2.67	2.66	65.3	4.0	
13	2610.10	0.55	12.2	2.67	2.67	67.2	5.8	
15	2610.30	2.46	14.3	2.68	2.66	61.2	12.5	
17	2610.55	0.60	13.1	2.66	2.66	72.5	3.6	
19	2610.70	0.26	10.9	2.66	2.65	70.4	4.1	
21V	2610.78	0.20	13.6	2.66	2.65	70.8	5.6	
23	2610.90	0.04	7.1	2.63	2.63			
25	2611.10	0.05	8.4	2.65	2.64	56.9	2.4	
27	2611.30	0.01	5.6	2.97	3.07			pyr
29	2611.50	0.02	8.0	2.70	2.63			pyr
31	2611.74	<0.01	3.2	2.60	2.61			frac
33V	2611.82	<0.01	3.0	2.58	2.61			short sample
49	2613.10	<0.01	3.6	3.20	2.88			pyr
51	2613.30	<0.01	3.1	2.64	2.65			
85	2616.03	<0.01	5.3	2.67	2.71			
89	2616.48	0.05	8.9	2.66	2.63			
91	2616.65	0.01	6.5	2.64	2.64			
93	2616.85	0.07	9.4	2.77	2.71			pyr
95V	2616.97	<0.01	7.1	2.63	2.66			
97	2617.05	0.01	5.8	2.65	2.64			
99	2617.25	0.24	10.3	2.72	2.72			
101	2617.45	0.58	11.5	2.75	2.76			pyr
103	2617.60	0.03	8.3	2.88	2.86			pyr
109	2618.05	<0.01	3.0	2.63	2.61	55.7	2.7	
111	2618.25	<0.01	2.6	2.59	2.61			
113	2618.48	0.01	5.4	2.64	2.63			
115	2618.65	0.01	5.4	2.66	2.62			
117	2618.85	0.05	6.1	2.67	2.60	59.9	2.5	frac/mounted
119V	2618.97	<0.01	7.1	2.82	2.80			pyr

Sample Number	Depth (metres)	Permeability to Air (milliDarcys)	Porosity (percent)	Grain Density		Fluid Saturations		Remarks
				Calculated (g/cm <sup>3</sup> )	Absolute (g/cm <sup>3</sup> )	Water (%)	Oil (%)	
121	2619.05	0.02	7.1	2.71	2.71			
123	2619.25	0.01	5.1	2.65	2.65	55.9	2.2	
125	2619.45	0.01	4.8	2.64	2.58			
127	2619.65	0.01	6.9	2.62	2.58			
129	2619.80	0.22	11.4	2.67	2.66	73.0	0.8	
131V	2619.97	0.03	11.2	2.68	2.65			
133	2620.05	<0.01	3.6	2.73	2.73			pyr
135	2620.25	<0.01	3.4	2.72	2.72			pyr
137	2620.45	0.16	10.6	2.65	2.64	65.3	1.5	frac
139	2620.65	0.01	6.9	2.85	3.07			pyr
141	2620.85	0.16	10.4	2.85	2.82	70.3	3.9	pyr
143V	2620.92	0.01	9.8	2.76	2.70			pyr
145	2621.05	1.12	12.4	2.66	2.65			
147	2621.25	0.87	12.7	2.67	2.68			
149	2621.45	0.03	7.9	2.67	2.67	63.4	6.3	
151	2621.65	<0.01	2.8	2.63	2.65			
153	2621.85	0.01	4.9	2.65	2.65			
155V	2621.95	<0.01	3.1	2.62	2.62			short sample
157	2622.05	0.01	5.6	2.65	2.64	60.0	3.1	
159	2622.25	0.01	6.3	2.66	2.66			
161	2622.45	0.01	5.6	2.64	2.65			
163	2622.65	0.02	7.7	2.66	2.66	78.7	2.9	
165	2622.85	0.02	8.4	2.67	2.66			
167V	2622.93	<0.01	6.4	2.66	2.64			
169	2623.05	0.01	6.3	2.66	2.65			
171	2623.25	<0.01	3.3	2.64	2.65	84.4	2.6	
173	2623.45	<0.01	3.0	2.63	2.63			frac/mounted
175	2623.65	0.01	4.5	2.66	2.66			C lam
177	2623.85	0.01	5.8	2.65	2.64	79.4	1.9	
179V	2623.97	0.01	7.1	2.66	2.68			
181	2624.05	0.01	4.9	2.65	2.65			
183	2624.25	0.01	5.7	2.65	2.66			short sample
185	2624.45	0.02	5.5	2.67	2.67	71.3	2.0	
187	2624.65	0.08	9.9	2.69	2.68			
189	2624.80	0.07	8.9	2.74	2.75			
191V	2624.97	0.02	7.6	3.11	2.95	62.0	3.2	pyr
193	2625.05	0.02	6.0	2.75	2.74			frac
195	2625.27	0.03	7.8	2.68	2.67			
197	2625.47	0.04	9.0	2.68	2.67			
199	2625.65	0.03	8.8	2.67	2.71	66.4	2.2	
201	2625.85	0.06	8.7	2.69	2.67			
203V	2625.97	0.01	8.1	2.68	2.66			
205	2626.05	0.06	8.7	2.68	2.67			
207	2626.25	0.02	6.5	2.68	2.68	85.5	3.7	
209	2626.45	0.08	8.3	2.73	2.75			
211	2626.65	0.03	6.6	2.73	2.73			
213	2626.85	0.03	6.9	2.70	2.68			frac/mounted

907511 ~~143~~  
143

Sample Number	Depth (metres)	Permeability to Air (milliDarcys)	Porosity (percent)	Grain Density		Fluid Saturations		Remarks
				Calculated (g/cm <sup>3</sup> )	Absolute (g/cm <sup>3</sup> )	Water (%)	Oil (%)	
215V	2626.97	0.04	10.7	2.72	2.71	69.7	2.2	
217	2627.05	0.04	7.9	2.70	2.69			
219	2627.25	0.01	6.8	2.69	2.68			
221	2627.42	0.01	5.6	2.79	2.75			pyr
223	2627.65	0.01	6.3	2.68	2.67	75.8	0.0	
225	2627.85	0.02	7.3	2.67	2.66			
227V	2627.97	0.01	8.1	2.67	2.68			
229	2628.05	0.05	8.4	2.67	2.66			
231	2628.25	0.05	9.2	2.67	2.67	67.4	3.3	
233	2628.45	0.10	10.5	2.67	2.68			
235	2628.63	0.06	7.1	2.66	2.65			
237	2628.85	0.05	7.2	2.74	2.66			
239V	2628.97	0.01	7.2	2.66	2.64	70.5	5.5	
241	2629.05	0.02	6.7	2.65	2.63			frac
243	2629.27	0.03	4.9	2.65	2.66			frac
245	2629.45	0.25	11.8	2.67	2.65	73.2	2.9	
247	2629.65	0.04	5.9	2.66	2.64			
249	2629.85	0.02	4.2	2.70	2.63			
251V	2629.93	<0.01	2.9	2.60	2.58	72.3	0.0	frac

907511 ~~144~~  
144

*APPENDIX II*

**POROSITY vs PERMEABILITY  
AT OVERBURDEN**



907511 <sup>145</sup> ~~145~~

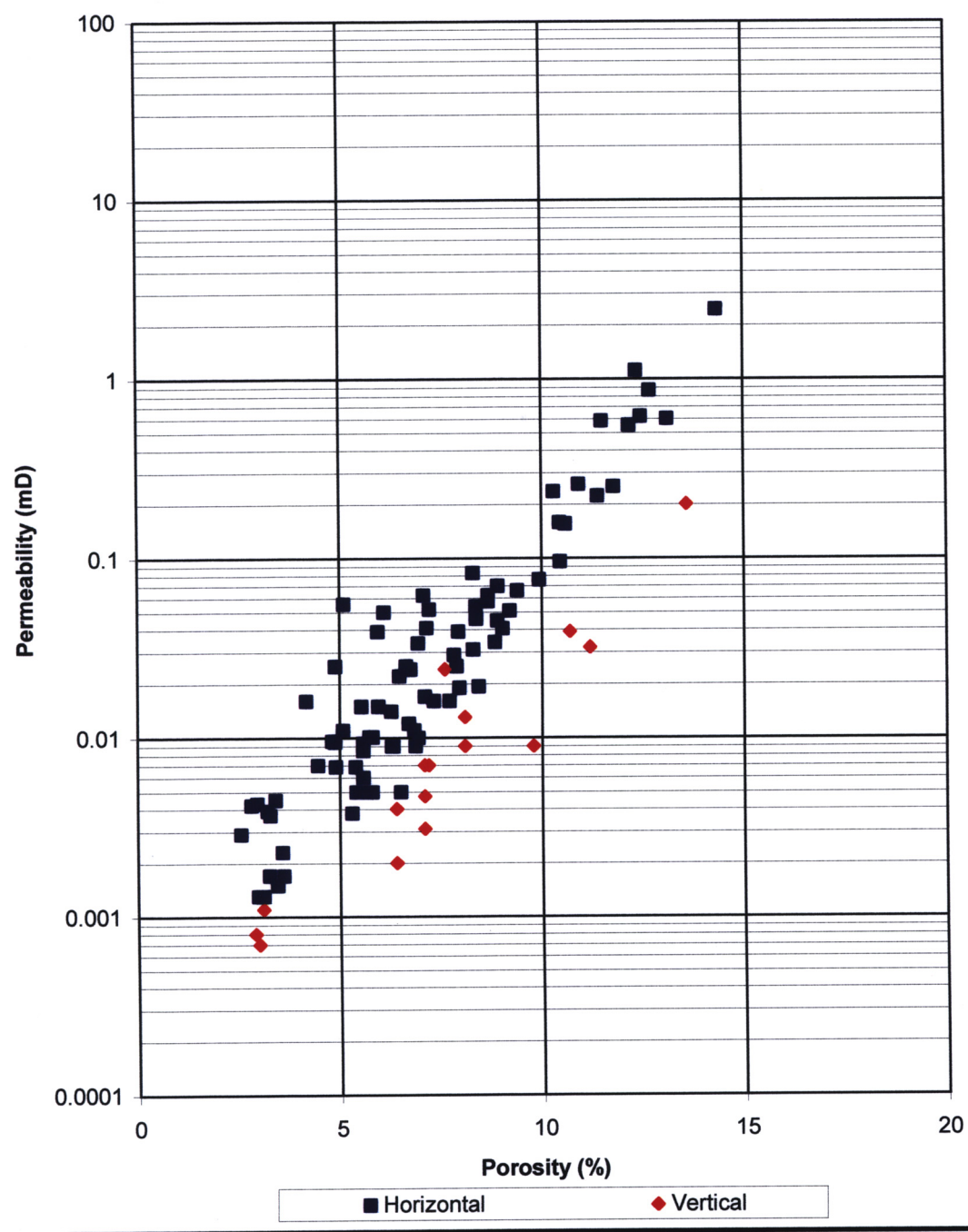
PE 907511-15



### POROSITY vs PERMEABILITY Overburden



**Client:** Esso Australia Ltd  
**Well:** Turrum-7  
**Depth:** 2609.00m - 2635.10m



907511 ~~146~~

146

***APPENDIX III***

**CORE PLOT**

907511 ~~100~~

147

PE908188

This is an enclosure indicator page.  
The enclosure PE908188 is enclosed within the  
container PE907511 at this location in this  
document.

The enclosure PE908188 has the following characteristics:

ITEM\_BARCODE = PE908188  
CONTAINER\_BARCODE = PE907511  
    NAME = Turrum-7 Core Plot Log  
    BASIN = GIPPSLAND  
    ONSHORE? = N  
    DATA\_TYPE = WELL  
DATA\_SUB\_TYPE = WELL\_LOG  
    DESCRIPTION = Turrum-7 Core Plot (Log), Core 1:  
                  2609.00m to 2635.10m, Scale 1:200 -  
                  showing Porosity, Permeability,  
                  Saturation and Density  
    REMARKS =  
    DATE\_WRITTEN =  
DATE\_PROCESSED =  
DATE\_RECEIVED = 06-APR-2000  
RECEIVED\_FROM = Esso Australia Ltd  
    WELL\_NAME = Turrum-7  
    CONTRACTOR = Esso Australia Ltd  
    AUTHOR =  
    ORIGINATOR = Esso Australia Ltd  
    TOP\_DEPTH = 2609  
    BOTTOM\_DEPTH = 2635.1  
ROW\_CREATED\_BY = DN07\_SW

(Inserted by DNRE - Vic Govt Mines Dept)

907511 ~~141~~  
148



**PETROLOGY & RESERVOIR QUALITY  
HIGHLIGHTING FORMATION CHARACTERISATIONS  
LIKELY TO AFFECT RESERVOIR POTENTIAL**

**of**

**TURRUM-7**

**for**

**ESSO AUSTRALIA LTD**

**by**

**ACS LABORATORIES PTY LTD**

907511 ~~102~~

149

21 December, 1999



Esso Australia Ltd  
12 Riverside Quay  
SOUTHBANK VIC 3006

Attention: Phil Burnett

**FINAL REPORT: 0423-01**

**CLIENT REFERENCE:** Contract No. 2710080 RFS No. 5  
Job No. T7002  
AFE No. L61019005

**MATERIAL:** 12 off-cut Core Samples

**LOCALITY:** Turrum-7

**WORK REQUIRED:** Petrology and Reservoir Quality

Please direct technical enquiries regarding this work to the signatories below under whose supervision the work was carried out.

A handwritten signature in black ink, appearing to read 'Peter N Crozier', with a long horizontal line extending to the right.

**PETER N CROZIER**  
Operations Manager

ACS Laboratories Pty Ltd shall not be liable or responsible for any loss, cost, damages or expenses incurred by the client, or any other person or company, resulting from any information or interpretation given in this report. In no case shall ACS Laboratories Pty Ltd be responsible for consequential damages including, but not limited to, lost profits, damages for failure to meet deadlines and lost production arising from this report.

Brisbane  
Laboratory:

P.O. Box 396, Chermside South Qld 4032, Australia  
☎: 61 7 3350 1222 Facsimile: 3359 0666  
E-mail: [acs.bris@acslabs.com.au](mailto:acs.bris@acslabs.com.au)

ACS Laboratories Pty Ltd  
ACN: 008 273 005

907511 ~~100~~  
150

**PETROLOGY & RESERVOIR QUALITY  
HIGHLIGHTING FORMATION CHARACTERISATIONS  
LIKELY TO AFFECT RESERVOIR POTENTIAL**

of

**TURRUM-7 CORE SAMPLES**

A final report prepared for

**ESSO AUSTRALIA LTD**

by

**ACS LABORATORIES PTY LTD**

in conjunction with

**DR GHAZI KRAISHAN (NCPGG)**

December 1999

This report is divided into two parts:

Part A presents an executive summary (Chapter 1), introduces this investigation (Chapter 2), presents the methods of investigations (Chapter 3), summarises the main results (Chapter 4) and presents an integrated model which discusses sediment provenance, environment of deposition and reservoir character (Chapter 5). Photomicrographs referenced in the text are located at the end of Part A.

Part B presents detailed thin section descriptions (Appendix I) and XRD traces (Appendix II). Representative photomicrographs are provided with each description (Appendix I).

**PART A**

1.	<b>EXECUTIVE SUMMARY</b> .....	1
2.	<b>INTRODUCTION</b> .....	2
3.	<b>METHODS</b> .....	3
4.	<b>RESULTS</b>	
	4.1 <b>Lithology</b> .....	5
	4.2 <b>Texture</b> .....	7
	4.3 <b>Composition</b> .....	7
	4.4 <b>XRD Bulk Mineralogy</b> .....	8
	4.5 <b>XRD Clay Mineralogy</b> .....	8
	4.6 <b>Scanning Electron Microscopy (SEM)</b> .....	23
	4.7 <b>Diagenesis</b> .....	25
	4.8 <b>Reservoir Quality</b> .....	25
5.	<b>SUMMARY AND CONCLUSIONS</b>	
	5.1 <b>Sediment Provenance</b> .....	32
	5.2 <b>Environment of Deposition</b> .....	32
	5.3 <b>Reservoir Potential</b> .....	32
6.	<b>REFERENCES</b> .....	33

**PART B****APPENDIX I - THIN SECTION DESCRIPTIONS**

Sample # 008C,	2609.65 m .....	45
Sample # 016C,	2610.30 m .....	48
Sample # 028C,	2611.30 m .....	53
Sample # 092C,	2616.65 m .....	56
Sample # 100C,	2617.25 m .....	59
Sample # V132C,	2619.97 m .....	64
Sample # 150C,	2621.45 m .....	69
Sample # 152C,	2621.65 m .....	74
Sample # 178C,	2623.85 m .....	77
Sample # 210C,	2626.45 m .....	80
Sample # 234C,	2628.45 m .....	85
Sample # 244C,	2629.27 m .....	91

**APPENDIX II - XRD TRACES**



## 1. EXECUTIVE SUMMARY

Esso Australia Ltd submitted 12 core samples collected from Turrum-7 well for petrographic analysis including detailed thin section description, X-ray diffraction and scanning electron microscopy. The main objectives of this study were to: undertake thin section descriptions including sediment classification, description of texture and composition, verify clay types, texture, grain size, shape, pore throat shape, clay matrix and pore bridging/grain coating clay identification using scanning electron microscope (SEM). SEM was used specifically to examine the morphology of the clay minerals. Particular attention was paid to observing:

- migration and/or mashing of fine clay crystallites in the pore space
- corrosion and/or dissolution of framework grains or authigenic phases
- change of habit of existing phases by collapse or swelling

Finally, the study aimed to present the sediment provenance, style and extent of diagenetic modification and reservoir potential.

The studied samples have similar mineralogy. Framework composition is dominated by monocrystalline quartz with minor to trace polycrystalline quartz, metamorphic and sedimentary rock fragments. Quartz grains are angular to rounded and exhibit slightly to strong undulose extinction with few coarse grains showing straight undulose extinction. Feldspar is a minor component and comprises orthoclase and cross hatched twinning to 'tartan' twinning (microcline). Plagioclase was absent in most of the samples. Micaceous schist, metaquartzite and chert are the main lithic fragments but siltstone and mudstone also occur in trace to rare amounts. Muscovite is moderate and altered in the studied samples. It is either disseminated or concentrated in very thin lamellae parallel to the bedding planes. The heavy mineral suite includes tourmaline, zircon and opaque grains. Detrital matrix is present in moderate amounts in some of the samples. Dispersed organic matter is minor in the samples and comprises coalified wood and plant materials. These sandstones are classified as sublitharenite, feldspathic litharenite, litharenite and lithwacke.

Routine core analysis (RCA) results show that Turrum-7 sandstone samples have low porosity and permeability, and fair to poor reservoir quality. RCA shows that ambient porosity for the studied samples ranges from 2.8% to 14.3% and air permeability ranges from 0 mD to 2.46 mD. Petrographical studies revealed that visual porosity of the studied samples is very low ranging from traces to 11.0% with an average of 5.5%, most of which is primary intergranular porosity. Highly altered ductile lithic fragments and authigenic clay masses contain considerable amounts of microporosity. Macroporosity is poorly developed and moderately affected by subsequent diagenetic modifications. The framework grains show mainly suture to concavo-convex contacts, suggesting that the effect of the compaction process in destroying the reservoir quality was severe. It seems likely that compaction and precipitation of authigenic minerals has had a large effect on the reservoir quality in the Turrum-7 core samples. Porosity reduction has occurred predominantly where the ductile lithic

fragments are abundant. Compaction has reduced the intergranular primary porosity by up to 56% of the original intergranular porosity. Cementation of authigenic minerals has further contributed to the porosity loss and reduced up to 33% of the original intergranular porosity.

SEM observations reveal that the samples contain very low visual porosity with dominant authigenic clay minerals. The pores are poorly developed and range in size from 1 micron up to a few microns. Pore throats are much smaller with an average size of much less than 1 micron. The macro-pores are poorly interconnected suggesting very low permeability and fair to poor reservoir quality. The pores are filled with authigenic clay minerals and minor quartz cement. Kaolinite is the dominant type of cement and occurs as pseudo hexagonal book-like crystals filling much of the pore spaces and restricting the reservoir potential. Illite is also common and occurs as fibrous to hairy crystals filling and bridging the pore spaces and pore throats. Both authigenic minerals formed due to alteration of feldspar and ductile lithic grains. Quartz cement is minor to moderate in some samples and occurs as thin, occasionally thick, euhedral overgrowths.

Based on the integration of detailed petrographic description with RCA, this study concludes that the reservoir potential of the studied samples is poor. Visual porosity is very low. Precipitation of authigenic minerals and mechanical compaction has had a major effect on reducing the primary intergranular porosity. Fines migration and invasion of fines from the wellbore into the formation should be minimal in the samples studied. Given that the cement of the studied samples is present in minor amounts and predominantly composed of authigenic clays, dissolution of this cement is unlikely. Since smectite or illite/smectite mixed layer were not detected, swelling is unlikely to occur within the samples.

## 2. INTRODUCTION

Esso Australia Ltd submitted 12 core samples from Turrum-7 well for a petrographic study involving detailed thin section description. Detailed thin section description and SEM studies were carried out on all samples. The following is a summary of the aims of this study:

- Undertake thin section descriptions to include sediment classification, description of texture and composition.
- Verify clay types, texture, grain size, shape, pore throat shape, clay matrix and pore bridging/grain coating clay identification using scanning electron microscope (SEM). SEM was used specifically to examine whether any damage effects could have occurred, in particular the morphology of the clay minerals. Particular attention was paid to observing:
  - a) migration and/or mashing of fine clay crystallites in the pore space

- b) corrosion and/or dissolution of framework grains or authigenic phases
  - c) change of habit of existing phases by collapse or swelling
- Presentation of a sediment provenance, style and extent of diagenetic modification and reservoir potential.

### 3. METHODS

Samples were supplied as off-cuts of core materials. Thin sections were cut perpendicular to the bedding plane. All samples were impregnated with blue-stained araldite prior to thin section preparation in order to facilitate porosity recognition. The modal composition for all samples was determined using standard techniques (Zuffa, 1985; Pettijohn et al. 1987) and image analysis using video camera.

All thin sections were stained with Alizarin Red-S and potassium ferricyanide to aid different carbonate assemblages identification (Dickson, 1965) and were stained with sodium cobaltinitrite to differentiate potassium feldspar from plagioclase (Lainz et al. 1964). Classification of clastic rocks was based on the relative proportion of detrital quartz, feldspar and rock fragments (Folk, 1974). Other detrital components, such as mica and heavy minerals, as well as all authigenic phases, are not included in the common sandstone classification.

The type of porosity is reported according to the classification of Schmidt and McDonald (1979). Furthermore, the point count data was compared to the routine core analysis (RCA) data to evaluate the effect of diagenetic modifications on reservoir quality.

X-ray Diffraction (XRD) analyses were carried out on 11 samples. Whole-rock samples were X-rayed for their bulk mineralogy. The samples were crushed in an agate swing mill prior to sub-samples being micronised in a McCrone mill using agate grinding elements and ethanol as a fluid. The samples were then oven-dried at less than 60°C to prevent collapse of clay structures.

Portions of the swing mill powdered samples were dispersed in water to extract the fine fraction containing an enhanced clay fraction. The pipetted fraction was allowed to dry slowly to produce an orientated thin film which was used to identify the clays present in the samples. Two X-ray runs for the clay fraction (< 2 µm) were made: 1) air dried at room temperature, and 2) after exposing the samples to ethylene glycol vapour overnight at 60°.

X-ray analyses for both whole-rock as a randomly orientated powder and orientated clay fraction samples were carried out on a *Philips PW 1840* vertical X-ray Diffractometer system with a *Philips PW 1729* high voltage generator using monochromic Cobalt K<sub>α</sub> radiation, at the following setting: cobalt anode X-ray tube energised at 40kV and 40mA (Fe filtered), scan speed 0.02° 2θ/sec or 1.0° 2θ/min for

the randomly oriented bulk samples and a scan speed  $0.05^\circ$   $2\theta$ /sec or  $2.0^\circ$   $2\theta$ /min for the oriented clay fraction and 0.2 mm receiving slit. The instrument was fitted with an automatic divergence slit. Whole-rock samples were scanned between  $3^\circ$  -  $75^\circ$   $2\theta$ , whilst the oriented clay samples were scanned between  $3^\circ$  -  $40^\circ$   $2\theta$ . Time constant was 1.0 sec.

Mineral identification of both whole-rock samples and clay fraction was checked by comparison with Joint Committee on Powder Diffraction Standards (JCPDS) files using Traces™ software. The identification of clay was based on the position of the main peaks (001, 002, 003 etc.) for each mineral.

A scanning electron microscope equipped with an energy-dispersive X-ray system (SEM-EDS) was used to study six samples after a detailed petrographic study. Samples were examined as fracture mounts. SEM was used specifically to examine the morphology of the clay minerals and the distribution and size of the pore throat.

A summary of all techniques used in this study is presented in Table 1.

**TABLE 1:** Summary of sample details and core analyses of Turrum-7 core samples.

Sample No.	Depth (m)	PETROLOGICAL ANALYSIS					CORE ANALYSIS		
		MA	PM	SEM	XRD	Clay	$\phi$	K	$g/cm^3$
008C	2609.65	*	*		*	*	*	*	*
016C	2610.30	*	*	*	*	*	*	*	*
028C	2611.30	*	*				*	*	*
092C	2616.65	*	*		*	*	*	*	*
100C	2617.25	*	*	*	*	*	*	*	*
V132C	2619.97	*	*	*	*	*	*	*	*
150C	2621.45	*	*	*	*	*	*	*	*
152C	2621.65	*	*		*	*	*	*	*
178C	2623.85	*	*		*	*	*	*	*
210C	2626.45	*	*	*	*	*	*	*	*
234C	2628.45	*	*	*	*	*	*	*	*
244C	2629.27	*	*		*	*	*	*	*

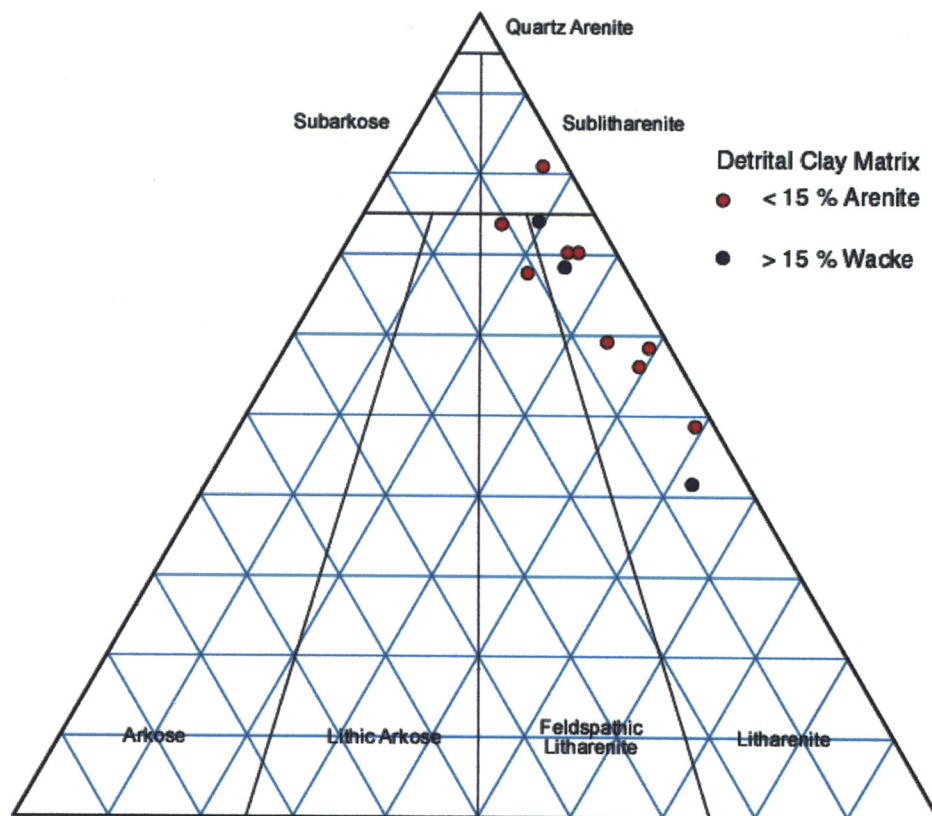
MA = modal analysis, PM = photomicrography, SEM = Scanning electron microscope, XRD = bulk mineralogy, Clay =  $< 2 \mu m$  clay mineralogy,  $\phi$  = core porosity, K = air permeability,  $g/cm^3$  = grain density.

## 4. RESULTS

A summary of the main lithological characteristics of the 12 core samples of Turrum-7 is given in Table 2. Grain size analysis and degree of sorting are presented in Table 3. The modal analysis of detrital, authigenic and porosity components are shown in Tables 4 and 5. Detailed petrographic description of each sample is given in Appendix I. Bulk and less than 2  $\mu\text{m}$  clay fraction mineralogy are presented in Tables 6 and 7, and Appendix II. Routine core analysis (RCA) results are summarised in Table 8. Photomicrographs referenced in the text below are presented at the end of Part A. Representative thin section and SEM photomicrographs of each sample are also given with the relevant thin section description in Appendix I.

### 4.1 Lithology

The Turrum-7 sandstone samples are composed mostly of quartz with considerable amounts of lithic fragments. Feldspar is a minor component most of which is potassium feldspar. The presence of trace to minor amounts of depositional matrix in most of the samples strongly suggests a moderate to low energy sedimentation. The average grain composition of the studied samples is  $Q_{63.8} F_{5.7} R_{30.5}$ . The Turrum-7 sandstones are classified as sublitharenite, feldspathic litharenite, litharenite and lithwacke (Fig. 1).



PE907511\_16

**Figure 1:** QFR ternary diagram showing the present-day framework grain composition of the Turrum-7 sands. Turrum-7 sands are classified as sublitharenite, feldspathic litharenite, litharenite and lithwacke (n = 12 samples), (after Folk, 1974).

**TABLE 2:** Summary of lithological descriptions of Turrum-7 core samples.

Sample No.	Depth (m)	Lithology	Brief Description
008C	2609.65	Litharenite	Creamy to light brown, grain supported, small scale to ripple cross stratification and minor evidence of bioturbation, moderately to well sorted, very fine-grained sandstone. Quartz grains are angular to subrounded. Minor authigenic minerals and very low visual porosity.
016C	2610.30	Litharenite	Creamy, grain supported, small scale cross stratification, well sorted, fine-grained sandstone. Quartz grains are mainly subangular to rounded. Considerable amount of authigenic clays and moderate visual porosity.
028C	2611.30	Sublitharenite	Dark brown to black, grain supported, massive with minor evidence of bioturbation, moderately sorted, silty to very fine-grained sandstone. Quartz grains are angular to subrounded. Considerable amounts of authigenic minerals and low visual porosity.
092C	2616.65	Litharenite	Creamy, grain supported, horizontal to small scale cross stratification, moderately to well sorted, fine-grained sandstone. Quartz grains are mainly subangular to rounded. Authigenic minerals are dominant and low visual porosity.
100C	2617.25	Litharenite	Creamy, grain supported, horizontally laminated to small scale cross stratification, well sorted, fine to medium-grained sandstone. Quartz grains are subangular to rounded. Considerable amounts of authigenic minerals and moderate visual porosity.
V132C	2619.97	Litharenite	Creamy, grain supported, horizontal to small scale cross stratification, well sorted, fine to medium-grained sandstone. Quartz grains are subangular to rounded. Moderate authigenic minerals and moderate visual porosity.
150C	2621.45	Litharenite	Creamy, grain supported, horizontal to small scale cross stratification, moderately to well sorted, medium-grained sandstone. Quartz grains are subangular to rounded. Considerable amounts of authigenic minerals and moderate to low visual porosity.
152C	2621.65	Lithwacke	Creamy to brown, grain supported, horizontal to small scale cross stratification, moderately sorted, very fine-grained sandstone. Quartz grains are angular to subrounded. Moderate authigenic minerals and very low visual porosity.
178C	2623.85	Lithwacke	Creamy to brown, grain supported, horizontal to small scale cross stratification with evidence of local bioturbation, moderately sorted, very fine-grained sandstone. Quartz grains are angular to subrounded. Moderate authigenic minerals and low visual porosity.
210C	2626.45	Feldspathic Litharenite	Creamy, grain supported, horizontal to small scale cross stratification, well sorted, fine to medium-grained sandstone. Quartz grains are subangular to rounded. Considerable amounts of authigenic minerals and moderate visual porosity.
234C	2628.45	Feldspathic Litharenite	Creamy, grain supported, horizontal to small scale cross stratification, well sorted, medium-grained sandstone. Quartz grains are mainly subangular to rounded. Common authigenic minerals and moderate visual porosity.
244C	2629.27	Lithwacke	Creamy to brown, grain supported, moderately sorted, medium-grained sandstone. Quartz grains are mainly angular to subrounded. Moderate authigenic minerals and very low visual porosity.

## 4.2 Texture

The samples show a narrow range of grain size from fine to silty very fine-grained to medium-grained (Table 3). Parallel grain alignment and laminations to small scale cross stratifications are common and occur in continuous to discontinuous thin streaks that best developed in the fine grain samples. The samples are characterised by strongly homogeneous grain fabrics. All samples are grain-supported. The degree of sorting is, in general, moderate to well.

Detrital grains range typically from angular to rounded. All samples underwent severe compaction leading to a predominance of point and suture grain contacts between detrital grains (Plate 1). Ductile deformation during early burial is evident by the presence of squeezed lithic grains and detrital depositional matrix (Plate 2) some mica flakes (Plate 3) and stylolites (Plate 4).

## 4.3 Composition

The framework component of all samples is dominated by monocrystalline quartz (21.4% - 46.4%, Table 4) with an average of  $34.1\% \pm 7.3$  (Table 5). Table 5 summarises the range, average and standard deviation of the main components of the Turrum-7 sandstone samples. Monocrystalline quartz commonly displays strong to slightly undulose extinction and rarely contains vacuoles and trains of vacuoles. Mineral inclusions in quartz grains are rare and comprise acicular rutile or prismatic tourmaline. Polycrystalline quartz grains are present in minor to trace amounts (1.4% - 3.6%, Table 4) with an average of  $2.2\% \pm 0.6$  (Table 5). Polycrystalline quartz grains predominantly occur as equant to subequant rounded coarse grains and display strong undulose extinction.

Feldspar is minor component ranging from 0.8% to 6.2% and an average of  $3.2\% \pm 1.5$  (Table 5). Plagioclase is entirely absent in most studied samples. Lithic grains are common components (6% - 30%) and comprise micaceous metamorphic schist (Plate 5), metaquartzite, rounded sedimentary chert and rare siltstone and claystone. Muscovite is present in minor amounts (2.2% - 10.6%, Table 4) with an average of 5.8% (Table 5), most of which is derived from the disintegration of the micaceous schist rock fragments. It is either disseminated or concentrated along thin laminae parallel to bedding plane (Plate 6). Brown and blue tourmaline and zircon are found as accessory minerals in many samples. Clay depositional matrix constitutes a moderate component (0.8% - 18.8%, Table 4) with an average of 7% (Table 5). It comprises organic rich silty to very fine-grained sandstone (Plate 7) and where abundant it occludes the intergranular porosity (Plate 5). Organic matter and coalified wood particles are present in minor amounts (Plate 7).

Authigenic phases are dominated by siderite (0% - 19.2%) with an average of  $4.1\% \pm 5.6$ . It occurs as micro spar with a grain size ranging between 5 to 20  $\mu\text{m}$ . It fills some of the pore spaces (Plate 8), and coats some of the detrital grains. It also replaces organic matter and organic-rich detrital matrix (Plate 9). Kaolinite (0% to 10.4%) and quartz cements (0% - 10%) are moderate authigenic components with an

average of 4.6% and 2.4% respectively. Kaolinite occurs as pseudo hexagonal book-like crystals filling much of the pore spaces and restricting the primary intergranular porosity (Plate 10). Quartz cement occurs as euhedral to anhedral thick overgrowths in the cleaner part of the samples (Plates 11 and 12). Pyrite is also present in moderate amounts (0% - 18.4%) and occurs as spheroidal aggregates of discrete, equigranular microcrysts; less than one  $\mu\text{m}$  in size (framboidal pyrite). The framboidal pyrite is associated with the argillaceous detrital matrix and organic materials. Pyrite also occurs as large cubes filling some of the pore spaces and replacing both detrital and authigenic grains. Dolomite or ferroan dolomite is present in trace amounts (0% to 2.6%) with an average of  $0.3\% \pm 0.7$ . It occurs as pore filling. It fills locally the pore spaces around the detrital and authigenic minerals (Plate 13).

#### 4.4 XRD Bulk Mineralogy

The X-ray diffraction results of the whole-rock samples are summarised in Table 6. The studied samples are dominated by quartz, major amounts of kaolinite and muscovite (mica including illite), minor to traces amounts of potassium feldspar, siderite and pyrite. The relative abundance of each mineral was assessed by comparison of the main peak heights. The identification of the minerals was based on Joint Committee on Powder Diffraction Standards files (JCPDS) using Traces™ software. It is believed that kaolinite and mica (illite) originated as alteration products of the micaceous metamorphic schist.

#### 4.5 XRD Clay Mineralogy

The clay fraction  $< 2 \mu\text{m}$  mineralogy of the samples studied from Turrum-7 well is presented in Table 7 and Appendix II. XRD patterns of the  $< 2 \mu\text{m}$  size fraction show that minor amounts of clay minerals have been recognised in the studied samples and are dominated by kaolinite and mica (illite). The main peak of kaolinite occurs at  $12.4^\circ 2\theta$  ( $7.14 \text{ \AA}$ ). Glycolation of the samples produced no detectable change of peak positions for both kaolinite and mica (illite).



**TABLE 3:** Summary of the grain size analysis and degree of sorting and angularity of Turrum-7 core samples.

Sample Number	Depth Metre	MGS mm	MGS Phi	MxGS mm	Sorting Degree	Roundness Degree
008C	2609.65	0.10	3.32	0.55	Moderate to Well	Angular to Subrounded
016C	2610.30	0.18	2.47	0.40	Well	Subangular to Rounded
028C	2611.30	0.05	4.32	0.25	Moderate	Angular to Subrounded
092C	2616.65	0.15	2.74	0.30	Moderate to Well	Subangular to Rounded
100C	2617.25	0.26	1.94	0.70	Well	Subangular to Rounded
V132C	2619.97	0.24	2.06	0.65	Well	Subangular to Rounded
150C	2621.45	0.25	2.00	0.50	Moderate to Well	Subangular to Rounded
152C	2621.65	0.05	4.32	0.35	Moderate	Angular to Subrounded
178C	2623.85	0.10	3.32	0.50	Moderate	Angular to Subrounded
210C	2626.45	0.20	2.32	0.60	Well	Subangular to Rounded
234C	2628.45	0.30	1.74	0.80	Well	Subangular to Rounded
244C	2629.27	0.15	2.74	0.45	Moderate	Angular to Subrounded

MGS = average grain size, MxGS = maximum grain size.

**TABLE 4:** Composition of Turrum-7 core samples. All values are in per cent based on image analysis.

Sample Number	008C	016C	028C	092C	100C	V132C
Depth (m)	2609.65	2610.30	2611.30	2616.65	2617.25	2619.97
Lithology	Litharenite	Sublitharenite	Sublitharenite	Litharenite	Litharenite	Litharenite
Grain Size (mm)	0.10	0.18	0.05	0.15	0.26	0.24
Sorting	Mod to Well	Well	Moderate	Mod to Well	Well	Well
<b>Framework Grains (TOTFWG)</b>						
<b>QUARTZ (TOTQTZG)</b>						
Mono (QZMO)	46.4	42.6	27.2	34.6	29.4	31.0
Poly (QZPO)	1.4	2.2	1.6	2.8	3.6	2.8
Undif. (QZUD)	0.0	0.0	0.0	0.0	0.0	0.0
<b>FELDSPAR (TOTFSP)</b>						
K-Spar (KSKE)	2.8	3.6	0.8	1.6	2.8	3.0
Plag. (FSPL)	0.0	0.0	0.0	0.0	0.0	0.4
Plutonic (FSPL)	0.0	0.0	0.0	0.0	0.0	0.0
Intergrowths (FSIG)	0.0	0.0	0.0	0.0	0.0	0.0
Undif. (FSUD)	0.0	0.0	0.0	0.0	0.0	0.0
<b>ROCK FRAGMENTS (TOTRKF)</b>						
<b>SEDIMENTARY (TOTSRKF)</b>						
Carbonate (RSCB)	0.0	0.0	0.0	0.0	0.0	0.0
Clay-Rich (RSCL)	0.0	0.0	0.0	0.4	0.0	0.0
Chert (RSCT)	0.4	0.8	0.4	1.0	1.0	0.8
Quartz-Rich (RSQZ)	0.0	0.0	0.0	0.0	0.0	0.0
Undif. (RSUN)	0.0	0.0	0.0	0.0	0.0	0.0
<b>METAMORPHIC (TOTMRKF)</b>						
Mica-Poor (RMMP)	1.4	2.0	0.8	1.6	2.2	1.6
Mica-Rich (RMIMR)	16.0	12.2	4.8	21.8	19.6	17.4
Undif. (RMUN)	0.0	0.0	0.0	0.0	0.0	0.0
<b>VOLCANIC (TOTVRKF)</b>						
Felsic (RVFS)	0.0	0.8	0.0	0.4	0.4	0.2
Mafic (RVMF)	0.0	0.0	0.0	0.0	0.0	0.0
Undif. (RVUN)	0.0	0.0	0.0	0.0	0.0	0.0
Undif. (RFUN)	0.0	0.0	0.0	0.0	0.0	0.0

**TABLE 4:** Composition of Turrum-7 core samples. All values are in per cent based on image analysis. (Continued)

Sample Number	008C	016C	028C	092C	100C	V132C
Depth (m)	2609.65	2610.30	2611.30	2616.65	2617.25	2619.97
<b>OTHER GRAINS (TOTOGS)</b>						
Glaucony (OGGL)	0.0	0.0	0.0	0.0	0.0	0.0
Fossils & Shells (OGFL)	0.0	0.0	0.0	0.0	0.0	0.0
Heavy/Opaque (OGHV)	0.8	0.8	0.4	0.6	0.0	1.2
Biotite (OMBT)	0.6	0.4	Tr	Tr	Tr	0.0
Muscovite (OMMS)	6.2	4.2	2.2	5.4	4.2	9.4
Undif. Micas (OMUN)	0.0	0.0	0.0	0.0	0.0	0.0
Phosphatic (OGPH)	0.0	0.0	0.0	0.0	0.0	0.0
Plant (OGPL)	0.0	0.0	0.0	0.0	0.0	0.0
<b>UNDIFFERENTIATED (GRUN)</b>						
<b>TOTAL POREFILL (TOTPF)</b>						
<b>TOTAL MATRIX (TOTMXP)</b>						
<b>DETITAL MATRIX (DEMTX)</b>						
Carbonate (MXCB)	0.0	0.0	0.0	0.0	0.0	0.0
Clay (MXCL)	8.8	0.8	3.8	5.2	1.2	4.8
Organic (MXOR)	3.0	0.6	2.6	3.8	1.0	2.0
Siliceous (MXSI)	0.0	0.0	0.0	0.0	0.0	0.0
Undif. (MXUN)	0.0	0.0	0.0	0.0	0.0	0.0
<b>AUTHIGENIC CLAYS (TOTCLAY)</b>						
Chlorite (CLCH)	0.0	0.0	0.0	0.0	0.0	0.0
Illite/Smectite (CLIS)	Tr	Tr	Tr	Tr	Tr	Tr
Kaolinite (CLKT)	2.8	7.6	0.0	4.0	5.0	5.6
Undif. (CLUN)	0.0	0.0	0.0	0.0	0.0	0.0
<b>TOTAL POREFILL CEMENTS (TOTPFCMT)</b>						
<b>CARBONATE CEMENTS (TOTCARB)</b>						
Calcite (CBCA)	0.0	0.0	0.0	0.0	0.0	0.0
Dolomite (CBDO)	0.0	0.0	0.0	0.0	0.0	Tr
Siderite (CBSD)	0.0	0.0	19.2	1.2	7.2	2.0
Undif. (CBUN)	0.0	0.0	0.0	0.0	0.0	0.0

**TABLE 4:** Composition of Turrum-7 core samples. All values are in per cent based on image analysis. (Continued)

Sample Number	008C	016C	028C	092C	100C	V132C
Depth (m)	2609.65	2610.30	2611.30	2616.65	2617.25	2619.97
<b>QUARTZ &amp; FELDSPAR CEMENTS (TOTSIIL)</b>						
Quartz (CMQZ)	Tr	6.8	1.4	Tr	7.4	1.2
Other Siliceous (CMSI)	0.0	0.0	0.0	0.0	0.0	0.0
Feldspar (CMFS)	0.0	0.0	0.0	0.0	0.0	0.0
<b>OTHER CEMENTS (TOTOCMT)</b>						
Anhydrite/Gypsum (CMAN)	0.0	0.0	0.0	0.0	0.0	0.0
Hydrocarbons (CMHC)	0.0	0.0	0.0	0.0	0.0	0.0
Pyrite (CMPY)	2.0	0.8	5.0	1.8	0.8	2.0
Iron Oxide (CM FE)	Tr	Tr	0.0	Tr	Tr	0.0
Zeolite (CMZE)	0.0	0.0	0.0	0.0	0.0	0.0
Undif. (CMUN)	0.0	0.0	0.0	0.0	0.0	0.0
<b>REPLACEMENT (TOTREP)</b>						
<b>CARBONATE (TOTRCARB)</b>						
Calcite (ICCA)	0.0	0.0	0.0	0.0	0.0	0.0
Dolomite (ICDO)	0.0	0.0	0.0	0.0	0.0	0.0
Siderite (ICSD)	0.0	0.0	8.4	4.2	4.0	2.6
Undif. (ICUN)	0.0	0.0	0.0	0.0	0.0	0.0
<b>CLAYS (TOTCLAY)</b>						
Chlorite (IRCH)	0.0	0.0	0.0	0.0	0.0	0.0
Kaolinite (IRKT)	1.0	1.6	Tr	1.8	1.4	2.6
Illite/Smectite (IRIS)	Tr	Tr	Tr	Tr	Tr	Tr
Undif. (IRCL)	0.0	0.0	0.0	0.0	0.0	0.0
<b>SILICA (TOTRSIL)</b>						
QTZ, CHERT, OPAL or Chalcedony (IRSI)	0.0	0.0	0.0	0.0	0.0	0.0
<b>OTHER (TOTORREP)</b>						
Pyrite (IRPY)	2.6	1.2	18.4	3.2	Tr	1.0
Zeolite (IRZE)	0.0	0.0	0.0	0.0	0.0	0.0
Undif. (IRUN)	0.0	0.0	0.0	0.0	0.0	0.0

**TABLE 4:** Composition of Turrum-7 core samples. All values are in per cent based on image analysis. (Continued)

Sample Number	008C	016C	028C	092C	100C	V132C
Depth (m)	2609.65	2610.30	2611.30	2616.65	2617.25	2619.97
<b>POROSITY (TOTPORO)</b>						
Primary Intergranular (PVIG)	2.8	8.8	2.2	3.2	6.8	7.2
Primary Intragranular (PVPR)	0.0	0.0	0.0	0.0	0.0	0.0
Fracture (PVFR)	0.0	0.0	0.0	0.0	0.0	0.0
Undif. (PVUN)	0.0	0.0	0.0	0.0	0.0	0.0
Secondary Intergranular (PVSE)	1.0	2.2	0.8	1.4	2.0	1.2
Secondary Intragranular (PVSC)	Tr	Tr	Tr	Tr	Tr	Tr

907511 ~~165~~  
165

TABLE 4: Composition of Turrum-7 core samples. All values are in per cent based on image analysis. (Continued)

Sample Number	150C	152C	178C	210C	234C	244C
Depth (m)	2621.45	2621.65	2623.85	2626.45	2628.45	2629.27
Lithology	Litharenite	Litharenite	Sublitharenite	Feldspathic Litharenite	Feldspathic Litharenite	Litharenite
Grain Size (mm)	0.25	0.05	0.10	0.20	0.30	0.15
Sorting	Mod to Well	Moderate	Moderate	Well	Well	Moderate
<b>Framework Grains (TOTFWG)</b>						
<b>QUARTZ (TOTQTZG)</b>						
Mono (QZMO)	27.0	21.4	41.2	36.6	34.4	37.6
Poly (QZPO)	2.4	1.4	2.0	2.4	2.4	1.8
Undif. (QZUD)	0.0	0.0	0.0	0.0	0.0	0.0
<b>FELDSPAR (TOTFSP)</b>						
K-Spar (KSKF)	1.8	2.8	3.8	6.2	5.4	4.2
Plag. (FSPL)	0.0	0.0	0.0	0.0	0.0	0.0
Plutonic (FSPR)	0.0	0.0	0.0	0.0	0.0	0.0
Intergrowths (FSIG)	0.0	0.0	0.0	0.0	0.0	0.0
Undif. (FSUD)	0.0	0.0	0.0	0.0	0.0	0.0
<b>ROCK FRAGMENTS (TOTRKF)</b>						
<b>SEDIMENTARY (TOTSRKF)</b>						
Carbonate (RSCB)	0.0	0.0	0.0	0.0	0.0	0.0
Clay-Rich (RSCL)	0.4	0.0	0.2	0.0	0.0	0.6
Chert (RSCT)	0.6	0.8	0.4	1.0	Tr	0.8
Quartz-Rich (RSQZ)	0.0	0.0	0.0	0.0	0.0	0.0
Undif. (RSUN)	0.0	0.0	0.0	0.0	0.0	0.0
<b>METAMORPHIC (TOTMRKF)</b>						
Mica-Poor (RMMP)	1.0	2.8	0.6	1.0	1.2	1.0
Mica-Rich (RMMR)	27.4	25.2	10.0	10.4	6.6	11.8
Undif. (RMUN)	0.0	0.0	0.0	0.0	0.0	0.0
<b>VOLCANIC (TOTVRKF)</b>						
Felsic (RVFS)	0.6	0.0	0.4	0.4	0.4	0.4
Mafic (RVMF)	0.0	0.0	0.0	0.0	0.0	0.0
Undif. (RVUN)	0.0	0.0	0.0	0.0	0.0	0.0
Undif. (RFUN)	0.0	0.0	0.0	0.0	0.0	0.0

**TABLE 4:** Composition of Turrum-7 core samples. All values are in per cent based on image analysis. (Continued)

Sample Number	150C	152C	178C	210C	234C	244C
Depth (m)	2621.45	2621.65	2623.85	2626.45	2628.45	2629.27
<b>OTHER GRAINS (TOTOGS)</b>						
Glaucony (OGGL)	0.0	0.0	0.0	0.0	0.0	0.0
Fossils & Shells (OGFL)	0.0	0.0	0.0	0.0	0.0	0.0
Heavy/Opaque (OGHV)	1.0	0.6	0.8	1.0	0.8	0.4
Biotite (OMBT)	Tr	0.4	0.0	0.0	0.0	0.0
Muscovite (OMMS)	4.6	10.6	5.8	7.0	4.2	6.2
Undif. Micas (OMUN)	0.0	0.0	0.0	0.0	0.0	0.0
Phosphatic (OGPH)	0.0	0.0	0.0	0.0	0.0	0.0
Plant (OGPL)	0.0	0.0	0.0	0.0	0.0	0.0
<b>UNDIFFERENTIATED (GRUN)</b>						
<b>TOTAL POREFILL (TOTPF)</b>						
<b>TOTAL MATRIX (TOTMXP)</b>						
<b>DETRITAL MATRIX (DETMX)</b>						
Carbonate (MXCB)	0.0	0.0	0.0	0.0	0.0	0.0
Clay (MXCL)	5.2	18.8	15.2	1.2	1.2	17.8
Organic (MXOR)	0.0	3.6	1.4	0.8	0.8	3.0
Siliceous (MXSI)	0.0	0.0	0.0	0.0	0.0	0.0
Undif. (MXUN)	0.0	0.0	0.0	0.0	0.0	0.0
<b>AUTHIGENIC CLAYS (TOTCLAY)</b>						
Chlorite (CLCH)	0.0	0.0	0.0	0.0	0.0	0.0
Illite/Smectite (CLIS)	Tr	Tr	Tr	Tr	Tr	Tr
Kaolinite (CLKT)	6.0	1.6	4.0	5.8	10.4	2.6
Undif. (CLUN)	0.0	0.0	0.0	0.0	0.0	0.0
<b>TOTAL POREFILL CEMENTS (TOTPFCMT)</b>						
<b>CARBONATE CEMENTS (TOTCARB)</b>						
Calcite (CBCA)	0.0	0.0	0.0	0.0	0.0	0.0
Dolomite (CBDO)	0.0	0.0	0.4	2.6	0.0	0.0
Siderite (CBSD)	3.4	Tr	3.0	9.6	1.4	2.2
Undif. (CBUN)	0.0	0.0	0.0	0.0	0.0	0.0

**TABLE 4:** Composition of Turrum-7 core samples. All values are in per cent based on image analysis. (Continued)

Sample Number	150C	152C	178C	210C	234C	244C
Depth (m)	2621.45	2621.65	2623.85	2626.45	2628.45	2629.27
<b>QUARTZ &amp; FELDSPAR CEMENTS (TOTSIIL)</b>						
Quartz (CMQZ)	0.0	0.0	0.0	Tr	10.0	2.2
Other Siliceous (CMSI)	0.0	0.0	0.0	0.0	0.0	0.0
Feldspar (CMFS)	0.0	0.0	0.0	0.0	0.0	0.0
<b>OTHER CEMENTS (TOTOCMT)</b>						
Anhydrite/Gypsum (CMAN)	0.0	0.0	0.0	0.0	0.0	0.0
Hydrocarbons (CMHC)	Tr	0.0	0.0	0.0	4.0	0.0
Pyrite (CMPY)	1.8	Tr	1.2	0.8	2.2	1.2
Iron Oxide (CMFE)	Tr	0.0	0.0	0.0	0.0	0.0
Zeolite (CMZE)	0.0	0.0	0.0	0.0	0.0	0.0
Undif. (CMUN)	0.0	0.0	0.0	0.0	0.0	0.0
<b>REPLACEMENT (TOTREP)</b>						
<b>CARBONATE (TOTRCARB)</b>						
Calcite (ICCA)	0.0	0.0	0.0	0.0	0.0	0.0
Dolomite (ICDO)	0.0	0.0	Tr	0.0	0.0	0.0
Siderite (ICSD)	3.8	3.6	1.8	3.6	1.4	Tr
Undif. (ICUN)	0.0	0.0	0.0	0.0	0.0	0.0
<b>CLAYS (TOTCLAY)</b>						
Chlorite (IRCH)	0.0	0.0	0.0	0.0	0.0	0.0
Kaolinite (IRKT)	5.4	1.8	1.4	1.8	4.6	2.0
Illite/Smectite (IRIS)	Tr	Tr	Tr	Tr	Tr	Tr
Undif. (IRCL)	0.0	0.0	0.0	0.0	0.0	0.0
<b>SILICA (TOTRSIL)</b>						
QTZ, CHERT, OPAL or Chalcedony (IRSI)	0.0	0.0	0.0	0.0	0.0	0.0
<b>OTHER (TOTORREP)</b>						
Pyrite (IRPY)	2.2	4.6	2.6	1.4	0.6	1.0
Zeolite (IRZE)	0.0	0.0	0.0	0.0	0.0	0.0
Undif. (IRUN)	0.0	0.0	0.0	0.0	0.0	0.0



**TABLE 4:** Composition of Turrum-7 core samples. All values are in per cent based on image analysis. (Continued)

Sample Number	150C	152C	178C	210C	234C	244C
Depth (m)	2621.45	2621.65	2623.85	2626.45	2628.45	2629.27
<b>POROSITY (TOTPORO)</b>						
Primary Intergranular (PVIG)	3.8	Tr	3.0	4.8	6.8	2.4
Primary Intragranular (PVPR)	0.0	0.0	0.0	0.0	0.0	0.0
Fracture (PVFR)	0.0	0.0	0.0	0.0	0.0	0.0
Undif. (PVUN)	0.0	0.0	0.0	0.0	0.0	0.0
Secondary Intergranular (PVSE)	1.6	Tr	0.8	1.6	1.2	0.8
Secondary Intragranular (PVSC)	Tr	Tr	Tr	Tr	Tr	Tr

**TABLE 5:** Summary of the modal analysis of Turrum-7 core samples.

	Average	Min	Max	STDEV
<b>Framework Grains (TOTFWG)</b>				
<b>QUARTZ (TOTQTZG)</b>				
Mono (QZMO)	34.1	21.4	46.4	7.3
Poly (QZPO)	2.2	1.4	3.6	0.6
Undif. (QZUD)	0.0	0.0	0.0	0.0
<b>FELDSPAR (TOTFSP)</b>				
K-Spar (KSKF)	3.2	0.8	6.2	1.5
Plag. (FSPL)	0.03	0.0	0.4	0.1
Plutonic (FSPL)	0.0	0.0	0.0	0.0
Intergrowths (FSIG)	0.0	0.0	0.0	0.0
Undif. (FSUD)	0.0	0.0	0.0	0.0
<b>ROCK FRAGMENTS (TOTRKF)</b>				
<b>SEDIMENTARY (TOTSRKF)</b>				
Carbonate (RSCB)	0.0	0.0	0.0	0.0
Clay-Rich (RSCL)	0.1	0.0	0.6	0.2
Chert (RSCT)	0.7	0.0	1.0	0.3
Quartz-Rich (RSQZ)	0.0	0.0	0.0	0.0
Undif. (RSUN)	0.0	0.0	0.0	0.0
<b>METAMORPHIC (TOTMRKF)</b>				
Mica-Poor (RMMP)	1.4	0.6	2.8	0.6
Mica-Rich (RMMR)	15.3	4.8	27.4	7.2
Undif. (RMUN)	0.0	0.0	0.0	0.0
<b>VOLCANIC (TOTVRKF)</b>				
Felsic (RVFS)	0.3	0.0	0.8	0.2
Mafic (RVMF)	0.0	0.0	0.0	0.0
Undif. (RVUN)	0.0	0.0	0.0	0.0
Undif. (RFUN)	0.0	0.0	0.0	0.0

**TABLE 5:** Summary of the modal analysis of Turrum-7 core samples. (Continued)

	Average	Min	Max	STDEV
<b>OTHER GRAINS (TOTOGS)</b>				
Glaucouy (OGGL)	0.0	0.0	0.0	0.0
Fossils & Shells (OGFL)	0.0	0.0	0.0	0.0
Heavy/Opaque (OGHV)	0.7	0.0	1.2	0.3
Biotite (OMBT)	0.1	0.0	0.6	0.2
Muscovite (OMMS)	5.8	2.2	10.6	2.3
Undif. Micas (OMUN)	0.0	0.0	0.0	0.0
Phosphatic (OGPH)	0.0	0.0	0.0	0.0
Plant (OGPL)	0.0	0.0	0.0	0.0
<b>UNDIFFERENTIATED (GRUN)</b>				
<b>TOTAL POREFILL (TOTPF)</b>				
<b>TOTAL MATRIX (TOTMXP)</b>				
<b>DETRITAL MATRIX (DEMTX)</b>				
Carbonate (MXCB)	0.0	0.0	0.0	0.0
Clay (MXCL)	7.0	0.8	18.8	6.7
Organic (MXOR)	1.9	0.0	3.8	1.3
Siliceous (MXSI)	0.0	0.0	0.0	0.0
Undif. (MXUN)	0.0	0.0	0.0	0.0
<b>AUTHIGENIC CLAYS (TOTCLAY)</b>				
Chlorite (CLCH)	0.0	0.0	0.0	0.0
Illite/Smectite (CLIS)	0.0	0.0	0.0	0.0
Kaolinite (CLKT)	4.6	0.0	10.4	2.8
Undif. (CLUN)	0.0	0.0	0.0	0.0
<b>TOTAL POREFILL CEMENTS (TOTPFCMT)</b>				
<b>CARBONATE CEMENTS (TOTCARB)</b>				
Calcite (CBCA)	0.0	0.0	0.0	0.0
Dolomite (CBDO)	0.3	0.0	2.6	0.7
Siderite (CBSD)	4.1	0.0	19.2	5.6
Undif. (CBUN)	0.0	0.0	0.0	0.0

**TABLE 5:** Summary of the modal analysis of Turrum-7 core samples. (Continued)

		Average	Min	Max	STDEV
<b>QUARTZ &amp; FELDSPAR CEMENTS (TOTSILJ)</b>					
	Quartz (CMQZ)	2.4	0.0	10.0	3.6
	Other Siliceous (CMSI)	0.0	0.0	0.0	0.0
	Feldspar (CMFS)	0.0	0.0	0.0	0.0
<b>OTHER CEMENTS (TOTOCMT)</b>					
	Anhydrite/Gypsum (CMAN)	0.0	0.0	0.0	0.0
	Hydrocarbons (CMHC)	0.3	0.0	4.0	1.2
	Pyrite (CMPY)	1.6	0.0	5.0	1.2
	Iron Oxide (CM FE)	0.0	0.0	0.0	0.0
	Zeolite (CMZE)	0.0	0.0	0.0	0.0
	Undif. (CMUN)	0.0	0.0	0.0	0.0
<b>REPLACEMENT (TOTREP)</b>					
<b>CARBONATE (TOTRCARB)</b>					
	Calcite (ICCA)	0.0	0.0	0.0	0.0
	Dolomite (ICDO)	0.0	0.0	0.0	0.0
	Siderite (ICSD)	2.8	0.0	8.4	2.4
	Undif. (ICUN)	0.0	0.0	0.0	0.0
<b>CLAYS (TOTCLAY)</b>					
	Chlorite (IRCH)	0.0	0.0	0.0	0.0
	Kaolinite (IRKT)	2.1	0.0	5.4	1.5
	Illite/Smectite (IRIS)	0.0	0.0	0.0	0.0
	Undif. (IRCL)	0.0	0.0	0.0	0.0
<b>SILICA (TOTRSILJ)</b>					
	QTZ, CHERT, OPAL or Chalcedony (IRSI)	0.0	0.0	0.0	0.0
<b>OTHER (TOTORREP)</b>					
	Pyrite (IRPY)	3.2	0.0	18.4	4.9
	Zeolite (IRZE)	0.0	0.0	0.0	0.0
	Undif. (IRUN)	0.0	0.0	0.0	0.0

**TABLE 5:** Summary of the modal analysis of Turrum-7 core samples. (Continued)

	Average	Min	Max	STDEV
<b>POROSITY (TOTPORO)</b>				
Primary Intergranular (PVIC)	4.7	2.2	8.8	2.3
Primary Intragranular (PVPR)	0.0	0.0	0.0	0.0
Fracture (PVFR)	0.0	0.0	0.0	0.0
Undif. (PVUN)	0.0	0.0	0.0	0.0
Secondary Intergranular (PVSE)	1.3	0.8	2.2	0.5
Secondary Intragranular (PVSC)	0.0	0.0	0.0	0.0

Min = minimum, Max = maximum STDEV = standard deviation.

**TABLE 6:** Qualitative bulk XRD results from selected core samples from Turrum-7.

Sample Number	Depth (metre)	Quartz	Kaolinite	Muscovite (and Illite)	K-feldspar	Pyrite	Siderite
008c	2609.65m	A	M	M	T		
016c	2610.3m	A	M	M	T	T	
092c	2616.65m	A	M	M			
100c	2617.25m	A	M	M	T	T	m
V132c	2619.97m	A	M	M	m		
150c	2621.45m	A	M	M	T		
152c	2621.65m	A	M	M	T		
178c	2632.85m	A	M	M	T		
210c	2626.45m	A	M	M	T		
234c	2628.45m	A (60%)	M (20%)	M (14%)	T (0.5%)		M (5%)
244c	2629.27m	A	M	M	T	T	

A = abundant (nominally more than 40 wt%), M = major (nominally > 10%), m = minor (nominally > 1%, < 10%), T = trace (nominally < 1%).

**TABLE 7:** Qualitative clay XRD results from selected core samples from Turrum-7 well.

Sample Number	Depth (metre)	Kaolinite	Chlorite	Muscovite Including Illite	Illite/Smectite	Smectite
008C	2609.65m	M		M		
016C	2610.3m	M		M		
092C	2616.65m	M		M		
100C	2617.25m	M		M		
V132C	2619.97m	M		M		
150C	2621.45m	M		M		
152C	2621.65m	M		M		
178C	2632.85m	M		M		
210C	2626.45m	M		M		
234C	2628.45m	M		M		
244C	2629.27m	M		m		

A = abundant (nominally more than 40 wt%), M = major (nominally > 10%), m = minor (nominally > 1%, < 10%), T = trace (nominally < 1%).

#### 4.6 Scanning Electron Microscopy (SEM)

The samples comprise a fine to medium-grained, moderately to well sorted sandstone with moderate amounts of authigenic clay mineral assemblage. Kaolinite and illite are the most common form of authigenic clays. Kaolinite occurs as fine to large pseudo hexagonal book-like crystals, ranging in size from 5  $\mu\text{m}$  up to 20  $\mu\text{m}$  (Plate 10). It occurs as pore filling, filling much of the pore spaces and pore throat and restricting the reservoir quality. Kaolinite also occurs around altered ductile lithic fragments and around altered feldspar grains, suggesting a direct relation between these components (Plate 14). Illite occurs as a late fibrous to hairy crystals around kaolinite and altered lithic fragments and altered feldspar grains (Plates 14 and 15). Illite crystals range in size from less than 1  $\mu\text{m}$  up to 5  $\mu\text{m}$ . They are bridging the pore spaces (Plate 16) and throats and reducing permeability. Fines migration and invasion of fines from the wellbore into the formation should be minimal in the samples studied. Given that the cement of the studied samples is predominantly composed of authigenic clays, dissolution of this cement is unlikely. Since smectite or illite/smectite mixed layer were not detected, swelling is unlikely to occur within the samples. SEM has also shown that quartz overgrowths are minor and has locally reduced the reservoir quality (Plate 12).

Based on SEM observations, most samples of Turrum-7 have fair to low amounts of porosity. The pores are small, most of which are less than 10  $\mu\text{m}$  and occasionally less than 1  $\mu\text{m}$  (Plate 12). The distribution of the pore throat is irregular with poor interconnection implying very poor permeability (Fig.2). The pores are poorly interconnected in a 3-D network giving poor permeability (Plate 17) and have triangular shape suggesting that most of the pores are of intergranular primary origin. Secondary porosity development is resulted from partial to complete dissolution of feldspar grains and ductile lithic fragments. Feldspar displays skeletal or sieve to honeycomb structure suggesting severe dissolution (Plate 18). Fine, and a few loose, kaolinite plates could possibly move to block additional pore throats during fluid migration. In some clean samples, fines migration during fluid extraction may cause a reduction in permeability since the size of the fines is similar to, or smaller than, most of the pore throats.

Figure 2 is an overview providing detailed texture, reservoir properties of six selected samples for SEM studies.

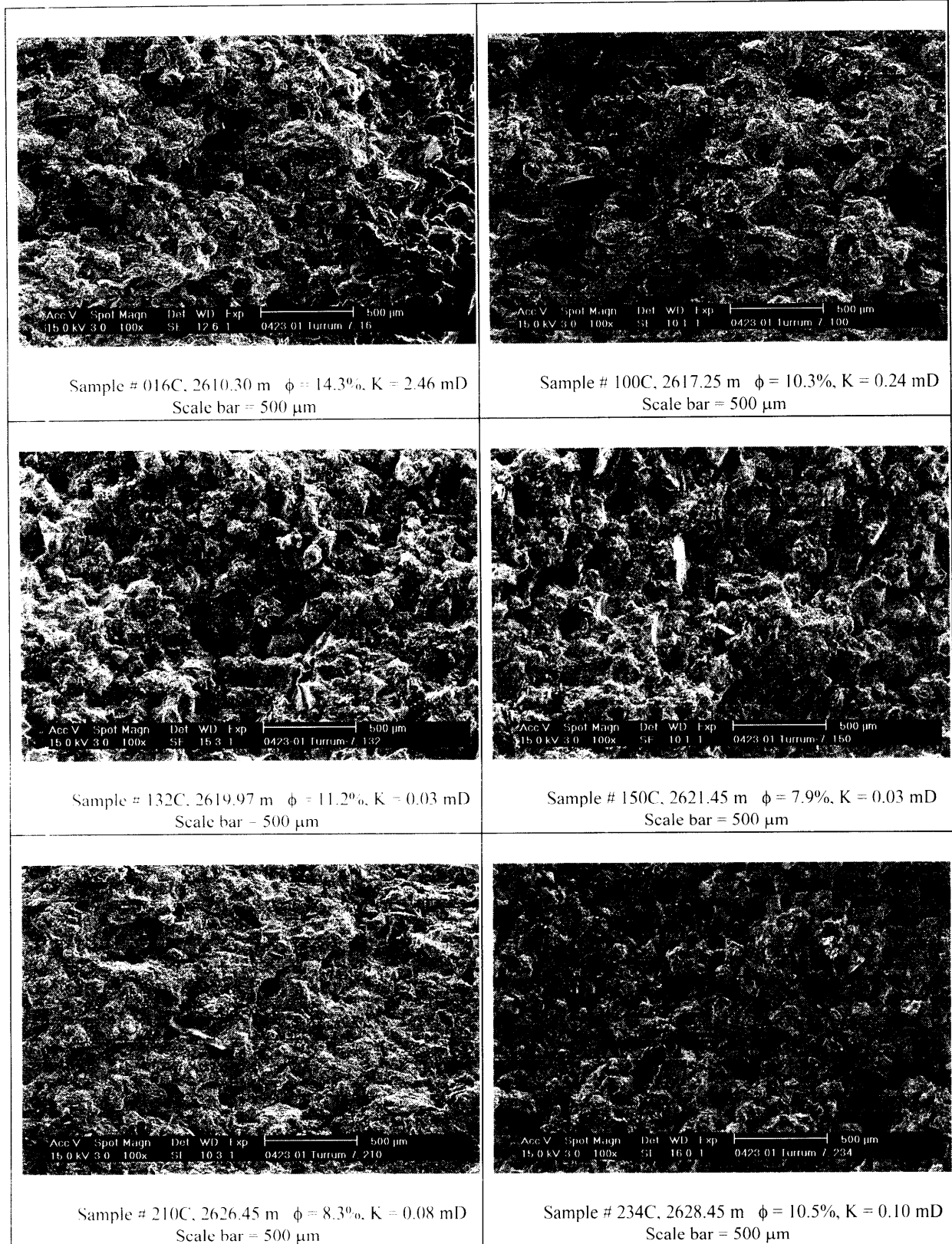


**Figure 2.** Overview of textural characteristics and reservoir parameters of selected core samples from Turrum-7.



#### 4.7 Diagenesis

Only the major diagenetic events are summarised below and the reader is referred to the thin section descriptions in Appendix I for a detailed discussion. As far as possible, diagenetic processes are discussed in chronological order. The following gives the relative timing of authigenic minerals and other diagenetic modifications observed during petrographic study.

- Early compaction has affected all samples and has resulted in closer packing of grains and well-developed parallel alignment of elongated detrital grains.
- Framboidal pyrite could have occurred during the early sulphate reduction.
- Micro spar siderite cement occurred early in the diagenetic history at the end of the early sulphate reduction.
- Alteration and dissolution of feldspar, ductile lithic fragments and mica could have been responsible for the formation of kaolin.
- After kaolin precipitation quartz cements have occurred as overgrowths. The quartz overgrowths postdated or at least formed simultaneously with the precipitation of kaolin.
- Traces of ferroan dolomite have formed later in the diagenetic history probably during the late reduction.
- Alteration of lithic fragments and potassium feldspar has continued to the late stage of diagenetic history and this has resulted in development of local secondary porosity and precipitation of authigenic illite. Authigenic illite occurs as fibrous to hairy crystals on the surface of kaolinite and altered feldspar grains and ductile lithic fragments. It also bridges the pore spaces and pore throats.
- Later in the diagenetic history, large cubic crystalline pyrite has occurred as pore filling around thin coal beds, organic-rich detrital matrix and coalified wood materials.

#### 4.8 Reservoir Quality

The results from routine core analysis (RCA) show that porosity for the studied samples ranges from 2.8% to 14.3% and air permeability ranges from 0 mD to 2.46 mD. Many of Turrum-7 sandstones are matrix-rich and have fair to poor reservoir characteristics.

Petrographic observations reveal that porosity is moderate to very low and presents mainly as primary pores as well as microporosity. Visible porosity dominantly occurs as primary intergranular porosity (Plate 19) and has been largely occluded by both compactional and cementation processes. Secondary pores are less dominant and comprise enlarged and elongated pores. Secondary porosity is mostly resulted from partial to complete dissolution of potassium feldspar. Potassium feldspar displays some sieve and skeletal structures (Plate 20), suggesting partial dissolution to increase

the visual porosity. Kaolinite and altered ductile lithic fragments contain considerable amounts of microporosity. There is a good relationship between total porosity and estimated visual porosity (Fig. 3) and between air permeability and visual porosity (Fig. 4).

The porosity of all samples is low to fair and depends upon a combination of texture, original framework components and diagenesis involving compaction.

The textural control on the reservoir quality is clear and is indicated by the relationship between grain size and both total porosity and air permeability on the other side (Figs 5 and 6). Many of the studied samples are matrix-rich (Table 4). Detrital matrix, including organic matter, has one of the major controls on the reservoir quality of Turrum-7 sandstones. The relatively good inverse relationship between total detrital matrix and air permeability suggests that the original framework components has occluded both total porosity (Fig. 7) and air permeability (Fig. 8).

Compaction is severe and is evident by concavo-convex, suture grain contacts, rearrangement of the grains, as well as by squeezed ductile deformation of lithic fragments, bent mica flakes and the presence of stylolites (Plates 1, 2, 3 and 4). Compaction processes have contributed to the porosity loss and destroyed up to 96% of the intergranular porosity. The intergranular volume (IGV) versus total cement diagram of Houseknecht (1987, 1989), modified by Ehrenberg (1989, 1990), was used to evaluate the effect of compaction processes on reservoir quality. The original porosity of the samples was assumed to be 40%. The grain size analysis shows that Turrum-7 sandstones are in general, moderately to well sorted and displays a unimodal grain-size distribution.

The IGV and total cement mean value data are shown in Table 9. The IGV versus total cement diagram (Fig. 9) of Turrum-7 sandstones shows that both compaction and cementation processes have played significant roles in destroying the original intergranular porosity. The mean values of the IGV and total cement are 17.7% and 13.4% respectively, Table 9. This means that, on average, around 56% of the intergranular porosity has been lost by compaction processes, whereas cementation has removed, on average, 33% of the intergranular porosity. Both processes in combination have destroyed, on average, 89% of the intergranular porosity. Therefore the remaining intergranular primary porosity, on average, is slightly less than 5%.

Precipitation of authigenic minerals (particularly siderite and kaolinite) has further contributed to the porosity loss by up to 70% of the primary intergranular porosity (Fig. 9).

**TABLE 8:** Routine core analysis (RCA) results for the Turrum-7 core samples near the selected core samples for petrographic study.

Sample Number	Depth (metres)	Permeability to Air (milliDarcys)	Porosity (per cent)	Grain Density	
				Calculated (g/cm <sup>3</sup> )	Absolute (g/cm <sup>3</sup> )
7	2609.65	0.01	6.7	2.64	2.64
15	2610.30	2.46	14.3	2.68	2.66
27	2611.30	0.01	5.6	2.97	3.07
91	2616.65	0.01	6.5	2.64	2.64
99	2617.25	0.24	10.3	2.72	2.72
131V	2619.97	0.03	11.2	2.68	2.65
149	2621.45	0.03	7.9	2.67	2.67
151	2621.65	0.00	2.8	2.63	2.65
177	2623.85	0.01	5.8	2.65	2.64
209	2626.45	0.08	8.3	2.73	2.75
233	2628.45	0.10	10.5	2.67	2.68
243	2629.27	0.03	4.9	2.65	2.66

**TABLE 9.** The effect of mechanical compaction and cementation processes on the primary intergranular porosity of the Turrum-7 sandstones.

Sample No.	Depth (m)	Total Cement (%)	IGV (%)	PDTC <sup>1</sup> (%)	PDMC <sup>2</sup> (%)
008C	2609.65	4.8	7.6	12.0	81.0
016C	2610.30	15.2	24.0	38.0	40.0
028C	2611.30	25.6	27.8	64.0	30.5
092C	2616.65	7.0	10.2	17.5	74.5
100C	2617.25	20.4	27.2	51.0	32.0
V132C	2619.97	10.8	18.0	27.0	55.0
150C	2621.45	11.2	15.0	28.0	62.5
152C	2621.65	1.6	1.6	4.0	96.0
178C	2623.85	8.6	11.6	21.5	71.0
210C	2626.45	18.8	23.6	47.0	41.0
234C	2628.45	28.0	34.8	70.0	13.0
244C	2629.27	8.2	10.6	20.5	73.5
Average		13.4	17.7	33.4	55.8

<sup>1</sup> PDTC = Porosity Destroyed by Total Cement

<sup>2</sup> PDMC = Porosity Destroyed by Mechanical Compaction

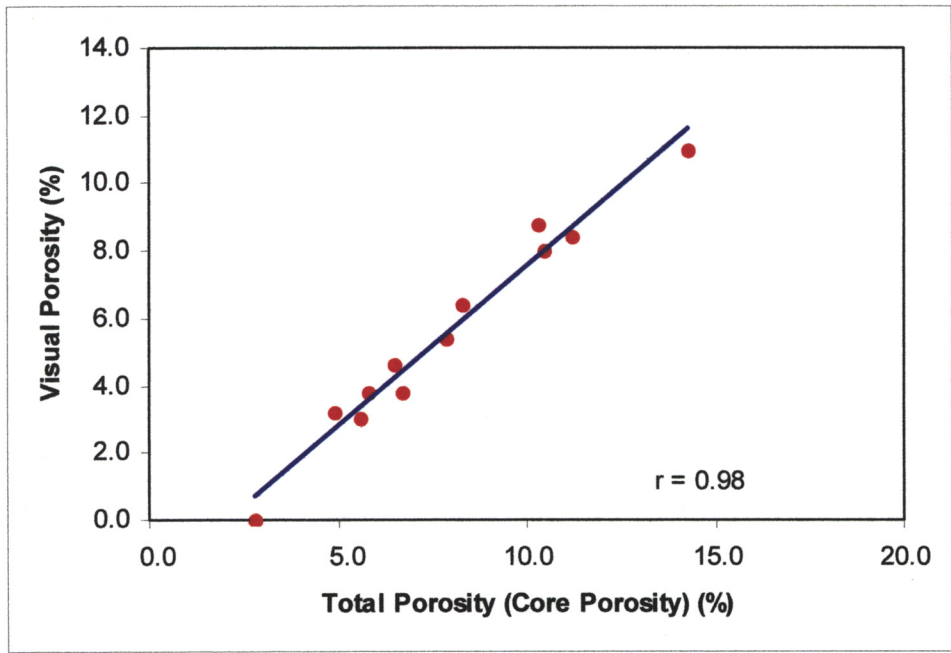


**Figure 3:** Relation between visual porosity and total porosity (core porosity). Note the high correlation coefficient  $r = 0.98$  between both components.

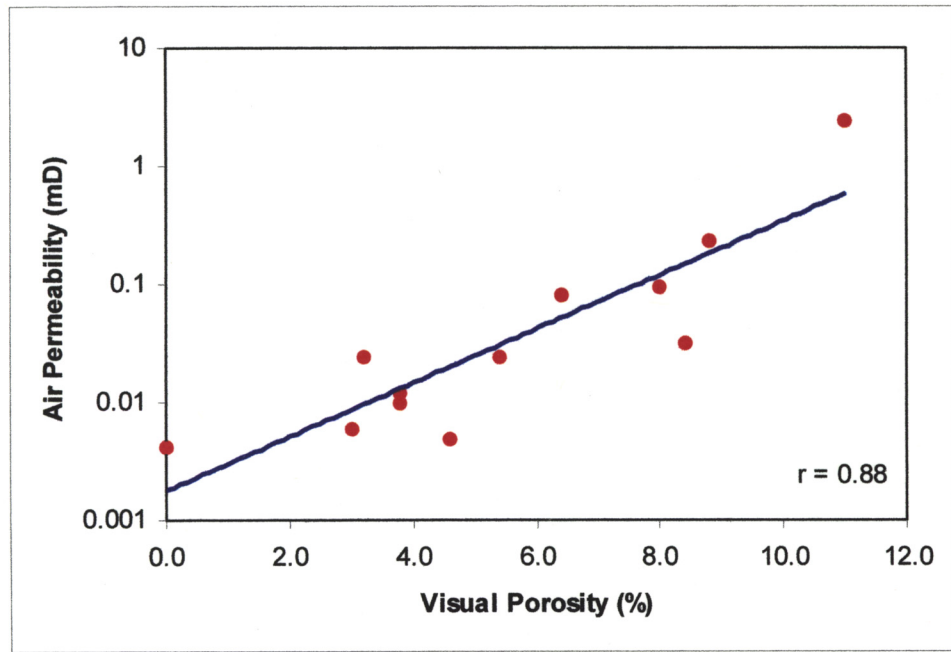


**Figure 4:** Relation between visual porosity and air permeability. Note the high correlation coefficient  $r = 0.88$  between both components.

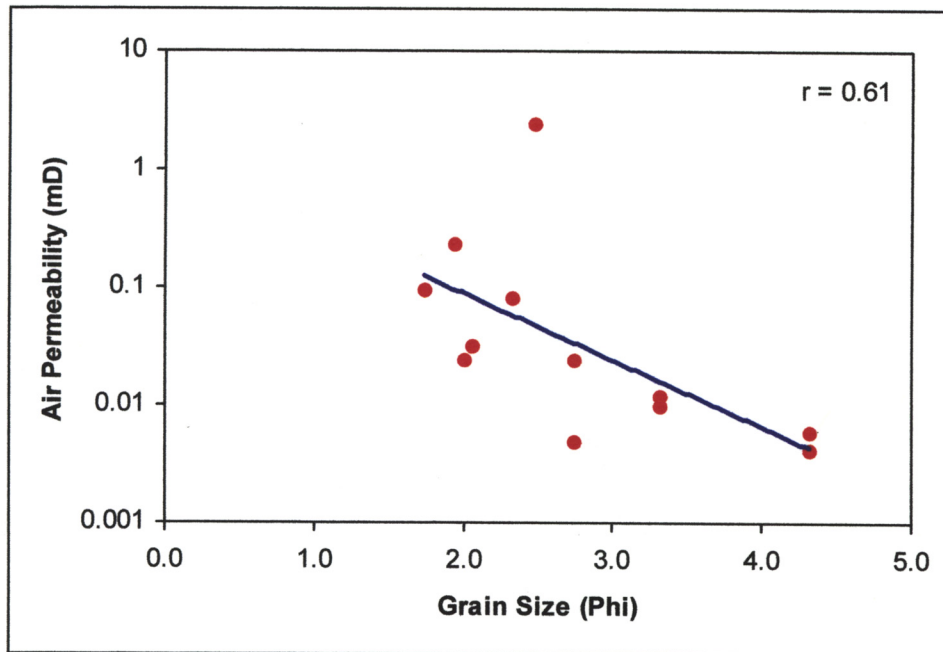


**Figure 5:** Relation between rock grain size and air permeability. The relatively high correlation coefficient  $r = 0.61$  between both components suggests a major control of textural variety on the reservoir quality

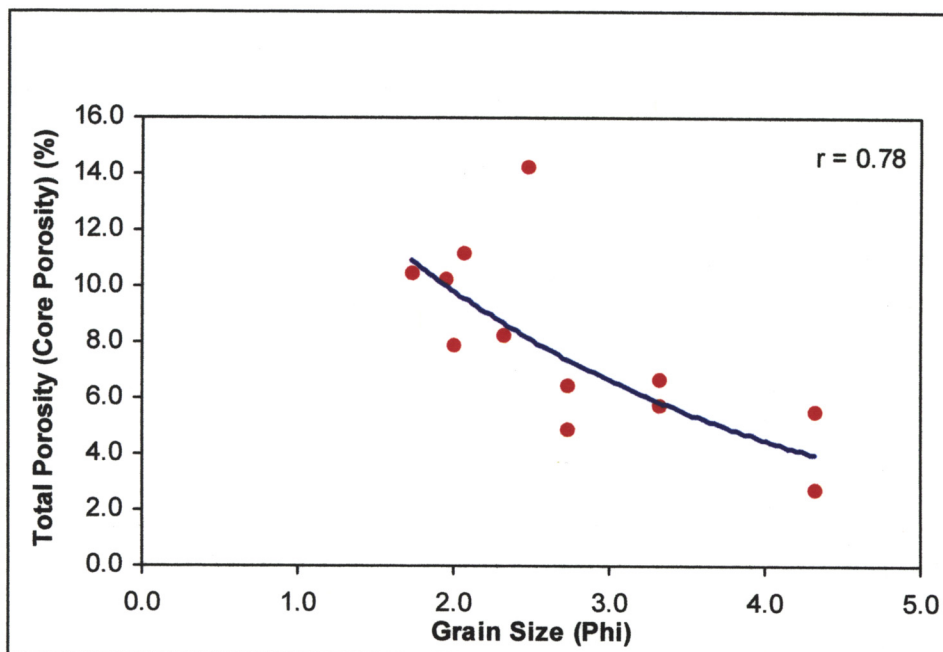


**Figure 6:** Relation between rock grain size and total porosity (core porosity). The relatively high correlation coefficient  $r = 0.78$  between both components suggests a major control of textural variety on the reservoir quality

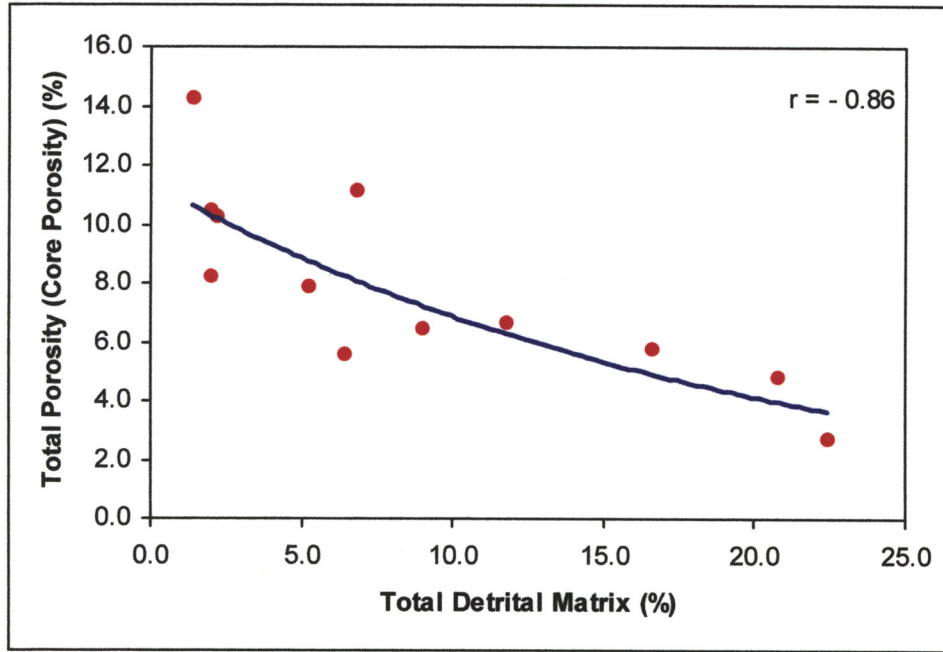


**Figure 7:** Relation between total detrital matrix and total porosity (core porosity). The relatively high inverse correlation coefficient  $r = -0.86$  between both components suggests a major control of original framework components on the reservoir quality.

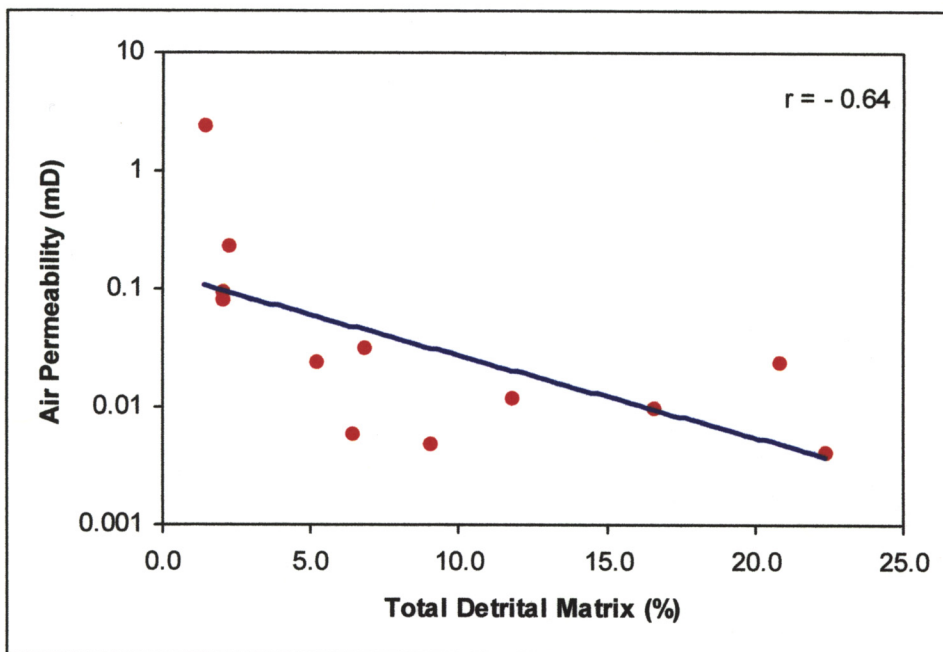


**Figure 8:** Relation between total detrital matrix and air permeability. The relatively good inverse correlation coefficient  $r = -0.64$  between both components suggests a major control of original framework components on the reservoir quality.

PE907511\_19

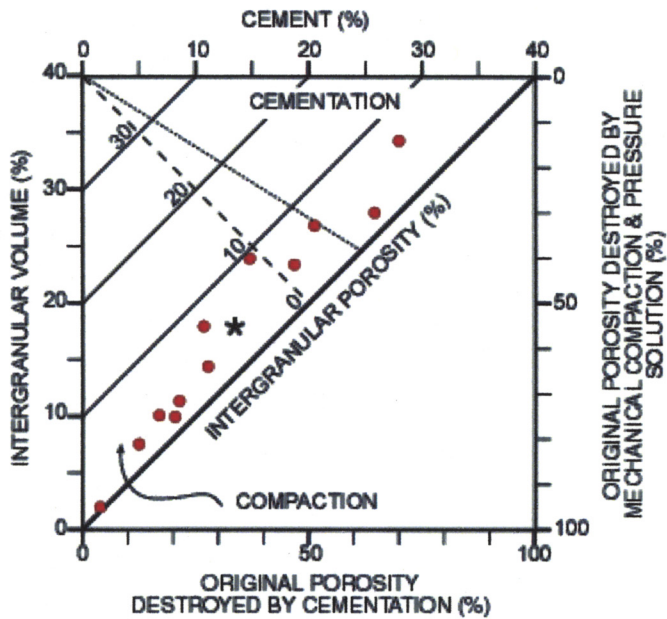


**Figure 9:** Intergranular volume vs total cement diagram for Turrum-7 sandstone samples to evaluate the relative importance of compaction and cementation process to porosity reduction (after Houseknecht (1987, 1989) and modified by Ehrenberg (1989, 1990). \* denotes the average.

## 5. SUMMARY AND CONCLUSIONS

### 5.1 Sediment Provenance

All samples exhibit similar sediment provenance. The amount of lithic fragments is moderate and sediment provenance can be precisely estimated. The presence of a high proportion of micaceous schist and rounded sedimentary chert, is interpreted to reflect contribution from both metamorphic source and an older sedimentary source, i.e. a recycled cratonic region.

### 5.2 Environment of Deposition

Interpretation of sedimentary environments is based mainly on the observations of thin sections. These could not be predicted precisely for each thin section as the studied sandstone samples from Turrum-7 lack diagnostic features of certain depositional environments, such as glaucony, calcareous fossils and coals. However, the sandstones of Turrum-7 were probably deposited by moderate to low energy sedimentation. The depositional environments range from meandering fluvial to tidal or lower shoreface and upper offshore. This is indicated by the texture, the degree of sorting, the presence of detrital clay matrix and the presence of trace fossils (bioturbation), as evidenced by the mixed nature of fine grained sands and silt, in the studied samples. Sedimentary structures, as evidenced in the thin sections, are mainly horizontal continuous to discontinuous laminations, with small scale cross to ripple laminations.

### 5.3 Reservoir Potential

Given the detailed petrographic analysis, it seems most likely that texture, original framework components and diagenetic modifications including compaction have affected reservoir potential of the Turrum-7 sandstones. The presence of detrital matrix and ductile rock fragments has made a major impact on the reservoir quality. Compaction has effected the reservoir quality to some degree, where ductile rock fragments and detrital matrix are dominant. Contacts between framework grains contain concavo-convex and suture contacts, indicating however, that compaction has had a severe effect in reducing the reservoir quality. Cementation of authigenic minerals has further contributed to the porosity loss. Authigenic clays and altered ductile rock fragments contain considerable amounts of microporosity between their grains.

The measured porosity of the nearest core plugs to the studied samples ranges from 2.8% to 14.3% and air permeability ranges from 0 mD to 2.46 mD. SEM revealed that the pores are poorly developed and almost reduced by compaction and precipitation of authigenic minerals. The pores are small ranging in size from 1 micron up to 10 microns. The pore throats are much smaller with an average of less than 1 micron. Microporosity is well developed between kaolinite booklets and accounts for as much as 50% of the kaolinite masses. The macro-pores are poorly interconnected suggesting very low permeability and fair to poor reservoir quality. Fines migration and invasion of fines from the wellbore into the formation should be minimal in the samples studied. Dissolution of the matrix cement is unlikely.



## 6. REFERENCES

- Dickson, J. A. D., 1966—Carbonate identification and genesis as revealed by staining. *J. Sediment. Petrol.*, 36, 491-505.
- Ehrenberg, S. N., 1989—Assessing the relative importance of compaction processes and cementation to reduction of porosity in sandstones: discussion; compaction and porosity evolution of Pliocene sandstones, Ventura basin, California: discussion. *Am. Assoc. Petrol. Geol. Bull.*, 73, 1274-1276.
- Ehrenberg, S. N., 1990—Relationship between diagenesis and reservoir quality in sandstones of the Gran Formation, Haltenbanken, Mid-Norwegian continental shelf. *Am. Assoc. Petrol. Geol. Bull.*, 74, 1538-1558.
- Folk, R. L., 1974—*Petrology of Sedimentary Rocks*. Austin, Texas, Hemphill Publishing Co., 182 p.
- Houseknecht, D. W., 1987—Assessing the relative importance of compaction processes and cementation to reduction of porosity in sandstones. *Am. Assoc. Petrol. Geol. Bull.*, 71, 633-642.
- Houseknecht, D. W., 1989—Assessing the relative importance of compaction processes and cementation to reduction of porosity in sandstones: reply. *Am. Assoc. Petrol. Geol. Bull.*, 73, 1277-1279.
- Laniz, R. V., Stevens, R. E. and Norman, M. B., 1964—Staining of Plagioclase Feldspar and other Minerals with F. D. and C. Red No. 2. U.S. Geol. Survey Prof. Paper 501-B, 152-153.
- Pettijohn, F. J., Potter, P. E. and Siever, R., 1987—*Sand and Sandstone*. New York, Springer-Verlag, 553 p.
- Schmidt, V. and McDonald, D. A., 1979—Texture and recognition of secondary porosity in sandstones. In: Scholle, P. A. and Schluger, P. R. (eds.), *Aspects of Diagenesis*. Soc. Econ. Palaeontologists and Mineralogists, Spec. Pub., 26, 209-225.
- Zuffa, G. G., 1985—Optical Analysis of Arenites: Influence of Methodology on Compositional Results. In: Zuffa, G. G., (ed.), *Provenance of Arenites*, North Atlantic Treaty Organization (NATO), Advanced Study Institute Series, V. C. D. Reidel Publishing Company, Dordrecht, 168-189.

PE907511-21

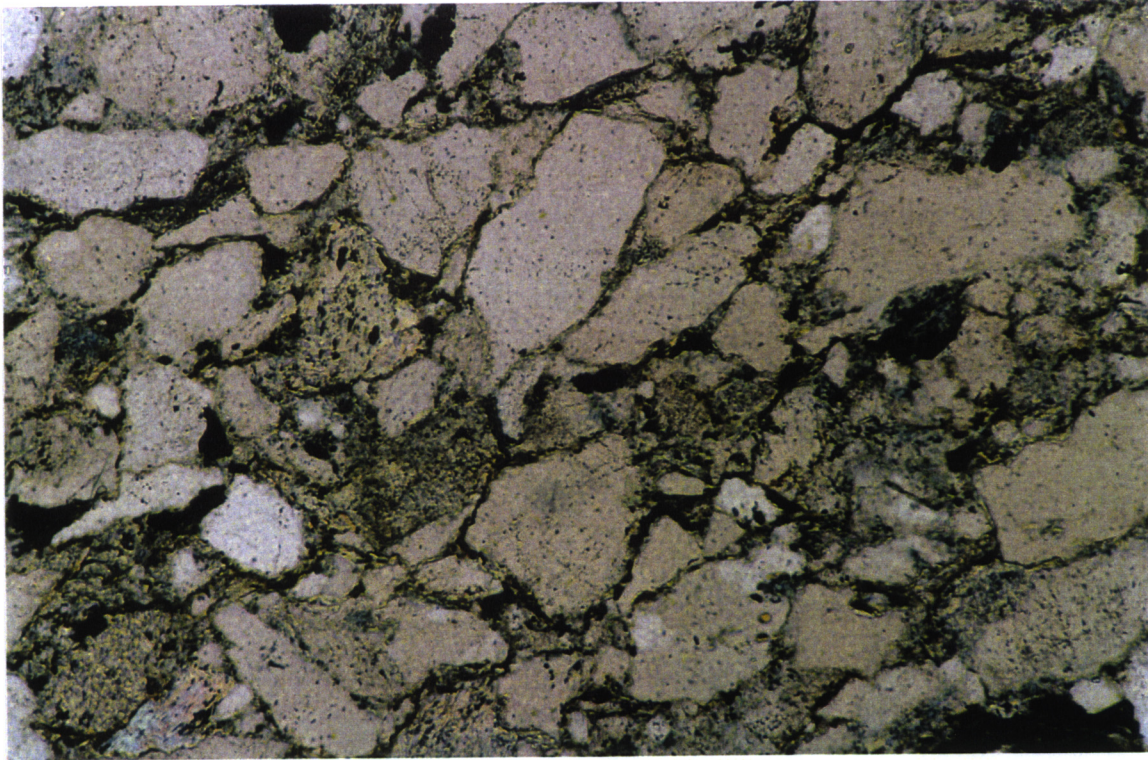


**Plate 1: (Sample No. 234C, 2628.45 m):** Thin section photomicrograph of feldspathic litharenite comprising well sorted, medium-grained sandstone. Note the concavo-convex and suture contacts between grains, indicating mechanical compaction. Also note squeezed ductile lithic fragments. Plane polarised light. Scale bar = 200  $\mu$ m.

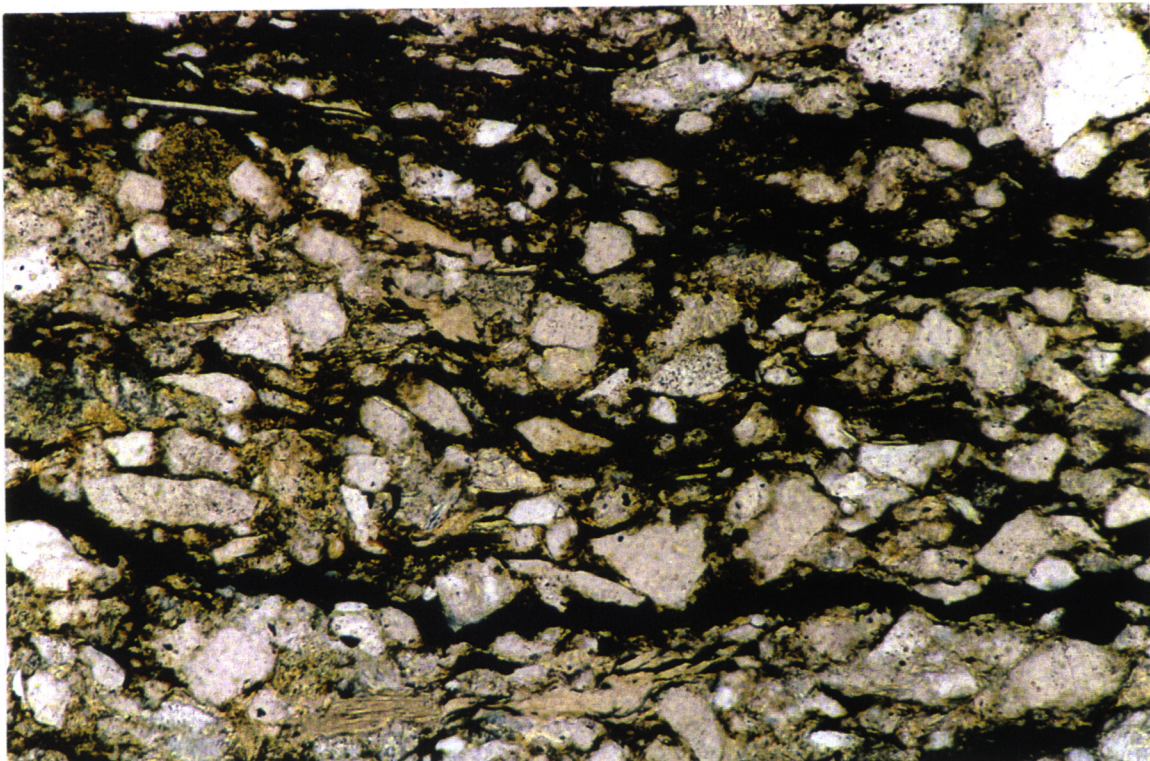


**Plate 2: (Sample No. 178C, 2623.85 m):** Thin section photomicrograph of lithwacke showing severe effects of compaction as indicated by the squeezed detrital depositional matrix. Plane polarised light. Scale bar = 200  $\mu$ m.

PE907511-22

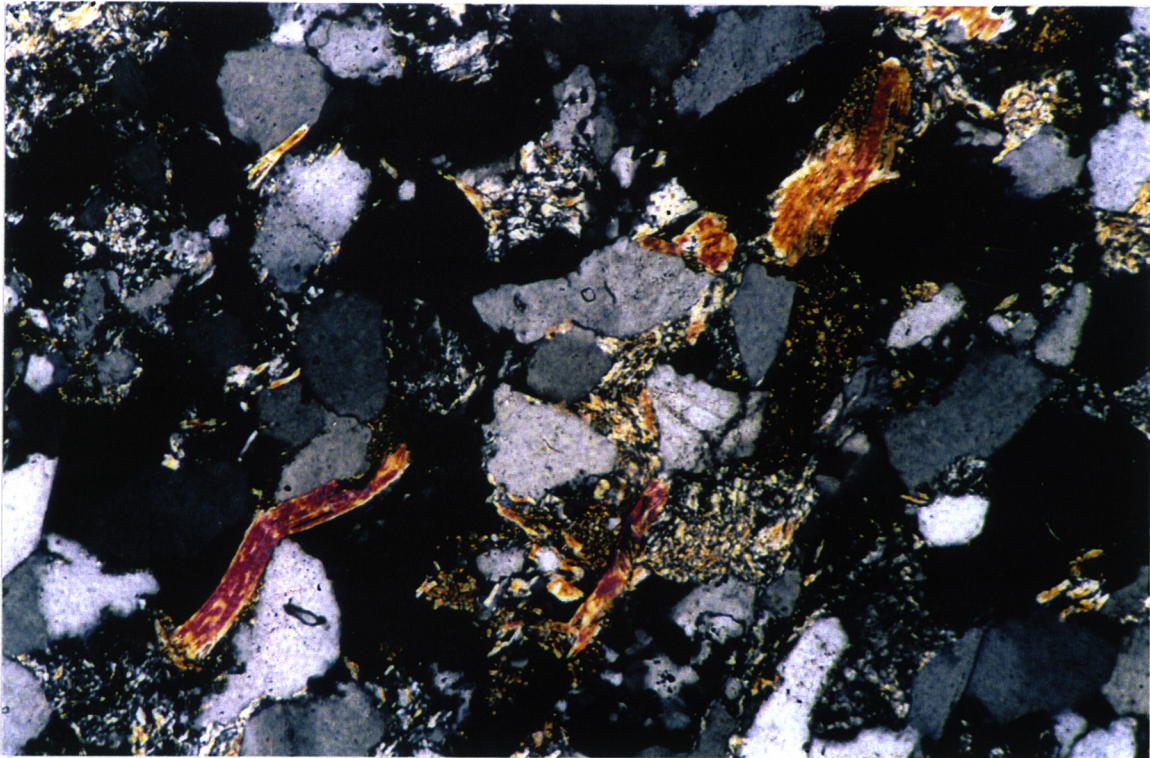


**Plate 3: (Sample No. 100C, 2617.25 m):** Thin section photomicrograph showing disintegrated metamorphic mica schist to produce muscovite. Note that mica flakes are squeezed between rigid quartz grains suggesting a severe mechanical compaction. Crossed polars. Scale bar = 200  $\mu\text{m}$ .

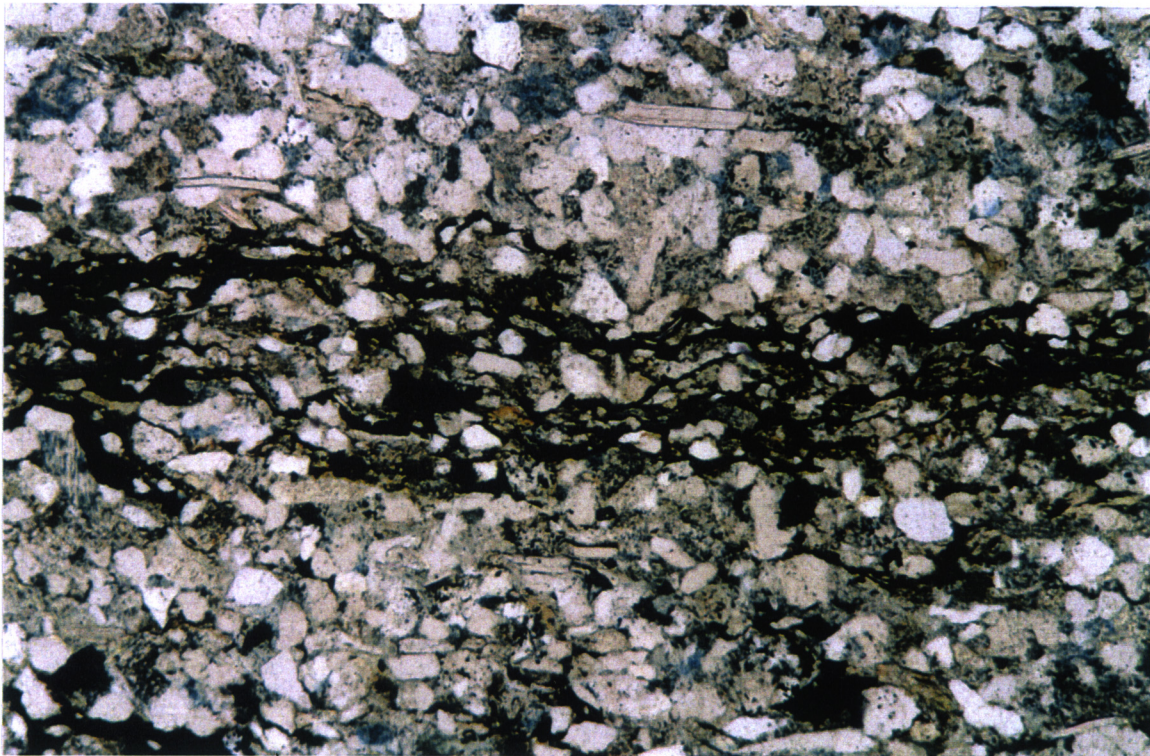


**Plate 4: (Sample No. 092C, 2616.65 m):** Thin section photomicrograph showing general view of compacted sample. The effect of mechanical compaction in reducing the reservoir quality was severe and is indicated by the presence of micro stylolites. Plane polarised light. Scale bar = 200  $\mu\text{m}$ .

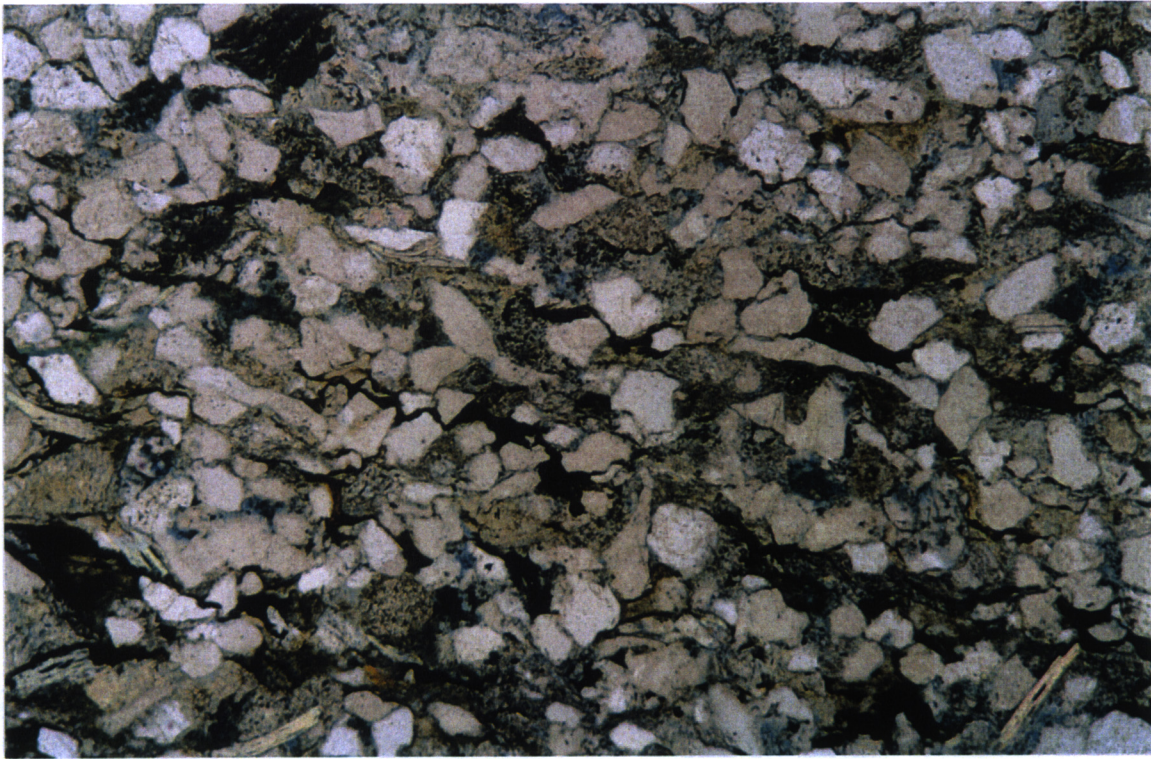


**Plate 5: (Sample No. V132C, 2619.97 m):** Thin section photomicrograph showing general view of well sorted, fine to medium-grained litharenite. Lithic fragments are abundant and during compaction the ductile lithic grains are squeezed and rearranged to reduce the primary intergranular porosity and reservoir quality. Plane polarised light. Scale bar = 200  $\mu\text{m}$ .



**Plate 6: (Sample No. V132C, 2619.97 m):** Thin section photomicrograph showing mica. It is either disseminated or concentrated along the bedding plane. It has originated as a result of alteration metamorphic mica schist. Plane polarised light. Scale bar = 200  $\mu\text{m}$ .

PE907511-24

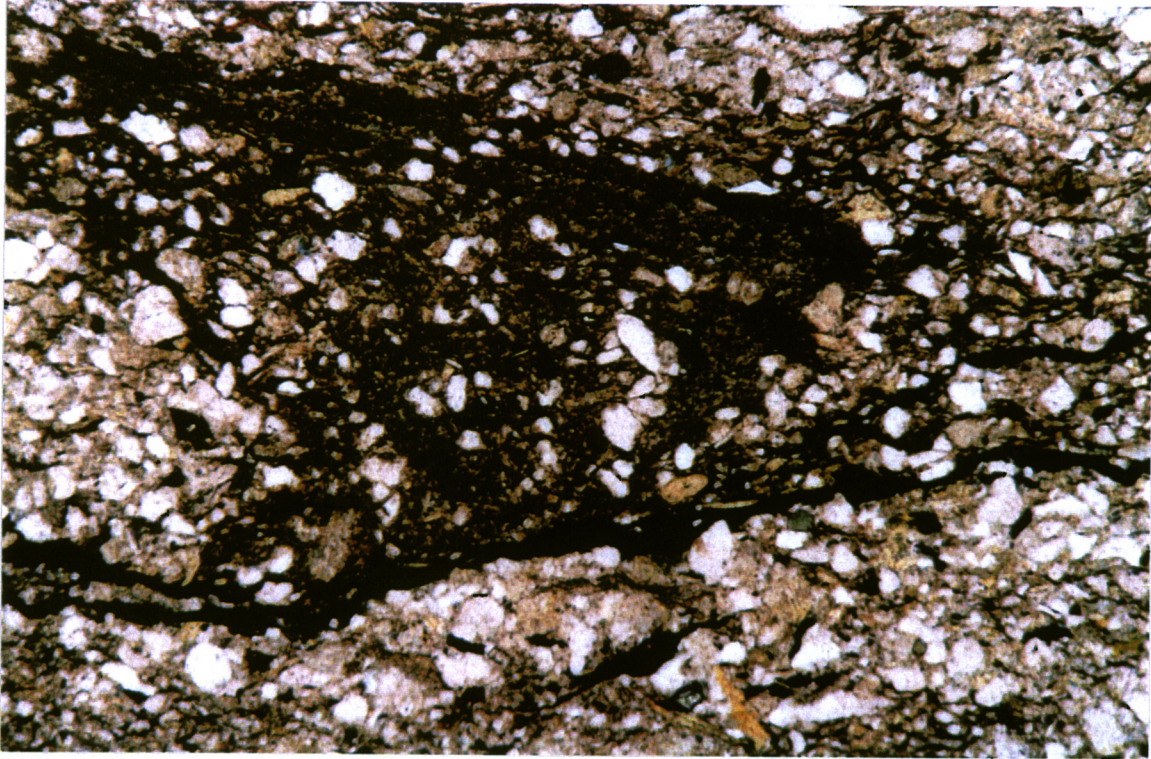


**Plate 7: (Sample No. 178C, 2623.85 m):** Thin section photomicrograph showing moderate amounts of detrital depositional matrix. It comprises organic rich silty to very fine-grained sandstone and where abundant it occludes the intergranular porosity. Plane polarised light. Scale bar = 200  $\mu\text{m}$ .

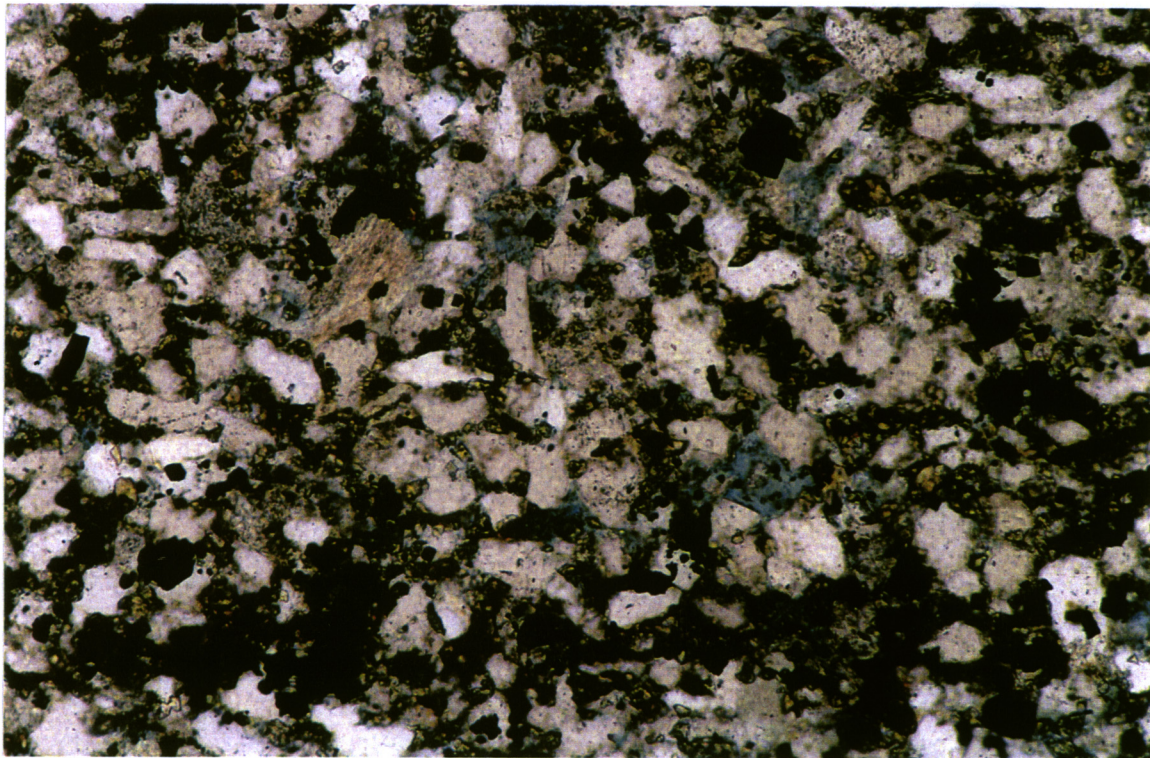


**Plate 8: (Sample No. 028C, 2611.30 m):** Thin section photomicrograph showing siderite cement. It occurs as micro spar crystals ranging in size from 2 to 20  $\mu\text{m}$  filling much of the pore spaces and restricting the reservoir quality in this sample. Plane polarised light. Scale bar = 200  $\mu\text{m}$ .

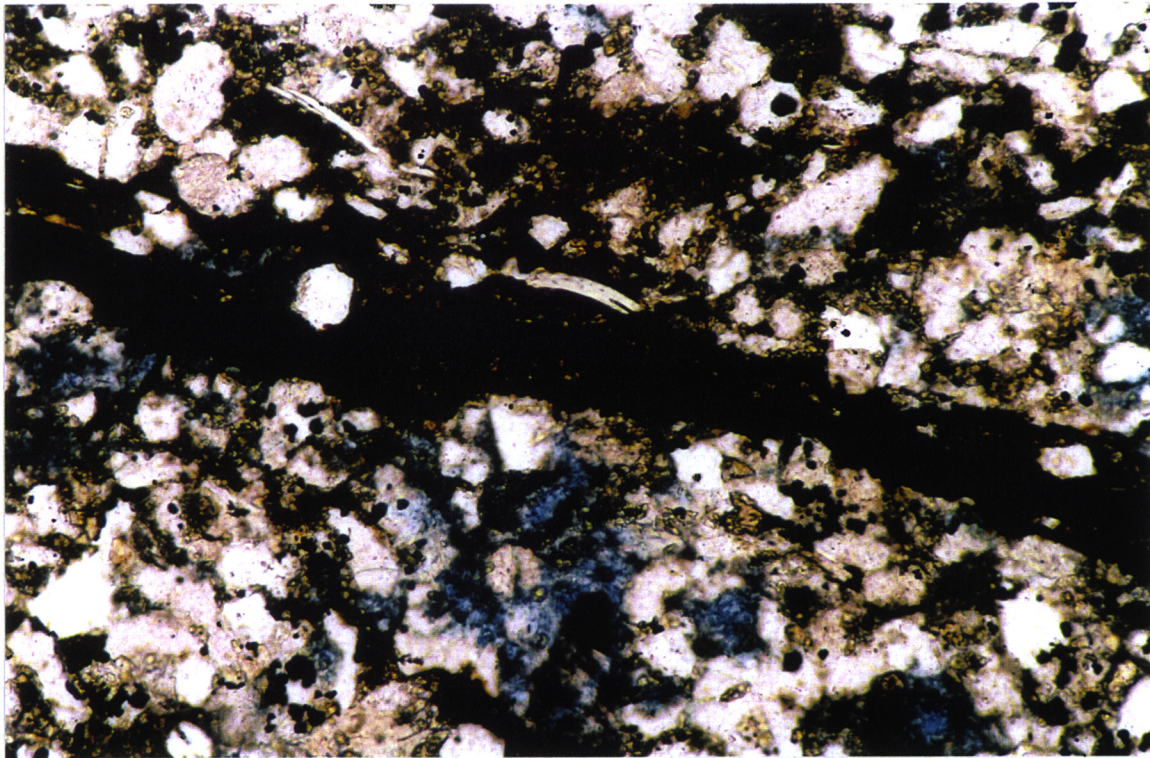


**Plate 9: (Sample No. 028C, 2611.30 m):** Thin section photomicrograph showing siderite cement. It occurs around organic matter and organic-rich detrital clay matrix. Plane polarised light. Scale bar = 200  $\mu\text{m}$ .

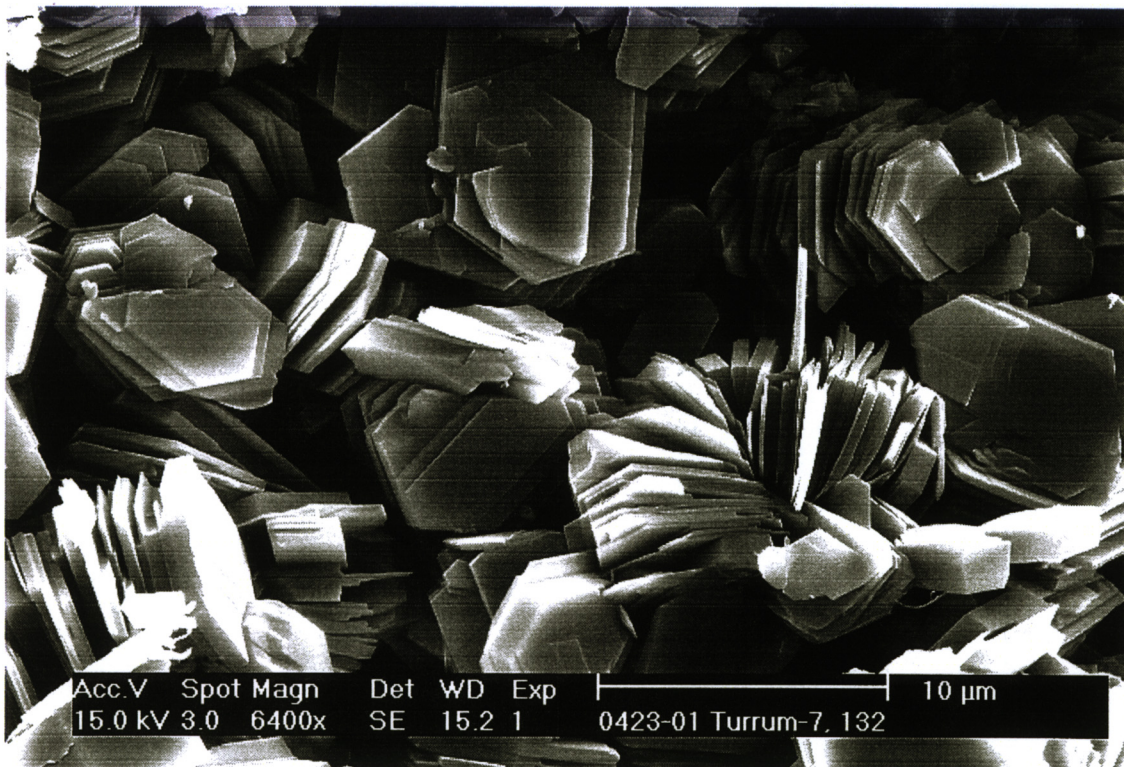


**Plate 10: (Sample No. V132C, 2619.97 m):** SEM photomicrograph showing authigenic kaolinite. Kaolinite occurs as pseudo hexagonal book-like crystals filling much of the pore spaces and restricting the reservoir quality. Note the amount of microporosity between kaolinite booklets. Scale bar = 10  $\mu\text{m}$ .

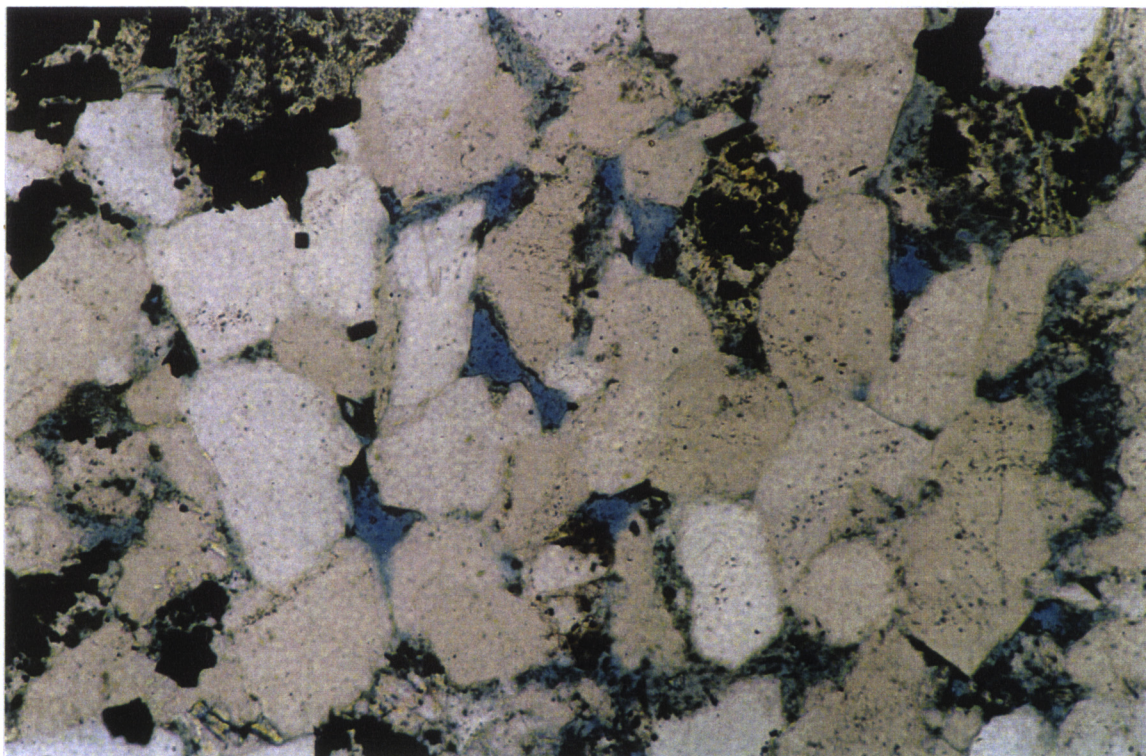


**Plate 11: (Sample No. 234C, 2628.45 m):** Thin section photomicrograph showing quartz cement. Quartz cementation occurs as thick overgrowths with porosity locally preserved. Note the presence of cubic pyrite filling some pore spaces and replacing lithic fragments. Plane polarised light. Scale bar = 200  $\mu\text{m}$ .

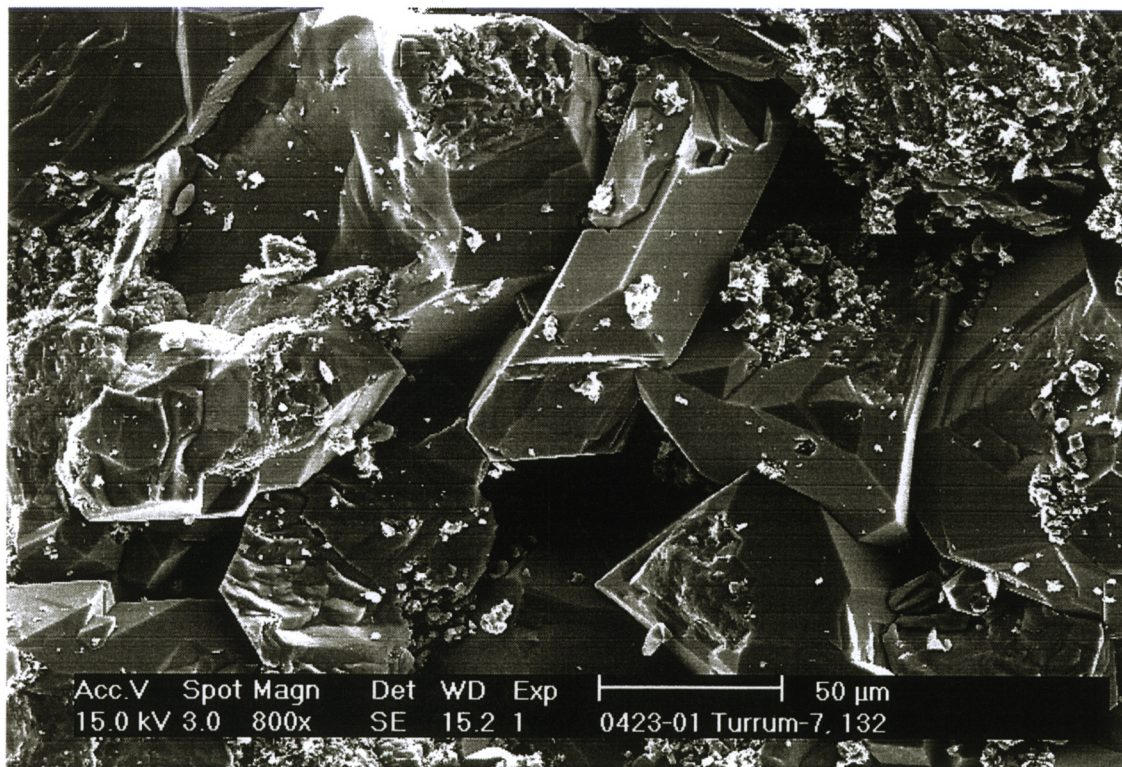


**Plate 12: (Sample No. V132C, 2619.97 m):** SEM photomicrograph showing quartz cement. Quartz cementation occurs as thick overgrowths. Although of quartz cementation porosity is locally still preserved. Note that the pores are fairly interconnected implying fair to low permeability in 3-D and fair reservoir quality. Scale bar = 50  $\mu\text{m}$ .

PE907511-27

907511 ~~192~~  
192

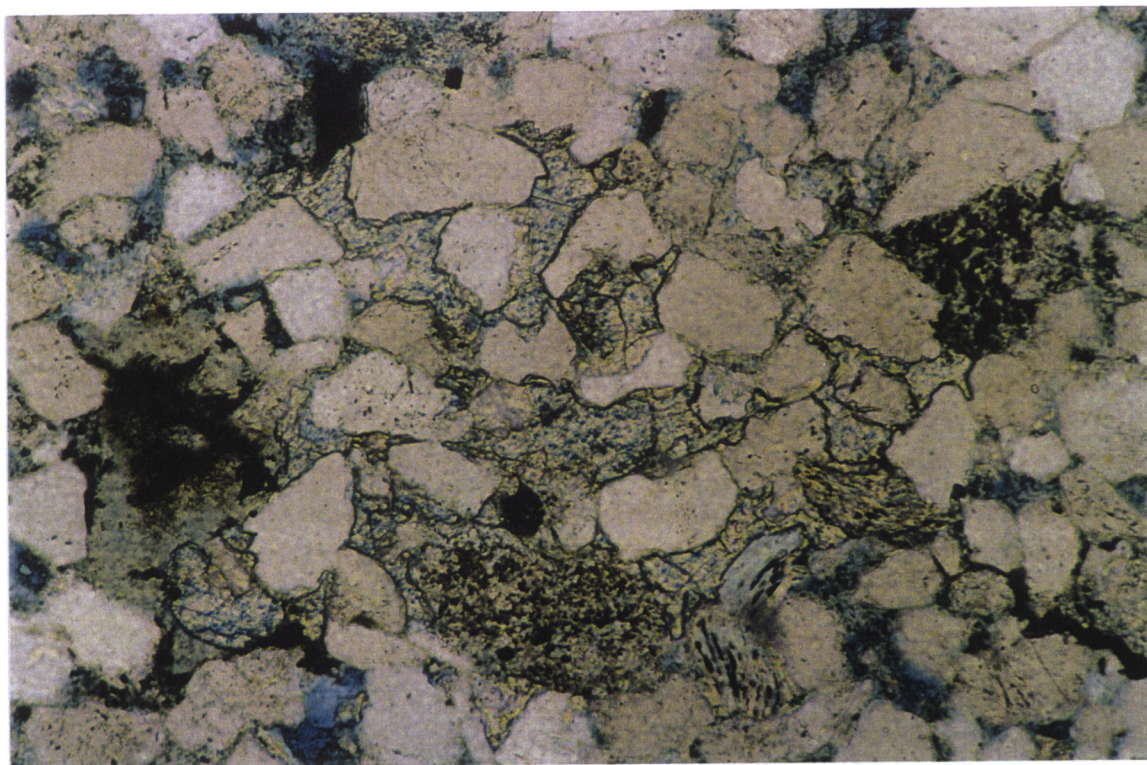


**Plate 13: (Sample No. V132C, 2619.97 m):** Thin section photomicrograph showing traces of ferroan dolomite cement filling the pore spaces. Plane polarised light. Scale bar = 200 µm.

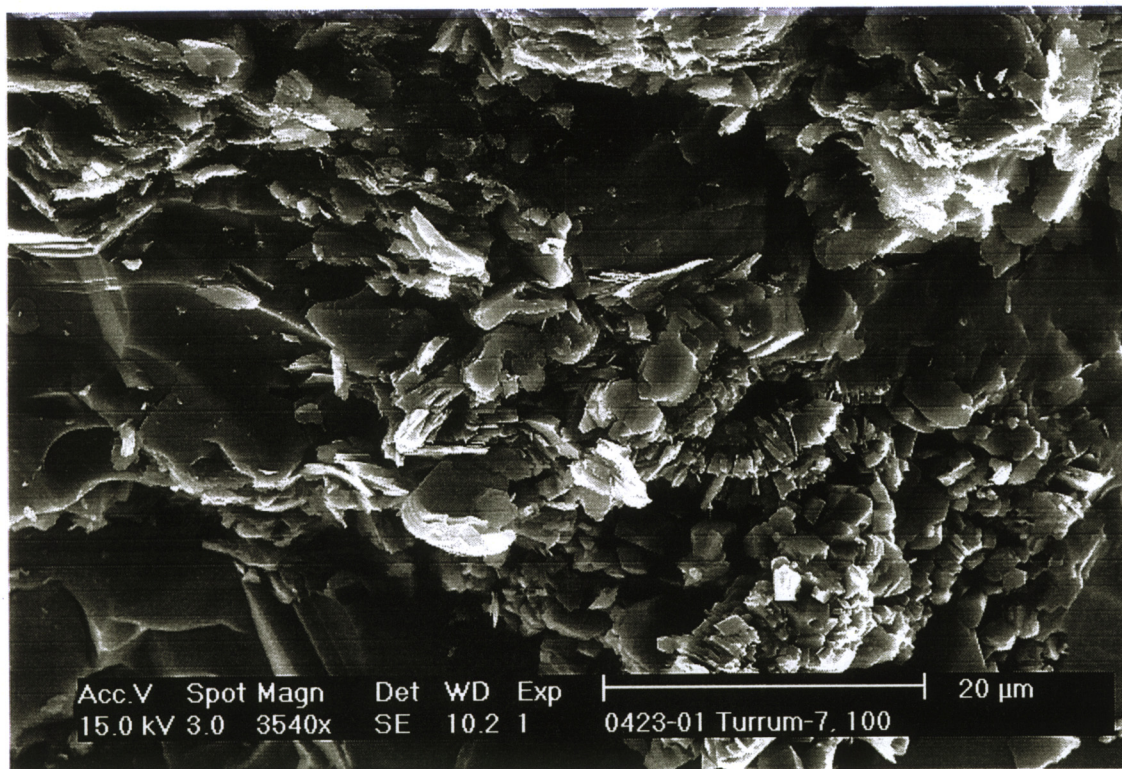
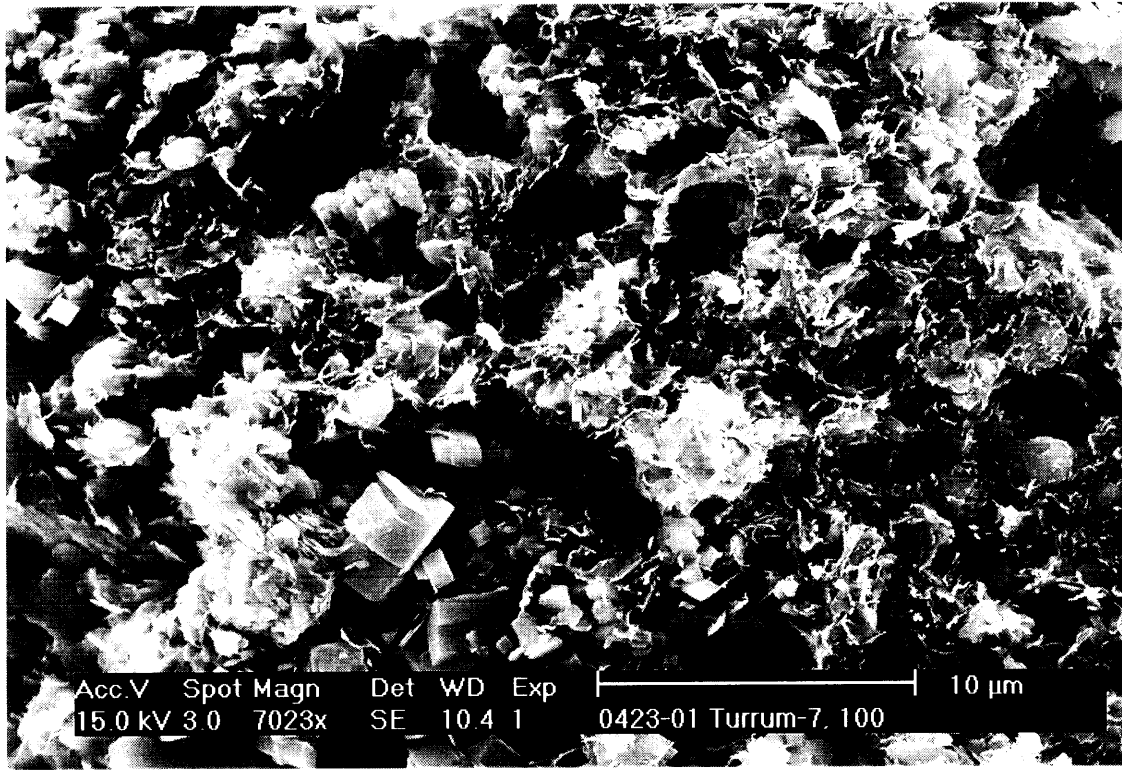


**Plate 14: (Sample No. 100C, 2617.25 m):** SEM photomicrograph showing authigenic kaolinite booklets on the surface of altered lithic fragment. Scale bar = 20 µm.

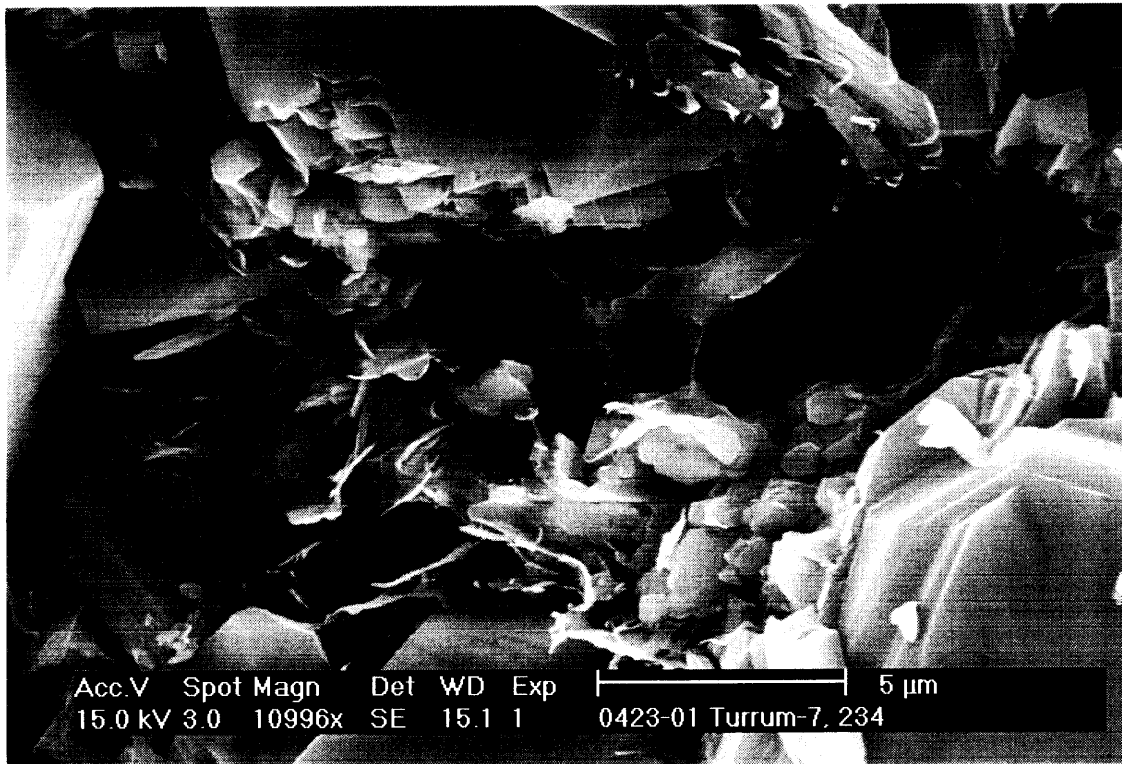


PE 907511-28

193  
907511 ~~193~~



**Plate 15: (Sample No. 100C, 2617.25 m):** SEM photomicrograph showing authigenic kaolinite and illite. Both authigenic minerals originated as a result of alteration of ductile mica schist lithic fragments. Both authigenic minerals have major control on the reservoir quality. Scale bar = 10  $\mu$ m.

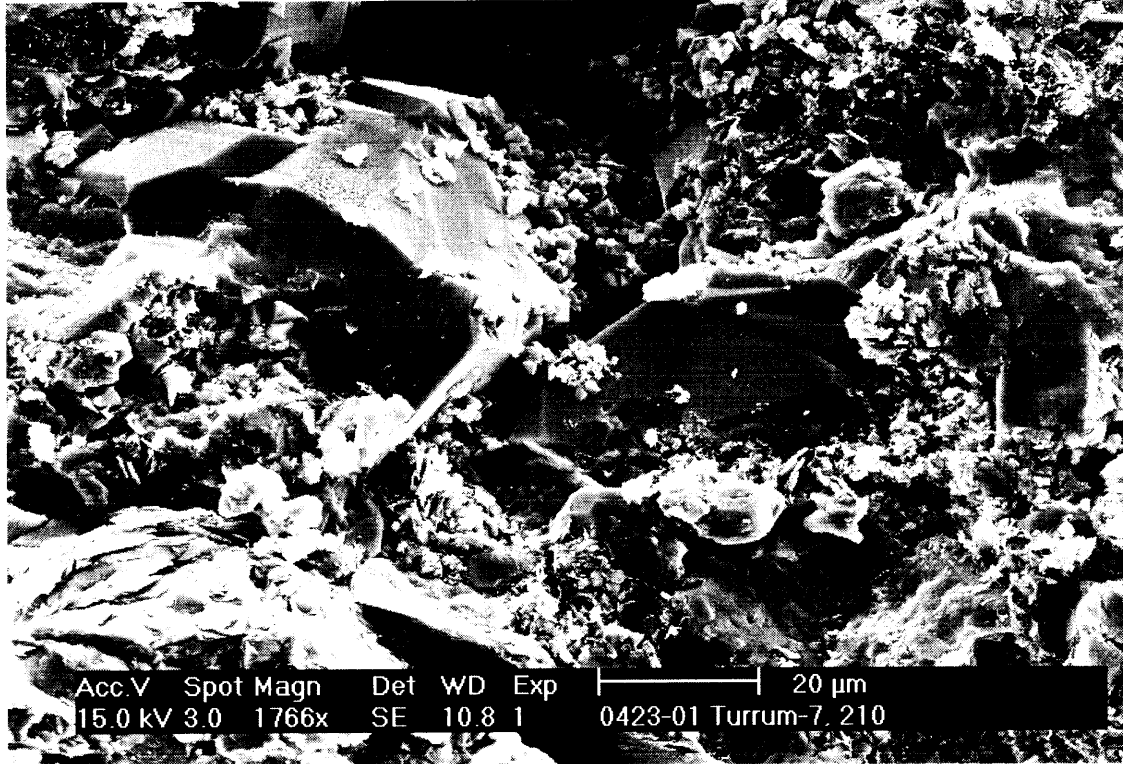


**Plate 16: (Sample No. 234C, 2628.45 m):** SEM photomicrograph showing authigenic fibrous to hairy illite filling some of the pore spaces. It also bridges the pores and pore throats and restricts the permeability and reservoir quality. Scale bar = 5  $\mu$ m.

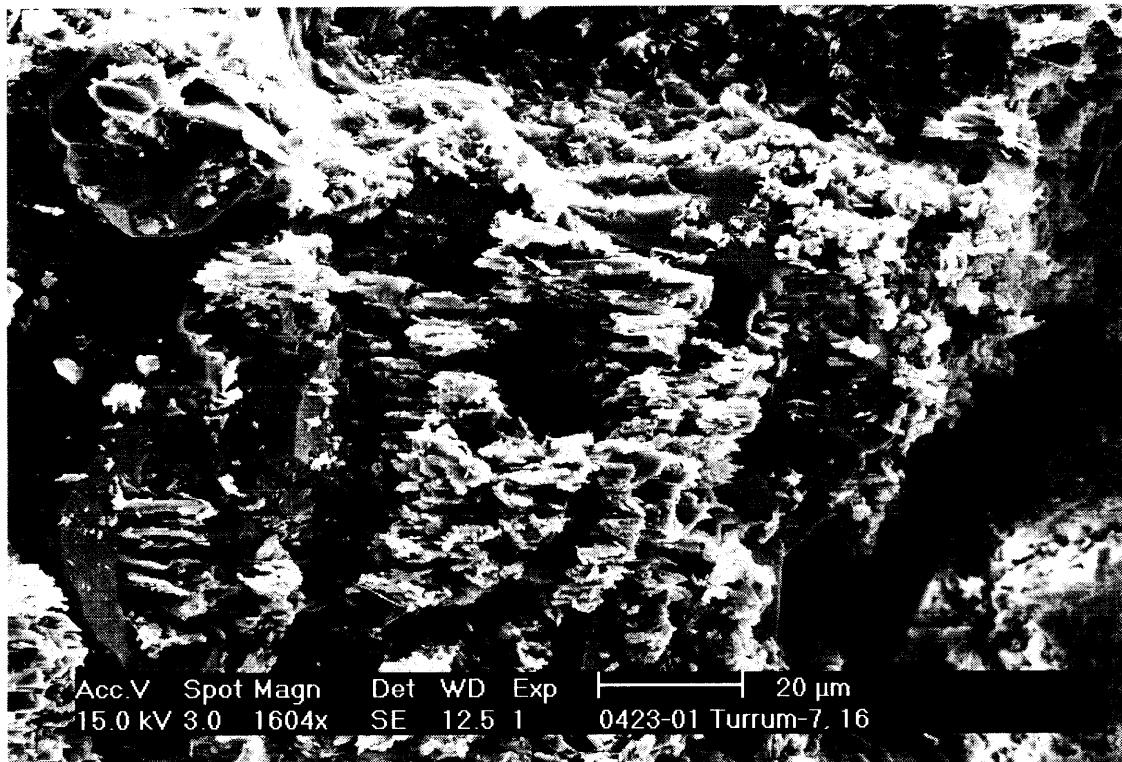
262645127

907511

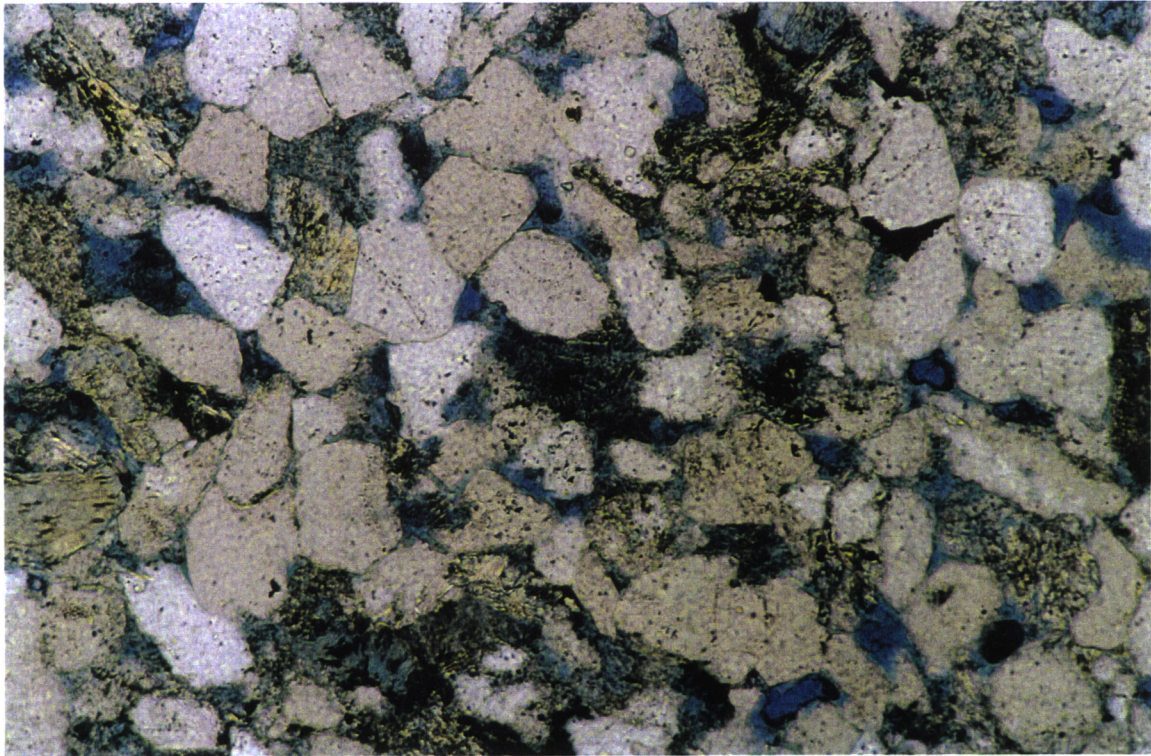
194  

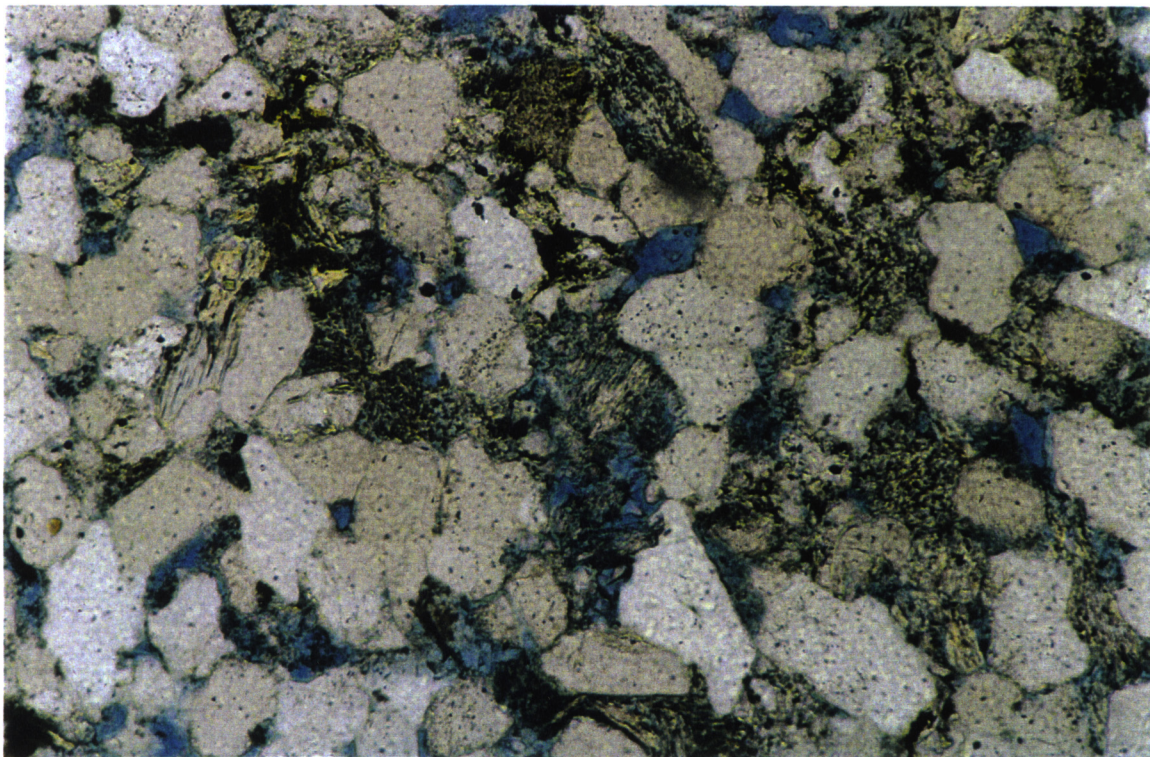
**Plate 17: (Sample No. 210C, 2626.45 m):** SEM photomicrograph of feldspathic litharenite comprising well sorted, subangular to rounded fine to medium-grained sandstone with moderate visual porosity. The pores are poorly interconnected in a 3-D network giving poor permeability. Scale bar = 20  $\mu\text{m}$ .



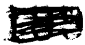
**Plate 18: (Sample No. 016C, 2610.30 m):** SEM photomicrograph showing secondary porosity development due to partial to complete dissolution of potassium feldspar grains. Scale bar = 20  $\mu\text{m}$ .



**Plate 19: (Sample No. 016C, 2610.30 m):** Thin section photomicrograph of litharenite comprising well sorted, subangular to rounded fine-grained sandstone with moderate visual porosity. Visual porosity occurs mostly as large triangles suggesting a primary intergranular origin. Plane polarised light. Scale bar = 200  $\mu\text{m}$ .



**Plate 20: (Sample No. 016C, 2610.30 m):** Thin section photomicrograph of litharenite showing minor secondary porosity as a result of partial to complete dissolution of potassium feldspar and lithic fragments. Potassium feldspar displays sieve to skeletal structure providing good interconnection to pore spaces. Plane polarised light. Scale bar = 200  $\mu\text{m}$ .

907511   
196

*APPENDIX I*

**DETAILED THIN SECTION DESCRIPTIONS**

**SAMPLE:** NO. 008C (2609.65 m)

**Lithology:** Litharenite

**Texture:** Creamy to light brown, grain supported, small scale to ripple cross stratification and minor evidence of bioturbation, moderately to well sorted, very fine-grained sandstone. Quartz grains are angular to subrounded. Minor authigenic minerals and very low visual porosity.

**Composition:** The framework component of the sample is dominated by monocrystalline quartz (46.4%) and trace polycrystalline quartz (1.4%). Minor to trace amount of potassium feldspar is present (2.8%). Lithic fragments are common (17.8%). Mica is another minor component most of which is muscovite (6.2%). Biotite is trace component (0.6%) and almost altered. Both muscovite and biotite are resulted from the alteration of metamorphic mica schist. Depositional clay matrix is minor component and comprise organic-rich silty to very fine-grained sandstone. Dispersed organic matter is also present in minor amount (3%). Authigenic minerals comprise minor pyrite (4.6%), kaolinite (3.8%) with traces of illite and quartz. There are low amounts of visible porosity (3.8%).

Monocrystalline quartz occurs normally as subangular to rounded grains and displays strongly undulose extinction with many grains containing fluid and igneous inclusions. Lithic fragments predominantly comprise metamorphic mica schist and rounded sedimentary chert.

The amount of visual porosity (Plate 21) in this sample is very low (3.8%) most of which is primary intergranular porosity. Secondary porosity is less common and resulted from partial dissolution of potassium feldspar and alteration of ductile lithic grains. The main agent controlling the reservoir quality in this sample is the mechanical compaction. Mechanical compaction has reduced around 81% of the primary intergranular porosity, whilst cementation of authigenic minerals has occluded around 12%.

**XRD:** XRD results show that quartz is the dominant component with major kaolinite and mica (including illite) and traces of potassium feldspar (Table 6 and Appendix II). The clay fraction (< 2  $\mu\text{m}$ ) is dominated by kaolinite and mica (muscovite and illite) (Table 7 and Appendix II).

**SEM:** No SEM photos.

**Diagenesis:**

The diagenesis of this sample can be summarised as follows:

- Early compaction has affected this sample and has resulted in closer packing of grains and well-developed parallel alignment of elongated detrital grains.
- Framboidal pyrite could have occurred during the early sulphate reduction.
- Alteration and dissolution of feldspar, ductile lithic fragments and mica could have been responsible for the formation of kaolin.
- After kaolin precipitation quartz cements have occurred as overgrowths. The quartz overgrowths postdated or at least formed simultaneously with the precipitation of kaolin.
- Alteration of lithic fragments and potassium feldspar has continued to the late stage of diagenetic history and this has resulted in development of local secondary porosity and precipitation of authigenic illite. Authigenic illite occurs as fibrous to hairy crystals on the surface of kaolinite, altered feldspar grains and ductile lithic fragments. It also bridges the pore spaces and pore throats.
- Later in the diagenetic history, large cubic crystalline pyrite has occurred as pore filling around thin coal beds, organic-rich detrital matrix and coalified wood materials.

**Env. Deposition:**

The sorting and moderate rounding in this fine-grained sandstone suggests deposition in a moderate to low energy environment. Sedimentary structures are dominated by small scale cross to ripple stratification with minor evidence of bioturbation. Possible environments include meandering fluvial to tidal to lower shoreface.

**Res. Potential:**

Visible porosity is low (3.8%) and the pores are poorly interconnected in a 3-D network giving a low permeability. The reservoir quality is fair to poor.

PE907511-31

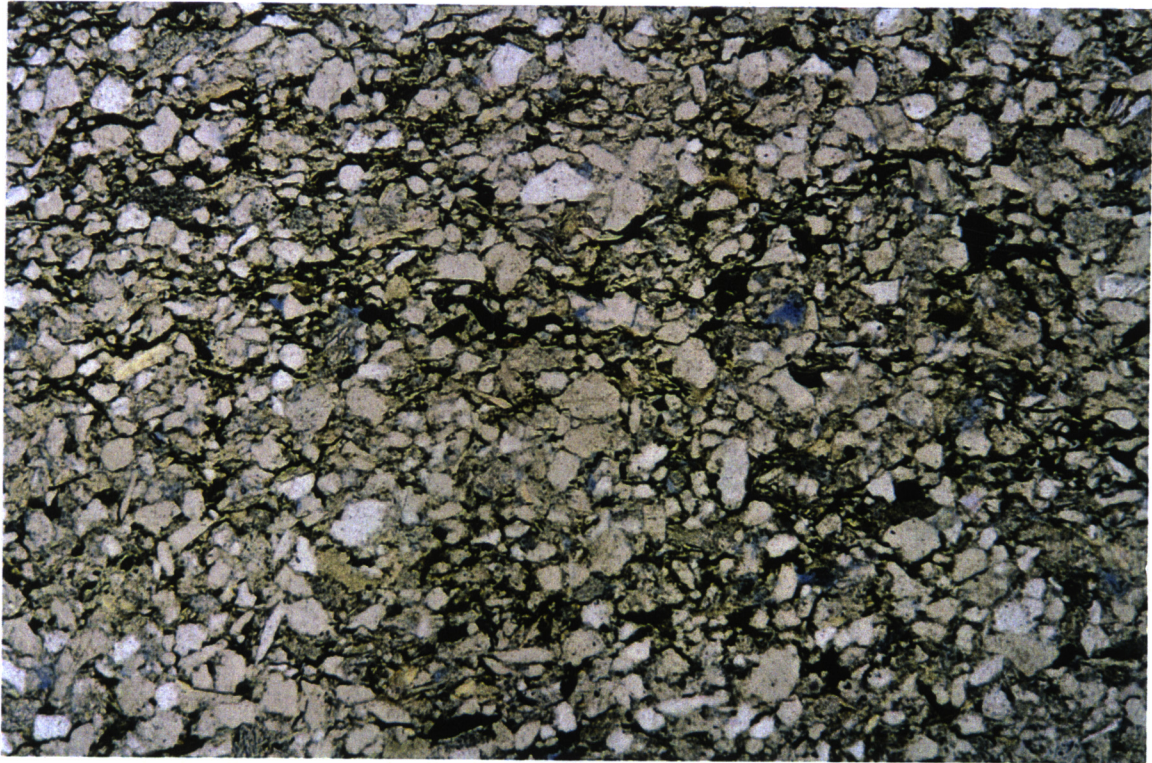


**Plate 21A: (Sample No. 008C, 2609.65 m):** Thin section photomicrograph showing generalised view of moderately to well sorted, very fine-grained sandstone with trace to minor amounts of intergranular porosity. Note the presence of stylolites indicating compaction. Plane polarised light. Scale bar = 500  $\mu\text{m}$ .



**Plate 21B: (Sample No. 008C, 2609.65 m):** Thin section photomicrograph showing local triangular pore spaces between authigenic and detrital grains. Plane polarised light. Scale bar = 200  $\mu\text{m}$ .

**SAMPLE:** NO. 016C (2610.30 m)

**Lithology:** Litharenite

**Texture:** The sample depicts a creamy, grain supported, small scale cross stratification, well sorted, fine-grained sandstone. Quartz grains are mainly subangular to rounded. Considerable amount of authigenic clays and moderate visual porosity.

**Composition:** Monocrystalline quartz is the dominant framework component (42.6%) with minor to trace amounts of polycrystalline quartz grains (2.2%). Potassium feldspar is present in minor amounts (3.6%). Lithic fragments are common (15.8%) and comprise predominantly mica schist. Mica is another minor component most of which is muscovite (4.2%). Biotite is trace component (0.4%) and almost altered. Both muscovite and biotite are resulted from the alteration of metamorphic mica schist. Depositional matrix and organic matter are trace components in this sample comprising 0.8% and 0.6% respectively. Authigenic minerals are trace and dominated by kaolinite (9.2%), authigenic quartz (6.8%) pyrite (2%) and traces of illite and iron oxide. There are very moderate amounts of visual porosity (11%).

Monocrystalline quartz grains show strong undulose extinction. Straight undulose extinction is less common. Many of the monocrystalline grains contain fluid and igneous inclusions. Polycrystalline quartz occurs predominantly as equant to sub equant grains.

Porosity is moderate in this sample and scattered throughout the sample, usually as triangular pores between detrital and authigenic minerals (Plate 22). This suggests that the porosity is largely intergranular primary.

**XRD:** Quartz is the dominant component with major kaolinite and mica (including illite), and traces of potassium feldspar and pyrite, (Table 6 and Appendix II). The clay fraction (< 2  $\mu\text{m}$ ) is dominated by kaolinite and mica (muscovite and illite), (Table 7 and Appendix II).

**SEM:** The sample comprises a well sorted, fine-grained sandstone with moderate amounts of authigenic clay mineral assemblage (Plates 23 and 24). Kaolinite occurs as fine to large pseudo hexagonal book-like crystals, ranging in size from 5  $\mu\text{m}$  up to 20  $\mu\text{m}$  (Plate 24). It occurs as pore filling, filling much of the pore spaces and pore throat and restricting the reservoir quality. SEM has also shown that quartz overgrowths are minor and has locally reduced the reservoir quality (Plates 24 and 25). Illite occurs as a late fibrous to hairy crystals around kaolinite, altered lithic fragments and altered feldspar grains (Plate 26).



The pores are small, most of which are less than 10  $\mu\text{m}$  and occasionally less than 1  $\mu\text{m}$  (Plate 23). The distribution of the pore throat is irregular with moderate interconnection implying moderate permeability (Plate 23).

**Diagenesis:**

The diagenesis of this sample can be summarised as follows:

- Early compaction has affected this sample and has resulted in closer packing of grains and well-developed parallel alignment of elongated detrital grains.
- Framboidal pyrite could have occurred during the early sulphate reduction.
- Alteration and dissolution of feldspar, ductile lithic fragments and mica could have been responsible for the formation of kaolin.
- After kaolin precipitation quartz cements have occurred as overgrowths. The quartz overgrowths postdated or at least formed simultaneously with the precipitation of kaolin.
- Alteration of lithic fragments and potassium feldspar has continued to the late stage of diagenetic history and this has resulted in development of local secondary porosity and precipitation of authigenic illite. Authigenic illite occurs as fibrous to hairy crystals on the surface of kaolinite, altered feldspar grains and ductile lithic fragments. It also bridges the pore spaces and pore throats.
- Later in the diagenetic history, large cubic crystalline pyrite has occurred as pore filling around thin coal beds, organic-rich detrital matrix and coalified wood materials.

**Env. Deposition:**

This well sorted, fine-grained sandstone with small scale cross stratification was probably deposited in a moderate energy environment. A precise depositional environment could not be constrained, however, from the general view and comparing with other samples, depositional environment is likely to be tidal to lower shoreface.

**Res. Potential:**

The sample shows a moderate reservoir potential with moderate porosity (11%). Compaction and cementation have almost equal effect on reducing the intergranular primary porosity.

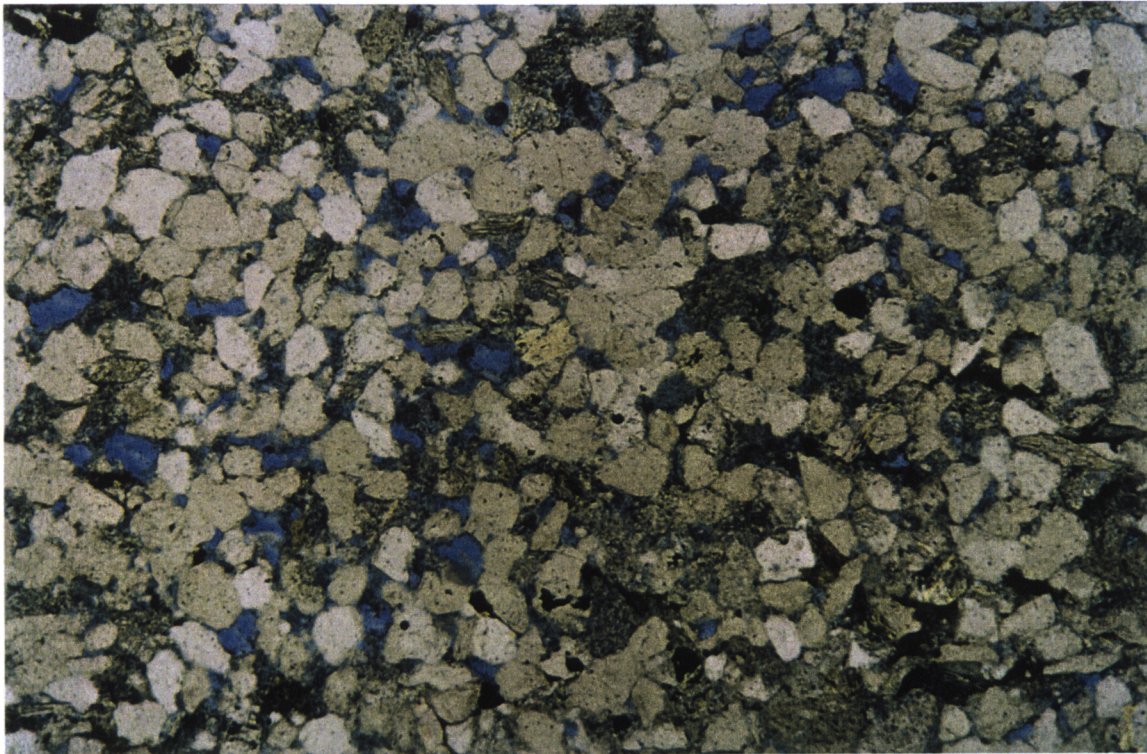


**Plate 22A: (Sample No. 016C, 2610.30 m):** Thin section photomicrograph showing generalised view of well sorted, subangular to rounded fine-grained sandstone with moderate amounts of intergranular porosity. Plane polarised light. Scale bar = 500  $\mu\text{m}$ .

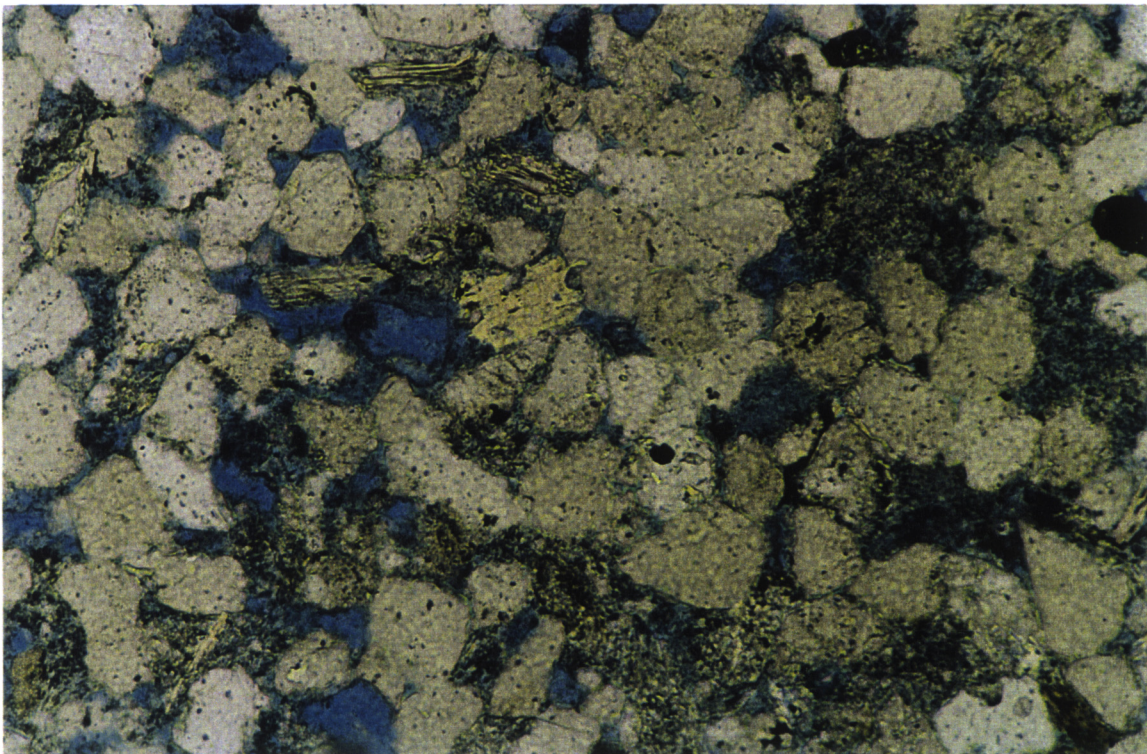


**Plate 22B: (Sample No. 016C, 2610.30 m):** Thin section photomicrograph showing triangular pore and minor secondary porosity. Secondary porosity has resulted from partial to complete dissolution of feldspar grains and lithic fragments. Plane polarised light. Scale bar = 200  $\mu\text{m}$ .

907511 ~~907511~~ 203



**Plate: 23: (Sample No. 016C, 2610.30 m):** SEM photomicrograph showing general view of the sample. Note the pores and pore throats are slightly interconnected giving fair permeability. Scale bar = 100  $\mu$ m.

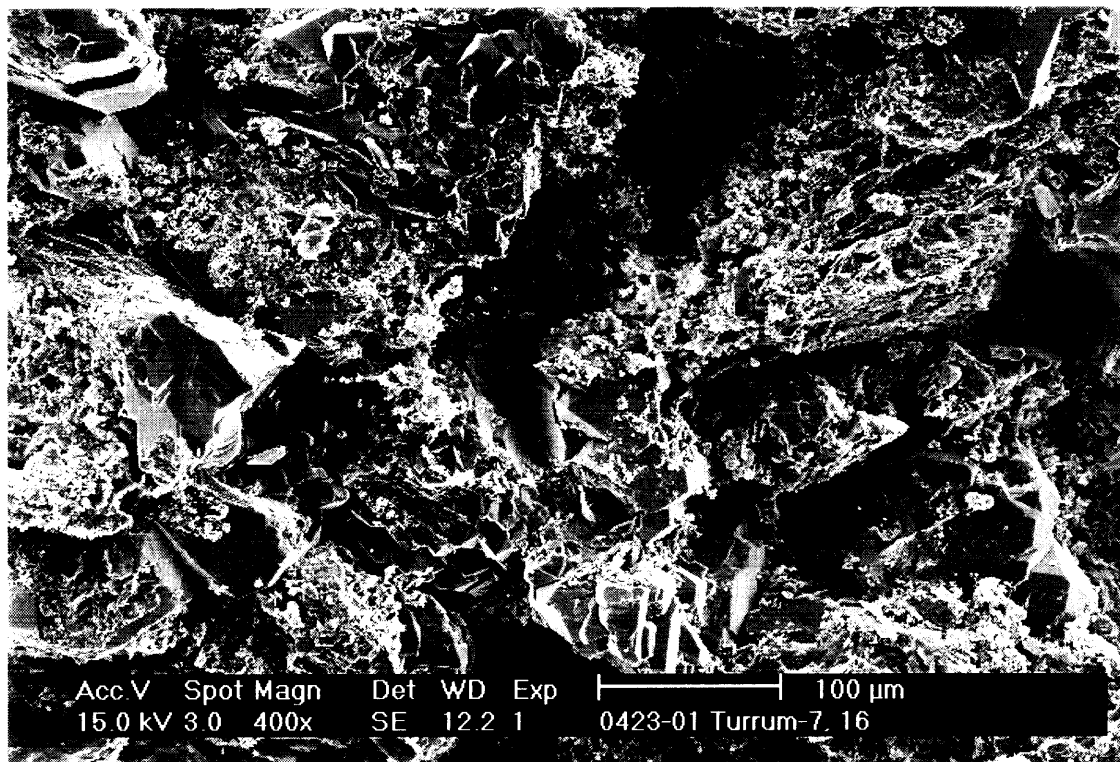


**Plate: 24: (Sample No. 016C, 2610.30 m):** SEM photomicrograph showing general view of the sample exhibiting minor amounts of quartz overgrowths and kaolinite. Kaolinite occurs as pore filling restricting the primary pores. Fibrous to hairy illite occurs later on the surface of the kaolinite booklets as a result of late alteration of feldspar and lithic fragments. Scale bar = 20  $\mu$ m.

204  
907511

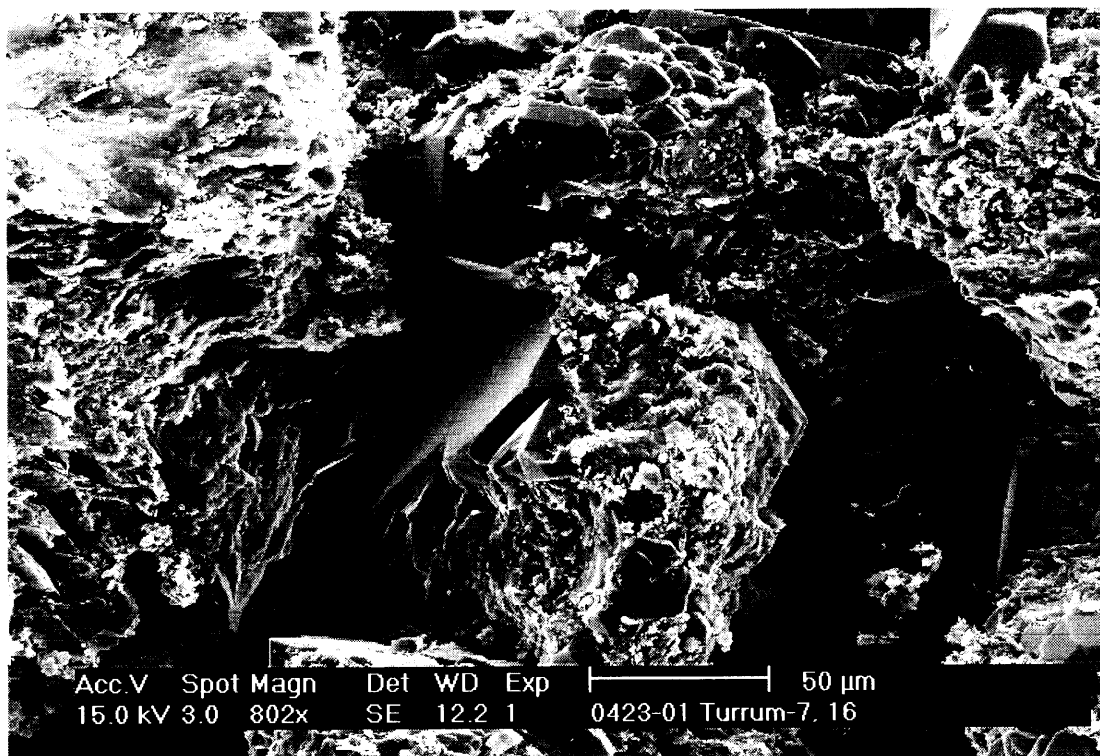


**Plate: 25: (Sample No. 016C, 2610.30 m):** SEM photomicrograph showing relatively large pore spaces. Note the pores and pore throats are slightly interconnected giving fair permeability. Scale bar = 50  $\mu$ m.

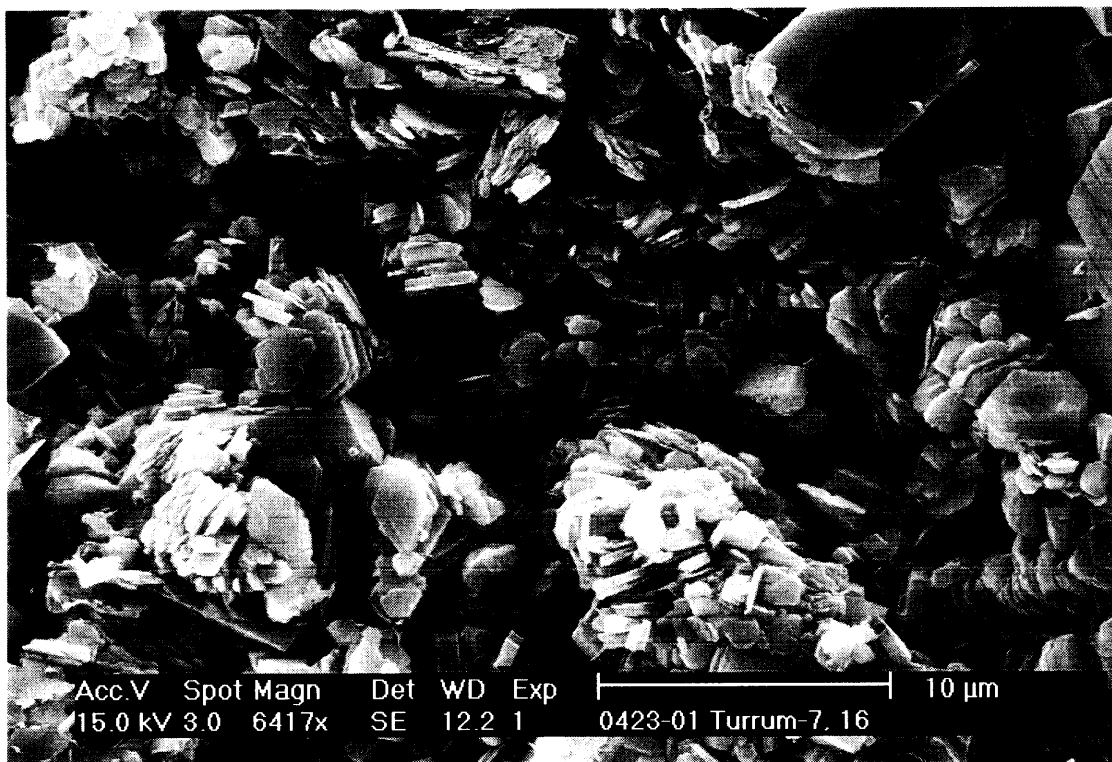


**Plate: 26: (Sample No. 016C, 2610.30 m):** SEM photomicrograph showing kaolinite booklets. Kaolinite occurs as pore filling pseudo hexagonal crystals ranging in size from less than 5  $\mu$ m up to 10  $\mu$ m. Local ragged kaolinite crystals suggest probable local corrosion or detrital origin. Scale bar = 10  $\mu$ m.

**SAMPLE:** NO. 028C (2611.30 m)

205  
907511 ~~907511~~

**Lithology:** Sublitharenite

**Texture:** The sample is dark brown to black, grain supported, massive with minor evidence of bioturbation, moderately sorted, silty to very fine-grained sandstone. Quartz grains are angular to subrounded. There are considerable amounts of authigenic minerals and low visual porosity.

**Composition:** The dominant framework component is monocrystalline quartz (27.2%). Polycrystalline quartz grains (1.6%) and potassium feldspar (0.8%) are present in trace amounts. Lithic fragments are minor components (6%) and predominantly comprise mica schist and chert. Mica is a minor component (2.2%). Detrital depositional clay matrix is also minor (3.8%). It comprises organic-rich silt to claystone. Dispersed organic matter is minor (2.6%). Authigenic minerals comprise siderite (27.6%) and pyrite (23.4%) with traces of authigenic kaolinite, and quartz (1.4%). There is a very low amount of visible porosity (3%).

Monocrystalline quartz displays strongly undulose extinction with some of the quartz grains containing fluid, igneous inclusions or needle-like minerals and biotite.

There is very low amount of porosity (3%) evident in this sample, mostly as scattered primary pores between detrital and authigenic minerals (Plate 27). Cementation is the main control, on the reservoir quality of this sample. Siderite and pyrite are dominant. Siderite occurs as pore filling micro spar crystals filling much of the pore spaces. It also replaces detrital matrix and organic matter. Pyrite is local in this sample and occurs as both early framboidal and late cubic crystals on the form of nodule.

**XRD:** No XRD run was taken for this sample.

**SEM:** No SEM photomicrographs for this sample.

**Diagenesis:** The diagenesis of this sample can be summarised as follows:

- Early compaction has affected this sample and has resulted in closer packing of grains and well-developed parallel alignment of elongated detrital grains.
- Framboidal pyrite could have occurred during the early sulphate reduction.

- Micro spar siderite cement occurred early in the diagenetic history at the end of the early sulphate reduction.
- Alteration and dissolution of feldspar, ductile lithic fragments and mica could have been responsible for the formation of kaolin.
- After kaolin precipitation quartz cements have occurred as overgrowths. The quartz overgrowths postdated or at least formed simultaneously with the precipitation of kaolin.
- Alteration of lithic fragments and potassium feldspar has continued to the late stage of diagenetic history and this has resulted in development of local secondary porosity and precipitation of authigenic illite. Authigenic illite occurs as fibrous to hairy crystals on the surface of kaolinite, altered feldspar grains and ductile lithic fragments. It also bridges the pore spaces and pore throats.
- Later in the diagenetic history, large cubic crystalline pyrite has occurred as pore filling around thin coal beds, organic-rich detrital matrix and coalified wood materials.

**Env. Deposition:** The very fine grain size, moderate sorting and moderate roundness of detrital grains in the sandstone, with the presence of bioturbation, indicate a low energy environment of deposition. Deposition may have possibly occurred in a meandering fluvial to tidal or upper offshore environment.

**Res. Potential:** The reservoir potential of this sample is poor. Visible porosity is very low in the sample (3%) with primary porosity being more common than secondary porosity. The primary pores have been partly to completely reduced in size by cementation. The pores are poorly interconnected giving a low permeability.

PE907511-35



**Plate 27A: (Sample No. 028C, 2611.30 m):** Thin section photomicrograph of sublitharenite comprising moderately sorted, silty to very fine-grained sandstone with very low proportion of intergranular porosity (blue) due to cementation by siderite and pyrite (black). Plane polarised light. Scale bar = 500  $\mu\text{m}$ .

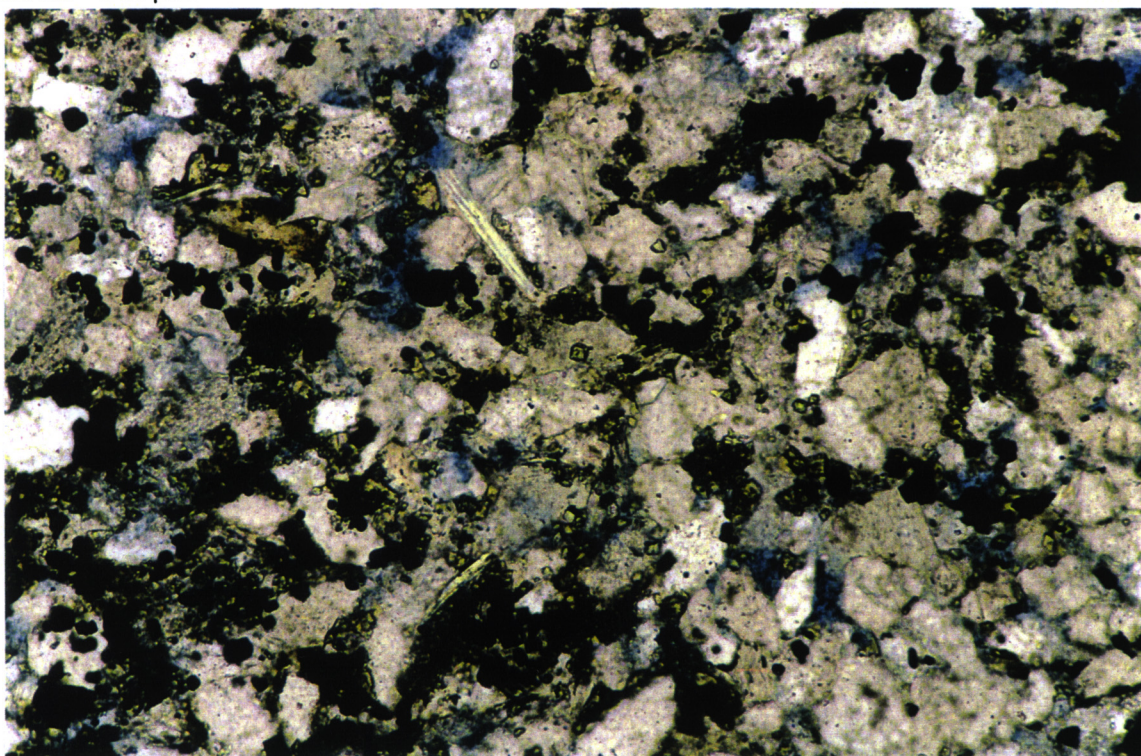


**Plate 27B: (Sample No. 028C, 2611.30 m):** Thin section photomicrograph showing micro spar siderite crystals filling the pore spaces and coating many of the detrital quartz grains. Precipitation of siderite and pyrite has occluded the reservoir quality in this sample. Plane polarised light. Scale bar = 200  $\mu\text{m}$ .

**SAMPLE:** NO. 092C (2616.65 m)

**Lithology:** Litharenite

**Texture:** The sample is creamy, grain supported, horizontal to small scale cross stratification, moderately to well sorted, fine-grained sandstone. Quartz grains are mainly subangular to rounded. Authigenic minerals are dominant and low visual porosity.

**Composition:** The sample is dominated by monocrystalline quartz (34.6%) with traces of minor polycrystalline quartz grains (2.8%) and potassium feldspar (1.6%). Lithic fragments are common (25.2%) and comprise predominantly mica schist (21.8%) and traces of quartzite (1.6%), rounded sedimentary chert (1%) and clay rich sedimentary rock fragments (0.4%). Mica is minor (5.4%), and most of which is muscovite. Detrital depositional matrix is another minor component (5.2%). Organic matter is traces (1%). Authigenic minerals comprise authigenic kaolinite (5.8%), siderite (5.4%), pyrite (5%), and traces of quartz. There are minor amounts of visible porosity (4.6%) in the sample.

Quartz is mainly monocrystalline and displays slight to strong undulose extinction with few grains having straight undulose extinction. Many of the quartz grains contain needle-like minerals, probably tourmaline and/or rutile. Lithic fragments are predominantly metamorphic mica schist and traces of rounded sedimentary chert. Mica is mainly muscovite and occurs as disseminated flakes.

Kaolinite is the dominant authigenic mineral and forms randomly oriented booklets that fill some of the spaces between detrital grains. Individual crystals are pseudo-hexagonal and range in size from less than 5  $\mu\text{m}$  up to 10  $\mu\text{m}$ .

Porosity is scattered locally throughout the sample (4.6%), usually as triangular pores between detrital and authigenic minerals (Plate 28). Secondary porosity is less common than the primary pores.

**XRD:** The sample is dominated by quartz, major kaolinite and mica (muscovite and illite) (Table 6, and Appendix II). The clay fraction (< 2  $\mu\text{m}$ ) is dominated by kaolinite and mica (muscovite and illite), (Table 7 and Appendix II).

**SEM:** No SEM photos were taken for this sample.



**Diagenesis:**

The diagenesis of this sample can be summarised as follows:

- Early compaction has affected this sample and has resulted in closer packing of grains and well-developed parallel alignment of elongated detrital grains.
- Framboidal pyrite could have occurred during the early sulphate reduction.
- Micro spar siderite cement occurred early in the diagenetic history at the end of the early sulphate reduction.
- Alteration and dissolution of feldspar, ductile lithic fragments and mica could have been responsible for the formation of kaolin.
- After kaolin precipitation quartz cements have occurred as overgrowths. The quartz overgrowths postdated or at least formed simultaneously with the precipitation of kaolin.
- Alteration of lithic fragments and potassium feldspar has continued to the late stage of diagenetic history and this has resulted in development of local secondary porosity and precipitation of authigenic illite. Authigenic illite occurs as fibrous to hairy crystals on the surface of kaolinite, altered feldspar grains and ductile lithic fragments. It also bridges the pore spaces and pore throats.
- Later in the diagenetic history, large cubic crystalline pyrite has occurred as pore filling around thin coal beds, organic-rich detrital matrix and coalified wood materials.

**Env. Deposition:**

The moderate to well sorting and moderate rounding nature in this fine-grained sandstone, along with the main sedimentary structures, indicates deposition in a low to moderate energy environment. Sedimentary structures are predominantly horizontal to small scale cross stratification, suggesting a meandering fluvial to lower shoreface environment.

**Res. Potential:**

Reservoir potential of this sample is fair to poor (4.6%). Compaction has contributed by up to 75% of the porosity loss while cementation has occluded around 17% of the original intergranular porosity. The sample has fair to low reservoir characteristics.

PE907511-36

210  
907511 ~~210~~



**Plate 28A: (Sample No. 092C, 2616.65 m):** Thin section photomicrograph showing general view of moderately to well sorted, fine-grained subangular to rounded litharenite with low amounts of primary intergranular porosity (blue). Plane polarised light. Scale bar = 500  $\mu$ m.

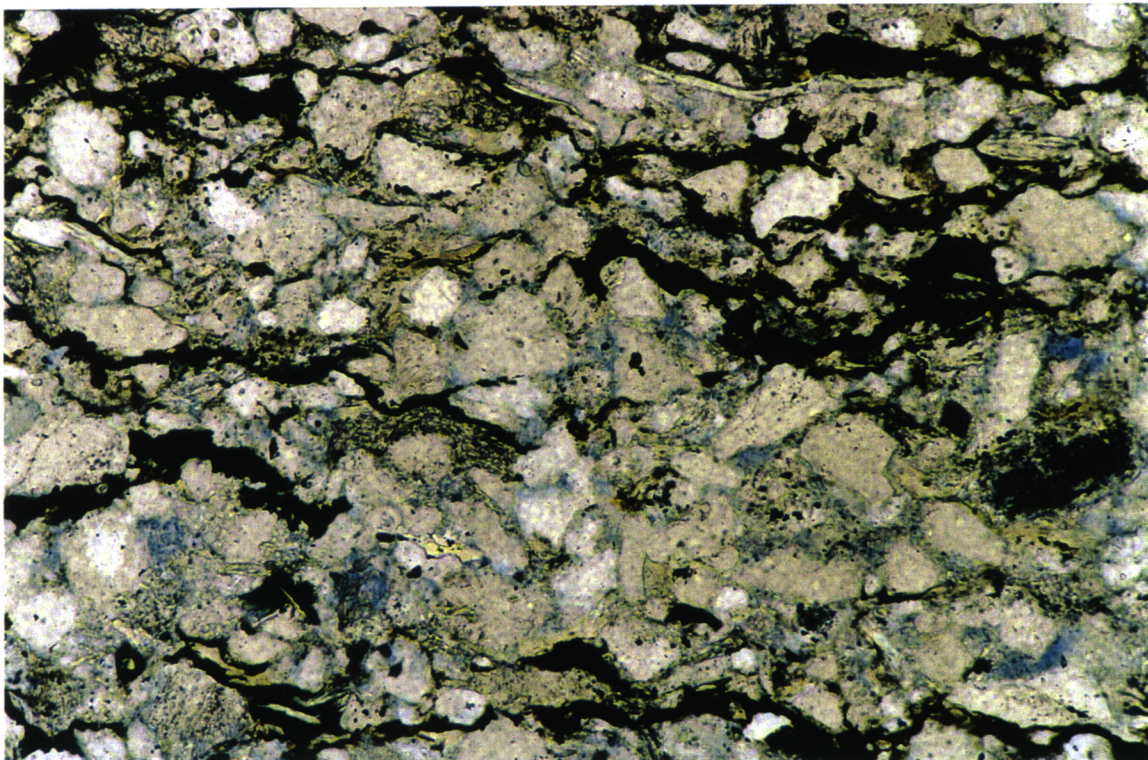


**Plate 28B: (Sample No. 092C, 2616.65 m):** Thin section photomicrograph of quartz arenite with low amounts of visual porosity. Note the presence of low amplitude stylolites indicating mechanical compaction. Plane polarised light. Scale bar = 200  $\mu$ m.

**SAMPLE:** NO. 100C (2617.25 m)

**Lithology:** Litharenite

**Texture:** The sample consists of creamy, grain supported, horizontally laminated to small scale cross stratification, well sorted, fine to medium-grained sandstone. Quartz grains are subangular to rounded. There are considerable amounts of authigenic minerals and moderate visual porosity.

**Composition:** Monocrystalline quartz is the main framework component and constitutes 29.4% of the sample. Polycrystalline quartz grains are minor (3.6%). Minor to trace amounts of potassium feldspar are present (2.8%). Lithic fragments are common (23.2%) and dominated by metamorphic micaceous schist (19.6%), quartzite (2.2%) and rounded sedimentary chert (1%). Mica is minor (4.2%) and dominated by muscovite. Detrital clay matrix and organic matter are trace components, 1.2% and 1% respectively. Authigenic minerals comprise siderite (11.2%), quartz overgrowth (7.4%), authigenic kaolinite (6.4%) and traces of pyrite (0.8%). Visible porosity is present in minor amounts in the sample (8.8%).

Monocrystalline quartz shows strongly undulose extinction. Few quartz grains contain fluid, igneous inclusions and needle-like minerals (tourmaline).

Porosity is minor in this sample (Plate 29). It occurs as both intergranular primary and secondary in origin. Secondary porosity is less common and originated by partial dissolution of feldspar, mica and ductile rock fragments.

**XRD:** Quartz is the dominant component of this sample with major kaolinite and mica (muscovite and illite), minor siderite and traces of potassium feldspar and pyrite, (Table 6 and Appendix II). The clay fraction (< 2  $\mu\text{m}$ ) is dominated by kaolinite and mica (muscovite and illite) (Table 7 and Appendix II).

**SEM:** The sample comprises a well sorted, fine to medium-grained sandstone with moderate amounts of authigenic clay mineral assemblage (Plate 30). Kaolinite occurs as fine to large pseudo hexagonal book-like crystals, ranging in size from 5  $\mu\text{m}$  up to 20  $\mu\text{m}$ . It occurs as pore filling, filling much of the pore spaces and pore throat and restricting the reservoir quality (Plate 31). Kaolinite also occurs around altered ductile lithic fragments and around altered feldspar grains (Plate 31), suggesting a direct relation between these components. Illite occurs as a late fibrous to hairy crystals around kaolinite, altered lithic fragments and altered feldspar grains. Illite crystals range in size from less than

1  $\mu\text{m}$  up to 5  $\mu\text{m}$ . They are bridging the pore spaces and throats and reducing permeability (Plate 32). SEM shows that quartz overgrowths are minor and have locally reduced the reservoir quality (Plate 33).

The pores are small, most of which are less than 10  $\mu\text{m}$  and occasionally less than 1  $\mu\text{m}$  (Plate 30).

**Diagenesis:**

The diagenesis of this sample can be summarised as follows:

- Early compaction has affected this sample and has resulted in closer packing of grains and well-developed parallel alignment of elongated detrital grains.
- Framboidal pyrite could have occurred during the early sulphate reduction.
- Micro spar siderite cement occurred early in the diagenetic history at the end of the early sulphate reduction.
- Alteration and dissolution of feldspar, ductile lithic fragments and mica could have been responsible for the formation of kaolin.
- After kaolin precipitation quartz cements have occurred as overgrowths. The quartz overgrowths postdated or at least formed simultaneously with the precipitation of kaolin.
- Alteration of lithic fragments and potassium feldspar has continued to the late stage of diagenetic history and this has resulted in development of local secondary porosity and precipitation of authigenic illite. Authigenic illite occurs as fibrous to hairy crystals on the surface of kaolinite, altered feldspar grains and ductile lithic fragments. It also bridges the pore spaces and pore throats.
- Later in the diagenetic history, large cubic crystalline pyrite has occurred as pore filling around thin coal beds, organic-rich detrital matrix and coalified wood materials.

**Env. Deposition:**

The well sorted nature, fine to medium grain size and horizontally laminated to small scale cross stratification in this sandstone sample, suggests a low to moderate energy depositional environment. The probable depositional environment of this sample is meandering fluvial to tidal to lower shoreface.

**Res. Potential:**

The sample has a moderate reservoir quality (8.8%). Precipitation of authigenic minerals apparently rather than mechanical compaction has affected the reservoir quality in this sample.

PE 907511 - 37

907511 ~~213~~ 213

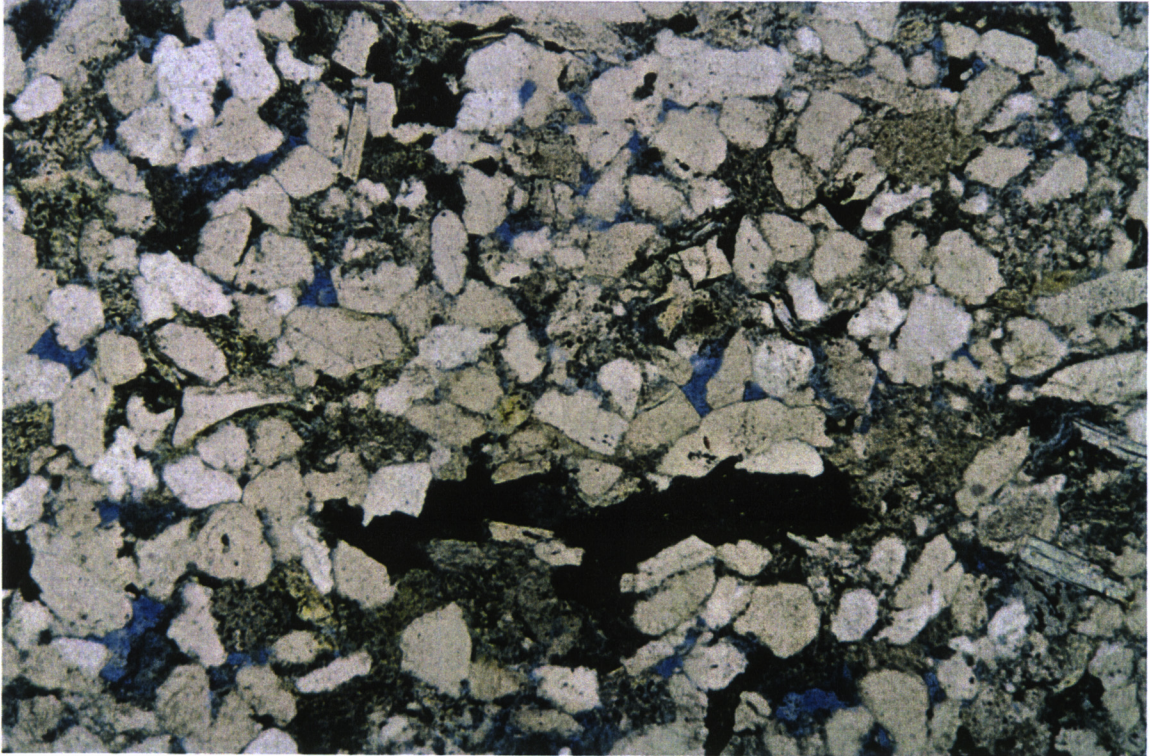


**Plate 29A: (Sample No. 100C, 2617.25 m):** Thin section photomicrograph showing general view of litharenite comprising well sorted, fine to medium-grained, subangular to rounded sandstone with moderate visual porosity. Note siderite cement patchily distributed. Plane polarised light. Scale bar = 500  $\mu\text{m}$ .

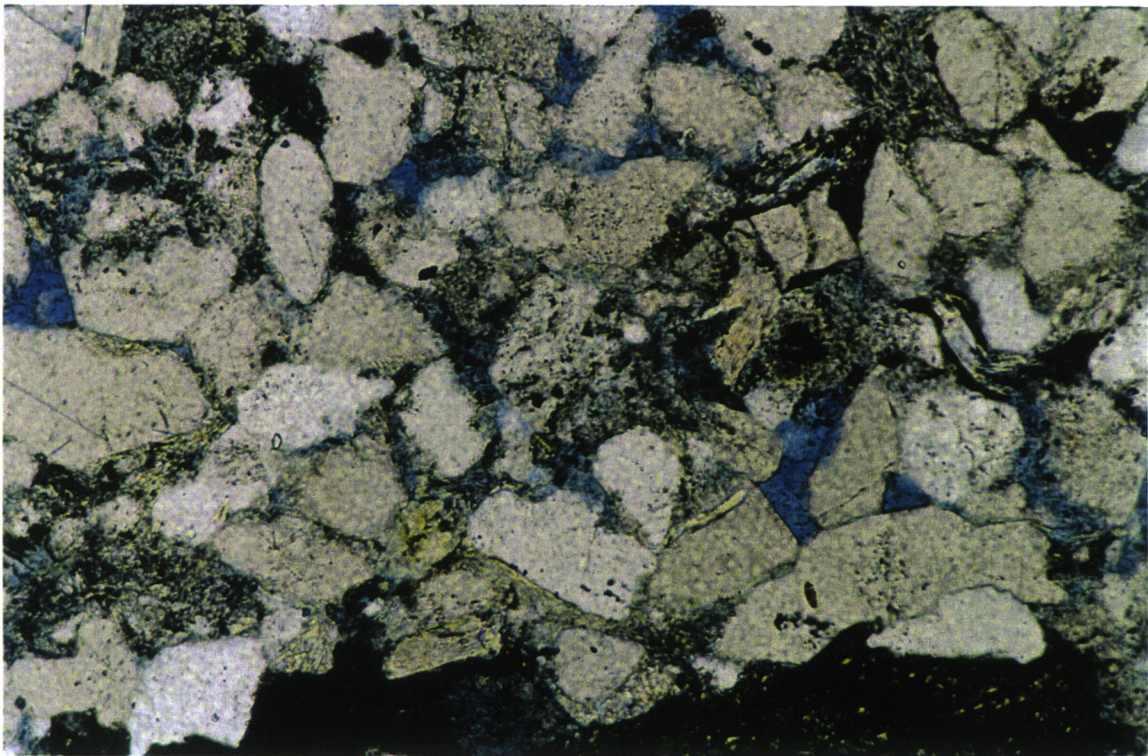


**Plate 29B: (Sample No. 100C, 2617.25 m):** Thin section photomicrograph showing moderate triangular visual porosity, implying that most of it was originated as primary intergranular porosity. Plane polarised light. Scale bar = 200  $\mu\text{m}$ .

907511-38

907511 <sup>214</sup> ~~38~~

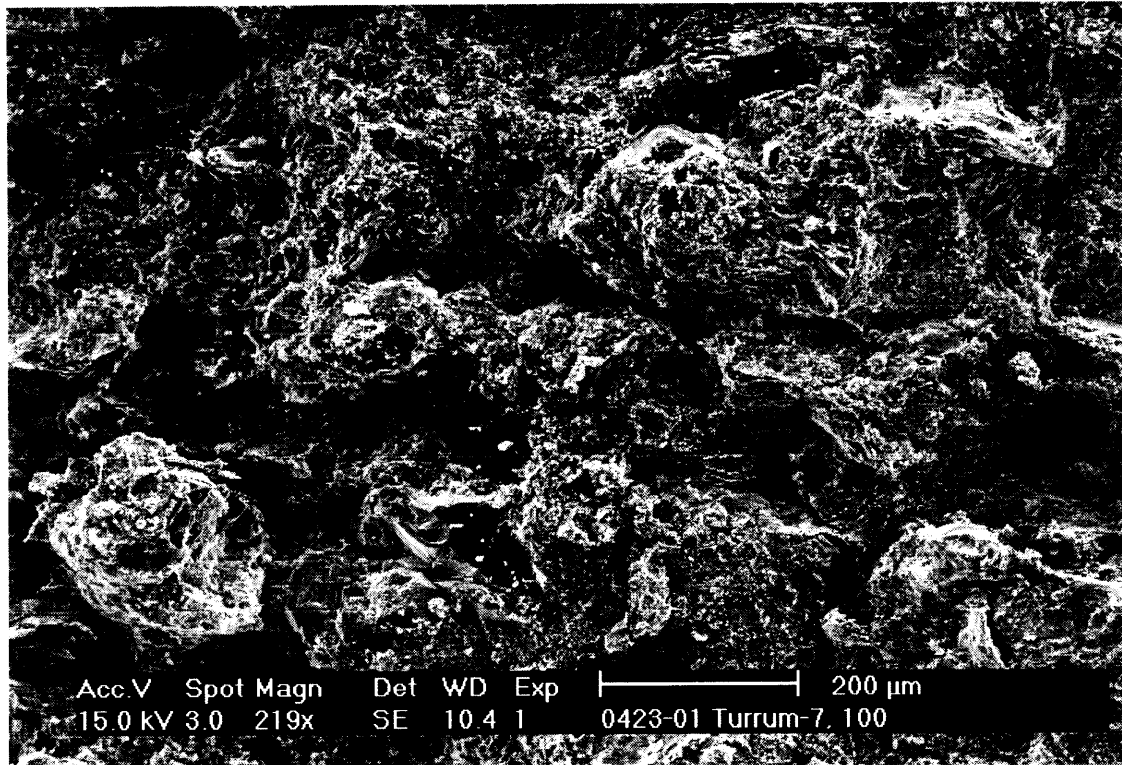


**Plate 30: (Sample No. 100C, 2617.25 m):** SEM photomicrograph showing general view of the sample with minor amounts of visual porosity. The pores are moderately to poorly interconnected giving low permeability in 3-D dimensions. Scale bar = 200 μm.

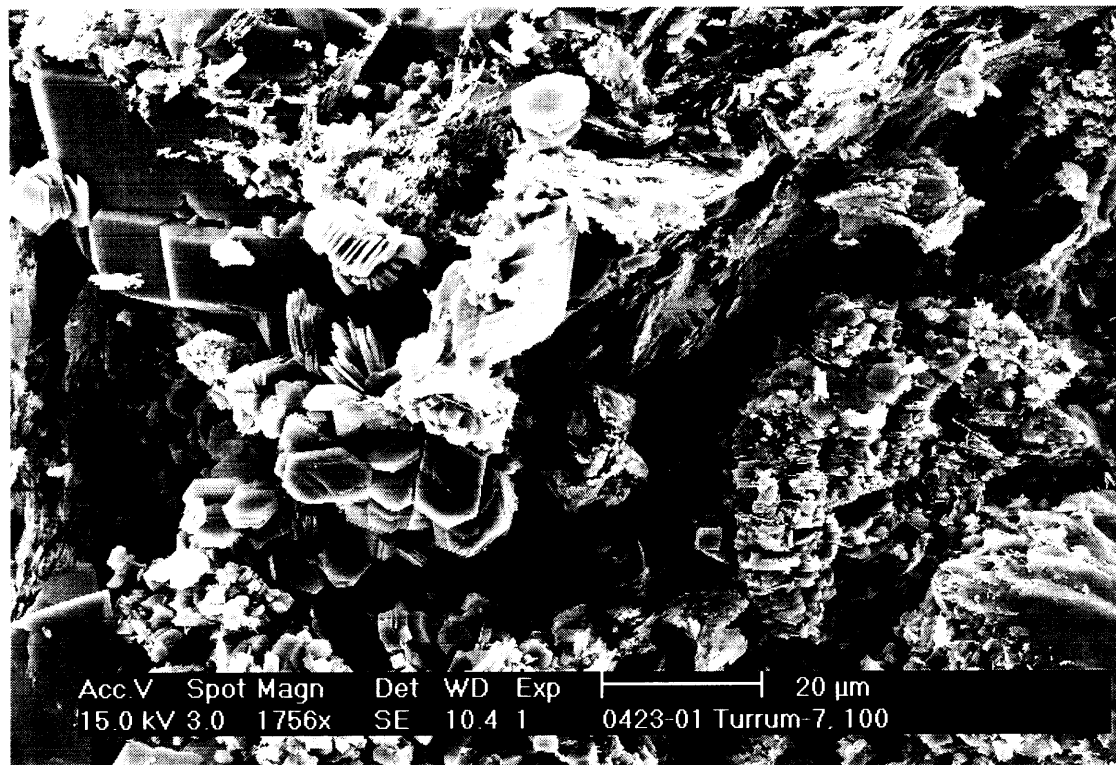


**Plate 31: (Sample No. 100C, 2617.25 m):** SEM photomicrograph showing pore filling kaolinite crystals filling much of the pore spaces. Note that kaolinite crystals are engulfed by quartz overgrowths suggesting at least simultaneous occurrence of both authigenic minerals. Kaolinite formed due to alteration of feldspar and lithic fragments. Scale bar = 20 μm.

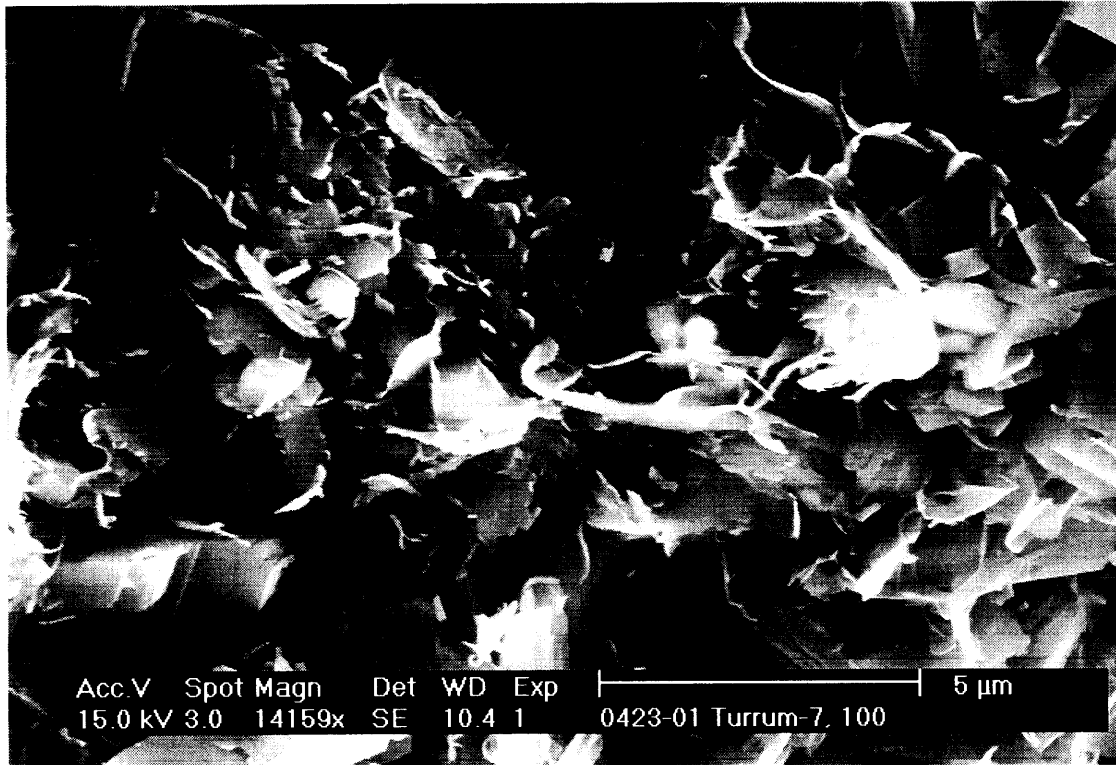


**Plate 32: (Sample No. 100C, 2617.25 m):** SEM photomicrograph showing fibrous to hairy authigenic illite filling and bridging the pores and pore throats. Illite formed due to alteration of mica schist lithic fragments. The pores are poorly interconnected giving low permeability in 3-D dimensions. Scale bar = 5 μm.

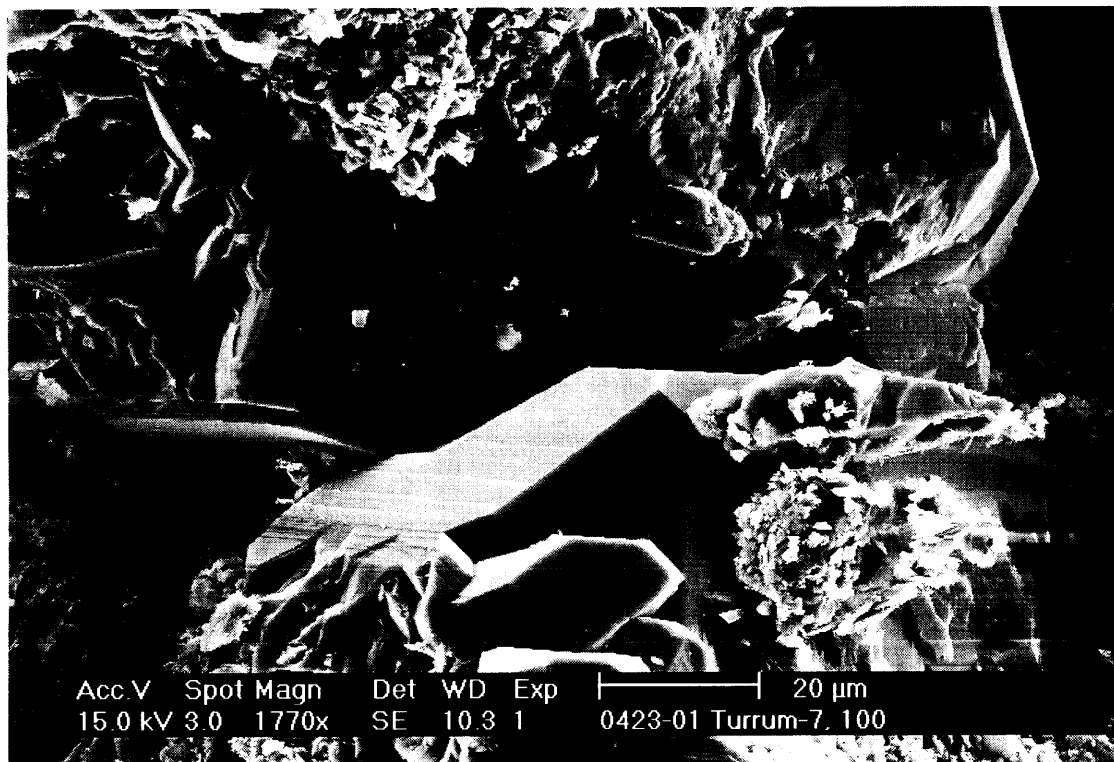


**Plate 33: (Sample No. 100C, 2617.25 m):** SEM photomicrograph showing quartz cement. Quartz cement occurs as large euhedral overgrowths. Note that kaolinite crystals are engulfed by quartz overgrowths suggesting at least simultaneous occurrence of both authigenic minerals. Scale bar = 20 μm.

**SAMPLE:** NO. V132C (2619.97 m)

**Lithology:** Litharenite

**Texture:** The sample is creamy, grain supported, horizontal to small scale cross stratification, well sorted, fine to medium-grained sandstone. Quartz grains are subangular to rounded. Moderate authigenic minerals and moderate visual porosity.

**Composition:** Monocrystalline quartz is the dominant framework component of this sample (31%). Polycrystalline quartz grains (2.8%) and potassium feldspar (3%) are minor components. Lithic fragments (20%) are common. Mica is minor component (9.4%) and comprises muscovite. Detrital depositional clay matrix is minor (4.8%). It consists of organic-rich silt to claystone. Dispersed organic matter is trace (2%). Authigenic minerals comprise kaolinite (8.2%), siderite (4.6%), pyrite (3%) and traces of quartz (1.2%). There are minor amounts of visible porosity (8.4%) in the sample (Plate 34).

Monocrystalline quartz grains exhibit subangular to rounded and display strongly undulose extinction with many grains containing fluid and igneous inclusions. Lithic fragments comprise metamorphic micaceous schist and rounded sedimentary chert.

There is a minor visual porosity (when the thin section is held to the light, Plate 34). Porosity mainly occurs as triangular pores between detrital and authigenic minerals. This suggests that the porosity is largely intergranular primary. Secondary porosity is much less common than in the primary pores. Secondary porosity was formed by minor dissolution of feldspar and ductile rock fragments.

**XRD:** The sample is dominated by quartz, major kaolinite and mica (muscovite and illite) and minor amounts of potassium feldspar, (Table 6 and Appendix II). The clay fraction (< 2  $\mu\text{m}$ ) is dominated by kaolinite and mica (muscovite and illite), (Table 7 and Appendix II).

**SEM:** The sample comprises a well sorted, fine to medium-grained sandstone with moderate amounts of authigenic clay mineral assemblage (Plate 35). Kaolinite occurs as fine to large pseudo hexagonal book-like crystals, ranging in size from 5  $\mu\text{m}$  up to 20  $\mu\text{m}$ . It occurs as pore filling, filling much of the pore spaces and pore throat and restricting the reservoir quality (Plate 36). SEM has also shown that quartz overgrowths are minor and has locally reduced the reservoir quality (Plate 37). Illite occurs as a late fibrous to hairy crystals around kaolinite, altered lithic fragments and altered feldspar grains. Illite crystals range in size from less than 1  $\mu\text{m}$  up to 5  $\mu\text{m}$ . They are bridging the pore spaces and throats and reducing permeability (Plate 38).



The pores are small, most of which are less than 10  $\mu\text{m}$  and occasionally less than 1  $\mu\text{m}$  (Plate 35). The pores are moderately interconnected in a 3-D network giving low permeability (Plate 35).

**Diagenesis:**

The diagenesis of this sample can be summarised as follows:

- Early compaction has affected this sample and has resulted in closer packing of grains and well-developed parallel alignment of elongated detrital grains.
- Framboidal pyrite could have occurred during the early sulphate reduction.
- Micro spar siderite cement occurred early in the diagenetic history at the end of the early sulphate reduction.
- Alteration and dissolution of feldspar, ductile lithic fragments and mica could have been responsible for the formation of kaolin.
- After kaolin precipitation quartz cements have occurred as overgrowths. The quartz overgrowths postdated or at least formed simultaneously with the precipitation of kaolin.
- Alteration of lithic fragments and potassium feldspar has continued to the late stage of diagenetic history and this has resulted in development of local secondary porosity and precipitation of authigenic illite. Authigenic illite occurs as fibrous to hairy crystals on the surface of kaolinite, altered feldspar grains and ductile lithic fragments. It also bridges the pore spaces and pore throats.
- Later in the diagenetic history, large cubic crystalline pyrite has occurred as pore filling around thin coal beds, organic-rich detrital matrix and coalified wood materials.

**Env. Deposition:**

The well sorted, fine to medium grain size and horizontal to small scale cross stratification, indicate a moderate to low-energy environment of deposition. The probable depositional environment is meandering fluvial. A precise depositional environment is hard to constrain, but from the general view and comparing with other samples, depositional environments could be tidal to lower shoreface.

**Res. Potential:**

The visible porosity is minor and consists predominantly of primary pores. The pores are poorly interconnected providing low porosity and permeability. Reservoir potential of this sample is fair to poor.

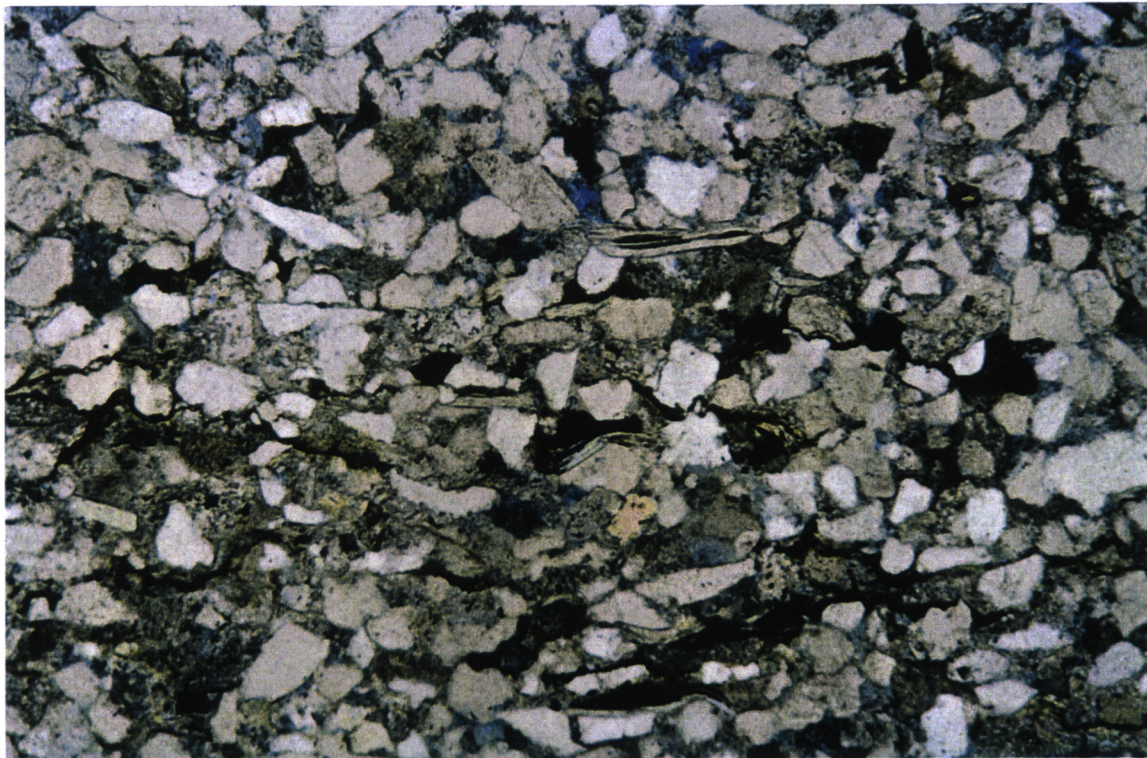


**Plate 34A: (Sample No. V132C, 2619.97 m):** Thin section photomicrograph showing general view of litharenite comprising well sorted, fine to medium-grained sandstone subangular to rounded sandstone. Plane polarised light. Scale bar = 500  $\mu\text{m}$ .

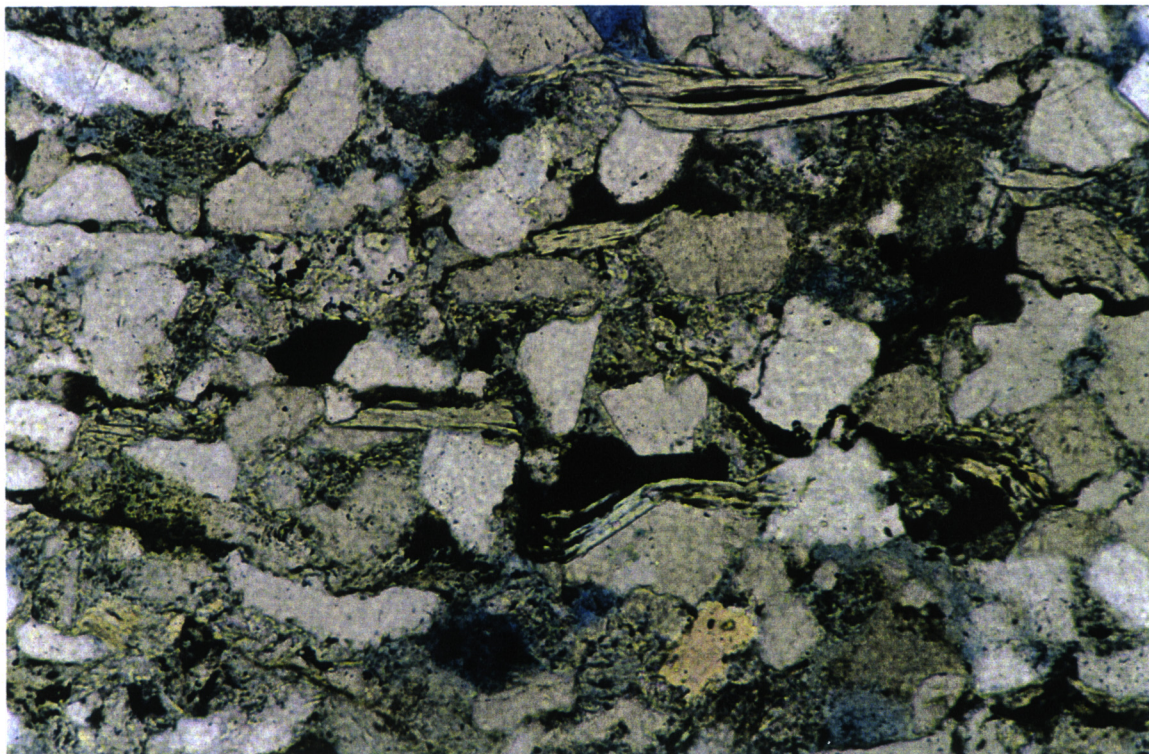


**Plate 34B: (Sample No. V132C, 2619.97 m):** Thin section photomicrograph showing minor amounts of visual porosity. Note also the presence of mica squeezed between rigid grains indicating mechanical compaction. Plane polarised light. Scale bar = 200  $\mu\text{m}$ .

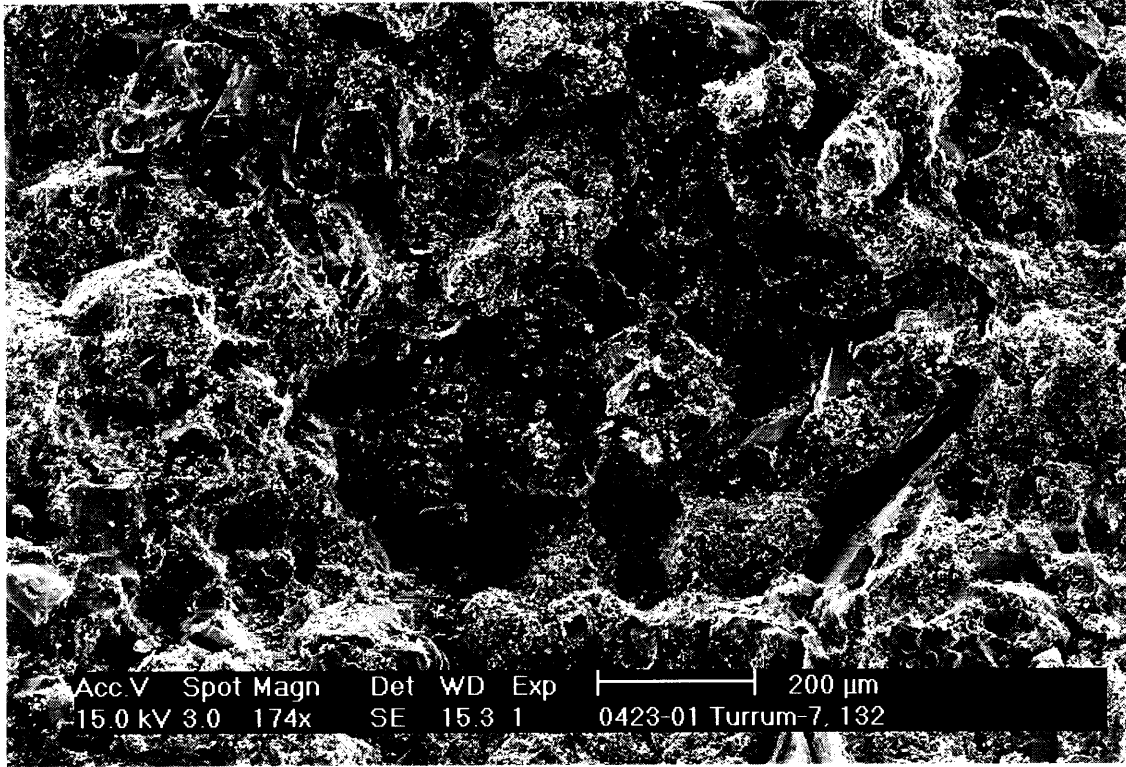


**Plate 35: (Sample No. V132C, 2619.97 m):** SEM photomicrograph showing general view of the sample with minor amounts of visual porosity. The pores are moderately to poorly interconnected giving low permeability in 3-D. Scale bar = 200 µm.

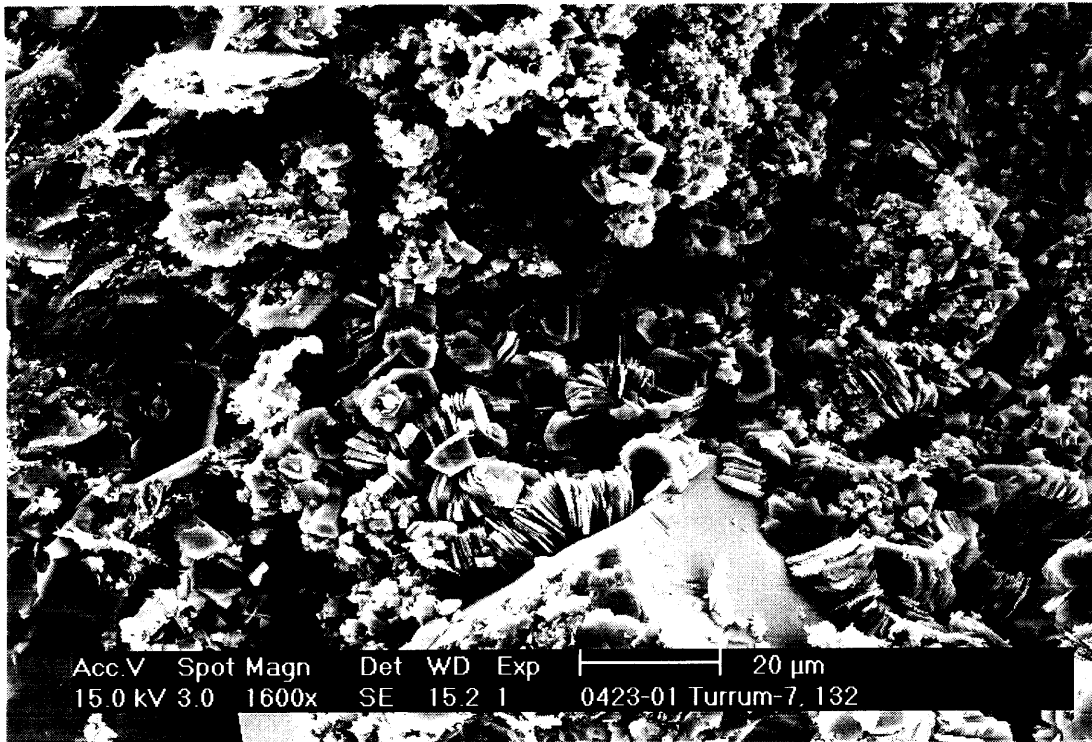


**Plate 36: (Sample No. V132C, 2619.97 m):** SEM photomicrograph showing pore filling authigenic kaolinite. Kaolinite occurs as pseudo hexagonal book-like crystals filling much of the pore spaces and restricting the intergranular primary porosity. Note alteration of lithic fragments. Scale bar = 20 µm.

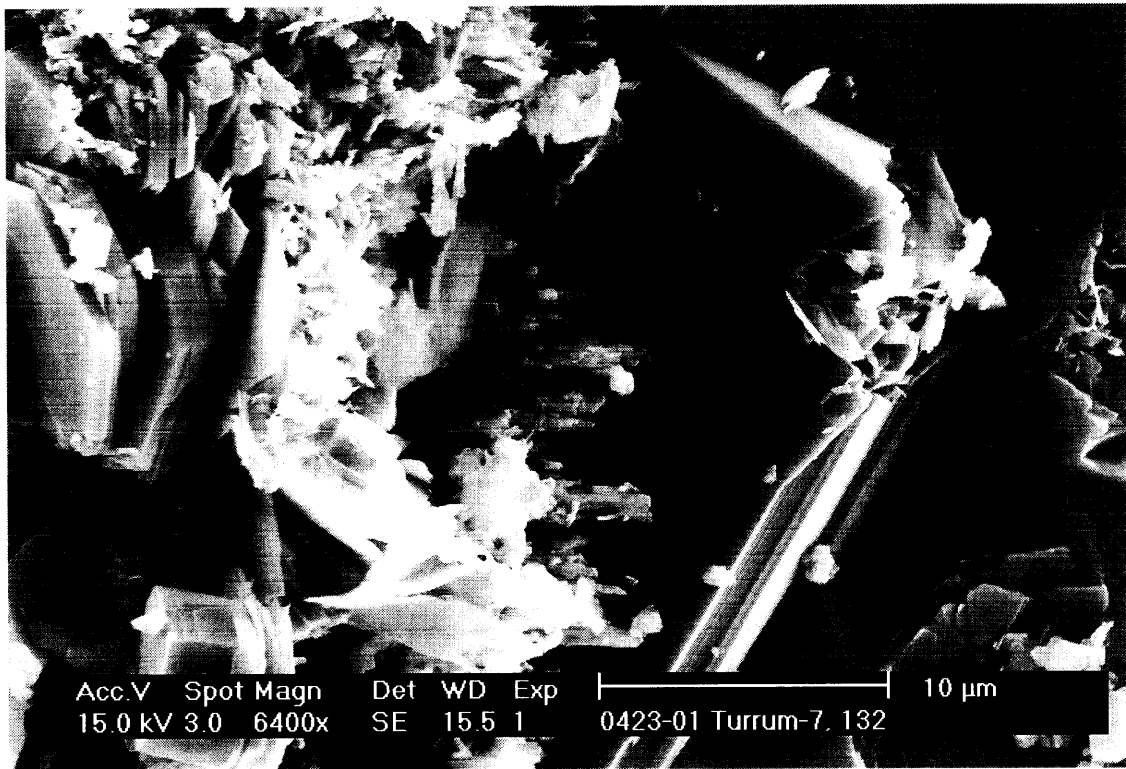


**Plate 37: (Sample No. V132C, 2619.97 m):** SEM photomicrograph showing alteration of feldspar grain to form kaolinite. Note that kaolinite crystals are engulfed by the quartz cement suggesting at least simultaneous occurrence of both authigenic minerals. Scale bar = 10 µm.

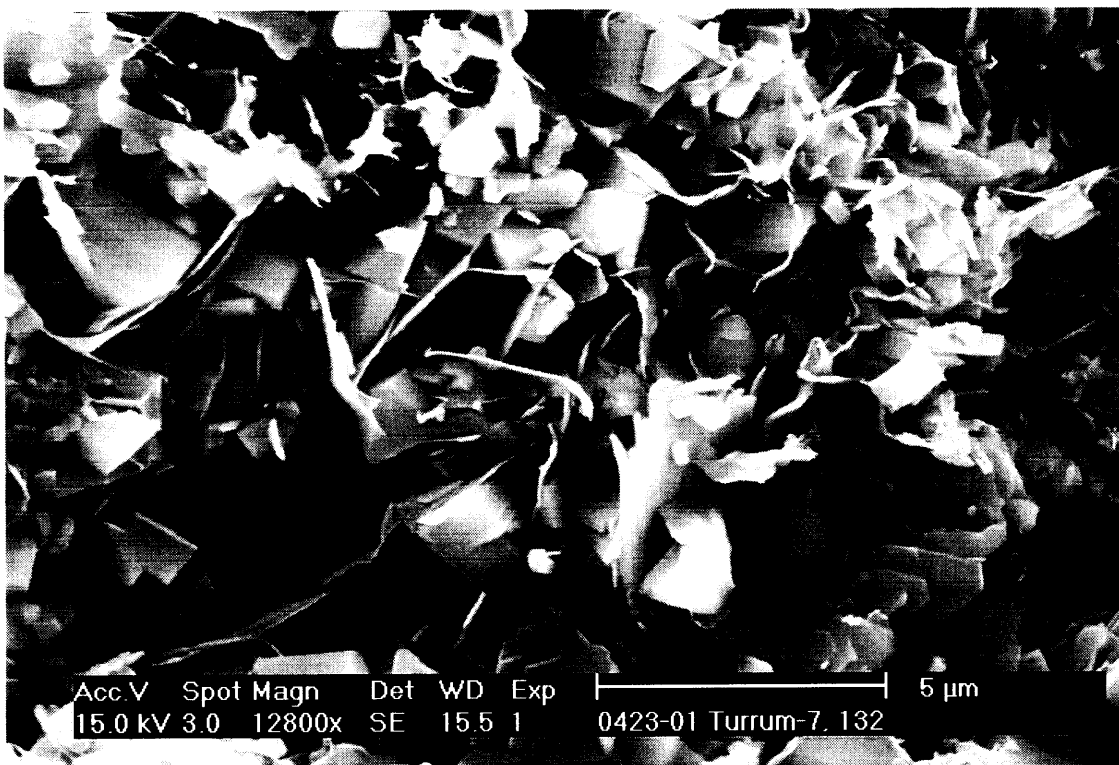


**Plate 38: (Sample No. V132C, 2619.97 m):** SEM photomicrograph showing fibrous to hairy authigenic illite on the surface of kaolinite booklets. Illite bridges the pores and pore throats, restricting the intergranular porosity and reducing permeability. Scale bar = 5 µm.

**SAMPLE:** NO. 150C (2621.45 m)

**Lithology:** Litharenite

**Texture:** The sample consists of creamy, grain supported, horizontal to small scale cross stratification, moderately to well sorted, medium-grained sandstone. Quartz grains are subangular to rounded. There are considerable amounts of authigenic minerals and moderate to low visual porosity.

**Composition:** The framework components of this sample are dominated by lithic fragments (30%) and monocrystalline quartz (27%). Polycrystalline quartz (2.4%), potassium feldspar (1.8%) and mica (4.6%) are trace to minor components. Mica is mainly muscovite. Detrital depositional clay matrix is minor (5.2%) and comprises organic-rich silt to claystone. Authigenic minerals are dominated by kaolinite (11.4%), siderite (7.2%) and pyrite (4%). There are minor amounts of visible porosity in this sample (5.4%).

Monocrystalline quartz exhibits strong undulose extinction with few grains showing straight undulose extinction. Lithic grains are predominantly mica schist with traces of quartzite and rounded sedimentary chert.

Visible porosity is minor (Plate 39) most of which is primary in origin. Mechanical compaction is the main factor controlling the reservoir quality in this sample. It reduces around 63% of the primary intergranular porosity meanwhile cementation of authigenic minerals has occluded around 28%.

**XRD:** Quartz is dominant with major kaolinite and mica (muscovite and illite), and traces of potassium feldspar, (Table 6 and Appendix II). The clay fraction (< 2  $\mu\text{m}$ ) is dominated by kaolinite and mica (muscovite and illite) Table 7 and Appendix II).

**SEM:** The sample comprises a moderately to well sorted, medium-grained sandstone with moderate amounts of authigenic clay mineral assemblage (Plate 40). Kaolinite occurs as fine to large pseudo hexagonal book-like crystals, ranging in size from 5  $\mu\text{m}$  up to 20  $\mu\text{m}$ . It occurs as pore filling, filling much of the pore spaces and pore throat and restricting the reservoir quality (Plate 41). Illite occurs as a late fibrous to hairy crystals around kaolinite, altered lithic fragments and altered feldspar grains. Illite crystals range in size from less than 1  $\mu\text{m}$  up to 5  $\mu\text{m}$  (Plate 42). They are bridging the pore spaces and throats and reducing permeability. SEM shows that quartz overgrowths are minor and have locally reduced the reservoir quality (Plate 43).

The pores are small, most of which are less than 10  $\mu\text{m}$  and occasionally less than 1  $\mu\text{m}$  (Plate 40). The distribution of the pore throat is irregular with poor interconnection implying low permeability (Plate 40).

**Diagenesis:**

The diagenesis of this sample can be summarised as follows:

- Early compaction has affected this sample and has resulted in closer packing of grains and well-developed parallel alignment of elongated detrital grains.
- Framboidal pyrite could have occurred during the early sulphate reduction.
- Micro spar siderite cement occurred early in the diagenetic history at the end of the early sulphate reduction.
- Alteration and dissolution of feldspar, ductile lithic fragments and mica could have been responsible for the formation of kaolin.
- After kaolin precipitation quartz cements have occurred as overgrowths. The quartz overgrowths postdated or at least formed simultaneously with the precipitation of kaolin.
- Alteration of lithic fragments and potassium feldspar has continued to the late stage of diagenetic history and this has resulted in development of local secondary porosity and precipitation of authigenic illite. Authigenic illite occurs as fibrous to hairy crystals on the surface of kaolinite, altered feldspar grains and ductile lithic fragments. It also bridges the pore spaces and pore throats.
- Later in the diagenetic history, large cubic crystalline pyrite has occurred as pore filling around thin coal beds, organic-rich detrital matrix and coalified wood materials.

**Env. Deposition:**

The medium sand size detrital grains in this sample range from subangular to rounded and moderate to well sorting. These features suggest deposition in a moderate to low energy environment. The environment of deposition was most probably meandering fluvial to tidal to lower shoreface.

**Res. Potential:**

The sample shows a poor reservoir potential with low visible porosity (4.4%). The porosity is poorly interconnected in a 3-D network giving a low permeability and reservoir quality.

PE907511-43

907511 ~~223~~ 223

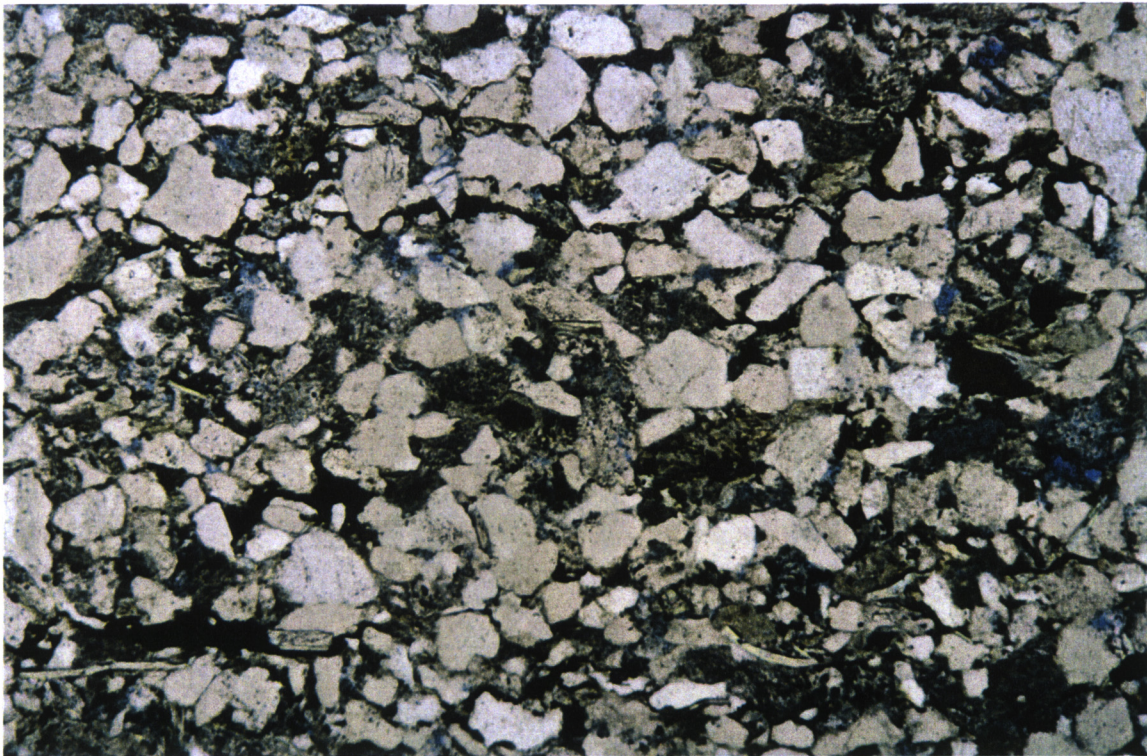


**Plate 39A: (Sample No. 150C, 2621.45 m):** Thin section photomicrograph showing general view of litharenite. The sample comprises moderately to well sorted, medium-grained, subangular to rounded sandstone. Minor visible porosity and fair to poor reservoir quality. Plane polarised light. Scale bar = 500  $\mu\text{m}$ .

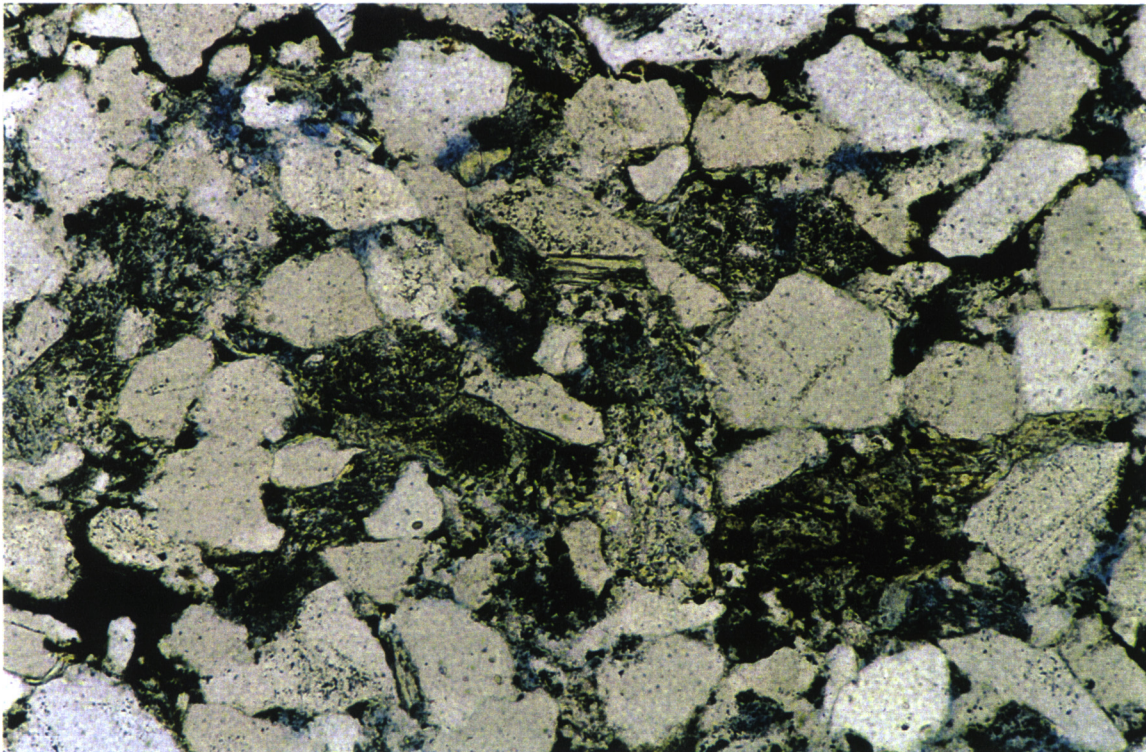


**Plate 39B: (Sample No. 150C, 2621.45 m):** Enlarged view of Plate 39.A. Plane polarised light. Scale bar = 200  $\mu\text{m}$ .

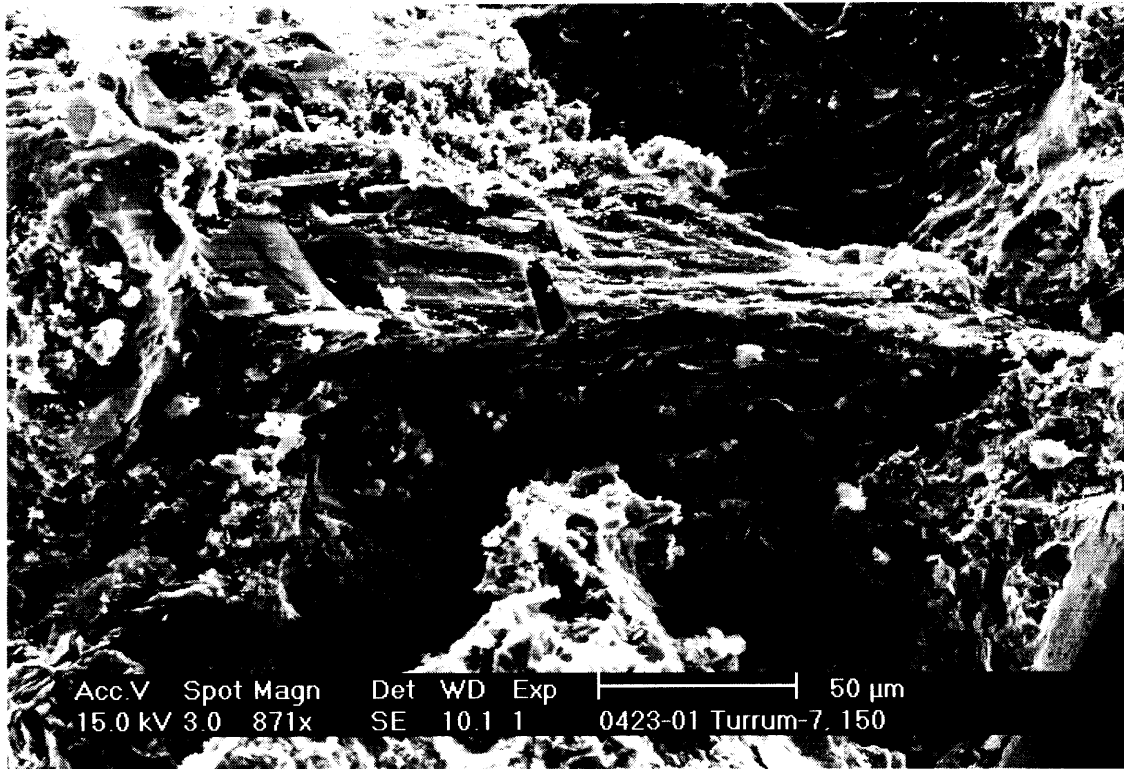


**Plate 40: (Sample No. 150C, 2621.45 m):** SEM photomicrograph showing general view of the sample. The pores are partially to completely filled with authigenic clays. The pores and pore throat are poorly connected giving a low permeability. Scale bar = 50 μm.

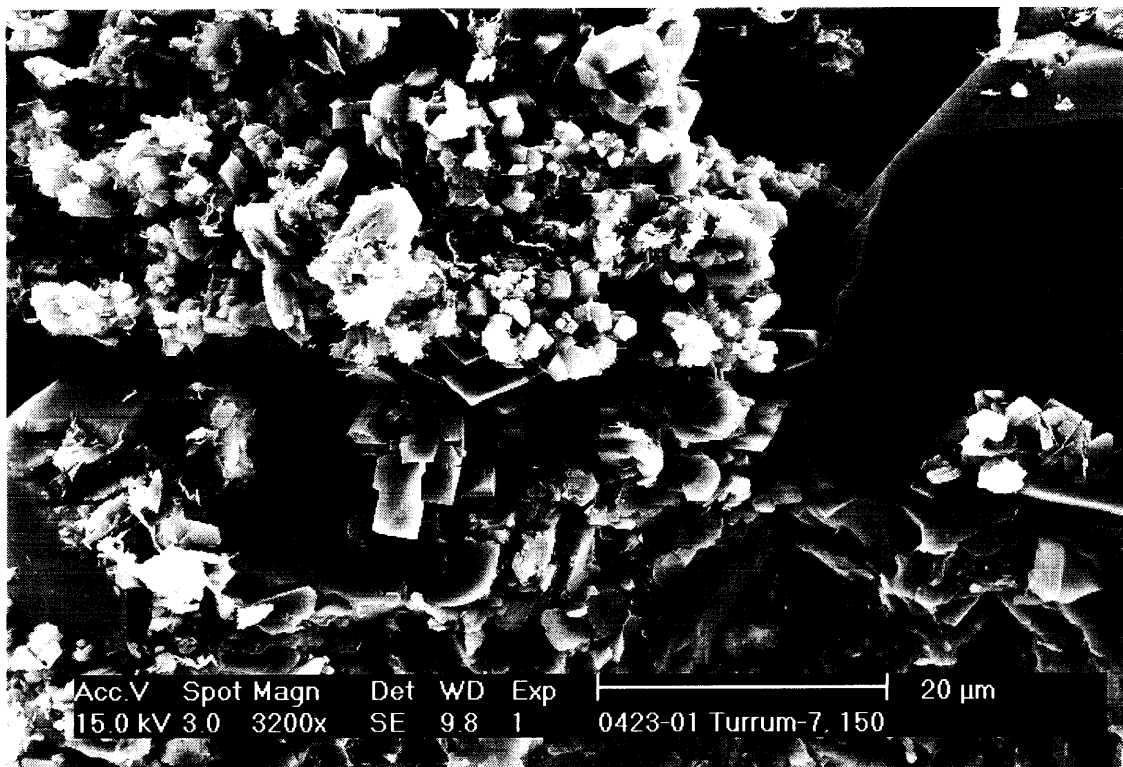


**Plate 41: (Sample NO. 150C, 2621.45 m):** SEM photomicrograph showing pore filling kaolinite. Note that illite has developed on the surface of kaolinite crystals. The poorly connected pore spaces and pore throat give low permeability and reservoir quality. Scale bar = 20 μm.



907511 ~~225~~  
225

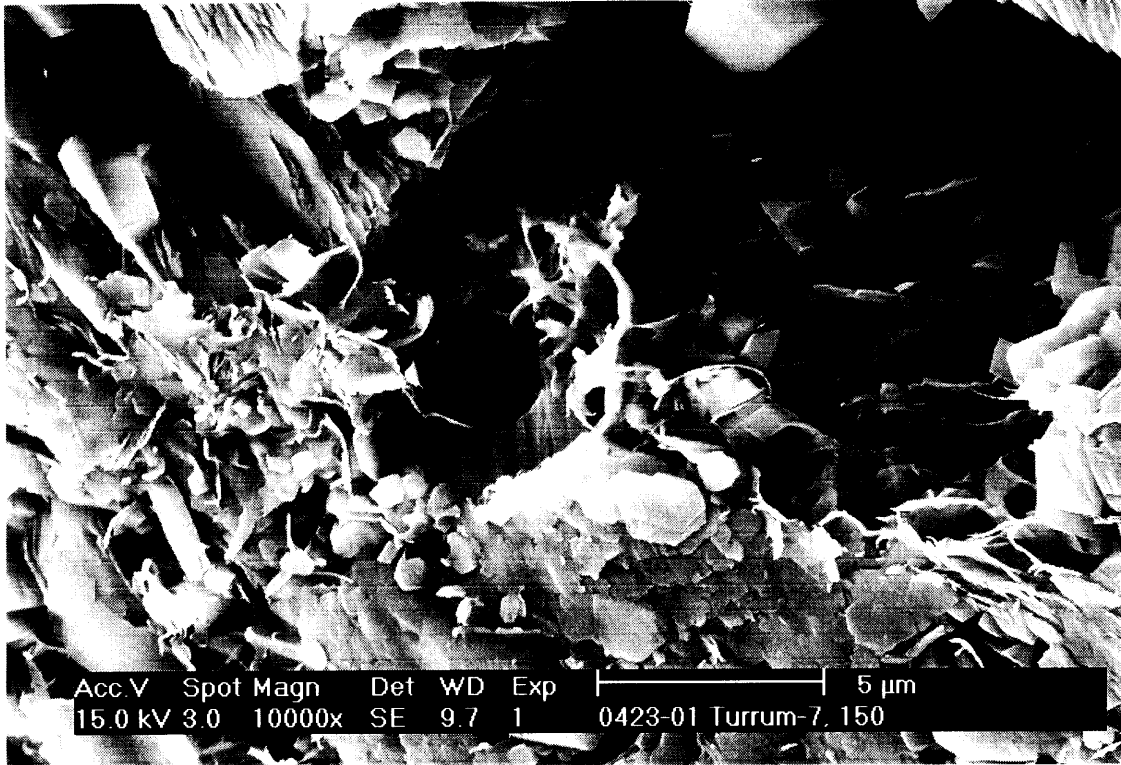


**Plate 42: (Sample No. 150C, 2621.45 m):** SEM photomicrograph showing authigenic hairy to fibrous illite filling and bridging the pores and pore throats and restricting the reservoir quality. Scale bar = 5 μm.

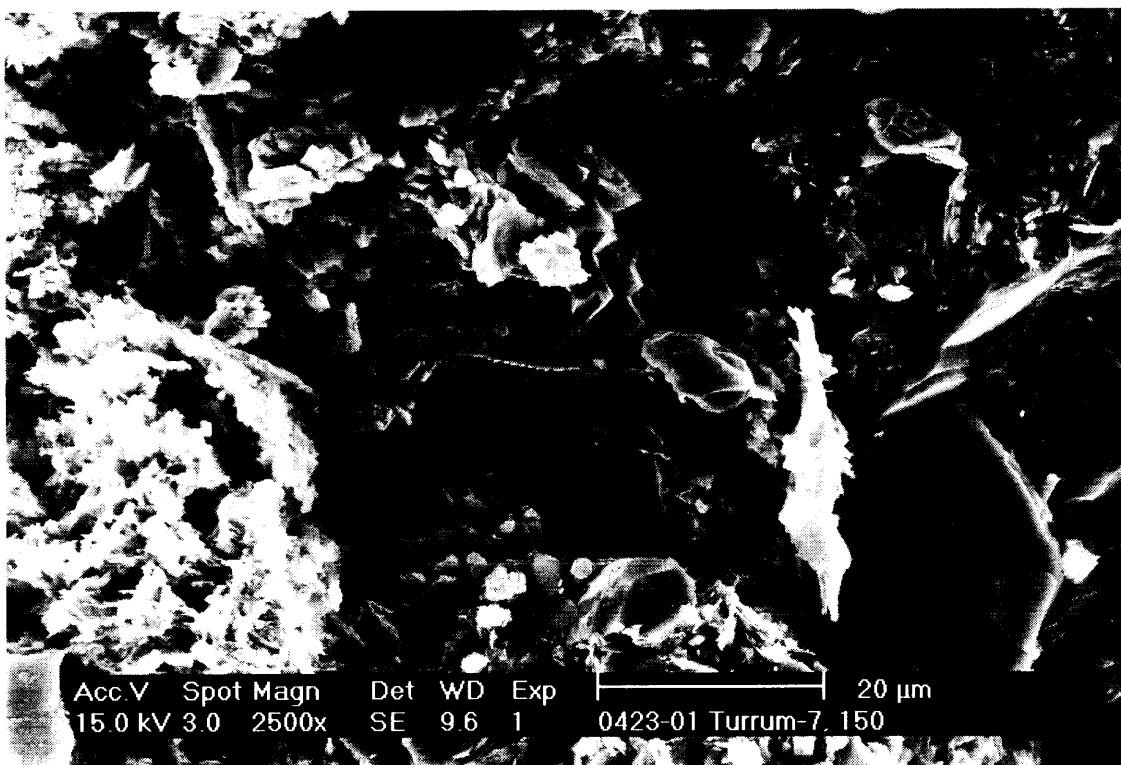


**Plate 43: (Sample No. 150C, 2621.45 m):** SEM photomicrograph showing small pores and pore throats. The poorly connected pore spaces and pore throat give low permeability and low reservoir quality. Scale bar = 20 μm.

**SAMPLE:** NO. 152C (2621.65 m)

**Lithology:** Lithwacke

**Texture:** Creamy to brown, grain supported, horizontal to small scale cross stratification, moderately sorted, very fine-grained sandstone. Quartz grains are angular to subrounded. Moderate authigenic minerals and very low visual porosity.

**Composition:** The framework component of the sample is dominated by lithic fragments (28.8%) and monocrystalline quartz (21.4%). Polycrystalline quartz grains (1.4%) and potassium feldspar (2.8%) are trace components. Detrital depositional clay matrix is present in significant amounts (18.8%) and comprises organic-rich silty to very fine-grained sandstone. Dispersed organic matter and coal thin laminae are present in minor amounts (3.6%). Mica (muscovite) is present as a minor component (10.6%). Authigenic minerals comprise pyrite (4.6%), siderite (3.6%) and kaolinite (3.4%). There are trace amounts of visible porosity (Plate 44).

Monocrystalline quartz occurs normally as subangular to rounded grains and displays strongly undulose extinction with many grains containing fluid and igneous inclusions. Lithic fragments predominantly comprise metamorphic mica schist and rounded sedimentary chert.

The amount of visual porosity (Plate 44) in this sample is very low due to the abundant of detrital depositional clay matrix. The main agent controlling the reservoir quality in this sample is the mechanical compaction and the presence of detrital matrix.

**XRD:** XRD results show that quartz is the dominant component with major kaolinite and mica (muscovite and illite) and minor potassium feldspar, (Table 6 and Appendix II). The clay fraction (< 2 mm) is dominated by kaolinite and mica (muscovite and illite), (Table 7 and Appendix II).

**SEM:** No SEM photomicrographs were taken for this sample.

**Diagenesis:** The diagenesis of this sample can be summarised as follows:

- Early compaction has affected this sample and has resulted in closer packing of grains and well-developed parallel alignment of elongated detrital grains.
- Framboidal pyrite could have occurred during the early sulphate reduction.

- Micro spar siderite cement occurred early in the diagenetic history at the end of the early sulphate reduction.
- Alteration and dissolution of feldspar, ductile lithic fragments and mica could have been responsible for the formation of kaolin.
- After kaolin precipitation quartz cements have occurred as overgrowths. The quartz overgrowths postdated or at least formed simultaneously with the precipitation of kaolin.
- Alteration of lithic fragments and potassium feldspar has continued to the late stage of diagenetic history and this has resulted in development of local secondary porosity and precipitation of authigenic illite. Authigenic illite occurs as fibrous to hairy crystals on the surface of kaolinite, altered feldspar grains and ductile lithic fragments. It also bridges the pore spaces and pore throats.
- Later in the diagenetic history, large cubic crystalline pyrite has occurred as pore filling around thin coal beds, organic-rich detrital matrix and coalified wood materials.

**Env. Deposition:** The moderate sorting and moderate rounding in this very fine-grained sandstone, with abundant detrital depositional clay matrix, suggests deposition in a low energy environment. Possible environments include tidal to lower shoreface to upper offshore.

**Res. Potential:** Visible porosity is very low (traces) and the pores are poorly interconnected in a 3-D network giving a very low permeability. The reservoir quality is poor.

PE907511-45

907511 ~~201~~ 228



**Plate 44A: (Sample No. 152C, 2621.65 m):** Thin section photomicrograph showing generalised view of moderately sorted, very fine-grained, angular to subrounded sandstone with trace amounts of intergranular porosity. Plane polarised light. Scale bar = 500  $\mu\text{m}$ .

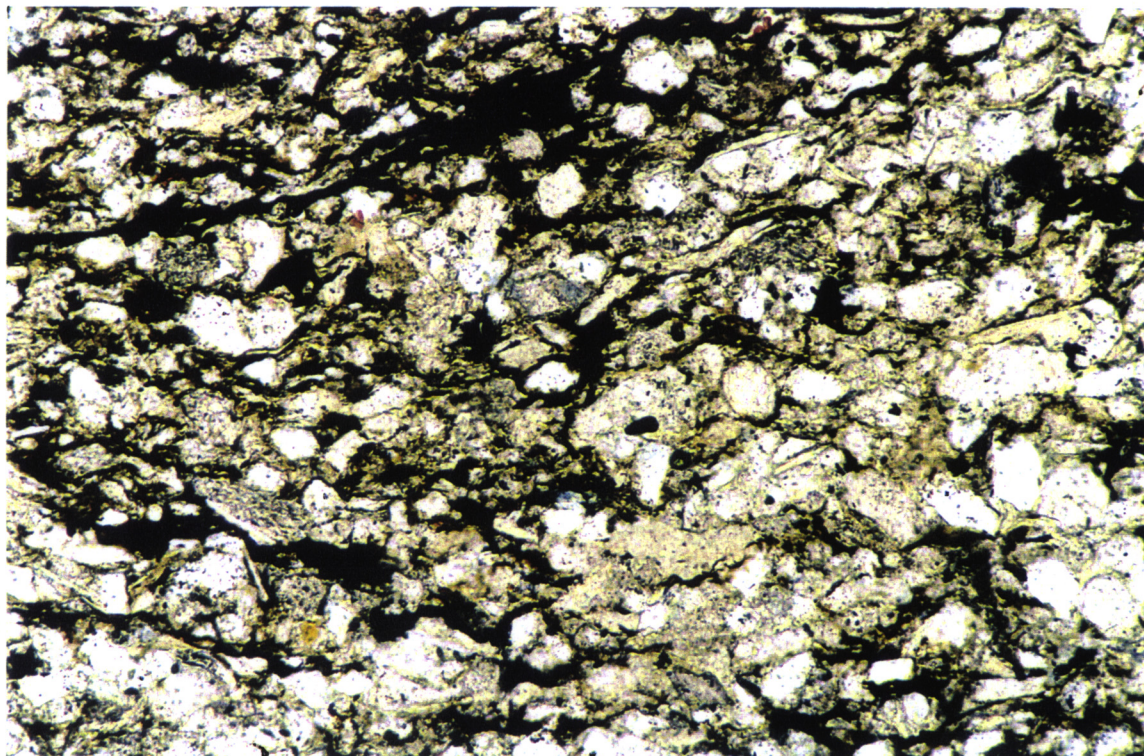


**Plate 44B: (Sample No. 152C, 2621.65 m):** The dirty part of the sample with high proportion of detrital depositional matrix. Note trace visual porosity. Plane polarised light. Scale bar = 200  $\mu\text{m}$ .

**SAMPLE:** NO. 178C (2623.85 m)

**Lithology:** Lithwacke

**Texture:** The sample depicts a creamy to brown, grain supported, horizontal to small scale cross stratification with evidence of local bioturbation, moderately sorted, very fine-grained sandstone. Quartz grains are angular to subrounded. Moderate authigenic minerals and low visual porosity.

**Composition:** Monocrystalline quartz is the dominant framework component (41.2%) with trace amounts of polycrystalline quartz grains (2%). Potassium feldspar is minor (3.8%). Lithic grains (11.6%) are minor component and comprise mica schist, traces of quartzite and rounded sedimentary chert. Mica is minor (5.8%). Detrital depositional clay matrix is common (15.2%) and consists of organic-rich claystone. Organic matter is trace component in this sample comprising 1.4%. Authigenic minerals are minor and dominated by authigenic kaolinite (5.4%), siderite (3.8%), pyrite (3.8%) and traces of ferroan dolomite (0.4%). There are low amounts of visual porosity (3.8%).

Monocrystalline quartz grains show strong undulose extinction. Straight undulose extinction is less common. Many of the monocrystalline grains contain fluid and igneous inclusions. Polycrystalline quartz occurs predominantly as equant to sub equant grains.

Porosity, in general, is more abundant than in the previous sample. Porosity is locally scattered throughout the sample, usually as triangular pores between detrital and authigenic minerals (Plate 45). This suggests that the porosity is largely intergranular primary.

**XRD:** Quartz is the dominant component with major amount of kaolinite and mica (muscovite and illite), (Table 6 and Appendix II). The clay fraction (< 2  $\mu\text{m}$ ) is dominated by kaolinite and mica (muscovite and illite), (Table 7 and Appendix II).

**SEM:** No SEM photomicrographs were taken for this sample.

**Diagenesis:** The diagenesis of this sample can be summarised as follows:

- Early compaction has affected this sample and has resulted in closer packing of grains and well-developed parallel alignment of elongated detrital grains.
- Framboidal pyrite could have occurred during the early sulphate reduction.

- Micro spar siderite cement occurred early in the diagenetic history at the end of the early sulphate reduction.
- Alteration and dissolution of feldspar, ductile lithic fragments and mica could have been responsible for the formation of kaolin.
- After kaolin precipitation quartz cements have occurred as overgrowths. The quartz overgrowths postdated or at least formed simultaneously with the precipitation of kaolin.
- Traces of ferroan dolomite have formed later in the diagenetic history probably during the late reduction.
- Alteration of lithic fragments and potassium feldspar has continued to the late stage of diagenetic history and this has resulted in development of local secondary porosity and precipitation of authigenic illite. Authigenic illite occurs as fibrous to hairy crystals on the surface of kaolinite, altered feldspar grains and ductile lithic fragments. It also bridges the pore spaces and pore throats.
- Later in the diagenetic history, large cubic crystalline pyrite has occurred as pore filling around thin coal beds, organic-rich detrital matrix and coalified wood materials.

**Env. Deposition:** The moderate sorting and very fine grain size in this unit, with the dominant sedimentary structures and local evidence of bioturbation, suggest low energy of depositional environment. The presence of a detrital depositional environment, with local bioturbation environments, indicates a depositional environment below the wave action that could be lower shoreface to upper offshore.

**Res. Potential:** The sample shows a poor reservoir potential with low porosity (3.8%). Compaction rather than cementation, was the main agent responsible for reducing the intergranular primary porosity. Compaction has reduced around 71% of the primary intergranular porosity, whilst cementation has occluded around 22%.

PE907511-46



**Plate 45A: (Sample No. 178C, 2623.85 m):** Thin section photomicrograph showing generalised view of moderately sorted, very fine-grained, angular to subrounded sandstone with considerable amounts of detrital matrix and very low intergranular porosity. Plane polarised light. Scale bar = 500 µm.



**Plate 45B: (Sample No. 178C, 2623.85 m):** Enlarged view of Plate 45A. Plane polarised light. Scale bar = 200 µm.

**SAMPLE:** NO. 210C (2626.45 m)

232  
907511 ~~232~~

**Lithology:** Feldspathic Litharenite

**Texture:** Creamy, grain supported, horizontal to small scale cross stratification, well sorted, fine to medium-grained sandstone. Quartz grains are subangular to rounded. There are considerable amounts of authigenic minerals and moderate visual porosity.

**Composition:** The dominant framework component is monocrystalline quartz (36.6%). Polycrystalline quartz grains are traces (2.4%). Potassium feldspar (6.2%) is minor component and comprises orthoclase and cross-hatched 'tartan' twinning. Lithic fragments (12.8%) are present in minor amounts and predominantly comprise mica schist, quartzite and rounded sedimentary chert. Mica is minor (7%) and consists of muscovite which largely originated from alteration of metamorphic mica schist. Detrital depositional clay matrix (1.2%) and organic matter (0.8%) are trace components. Authigenic minerals comprise siderite (13.2%), authigenic kaolinite (7.6%), ferraon dolomite (2.6%), pyrite (2.2%) and traces of quartz cement. There are minor amounts of visible porosity (6.4%).

Monocrystalline quartz displays strongly undulose extinction with some of the quartz grains containing fluid, igneous inclusions or needle-like minerals and biotite.

There is minor porosity (6.4%) evident in this sample, mostly as scattered primary pores between detrital and authigenic minerals (Plate 46).

**XRD:** The sample is dominated by quartz, with major amounts of kaolinite and mica (muscovite and illite), (Table 6 and Appendix II). The clay fraction (< 2  $\mu\text{m}$ ) is dominated by kaolinite and mica (muscovite and illite), (Table 7 and Appendix II).

**SEM:** The sample comprises a well sorted, fine to medium-grained sandstone with moderate amounts of authigenic clay mineral assemblage (Plate 47). Kaolinite occurs as fine to large pseudo hexagonal book-like crystals, ranging in size from 5  $\mu\text{m}$  up to 20  $\mu\text{m}$ . It occurs as pore filling, filling much of the pore spaces and pore throats, restricting the reservoir quality (Plate 48). SEM has also shown that quartz and siderite cements are minor and have locally reduced the reservoir quality (Plate 49). Illite occurs as late fibrous to hairy crystals around kaolinite, altered lithic fragments and altered feldspar grains. Illite crystals range in size from less than 1  $\mu\text{m}$  up to 5  $\mu\text{m}$ . They are bridging the pore spaces and throats and reducing permeability (Plate 50).



The pores are small, most of which are less than 10  $\mu\text{m}$  and occasionally less than 1  $\mu\text{m}$  (Plate 47). The distribution of the pore throat is irregular with moderate interconnection implying low permeability (Plate 47).

**Diagenesis:**

The diagenesis of this sample can be summarised as follows:

- Early compaction has affected this sample and has resulted in closer packing of grains and well-developed parallel alignment of elongated detrital grains.
- Framboidal pyrite could have occurred during the early sulphate reduction.
- Micro spar siderite cement occurred early in the diagenetic history at the end of the early sulphate reduction.
- Alteration and dissolution of feldspar, ductile lithic fragments and mica could have been responsible for the formation of kaolin.
- After kaolin precipitation quartz cements have occurred as overgrowths. The quartz overgrowths postdated or at least formed simultaneously with the precipitation of kaolin.
- Traces of ferroan dolomite have formed later in the diagenetic history probably during the late reduction.
- Alteration of lithic fragments and potassium feldspar has continued to the late stage of diagenetic history and this has resulted in development of local secondary porosity and precipitation of authigenic illite. Authigenic illite occurs as fibrous to hairy crystals on the surface of kaolinite, altered feldspar grains and ductile lithic fragments. It also bridges the pore spaces and pore throats.
- Later in the diagenetic history, large cubic crystalline pyrite has occurred as pore filling around thin coal beds, organic-rich detrital matrix and coalified wood materials.

**Env. Deposition:**

The fine to medium grain size, moderate sorting and moderate roundness of detrital grains in the sandstone indicates a moderate to low energy environment of deposition. Deposition may have occurred in a meandering fluvial to lower shoreface environment.

**Res. Potential:**

The reservoir potential of this sample is fair. Visible porosity is minor in the sample (6.4%) with primary porosity being more common than secondary porosity. Cementation rather than mechanical compaction is responsible for reducing the reservoir quality. It occludes up to 47% whilst compaction reduced around 41%.

907511 ~~XXXX~~  
234

PE907511\_47

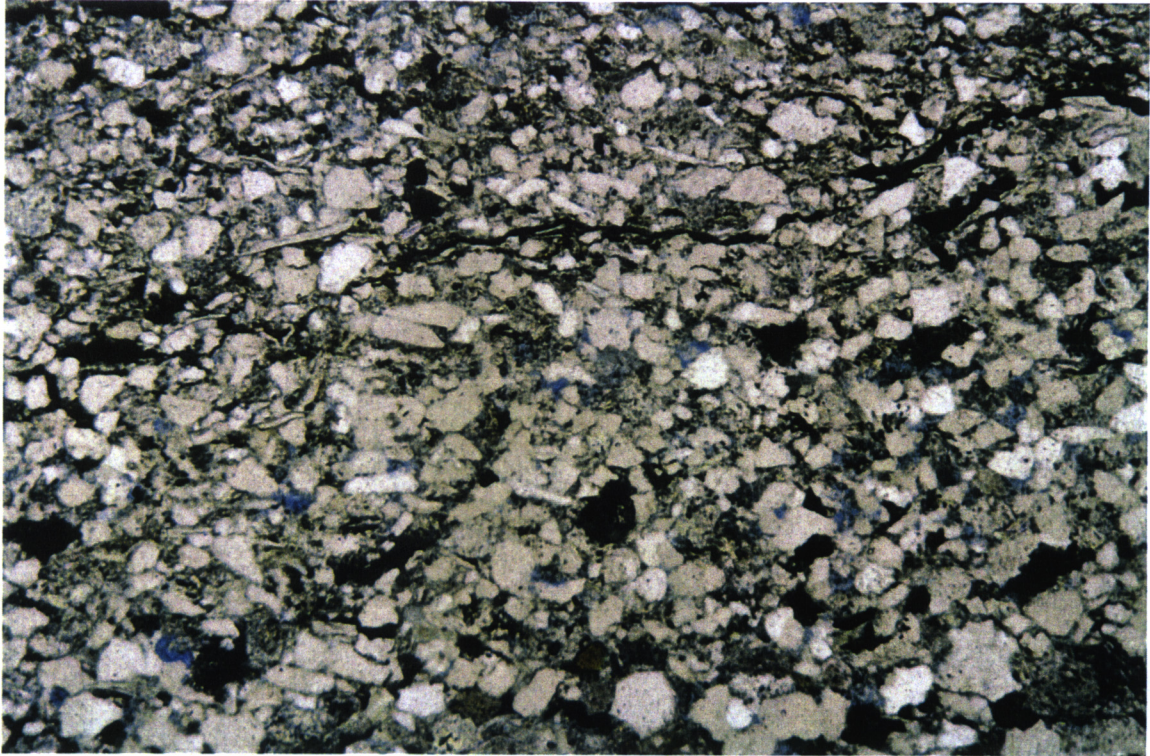


**Plate 46A: (Sample No. 210C, 2626.45 m):** Thin section photomicrograph of feldspathic litharenite comprising well sorted, fine to medium-grained, subangular to rounded sandstone with patches of intergranular porosity (blue). Plane polarised light. Scale bar = 500  $\mu\text{m}$ .

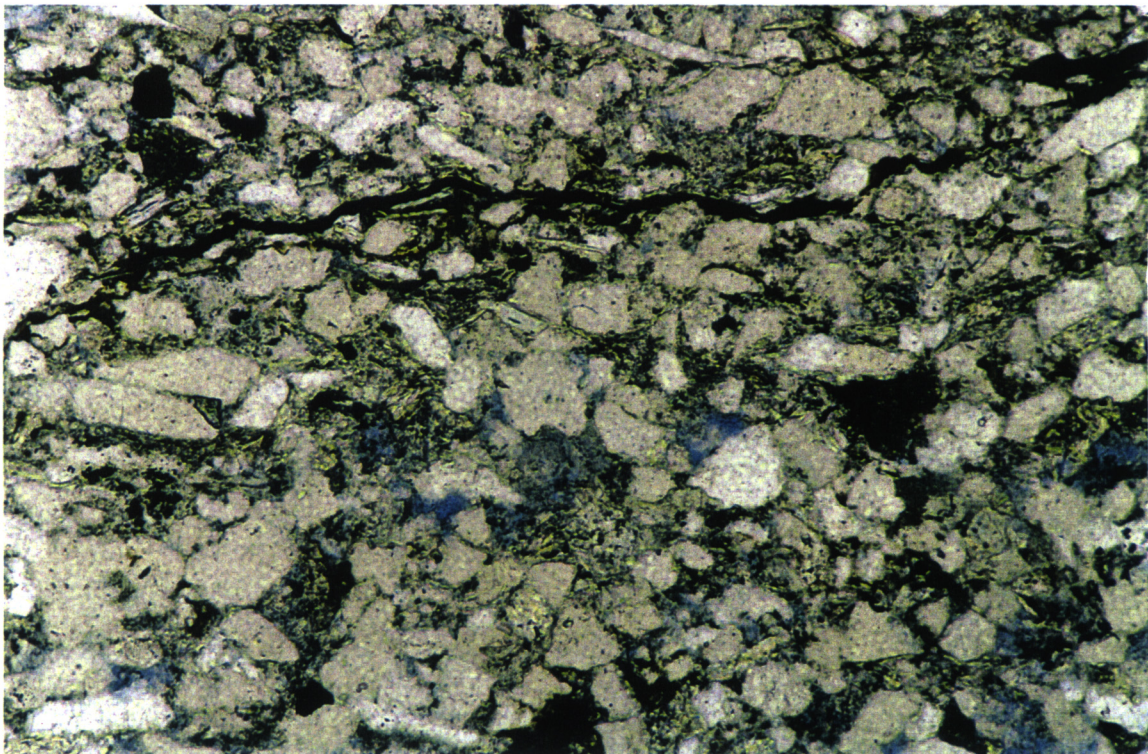


**Plate 46B: (Sample No. 210C, 2626.45 m):** Enlarged view of Plate 46A. Plane polarised light. Scale bar = 200  $\mu\text{m}$ .

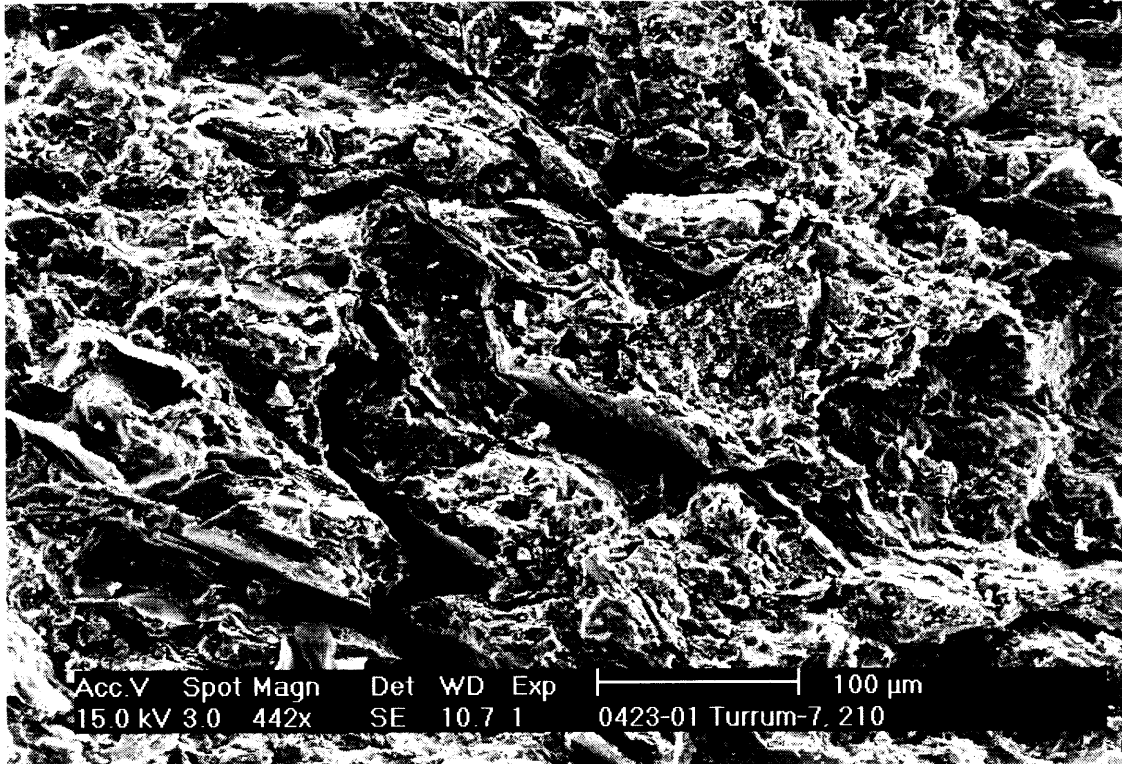


**Plate 47: (Sample No. 210C, 2626.45 m):** SEM photomicrograph showing general view of the sample. The sample contains minor visual porosity. The pores are small and poorly interconnected implying low permeability. Scale bar = 100 μm.

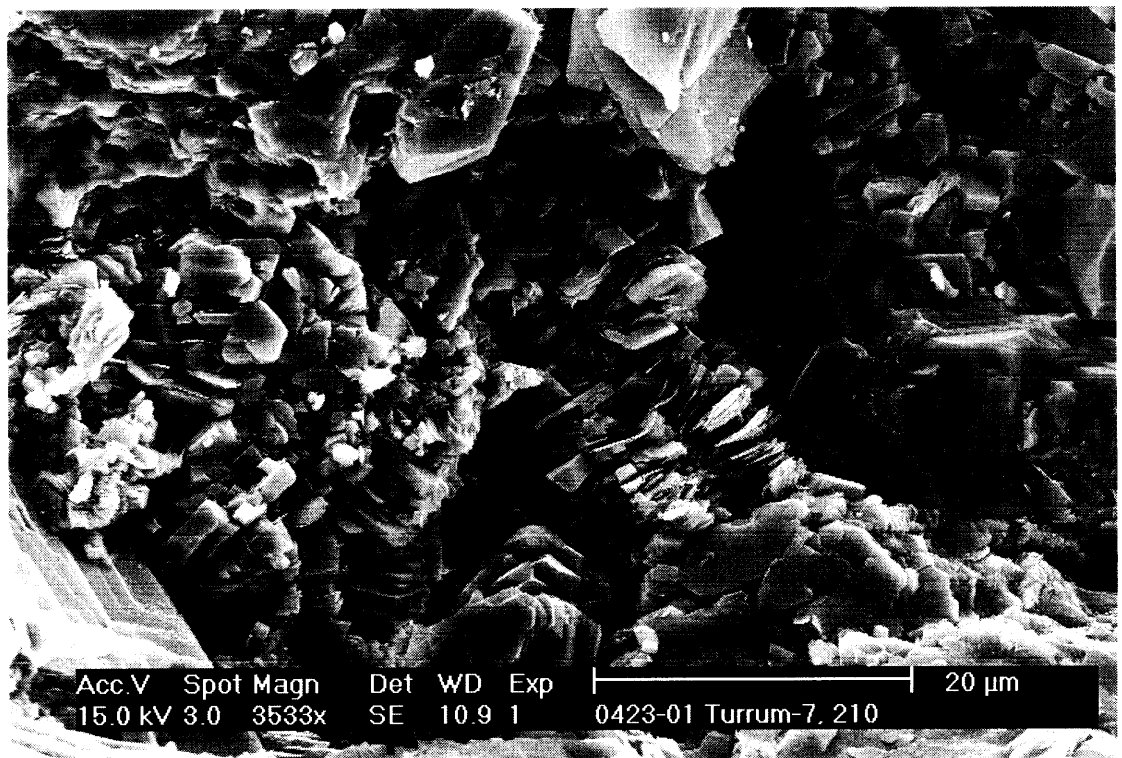


**Plate 48: (Sample No. 210C, 2626.45 m):** SEM photomicrograph showing pore filling kaolinite booklets. Kaolinite occurs as pore filling. It fills much of the pore spaces and restricts the reservoir quality. The pores are poorly interconnected in 3-D suggesting low permeability. Scale bar = 20 μm.

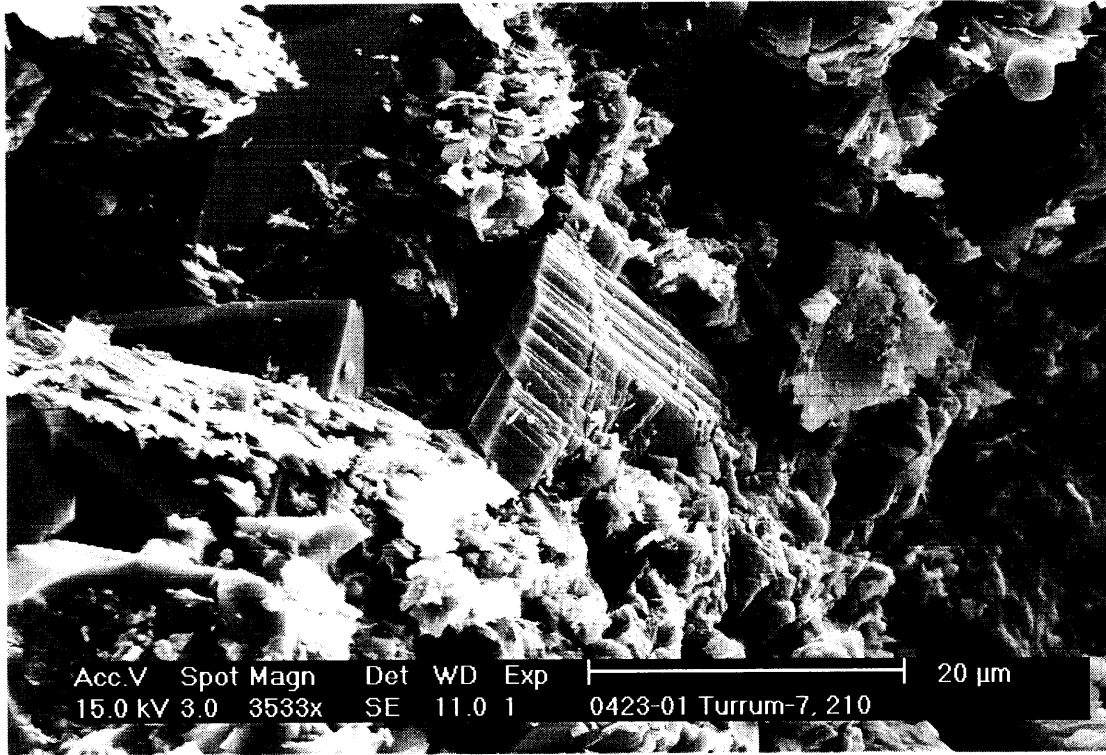


**Plate 49: (Sample No. 210C, 2626.45 m):** SEM photomicrograph showing different type of authigenic minerals filling and restricting the pores and pore throats. Quartz overgrowths, siderite, kaolinite and illite are common in this sample. Scale bar = 20 µm.

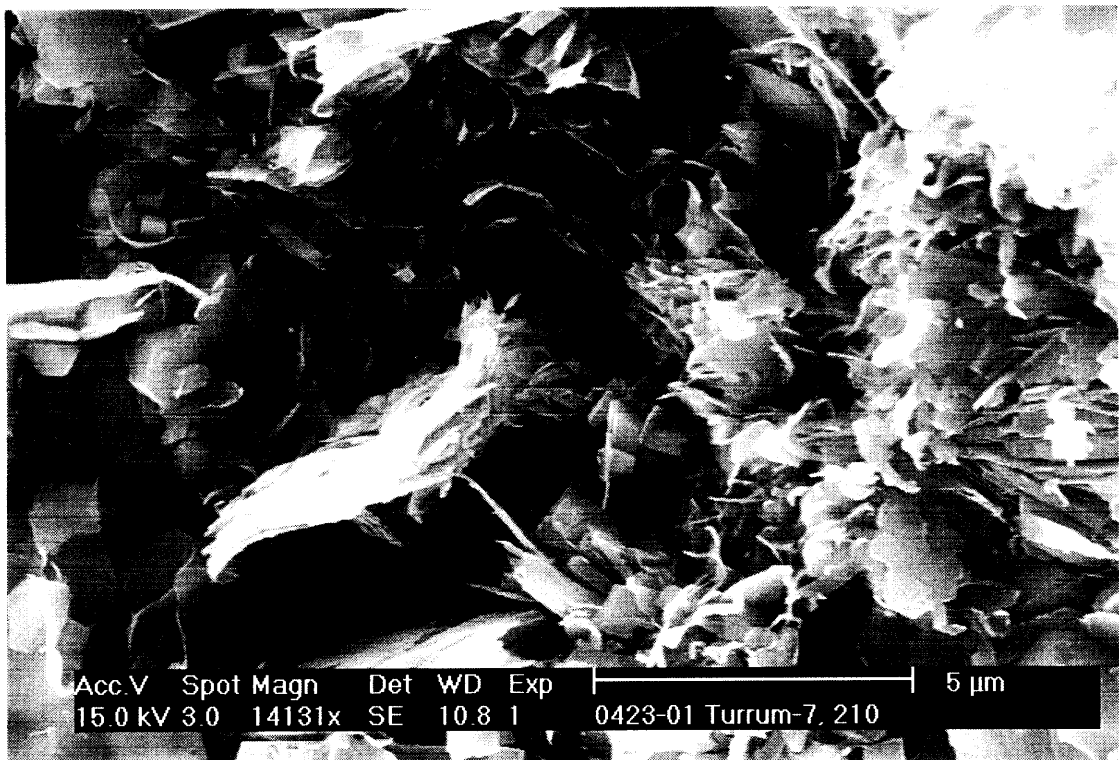


**Plate 50: (Sample No. 210C, 2626.45 m):** SEM photomicrograph showing authigenic fibrous to hairy illite filling and bridging the pores and pore throats. Authigenic illite has major influence in reducing the permeability in this sample. Scale bar = 5 µm.

**SAMPLE:** NO. 234C (2628.45 m)

**Lithology:** Feldspathic Litharenite

**Texture:** The sample is creamy, grain supported, horizontal to small scale cross stratification, well sorted, medium-grained sandstone. Quartz grains are mainly subangular to rounded. Authigenic minerals are common and moderate visual porosity.

**Composition:** The sample is dominated by monocrystalline quartz (34.4%) with trace amounts of polycrystalline quartz grains (2.4%). Potassium feldspar (5.4%) is minor component and consists of orthoclase and microcline displaying cross-hatched 'tartan' twinning. Lithic fragments (8.2%) are minor components and comprise mica schist, quartzite and rounded sedimentary chert. Mica is minor (4.2%). Detrital depositional clay matrix is also present in trace amounts (1.2%). It comprises organic-rich silt and mudstone. Dispersed organic matter or coalified wood and plant debris are present also in trace amounts (0.8%). Authigenic minerals comprise authigenic kaolinite (15%), quartz overgrowths (10%), pyrite (2.8%), siderite (2.8%). There are minor amounts of visible porosity (8%) in the sample.

Quartz is mainly monocrystalline and displays slightly to strong undulose extinction with few grains having straight undulose extinction. Many of the quartz grains contain needle-like minerals, probably tourmaline and/or rutile. Lithic fragments are predominantly metamorphic mica schist and traces of rounded sedimentary chert. Mica is mainly muscovite and occurs as disseminated flakes.

Porosity is locally scattered throughout the sample (8%), usually as triangular pores between detrital and authigenic minerals (Plate 51). Secondary porosity is less common than the primary pores. Cementation of authigenic minerals was the main agent responsible for reducing the primary intergranular porosity. It occluded around 70% of the original porosity and compaction has reduced around 13%.

**XRD:** The sample is dominated by quartz, major kaolinite, mica (muscovite and illite), and siderite, with traces of potassium feldspar, (Table 6, and Appendix II). The clay fraction (< 2  $\mu\text{m}$ ) is dominated by kaolinite and mica (muscovite and illite), (Table 7 and Appendix II).

**SEM:** The sample comprises a well sorted, medium-grained sandstone with moderate amounts of authigenic clay mineral assemblage (Plate 52). Secondary porosity development has resulted from partial to complete dissolution of feldspar grains and ductile lithic fragments. Feldspar displays skeletal or sieve to honeycomb structure suggesting severe

dissolution (Plate 53). SEM has also shown that quartz overgrowths are minor and have locally reduced the reservoir quality.

Kaolinite occurs as fine to large pseudo hexagonal book-like crystals, ranging in size from 5  $\mu\text{m}$  up to 20  $\mu\text{m}$ . It occurs as pore filling, filling much of the pore spaces and pore throats, restricting the reservoir quality (Plate 54). Illite occurs as a late fibrous to hairy crystals around kaolinite, altered lithic fragments and altered feldspar grains. Illite crystals range in size from less than 1  $\mu\text{m}$  up to 5  $\mu\text{m}$ . They are bridging the pore spaces and throats and reducing permeability (Plate 55).

The pores are small, most of which are less than 10  $\mu\text{m}$  and occasionally less than 1  $\mu\text{m}$  (Plate 52). The distribution of the pore throat is irregular with moderate interconnection implying very poor permeability (Plate 52).

#### **Diagenesis:**

The diagenesis of this sample can be summarised as follows:

- Early compaction has affected this sample and has resulted in closer packing of grains and well-developed parallel alignment of elongated detrital grains.
- Framboidal pyrite could have occurred during the early sulphate reduction.
- Micro spar siderite cement occurred early in the diagenetic history at the end of the early sulphate reduction.
- Alteration and dissolution of feldspar, ductile lithic fragments and mica could have been responsible for the formation of kaolin.
- After kaolin precipitation quartz cements have occurred as overgrowths. The quartz overgrowths postdated or at least formed simultaneously with the precipitation of kaolin.
- Alteration of lithic fragments and potassium feldspar has continued to the late stage of diagenetic history and this has resulted in development of local secondary porosity and precipitation of authigenic illite. Authigenic illite occurs as fibrous to hairy crystals on the surface of kaolinite, altered feldspar grains and ductile lithic fragments. It also bridges the pore spaces and pore throats.
- Later in the diagenetic history, large cubic crystalline pyrite has occurred as pore filling around thin coal beds, organic-rich detrital matrix and coalified wood materials.

**Env. Deposition:** The well sorting and rounding nature in this medium-grained sandstone, with the horizontal to small scale laminations, indicate deposition in a moderate to high energy environment. The moderate grain alignment (as seen in thin section) indicates deposition by traction currents, thus the environment of deposition may have been meandering fluvial to lower shoreface.

**Res. Potential:** Reservoir potential of this sample is fair (8%). Visible pores are partly to completely filled with quartz, kaolinite and siderite cements. Compaction has contributed by up to 13% of the porosity loss while cementation has occluded around 70% of the original intergranular porosity. The sample has fair reservoir characteristics.

PE907511\_50

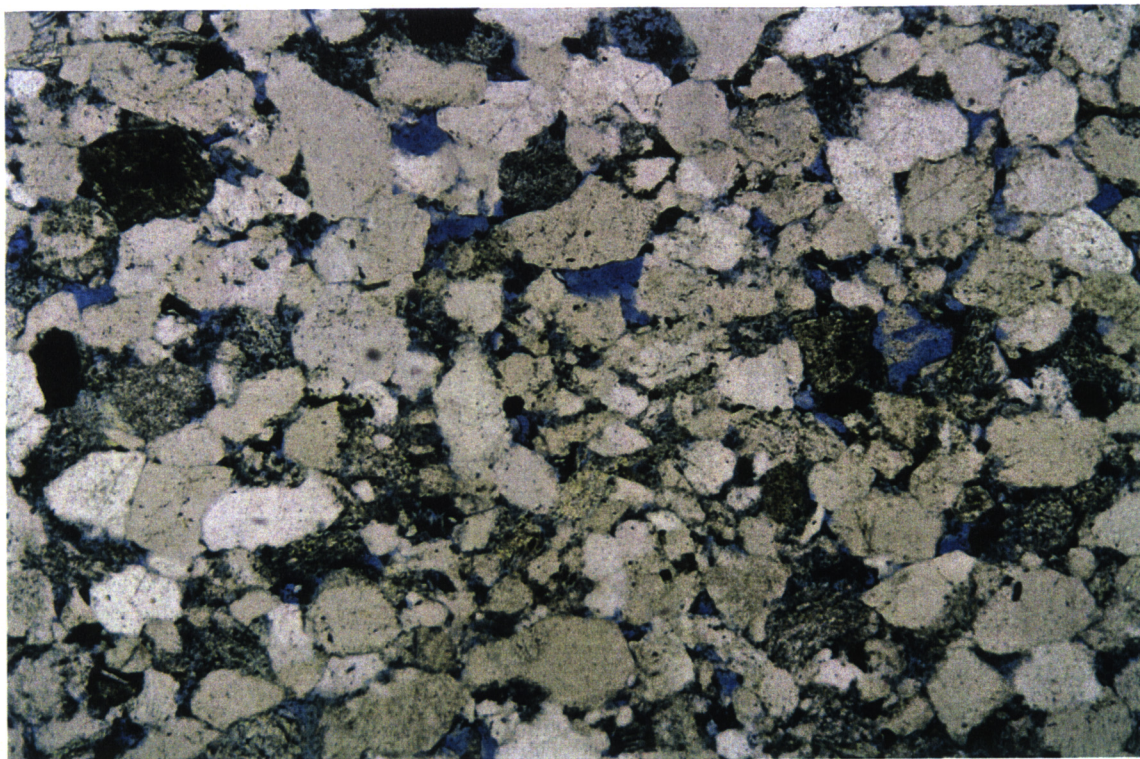


**Plate 51A: (Sample No. 234C, 2628.45 m):** Thin section photomicrograph showing general view of feldspathic litharenite comprising well sorted, medium-grained, subangular to rounded sandstone with moderate amounts of primary intergranular porosity (blue). Plane polarised light. Scale bar = 500  $\mu\text{m}$ .

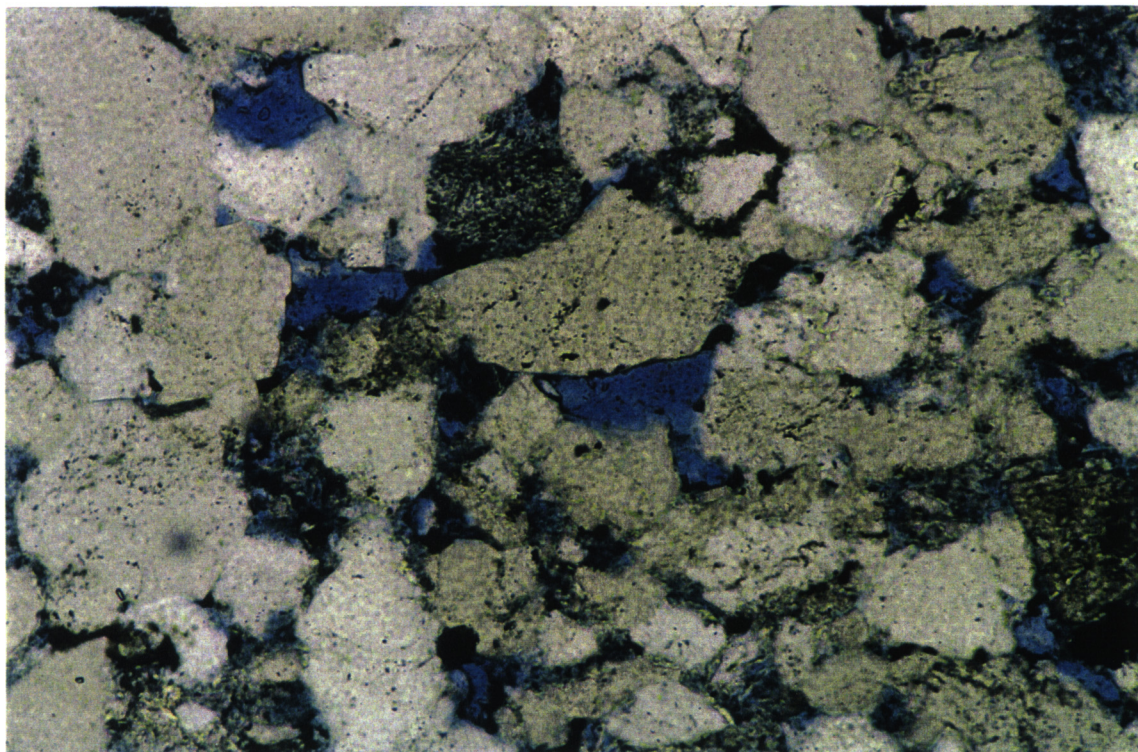


**Plate 51B: (Sample No. 234C, 2628.45 m):** Enlarged view of Plate 51A. Plane polarised light. Scale bar = 200  $\mu\text{m}$ .



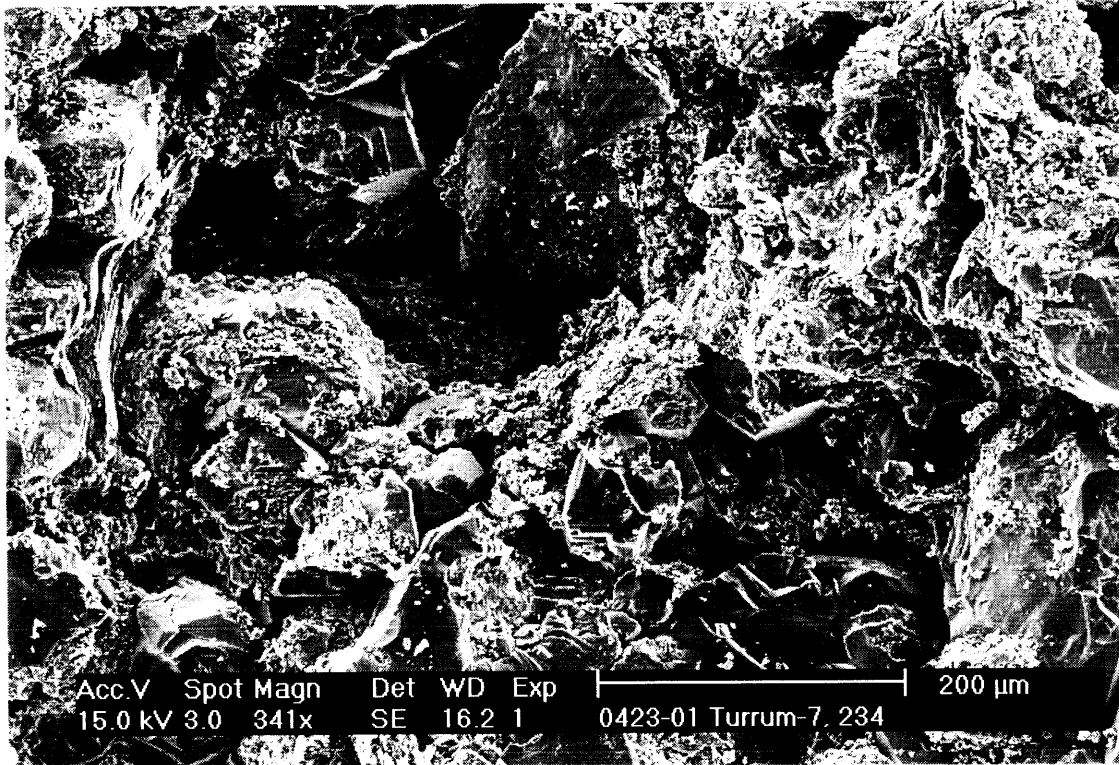


**Plate 52: (Sample No. 234C, 2628.45 m):** SEM photomicrograph showing general view of the sample with minor pore spaces. The pore spaces are moderately interconnected indicating fair to low permeability. Scale bar = 200 μm.

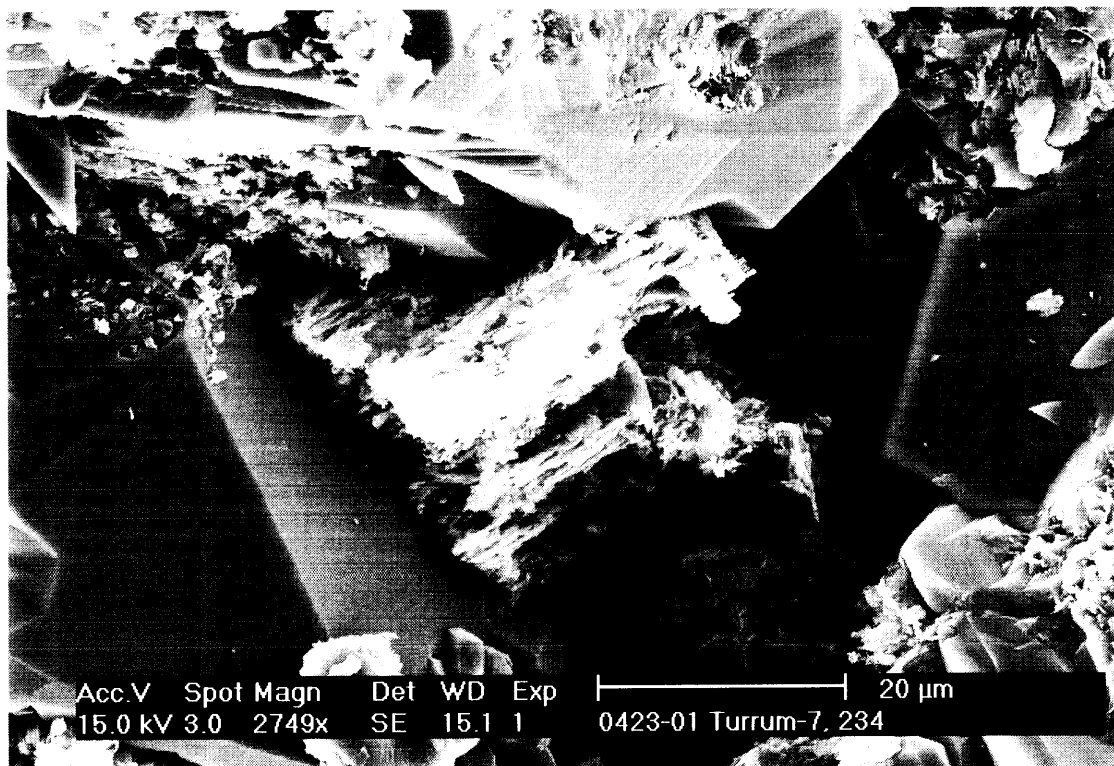


**Plate 53: (Sample No. 234C, 2628.45 m):** SEM photomicrograph showing minor amounts of visual porosity. Note quartz overgrowths and kaolinite filling many of the pore spaces. Note also feldspar dissolution and development of secondary porosity. Scale bar = 20 μm.

907511 <sup>242</sup> ~~242~~



**Plate 54: (Sample No. 234C, 2628.45 m):** SEM photomicrograph showing pore filling kaolinite booklets. Kaolinite occurs as pseudo hexagonal book-like crystals ranging in size from 5 to 20 µm. They fill much of the pore spaces and restrict the reservoir quality of this sample. Scale bar = 50 µm.

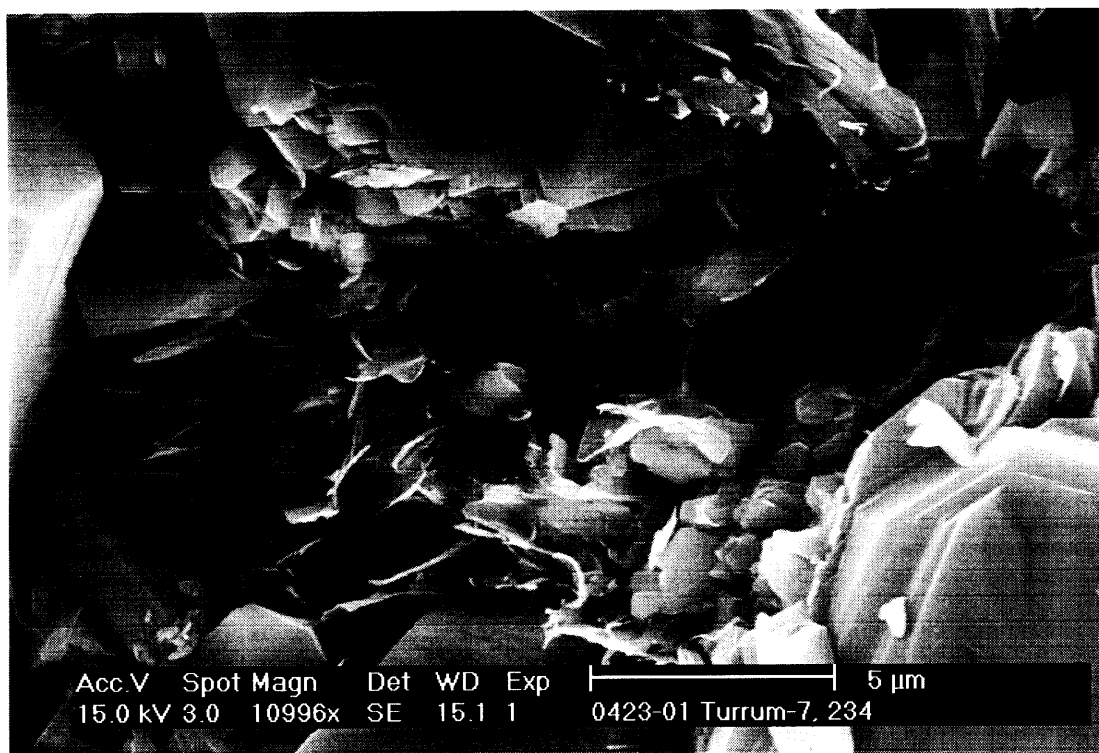


**Plate 55: (Sample No. 234C, 2628.45 m):** SEM photomicrograph showing authigenic fibrous to hairy illite. Authigenic illite bridges the pores and pore throats and restricts the permeability and reservoir quality. Scale bar = 5 µm.

**SAMPLE:** NO. 244C (2629.27 m)

**Lithology:** Lithwacke

**Texture:** The sample consists of creamy to brown, grain supported, moderately sorted, medium-grained sandstone. Quartz grains are mainly angular to subrounded. Moderate authigenic minerals and very low visual porosity.

**Composition:** Monocrystalline quartz is the main framework component and constitutes 37.6% of the sample. Polycrystalline quartz grains are trace (1.8%). Potassium feldspar is present also in minor amounts 4.2%. Lithic fragments are common (14.6%). Lithic grains are dominated by metamorphic micaceous schist (11.8%), quartzite (1%) and rounded sedimentary chert (0.8%). Mica is minor (6.2%) and consists of muscovite. Detrital depositional clay matrix is common (17.8%) and comprises organic-rich silt to claystone. Authigenic minerals comprise authigenic kaolinite (4.6%), siderite (2.2%), quartz overgrowths (2.2%) and pyrite (2.2%). Visible porosity is present in minor amounts in the sample (3.2%).

Monocrystalline quartz shows strongly undulose extinction. Few quartz grains contain fluid, igneous inclusions and needle-like minerals (tourmaline).

Porosity is low in this sample (Plate 56). It occurs as both intergranular primary and secondary in origin. Secondary porosity is less common and originated by partial dissolution of feldspar, mica and ductile rock fragments.

**XRD:** Quartz is the dominant component of this sample with major kaolinite and mica (muscovite and illite) and traces of potassium feldspar and pyrite, (Table 6 and Appendix II). The clay fraction (< 2 μm) is dominated by kaolinite and mica (muscovite and illite), (Table 7 and Appendix II).

**SEM:** No SEM photos were taken for this sample.

**Diagenesis:** The diagenesis of this sample can be summarised as follows:

- Early compaction has affected this sample and has resulted in closer packing of grains and well-developed parallel alignment of elongated detrital grains.
- Framboidal pyrite could have occurred during the early sulphate reduction.

- Micro spar siderite cement occurred early in the diagenetic history at the end of the early sulphate reduction.
- Alteration and dissolution of feldspar, ductile lithic fragments and mica could have been responsible for the formation of kaolin.
- After kaolin precipitation quartz cements have occurred as overgrowths. The quartz overgrowths postdated or at least formed simultaneously with the precipitation of kaolin.
- Alteration of lithic fragments and potassium feldspar has continued to the late stage of diagenetic history and this has resulted in development of local secondary porosity and precipitation of authigenic illite. Authigenic illite occurs as fibrous to hairy crystals on the surface of kaolinite, altered feldspar grains and ductile lithic fragments. It also bridges the pore spaces and pore throats.
- Later in the diagenetic history, large cubic crystalline pyrite has occurred as pore filling around thin coal beds, organic-rich detrital matrix and coalified wood materials.

**Env. Deposition:** The moderately sorted, medium-grained sandstone, with common detrital depositional clay matrix, suggests a low energy depositional environment. Accumulation of such amounts of detrital matrix could happen in an environment away from wave action. The probable depositional environment of this sample is lower shoreface to upper offshore.

**Res. Potential:** The sample has a fair to poor reservoir quality (3.2%). Reservoir quality apparently has been affected by mechanical compaction rather than precipitation of authigenic minerals.

PE907511\_53

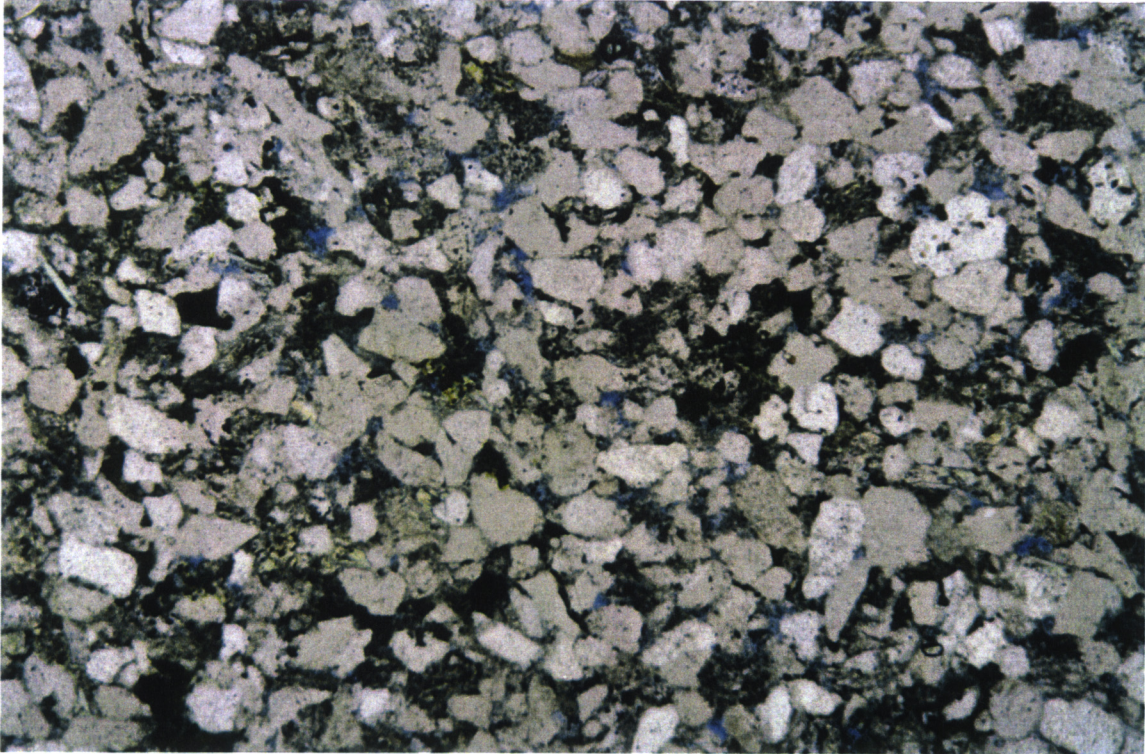


**Plate 56A: (Sample No. 244C, 2629.27 m):** Thin section photomicrograph showing general view of lithwacke comprising moderately sorted, medium-grained, angular to subrounded sandstone with moderate visual porosity. Plane polarised light. Scale bar = 500  $\mu\text{m}$ .

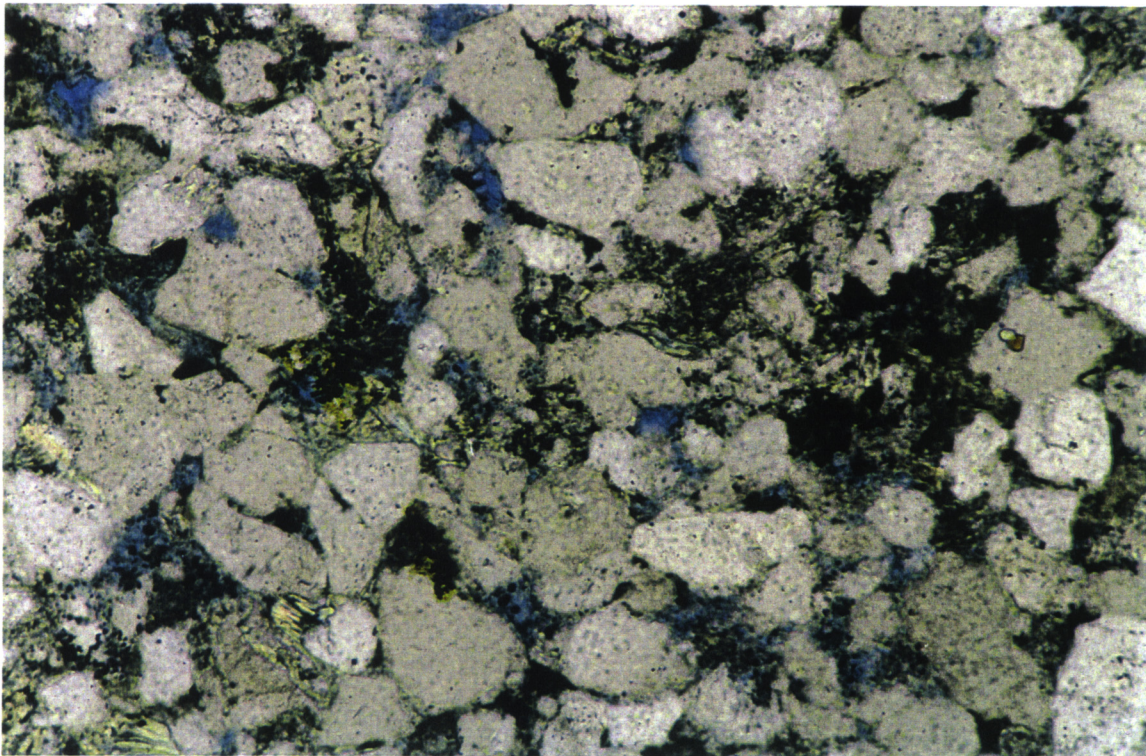


**Plate 56B: (Sample No. 244C, 2629.27 m):** Enlarged view of Plate 56A. Plane polarised light. Scale bar = 200  $\mu\text{m}$ .

907511 ~~246~~  
246

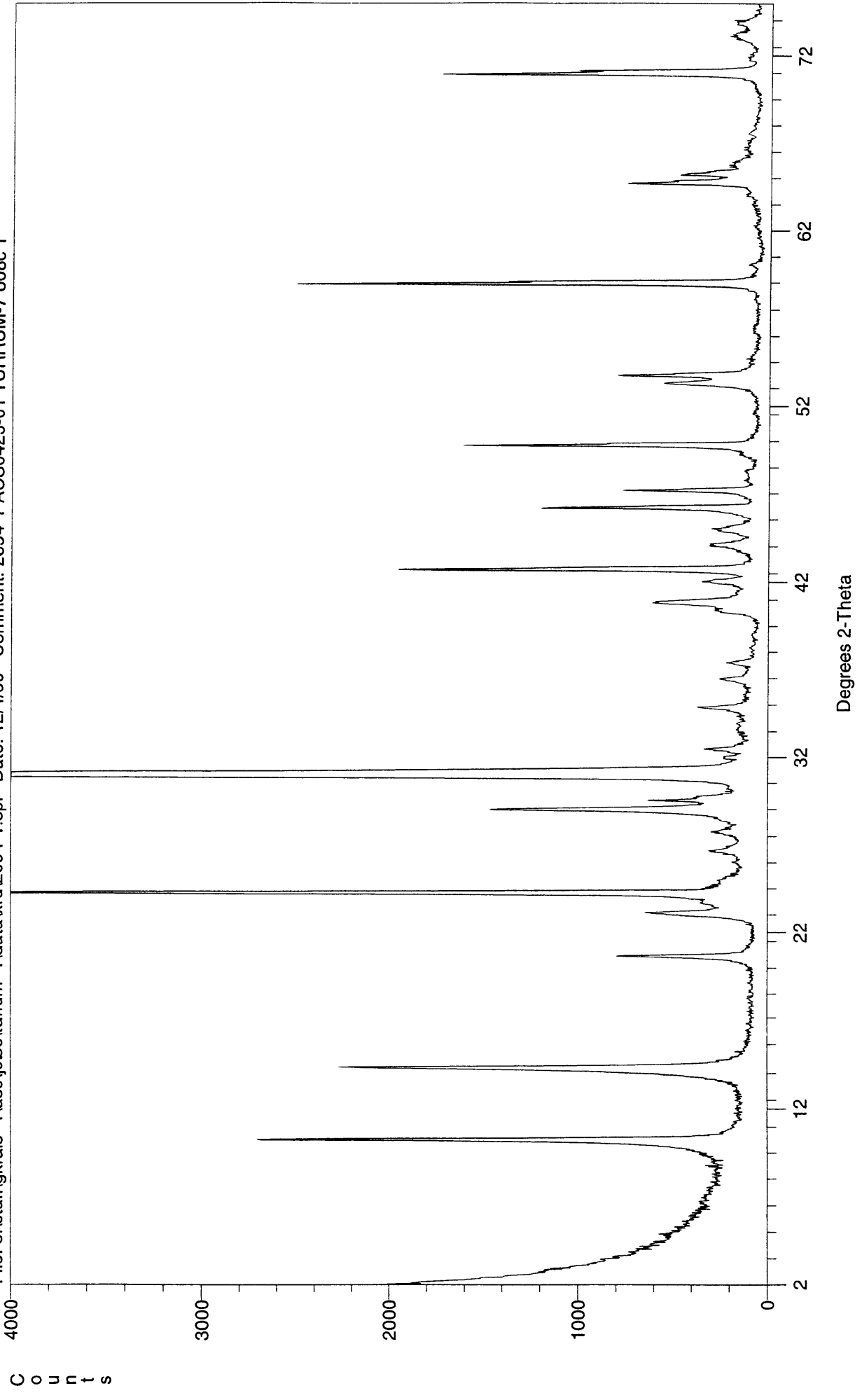
***APPENDIX II***

**XRD AND CLAY FRACTION (LESS THAN 2 mm) TRACES**

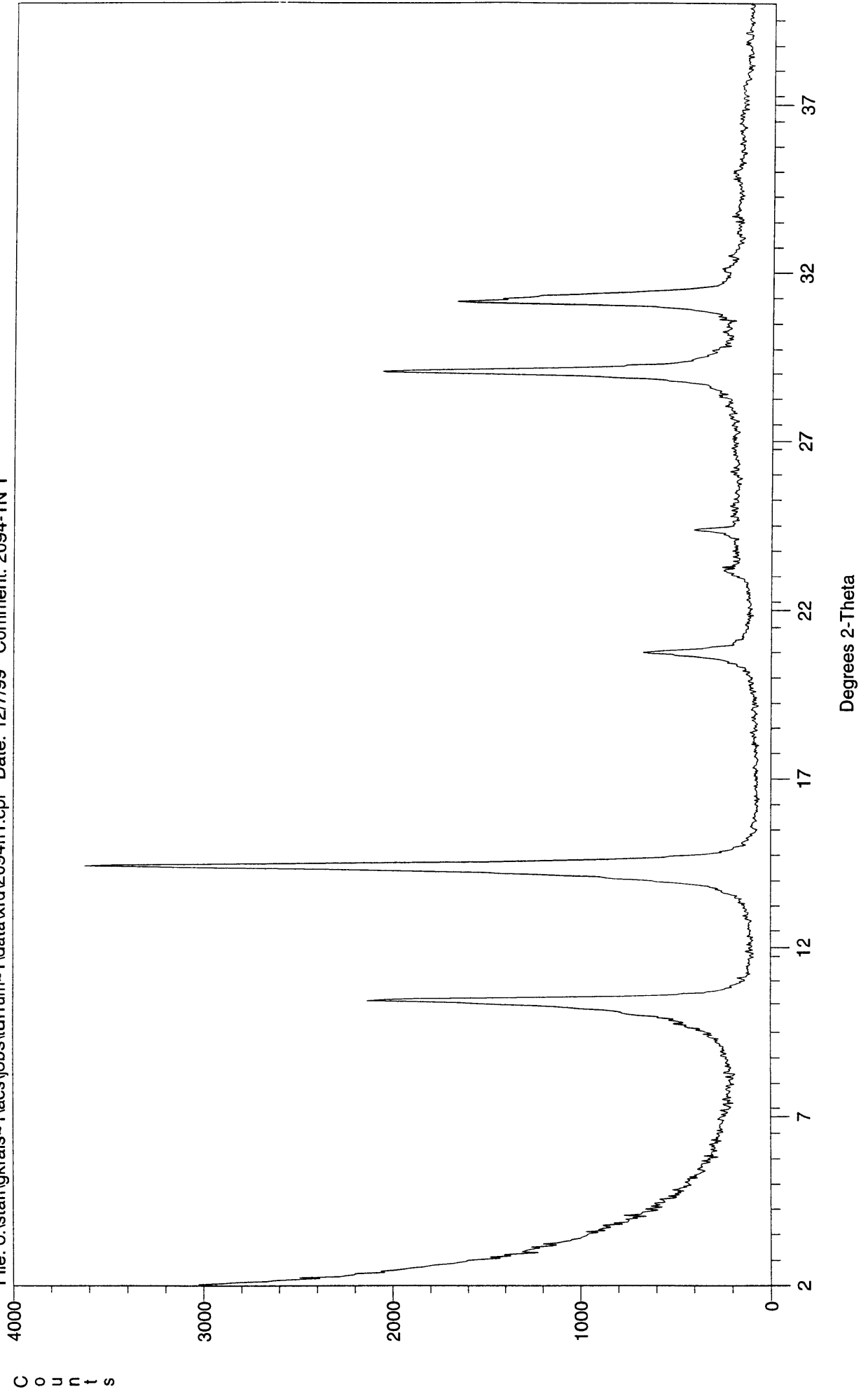
907511

247

File: o:\staff\krais~1\acs\jobs\turum~1\data\xrd\2094-1.cpi Date: 12/4/99 Comment: 2094-1 ACS0423-01 TURRUM-7 008c 1

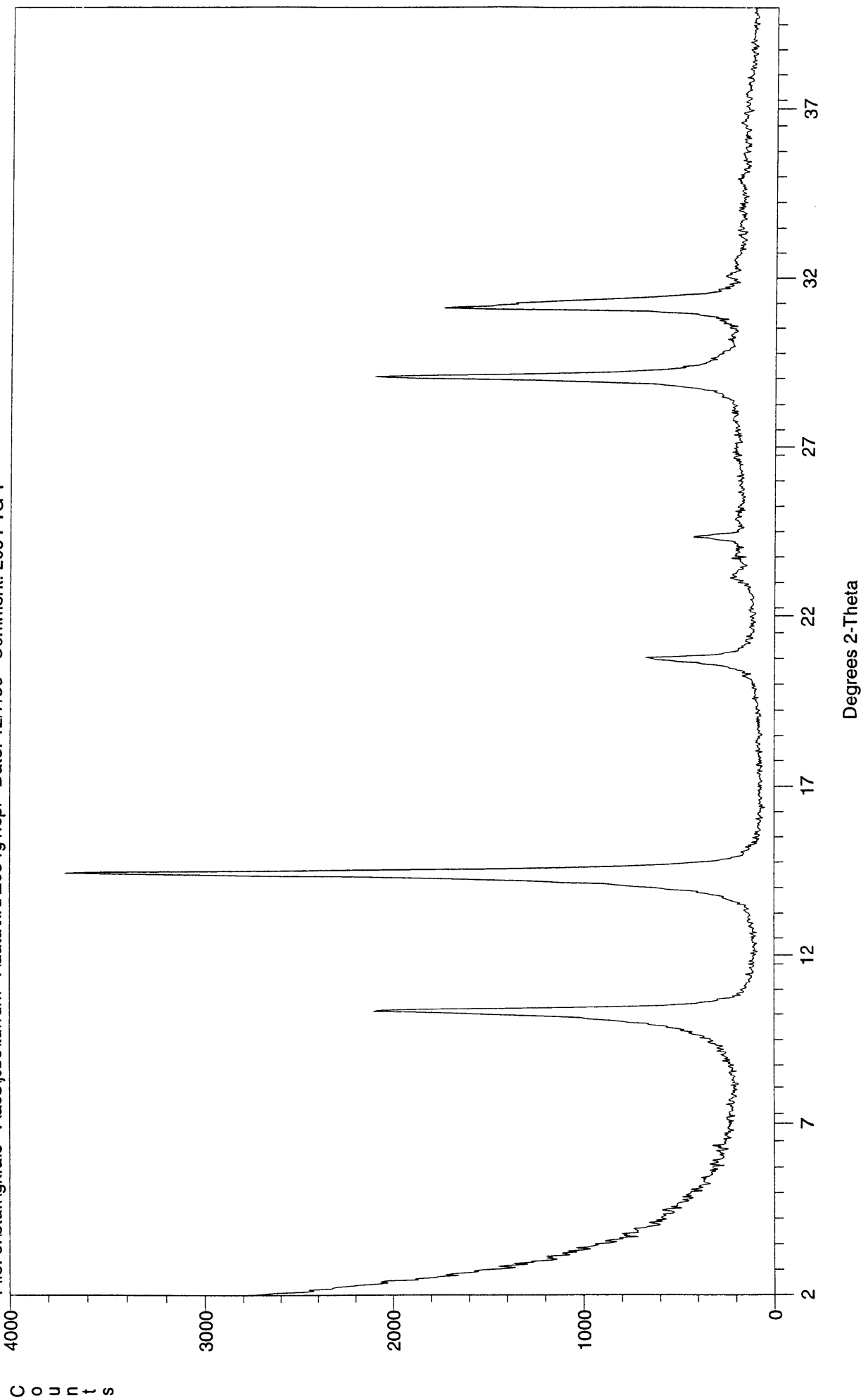


File: o:\staff\gkrais-1\acs\jobs\turrrum-1\data\xrd\2094n1.cpi Date: 12/7/99 Comment: 2094-1N 1

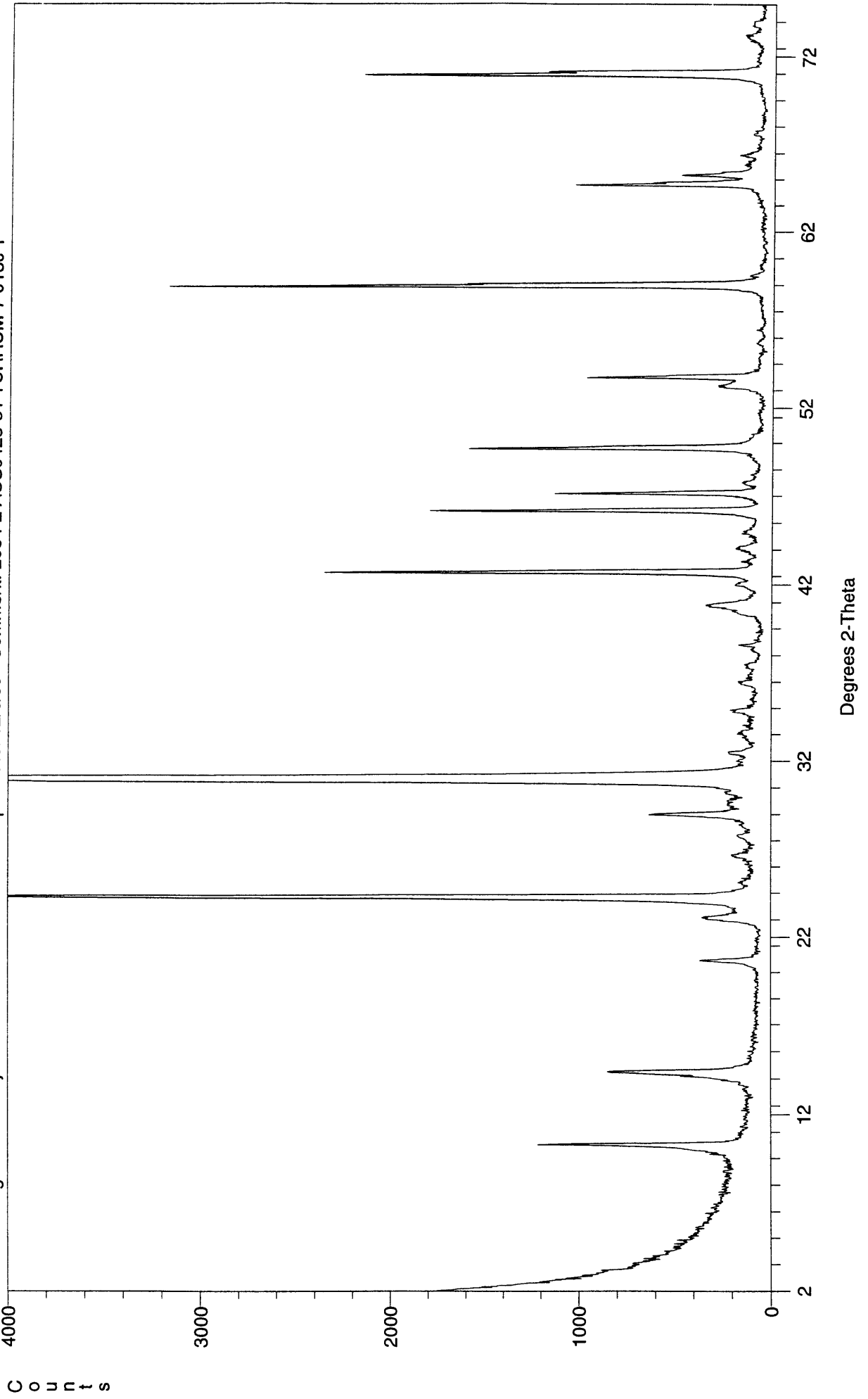




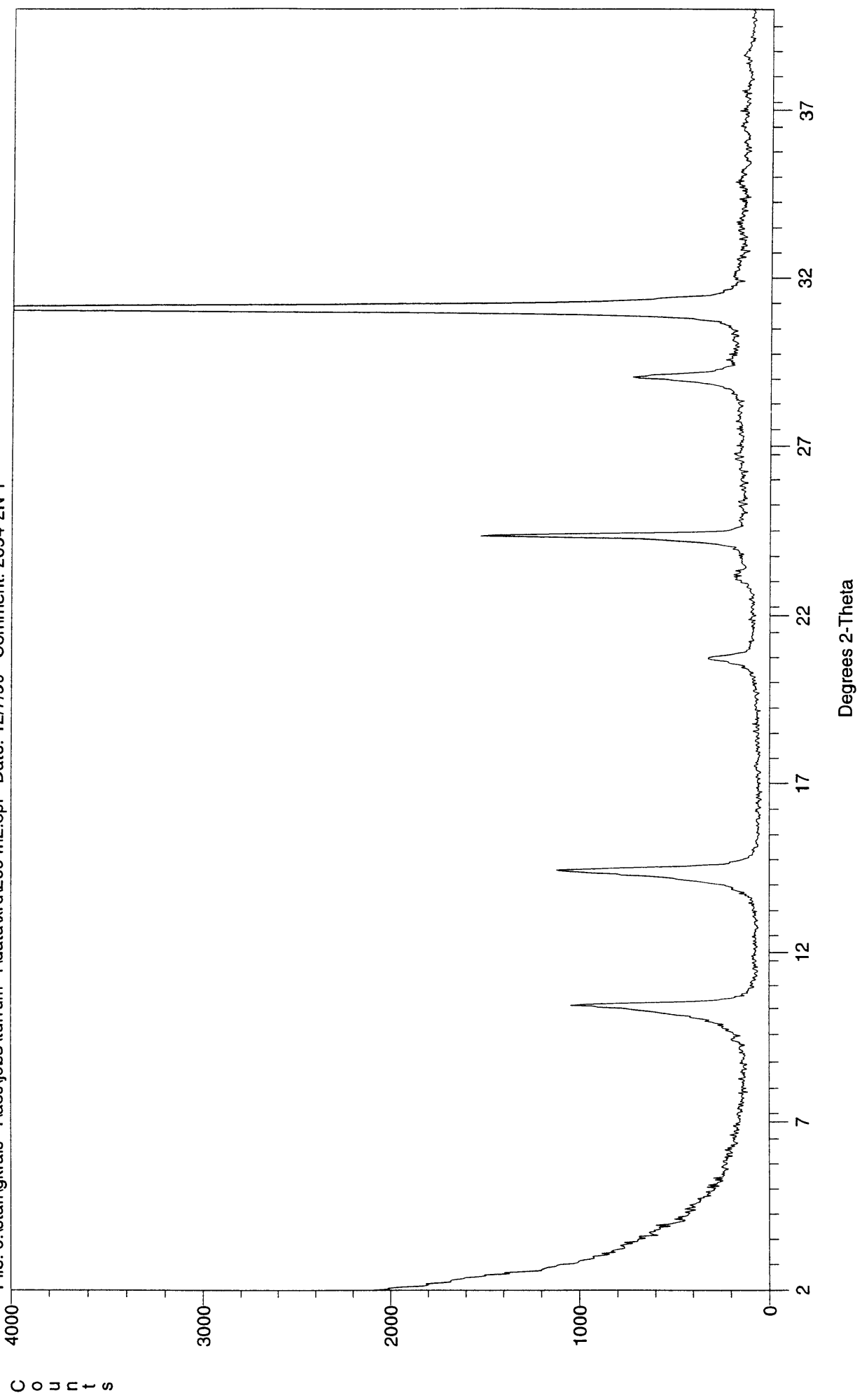
File: o:\staff\krais~1\acs\jobs\tururum~1\data\xrd\2094g1.cpi Date: 12/7/99 Comment: 2094-1G 1



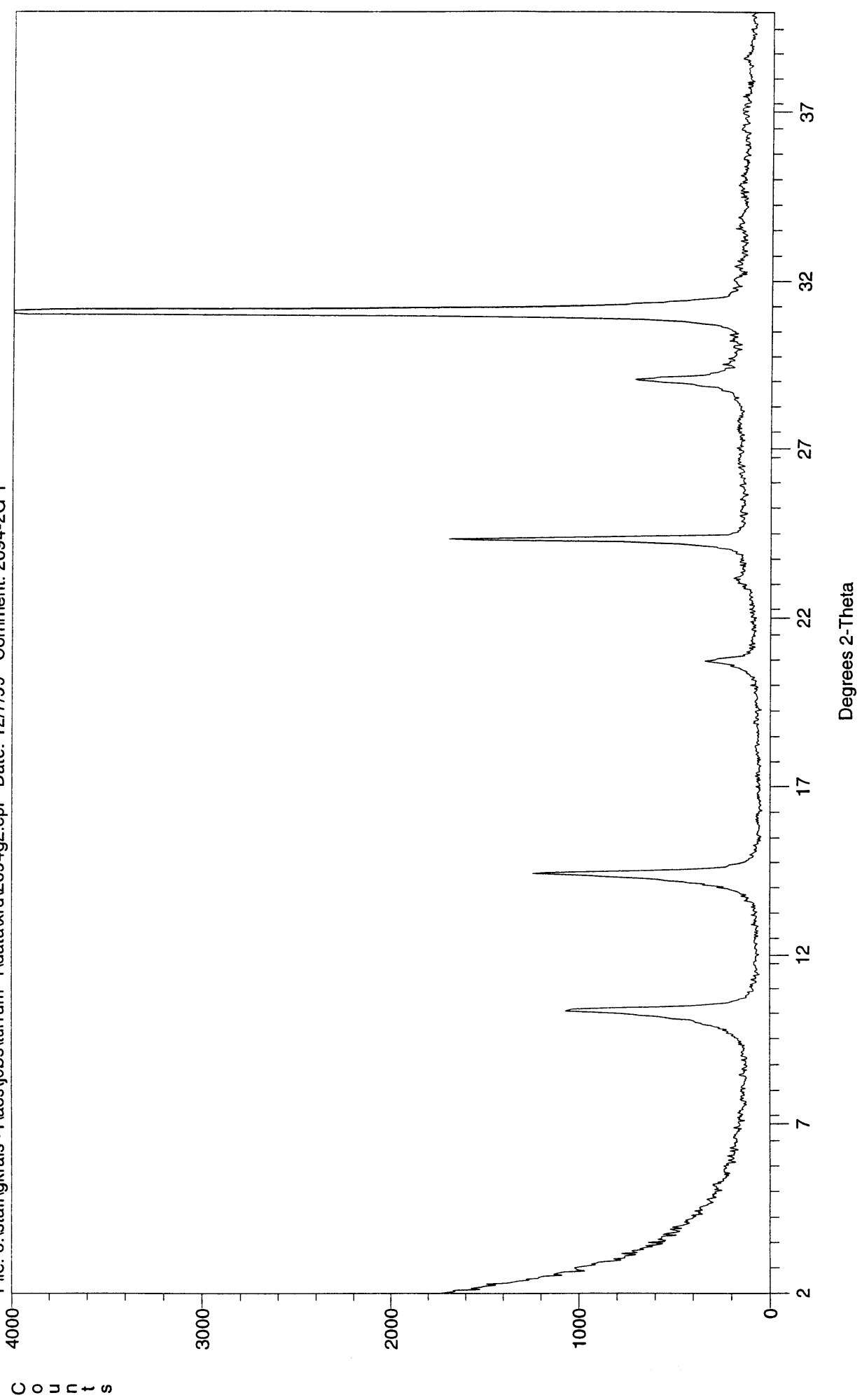
File: o:\staff\krais~1\acs\jobs\turrum~1\data\xrd\2094-2.cpi Date: 12/6/99 Comment: 2094-2 ACS0423-01 TURRUM-7 016c 1



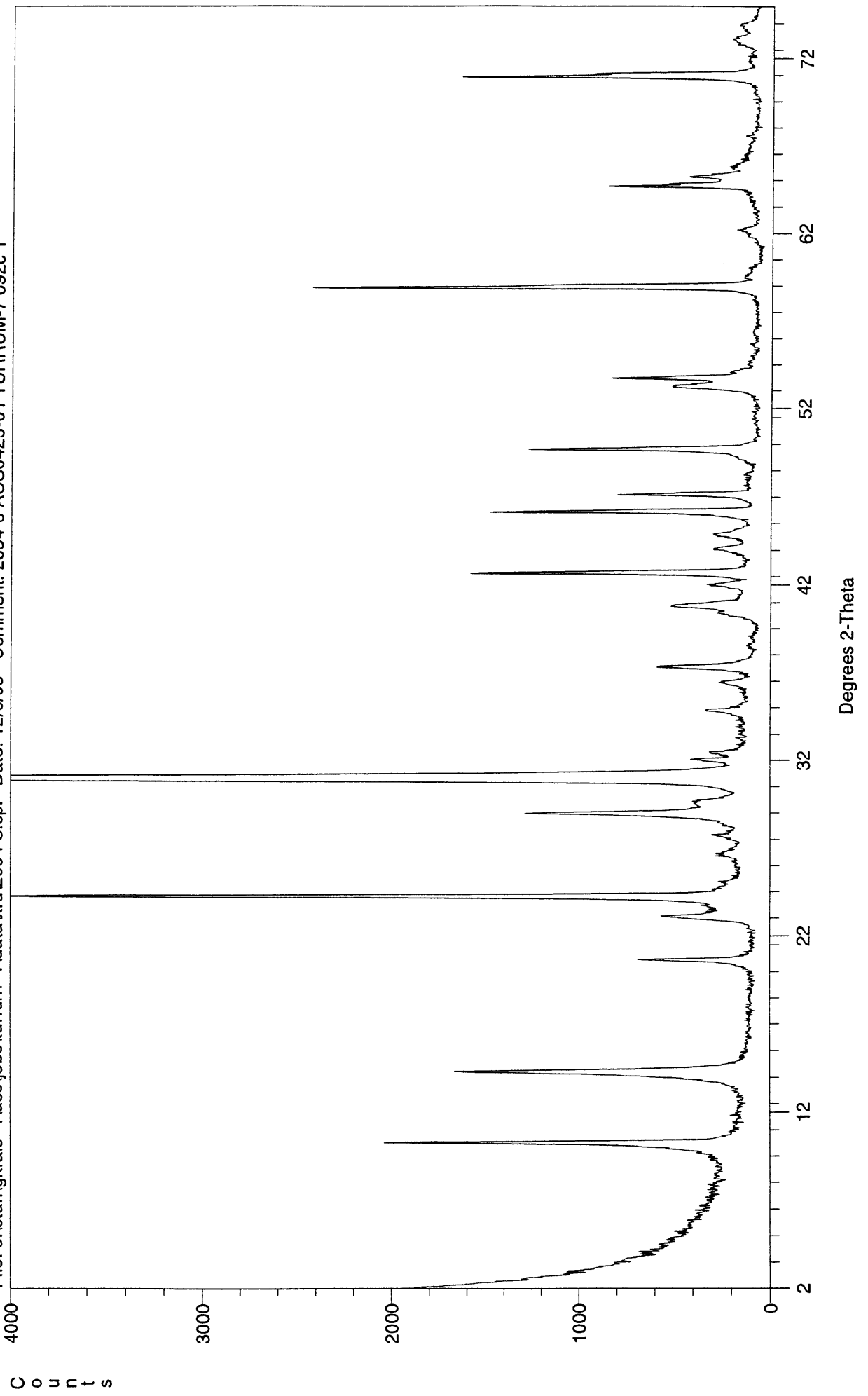
File: o:\staff\krais~1\acs\jobs\turrrum~1\data\xrd\2094n2.cpi Date: 12/7/99 Comment: 2094-2N 1



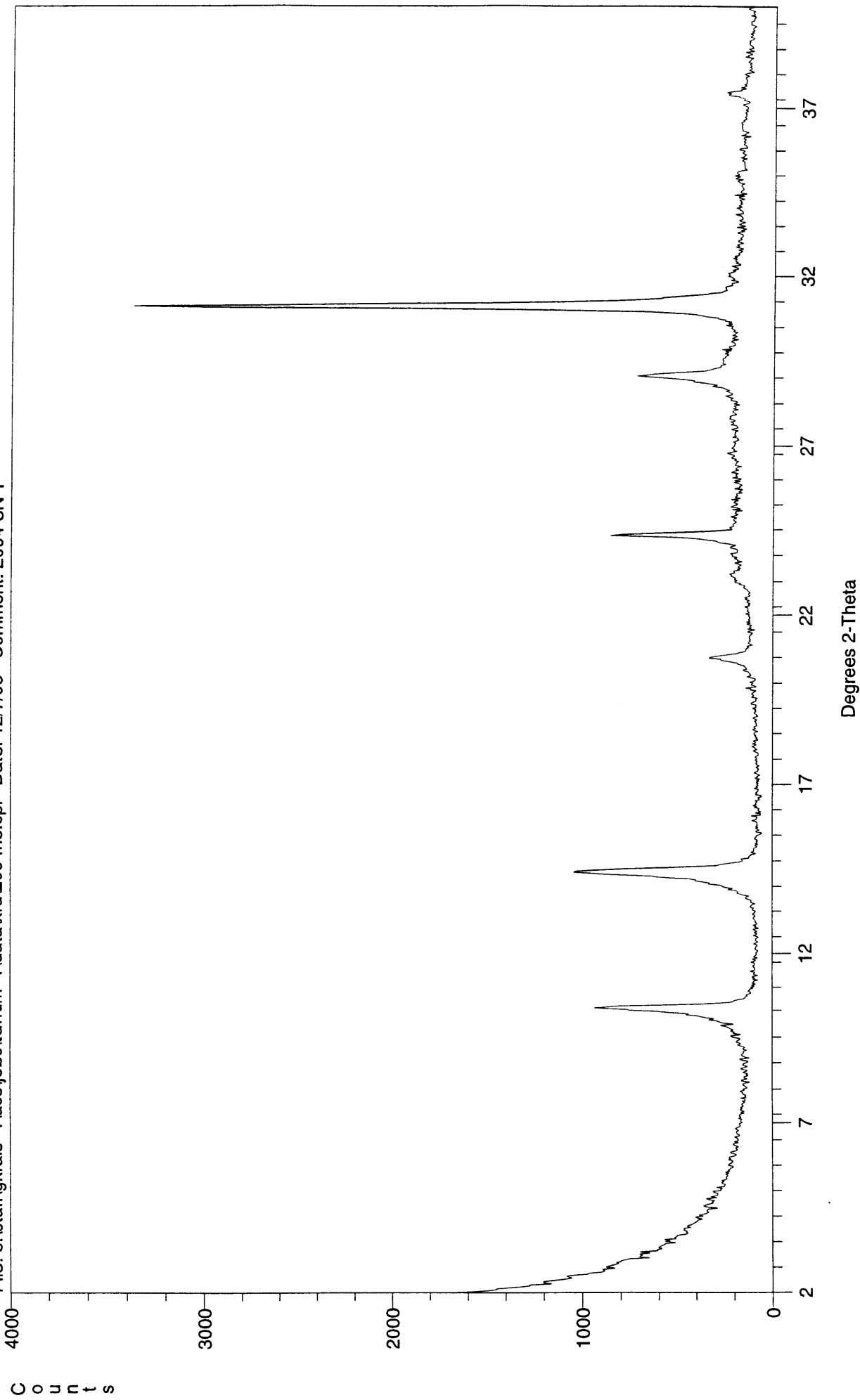
File: o:\staff\gkrais~1\acs\jobs\tururum~1\data\rd\2094g2.cpi Date: 12/7/99 Comment: 2094-2G 1



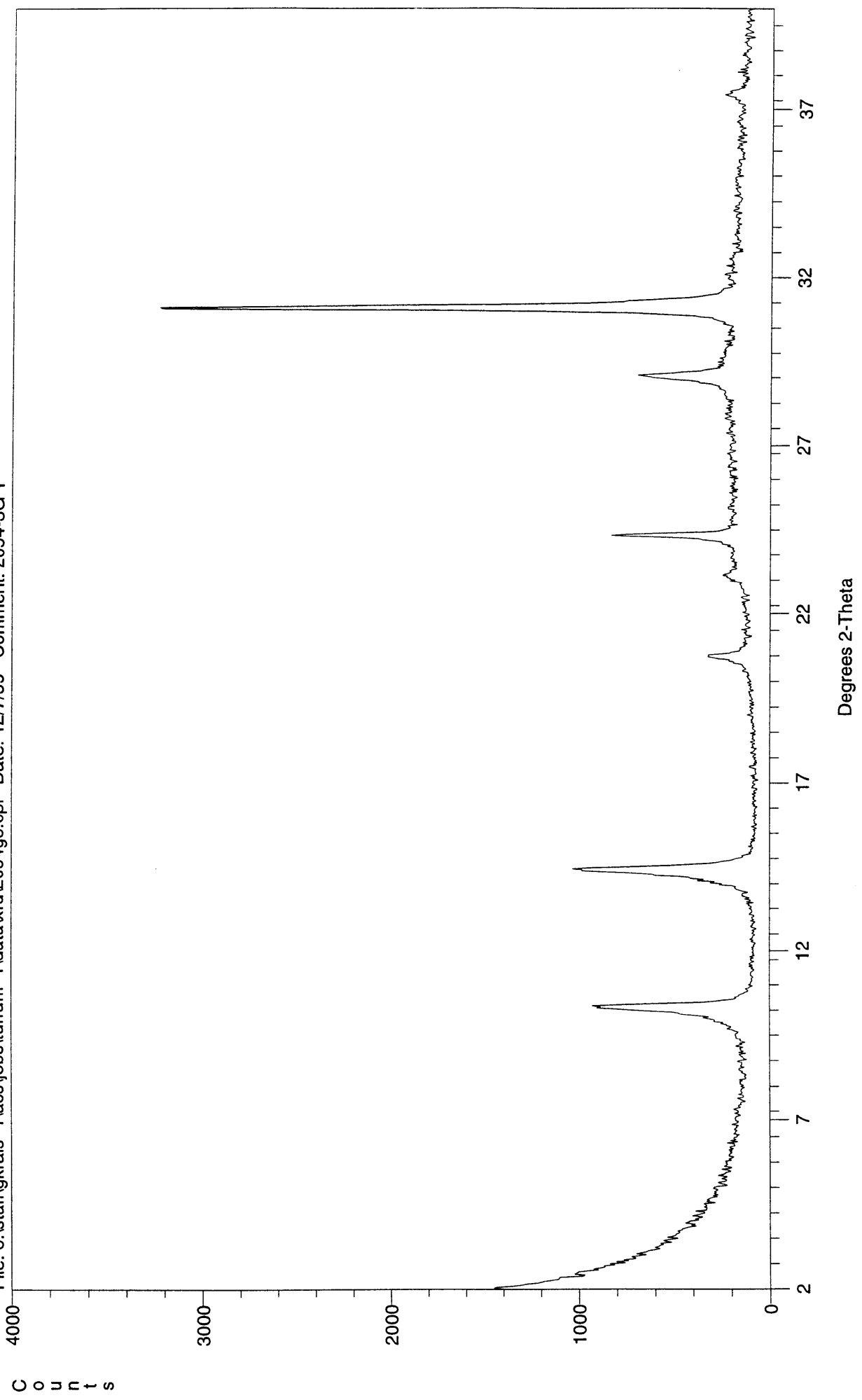
File: o:\staff\krais~1\acs\jobs\tururum~1\data\vr\d2094-3.cpi Date: 12/6/99 Comment: 2094-3 ACS0423-01 TURRUM-7 092c 1



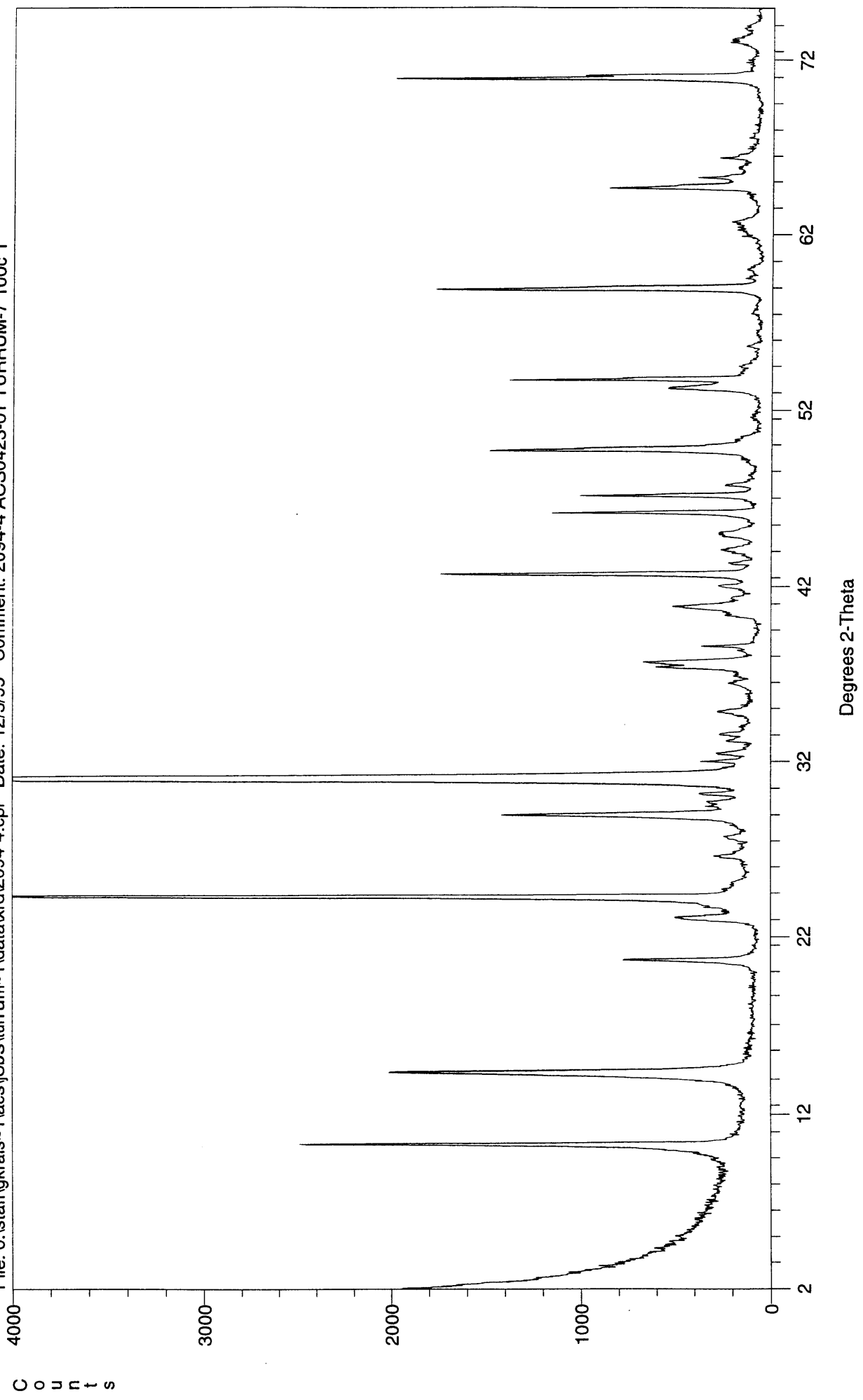
File: o:\staff\gkrais~1\acs\jobs\tururum~1\data\rd\2094n3.cpi Date: 12/7/99 Comment: 2094-3N 1



File: o:\staff\krais~1\acs\jobs\turrum~1\data\xrd\2094g3.cpi Date: 12/7/99 Comment: 2094-3G 1

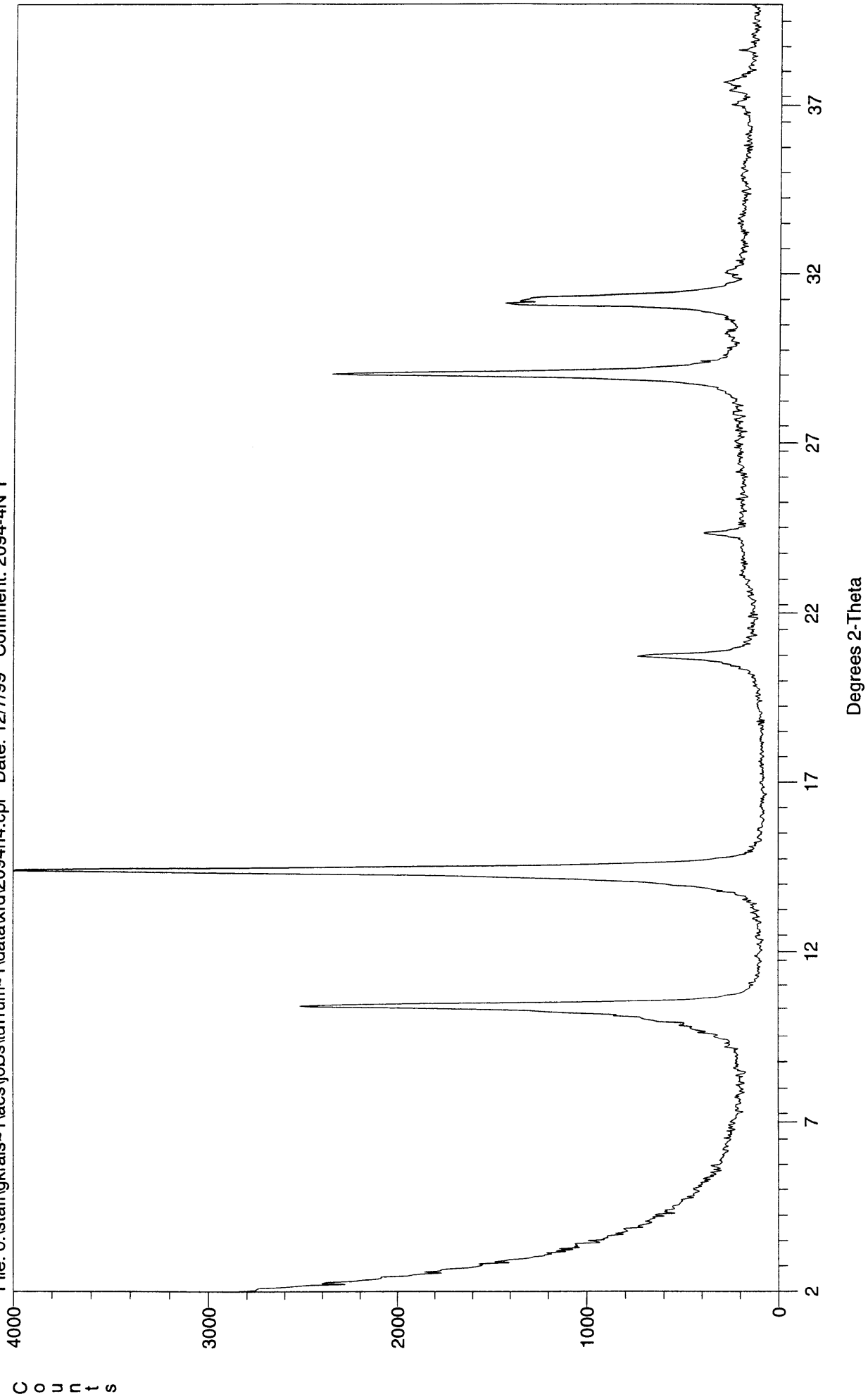


File: o:\staff\gkrais-1\acs\jobs\turrum-1\data\xrd\2094-4.cpi Date: 12/5/99 Comment: 2094-4 ACS0423-01 TURRUM-7 100c 1

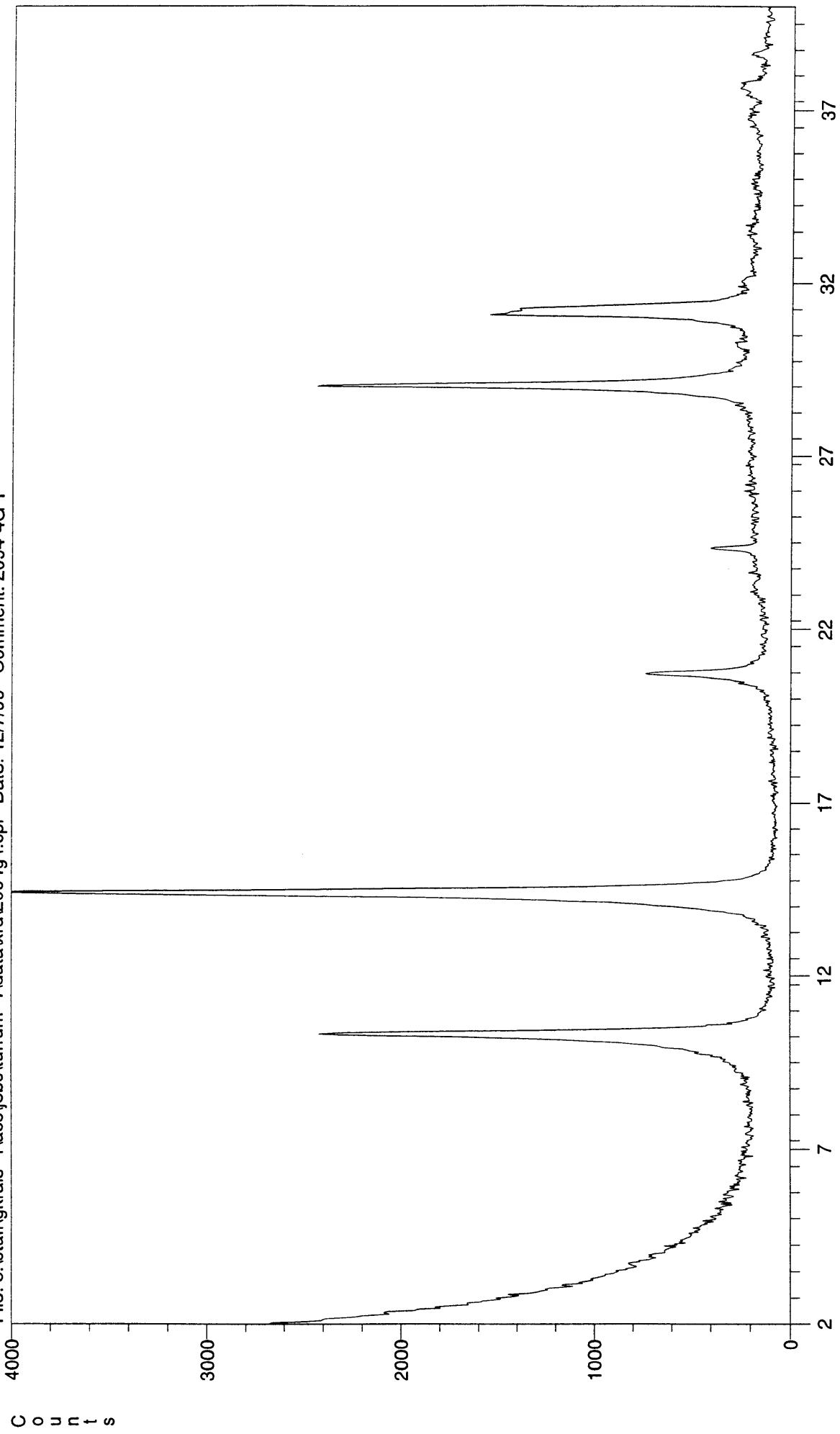




File: o:\staff\krais~1\acs\jobs\turrun~1\data\rd\2094n4.cpi Date: 12/7/99 Comment: 2094-4N 1

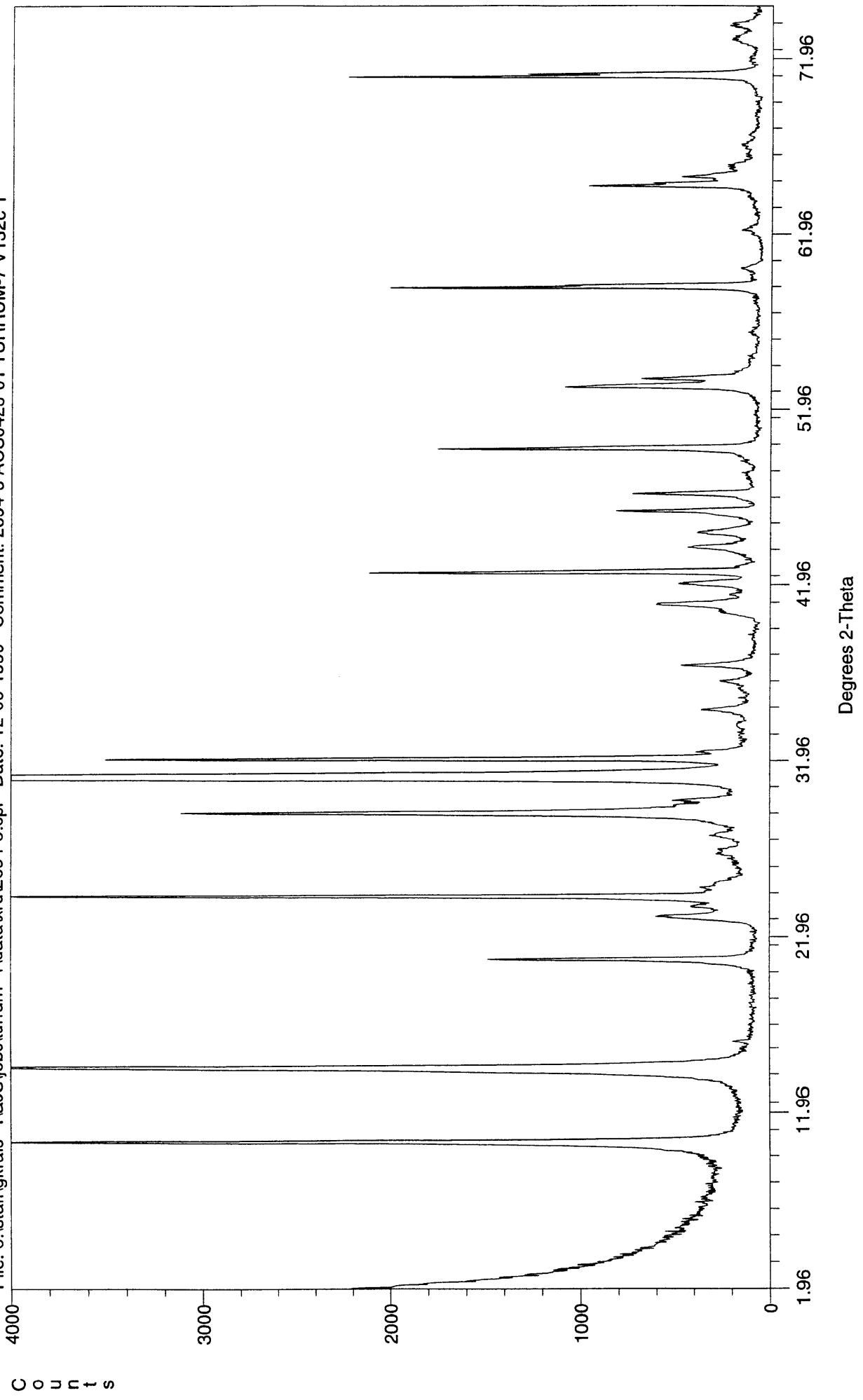


File: o:\staff\gkrais~1\acs\jobs\tururum~1\data\xrd\2094g4.cpi Date: 12/7/99 Comment: 2094-4G 1

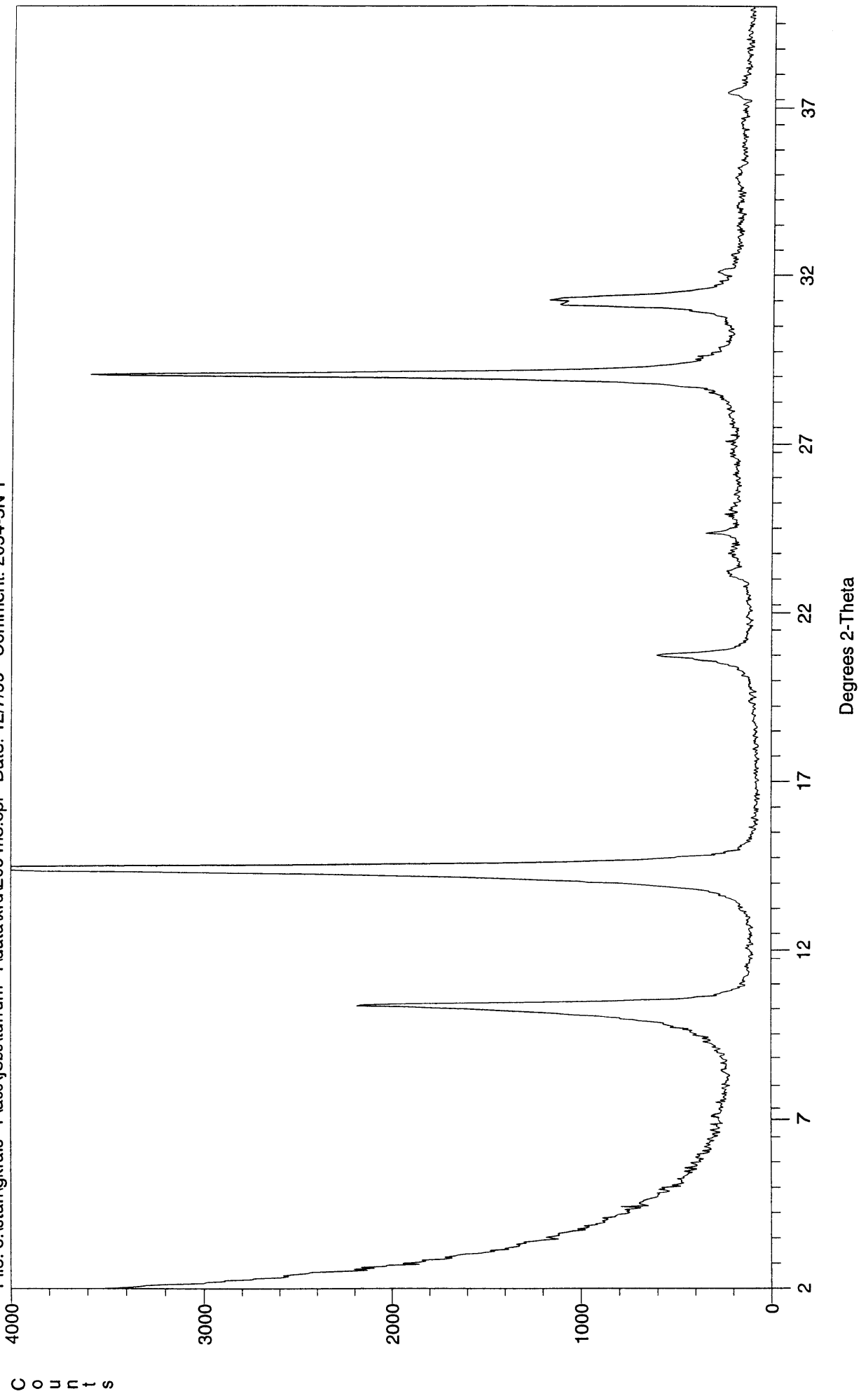


Degrees 2-Theta

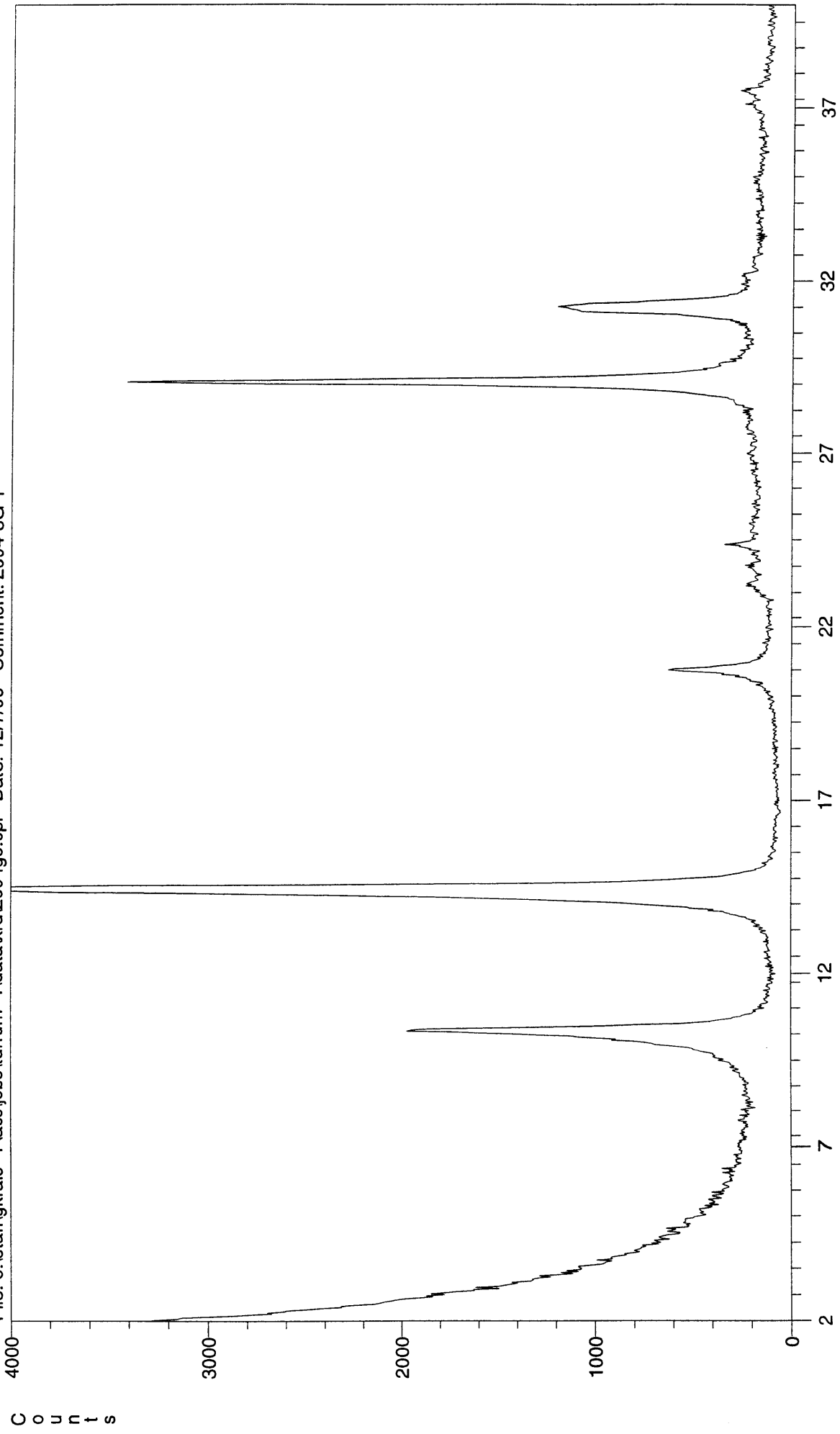
File: o:\staff\gkrais~1\data\rd\2094-5.cpi Date: 12-09-1999 Comment: 2094-5 ACS0423-01 TURRUM-7 V132c 1



File: o:\staff\gkrais~1\acs\jobs\tururum~1\data\xrd\2094n5.cpi Date: 12/7/99 Comment: 2094-5N 1

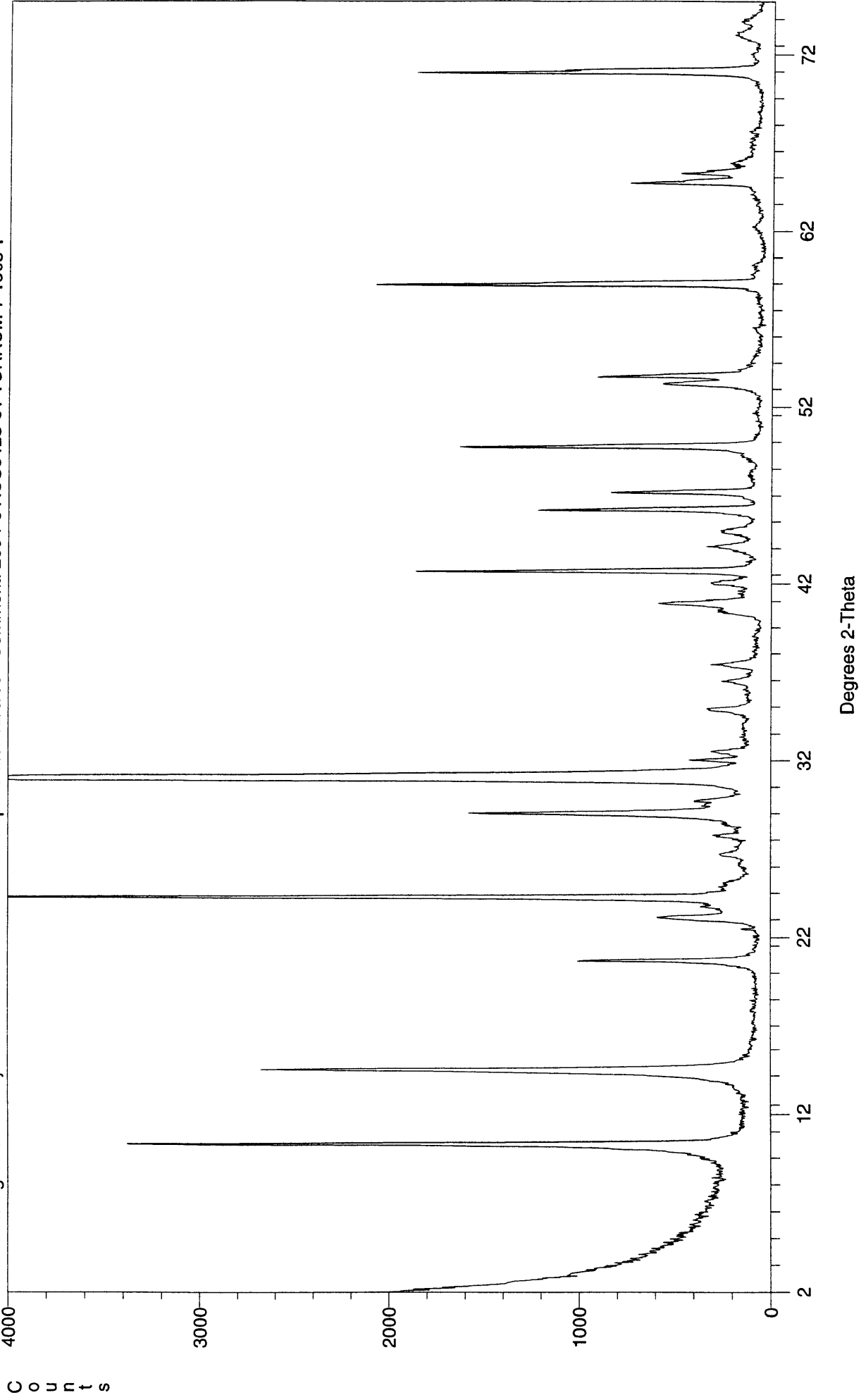


File: o:\staff\krais~1\acs\jobs\tururum~1\data\xrd\2094g5.cpi Date: 12/7/99 Comment: 2094-5G 1

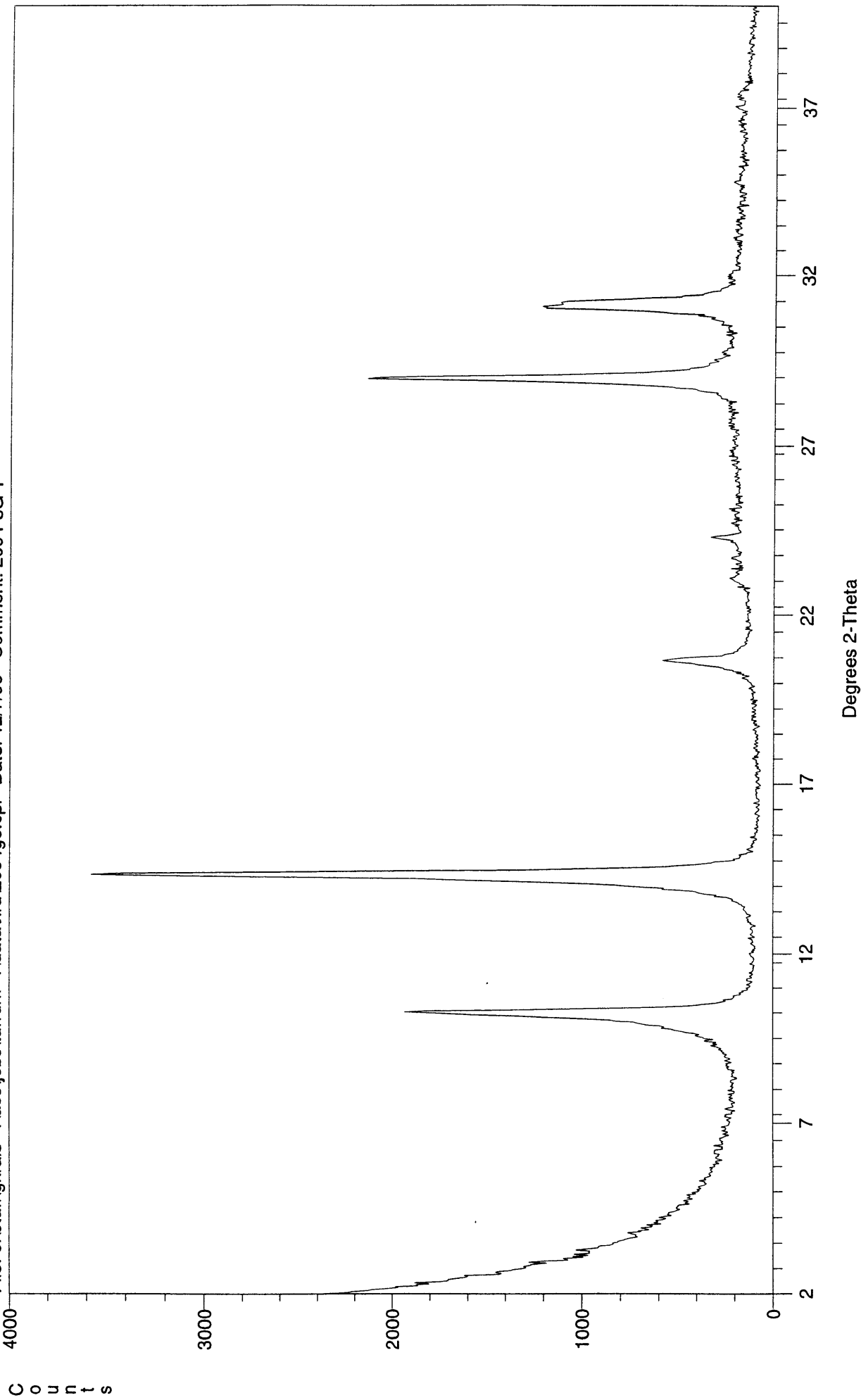


Degrees 2-Theta

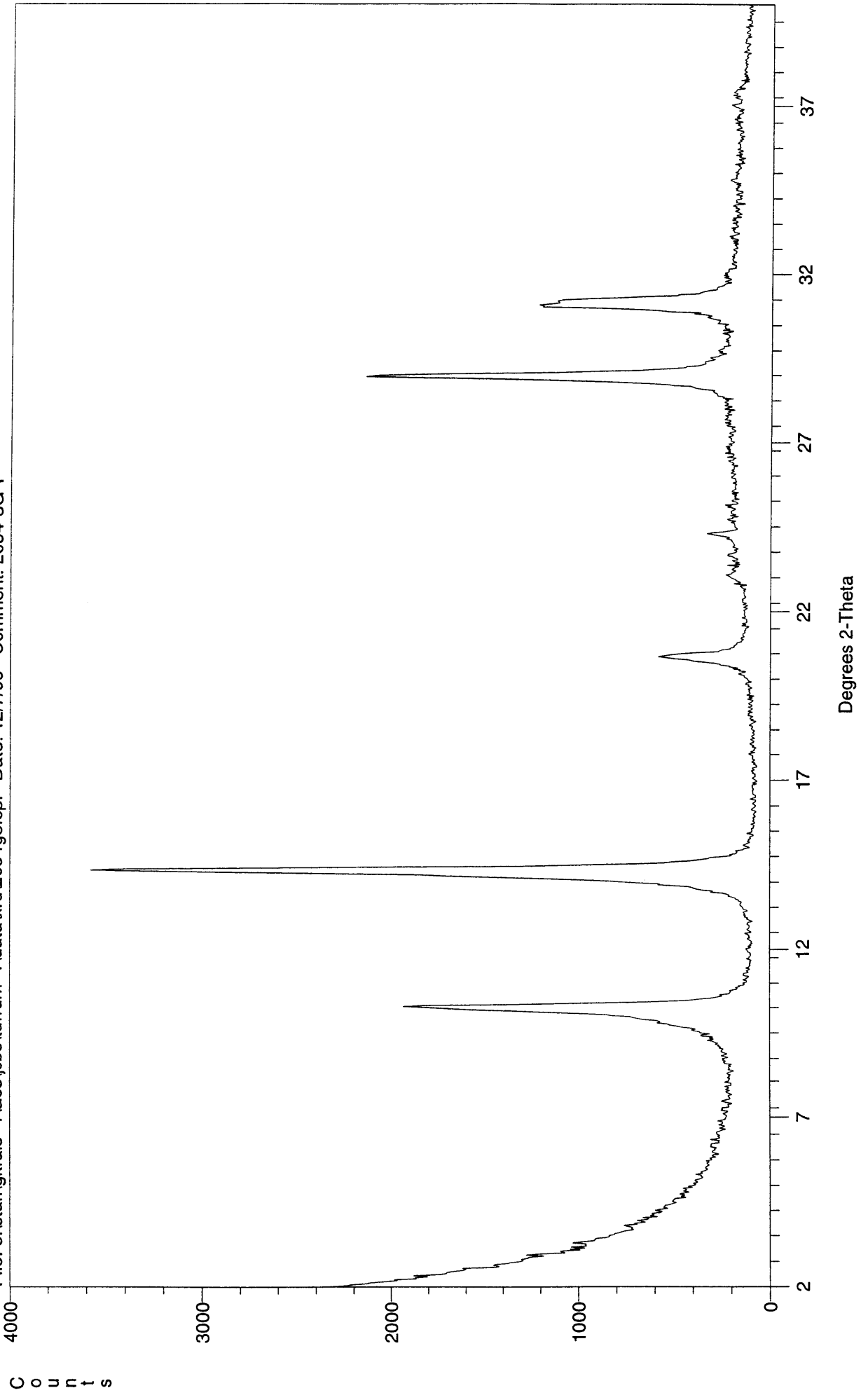
File: o:\staff\gkrais~1\acs\jobs\turrum~1\data\xrd\2094-6.cpi Date: 12/5/99 Comment: 2094-6 ACS0423-01 TURRUM-7 150c 1



File: o:\staff\gkrais~1\acs\jobs\tururum~1\data\xrd\2094g6.cpi Date: 12/7/99 Comment: 2094-6G 1

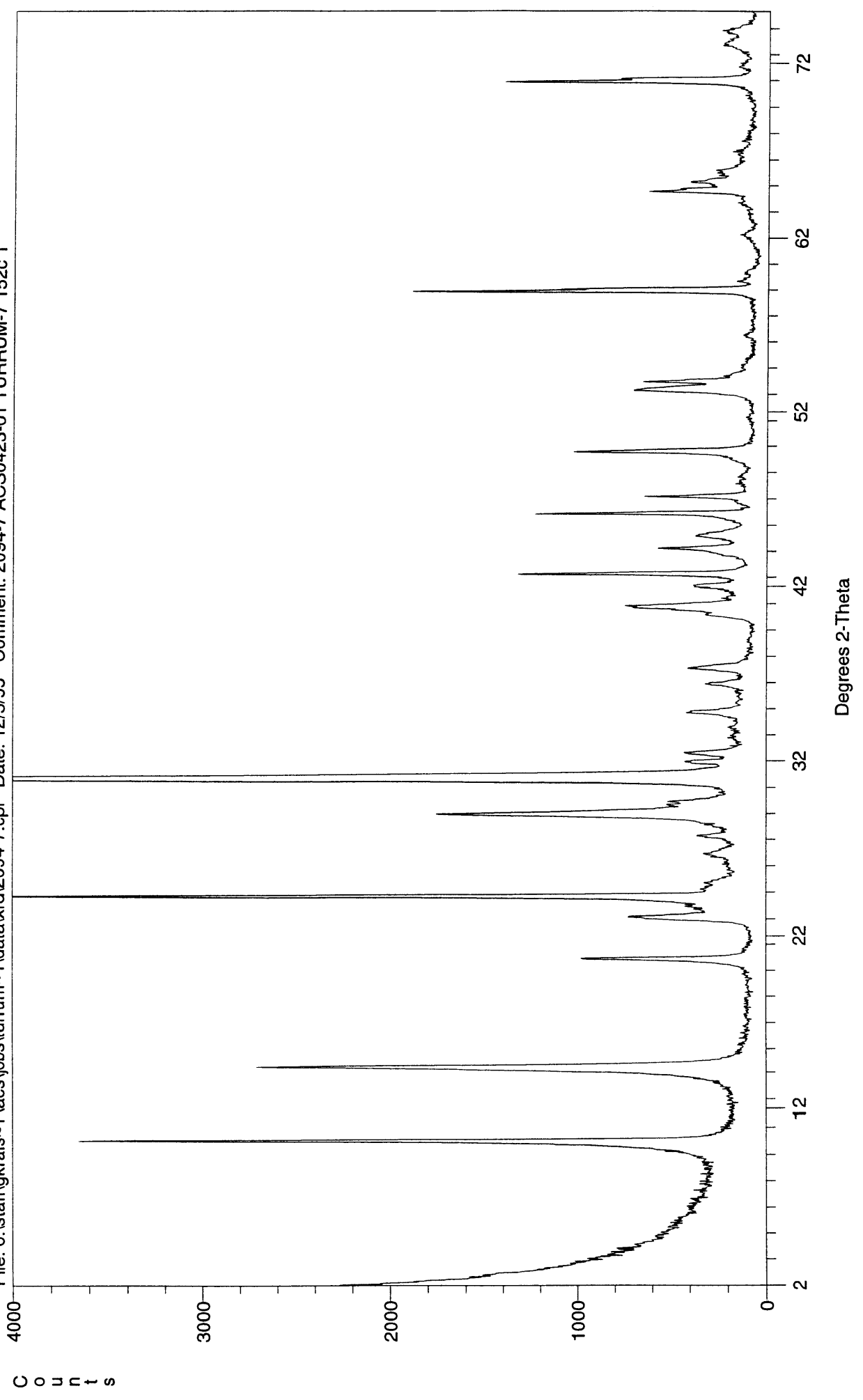


File: o:\staff\gkrais~1\acs\jobs\turrum~1\data\xrd\2094g6.cpi Date: 12/7/99 Comment: 2094-6G 1

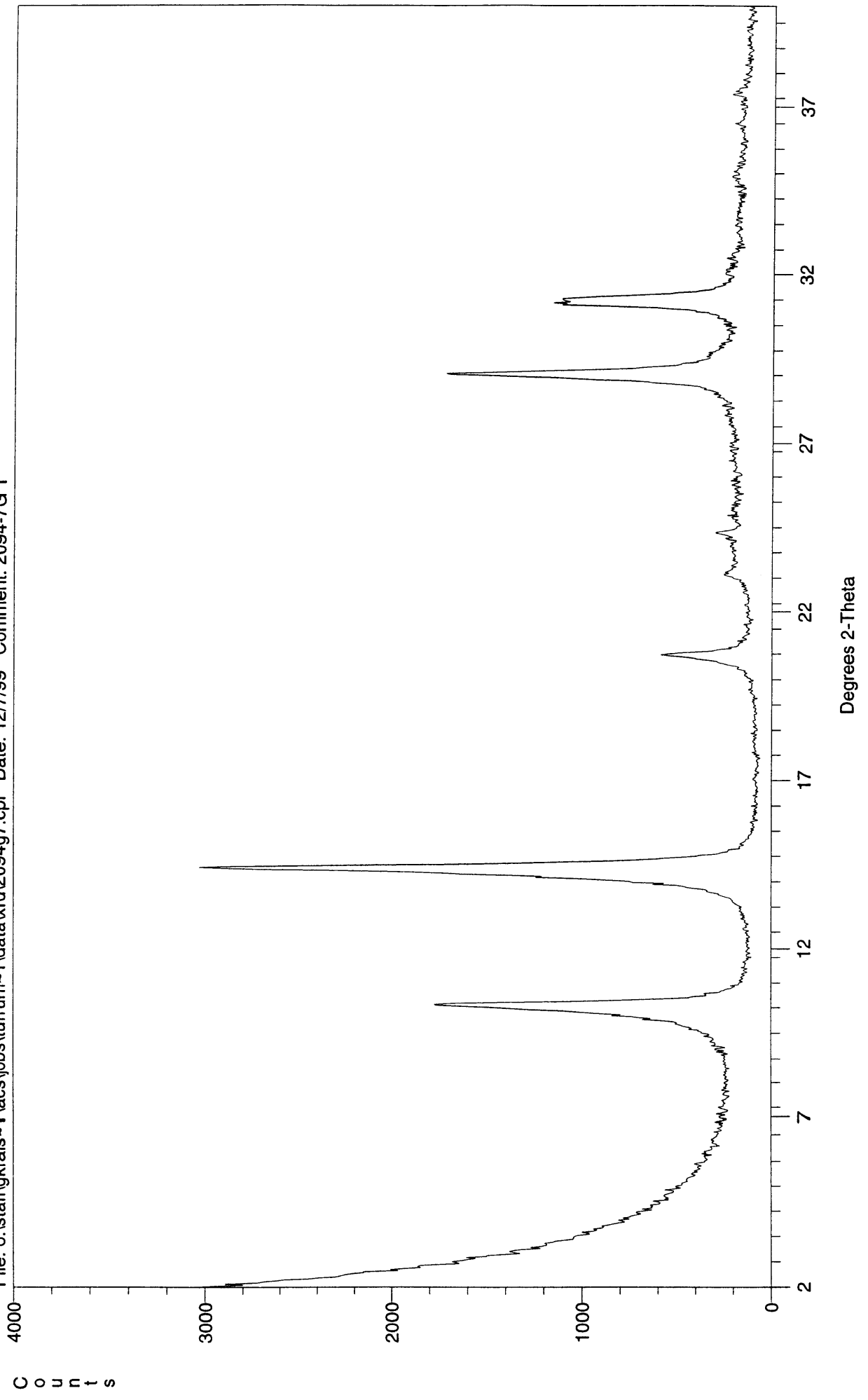




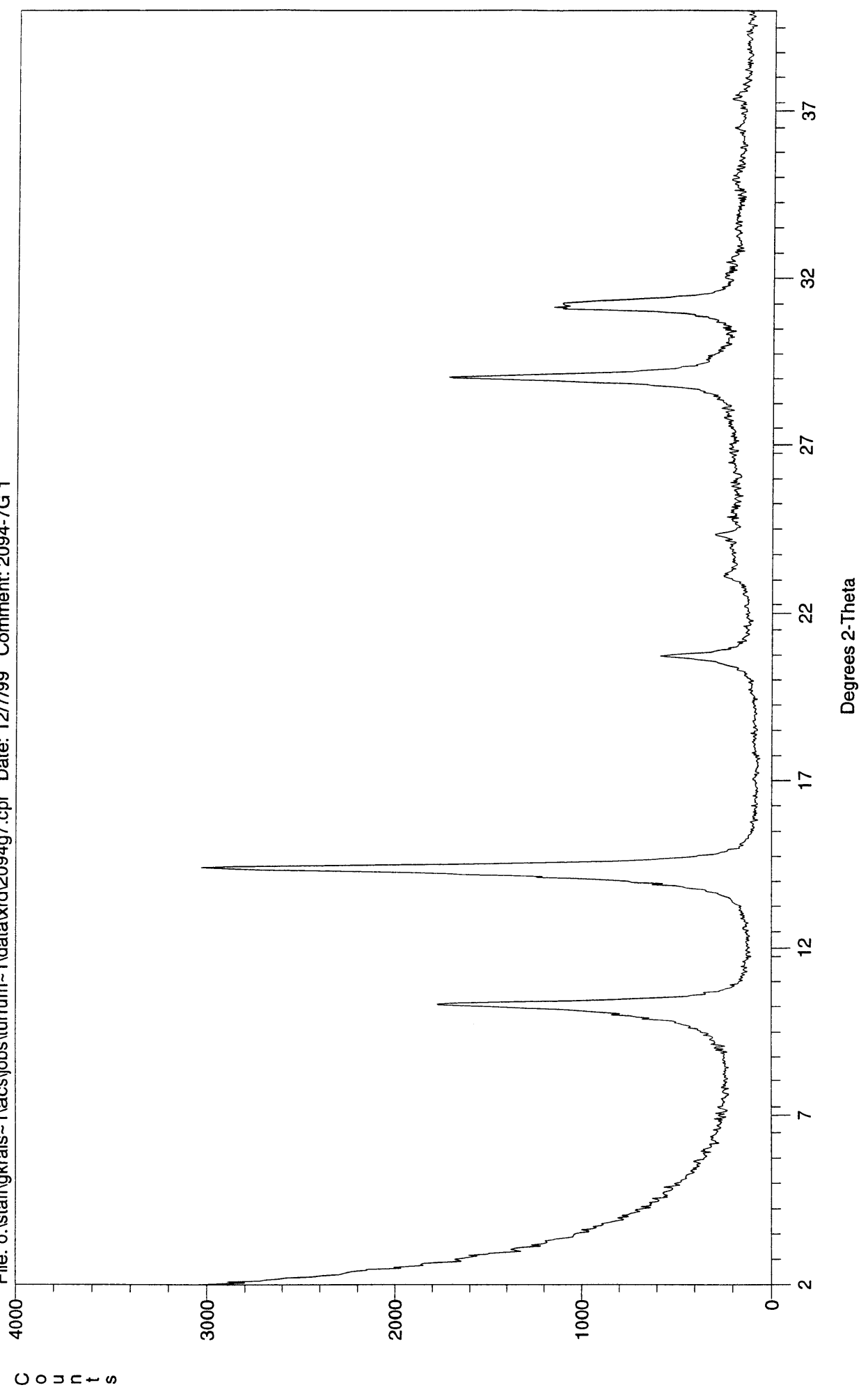
File: o:\staff\gkrais~1\acs\jobs\turrium~1\data\rd\2094-7.cpi Date: 12/5/99 Comment: 2094-7 ACS0423-01 TURRUM-7 152c 1



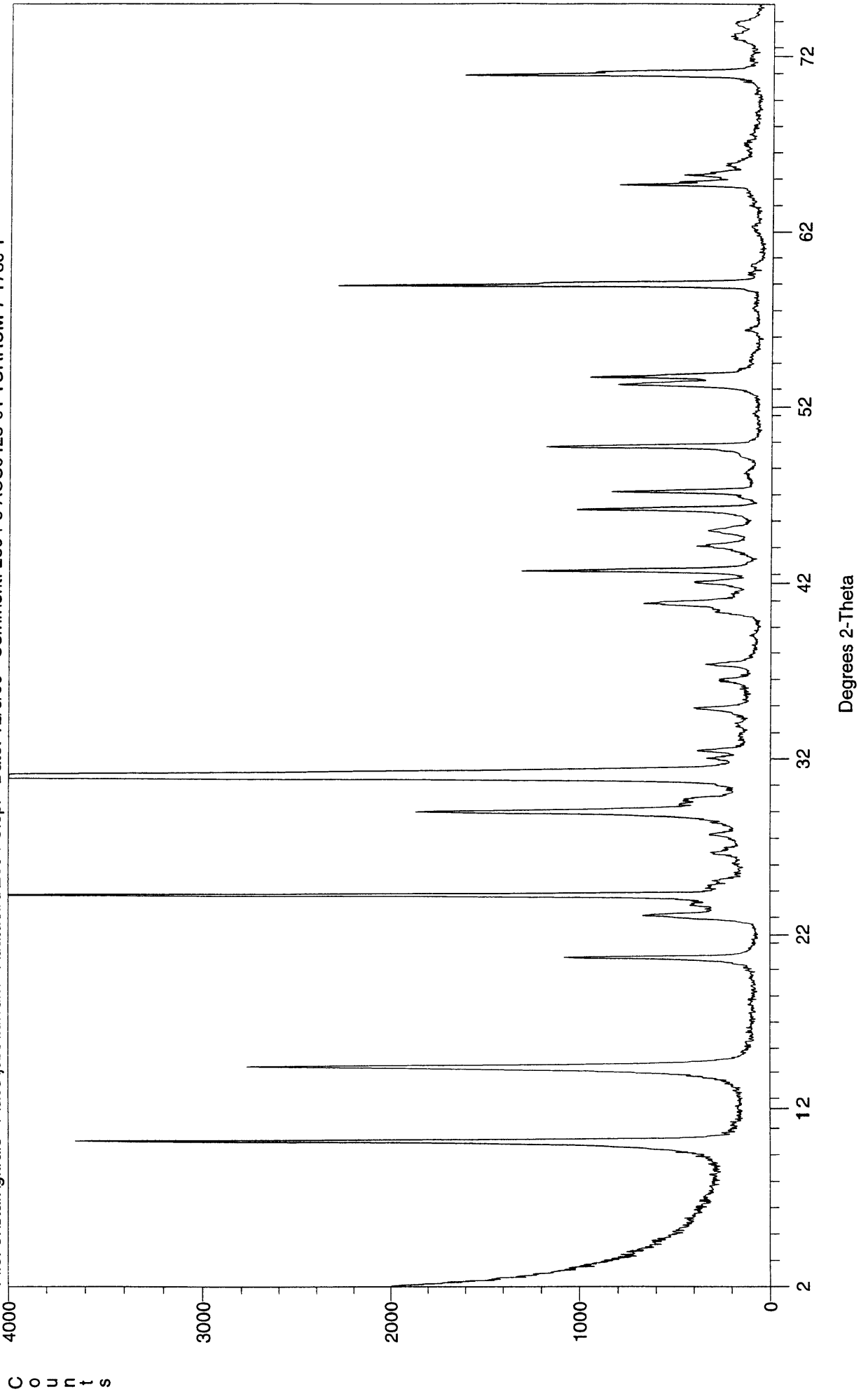
File: o:\staff\krais~1\acs\jobs\lurum~1\data\xrd\2094g7.cpi Date: 12/7/99 Comment: 2094-7G 1



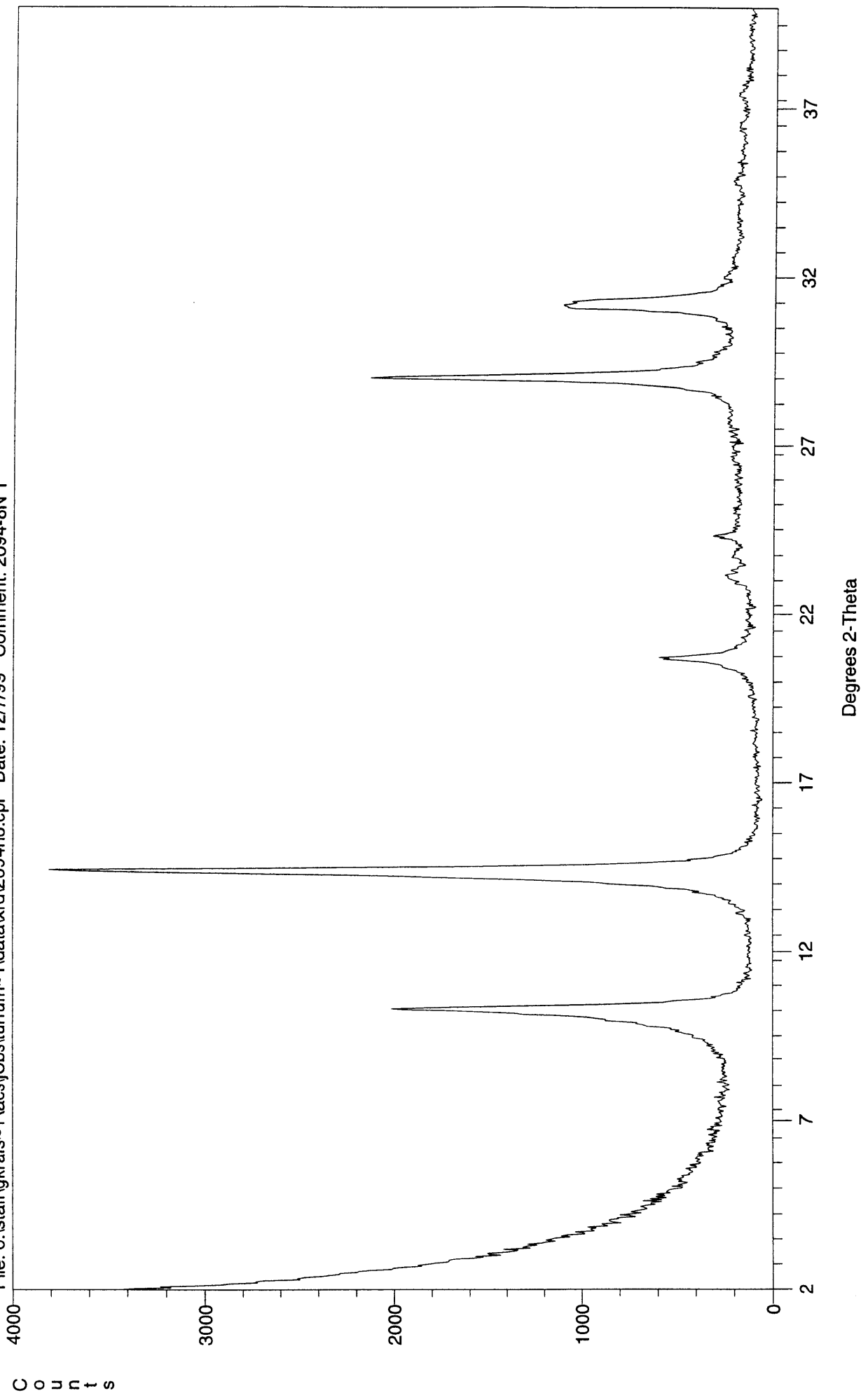
File: o:\staff\gkrais~1\acs\jobs\tururum~1\data\xrd\2094g7.cpi Date: 12/7/99 Comment: 2094-7G 1



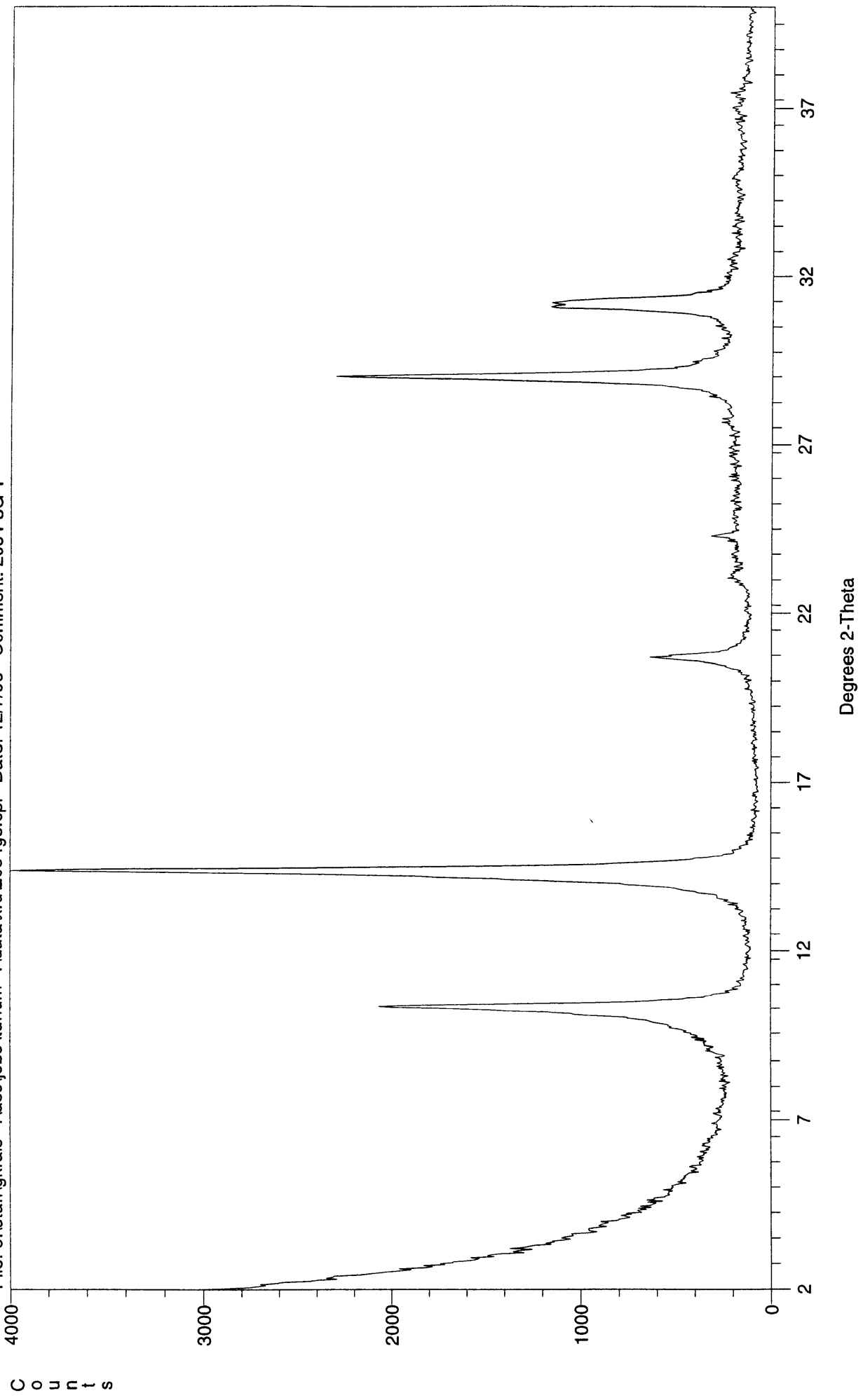
File: o:\staff\gkrais~1\acs\jobs\turrum~1\data\xrd\2094-8.cpi Date: 12/5/99 Comment: 2094-8 ACS0423-01 TURRUM-7 178c 1



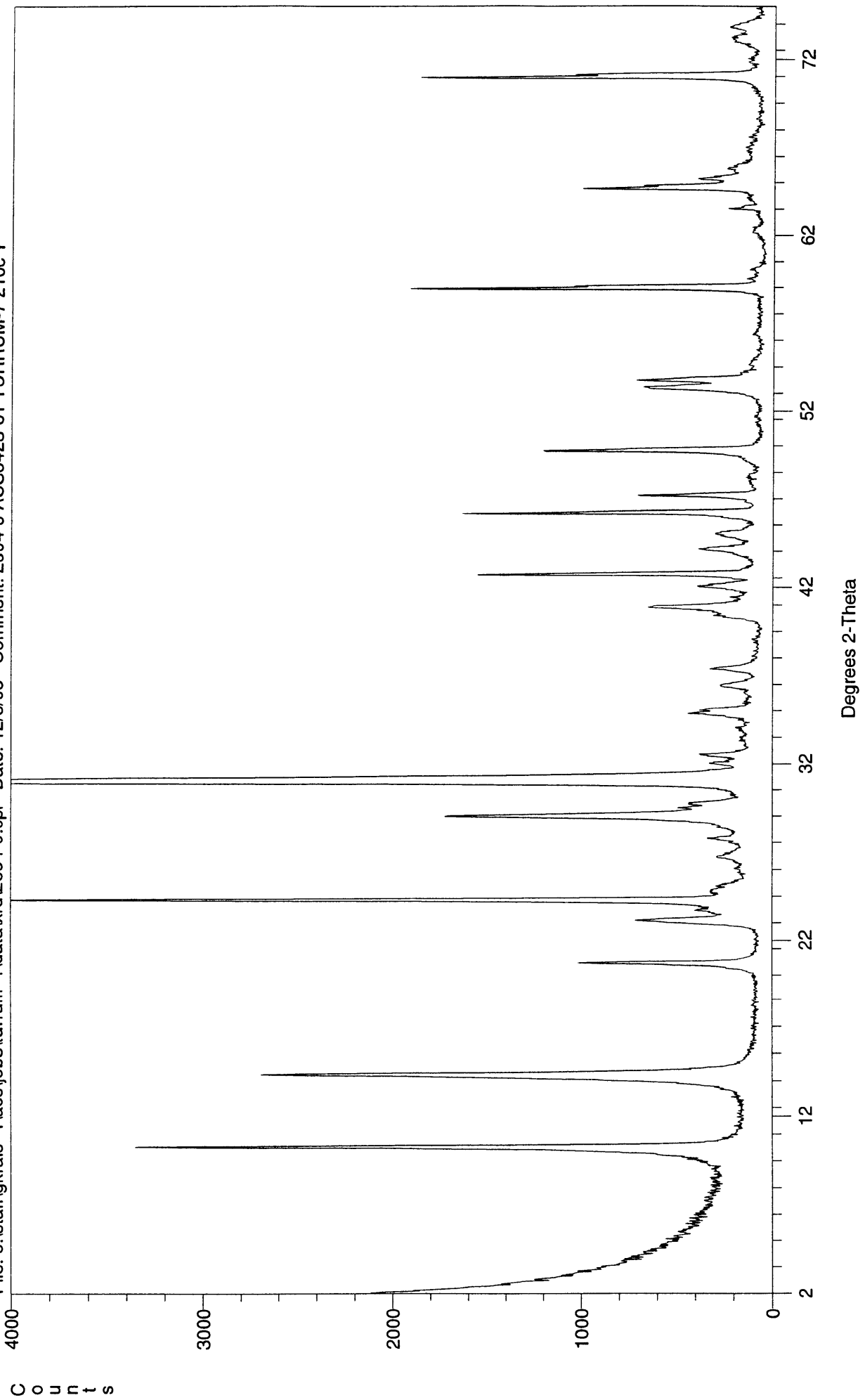
File: o:\staff\gkrais~1\acs\jobs\turruum~1\data\xrd\2094n8.cpi Date: 12/7/99 Comment: 2094-8N 1



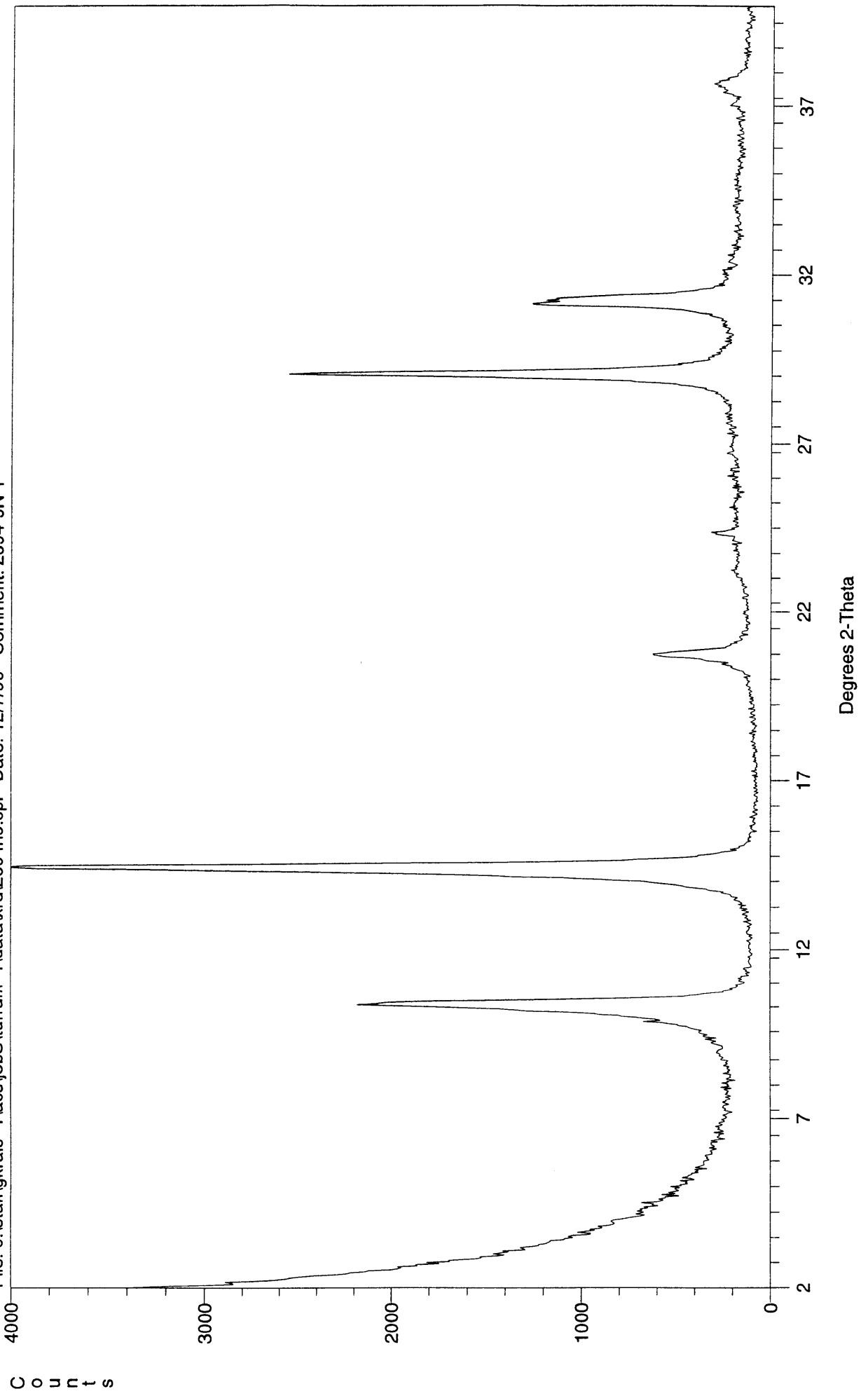
File: o:\staff\krais-1\acs\jobs\turrun-1\data\rd\2094g8.cpi Date: 12/7/99 Comment: 2094-8G 1



File: o:\staff\gkrais~1\acs\jobs\tururum~1\data\rd\2094-9.cpi Date: 12/5/99 Comment: 2094-9 ACS0423-01 TURURUM-7 210c 1

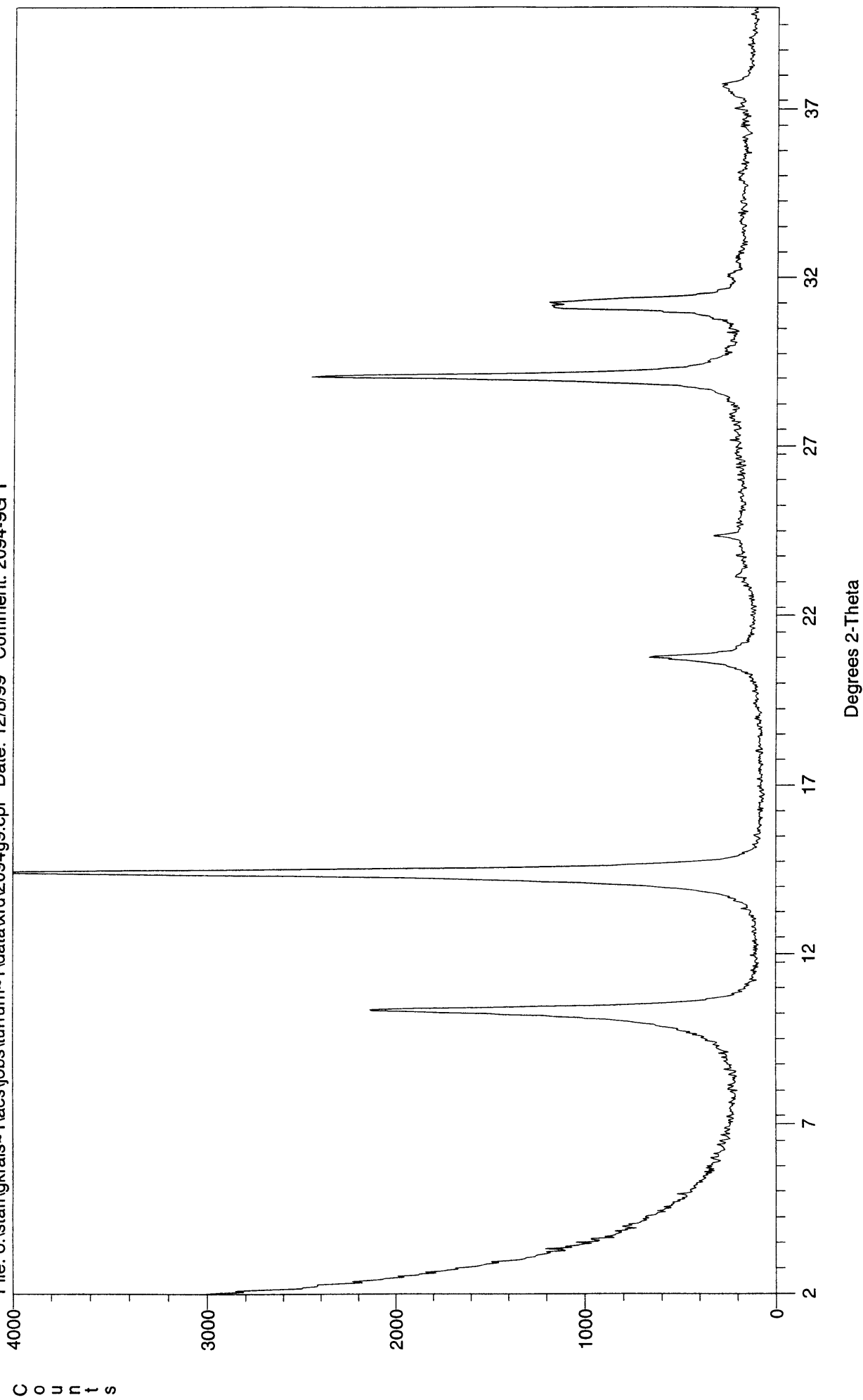


File: o:\staff\gkrais~1\acs\jobs\turum~1\data\xrd\2094n9.cpi Date: 12/7/99 Comment: 2094-9N 1

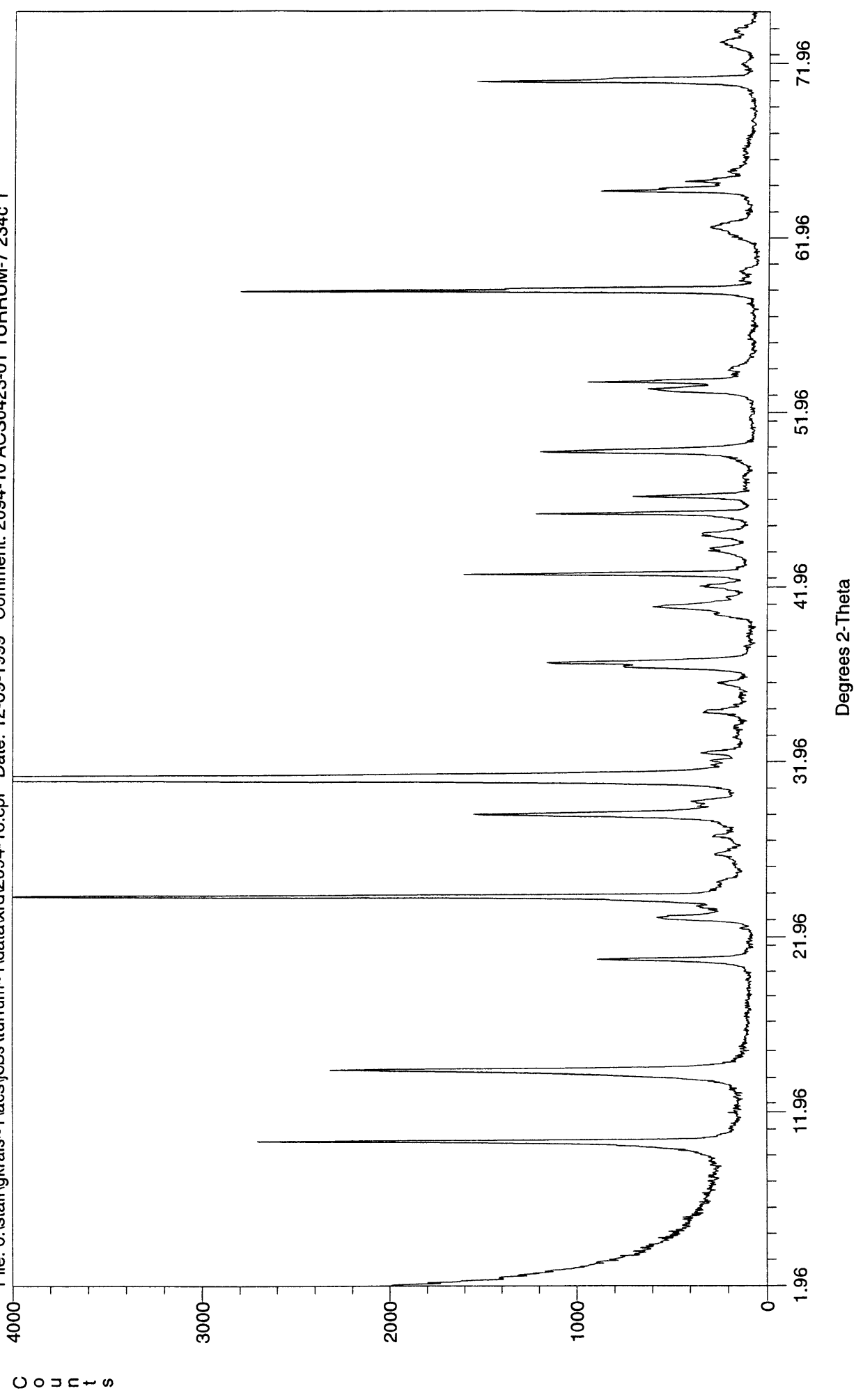




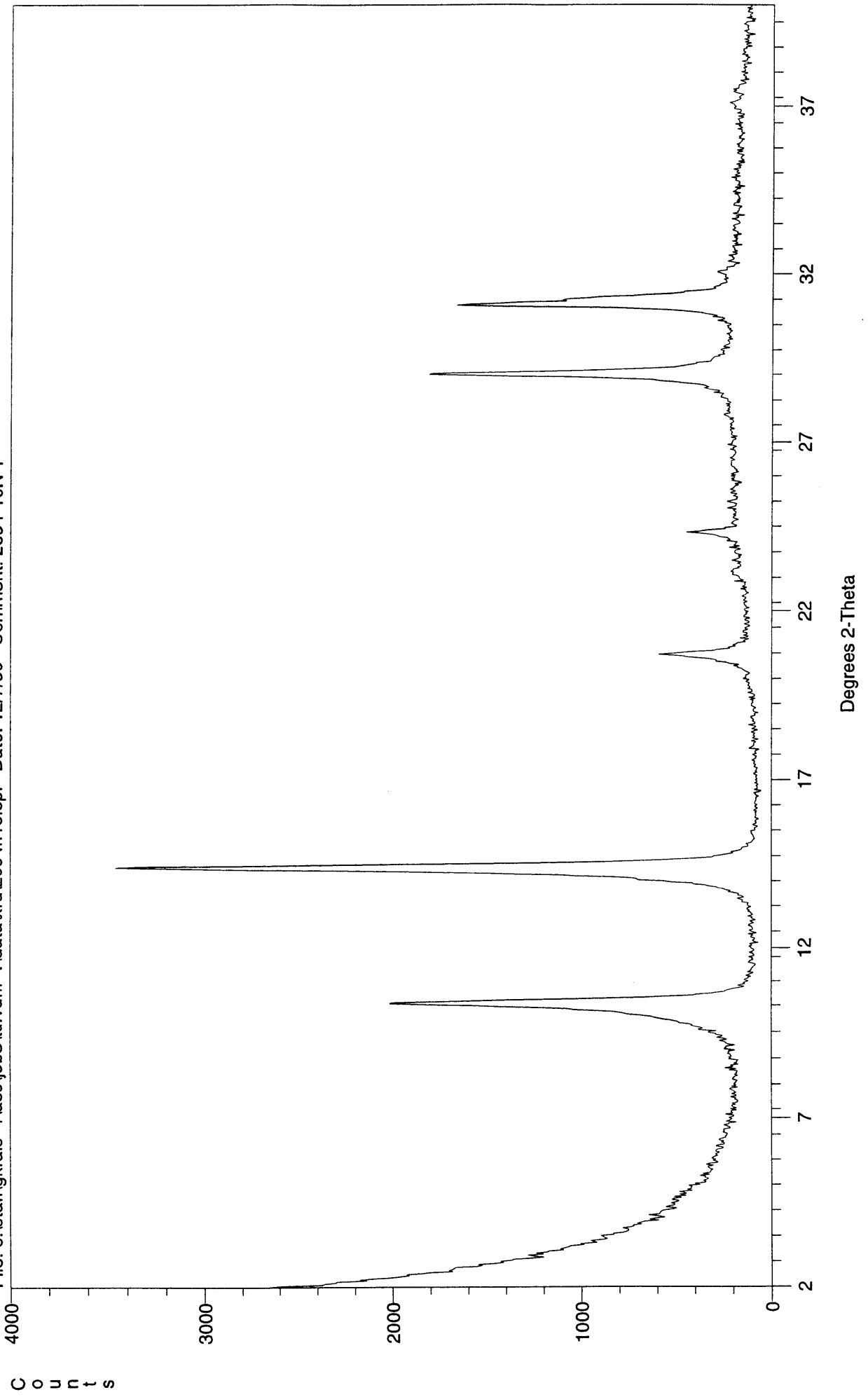
File: o:\staff\gkrais-1\acs\jobs\tururum-1\data\xrd\2094g9.cpi Date: 12/8/99 Comment: 2094-9G 1



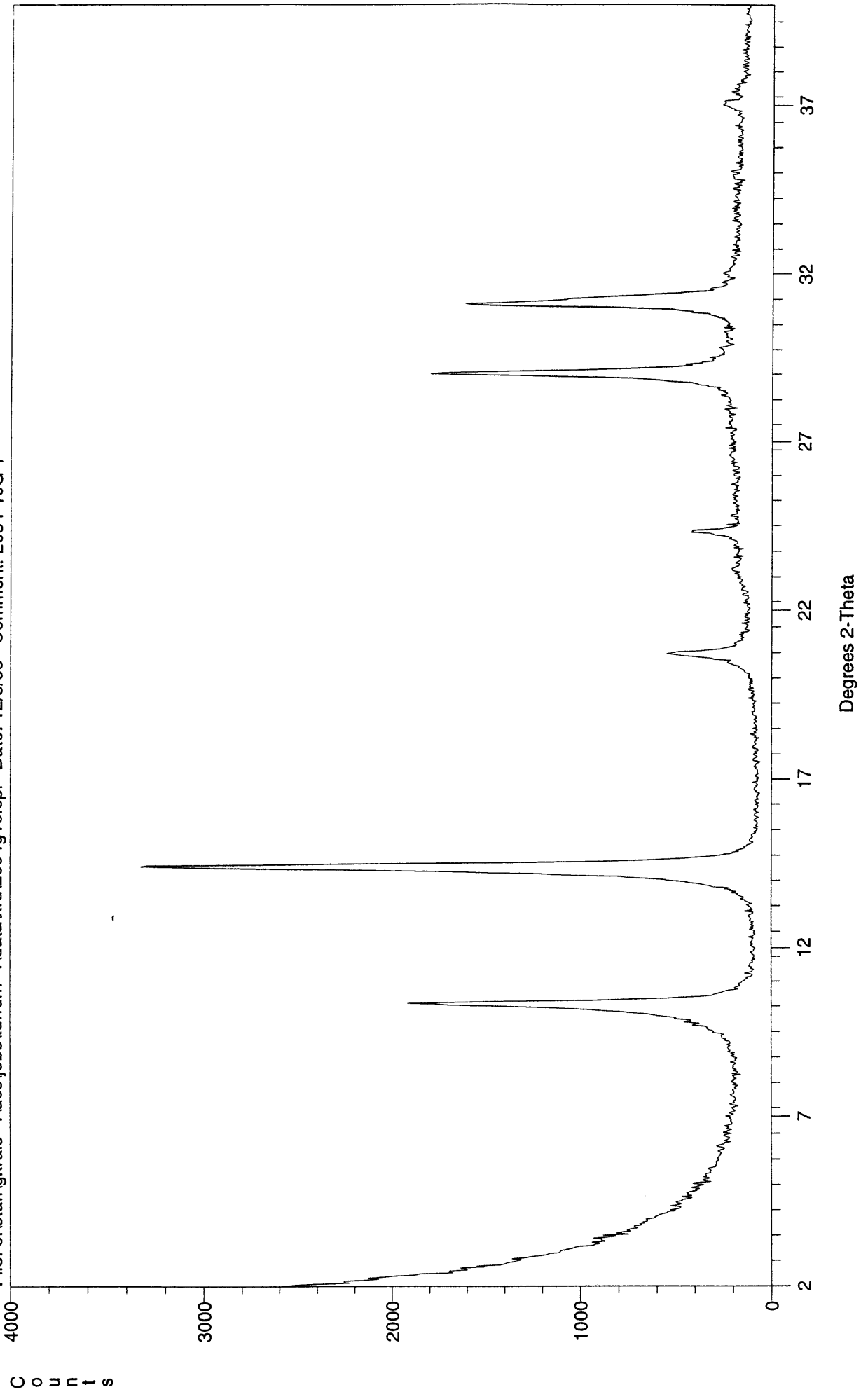
File: o:\staff\krais~1\acs\jobs\turrium~1\data\xrd\2094-10.cpi Date: 12-09-1999 Comment: 2094-10 ACS0423-01 TURRUM-7 234c 1



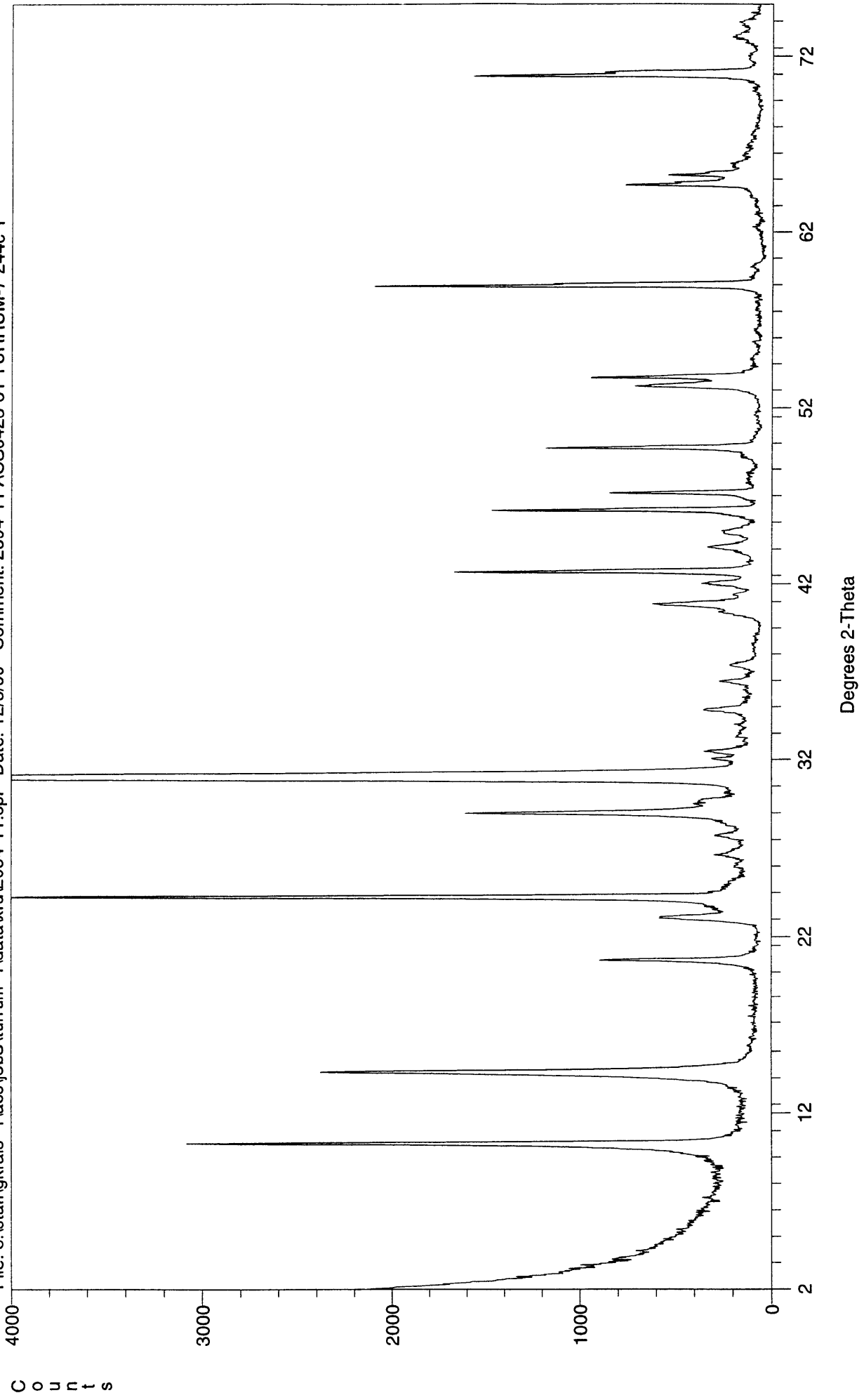
File: o:\staff\gkrais~1\acs\jobs\turru~1\data\rd\2094n10.cpi Date: 12/7/99 Comment: 2094-10N 1



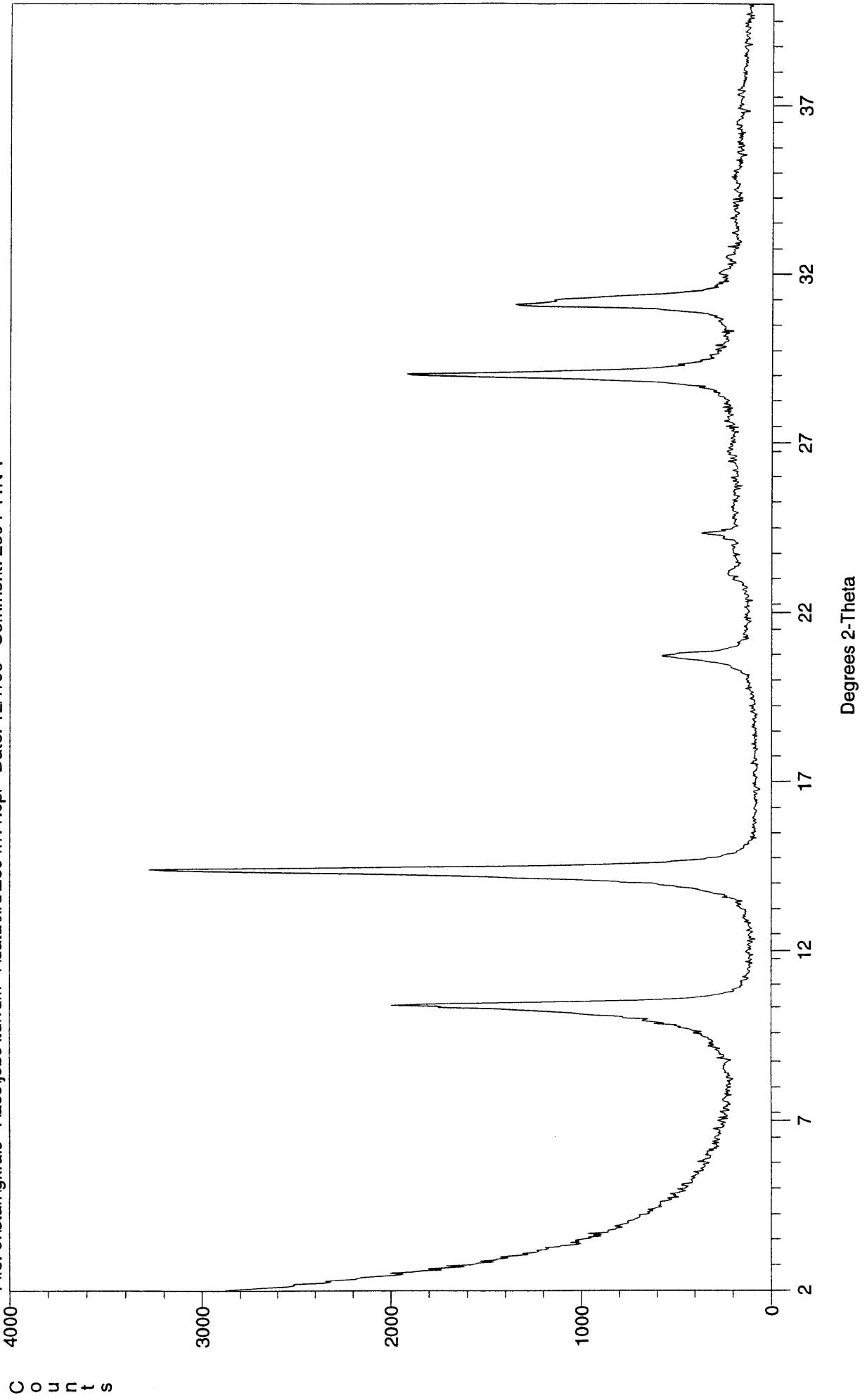
File: o:\staff\gkrais~1\acs\jobs\tururum~1\data\xrd\2094g10.cpi Date: 12/8/99 Comment: 2094-10G 1



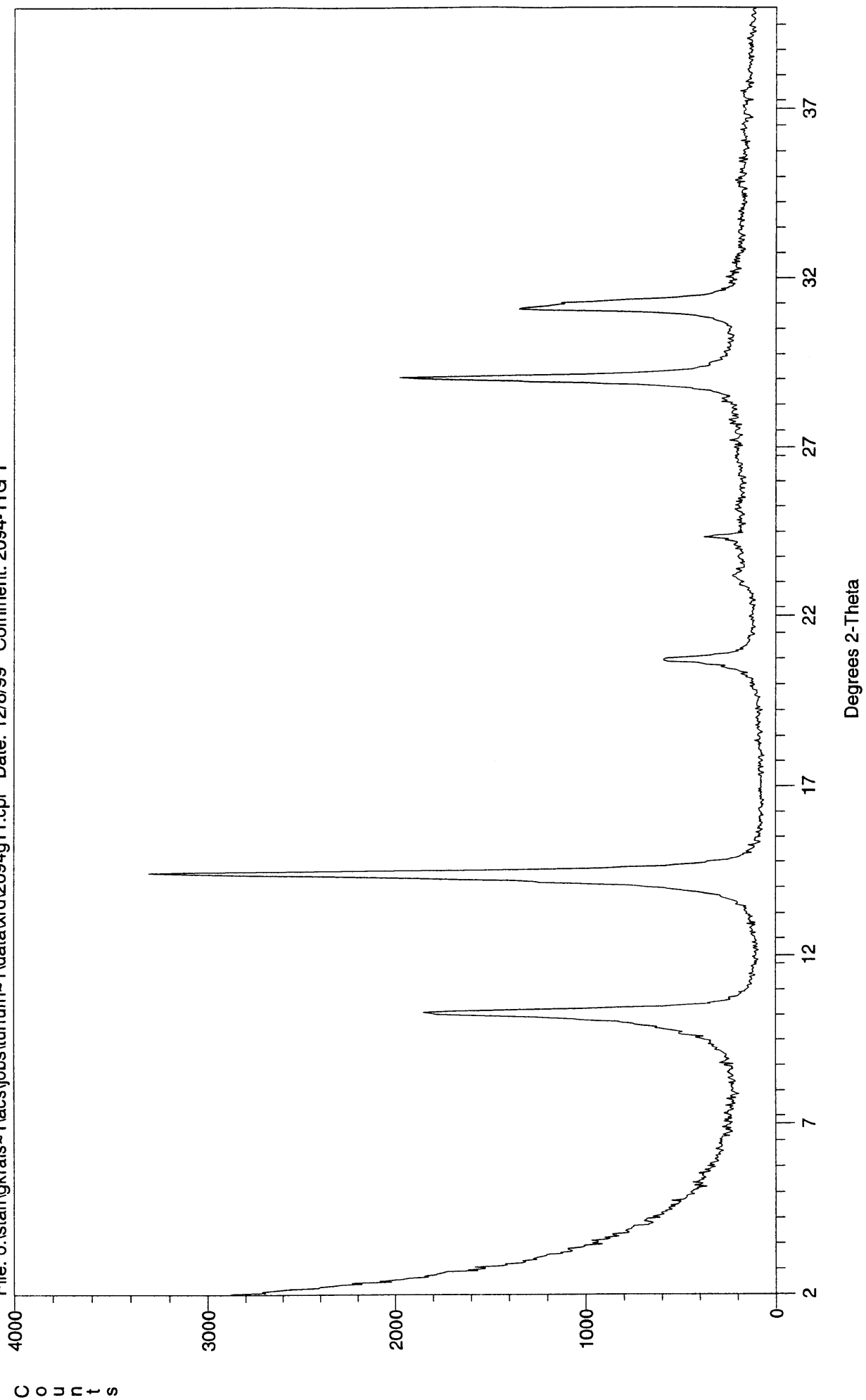
File: o:\staff\krais~1\acs\jobs\turru~1\data\rd\2094-11 .cpi Date: 12/5/99 Comment: 2094-11 ACS0423-01 TURRUM-7 244c 1



File: o:\staff\krais~1\acs\jobs\turum~1\data\xrd\2094n11.cpi Date: 12/7/99 Comment: 2094-11N 1



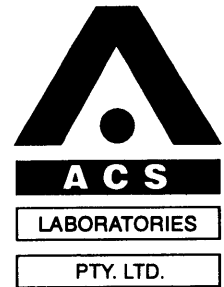
File: o:\staff\krais~1\acs\jobs\turnum~1\data\xrd\2094g11.cpi Date: 12/8/99 Comment: 2094-11G 1



907511 ~~288~~  
280



907511 ~~284~~  
281



**MERCURY INJECTION ANALYSIS FINAL REPORT**  
**of**  
***TURRUM-7***  
**for**  
***ESSO AUSTRALIA LTD***  
**by**  
**ACS LABORATORIES PTY LTD**

907511 ~~205~~  
282



23 December, 1999

Esso Australia Ltd  
Esso House  
12 Riverside Quay  
SOUTHBANK VIC 3006

Attention: Mr Phil Burnett

**FINAL REPORT: 0306(b)-02**  
**TURRUM-7**

**CLIENT REFERENCE:** Contract Number 2710080 RFS No.5  
AFE No. L61019005

**MATERIAL:** Core Plugs and Core Plug Offcuts

**LOCALITY:** Gippsland Basin, Bass Strait

**WORK REQUIRED:** Mercury Injection Analysis

Please direct technical inquiries regarding this work to the signatory below under whose supervision the work was conducted.

A handwritten signature in black ink, appearing to read 'Peter Crozier', with a horizontal line underneath.

**PETER CROZIER**  
Operations Manager

ACS Laboratories Pty. Ltd. shall not be liable or responsible for any loss, cost, damages or expenses incurred by the client, or any other person or company, resulting from any information or interpretation given in this report. In no case shall ACS Laboratories Pty. Ltd. be responsible for consequential damages including, but not limited to, lost profits, damages for failure to meet deadlines and lost production arising from this report.

Address: P.O. Box 396, Chermside South, Qld. 4032 Australia  
Telephone: 61 7 3350 1222 Facsimile: 61 7 3359 0666  
E-mail: acs.bris@acslabs.com.au

ACS Laboratories Pty Ltd  
ACN: 008 273 005

**CONTENTS**

**PAGE**

***CHAPTERS***

<b>1. INTRODUCTION .....</b>	<b>1</b>
<b>2. STUDY AIMS .....</b>	<b>3</b>
<b>3. SAMPLE TEST PROCEDURES</b>	
<b>3.1 Mercury Injection Capillary Pressure .....</b>	<b>5</b>

***APPENDIX***

<b>I. MERCURY INJECTION CAPILLARY PRESSURE RESULTS</b>	
--------------------------------------------------------	--

907511 ~~284~~  
284

***CHAPTER 1***

**INTRODUCTION**

## 1. INTRODUCTION

A suite of 12 contingency plug offcuts from Turrum-7 were received at ACS Laboratories Brisbane office on 4 November, 1999. These samples required mercury injection analysis and detailed petrographic descriptions. The petrographic work is reported in a separate final report number 0423-01.

The following report includes tabular data of mercury injection capillary pressures and plots showing these as capillary pressure versus saturation and intrusion vs pore throat diameter.

***CHAPTER 2***

**STUDY AIMS**

**2. STUDY AIMS**

The analysis was performed with the following aims:

1. To determine pore throat entry pressures and pore size distribution through the provision of mercury injection capillary pressure data.

## ***CHAPTER 3***

### **SAMPLE TEST PROCEDURES**

#### **3.1 Mercury Injection Capillary Pressure**



### 3. SAMPLE TEST PROCEDURES

#### 3.1 Mercury Injection Capillary Pressure

A suite of mercury injection capillary pressure analyses was performed on selected contingency plug offcuts. Samples of sufficient volume to fill the sample chamber (circa 2cm<sup>3</sup>) were utilised for capillary pressure determinations by the mercury injection technique. The mercury injection apparatus used was a semi-automatic Micromeritics Autopore 9410 which can operate up to a pressure of 60,000 psia, and can measure intrusions as small as 0.0001cm<sup>3</sup>.

The Micromeritics Autopore records mercury intrusion by measuring the capacitance change between the capillary of mercury contained in the penetrometer and an outer metal sheath as mercury invades the samples. For pressure up to 24 psia, air pressure was used. Hydraulic oil was used to achieve the higher pressures. No volume corrections for pressure effects were made, since below 24 psia they are negligible, whilst for higher pressures the penetrometer experiences equal external and internal pressures and mercury compression is offset by penetrometer compression.

All samples were placed into calibrated glass penetrometers. These consist of a sample chamber and attached precision bore capillary. Once the samples were placed into the penetrometer, a vacuum was applied until less than 50 micrometres of mercury had been achieved. Mercury was then introduced into the penetrometer and the run commenced along pre-defined pressure points on a logarithmic scale. After equilibration at each pressure point, a capacitance reading was taken which was then converted into an equivalent intrusion volume. Pore throat diameter for intrusion pressure can be calculated as such:

$$D = \frac{4T \cos\theta C}{P_c}$$

<i>where</i>	<i>D</i>	=	<i>pore throat diameter (microns)</i>
	<i>T</i>	=	<i>interfacial tension (dynes/cm)</i>
	$\theta$	=	<i>contact angle (degrees)</i>
	<i>P<sub>c</sub></i>	=	<i>capillary pressure (psi)</i>
	<i>C</i>	=	<i>conversion constant</i>
		=	<i>145 x 10<sup>3</sup></i>

Any apparent inconsistencies between the reported values of Intrusion (percent) and Saturation (percent) are a rounding effect. All intrusion however accumulates to 100% saturation at maximum pressure.

The first two points on the pore size distribution plot have been removed at the request of Esso representatives, because these points were due to surface irregularities.

907511 ~~290~~  
290

*APPENDIX I*

**MERCURY INJECTION CAPILLARY PRESSURE RESULTS**

**CAPILLARY PRESSURE**

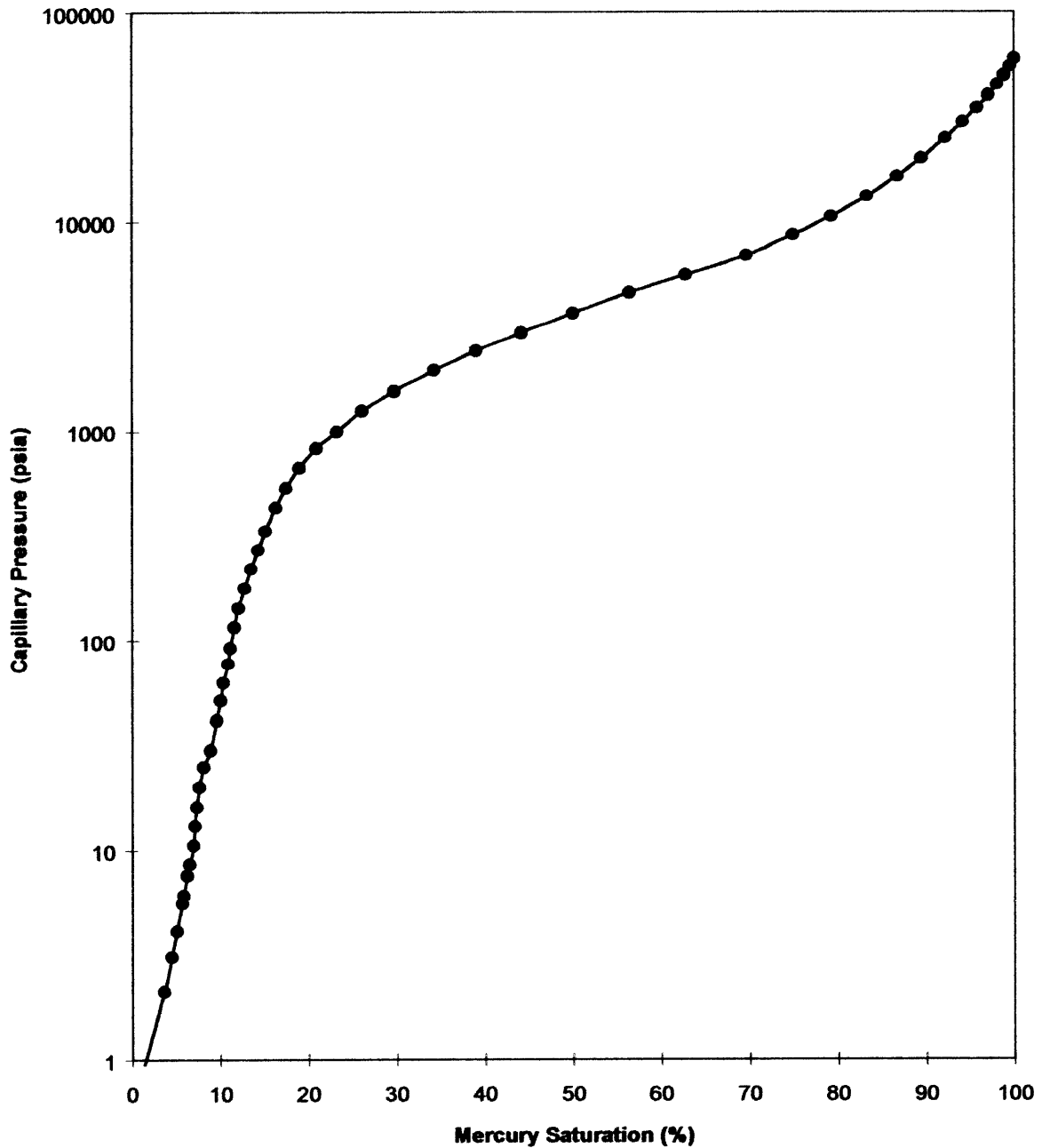
**Client** Esso Australia Ltd  
**Well** Turrum-7  
**Test Method** Air/Mercury Capillary Pressure Drainage  
**Sample** 008c  
**Depth** 2609.65 m

Pressure (psia)	Intrusion (percent)	Saturation (percent)	Pore Diameter (mm)
0.58	0.0	0.0	368.0
2.11	3.6	3.6	101.0
3.10	0.9	4.5	68.4
4.11	0.6	5.1	51.6
5.58	0.6	5.7	38.0
6.08	0.2	5.8	34.9
7.56	0.4	6.2	28.0
8.58	0.3	6.5	24.7
10.6	0.4	7.0	20.1
13.0	0.2	7.1	16.3
16.1	0.2	7.3	13.2
20.0	0.3	7.6	10.6
25.0	0.5	8.1	8.48
30.0	0.8	8.9	7.07
40.8	0.7	9.6	5.20
50.4	0.4	10.0	4.20
60.9	0.3	10.3	3.48
76.2	0.6	10.9	2.78
91.7	0.3	11.2	2.31
116	0.4	11.6	1.83
143	0.5	12.1	1.49
177	0.7	12.8	1.20
220	0.7	13.5	0.965
270	0.8	14.3	0.785
332	0.9	15.1	0.638
429	1.2	16.3	0.494
532	1.1	17.5	0.398

Pressure (psia)	Intrusion (percent)	Saturation (percent)	Pore Diameter (mm)
665	1.5	19.0	0.319
828	1.9	20.9	0.256
992	2.3	23.2	0.214
1246	2.9	26.1	0.170
1550	3.6	29.7	0.137
1954	4.5	34.3	0.108
2419	4.8	39.0	0.0876
2948	5.1	44.2	0.0719
3643	5.9	50.0	0.0582
4582	6.4	56.4	0.0463
5579	6.4	62.8	0.0380
6888	6.9	69.6	0.0308
8636	5.3	74.9	0.0245
10573	4.3	79.3	0.0201
13163	4.1	83.3	0.0161
16375	3.5	86.8	0.0129
20000	2.7	89.5	0.0106
24952	2.7	92.2	0.0085
29882	2.0	94.2	0.0071
34943	1.6	95.8	0.0061
40026	1.3	97.1	0.0053
45071	1.0	98.1	0.0047
50001	0.8	98.9	0.0042
55113	0.6	99.5	0.0038
59987	0.5	100.0	0.0035

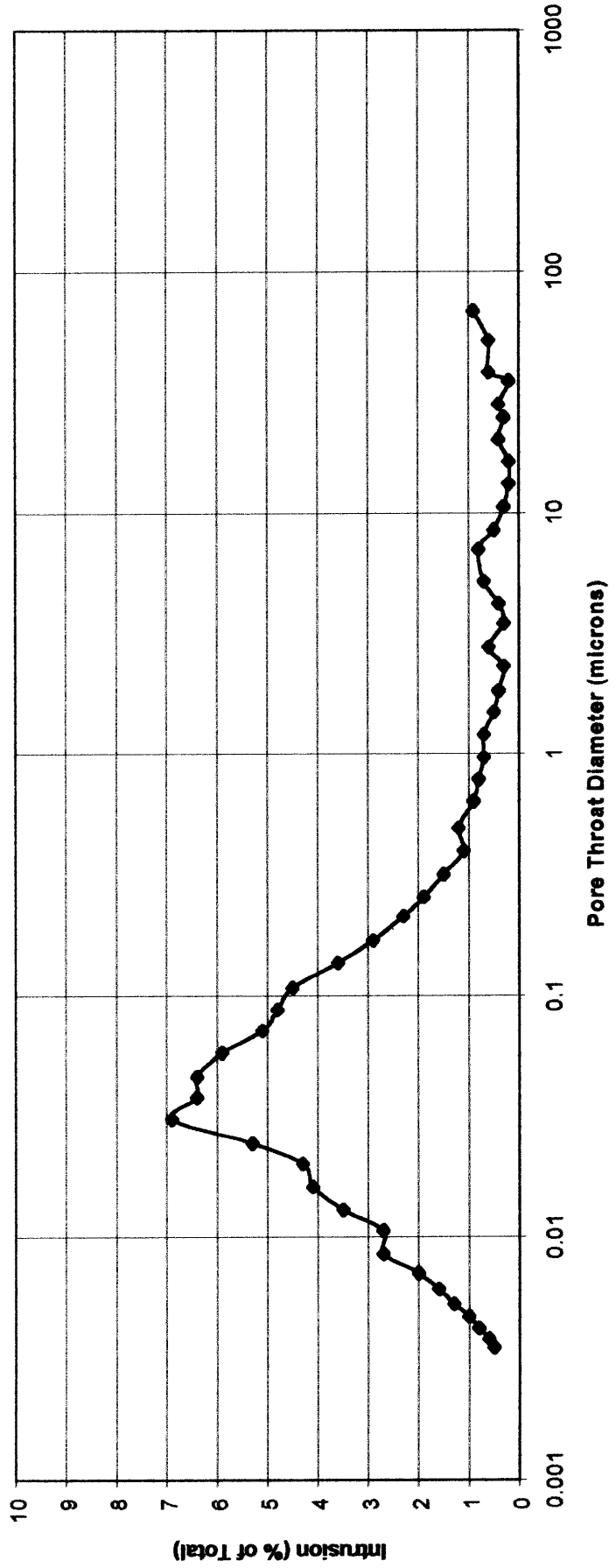
### CAPILLARY PRESSURE

**Client**                    Esso Australia Ltd  
**Well**                        Turrum-7  
  
**Test Method**            Air/Mercury Capillary Pressure Drainage  
  
**Sample**                    008c  
**Depth**                    2609.65 m



# PORE SIZE DISTRIBUTION

**Client** Esso Australia Ltd  
**Well** Turrum-7  
**Test Method** Air/Mercury Capillary Pressure Drainage  
**Sample** 008c  
**Depth** 2609.65 m



**CAPILLARY PRESSURE**

**Client** Esso Australia Ltd  
**Well** Turrum-7  
**Test Method** Air/Mercury Capillary Pressure Drainage  
**Sample** 016c  
**Depth** 2610.30 m

Pressure (psia)	Intrusion (percent)	Saturation (percent)	Pore Diameter (mm)
0.58	0.0	0.0	368.0
2.12	2.7	2.7	99.9
3.10	0.6	3.3	68.5
4.10	0.4	3.6	51.7
5.58	0.4	4.0	38.0
6.08	0.1	4.2	34.9
7.58	0.3	4.4	28.0
8.58	0.2	4.6	24.7
10.6	0.3	4.9	20.1
13.0	0.4	5.3	16.2
16.0	0.4	5.7	13.2
20.0	0.6	6.2	10.6
25.0	0.9	7.2	8.48
30.0	2.0	9.2	7.07
40.2	6.4	15.6	5.27
50.8	8.1	23.6	4.18
60.8	6.1	29.7	3.49
75.9	7.1	36.8	2.79
90.3	5.1	41.8	2.35
117	6.3	48.2	1.82
141	4.4	52.5	1.50
175	4.4	56.9	1.21
220	4.6	61.5	0.964
273	4.2	65.7	0.776
329	3.4	69.1	0.645
422	4.6	73.7	0.503
537	4.3	78.0	0.395

---

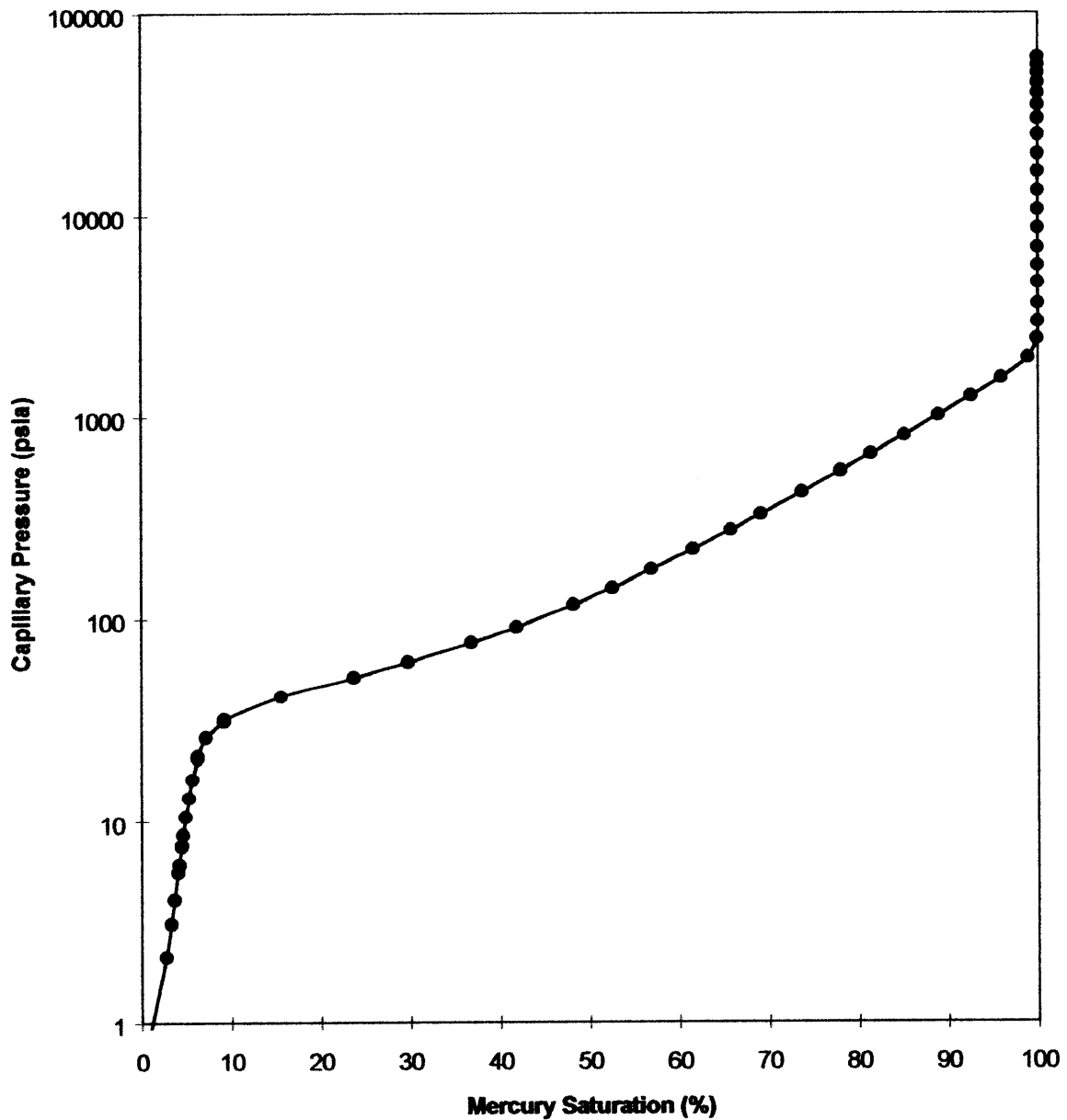
Pressure (psia)	Intrusion (percent)	Saturation (percent)	Pore Diameter (mm)
651	3.4	81.4	0.326
807	3.7	85.1	0.263
1010	3.8	88.9	0.210
1261	3.7	92.6	0.168
1556	3.4	95.9	0.136
1954	3.0	98.9	0.108
2423	1.0	99.9	0.0875
2955	0.1	100.0	0.0717
3634	0.0	100.0	0.0583
4600	0.0	100.0	0.0461
5594	0.0	100.0	0.0379
6870	0.0	100.0	0.0309
8576	0.0	100.0	0.0247
10556	0.0	100.0	0.0201
13168	0.0	100.0	0.0161
16358	0.0	100.0	0.0130
19995	0.0	100.0	0.0106
24926	0.0	100.0	0.0085
30007	0.0	100.0	0.0071
35008	0.0	100.0	0.0061
40130	0.0	100.0	0.0053
45016	0.0	100.0	0.0047
50161	0.0	100.0	0.0042
55111	0.0	100.0	0.0038
60048	0.0	100.0	0.0035

---



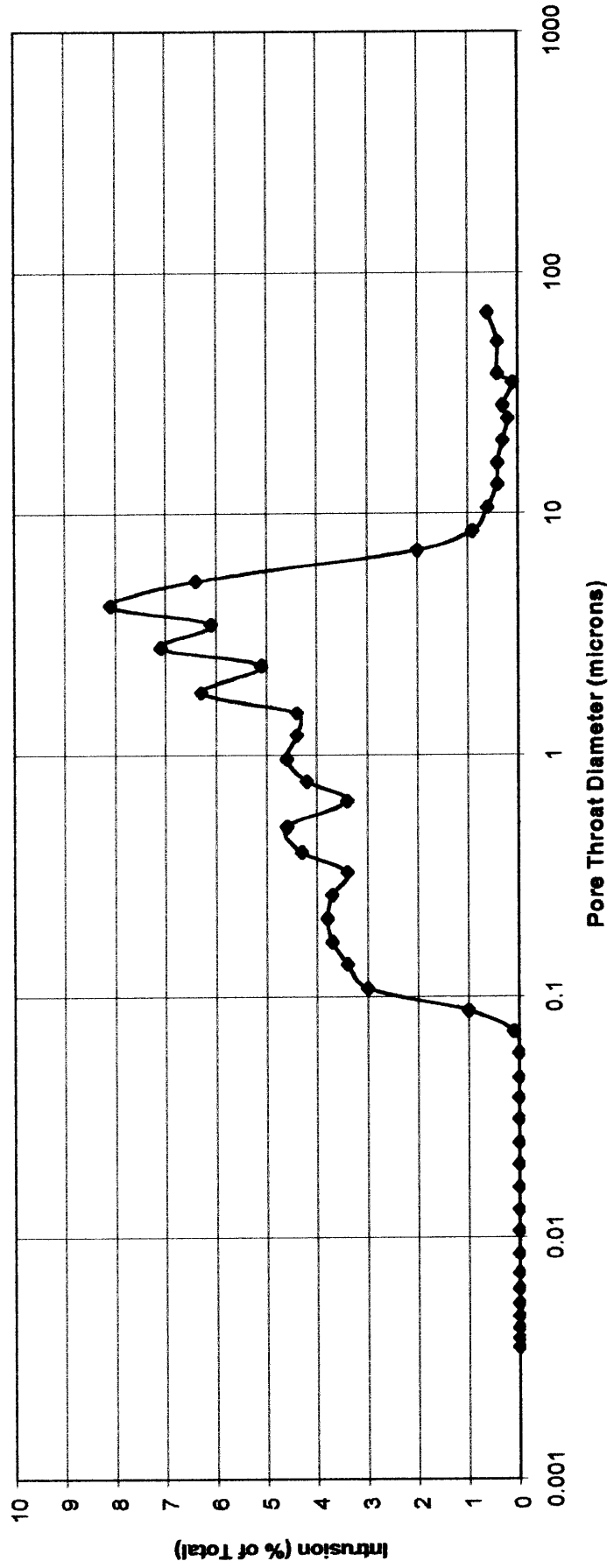
### CAPILLARY PRESSURE

**Client**                    Esso Australia Ltd  
**Well**                        Turrum-7  
  
**Test Method**            Air/Mercury Capillary Pressure Drainage  
  
**Sample**                    016c  
**Depth**                    2610.30 m



# PORE SIZE DISTRIBUTION

**Client** Esso Australia Ltd  
**Well** Turrum-7  
**Test Method** Air/Mercury Capillary Pressure Drainage  
**Sample** 016c  
**Depth** 2610.30 m



907511 ~~301~~  
298

**CAPILLARY PRESSURE**

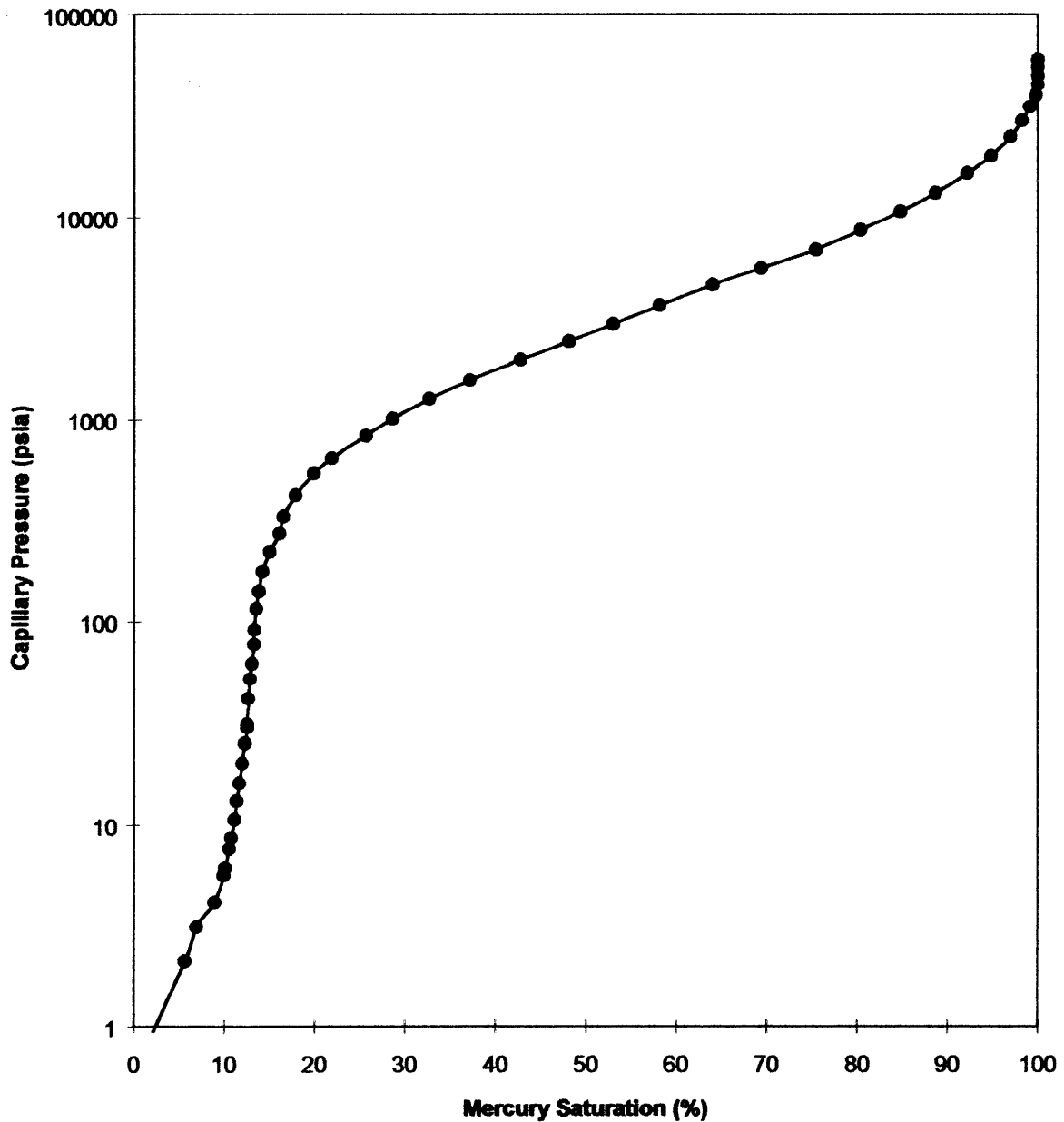
**Client** Esso Australia Ltd  
**Well** Turrum-7  
**Test Method** Air/Mercury Capillary Pressure Drainage  
**Sample** 028c  
**Depth** 2611.30 m

Pressure (psia)	Intrusion (percent)	Saturation (percent)	Pore Diameter (mm)
0.58	0.0	0.0	368.0
2.11	5.7	5.7	101.0
3.10	1.3	7.0	68.4
4.11	2.0	8.9	51.6
5.58	1.0	10.0	38.0
6.08	0.2	10.1	34.9
7.56	0.4	10.6	28.0
8.58	0.2	10.8	24.7
10.6	0.4	11.2	20.1
13.0	0.2	11.4	16.3
16.1	0.3	11.7	13.2
20.0	0.3	12.0	10.6
25.0	0.3	12.3	8.48
30.0	0.3	12.6	7.07
41.1	0.1	12.7	5.16
51.7	0.2	12.9	4.10
61.4	0.2	13.1	3.45
76.1	0.2	13.3	2.79
91.1	0.0	13.3	2.33
116	0.2	13.6	1.83
141	0.3	13.9	1.50
176	0.4	14.3	1.20
222	0.8	15.1	0.957
272	1.0	16.1	0.780
330	0.4	16.5	0.642
419	1.4	17.9	0.505
541	2.0	19.9	0.392

Pressure (psia)	Intrusion (percent)	Saturation (percent)	Pore Diameter (mm)
642	2.0	21.9	0.330
829	3.8	25.7	0.256
1008	3.0	28.6	0.210
1257	4.1	32.7	0.169
1554	4.5	37.2	0.136
1963	5.6	42.8	0.108
2420	5.4	48.2	0.0876
2944	4.9	53.0	0.0720
3644	5.2	58.2	0.0582
4623	5.9	64.0	0.0459
5582	5.4	69.4	0.0380
6884	6.0	75.5	0.0308
8626	4.9	80.4	0.0246
10589	4.4	84.8	0.0200
13134	3.9	88.7	0.0161
16421	3.5	92.2	0.0129
19981	2.6	94.8	0.0106
24916	2.1	97.0	0.0085
29910	1.3	98.2	0.0071
35017	0.9	99.1	0.0061
40087	0.6	99.8	0.0053
44954	0.2	100.0	0.0047
49921	0.0	100.0	0.0042
55005	0.0	100.0	0.0039
59950	0.0	100.0	0.0035

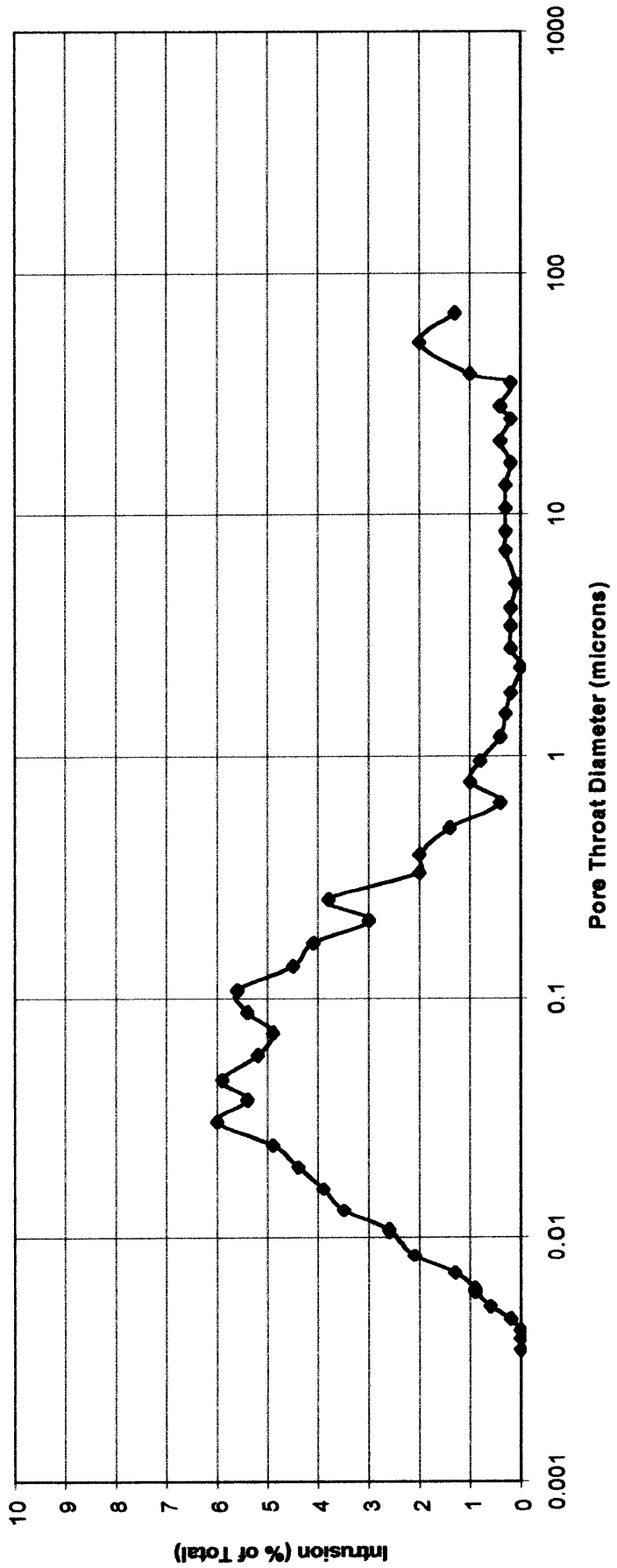
## CAPILLARY PRESSURE

**Client**                    Esso Australia Ltd  
**Well**                        Turrum-7  
  
**Test Method**            Air/Mercury Capillary Pressure Drainage  
  
**Sample**                    028c  
**Depth**                     2611.30 m



**PORE SIZE DISTRIBUTION**

**Client** Esso Australia Ltd  
**Well** Turrum-7  
**Test Method** Air/Mercury Capillary Pressure Drainage  
**Sample** 028c  
**Depth** 2611.30 m



**CAPILLARY PRESSURE**

**Client** Esso Australia Ltd  
**Well** Turrum-7  
**Test Method** Air/Mercury Capillary Pressure Drainage  
**Sample** 092c  
**Depth** 2616.65 m

Pressure (psia)	Intrusion (percent)	Saturation (percent)	Pore Diameter (mm)
0.55	0.0	0.0	385.0
2.11	3.2	3.2	100.0
3.10	0.6	3.8	68.3
4.09	0.5	4.3	51.8
5.58	0.5	4.7	38.0
6.09	0.2	5.0	34.8
7.59	0.4	5.3	27.9
8.58	0.2	5.6	24.7
10.6	0.4	6.0	20.1
13.1	0.4	6.4	16.2
16.0	0.5	6.9	13.2
20.0	0.6	7.5	10.6
25.0	0.8	8.3	8.48
30.0	0.8	9.1	7.07
40.7	0.7	9.8	5.21
51.1	0.8	10.5	4.15
61.6	0.6	11.1	3.44
76.3	0.6	11.7	2.78
92.2	0.5	12.3	2.30
117	0.7	13.0	1.81
141	0.4	13.4	1.50
176	0.6	14.0	1.21
222	0.6	14.6	0.953
272	0.7	15.3	0.779
330	1.2	16.5	0.642
424	1.1	17.6	0.500
529	1.7	19.3	0.401

---

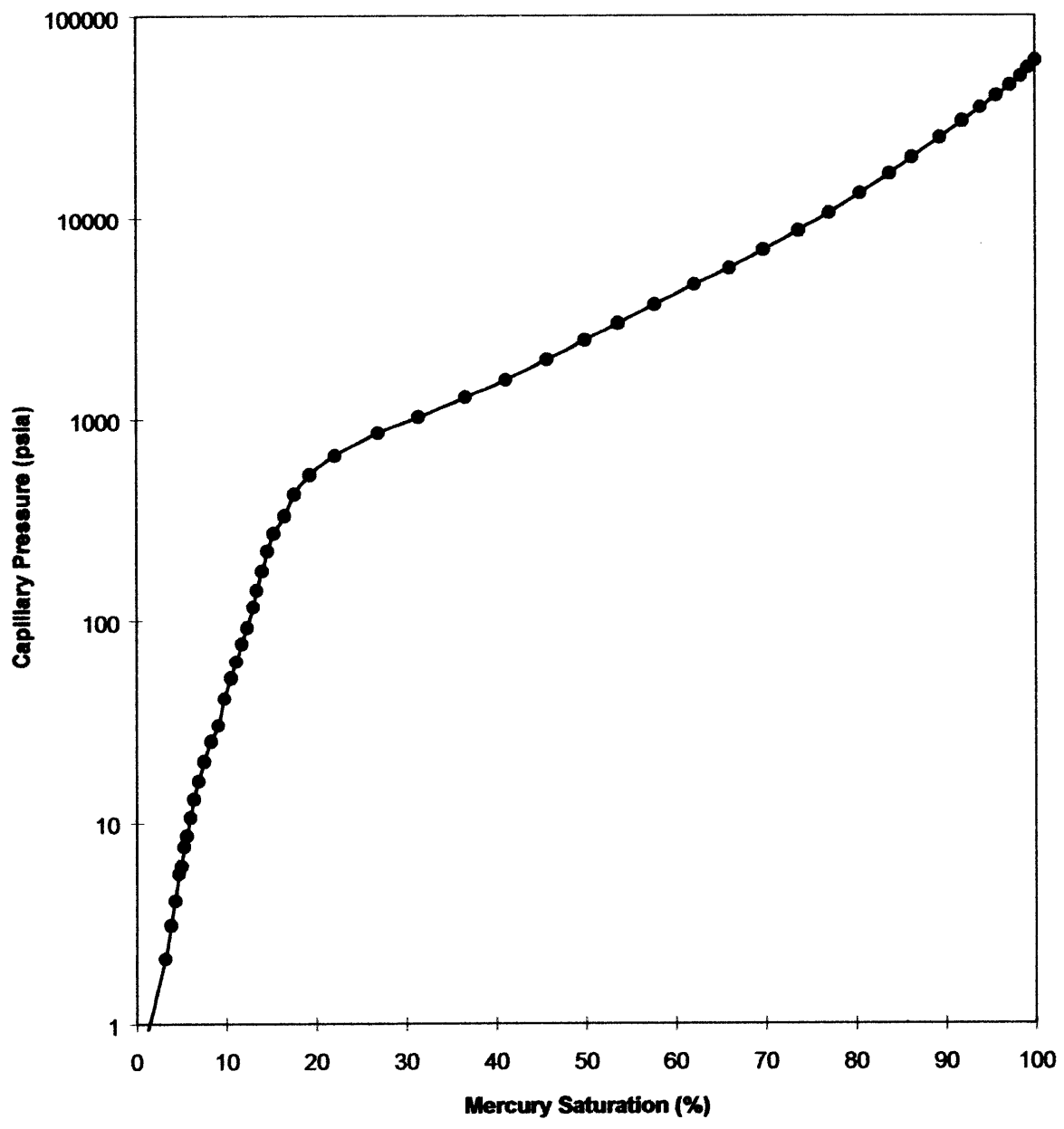
Pressure (psia)	Intrusion (percent)	Saturation (percent)	Pore Diameter (mm)
660	2.8	22.1	0.321
854	4.8	26.9	0.248
1019	4.5	31.4	0.208
1276	5.2	36.6	0.166
1556	4.4	41.1	0.136
1964	4.7	45.7	0.108
2446	4.2	49.9	0.0867
2970	3.7	53.6	0.0714
3682	4.1	57.7	0.0576
4637	4.4	62.1	0.0457
5596	3.9	66.0	0.0379
6884	3.8	69.8	0.0308
8595	3.8	73.7	0.0247
10549	3.4	77.1	0.0201
13143	3.4	80.5	0.0161
16458	3.3	83.8	0.0129
19910	2.6	86.3	0.0106
24914	3.0	89.4	0.0085
29974	2.5	91.9	0.0071
34906	2.0	93.9	0.0061
40069	1.8	95.7	0.0053
45060	1.5	97.2	0.0047
50066	1.2	98.4	0.0042
54920	0.9	99.2	0.0039
60028	0.8	100.0	0.0035

---



### CAPILLARY PRESSURE

**Client**                    Esso Australia Ltd  
**Well**                      Turrum-7  
  
**Test Method**            Air/Mercury Capillary Pressure Drainage  
  
**Sample**                  092c  
**Depth**                    2616.65 m

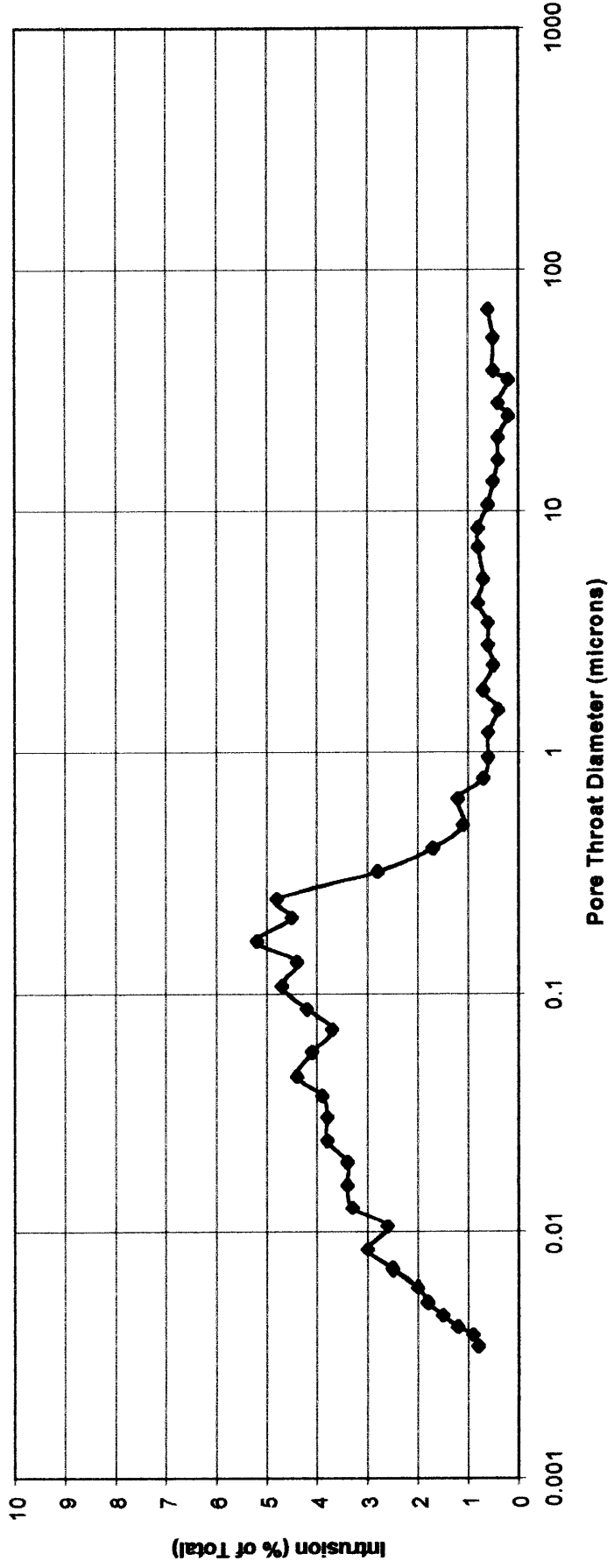


# PORE SIZE DISTRIBUTION

**Client** Esso Australia Ltd  
**Well** Turrum-7

**Test Method** Air/Mercury Capillary Pressure Drainage

**Sample** 092c  
**Depth** 2616.65 m



907511 ~~306~~  
306

**CAPILLARY PRESSURE**

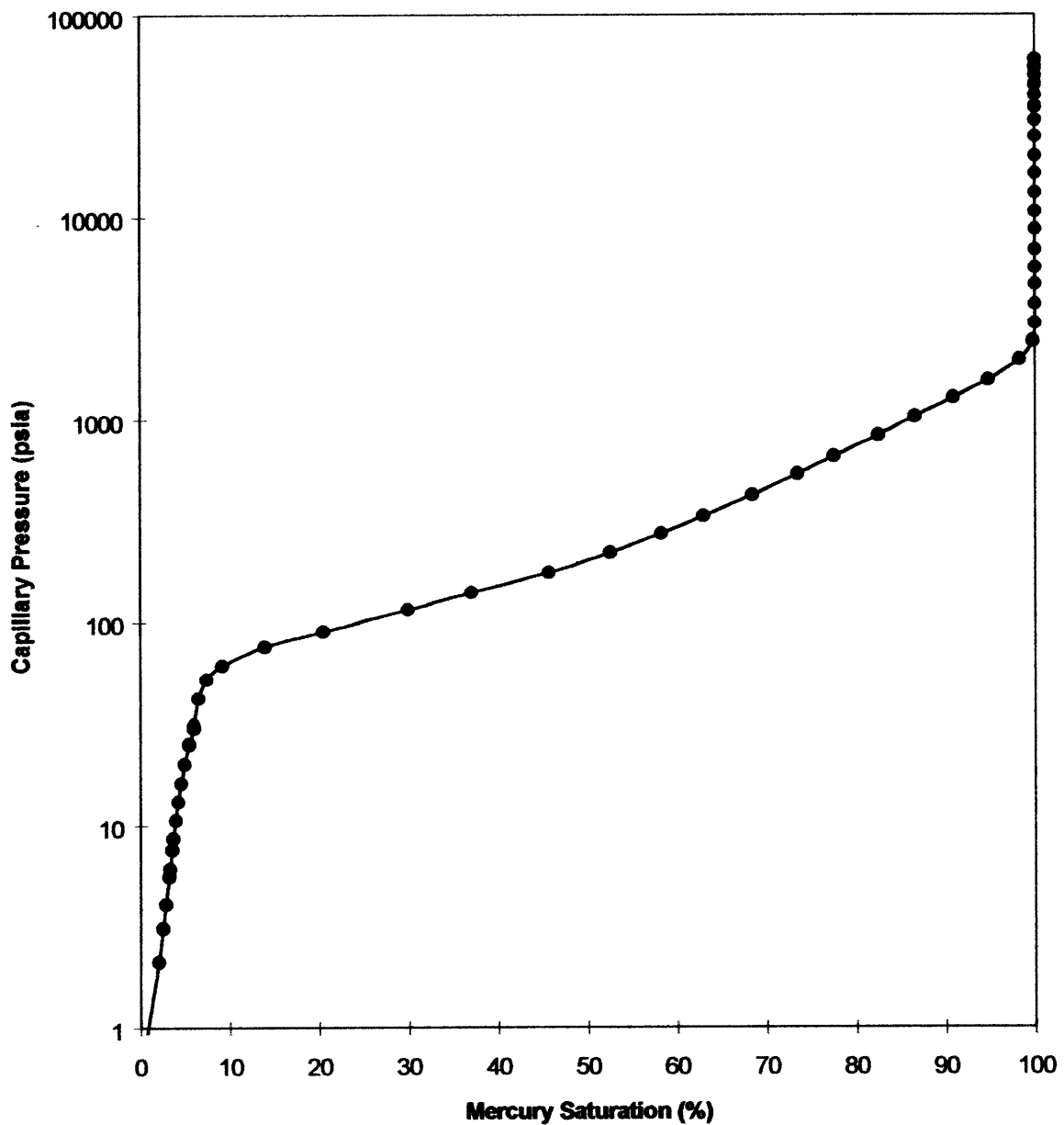
**Client** Esso Australia Ltd  
**Well** Turrum-7  
**Test Method** Air/Mercury Capillary Pressure Drainage  
**Sample** 100c  
**Depth** 2617.25 m

Pressure (psia)	Intrusion (percent)	Saturation (percent)	Pore Diameter (mm)
0.58	0.0	0.0	366.0
2.12	2.1	2.1	99.8
3.11	0.5	2.5	68.2
4.11	0.3	2.9	51.6
5.61	0.4	3.2	37.8
6.09	0.1	3.3	34.8
7.60	0.2	3.5	27.9
8.60	0.1	3.7	24.6
10.6	0.3	4.0	20.1
13.1	0.3	4.2	16.2
16.1	0.3	4.6	13.2
20.0	0.4	5.0	10.6
25.0	0.5	5.5	8.47
30.0	0.6	6.0	7.07
40.6	0.5	6.5	5.22
50.9	0.9	7.4	4.16
60.0	1.8	9.2	3.53
75.1	4.7	13.9	2.82
89.6	6.5	20.5	2.37
115	9.5	29.9	1.84
140	7.1	37.0	1.52
175	8.7	45.7	1.21
220	6.8	52.5	0.965
273	5.7	58.2	0.777
333	4.7	62.9	0.637
424	5.4	68.4	0.501
537	5.1	73.4	0.395

Pressure (psia)	Intrusion (percent)	Saturation (percent)	Pore Diameter (mm)
654	4.1	77.5	0.324
836	5.0	82.5	0.254
1026	4.1	86.6	0.207
1275	4.3	90.8	0.166
1559	3.9	94.7	0.136
1973	3.5	98.3	0.107
2426	1.5	99.7	0.0874
2972	0.3	100.0	0.0713
3681	0.0	100.0	0.0576
4618	0.0	100.0	0.0459
5574	0.0	100.0	0.0380
6874	0.0	100.0	0.0308
8637	0.0	100.0	0.0245
10561	0.0	100.0	0.0201
13134	0.0	100.0	0.0161
16396	0.0	100.0	0.0129
19991	0.0	100.0	0.0106
24900	0.0	100.0	0.0085
30023	0.0	100.0	0.0071
34938	0.0	100.0	0.0061
40053	0.0	100.0	0.0053
45061	0.0	100.0	0.0047
49981	0.0	100.0	0.0042
55037	0.0	100.0	0.0039
59964	0.0	100.0	0.0035

**CAPILLARY PRESSURE**

**Client** Esso Australia Ltd  
**Well** Turrum-7  
**Test Method** Air/Mercury Capillary Pressure Drainage  
**Sample** 100c  
**Depth** 2617.25 m

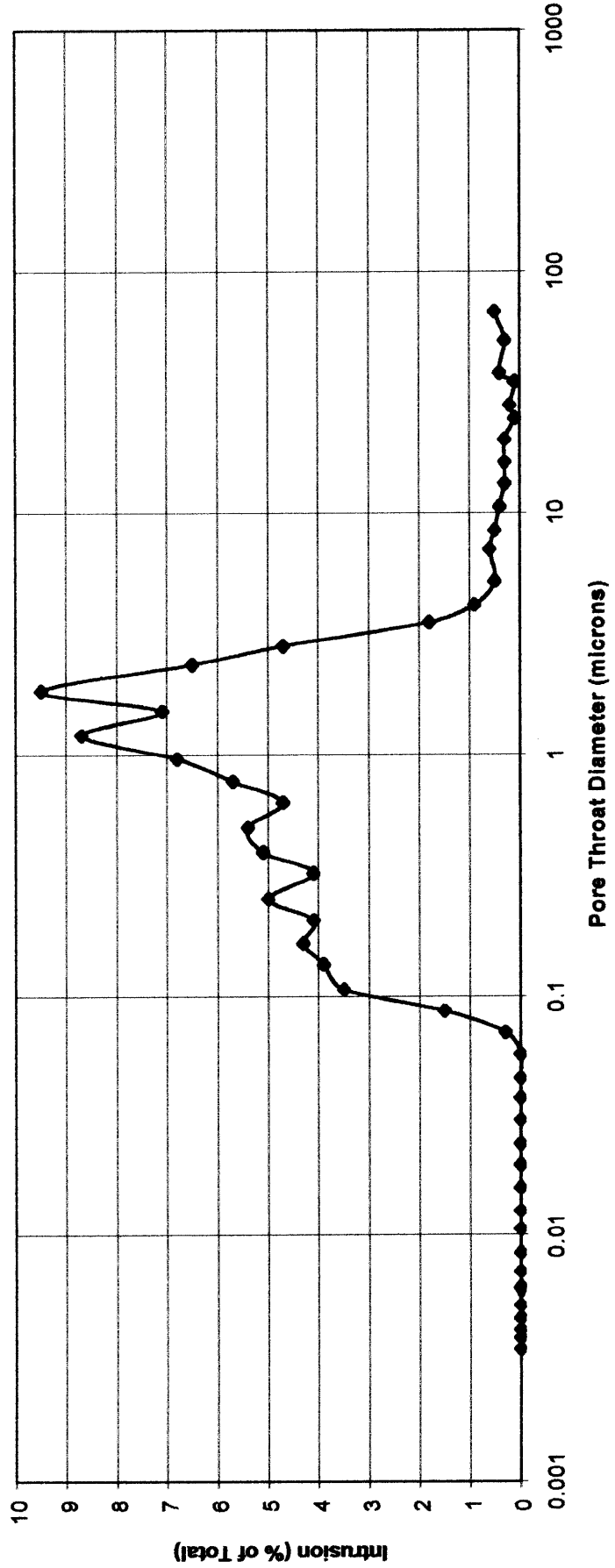


# PORE SIZE DISTRIBUTION

**Client Well** Esso Australia Ltd  
Turrum-7

**Test Method** Air/Mercury Capillary Pressure Drainage

**Sample Depth** 100c  
2617.25 m



907511 ~~XXXX~~  
310

**CAPILLARY PRESSURE**

**Client** Esso Australia Ltd  
**Well** Turrum-7  
**Test Method** Air/Mercury Capillary Pressure Drainage  
**Sample** V132c  
**Depth** 2619.97 m

Pressure (psia)	Intrusion (percent)	Saturation (percent)	Pore Diameter (mm)
0.57	0.0	0.0	373.0
2.11	2.8	2.8	101.0
3.12	0.7	3.5	68.0
4.10	0.5	4.0	51.7
5.60	0.4	4.3	37.8
6.11	0.3	4.6	34.7
7.59	0.3	4.9	27.9
8.58	0.2	5.1	24.7
10.6	0.2	5.3	20.0
13.1	0.3	5.6	16.2
16.0	0.4	5.9	13.2
20.0	0.5	6.4	10.6
25.0	0.3	6.8	8.47
30.0	0.4	7.2	7.07
40.8	0.4	7.6	5.19
50.5	0.4	8.0	4.20
61.3	0.3	8.3	3.46
76.0	0.6	8.9	2.79
92.2	0.5	9.4	2.30
116	0.8	10.2	1.83
142	2.2	12.4	1.49
175	3.2	15.6	1.21
220	5.2	20.8	0.964
271	5.8	26.6	0.784
329	6.3	32.9	0.644
420	7.2	40.1	0.505
536	5.8	45.8	0.395

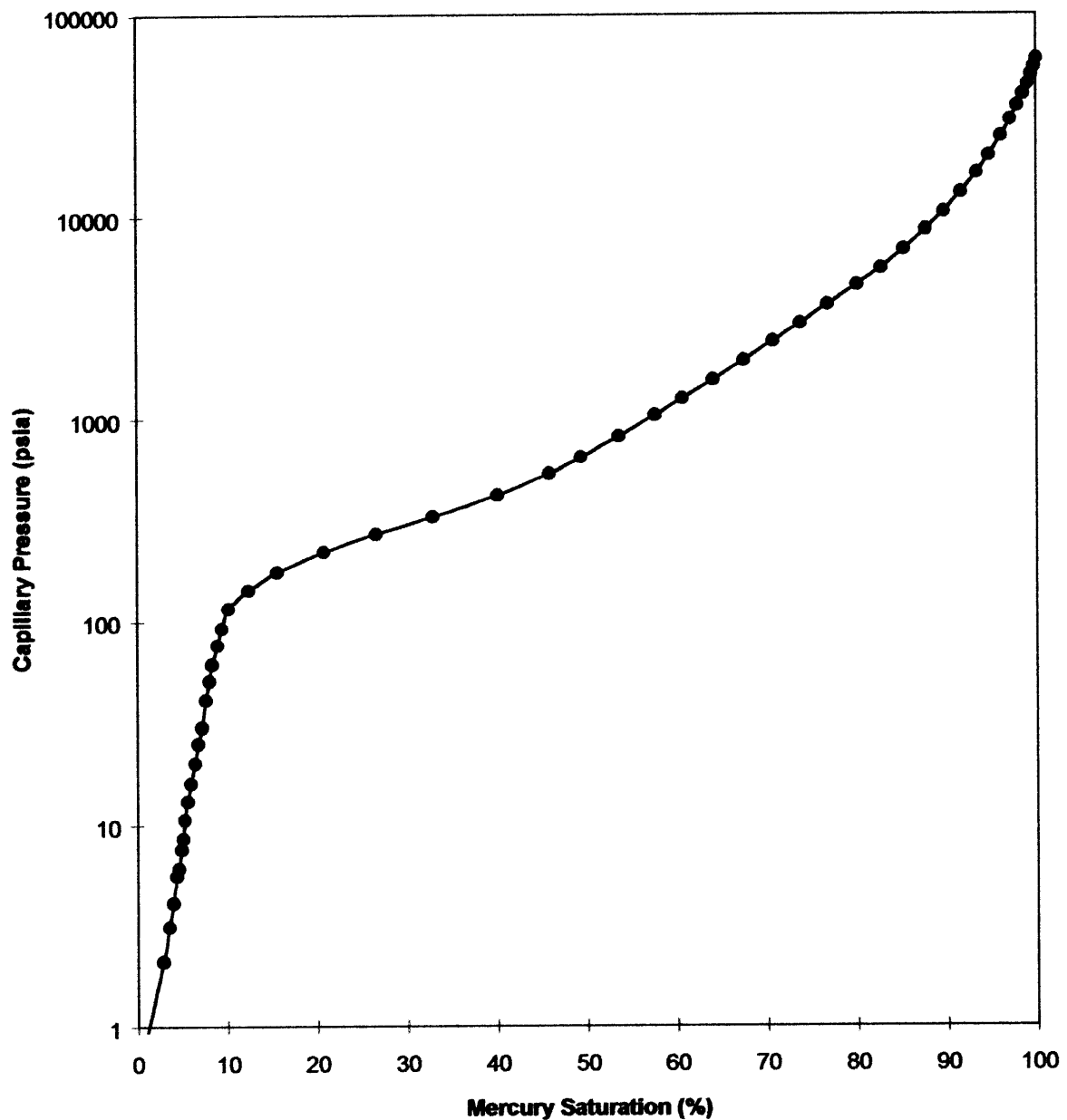
907511 ~~312~~  
312

Pressure (psia)	Intrusion (percent)	Saturation (percent)	Pore Diameter (mm)
645	3.5	49.4	0.329
818	4.2	53.6	0.259
1041	4.0	57.6	0.204
1264	3.1	60.7	0.168
1566	3.4	64.0	0.135
1949	3.4	67.4	0.109
2420	3.3	70.7	0.0876
2966	3.0	73.7	0.0715
3659	3.1	76.8	0.0579
4612	3.2	80.0	0.0460
5579	2.7	82.7	0.0380
6904	2.5	85.2	0.0307
8620	2.5	87.7	0.0246
10592	2.0	89.7	0.0200
13138	1.9	91.6	0.0161
16376	1.8	93.4	0.0129
20000	1.4	94.7	0.0106
24942	1.3	96.1	0.0085
29964	1.1	97.1	0.0071
34996	0.8	97.9	0.0061
39977	0.6	98.5	0.0053
44916	0.5	99.0	0.0047
50093	0.4	99.5	0.0042
54850	0.3	99.8	0.0039
59982	0.2	100.0	0.0035



**CAPILLARY PRESSURE**

**Client** Esso Australia Ltd  
**Well** Turrum-7  
**Test Method** Air/Mercury Capillary Pressure Drainage  
**Sample** V132c  
**Depth** 2619.97 m

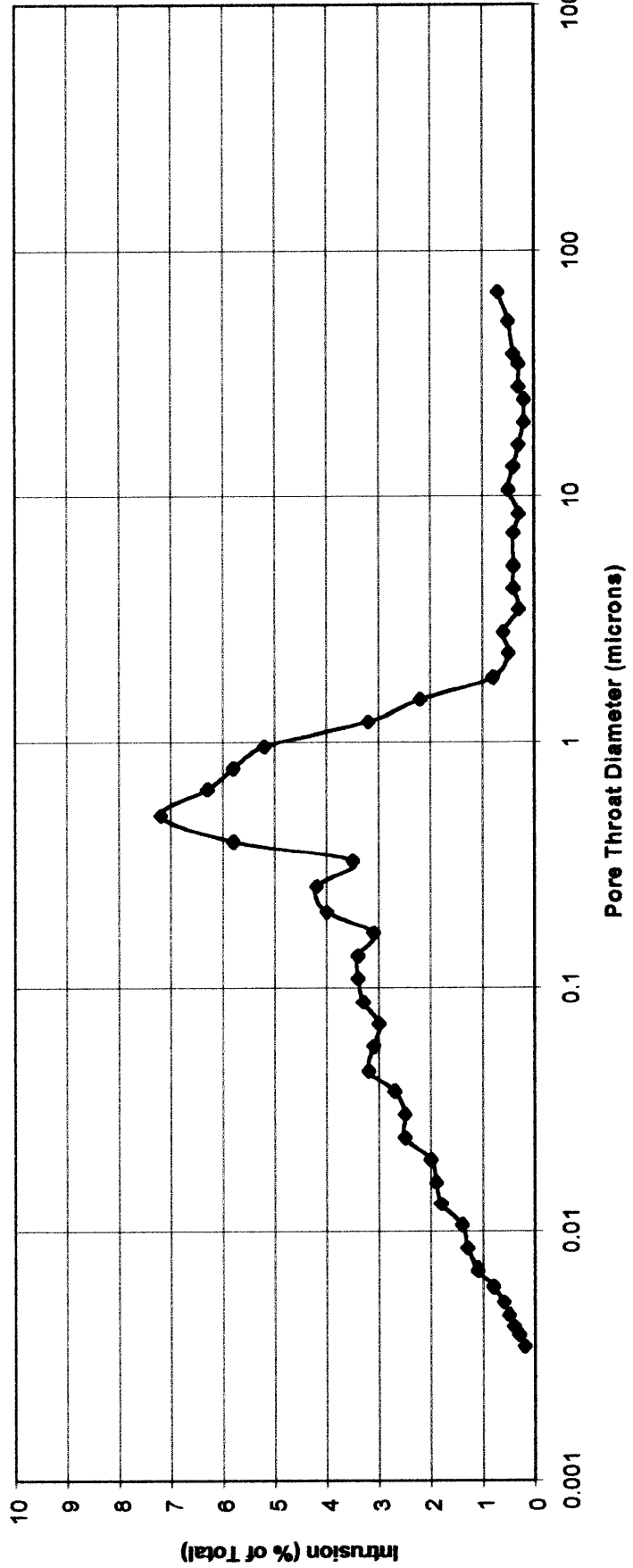


# PORE SIZE DISTRIBUTION

**Client** Esso Australia Ltd  
**Well** Turrum-7

**Test Method** Air/Mercury Capillary Pressure Drainage

**Sample** V132c  
**Depth** 2619.97 m



907511

314

**CAPILLARY PRESSURE**

**Client** Esso Australia Ltd  
**Well** Turrum-7  
**Test Method** Air/Mercury Capillary Pressure Drainage  
**Sample** 150c  
**Depth** 2621.45 m

Pressure (psia)	Intrusion (percent)	Saturation (percent)	Pore Diameter (mm)
0.58	0.0	0.0	368.0
2.12	2.0	2.0	99.9
3.10	0.5	2.5	68.5
4.10	0.4	2.9	51.7
5.58	0.4	3.2	38.0
6.08	0.1	3.3	34.9
7.58	0.2	3.6	28.0
8.58	0.2	3.7	24.7
10.6	0.3	4.0	20.1
13.0	0.1	4.1	16.2
16.0	0.1	4.2	13.2
20.0	0.2	4.4	10.6
25.0	0.1	4.6	8.48
30.0	0.4	5.0	7.07
40.4	0.4	5.8	5.25
50.5	0.4	6.2	4.20
61.2	0.3	6.5	3.46
75.5	0.4	6.9	2.81
91.8	0.2	7.0	2.31
116	0.3	7.3	1.83
141	0.3	7.6	1.50
176	0.4	8.0	1.20
221	0.6	8.6	0.959
269	0.9	9.5	0.787
332	1.6	11.1	0.638
426	3.2	14.3	0.497
522	4.7	19.0	0.406

---

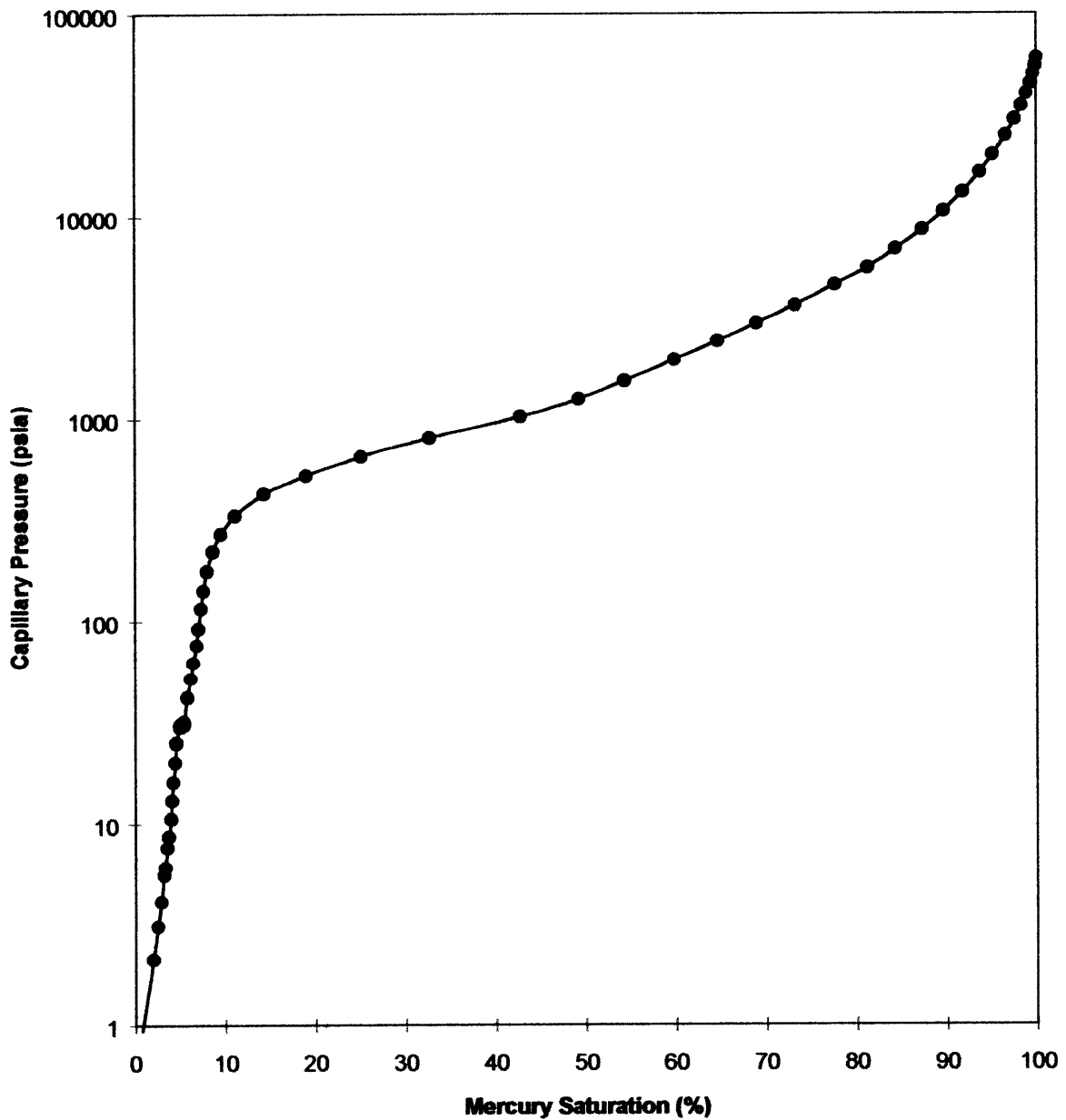
Pressure (psia)	Intrusion (percent)	Saturation (percent)	Pore Diameter (mm)
652	6.1	25.1	0.325
802	7.6	32.7	0.264
1020	10.1	42.8	0.208
1247	6.5	49.3	0.170
1541	5.1	54.3	0.138
1955	5.5	59.9	0.108
2416	4.8	64.6	0.0877
2949	4.3	69.0	0.0719
3636	4.3	73.2	0.0583
4586	4.4	77.6	0.0462
5584	3.7	81.3	0.0380
6868	3.1	84.4	0.0309
8599	3.0	87.4	0.0247
10603	2.4	89.7	0.0200
13149	2.1	91.8	0.0161
16455	1.9	93.7	0.0129
19978	1.4	95.1	0.0106
24906	1.4	96.6	0.0085
29950	1.0	97.6	0.0071
34974	0.8	98.3	0.0061
40063	0.6	98.9	0.0053
45067	0.4	99.3	0.0047
50122	0.3	99.7	0.0042
55019	0.2	99.9	0.0039
60050	0.1	100.0	0.0035

### CAPILLARY PRESSURE

**Client**                    Esso Australia Ltd  
**Well**                        Turrum-7

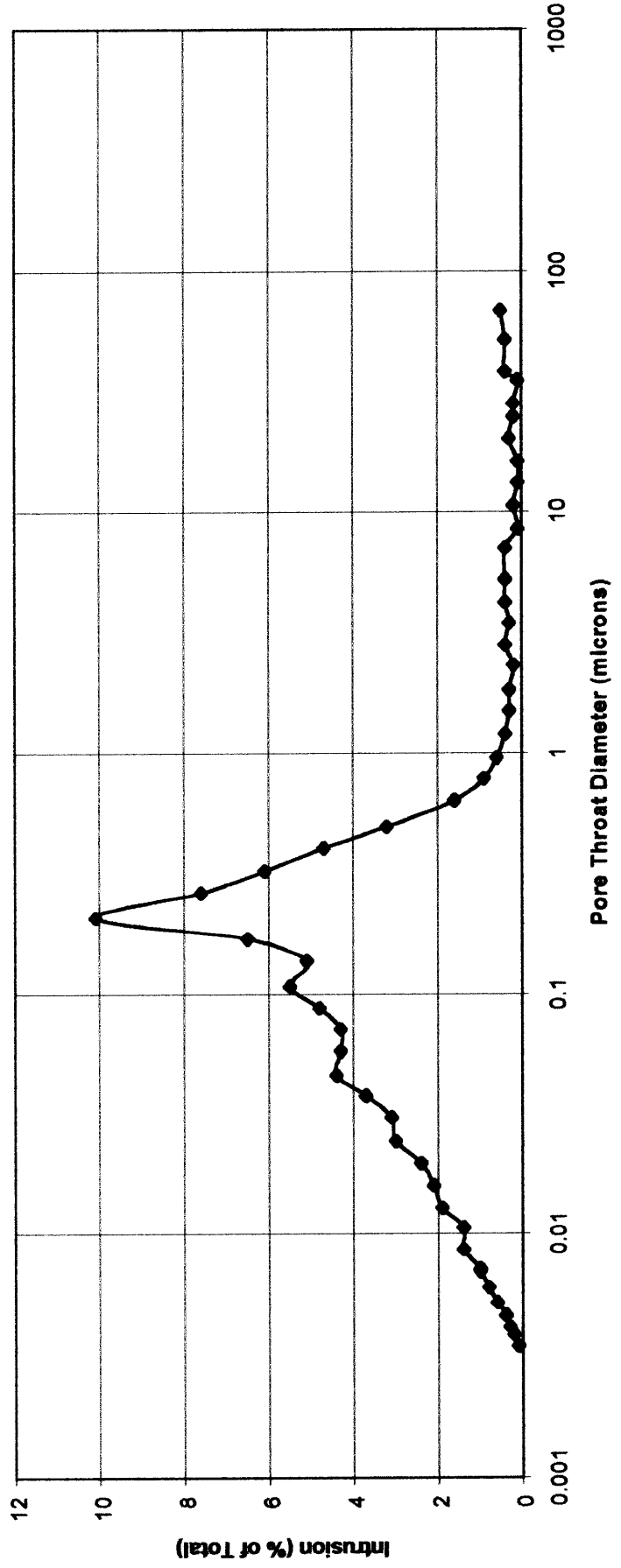
**Test Method**            Air/Mercury Capillary Pressure Drainage

**Sample**                    150c  
**Depth**                    2621.45 m



# PORE SIZE DISTRIBUTION

**Client** Esso Australia Ltd  
**Well** Turrum-7  
**Test Method** Air/Mercury Capillary Pressure Drainage  
**Sample** 150c  
**Depth** 2621.45 m



907511 ~~XXXXXX~~  
319

**CAPILLARY PRESSURE**

**Client** Esso Australia Ltd  
**Well** Turrum-7  
**Test Method** Air/Mercury Capillary Pressure Drainage  
**Sample** 152c  
**Depth** 2621.65 m

Pressure (psia)	Intrusion (percent)	Saturation (percent)	Pore Diameter (mm)
0.56	0.0	0.0	378.0
2.12	6.1	6.1	100.0
3.10	0.9	7.1	68.3
4.12	0.6	7.6	51.5
5.60	0.8	8.4	37.9
6.09	0.2	8.6	34.8
7.59	0.4	9.0	27.9
8.58	0.4	9.4	24.7
10.6	0.5	9.9	20.0
13.0	0.5	10.4	16.3
16.0	0.3	10.8	13.2
20.0	0.4	11.2	10.6
25.0	0.2	11.4	8.48
30.0	0.1	11.5	7.07
40.8	0.4	12.5	5.20
51.8	0.4	12.9	4.09
61.1	0.4	13.2	3.47
76.0	0.4	13.7	2.79
91.7	0.4	14.1	2.31
116	0.6	14.6	1.83
142	0.9	15.5	1.49
176	1.1	16.6	1.21
221	0.7	17.3	0.961
269	0.7	18.0	0.788
334	0.8	18.9	0.635
419	0.9	19.8	0.506
523	0.9	20.7	0.405

Pressure (psia)	Intrusion (percent)	Saturation (percent)	Pore Diameter (mm)
670	1.1	21.7	0.316
815	0.9	22.6	0.260
1021	1.1	23.7	0.208
1246	0.9	24.6	0.170
1553	1.1	25.7	0.137
1939	1.2	26.9	0.109
2423	1.3	28.2	0.0875
2939	1.2	29.5	0.0721
3632	1.4	30.9	0.0584
4565	1.8	32.7	0.0464
5590	1.9	34.6	0.0379
6876	2.1	36.8	0.0308
8601	2.8	39.6	0.0246
10577	3.2	42.8	0.0200
13140	4.2	46.9	0.0161
16362	5.2	52.1	0.0130
19933	5.8	57.9	0.0106
24912	8.5	66.4	0.0085
29966	6.7	73.1	0.0071
34954	6.2	79.4	0.0061
40109	5.6	85.0	0.0053
45049	4.6	89.6	0.0047
49898	3.9	93.5	0.0042
55027	3.5	97.0	0.0039
59897	3.0	100.0	0.0035

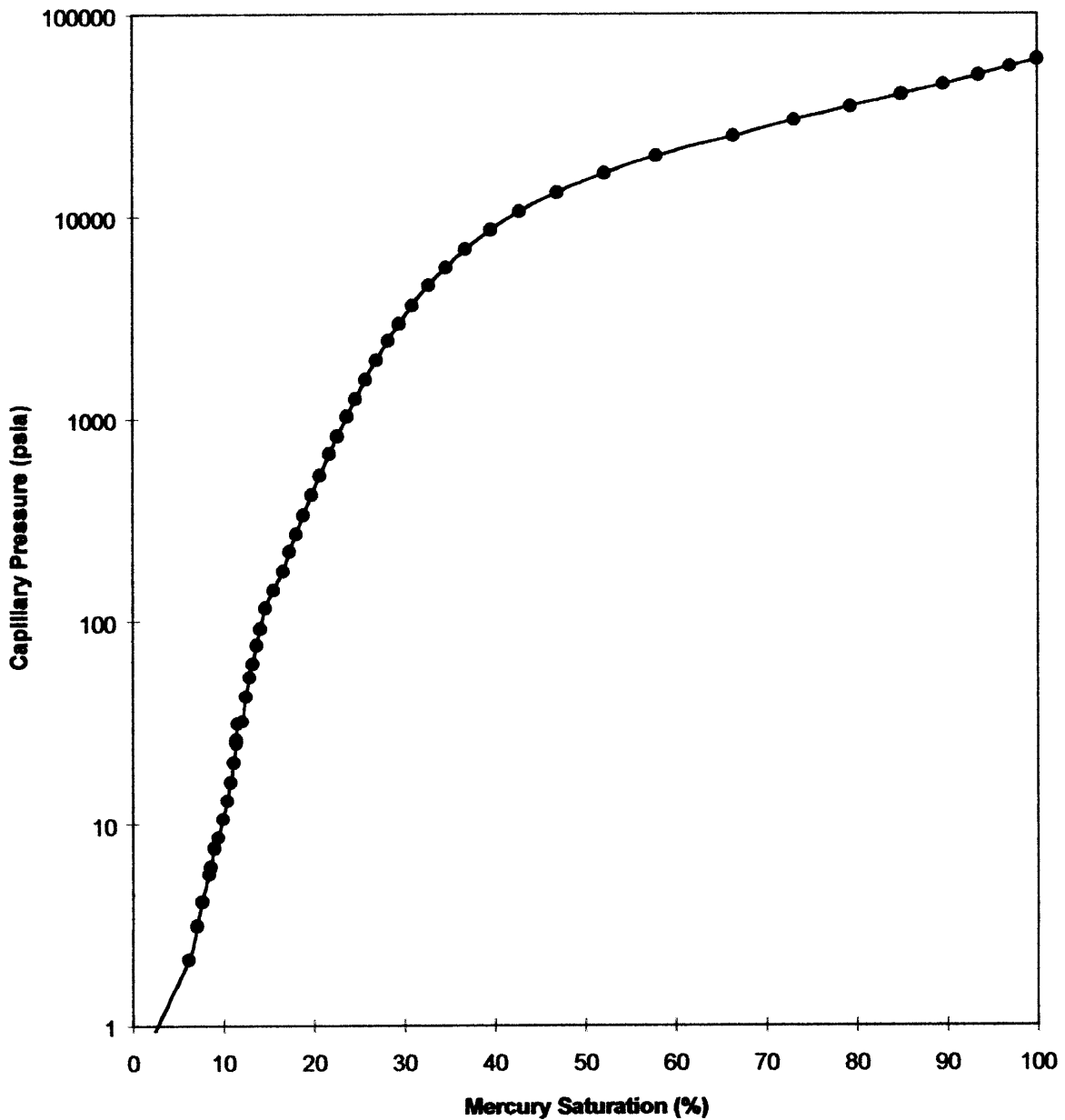


### CAPILLARY PRESSURE

**Client**            Esso Australia Ltd  
**Well**                Turrum-7

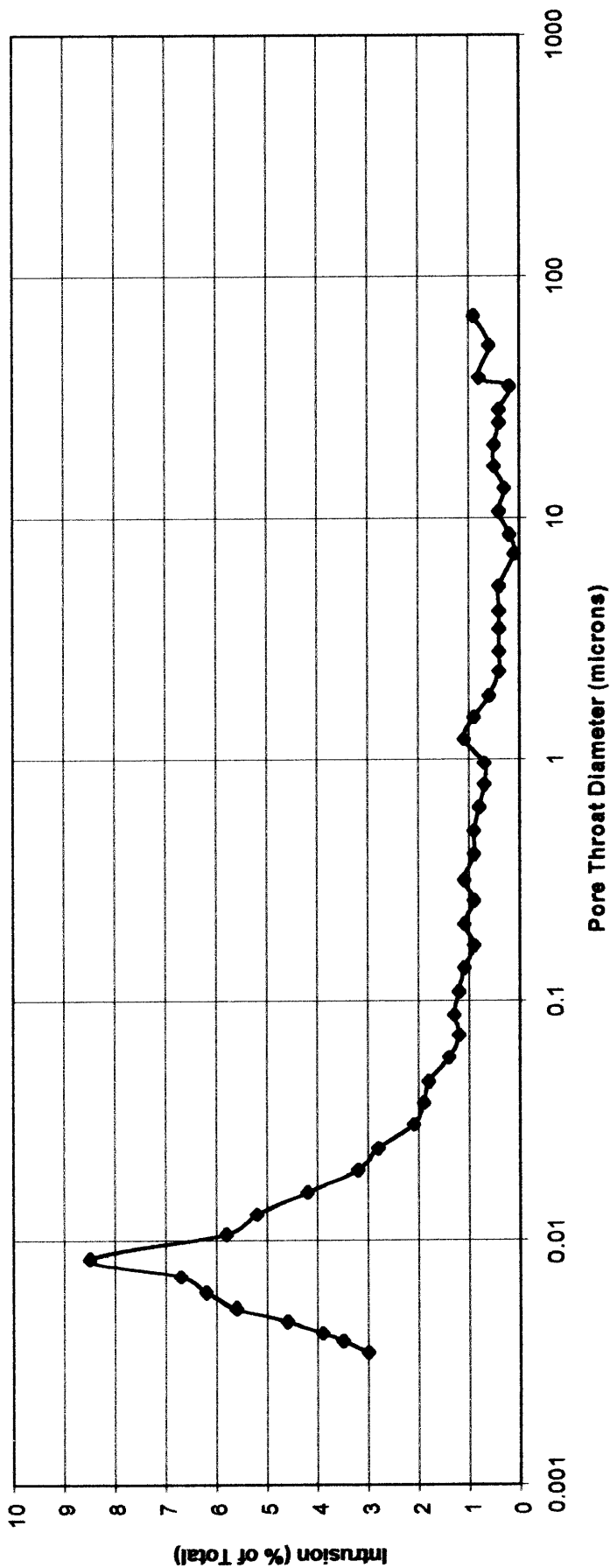
**Test Method**      Air/Mercury Capillary Pressure Drainage

**Sample**            152c  
**Depth**             2621.65 m



# PORE SIZE DISTRIBUTION

**Client** Esso Australia Ltd  
**Well** Turrum-7  
**Test Method** Air/Mercury Capillary Pressure Drainage  
**Sample** 152c  
**Depth** 2621.65 m



**CAPILLARY PRESSURE**

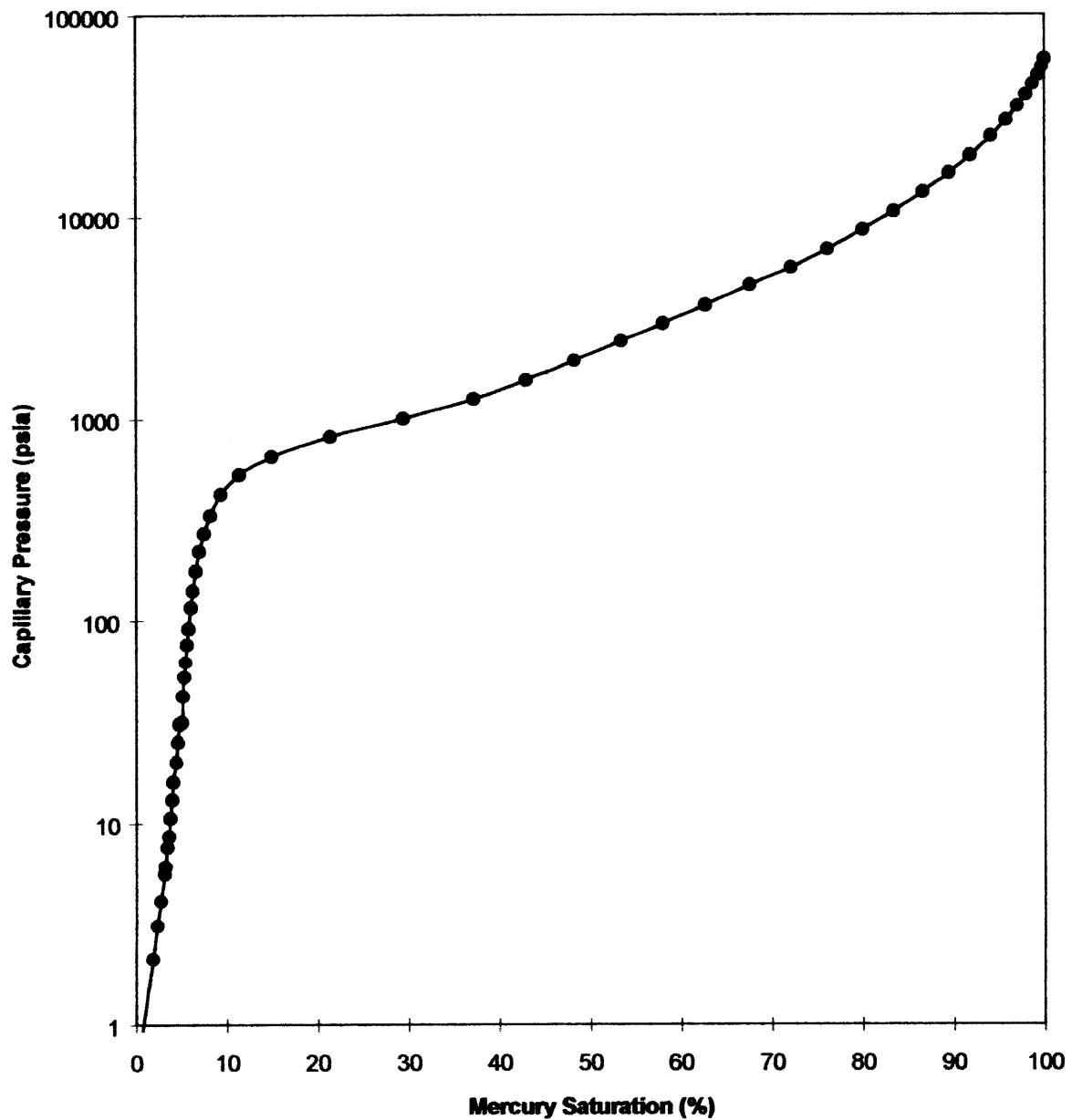
**Client** Esso Australia Ltd  
**Well** Turrum-7  
**Test Method** Air/Mercury Capillary Pressure Drainage  
**Sample** 178c  
**Depth** 2623.85 m

Pressure (psia)	Intrusion (percent)	Saturation (percent)	Pore Diameter (mm)
0.56	0.0	0.0	378.0
2.12	1.8	1.8	100.0
3.10	0.5	2.3	68.3
4.12	0.4	2.7	51.5
5.60	0.4	3.1	37.9
6.09	0.1	3.2	34.8
7.59	0.2	3.4	27.9
8.58	0.2	3.6	24.7
10.6	0.1	3.7	20.0
13.0	0.2	3.9	16.3
16.0	0.1	4.0	13.2
20.0	0.3	4.4	10.6
25.0	0.2	4.6	8.48
30.0	0.2	4.7	7.07
41.0	0.1	5.1	5.17
51.0	0.1	5.3	4.15
61.2	0.1	5.4	3.46
76.0	0.1	5.5	2.79
91.3	0.2	5.7	2.32
117	0.3	6.0	1.81
141	0.2	6.2	1.50
176	0.3	6.5	1.20
220	0.4	6.9	0.963
270	0.5	7.5	0.785
331	0.7	8.2	0.640
421	1.1	9.3	0.504
530	2.1	11.3	0.400

Pressure (psia)	Intrusion (percent)	Saturation (percent)	Pore Diameter (mm)
650	3.5	14.9	0.326
815	6.5	21.4	0.260
999	8.0	29.4	0.212
1243	7.7	37.2	0.171
1550	5.8	42.9	0.137
1933	5.3	48.2	0.110
2416	5.2	53.4	0.0878
2955	4.6	58.0	0.0718
3641	4.7	62.7	0.0582
4556	4.9	67.6	0.0465
5578	4.5	72.1	0.0380
6874	4.0	76.1	0.0308
8580	3.9	80.0	0.0247
10598	3.4	83.4	0.0200
13174	3.2	86.6	0.0161
16382	2.9	89.5	0.0129
19945	2.3	91.8	0.0106
24900	2.3	94.1	0.0085
29930	1.7	95.8	0.0071
35005	1.2	97.0	0.0061
40013	0.9	98.0	0.0053
44988	0.7	98.7	0.0047
49977	0.6	99.3	0.0042
54850	0.4	99.7	0.0039
59979	0.3	100.0	0.0035

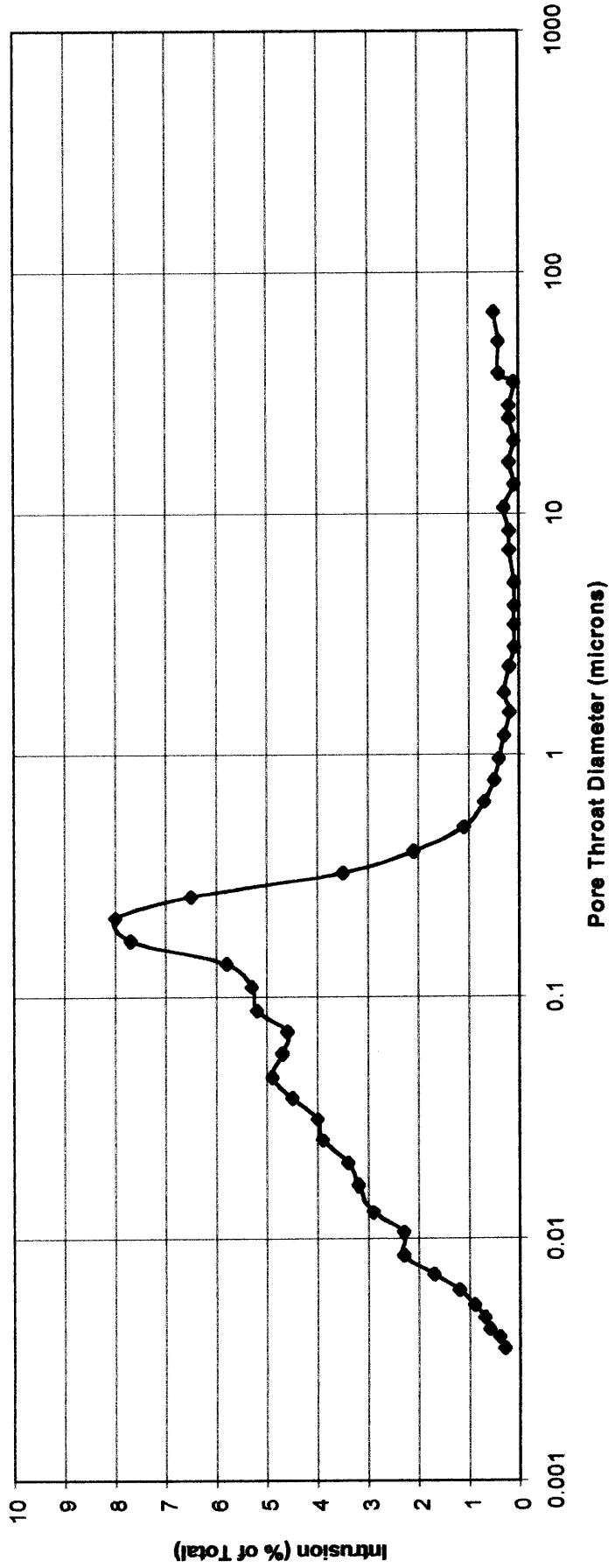
### CAPILLARY PRESSURE

**Client**            Esso Australia Ltd  
**Well**                Turrum-7  
  
**Test Method**      Air/Mercury Capillary Pressure Drainage  
  
**Sample**            178c  
**Depth**             2623.85 m



# PORE SIZE DISTRIBUTION

**Client** Esso Australia Ltd  
**Well** Turrum-7  
**Test Method** Air/Mercury Capillary Pressure Drainage  
**Sample** 178c  
**Depth** 2623.85 m



**CAPILLARY PRESSURE**

**Client** Esso Australia Ltd  
**Well** Turrum-7  
**Test Method** Air/Mercury Capillary Pressure Drainage  
**Sample** 210c  
**Depth** 2626.45 m

Pressure (psia)	Intrusion (percent)	Saturation (percent)	Pore Diameter (mm)
0.58	0.0	0.0	366.0
2.12	2.3	2.3	99.8
3.11	0.5	2.8	68.2
4.11	0.4	3.2	51.6
5.61	0.4	3.6	37.8
6.09	0.1	3.7	34.8
7.60	0.1	3.8	27.9
8.60	0.1	3.9	24.6
10.6	0.1	4.0	20.1
13.1	0.3	4.3	16.2
16.1	0.2	4.5	13.2
20.0	0.2	4.7	10.6
25.0	0.3	5.0	8.47
30.0	0.2	5.1	7.07
40.8	0.4	5.8	5.20
51.5	0.3	6.1	4.12
61.1	0.3	6.4	3.47
77.6	0.4	6.7	2.73
90.7	0.3	7.0	2.34
116	0.3	7.3	1.84
143	0.4	7.7	1.48
178	0.5	8.2	1.19
222	0.7	8.9	0.955
270	0.9	9.7	0.785
332	1.3	11.0	0.639
420	2.4	13.4	0.505
526	5.7	19.2	0.403

---

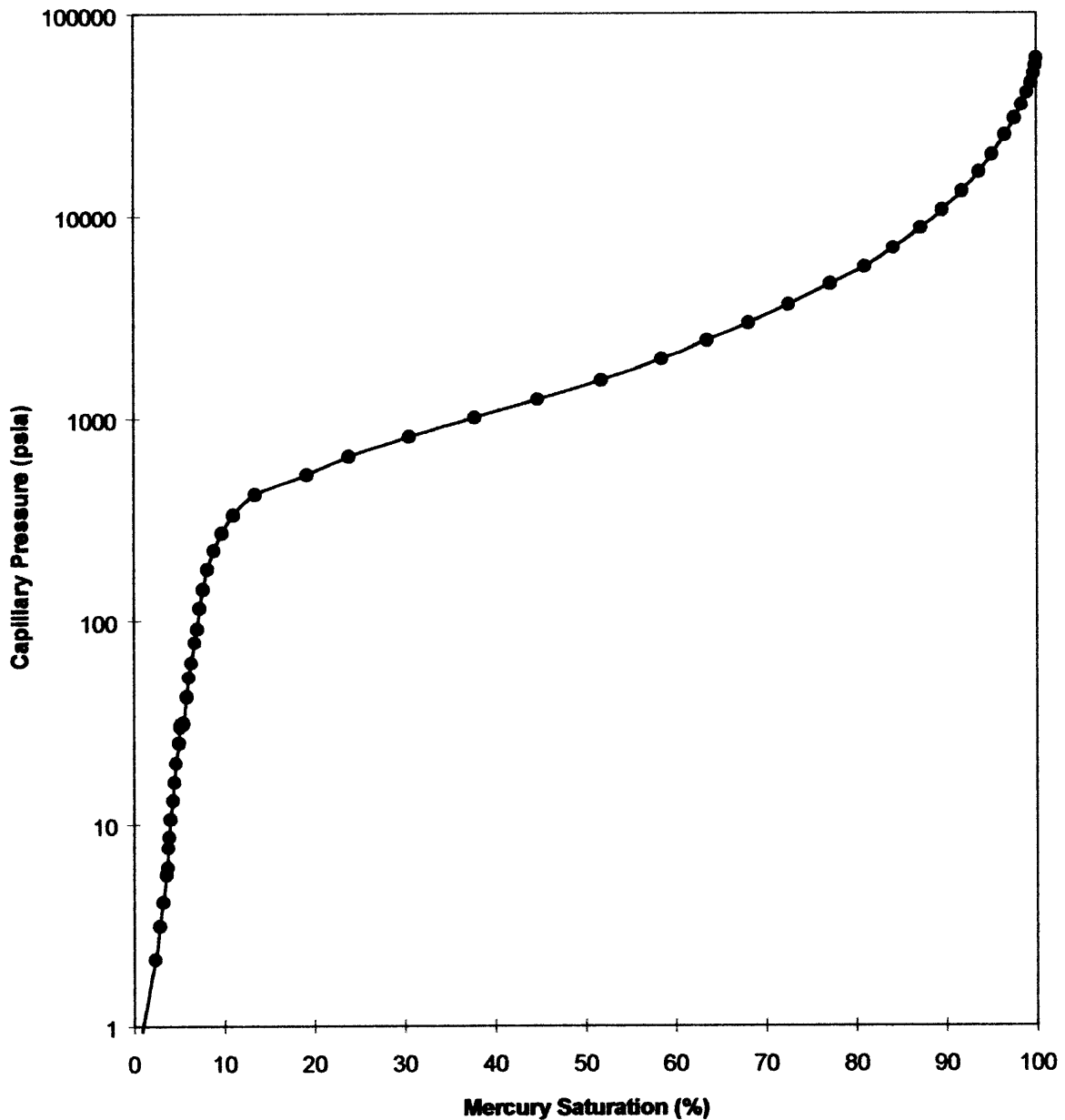
Pressure (psia)	Intrusion (percent)	Saturation (percent)	Pore Diameter (mm)
648	4.7	23.9	0.327
811	6.7	30.6	0.261
1007	7.2	37.8	0.211
1236	7.0	44.8	0.171
1537	7.0	51.8	0.138
1951	6.7	58.5	0.109
2407	5.0	63.5	0.0881
2947	4.6	68.1	0.0719
3632	4.5	72.6	0.0584
4588	4.6	77.2	0.0462
5577	3.8	81.0	0.0380
6893	3.2	84.2	0.0308
8629	3.0	87.2	0.0246
10567	2.3	89.6	0.0201
13149	2.2	91.8	0.0161
16388	1.9	93.7	0.0129
19955	1.5	95.1	0.0106
24884	1.4	96.5	0.0085
30003	1.1	97.6	0.0071
34987	0.8	98.4	0.0061
40168	0.6	99.0	0.0053
45081	0.4	99.4	0.0047
50001	0.3	99.7	0.0042
54934	0.2	99.9	0.0039
59899	0.1	100.0	0.0035

---



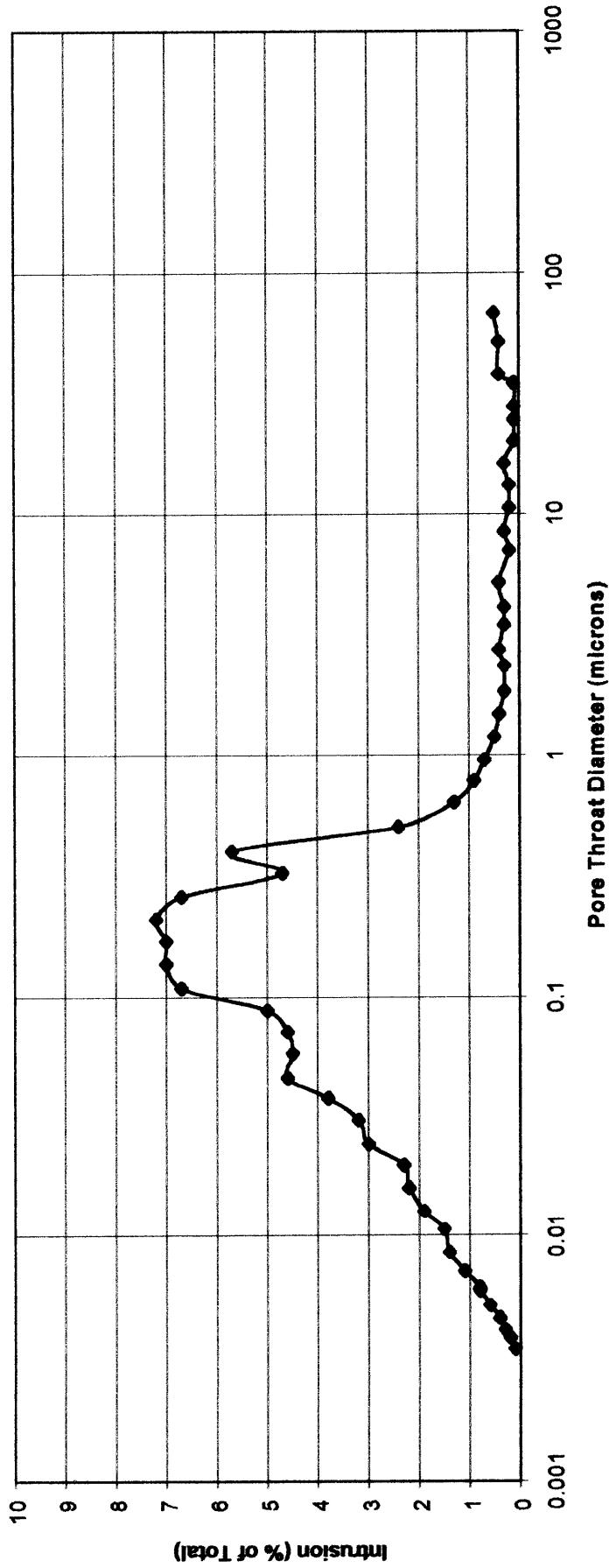
### CAPILLARY PRESSURE

**Client**                    Esso Australia Ltd  
**Well**                      Turrum-7  
  
**Test Method**            Air/Mercury Capillary Pressure Drainage  
  
**Sample**                  210c  
**Depth**                    2626.45 m



# PORE SIZE DISTRIBUTION

**Client** Esso Australia Ltd  
**Well** Turrum-7  
**Test Method** Air/Mercury Capillary Pressure Drainage  
**Sample** 210c  
**Depth** 2626.45 m



***CAPILLARY PRESSURE***

**Client** Esso Australia Ltd  
**Well** Turrum-7  
**Test Method** Air/Mercury Capillary Pressure Drainage  
**Sample** 234c  
**Depth** 2628.45 m

Pressure (psia)	Intrusion (percent)	Saturation (percent)	Pore Diameter (mm)
0.55	0.0	0.0	385.0
2.11	2.7	2.7	100.0
3.10	0.6	3.4	68.3
4.09	0.5	3.8	51.8
5.58	0.5	4.3	38.0
6.09	0.1	4.4	34.8
7.59	0.4	4.8	27.9
8.58	0.2	5.0	24.7
10.6	0.2	5.3	20.1
13.1	0.3	5.6	16.2
16.0	0.3	5.9	13.2
20.0	0.4	6.3	10.6
25.0	0.4	6.7	8.48
30.0	0.5	7.2	7.07
40.6	0.6	8.1	5.22
50.6	0.6	8.7	4.19
61.3	0.8	9.6	3.46
75.9	1.1	10.6	2.79
90.2	1.6	12.2	2.35
116	3.8	16.1	1.83
141	4.6	20.7	1.50
176	5.1	25.8	1.21
222	6.1	31.8	0.953
273	4.8	36.6	0.776
330	5.0	41.6	0.642
421	5.8	47.5	0.504
555	6.2	53.6	0.382

---

Pressure (psia)	Intrusion (percent)	Saturation (percent)	Pore Diameter (mm)
645	2.9	56.5	0.329
826	4.6	61.2	0.257
1024	3.9	65.0	0.207
1264	3.6	68.7	0.168
1566	3.6	72.2	0.135
1954	3.5	75.7	0.109
2425	3.2	78.9	0.0874
2949	2.6	81.5	0.0719
3643	2.6	84.1	0.0582
4594	2.5	86.5	0.0461
5592	1.9	88.5	0.0379
6877	1.6	90.1	0.0308
8595	1.6	91.7	0.0247
10587	1.2	92.9	0.0200
13139	1.2	94.1	0.0161
16400	1.1	95.2	0.0129
19929	0.8	96.0	0.0106
24910	0.9	96.9	0.0085
29974	0.7	97.6	0.0071
34982	0.5	98.1	0.0061
40094	0.5	98.7	0.0053
45015	0.4	99.1	0.0047
49959	0.3	99.4	0.0042
54964	0.3	99.8	0.0039
59983	0.2	100.0	0.0035

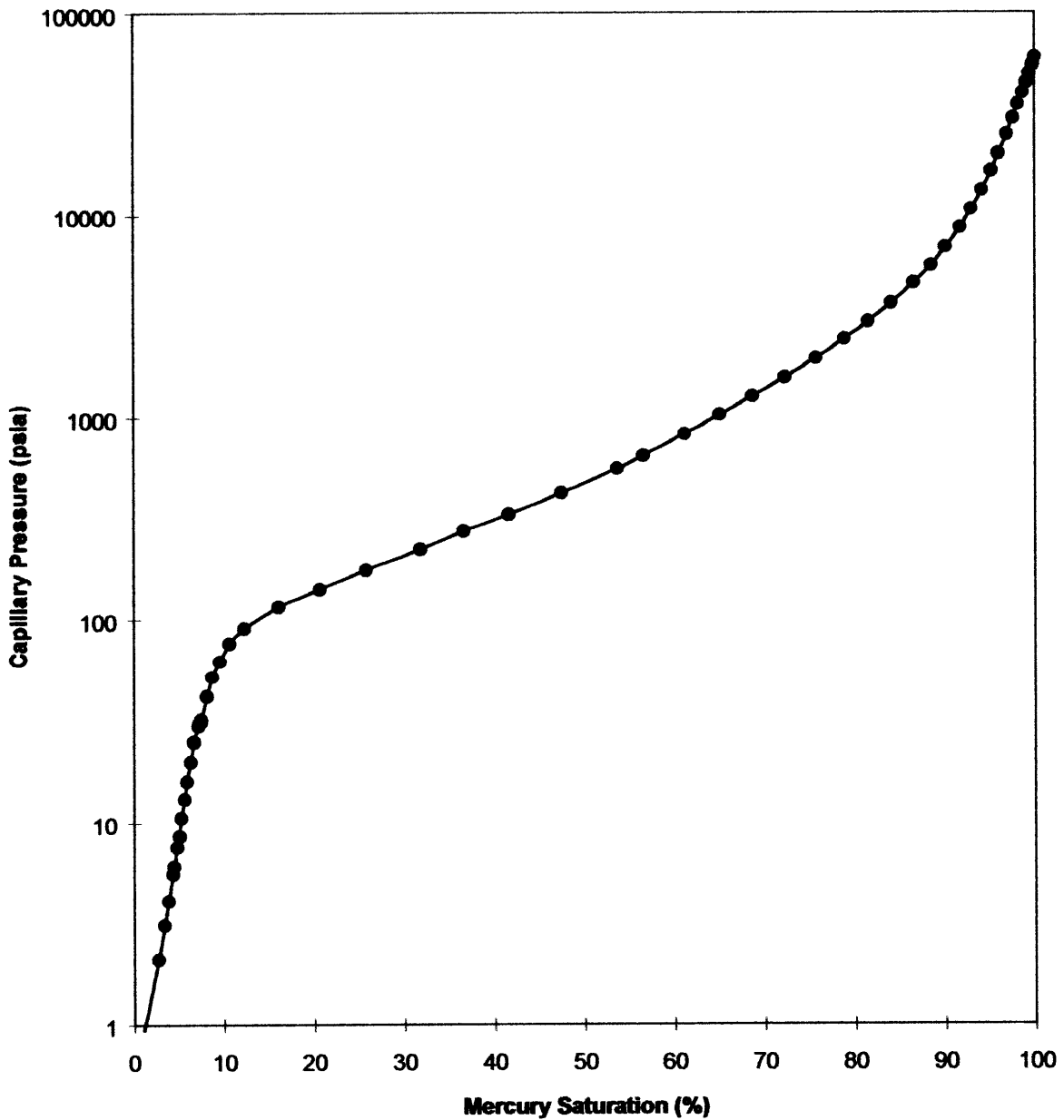
---

### CAPILLARY PRESSURE

**Client**            Esso Australia Ltd  
**Well**              Turrum-7

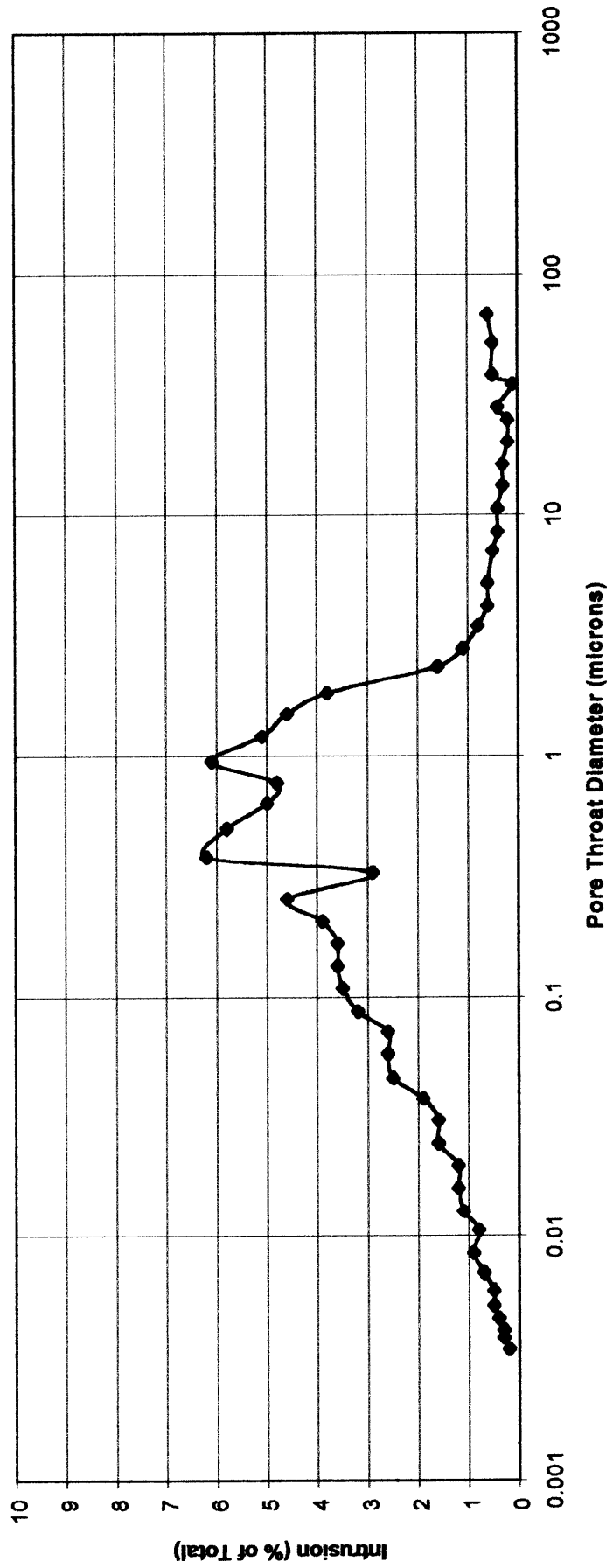
**Test Method**     Air/Mercury Capillary Pressure Drainage

**Sample**           234c  
**Depth**            2628.45 m



# PORE SIZE DISTRIBUTION

**Client** Esso Australia Ltd  
**Well** Turrum-7  
**Test Method** Air/Mercury Capillary Pressure Drainage  
**Sample** 234c  
**Depth** 2628.45 m



907511 [REDACTED]  
334

**CAPILLARY PRESSURE**

**Client** Esso Australia Ltd  
**Well** Turrum-7  
**Test Method** Air/Mercury Capillary Pressure Drainage  
**Sample** 244c  
**Depth** 2629.27 m

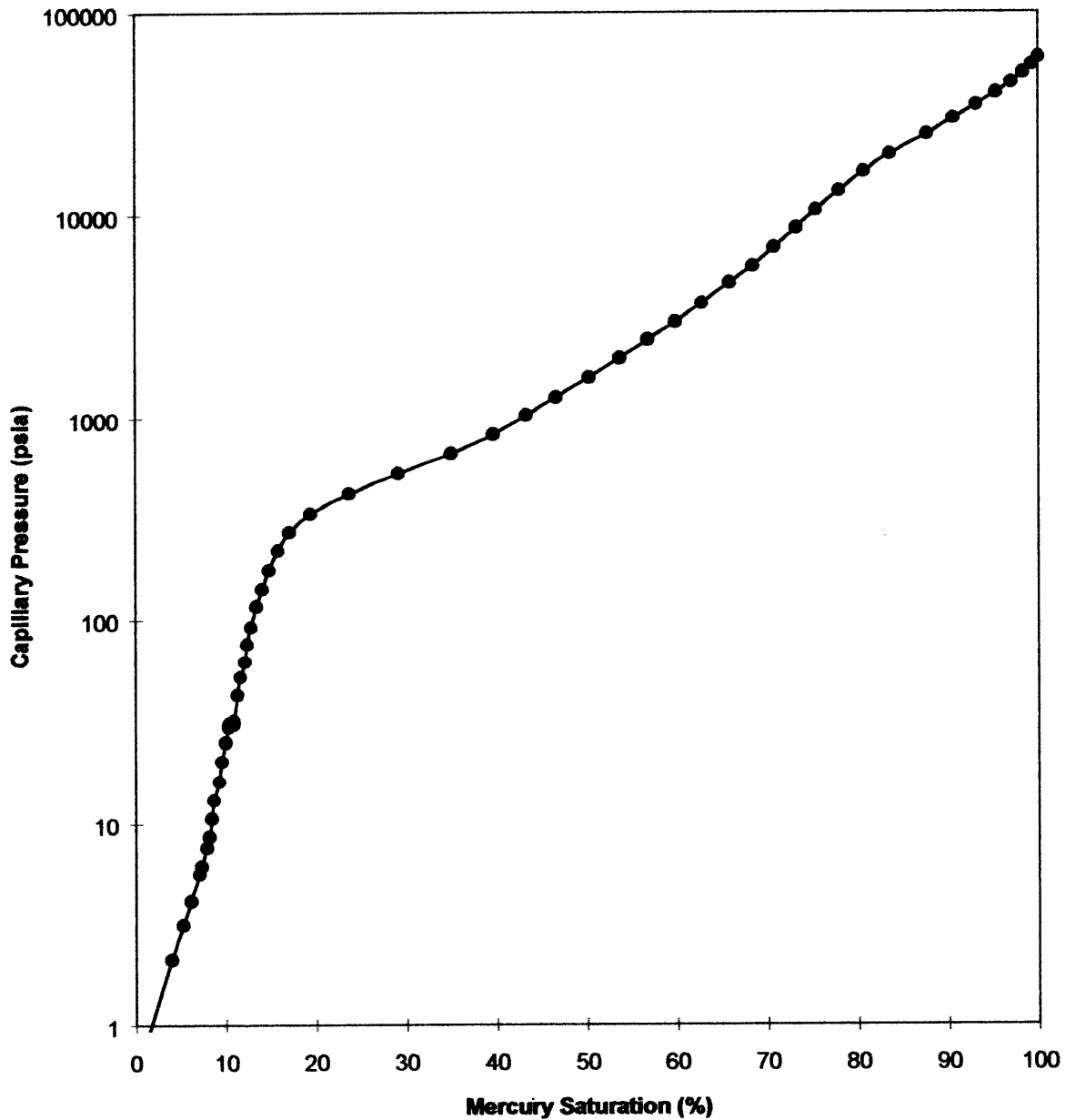
Pressure (psia)	Intrusion (percent)	Saturation (percent)	Pore Diameter (mm)
0.57	0.0	0.0	373.0
2.11	4.0	4.0	101.0
3.12	1.2	5.2	68.0
4.10	0.9	6.1	51.7
5.60	0.9	7.1	37.8
6.11	0.2	7.3	34.7
7.59	0.6	7.9	27.9
8.58	0.3	8.2	24.7
10.6	0.3	8.4	20.0
13.1	0.2	8.7	16.2
16.0	0.6	9.2	13.2
20.0	0.3	9.5	10.6
25.0	0.4	10.0	8.47
30.0	0.4	10.3	7.07
41.1	0.4	11.3	5.16
50.6	0.3	11.6	4.19
60.7	0.5	12.1	3.49
75.4	0.2	12.4	2.81
91.9	0.4	12.8	2.31
116	0.6	13.4	1.82
142	0.6	14.0	1.49
176	0.8	14.8	1.21
220	1.0	15.8	0.962
271	1.3	17.0	0.782
334	2.3	19.4	0.635
421	4.3	23.7	0.504
529	5.4	29.1	0.401

Pressure (psia)	Intrusion (percent)	Saturation (percent)	Pore Diameter (mm)
666	5.9	35.0	0.318
828	4.7	39.6	0.256
1026	3.6	43.3	0.207
1258	3.3	46.6	0.168
1578	3.6	50.2	0.134
1967	3.4	53.7	0.108
2419	3.1	56.8	0.0877
2972	3.0	59.8	0.0713
3665	2.9	62.7	0.0578
4632	3.1	65.8	0.0458
5596	2.5	68.4	0.0379
6893	2.4	70.7	0.0308
8624	2.5	73.2	0.0246
10566	2.2	75.4	0.0201
13147	2.6	77.9	0.0161
16404	2.8	80.7	0.0129
19975	2.9	83.6	0.0106
24992	4.1	87.6	0.0085
29997	2.9	90.6	0.0071
34932	2.6	93.1	0.0061
40070	2.2	95.3	0.0053
45157	1.7	97.0	0.0047
50156	1.3	98.3	0.0042
55110	1.0	99.3	0.0038
59955	0.7	100.0	0.0035



# CAPILLARY PRESSURE

**Client**            Esso Australia Ltd  
**Well**                Turrum-7  
  
**Test Method**      Air/Mercury Capillary Pressure Drainage  
  
**Sample**            244c  
**Depth**             2629.27 m

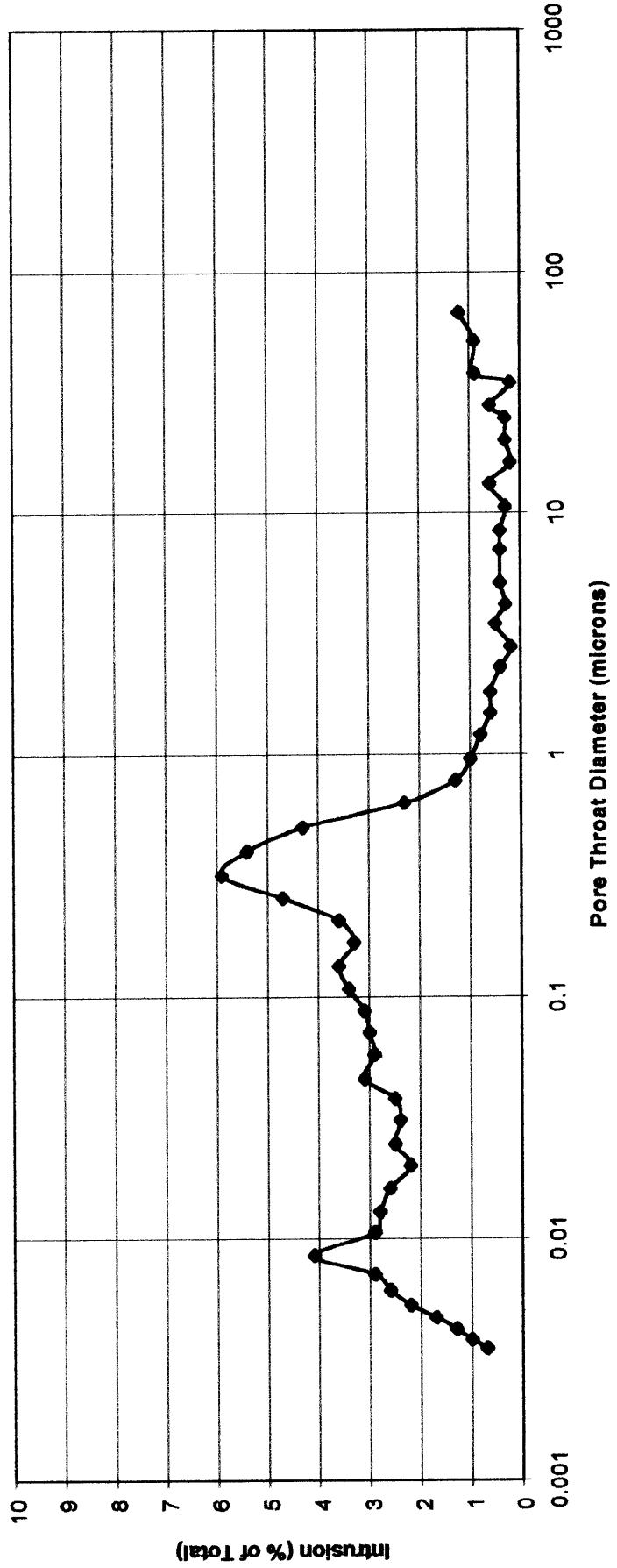


# PORE SIZE DISTRIBUTION

**Client** Esso Australia Ltd  
**Well** Turrum-7

**Test Method** Air/Mercury Capillary Pressure Drainage

**Sample** 244c  
**Depth** 2629.27 m



907511 ~~XXXXXX~~  
338

907511 5

339

907511 ~~3~~  
340

**APPENDIX 6**

**TURRUM 7**

**Well Seismic Processing Report**

Schlumberger Oilfield Australia Pty Limited  
A.C.N. 003 264 597  
Level 4, 150 Albert Road  
South Melbourne Victoria 3205  
Ph: (03) 9696 6266 Fax: (03) 9690 0309

***ESSO Australia Ltd.***

**WELL SEISMIC PROCESSING REPORT**

**VSP/Geogram**

***Turrum-7***

FIELD: TURRUM

COUNTRY: AUSTRALIA

COORDINATES: Longitude : 148 15'49.2257" E  
: Latitude : 38 15'52.2558" S

DATE OF VSP SURVEY: 14 Sep 1999

REFERENCE NO: AMF-561293/561294

INTERVAL: 2800-181 MKb

Prepared by:  
Yuri Solovyov (Schlumberger Geoquest)

## CONTENTS

<b>1.</b>	<b>Introduction</b>	4
<b>2.</b>	<b>Data Acquisition</b>	4
<b>3.</b>	<b>Well Seismic Edit</b>	5
3.1	Data quality	5
3.2	Transit Time Measurement	5
3.3	Correction to Datum	5
<b>4.</b>	<b>VSP Processing</b>	6
4.1	Stacking	6
4.2	Spherical Divergence Correction and Bandpass Filter	6
4.3	Velocity Filter	8
4.4	Waveshaping Deconvolution	8
<b>5.</b>	<b>Sonic Calibration Processing</b>	9
5.1	Sonic Calibration	9
5.2	Open Hole Logs	10
5.3	Correction to Datum and Velocity Modeling	11
5.4	Sonic Calibration Results	11
<b>6.</b>	<b>Synthetic Seismogram Processing</b>	11
6.1	Depth to Time Conversion	11
6.2	Primary Reflection Coefficients	11
6.3	Primaries with Transmission Loss	12
6.4	Primaries plus Multiples	12
6.5	Multiples Only	12
6.6	Wavelet	12
6.7	Polarity Convention	12
6.8	Convolution	12

<b>A Summary of Geophysical Listings</b>	13
A1 Well Seismic Report	13
A2 Drift & Sonic Adjustment	13
A3 Velocity Report	14
A4 Time to Depth Report	15
A5 Depth to Time Report	15

### List of Figures

1 Amplitude Spectrum	7
2 Schlumberger Wavelet Polarity Convention	17

## 1. Introduction

One vertical seismic profile was recorded with the Dual Combinable Seismic Acquisition Tool (CSAT) at the *Turrum-7* well. The survey was run on 14 September 1999.

Processing of the data consisted of performing the VSP processing, sonic calibration and generating a Geogram. This report describes the processing, explains the parameter choices and presents the results.

## 2. Data Acquisition

The data were acquired in one logging run using the three component Dual Combinable Seismic Acquisition Tool (CSAT). An Air Gun DHS-1500, with 500 cu in capacity was used as the source. The gun was positioned 6 meters below the sea level. The hydrophone was attached 3 m below the gun. Recording was made on the Schlumberger Maxis 500 Unit using DLIS format.

Table 1. Survey Parameters

Elevation of KB	26 M
Elevation of DF	26 M
Elevation of GL	-62 M
Energy Source	500 cu in. Airgun
Source Offset	45 M
Source Depth	6 M below Sea Level
Reference Sensor	Hydrophone
Hydrophone Offset	45 M
Hydrophone Depth	9 M below GL
Source & Hyd. Azimuth	45 Degr.
Tool Type	Dual CSAT
Tool Combination	Dual GAC geophone, 19 m spacing
De-coupled Geophones	Yes
Shaker Fitted	Yes
Number of Axis	3
Geophone Type	GAC
Frequency Response (GAC)	3-200 Hz
Sampling Rate	1 ms.
Recording Time	3.0 sec.
Acquisition Unit	MAXIS
Recording Format	DLIS



### 3. Well Seismic Edit

Each shot of the raw geophone data was evaluated and edited as necessary. The hydrophone data were also evaluated for signature changes and timing shifts.

The good shots at each level were stacked, using a median stacking technique, to increase the signal to noise ratio of the data. The transit time of each trace was re-computed after stacking.

#### 3.1 Data Quality

The overall quality of the data is good. Some tube wave noise was present in raw data. It was effectively reduced after velocity filtering.

#### 3.2 Transit Time Measurement

The transit time measured,  $\Delta t$ , corresponds to a difference between arrivals recorded by surface and downhole sensors. The reference time (zero time) is the physical recording of the source signal by accelerometers on the gun or sensors positioned near the source. In this case, a hydrophone positioned 3 m below the gun was used as the reference. First break picking algorithms were used on both the hydrophone and the geophone.

#### 3.3 Correction to Datum

Seismic Reference Datum (SRD) is at Mean Sea Level.

The source was positioned 6 meters below the sea level. A hydrophone was located 3 meter below airgun. A static correction of 5.9 msec (OWT) was thus applied to all data to correct it to SRD.

#### 4. VSP Processing

The vertical component of the VSP data was processed using the conventional zero offset vertical incidence processing chain. The following subsections describe the main aspects of the processing chain the final VSP data set.

- load data
- edit bad records and sort raw VSP traces
- Z component median stack
- peak break time
- bandpass filter : 5-110 HZ
- time varying gain :  $(T_0/T_1)^{\exp 1}$
- first break normalization gate : 100 MS
- static shifting to SRD : 0.0059 S
- wavefield separation (mean filter, 9 levels, 1 sample)
- waveshaping deconvolution (decon operator created by filtered unit impulse, 5-80 HZ,
- filter length : 1 S)
- upgoing wavefield enhancement (median filter, 7 levels, 1 sample)
- -90 deg phase rotation
- corridor stack : 0.1 S window, (all traces except the deepest 5)
- corridor stack : mask used

##### 4.1 Stacking

After reordering and selecting the raw shots, a median stack was performed on the vertical component data. In this method of stacking, at each sample time, the amplitudes of the input traces are read and sorted in ascending order. The output is the median amplitude value from this ordering. If an even number of traces are input, the first is dropped and a median calculated. Then the last is dropped and another median found. The final output is the average of these two median values. The surface sensor (hydrophone) breaks are used as the zero time for stacking. The break time of each trace is recomputed after stacking.

The data quality is average with some high frequency noise present on raw Z component. The Amplitude Spectrum of vertical component for each stacked level is presented in Figure 1.

##### 4.2 Spherical Divergence Correction and Bandpass Filter

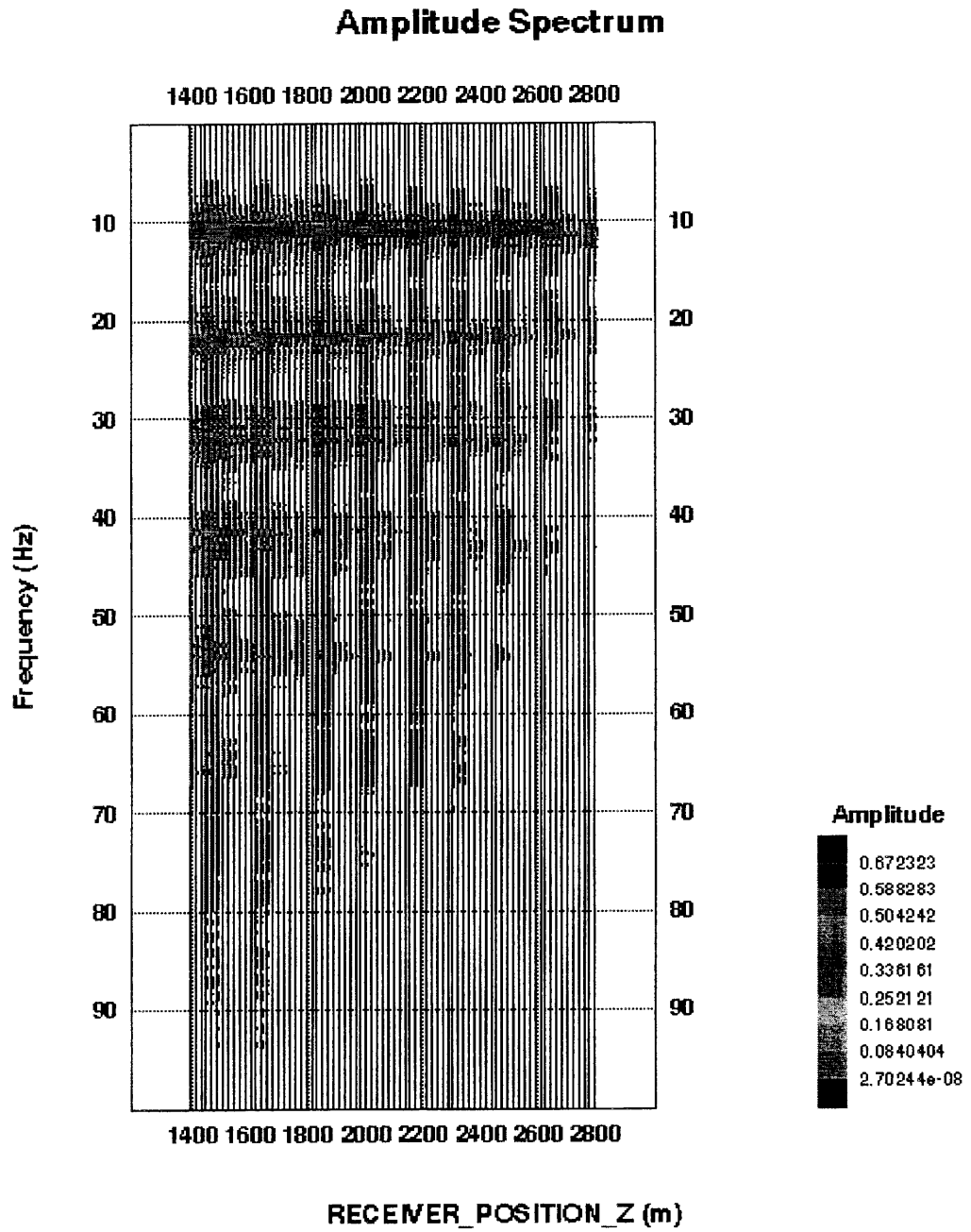
A bandpass filter of 5-110 hertz bandwidth was applied and time varying gain function of the exponential form :

$$Gain(T) = \left( \frac{T}{T_0} \right)^{\alpha}$$

where T is the recorded time,  $T_0$  is the first break time and  $\alpha = 1$

Trace equalization was applied by normalizing the RMS amplitude of the first break to correct for transmission losses of the direct wave. A normalization window of 100 millisecs was used. Static shifting to SRD= - 0.0059 s was applied to Z component stacked data. Stacked Z component data presented in Plot1.

Figure 1. Amplitude Spectrum



### 4.3 Velocity filter

907511 ~~348~~

348

The downgoing coherent energy is estimated using nine levels mean velocity filter. The filter array is moved down one level after each computation and the process is repeated level by level over the entire dataset. As a result, the deepest and shallowest levels are lost because of edge effects.

The residual wavefield is obtained by subtracting the downgoing coherent energy from the total wavefield. The residual wavefield is dominated by reflected compressional events (Plot 3).

The downgoing wavefield is displayed in one way time (Plot 2).

### 4.4 Waveshaping Deconvolution

The Waveshaping deconvolution operator is a double sided operator and is designed trace by trace opening 20 ms before the first break with a window length of 1 S. The desired outputs were chosen to be zero phase with a band width of 5-80 Hz. Once the design is made upon the downgoing wavefield, it is applied to the downgoing and subtracted wavefield at the same level. The upgoing compressional wavefield is enhanced in an exactly analogous manner to before.

The trace by trace deconvolution is applied in order to collapse the multiple sequence of shear arrivals, diffractions or out of plane reflections. The result of Waveshaping deconvolution on the upgoing wavefield, enhanced by 7 level median filter is shown in Plot 5.

The downgoing wavefield is displayed in one way time (Plot 4).

A corridor stack was computed on the data after  $-90$  deg rotation of the Waveshaping deconvolution output by defining a constant 100 ms timing window along the time depth curve and stacking the data onto a single trace. All traces were used except the deepest 5 traces. This trace under normal circumstances should satisfy the assumption of one dimensionality and provide the best seismic representation of the borehole. In addition to that the corridor stack within the Input mask, displayed in the plot, was computed. This is displayed in Plot 6 (Normal Polarity) and Plot 7 (Reversed Polarity).

## 5. Sonic Calibration Processing

### 5.1 Sonic Calibration

A 'drift' curve is obtained using the sonic log and the vertical check level times. The term 'drift' is defined as the seismic time (from check shots) minus the sonic time (from integration of edited sonic). Commonly the word 'drift' is used to identify the above difference, or to identify the gradient of drift versus increasing depth, or to identify a difference of drift between two levels.

The gradient of drift, that is the slope of the drift curve, can be negative or positive.

For a negative drift ( $\Delta\text{drift}/\Delta\text{depth} < 0$ ) the sonic time is greater than the seismic time over a certain section of the log.

For a positive drift ( $\Delta\text{drift}/\Delta\text{depth} > 0$ ), the sonic time is less than the seismic time over a certain section of the log.

The drift curve, between two levels, is then an indication of the error on the integrated sonic or an indication of the amount of correction required on the sonic to have the TTI of the corrected sonic match the check shot times.

Two methods of correction to the sonic log are used.

1. Uniform or block shift. This method applies a uniform correction to all the sonic values over the interval. This uniform correction is applied in the case of positive drift and is the average correction represented by the drift curve gradient expressed in  $\mu\text{sec}/\text{ft}$ .

2.  $\Delta T$  Minimum. In the case of negative drift a second method is used, called  $\Delta$  minimum. This applies a differential correction to the sonic log, where it is assumed that the greatest amount of transit time error is caused by the lower velocity sections of the log. Over a given interval the method will correct only  $\Delta t$  values which are higher than a threshold, the  $\Delta t_{\text{min}}$ . Values of  $\Delta$  which are lower than the threshold are not corrected. The correction is a reduction of the excess of  $\Delta t$  over  $\Delta t_{\text{min}}$ ,  $\Delta t - \Delta t_{\text{min}}$ .

$\Delta t - \Delta t_{\text{min}}$  is reduced through multiplication by a reduction coefficient which remains constant over the interval. This reduction coefficient, named  $G$ , can be defined as:

$$G = 1 + \frac{\text{drift}}{(\Delta t - \Delta t_{\text{min}})dZ}$$

Where drift is the drift over the interval to be corrected and the value  $(\Delta t - \Delta t_{\text{min}})dZ$  is the time difference between the integrals of the two curves  $\Delta t$  and  $\Delta t_{\text{min}}$ . only over the intervals where  $\Delta t > \Delta t_{\text{min}}$ .

Hence the corrected sonic:  $\Delta t = G(\Delta t - \Delta t_{\text{min}}) + \Delta t_{\text{min}}$ .

## 5.2 Open Hole Logs

The DT spliced from 2 service runs and edited for washouts (see Plots 6,7) was used for a drift computation.

The density log has been edited to take into account bad hole condition and extended from 638 mSRD to mean sea level, using constant value of 2.4 g/cm<sup>3</sup>.

The gamma ray, induction resistivity, neutron porosity and caliper logs are included as correlation curves.

## 5.3 Correction to Datum and Velocity Modeling

The sonic calibration processing has been referenced to mean sea level which the seismic reference datum. Static corrections are applied to correct for source offset and source depth.

## 5.4 Sonic Calibration Results


The top of the sonic log (638 metres below SRD) is chosen as the origin for the calibration drift curve.

The drift curve is the correction imposed upon the sonic log. The adjusted sonic curve is considered to be the best result using the available data. A list of shifts used on the sonic data is given in A2 Listing.

Raw sonic log, adjusted sonic log and integrated raw and adjusted travel times are displayed in Plot 8 - Drift Corrected Sonic.

Velocity Crossplot is presented in Plot 9.

## 6. Synthetic Seismogram Processing

907511   
351

GEOGRAM plots were generated using 20, 25, 30 and 40 HZ -90deg shifted 0 Phase Ricker Wavelets.

The presentations include both normal and reversed polarity on a time scale of 20 cm/sec (Plots 6,7).

GEOGRAM processing produces synthetic seismic traces based on reflection coefficients generated from sonic and density measurements in the well-bore. The steps in the processing chain are the following:

- Depth to time conversion
- Reflection coefficient generation
- Attenuation coefficient calculation
- Convolution
- Output

### 6.1 Depth to Time Conversion

Open hole logs are recorded from the bottom to top with a depth index. This data is converted to a two-way time index.

### 6.2 Primary Reflection Coefficients

Sonic and density data are averaged over chosen time intervals (normally 2 or 4 millisecs). Reflection coefficients are then computed using:

$$R = \frac{r_2 \cdot v_2 - r_1 \cdot v_1}{r_2 \cdot v_2 + r_1 \cdot v_1}$$

where:

$r_1$  = density of the layer above the reflection interface

$r_2$  = density of the layer below the reflection interface

$v_1$  = compressional wave velocity of the layer above the reflection interface

$v_2$  = compressional wave velocity of the layer below the reflection interface

This computation is done for each time interval to generate a set of primary reflection coefficients without transmission losses.

### 6.3 Primaries with Transmission Loss

Transmission loss on two-way attenuation coefficients is computed using:

$$A_n = (1 - R_1^2).(1 - R_2^2).(1 - R_3^2)...(1 - R_n^2)$$

A set of primary reflection coefficients with transmission loss is generated using:

$$Primary_n = R_n.A_{n-1}$$

### 6.4 Primaries plus Multiples

Multiples are computed from these input reflection coefficients using the transform technique from the top of the well to obtain the impulse response of the earth. The transform outputs primaries plus multiples.

### 6.5 Multiples Only

By subtracting previously calculated primaries from the above result we obtain multiples only.

### 6.6 Wavelet

A theoretical wavelet is chosen to use for convolution with the reflection coefficients previously generated. Choices available include:

- Klauder wavelet
- Ricker zero phase wavelet
- Ricker minimum phase wavelet
- Butterworth wavelet
- User defined wavelet

Time variant Butterworth filtering can be applied after convolution.

### 6.7 Polarity Convention

An increase in acoustic impedance gives a positive reflection coefficient, is written to tape as a negative number and is displayed as a white trough under normal polarity. Polarity conventions are displayed in figure 2.

### 6.8 Convolution

The standard procedure of convolving the wavelet with reflection coefficients; the output is the synthetic seismogram.



## A Summary of Geophysical Listings

Five geophysical data listings are appended to this report. Following is a brief description of the format of each listing.

### **A1 Check Shot Data**

1. Level number: the level number starting from the top level (includes any imposed shots).
2. Vertical depth from SRD: *dsrd*, the depth in metres from seismic reference datum.
3. Measured depth from KB: *dkb*, the depth in metres from kelly bushing.
4. Observed travel time HYD to GEO: *tim0*, the transit time picked from the stacked data by subtracting the surface sensor first break time from the downhole sensor first break time.
5. Vertical travel time SRD to GEO: *shtm*, is *timv* corrected for the vertical distance between source and datum.
6. Delta depth between shots:  $\Delta depth$ , the vertical distance between each level.
7. Delta time between shots:  $\Delta time$ , the difference in vertical travel time (*shtm*), between each level.
8. Interval velocity between shots: the average seismic velocity between each level,  $\Delta depth / \Delta time$
9. Average velocity SRD to GEO: the average seismic velocity from datum to the corresponding checkshot level,  $\frac{dsrd}{shtm}$

**Zone Set Data**

1. Knee number: the knee number starting from the highest knee. (The first knees listed will generally be at SRD and the top of sonic. The drift imposed at these knees will normally be zero.)
2. Measured depth from KB: the depth in metres from kelly bushing
3. Vertical depth from SRD: the depth in metres from seismic reference datum.
4. Selected Drift at knee: the value of drift imposed at each knee.
5. Shift: the change in drift divided by the change in depth between any two levels.
6. Delta-T: see section 4 of report for an explanation of  $\Delta t_{min}$ .
7. Reuction factor G: see section 4 of report.
8. Selected Drift Gradient: the gradient of the imposed drift curve.

**Sonic Adjustment Data**

1. Measured depth from KB: the depth in metres from kelly bushing
2. Vertical depth from SRD: the depth in metres from seismic reference datum.
3. Vertical shot time SRD to GEO: the calculated vertical travel time from datum to downhole geophone.
4. Adjusted Sonic Time.
5. Computed drift at level: the checkshot time minus the integrated raw sonic time.
6. Residual Shot Time - Adjusted Sonic Time.
7. Adjusted Interval Velocity.
8. Adjusted RMS Velocity.
9. Adjusted Average Velocity.

## A3 Velocity Report

907511 ~~355~~  
355

The data in this listing has been resampled in time.

1. Two way travel time from SRD: this is the index for the data in this listing. The first value is at SRD (0 millisecs) and the sampling rate is 2 millisecs.
2. Measured depth from KB: the depth from KB at each corresponding value of two way time.
3. Vertical depth from SRD: the vertical depth from SRD at each corresponding value of two way time.
4. Average velocity SRD to GEO: the vertical depth from SRD divided by half the two way time.
5. RMS velocity: the root mean square velocity from datum to the corresponding value of two way time.

$$v_{rms} = \sqrt{S \sum_{i=1}^n v_i^2 t_i / S \sum_{i=1}^n t_i}$$

where  $v_i$  is the velocity between each 2 millisecs interval.

6. Interval velocity: the velocity between each sampled depth. Typically, the sampling rate is 2 millisecs two way time, (1 millisecc one way time) therefore the interval velocity will be equal to the depth increment divided by 0.002. It is equivalent to column 9 from the Velocity Report.

907511 ~~356~~

356

**A4 Time to Depth**

1. Two Way Sonic Time from SRD
- 2-11. Depth at Time 0-9 ms: moveout times every 1 ms

**A5 Depth to Time Report**

1. Vertical Depth from SRD
- 2-11. Two Way Travel Time 0-27 m: moveout depths every 3 m.

### SCHLUMBERGER (SEG-1976) WAVELET POLARITY CONVENTION

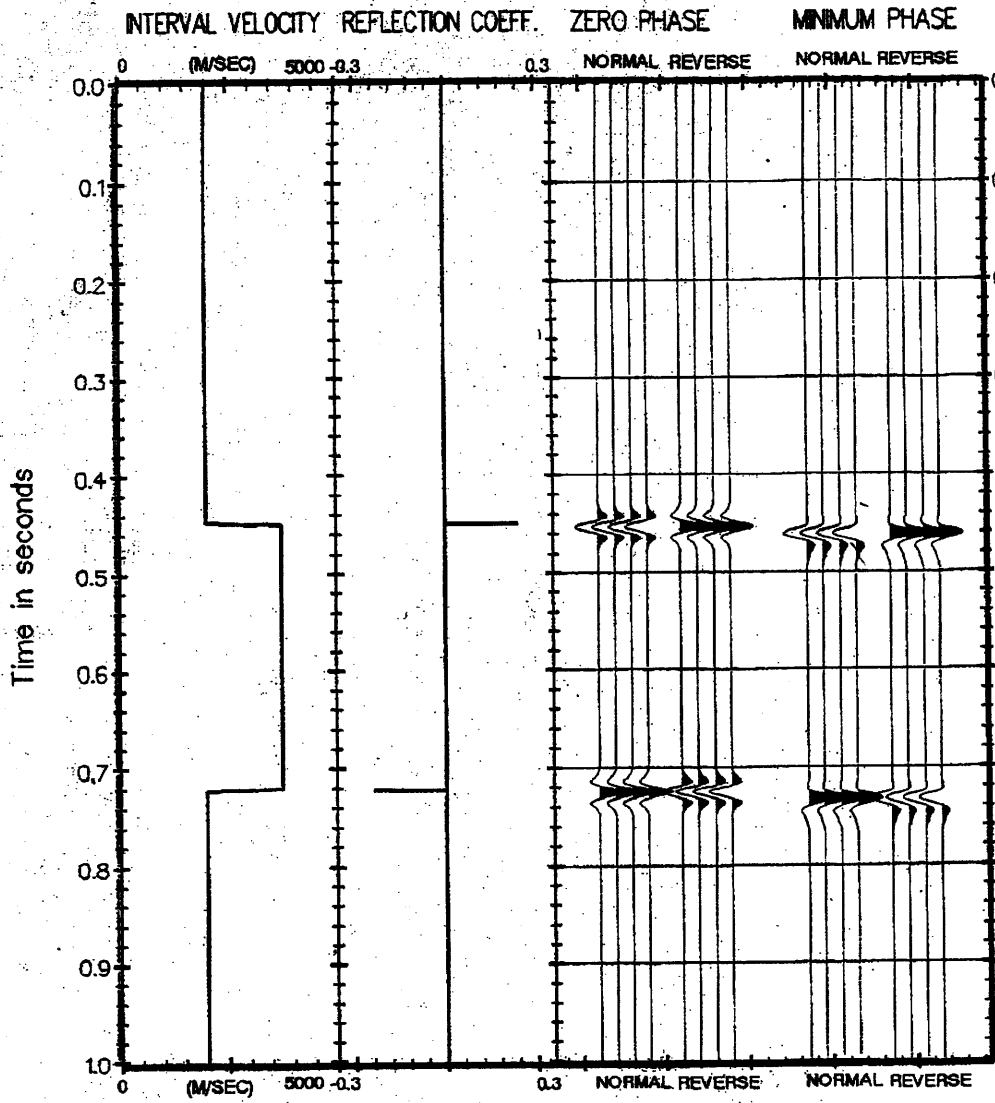


Figure 2. Schlumberger Wavelet Polarity Convention